frontiers | Research Topics

Metabolic modulation of cellular function

Edited by
Or Kakhlon, Ann Saada and Pablo Vicente Escriba

Published in
Frontiers in Cell and Developmental Biology
Frontiers in Molecular Biosciences

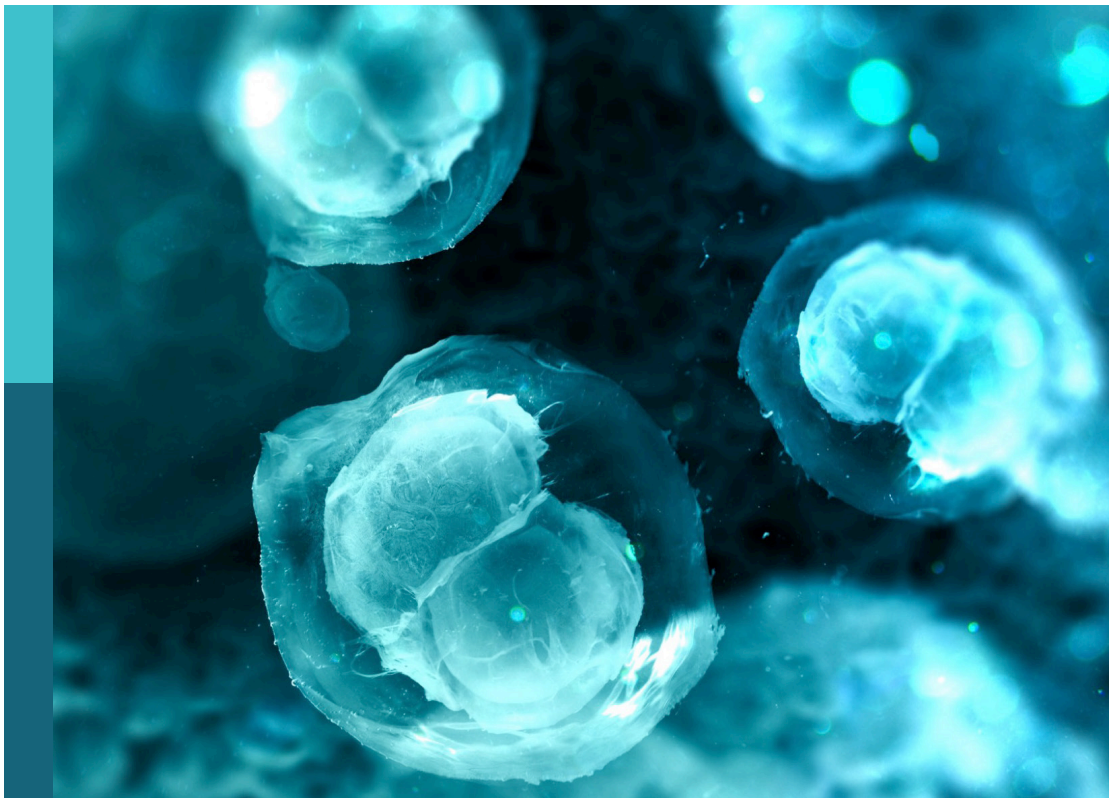

ISSN 1664-8714
ISBN 978-2-8325-4688-8
DOI 10.3389/978-2-8325-4688-8

About Frontiers

Frontiers is more than just an open access publisher of scholarly articles: it is a pioneering approach to the world of academia, radically improving the way scholarly research is managed. The grand vision of Frontiers is a world where all people have an equal opportunity to seek, share and generate knowledge. Frontiers provides immediate and permanent online open access to all its publications, but this alone is not enough to realize our grand goals.

Frontiers journal series

The Frontiers journal series is a multi-tier and interdisciplinary set of open-access, online journals, promising a paradigm shift from the current review, selection and dissemination processes in academic publishing. All Frontiers journals are driven by researchers for researchers; therefore, they constitute a service to the scholarly community. At the same time, the *Frontiers journal series* operates on a revolutionary invention, the tiered publishing system, initially addressing specific communities of scholars, and gradually climbing up to broader public understanding, thus serving the interests of the lay society, too.

Dedication to quality

Each Frontiers article is a landmark of the highest quality, thanks to genuinely collaborative interactions between authors and review editors, who include some of the world's best academicians. Research must be certified by peers before entering a stream of knowledge that may eventually reach the public - and shape society; therefore, Frontiers only applies the most rigorous and unbiased reviews. Frontiers revolutionizes research publishing by freely delivering the most outstanding research, evaluated with no bias from both the academic and social point of view. By applying the most advanced information technologies, Frontiers is catapulting scholarly publishing into a new generation.

What are Frontiers Research Topics?

Frontiers Research Topics are very popular trademarks of the *Frontiers journals series*: they are collections of at least ten articles, all centered on a particular subject. With their unique mix of varied contributions from Original Research to Review Articles, Frontiers Research Topics unify the most influential researchers, the latest key findings and historical advances in a hot research area.

Find out more on how to host your own Frontiers Research Topic or contribute to one as an author by contacting the Frontiers editorial office: frontiersin.org/about/contact

Metabolic modulation of cellular function

Topic editors

Or Kakhlon — Hadassah Medical Center, Israel

Ann Saada — Hebrew University of Jerusalem, Israel

Pablo Vicente Escriba — University of the Balearic Islands, Spain

Citation

Kakhlon, O., Saada, A., Escriba, P. V., eds. (2024). *Metabolic modulation of cellular function*. Lausanne: Frontiers Media SA. doi: 10.3389/978-2-8325-4688-8

Table of contents

frontiers | Frontiers in Cell and Developmental Biology

TYPE Editorial
PUBLISHED 18 March 2024
DOI 10.3389/fcell.2024.1395922

OPEN ACCESS

EDITED AND REVIEWED BY
Graça Soveral,
University of Lisbon, Portugal

*CORRESPONDENCE
Or Kakhlon,
ork@hadassah.org.il

RECEIVED 04 March 2024
ACCEPTED 08 March 2024
PUBLISHED 18 March 2024

CITATION
Kakhlon O, Saada A and Escriba PV (2024), Editorial: Metabolic modulation of cellular function.
Front. Cell Dev. Biol. 12:1395922.
doi: 10.3389/fcell.2024.1395922

Editorial: Metabolic modulation of cellular function

Or Kakhlon[1]*, Ann Saada[1] and Pablo V. Escriba[2]

[1]Hadassah Medical Center, Jerusalem, Israel, [2]University of the Balearic Islands, Palma de Mallorca, Spain

KEYWORDS

metabolism, metabolic pathways, drug discovery, cell fate, metabolomics

Editorial on the Research Topic
Metabolic modulation of cellular function

In this Research Topic, metabolic changes are described as sensors or mediators of biological processes in cells and organisms. These functions are performed by metabolites as substrates, products, and allosteric regulators of cellular enzymes and as substrates of post-translational and epigenetic modifications, enabling them to mediate cell signaling. This Research Topic showcases metabolites as a pool of molecules (metabolome) which regulate cell function, fate and structure. This definition implies that not all the constituents of pathways or mechanisms influenced by the metabolome are known *a priori*, i.e., these pathways/mechanisms are investigated by an *untargeted* approach. *Untargeted* studies can thus *generate* new hypotheses on how metabolites sense or mediate the phenotype(s) investigated, or even discover novel pathways converging to and diverging from known pathways. Alternatively, in *targeted* analyses, well-established metabolites and metabolic pathways are presumably implicated in new phenotypes. Only these metabolites are quantified to obtain steady-state levels and metabolic fluxes by mass spectrometry and isotope tracing, respectively. Targeted studies *test* hypotheses limited to specific research questions. Targeted and untargeted analyses may also be combined to unveil novel connections and networks involved in the phenotypes studied. Lastly, metabolite levels and fluxes are also diagnostic and efficacy biomarkers. Metabolic investigations involving hypotheses testing and biomarkers generation illustrate how metabolic changes can modulate cell function as represented in this Research Topic.

Three papers illustrate how metabolic reprogramming can directly determine cell fate with ensuing consequences on health and disease. Zhao et al. show that during acute kidney injury (AKI) many anabolic and catabolic pathways are modified. Beyond the reprogramming of well-known pathways such as fatty acid oxidation and glycolysis, AKI also implicates triglyceride overaccumulation, activation of polyol metabolism and amino acid and redox modifications. These broad metabolic alterations activate programmed cell death pathways: apoptosis, ferroptosis, necroptosis, pyroptosis and autophagic block. This review thus represents a hypothesis-generating study in which the involvement of broad-scale metabolic pathways serves as a fertile ground for the discovery of novel metabolic-based therapeutic interventions. Another interesting review linking metabolic reprogramming with programmed cell death is Yang et al. This review discusses Paneth cell (Lueschow and McElroy, 2020), epithelial cells in the intestinal crypt, which maintain intestinal health. Paneth cells are multi-functional cells regulating microbiota composition (by secreting the selective bactericidal α-defensin), and intestinal epithelial and stem cells death and growth. This review is unique to this Research Topic, inasmuch as it does not describe specific metabolic pathways,

but rather modulation of intestinal microbiota, which, on its own, is a key systemic metabolic modulator. Commensal microbiota determine intestinal metabolic homeostasis by both expressing metabolic enzymes not encoded by the host and cross-feeding between bacterial stains which produces nutrients for host consumption [*e.g.*, acetate produced by *Bifidobacterium* is a substrate for butyrate produced by *F. prausnitzii* (Lee et al., 2018)]. The third paper focusing on cell fate modulation by metabolic reprogramming is Sukjoi et al. The authors have previously shown that holocarboxylase synthetase (HLCS) is overexpressed and pro-oncogenic in the triple-negative breast cancer (TNBC) cell line MDA-MB-231. Here they test the hypothesis that HLCS knockdown is anti-carcinogenic and investigate which biochemical and metabolic changes HLCS knockdown causes. They show that HLCS knockdown is mainly associated with inhibition of proteins facilitating invasiveness and metastasis, such as SerpinB2 (Harris et al., 2017) and collagenase (Fields, 2013). The authors also suggest that HLCS knockdown inhibits malignant cell growth by suppressing the urea cycle: HLCS-mediated increase in argininosuccinate synthase can increase aspartate and ensuing nucleotide synthesis and constitutive proliferation.

Two papers describe diseases directly caused by metabolic dysfunction, possibly ameliorated by endogenous metabolic factors. Bourebaba et al. show that sex hormone binding globulin (SHBG) can lower saturated and pro-inflammatory fatty acids causing metabolic syndrome. Furthermore, SHBG induced lipolysis, repressed lipogenesis, increased insulin sensitivity by boosting insulin signaling receptors and attenuated pro-inflammatory factors demonstrating a comprehensive effect on metabolic syndrome. Shilian et al. discuss the role of the elongator complex, deficient in familial dysautonomia (FD), on acetyl-CoA synthesis/target acetylation through stabilization of the key metabolic enzyme ATP-citrate lyase (ACLY) which acetylates the cytoskeleton enabling neuritogenesis. Elongator deficiency leads to proteasomal degradation of microtubule associated protein Tau, reversible by deacetylase inhibitors. Moreover, Tau and neuritogenesis deficiencies can be corrected by ACLY overexpression demonstrating a novel potential metabolic therapy for FD through acetyl-CoA restoration.

Another set of articles uses knowledge on metabolic reprogramming as a platform for drug discovery. Arévalo et al.'s review provides an updated account of the long-known anti-leukemic efficacy of botanical drugs. They show that chemoresistant metabolic reprogramming in leukemia cells (glycolytic activation and OxPhos suppression) is modified by botanical compounds, *e.g.*, inhibition of glycolytic enzymes by alkaloids and enhancement of fatty acid oxidation by avocado-extracted lipid B. These metabolic modifications predispose originally chemoresistant leukemia cells to cytotoxic chemotherapy making botanical drugs preferred co-adjuvants. The approach presented in this review is illustrated in Granit et al.'s research article. The authors tackle cisplatin chemoresistance in TNBC purportedly caused by metabolic and ensuing epigenetic reprogramming. They show that the histone deacetylase inhibitor valproic acid (VPA) can mitigate cisplatin chemoresistance by inhibiting fatty acid oxidation and OxPhos through decreasing both acylcarnitines and carnitine as an FAO precursor. In a follow-up work Mizrahi et al., the authors show that VPA actually increases cisplatin chemoresistance by up-modulation of glycolysis and the anti-oxidant enzyme aldehyde dehydrogenase (ALDH) and that only combining VPA with the pro-oxidant ALDH inhibitor disulfiram can overcome these pro-resistance effects of VPA both in TNBC cells and in more patient-relevant TNBC organoids. The work by Gharaba et al. uses aberrant cell-morphological phenotype as a hypothesis-driven strategy for potential drug discovery. Newly discovered deficient nuclear actin cap in Huntington Disease (HD) fibroblasts is associated with aberrant cell motility as acceptedly manifested in Hutchinson-Gilford progeria syndrome, used as an actin cap lacking reference. The authors propose that the quantifiable correction of aberrant actin cap and motility might serve to assess potential HD drug efficiency and demonstrate this by correction of these phenotypes using the mitochondrial antioxidant Mito Q.

Other papers provide metabolic underpinnings for key organismal processes, embryonal development and aging. Sakai et al. show that hypoxia-triggered and glycolysis-enabled proliferation is necessary for neural tube closure of neuroepithelial cells, which is not influenced by OxPhos modulation. Fang et al. describe systemic metabolic biomarkers of aging showing their association with attrition over time of mitochondrial TCA cycle-dependent pathways and parallel increase in glycolytic flux. Many of these biomarkers are accumulated metabolites which do not degrade. As opposed to the systemic level, at the organ level, inter-organ metabolomic variability is caused by differences in aging onset, *e.g.*, glycolysis induced at different ages in different muscle types.

Lastly, Esterhuizen et al.'s perspective reviews the impact of environmental stressors on metabolic diseases concluding that this relationship is bidirectional: environmental stressors suppressing human physiology, and physiological stress, especially perturbed hormonal balance and immunity, predisposing to environmental diseases, especially due to compromised detoxification capacity.

In summary, this Research Topic comprises a diverse set of papers on the modulation of cell function via metabolic reprogramming. Most papers test hypotheses and tackle the involvement of metabolic reprogramming in cell fate determination, endogenous pathogenic mechanisms, drug and therapy discovery and key biological processes. All papers showcase that a deep understanding of the metabolic machinery is key to the deciphering of biological processes in health and disease.

Author contributions

OK: Conceptualization, Writing–original draft, Writing–review and editing. AS: Writing–review and editing. PE: Writing–review and editing.

Conflict of interest

The authors declare that the research was conducted in the absence of any commercial or financial relationships that could be construed as a potential conflict of interest.

The author(s) declared that they were an editorial board member of Frontiers, at the time of submission. This had no impact on the peer review process and the final decision.

Publisher's note

References

Fields, G. B. (2013). Interstitial collagen catabolism. *J. Biol. Chem.* 288 (13), 8785–8793. doi:10.1074/jbc.R113.451211

Harris, N. L. E., Vennin, C., Conway, J. R. W., Vine, K. L., Pinese, M., Cowley, M. J., et al. (2017). SerpinB2 regulates stromal remodelling and local invasion in pancreatic cancer. *Oncogene* 36 (30), 4288–4298. doi:10.1038/onc.2017.63

Lee, H. L., Shen, H., Hwang, I. Y., Ling, H., Yew, W. S., Lee, Y. S., et al. (2018). Targeted approaches for *in situ* gut microbiome manipulation. *Genes (Basel)* 9 (7), 351. doi:10.3390/genes9070351

Lueschow, S. R., and McElroy, S. J. (2020). The Paneth cell: the curator and defender of the immature small intestine. *Front. Immunol.* 11, 587. doi:10.3389/fimmu.2020.00587

frontiers | Frontiers in Cell and Developmental Biology

TYPE Original Research
PUBLISHED 26 October 2022
DOI 10.3389/fcell.2022.1015125

OPEN ACCESS

EDITED BY
Pablo Vicente Escriba,
University of the Balearic Islands, Spain

REVIEWED BY
Ketan Patel,
University of Reading, United Kingdom
Liberty Francois-Moutal,
Saint Louis University, United States

*CORRESPONDENCE
Miguel Weil,
miguelw@tauex.tau.ac.il

SPECIALTY SECTION
This article was submitted to Cellular Biochemistry,
a section of the journal
Frontiers in Cell and Developmental Biology

RECEIVED 09 August 2022
ACCEPTED 05 October 2022
PUBLISHED 26 October 2022

CITATION
Shilian M, Even A, Gast H, Nguyen L and Weil M (2022), Elongator promotes neuritogenesis via regulation of tau stability through acly activity.
Front. Cell Dev. Biol. 10:1015125.
doi: 10.3389/fcell.2022.1015125

Elongator promotes neuritogenesis *via* regulation of tau stability through acly activity

Michal Shilian[1], Aviel Even[1], Hila Gast[1], Laurent Nguyen[2] and Miguel Weil[1]*

[1]Laboratory for Neurodegenerative Diseases and Personalized Medicine, The Shmunis School of Biomedicine and Cancer Research, The George S. Wise Faculty for Life Sciences, Sagol School of Neurosciences, Tel Aviv University, Tel Aviv, Israel, [2]GIGA-Stem Cells and GIGA-Neurosciences, Interdisciplinary Cluster for Applied Genoproteomics (GIGAR), University of Liège, C.H.U. Sart Tilman, Belgium, BIOMED Research Institute, Hasselt, Belgium

The six subunits (Elp1 to Elp6) Elongator complex promotes specific uridine modifications in tRNA's wobble site. Moreover, this complex has been indirectly involved in the regulation of α-tubulin acetylation in microtubules (MTs) *via* the stabilization of ATP-Citrate Lyase (Acly), the main cytosolic source of acetyl-CoA production in cells, a key substrate used for global protein acetylation. Here, we report additional evidence that Elongator activity is important for proper cytoskeleton remodeling as cells lacking expression of Elp1 show morphology impairment; including distinct neurite process formation and disorganization and instability of MTs. Here, we show that loss of Elongator results in a reduction of expression of the microtubule associated protein Tau (MAPT). Tau, is a well-known key MT regulator in neurons whose lysines can be competitively acetylated or ubiquitylated. Therefore, we tested whether Tau is an indirect acetylation target of Elongator. We found that a reduction of Elongator activity leads to a decrease of lysine acetylation on Tau that favors its proteasomal degradation. This phenotype was prevented by using selective deacetylase or proteasomal inhibitors. Moreover, our data demonstrate that Acly's activity regulates the mechanism underlying Tau mediated neurite morphology defects found in Elp1 KD since both Tau levels and neurites morphology are restored due to Acly overexpression. This suggests a possible involvement of both Tau and Acly dysfunction in Familial Dysautonomia (FD), which is an autosomal recessive peripheral neuropathy caused by mutation in the *ELP1* gene that severely affects Elp1 expression levels in the nervous system in FD patients in a similar way as found previously in Elp1 KD neuroblastoma cells.

KEYWORDS

elongator complex, MAPT/Tau protein, neuritogenesis, protein acetylation, familial dysautonomia

Introduction

The best established cellular function of the Elongator complex is translation through modification of uridines in tRNA's wobble site. The Elongator complex promotes the formation of 5-methoxycarbonylmethyl (mcm5) and 5-carbamoylmethyl (ncm5) on side-chains of wobble uridines (U34) of selected tRNAs, thereby regulating protein translation. Reduced levels of modified anticodons caused by depletion of the Elongator complex results in a codon-dependent decrease in ribosomal translocation and affect protein synthesis rates globally (Huang, Johansson and Byström, 2005; Hermand, 2020). Moreover, this complex has a role in intracellular transport in the nervous system (Singh et al., 2010; Miśkiewicz et al., 2011) through acetylation of the α-tubulin in neuronal microtubules (MT) (Creppe et al., 2009; Solinger et al., 2010; Even et al., 2019; Even et al., 2021). Loss of Elongator activity is associated with both neurodegeneration and axonal transport defects (Solinger et al., 2010; Bento-Abreu et al., 2018) *in vivo*, and also leads to Familial Dysautonomia (FD). FD is an autosomal recessive neuropathy that affects the development and function of the autonomic and peripheral nervous system (PNS) (Riley and Day, 1949; Bar-Aluma, 2003). A point mutation in the gene coding for the Elongator scaffold subunit, *ELP1*, results in its splicing defects *via* exon skipping, further leading to a severe reduction of Elp1 protein levels in the FD patient nervous system (Anderson et al., 2001; Slaugenhaupt et al., 2001). Elongator is a complex made of two copies of six subunits (Elp1 to Elp6) where Elp3 acts as the catalytic ones (Winkler et al., 2002; Petrakis, Wittschieben and Svejstrup, 2004). Loss of Elp1 results in impaired Elongator activities, and removal of any Elongator subunits affects the Elongator assembly leading to comparable phenotype in eukaryotes, suggesting that all subunits are essential for the integrity and activity of the complex (Petrakis, Wittschieben and Svejstrup, 2004; Close et al., 2006; Esberg et al., 2006). Our FD neuroblastoma cell model, where Elp1 is knockdown, shows transcriptional changes and aberrant cell shape, expressed as cell adhesion problem that results from Contactin 1 overexpression, including distinct neurite process formation as well as disorganization and instability of microtubules (MTs) (Cohen-kupiec et al., 2010; Cheishvili et al., 2011; Cohen-Kupiec et al., 2011).

The nervous system homeostasis depends on the integrity, dynamics, and organization of MT cytoskeleton (Hirokawa et al., 1996), which is regulated by various microtubule associated proteins (MAPs). The key regulator MAP Tau (MAPT) is associated with MTs and promotes their assembly and stabilization in neurons. Tau likely plays a key role in axonal growth and in the establishment of neuronal polarity and strongly promotes neurite outgrowth during differentiation (Caceres, Potrebic and Kosik, 1991; Esmaeli-azad, Mccarty and Feinstein, 1994; Hirokawa et al., 1996). In contrast, Tau malfunction underlies neurodegeneration and is associated with frontotemporal dementia, Alzheimer, Parkinson and other Tauopathies (Froelich et al., 1998; Spillantini et al., 1998; Ludolph et al., 2009). Tau proteins undergo a large variety of posttranslational modifications (PTMs) that influence it structure and function (Martin, Latypova and Terro, 2011; Mietelska-Porowska et al., 2014). For example, Tau acetylation mediated by the acetyltransferase p300 and its deacetylation by Hdac6 regulates its turnover and stability (Min et al., 2010; Cook and Stankowski, 2014). Ubiquitination is another PTM that modulates turnover. Tau ubiquitination mediates its degradation in the cytosol by the ubiquitin proteasome system (UPS) (David et al., 2002). Interestingly, nearly all acetylation sites on Tau are alternately modified by ubiquitin (Min et al., 2010), and evidence from primary cultured neurons and *in vivo* experiments suggested that competition between acetylation and ubiquitylation of lysine sites in Tau (Min et al., 2010) takes place, that further affect its protein turnover.

We recently showed that loss of Elongator activity results in lower MT acetylation in projection neurons, across species. This phenotype results from a loss of stabilization of ATP-Citrate Lyase (Acly), thereby affecting the acetylase activity of alpha-Tat1 and ultimately resulting in abnormal vesicular transport in projection neurons *in vivo* and *in vitro* (Even et al., 2021). Acly is a transferase that catalyzes the conversion of citrate and coenzyme A to acetyl-CoA, which is one key substrate used for protein acetylation. It is thus possible that loss of Elongator indirectly impacts the activity of multiple acetyltransferases that mediated PTM processes in proteins of both the cytosol and the nucleus, as we have reported for α-tubulin in MTs (Even et al., 2021) and H3 histones by others (Martin et al., 2011) (Wellen et al., 2009), respectively.

Here, by combining cellular and molecular analyses in a neuroblastoma cell line depleted for Elp1 and also in several Elp3 depletion models *in vitro* and *in vivo* we show that loss of Elongator results in reduced Tau protein levels. This results in the abnormal morphology of the neurite's network. At the molecular level, the reduction of Tau level results from its increased instability that occurs upon changes in the balance between ubiquitylation and acetylation. The reduction of Elongator activity leads to a decrease of lysine acetylation on Tau protein that favors its proteasomal degradation. This results from Acly decreased activity under Elongator deficiency in these cells. Moreover, our data demonstrate that Acly's activity regulates the mechanism underlying Tau mediated neurite morphology defects found in Elp1 KD suggesting the possible involvement of Tau dysfunction in the FD peripheral neuropathy.

Materials and methods

Cell culture

SH-SY5Y human neuroblastoma-derived cell lines used in this work were cultured in polystyrene culture flasks (Corning) at 37°C with 5% CO2 in DMEM (Gibco, Invitrogen, 11965092)

medium supplemented with 10% Fetal Calf Serum (Gibco, Invitrogen, 10500056), 1 mM Sodium pyruvate (Gibco, Invitrogen, 11360070) and antibiotics (50 U/ml of penicillin, streptomycin and nystatin).

HEK293 cells were grown in the same conditions as above. The SHSY5Y human neuroblastoma FD model (Elp1 KD) and PLKO vector control were generated in our laboratory as previously described (Cohen-kupiec et al., 2010). The SHSY5Y human neuroblastoma Tau knockdown model (Tau KD) and control were kindly provided by Dr. Paganetti's Laboratory for Biomedical Neurosciences (LBN) Neurocenter of Southern Switzerland (NSI) (Sola et al., 2020).

Neuronal differentiation of neuroblastoma cells

For neuronal differentiation of neuroblastoma cell lines, 96 well tissue culture (microscopy grade) plates were pre-coated with 10 µg/ml Poly-D-Lysine (30–70 kDa, Sigma-Aldrich Corp., Israel) for 4 h at room temperature, then rinsed twice with PBS and incubated with 4 µg/ml Laminin (Sigma-Aldrich Corp., Israel) overnight at 4°C. The plates were rinsed once with PBS and neuroblastoma cells were seeded in full supplemented DMEM, after 24 h the cells were incubated with 10 µM retinoic acid for 5 days and then in serum-free medium (Gibco, Invitrogen, 11965092) with 2 nM BDNF (PeproTech Asia, Israel) for 3 days at 37°C with 5% CO2.

Animals

Brains from Elp3cKO and WT mice at P0-P2 were collected and snap frozen by the Laboratory of Molecular Regulation of Neurogenesis, University of Liège, Belgium and sent frozen to the Laboratory in Israel for analysis (Even et al., 2021). *Drosophila melanogaster* fly stocks were obtained from the Laboratory of Molecular Regulation of Neurogenesis, University of Liège, Belgium (Even et al., 2021). Flies were kept at 25°C in incubator with regular 12 h light and dark cycle. All crosses were performed at 25°C. UAS-RNAi carrying lines; UAS:RNAi Zpg (VDRC CG10125), UAS:RNAi Elp3 (VDRC CG15433) were crossed with Elav-Gal4 (BDSC 458) for WB analysis.

Image based cell HCA live phenotyping experiments

For live HCA microscopy experiments, 8,000 neuroblastoma cells were plated per well in 96-well plates (Grenier, Austria) in full supplemented DMEM and incubated overnight at 37°C, and 5% CO2 before starting neuronal differentiation with RA as described above. For live staining, culture media was removed and replaced with fluorescent dyes mix containing Hoechst 33342 (Merck-Sigma, United States) 1:10,000, CellTrace™ Calcein Green AM (Invitrogen, United States) 1:5,000 or Calcein Red-Orange AM (Invitrogen, United States) 1:5,000, diluted in HBSS. After 30 min incubation at 37°C, and 5% CO2 the plate was transferred to the IN Cell Analyzer 2,200 (GE Healthcare) for image acquisition under cell culture environmental conditions. Twenty images per fluorescent channel (fixed spacing fields) for each well were acquired in two different channels in less than 60 min. All images under a ×20 magnification were taken using the same acquisition protocol with constant exposures for each fluorescent channel. The multiple cell images were subsequently segmented and high content analyzed using IN Carta® Image Analysis Software. Two dimension principal component analysis (PCA) was applied based on morphological features, followed by a ranking of features contributing to the separation in the PCA analysis.

Immunofluorescence

Cells were plated on coverslips in 24 well plates at a density of 30,000 cells following neuronal differentiation (as described above). Cells were fixed by incubation in 4% PFA-sucrose in PBS for 10 min at RT and washed twice with PBS. Permeabilization was done using PBS + 0.1% Triton X for 10 min. Cells were incubated in blocking solution (PBS+0.05% Triton-X+10% FBS+ 2% BSA) for 1 h at RT. Following overnight incubation with primary antibodies (see Table 1) in blocking solution at 4°C, washing, and incubation with secondary antibodies (PBS+0.05% Triton-X+10% FBS+ 2% BSA) at RT for 1 h, nuclei were stained for 10 min with 1:10,000 Hoechst 33342/PBS and coverslips were washed and then mounted on microscope slides. Images of the stained cells were obtained using a confocal microscope Zeiss LSM 510 Meta. Fluorescence intensity levels of Tau labeled cells were measured by Fiji (https://imagej.net/Fiji/Downloads).

Real time quantitative PCR analysis

Total RNA was extracted with TRIzol Reagent (Ambion, Life Technologies) followed by RNA extraction performed following the manufacturer's instructions. After DNAse treatment (Roche), The concentration of total RNA was measured using a Nano Drop Spectrophotometer (Nano Drop Technologies, United States). Total RNA (300 ng) was reverse-transcribed into complementary DNA (cDNA) with Reverse It first Strand kit (ABgene) using oligo-dT as a primer according to the manufacturer's instructions.

RT-qPCR was performed using Quant Studio (Thermo) and TaqMan primers, HPRT gene Hs99999909_m1, was used as endogenous gene control. All quantitative real-time PCR

TABLE 1 List of Antibodies.

Protein	Company	Cat #	WB	IF	IP
Tau HT7	Invitrogen	MN1000B	1:1000	1:400	5ug
Tau	Abcam	ab64193	1:500		
Tau 5A6	Hybridoma Bank		1:500		
Elp1/IKAP	Abnova	PAB12857	1:1000		
Elp3	Jesper Svejstrup		1:1,000		
β-actin	Sigma-Aldrich	A3854	1:20,000		
α-Tubulin	Sigma-Aldrich	T9026	1:5,000		
Acetylated α-Tubulin	Sigma-Aldrich	T7451	1:15,000		
Acly	Cell Signaling	13390	1:1,000		
Hdac6	Santa Cruz Biotechnology	sc-5258	1:200		
p300	Cell Signaling	D8Z4E	1:1000		
Ac-Lysine	Sigma-Aldrich	SAB5200090	1:200		
Ubiquitin	Sigma-Aldrich	u0508	1:1000		
HA	Sigma	H6908			
HRP-conjugated donkey anti-rabbit	Abcam	ab 205722	1:10,000		
HRP-conjugated donkey anti-mouse	Abcam	ab97040	1:10,000		
goat anti mouse	Life technologies	A-10680		1:400	
goat anti rabbit	Life technologies	A-21244		1:400	

TaqMan analysis are presented as representative results in triplicates of 3 biological repeats.

Analyses were done using the 2-$^{\Delta\Delta}$CT method with the following primers; for *ELP1* Hs00932050_m1 and *MAPT* Hs00902194_m1.

Western blot

Cells were quickly homogenized on ice in RIPA buffer, protease inhibitor cocktail (Sigma-Aldrich, S8820) and 5 μM Trichostatin-A (TSA, Sigma-Aldrich, T8552) were added to the buffer to inhibit protein degradation and deacetylation. Protein concentration of each sample was measured by using the Protein Assay Kit (Pierce Biotechnology, Rockford) according to the manufacturer's instructions. Subsequently, samples were denatured by 10 min incubation in 70°C in loading buffer and reducing agent (life technology), and were loaded on SDS-page gel 4–12% gradient gels (life technology) in MES SDS running buffer (life technology) to be finally transferred to a nitrocellulose membrane in 7 min using an iBlot-2. Immunoblotting was performed with the primary and secondary antibodies listed in Table 1. We used 2 μg of protein lysate for α-tubulin acetylation analysis and 20–30 μg for all other proteins. Nitrocellulose membranes were imaged using Amersham Imager 600 (General Electric, 29083461) and band densitometry was measured using FIJI.

Cycloheximide pulse-chase assay

Differentiated neuroblastoma Elp1 KD and control cells were cultured in 6-well plates at 80% confluency before treatment with 50 μg/ml cycloheximide (CHX) (C7698 Sigma) for 0 h, 2 h, 8 h, 10 h, 24 h. All samples were harvested simultaneously by adding in each well 100 μL RIPA buffer (supplemented with complete proteinase inhibitor cocktail and TSA) and subsequent mechanical scraping. Following incubation on ice for 10 min, samples were centrifuged for 10 min at 8,000 x g to collect the supernatant. Protein concentration of each sample was measured by using the Protein Assay Kit (Pierce Biotechnology, Rockford) according to the manufacturer's instructions. following WB analysis (as described above).

Reagents and drug treatments

BMS 303141 (BMS), Tubastatin A (TubA), MG-132 and cycloheximide were obtained from Sigma-Aldrich (SML0784, SML0044, M7449, and C104450, respectively). MG-132 (20 μM) was added to fully differentiated cells 4 h prior to protein extraction. For ubiquitinated Tau MG-132 (17.5 μM) was added to HEK293 transfected cells 15 h prior to immunoprecipitation. Treatment of TubA, (2 μM) for 24 h alone or together with MG-132 (20 μM) for the last 4 h were added to fully differentiated cells, prior to protein extraction.

BMS (1 μM) was added to fully differentiated cells for 72 h prior to cells fixation and immunofluorescence analysis.

Acly activity assay

Acly activity assay was measured as previously described by us (Even et al., 2021) using 5 μg of protein extracts from differentiated neuroblastoma Elp1 KD and control cells.

Plasmids and transfections

HEK293 cells were transfected with 5–10 μg of plasmids pCAGGs hElp3 Flag IRES RFP, pCAGGs hElp3mKAT Flag IRES RFP (Laguesse et al., 2015), using calcium phosphate. 24 h post transfection, cells were lysed in IP lysis buffer on ice, following immunoprecipitation (as described below).

SH-SY5Y human neuroblastoma cells were infected using Adenoviruses MOI 1000 for 4 h; The Adenovirus vector is VB211014, pAV [Exp]-EGFP-EFS > hACLY [NM_001303274.1]:IRES:Neo for expression of human ACLY or pAV [Exp]-EGFP-EFS>hMAPT [NM_001377265.1]:IRES:Neo for expression of human MAPT, and the promotor was replaced by an EFS promoter. After 24 h cells were harvested and plated on PDL-Laminin coated 96 wells plate, 24 h later a shorter neuronal differentiation protocol (3 days RA and 3 days BDNF) was applied and image based cell HCA live phenotyping experiment was performed.

Immunoprecipitation analysis

Pierce Crosslink immunoprecipitation kit (#26147) was used following the manufacturer's instructions. For immunoprecipitation experiments, cells were lysed in IP buffer (supplied with the kit) and supplemented with protease inhibitors and TSA. About 300–1000 μg of cell lysates were incubated overnight at 4°C with the indicated antibodies. For Tau acetylation and ubiquitylation analysis, 5 μg of Tau HT7 (Invitrogen) were crosslinked using DSS to protein A/G. For detection by WB of acetylated Tau or ubiquitinated Tau, acetylated Lysine (Sigma) antibody or ubiquitin (Sigma) or HA (Sigma) and Tau (Abcam) or Tau HT7 (Invitrogen) were used. acetylated Tau or ubiquitinated Tau were measured as ac-Lys levels or ubiquitin levels divided by Tau levels.

Deacetylation assay

α-Tubulin deacetylation assay was performed using 10 μg of protein extracts from differentiated SHSY5Y neuroblastoma cells as previously described by us (Even et al., 2021).

In vitro α-tubulin assay

In vitro α-tubulin acetylation assay was performed using 25 μg of protein extracts from differentiated SHSY5Y neuroblastoma cells as previously described by us (Even et al., 2021).

Acetyl-CoA sample preparation and LC–MS/MS analysis

Acetyl-CoA sample preparation and LC–MS/MS analysis was performed as previously described by us (Even et al., 2021).

Analysis and statistics

All experiments were performed under single blinded conditions and statistical analyses were generated with GraphPad Prism Software 7.0.

Results

To investigate further and quantify the morphological differences previously observed between Elp1 KD and control neuroblastoma cells (Cohen-kupiec et al., 2010; Cheishvili et al., 2011) we applied live fluorescence microscopy image high content analysis (HCA) of Calcein AM live stained cells to visualize neurite morphologies. For the morphology experiments the neuroblastoma cells were seeded in 96 well plates and cultured in differentiation medium for 5 days containing 10% FBS medium with retinoic acid (RA), followed by serum-free medium supplemented with BDNF for 3 days. For neurite morphology analysis, we identified neurite processes using a specialized image analysis software in thousands of double stained cells, calcein AM (left panel) and Hoescht 222342 (mid panel), as represented in Figure 1A (right panel) for control and Elp1 KD respectively.

A two-dimensional principal component analysis was applied to identify the vectors from the data produced in these experiments that classify the difference in neurite morphology between control (in blue) and Elp1 KD (in light blue) cells (Figure 1B). Feature selection analysis show the list of critical features (Figure 1C) that best contribute to the classification difference between the groups. We focused in the most meaningful and relevant features that characterize the morphological differences of neurites between control and Elp1 KD for further analysis as shown in Figures 1D–I. All the selected neurites morphology features displayed distinct and significant differences between control and Elp1 KD cells (Figures 1D–I). Overall, the reduced neurite number, length

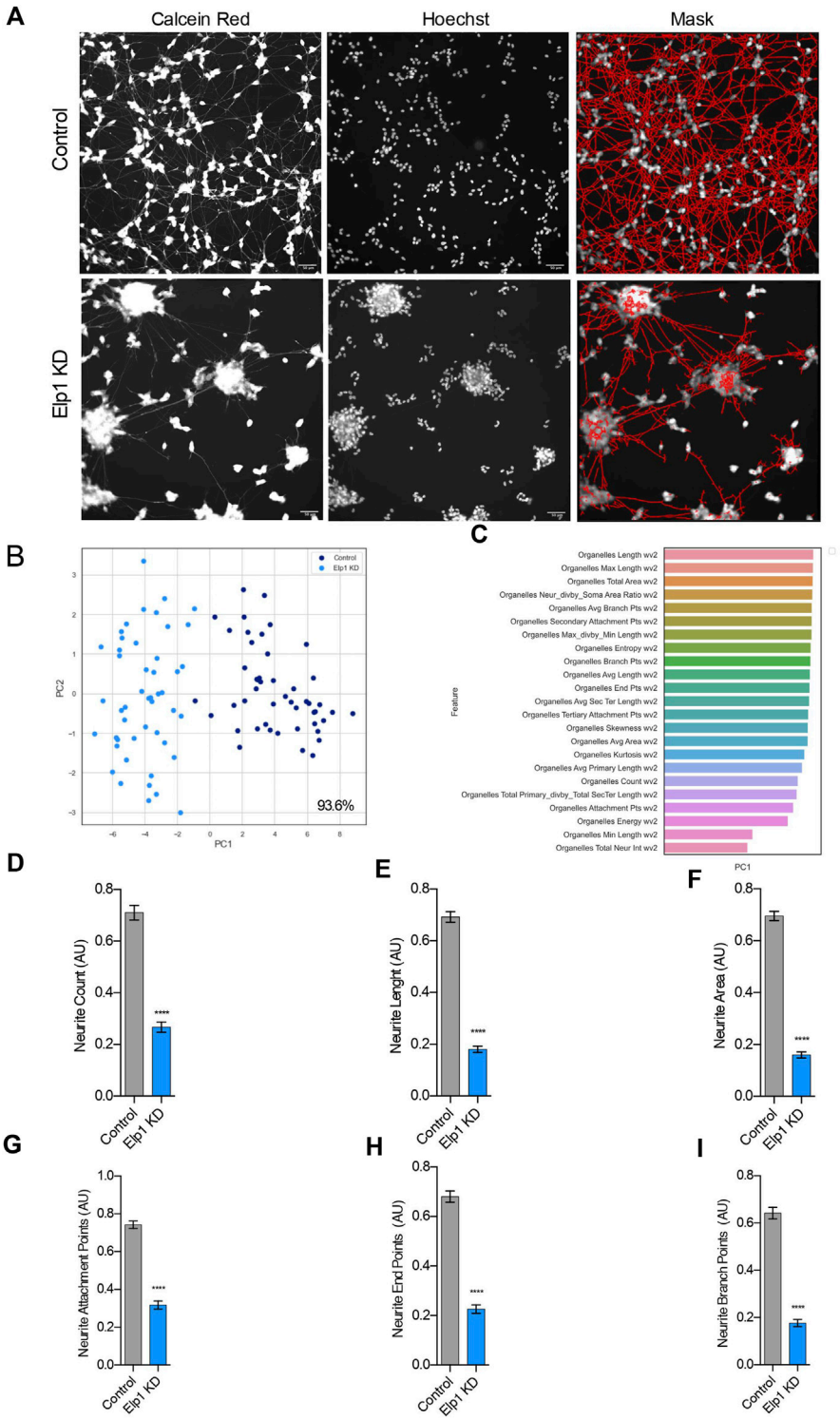

FIGURE 1
Elp1 is involved in neurite morphology, Depletion of Elp1 Causes Defective neurite outgrowth in differentiated SHSY5Y cells. **(A)** Representative images of Live fluorescence microscopy staining of differentiated SHSY5Y cells control *versus* Elp1 KD using Calcein AM (Red) and Hoechst (Blue) to visualize neurite morphology. on the right side; segmentation of neurites by InCarta software. Scale bar is 50 µm. **(B)** Two dimension principal component analysis (PCA) plot of stained cells based on morphological features. Symbols in dark blue represent the control cells; symbols in light blue represent Elp1KD cells. each circle represent data extracted from 20 fields coming from one well, each field contain hundreds of cells. PCA Score 93.6% **(C)** Plot of features contribution to the separation in the PCA analysis **(D–I)** Quantification of the selected morphology features including
(*Continued*)

FIGURE 1 (Continued)
Neurite Count **(D)**, Neurite Length **(E)**, Neurite Area **(F)**, Neurite Attachment Points **(G)**, Neurite End Points **(H)** and Neurite Branch Points **(I)**. All graphs show values of means ± SEM. Significance was determined by: d-i two-sided *t* test, Specifically, [**(D)** $p < 0.0001$; **(E)** $p < 0.0001$; **(F)** $p < 0.0001$; **(G)** $p < 0.0001$; **(H)** $p < 0.0001$; **(I)** $p < 0.0001$;] n = Number of wells (each well contains data from 20 fields, each field contains hundreds of cells): **(D–I)** Control n = 48; Elp1 KD *n* = 48.

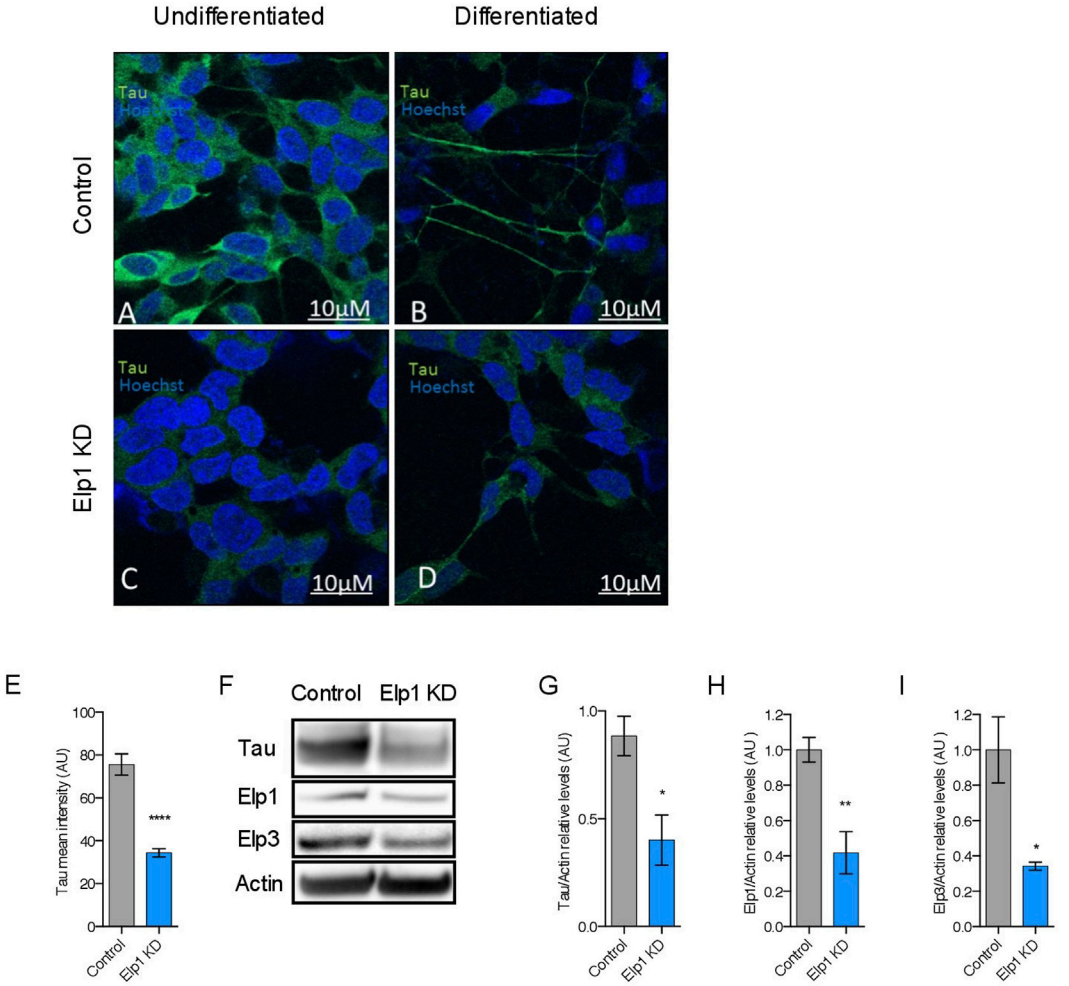

FIGURE 2
Elongator depletion leads to reduction in Tau protein expression. **(A–E)** Immunolabeling and quantification of Tau in Elp1 KD and control SHSY5Y cells. Tau is stained in green, before **(A,C)** and after differentiation **(B,D)**. Scale bar is 10 μm. **(F–I)** Western blotting to detect and quantify Tau, Elp1, Elp3 and ß-Actin in differentiated SHSY5Y extracts from Control and Elp1 KD cells. Histograms of proportion of Tau **(G)**, Elp1 **(H)** and Elp3 **(I)** expression to ß-Actin. All graphs show values of means ± SEM. Significance was determined by: eg-i two-sided *t* test, Specifically, [**(E)** $p < 0.0001$; **(G)** $p = 0.0114$; **(H)** $p = 0.0018$; **(I)** $p = 0.0249$;]. *n* = Number of wells (each well contains data from 20 fields, each field contains hundreds of cells): **(E)** Control *n* = 119; Elp1 KD n = 85; *n* = Number of experimental repeats: **(G)** Control *n* = 5; Elp1 KD *n* = 5; **(H)** Control *n* = 6; Elp1 KD *n* = 6; **(I)** Control n = 3; Elp1 KD *n* = 3.

and other morphological features in Elp1 KD cells suggest that Elp1 is required for neuritogenesis and depletion of Elp1 causes defective morphology of neurites. This result is in line with our previous studies where we found that Elp1 is involved in neuronal outgrowth and peripheral target innervation in chick embryos (Abashidze et al., 2014).

Since neurite growth and morphology rely on several cytoskeleton proteins, such as Microtubule associated proteins

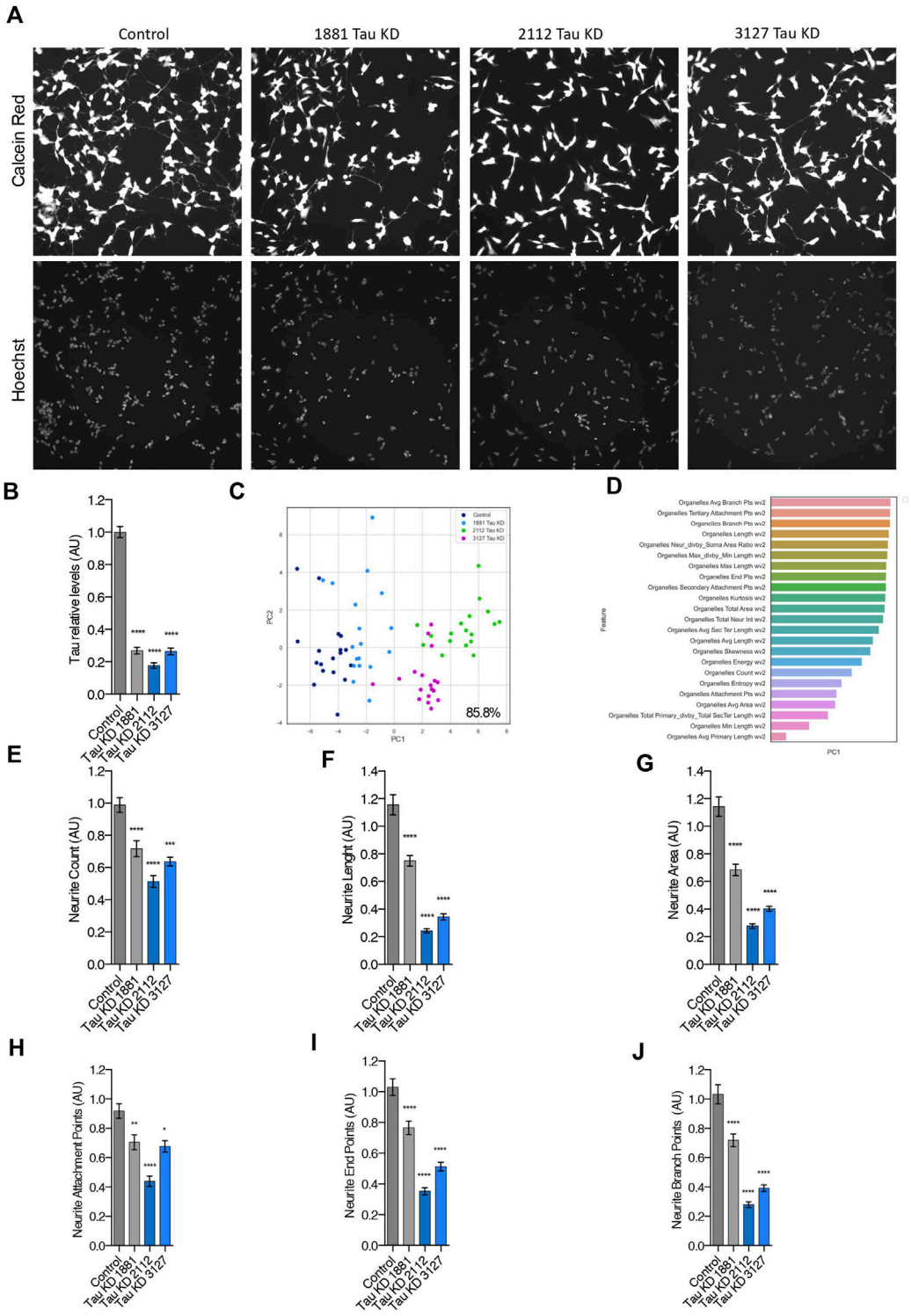

FIGURE 3
Depletion of Tau causes abnormal neurite morphology in differentiated SHSY5Y cells, similarly as in Elp1 depletion. **(A)** Representative images of Live fluorescence microscopy staining of differentiated SHSY5Y cells control *versus* Tau KD lines (Tau KD 1881; Tau KD 2112, Tau KD 3127) using Calcein AM (Red) and Hoechst (Blue) to visualize neurite morphology. Scale bar is 50 μm. **(B)** Immunolabeling and quantification of Tau levels **(C)** Two dimension principal component analysis (PCA) plot of stained cells based on morphological features. Symbols represent the control cells (dark blue); Tau KD 1881 cells (light blue), Tau KD 2112 (pink), Tau KD 3127 (green). each circle represent data extracted from 20 fields coming from one well, each field contain hundreds of cells. PCA Score 85.8% **(D)** Plot of features contribution to the separation in the PCA analysis **(E–J)** Quantification
(*Continued*)

FIGURE 3 (Continued)
of the selected morphology features including Neurite Count **(E)**, Neurite Length **(F)**, Neurite Area **(G)**, Neurite Attachment Points **(H)**, Neurite End Points **(I)** and Neurite Branch Points **(J)**. All graphs show values of means ± SEM. Significance was determined by: b, e-j two-sided one-way analysis of variance (ANOVA), Specifically, [**(B)** $p < 0.0001$, F = 250.3; **(E)** $p < 0.0001$, F = 23.93; **(F)** $p < 0.0001$, F = 77.28; **(G)** $p < 0.0001$, F = 69.46; **(H)** $p < 0.0001$, F = 22.06; **(I)** $p < 0.0001$, F = 56.87; **(J)** $p < 0.0001$, F = 54.18;] In addition, the post hoc multiple comparisons, to analyze statistical difference of each condition compared to control for **(B–J)** by Dunnett test, *$p < 0.05$, **$p < 0.01$, ***$p < 0.001$, and ****$p < 0.0001$. n = Number of wells (each well contains data from 20 fields, each field contains hundreds of cells): **(B)** Control n = 40; Tau KD 1881 n = 32; Tau KD 2112 n = 32; Tau KD 3127 n = 24; **(E–J)** Control n = 56; Tau KD 1881 n = 50; Tau KD 2112 n = 62; Tau KD 3127 n = 18.

(MAPs), we further aimed to investigate whether the observed Elp1-dependent neurites morphology differences in FD neuroblastoma model can be explained by deregulation of Tau (Microtubule Associated Protein Tau; MAPT).

To investigate the correlation between the neurite morphological features with Tau expression in Elp1 KD FD neuroblastoma cells, we measured Tau expression by immuno-fluorescence confocal microscopy analysis of Elp1 KD and control cells, using Tau antibodies before and after differentiation with RA and BDNF, as shown in representative images in Figure 2 A-D. Note the apparent morphological differences that exist in neurite length between control and Elp1 KD, especially after differentiation (Figures 2B,D respectively). Quantitative analysis of Tau fluorescence intensity in differentiated cells (Figure 2E) shows that Tau levels in control neuroblastoma cells both before and after differentiation (Figures 2A,C, respectively) are higher compared to Elp1 KD (Figures 2B,D, respectively). Western blot analysis on protein extracts obtained from differentiated control and Elp1 KD neuroblastoma cells shows a reduction by almost 60% of Tau protein level in Elp1 KD, as compared to control cells (Figures 2F,G). The severe reduction of Tau protein upon Elp1 deficiency is not exclusive to Elp1 KD neuroblastoma cells and is further supported *in vivo* in Elongator deficiency neuronal models in mice and flies (Supplementary Figure S1). Tau protein levels were measured by WB analysis in extracts made of adult mice brains of Elp3 KD (Supplementary Figure S1A, B) and adult fly heads, following neuronal (elav-driven) expression of Elp3 KD (Supplementary FigureS1C, D). These results showed reduced Tau protein levels in both Elp3 KD models, suggesting that loss of Elongator complex impacts Tau expression in human, flies and mouse neuronal models.

Since previous studies have suggested that Tau may function in neurite outgrowth and growth cone motility and that inactivation of Tau in whole DRG neurons resulted in reduced neurite number and length (Liu, Lee and Jay, 1999), we postulated that the abnormal neurite morphology observed in Elp1 KD neuroblastoma cells might arise from Tau depletion. To directly investigate this hypothesis, we performed live imaging HCA neurites morphological experiments (similar as shown in Figure 1) using three established Tau-knock down (Tau KD) neuroblastoma cells that express constitutively each one of three distinct Tau shRNAs and respective cell line control, obtained as a kind gift from Paganetti's lab that were generated as described by them (Sola et al., 2020). As shown in Figure 3 the two-dimensional principal component analysis applied to select the critical features from the data produced in these experiments resulted in the same selected critical neurite morphology features from the analysis done for the Elp1KD cells (Figures 3C,D). Measures from the selected morphology features show a reduced number of neurites per cell, reduction in neurite length and area, fewer attachment points, and reduces numbers of branch points and end points per neurite (Figures 3E–J). The reduction levels in all neurite morphology features correlated with Tau expression levels with Tau KD cell lines expressing different levels of Tau protein, with reduced Tau-expression corresponding to 73% for the 1881 shRNA, 82% for the 2112 shRNA and 74% reduced Tau in 3127 shRNA (Figure 3B). Altogether, these results suggest that the aberrant neurite morphology seen upon Elp1 KD may rely on reduced Tau levels.

It was previously suggested that the Elongator complex contributes to transcriptional elongation *via* RNAPII-associated chromatin remodeling (Close et al., 2006). To test the possibility that the reduction of Tau levels detected in Elp1 knockdown neuroblastoma cells results from a reduction in *MAPT* gene transcription, we performed quantitative real-time PCR analysis (qRT-PCR) as shown in Figure 4A. We observed that while Elp1 mRNA transcription is significantly reduced in Elp1 KD neuroblastoma cells (Figure 4A, left), the MAPT mRNA expression level is similar in both Elp1 KD neuroblastoma cells and control cells supporting the view that Tau expression in the FD model is probably regulated at the protein (Figure 4A, right).

To study if the reduced levels of Tau (see Figure 2) observed in Elp1 KD cells arises from its change of stability, we used the protein synthesis inhibitor cycloheximide (CHX) in pulse-chase experiments, as described in Figures 4B,C. Differentiated neuroblastoma cell lysates were prepared after different times of incubation with CHX and analyzed using primary Tau antibodies by WB analysis (Figure 4B). The turnover rate of Tau in Elp1 KD cells was compared to control cells, with a time of CHX treatment measured as Tau relative levels. Tau showed a faster signal decay in Elp1 KD cells, as compared to control cells, suggesting that Elp1 KD cells have a higher degradation rate of Tau (Figure 4C). To study whether the reduced stability of Tau in Elp1 KD cells correlates to the proteasome-mediated

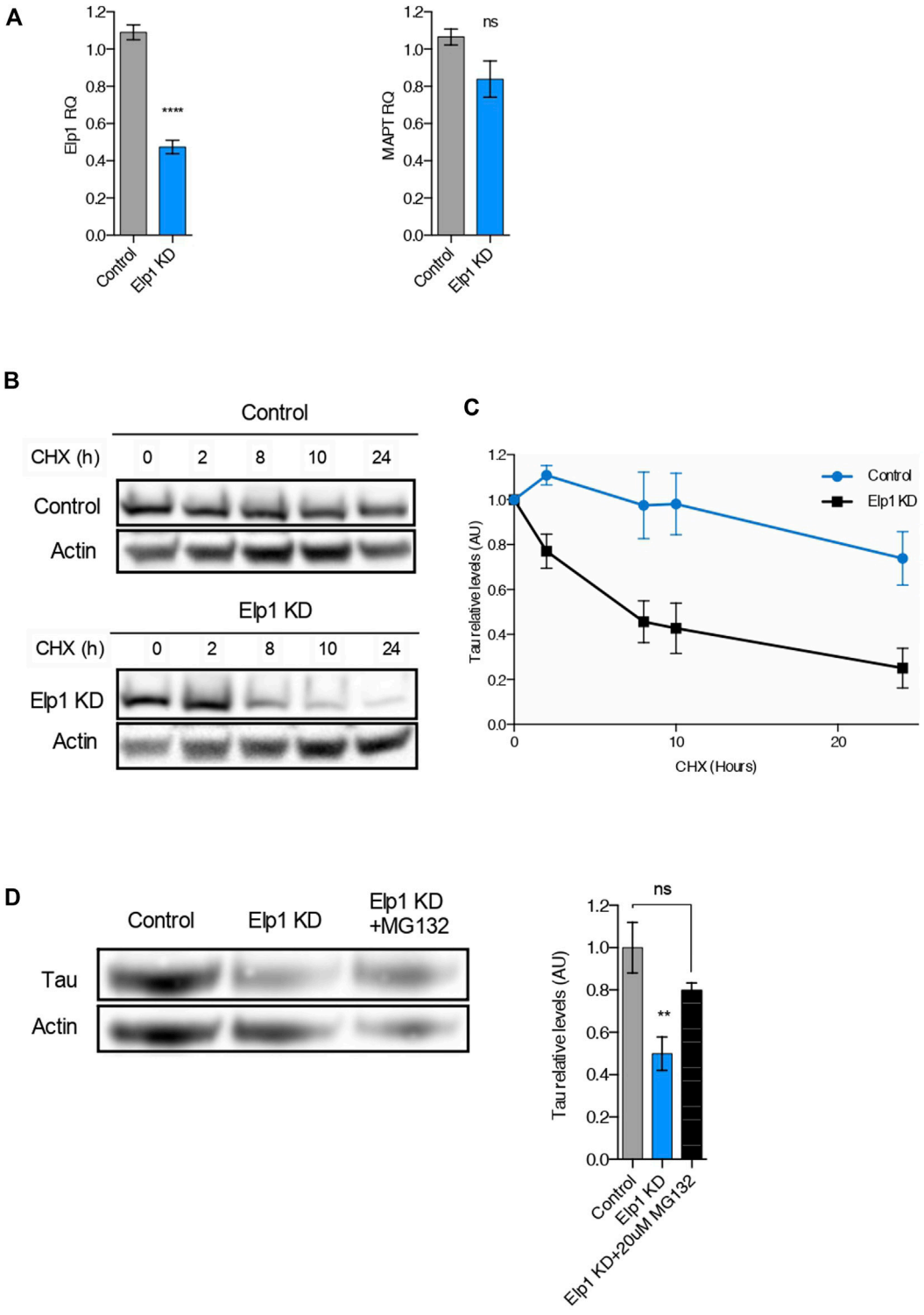

FIGURE 4
The reduction of Tau levels in ELP1 depletion is due to Tau protein instability. **(A)** qRT-PCR analysis of Elp1 mRNA (left) and MAPT mRNA (right) in differentiated SHSY5Y extracts from Control and Elp1 KD cells. **(B,C)** Immunoblotting and quantification of Tau and ß-Actin in differentiated SHSY5Y extracts from Control and Elp1 KD cells incubated with cycloheximide (CHX, 50 µg/ml) for 0, 2, 8, 10 and 24 h. **(D)** Immunoblotting and histogram of Tau and ß-Actin in differentiated SHSY5Y extracts from Control and Elp1 KD cells incubated with vehicle or MG-132 (20 µM) for 4 h. All graphs show values of means ± SEM. Significance was determined by: **(A)** two-sided *t* test, Specifically, [(a left) $p < 0.0001$; (a right) $p = 0.1349$;] **(C)** two-sided two-way ANOVA. Specifically, [$p = 0.0224$, F Interaction (4, 44) = 3.173] **(D)** two-sided one-way analysis of variance (ANOVA), Specifically, [$p = 0.0084$, F = 8.5;] In addition, the post hoc multiple comparisons, to analyze statistical difference of each condition compared to control by Dunnett test, $^{**}p < 0.01$. *n* = Number of experimental repeats: **(A)** Control *n* = 5; Elp1 KD *n* = 5; **(C)** Control *n* = 5; Elp1 KD *n* = 7; **(D)** Control *n* = 4; Elp1 KD *n* = 5; Elp1 KD + MG132 *n* = 3.

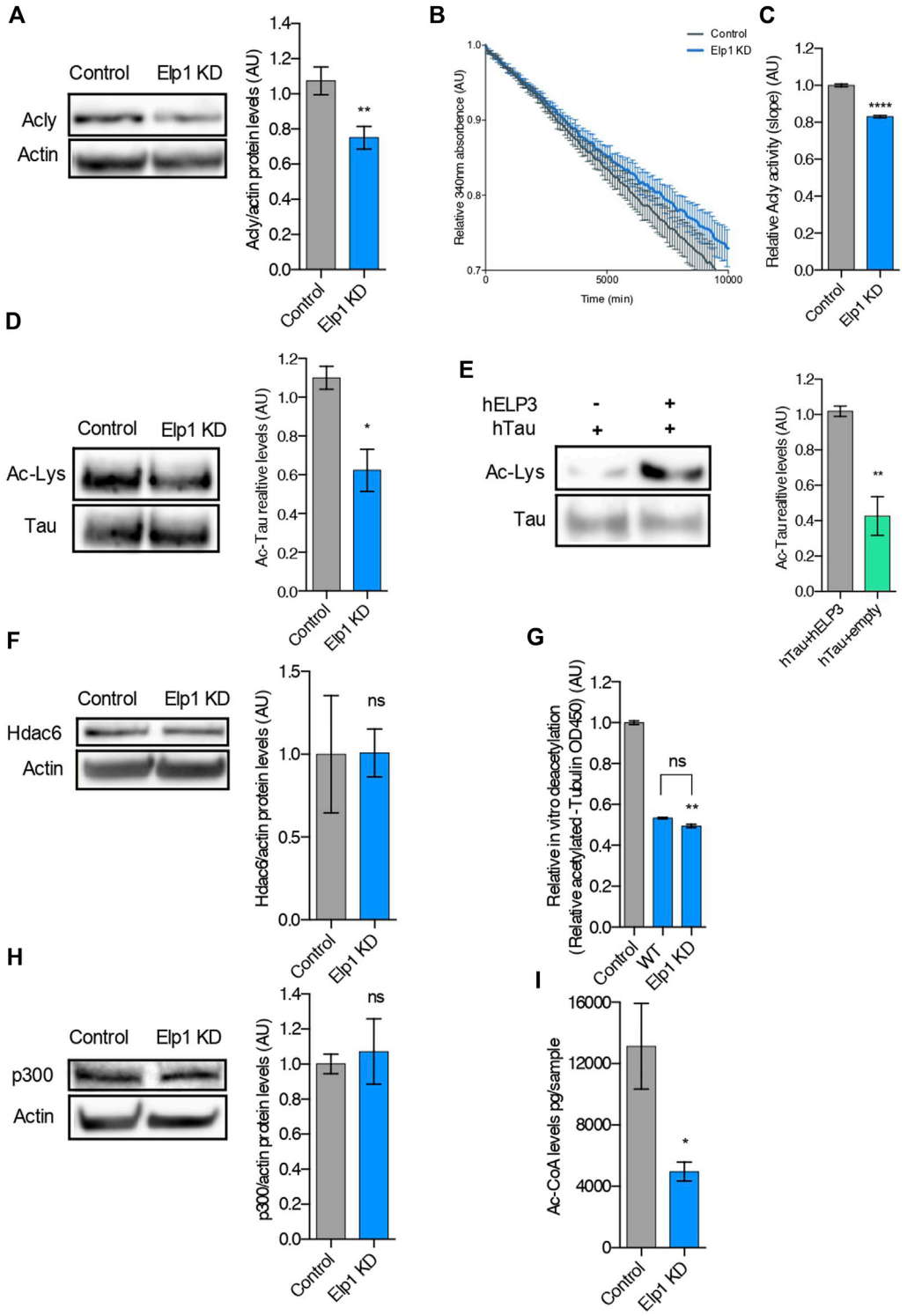

FIGURE 5
Tau is hypoacetylated, a result of impaired production of acetyl-CoA upon Elongator depletion. **(A)** Western blotting to detect and quantify Acly, and ß-Actin in control and Elp1KD cells extracts. Histograms of proportion of Acly expression to ß-Actin. **(B,C)** Analysis of Acly activity by malate dehydrogenase coupled method performed in control and Elp1KD cells lysates. Histogram of relative Acly activity over assay **(B)** and of slopes **(C)** from the linear phase of the reaction. **(D)** Immunoprecipitation followed by Western blotting to detect and quantify Acetylated Tau, in control and Elp1KD cells extracts. Histograms of proportion of acetylated lysine expression to Tau. **(E)** Immunoprecipitation followed by Western blotting to detect and quantify acetylated Tau, in extracts from HEK293 cells transfected with Tau, Elp3 or empty vector. Histograms of proportion of acetylated
(*Continued*)

FIGURE 5 (Continued)
lysine expression to Tau. **(F)** Western blotting to detect and quantify Hdac6, and ß-Actin in control and Elp1KD cells extracts. Histograms of proportion of Hdac6 expression to ß-Actin. **(G)** *In vitro* deacetylation assay of endogenously acetylated bovine brain tubulin incubated for 4 h with extracts of WT and Elp1KD cells, or without cells extract (control). **(H)** Immunoblotting to detect p300, ß-Actin in control and Elp1KD cells extracts and histograms of proportion of p300 expression to ß-Actin. **(I)** LC-MS quantification of Acetyl-CoA levels in control and Elp1KD cells lysates. All graphs show values of means ± SEM. Significance was determined by: **(A–I)** two-sided *t* test, Specifically, [**(A)** $p = 0.0059$; **(C)** $p < 0.0001$; **(D)** $p = 0.0256$; **(E)** $p = 0.0019$; **(F)** $p = 0.9833$; **(H)** $p = 0.7225$; **(I)** $p = 0.0456$;] **(G)** two-sided Kruskal Wallis one-way ANOVA, Specifically, [$p = 0.0003$, K = 9.346;] In addition, the post hoc multiple comparisons, to analyze statistical difference of each condition compared to control by Dunnett test, $^{**}p < 0.01$. *n* = Number of experimental repeats: **(A)** Control *n* = 8; Elp1 KD *n* = 9; **(C)** Control *n* = 3; Elp1 KD *n* = 3; **(D)** Control *n* = 3; Elp1 KD *n* = 3; **(E)** Control *n* = 4; Elp1 KD *n* = 4; **(F)** Control *n* = 3; Elp1 KD *n* = 3; **(G)** Control *n* = 6; WT *n* = 3; Elp1 KD *n* = 3; **(H)** Control *n* = 4; Elp1 KD *n* = 4; **(I)** Control *n* = 3; Elp1 KD *n* = 3.

degradation, we examined Tau protein levels in the presence or absence of the proteasomal inhibitor MG132 which blocks the proteasome-mediated degradation (Figure 4D). We found that MG132 increased Tau levels in Elp1 KD cells by almost 2 fold which was similar to levels observed in control cells. Altogether, these results led us to suggest that Elongator may indirectly regulate Tau protein turnover through the ubiquitin proteasome pathway (UPP).

Since we recently showed that loss of Elongator activity interferes with MT acetylation and axonal transport *via* reduction of Acly expression (Even et al., 2021), we perform experiments to investigate whether loss of Elp1 may trigger hypoacetylation of Tau (Figure 5). We observed a reduction of Acly protein expression levels also in our Elp1 KD neuroblastoma model (Figure 5A). We next measured Acly activity by performing an *in vitro* acetyl-CoA production assay (malate dehydrogenase coupled assay) (Wellen et al., 2009). For this, we incubated CoA and citrate (Acly substrates) with extracts from Elp1 KD and control neuroblastoma cells. Our results showed that Elp1 KD cells have reduced acetyl-CoA production activity (Figures 5B,C), suggesting that Elp1 depletion affects Acly activity correlated with its decreased expression levels.

It is known that Tau acetylation affects its turnover *via* protein stability (Cook and Stankowski, 2014; Min et al., 2010). To study whether the reduced stability of Tau in Elp1 KD cells results from its impaired acetylation, we measured Tau acetylation levels by immunoprecipitation followed by western blot analysis. For these experiments, we extracted protein from Elp1 KD and control neuroblastoma cells, immunoprecipitated Tau using specific antibodies and revealed by western blot using anti-pan acetyl lysine antibodies. The level of acetylated Tau, measured as ac-lysine levels above total Tau levels, was reduced in Elp1 KD neuroblastoma cells, as compared to control cells (Figure 5D). Next, to test whether Tau acetylation can be increased by Elongator activity, we transiently co-transfected HEK293T cells with Tau and ELP3 or with a control vector. Tau was next immunoprecipitated and subjected to western blot analysis to detect Tau acetylation levels. We observed an increase in acetylated Tau upon its over-expression with Elp3 (Figure 5E). These results suggest that the overall reduction of Tau expression upon reduction of Elongator activity results from the hypoacetylation of Tau.

Since loss of Elongator correlates with poor acetylation of α-tubulin lysine 40 (K40) in neuronal MTs (Creppe et al., 2009; Solinger et al., 2010), a defect shared by Elp1 KD neuroblastoma cells (Supplementary Figure S2A), we tested whether Tau hypoacetylation may arise from a change of expression or activity of Hdac6, the enzyme that also controls α-tubulin deacetylation (Kalebic et al., 2013). Since no change in Hdac6 expression in Elp1 KD cells and control cells (Figure 5F) was observed, we measured the activity of this enzyme in MT preparations. The deacetylation activity of Hdac6 for MTs was assessed *in vitro* by incubating free acetylated α-tubulin (from bovine brain extracts) with extracts from Elp1 KD or control cells (Figure 5G). Together with it, p300 levels, the acetyltransferase which acetylates Tau protein, showed no difference in Elp1 KD cells when compared to control in WB analysis (Figure 5H).

Moreover, we detected a reduction of acetyl-CoA levels in extracts from Elp1 KD cells, as compared to control by LC-MS metabolic analysis (Figure 5I). To assess that the hypoacetylation observed in both Tau and α-tubulin in Elp1 KD neuroblastoma model is caused by lack of acetyl-CoA; the acetyltransferase's substrate, we conducted an *in vitro* α-tubulin acetylation assay (Even et al., 2019). For this assay, pre-polymerized unacetylated MTs from HeLa cells were incubated with acetyl-CoA and cells extracts from Elp1 KD or control to assess the level of acetylation of α-tubulin. No differences in MT acetylation levels between the Elp1 KD and control cells upon addition of acetyl-CoA were observed (Supplementary Figure S2). Although indirectly, this suggests that Tau hypoacetylation might be a result of reduced Acly and impaired activity, causing a reduction in acetyl-CoA levels in the Elongator depletion background.

To further test whether the reduced level of Tau expression under Elongator depletion background relies on a change in Tau acetylation status and protein degradation, we tested if deacetylation inhibition of Hdac6, which is the known deacetylase of Tau (Noack, Leyk and Richter-Landsberg, 2014), may rescue Tau protein levels in Elongator depleted backgrounds (see Figure 6). To this hypothesis, we measured Tau acetylation in protein extracts from neuroblastoma cells

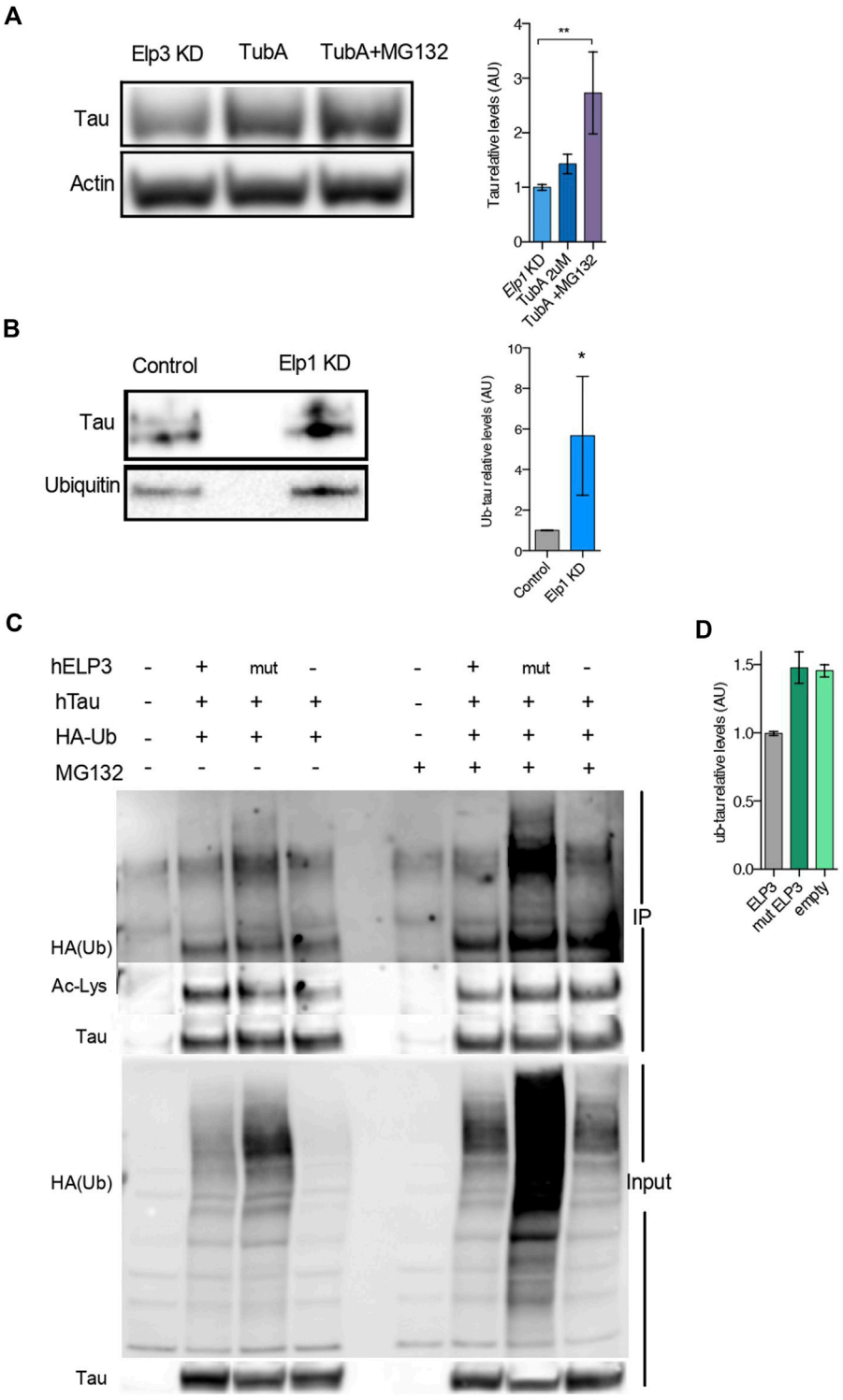

FIGURE 6
Elongator Deficiency Reduces Tau acetylation, Increases Tau ubiquitylation and induces its Degradation. **(A)** Immunoblotting and quantification of Tau and ß-Actin in differentiated SHSY5Y extracts from Control and Elp1 KD cells incubated with vehicle, Tubastatin A (TubA, 2 μM) for 24 h or Tubastatin A (TubA, 2 μM) for 24 h together with MG-132 (MG132 , 20 μM) for the last 4 h. **(B)** Immunoprecipitation followed by Western blotting to detect and quantify ubiquitylated Tau, in control and Elp1KD cells extracts. Histograms of proportion of ubiquitin expression to Tau. **(C–D)** Immunoprecipitation of Tau followed by Western blotting to detect and quantify ubiquitylated Tau; Lysates from HEK293 cells transfected with plasmids expressing WT Tau, HA-tagged ubiquitin and ELP3 or mutated ELP3 in the KAT domain or empty vector incubated with vehicle or MG-132
(*Continued*)

FIGURE 6 (Continued)
(MG132 , 17.5 μM) for 15 h. Immunoprecipitates (IP) and total soluble lysates (Input) were analyzed by western blotting, with either anti-HA or anti-acetylated lysine and anti Tau antibodies. **(D)** Histograms of proportion of ubiquitin expression to Tau incubated with MG-132 (edit graph add stat maybe quantify HA/Tau). All graphs show values of means ± SEM. Significance was determined by: **(A)** two-sided Kruskal Wallis one-way ANOVA, specifically, [$p = 0.0001$, K = 11.8;] In addition, the post hoc multiple comparisons, to analyze statistical difference of each condition compared to Elp1KD by Dunnett test, $*p < 0.05$, $**p < 0.01$. **(B)** two-sided *t* test, Specifically, [**(A)** $p = 0.0286$;]; *n* = Number of experimental repeats: **(A)** Elp1 KD $n = 6$; Elp1 KD + TubA $n = 6$; Elp1 KD + TubA MG132 $n = 5$; **(B)** Control $n = 4$; Elp1 KD $n = 4$.

treated with the selective Hdac6 inhibitor Tubastatin A (TubA), combined or not with the proteasomal inhibitor MG-132 treatment. We observed a synergistic increase of Tau level in Elp1 KD cells, as compared to their controls, upon co-inhibition of Hdac6 and proteasomal degradation (Figure 6A). This observation suggests that the stability of Tau is regulated by both UPP and acetylation.

To investigate whether Tau protein turnover is regulated by the UPP and whether Tau ubiquitin levels are affected in Elp1 KD cells, we performed a Western Blot analysis of immunoprecipitated Tau with anti-ubiquitin antibody. Our results show that the ubiquitination levels of Tau are significantly increased in the Elp1 KD cells (Figure 6B). Altogether, these results suggest that the reduction of Tau levels upon Elongator depletion is related to its hypoacetylation and increased ubiquitylation. According to that acetylation and ubiquitination of Tau potentially may occur on similar lysine residues, we hypothesized that Elongator depletion changes the balance of acetylation/ubiquitylation on some lysine residues.

To test this hypothesis, we co-transfected HEK293T cells with HA-tagged ubiquitin, and Tau together with either WT ELP3 (as the Elongator's functional catalytic subunit) or KAT domain mutant ELP3 or with empty vector, in the presence or absence of the proteasomal inhibitor MG132. We then performed an immunoprecipitation assay with Tau antibodies followed by immunoblotting using an anti-HA antibody and Anti-acetylated lysine antibody, to detect acetylation and ubiquitination of Tau in the same samples. We observed that the acetylation levels of Tau were reduced in mutant ELP3 overexpression and an empty vector control as compared to ELP3 overexpression. Our data showed a characteristic high molecular weight smear of polyubiquitin molecules conjugated to Tau in mutated ELP3 co-transfected cells. In contrast, we detected a reduced ubiquitin signal in cells transfected with ELP3 (Figure 6C HA-ub high molecular weight smear, lanes 2–4). In the presence of MG132, we observed that Tau polyubiquitination levels increased in mutant ELP3 expressing cells as well as with the empty vector when compared to control ELP3 expressing cells (Figure 6C; HA-ub single band, lanes 6–8 and 6E). The results showed that Tau is associated with polyubiquitin chains and that defects in Elp3 led to increased levels of Tau ubiquitylation at the expense of its acetylation (Figure 6D; ac-Lys single band, lanes 2–4). These results support the view that Elp3 is required for proper Tau acetylation and that mutant Elp3 impaired Tau acetylation, thereby disrupting the balance of acetylation/ubiquitylation of Tau lysine residues. These results suggest that the instability of Tau in cells depleted for Elongator activity results from changes in its post translational modifications leading to its degradation.

Having established the molecular network linking Tau instability with the depletion of Elongator's activity and its implication in neuritogenesis in neuroblastoma cells, we next investigated increasing Acly or Tau expression levels may rescue Elp1KD phenotype. Therefore, we simultaneously infected Elp1KD and control neuroblastoma cells with an adenovirus vector encoding for either Tau or Acly, 36 h prior their shorter RA-mediated differentiation to maximize the ectopic protein overexpression before neurite differentiation takes place. In order to investigate separately the Tau and Acly overexpression effects on neurite morphology, we compared the morphology data obtained from images of control neuroblastoma GFP and Elp1KD GFP infected cells, Elp1KD cells expressing human Tau and Elp1KD cells expressing human Acly (Figure 7). Figure 7A shows representative images of the neuroblastoma cell groups overexpressing the different proteins, GFP, Tau and Acly. Note that confluency in these experiments is lower due to viral infection affecting also the cell clumping phenotype in Elp1KD. As shown in Figure 7B, the two-dimensional principal component analysis applied to classify the difference in neurite morphology between GFP expressing control (in dark blue) and Elp1 KD (in pink), Elp1KD expressing Tau (hMAPT, in green) and Elp1KD expressing hACLY (in light blue) cells, resulted in 90.9% separation between the Elp1 groups overexpressing either Tau or Acly including the GFP neuroblastoma control group and the Elp1KD-GFP group. The selected neurite morphology features relevant for the PCA classification between the groups are shown in Figure 7C. Moreover, quantitative comparative analysis of the most relevant features between the groups are shown in Figures 7D–I where the overexpression effects of both Tau and Acly in Elp1 KD cells on each one of the morphological features in each of these graphs, is significantly different from the Elp1-KD-GFP group shown.

To establish a hierarchy between Tau and Acly in the system, we tested whether Acly is required for the stability of Tau protein by specifically inhibiting Acly using BMS-303141 (BMS) (Li et al., 2007) in control differentiated neuroblastoma cells (Figure 8). This treatment reduced significantly the level of Tau protein compared

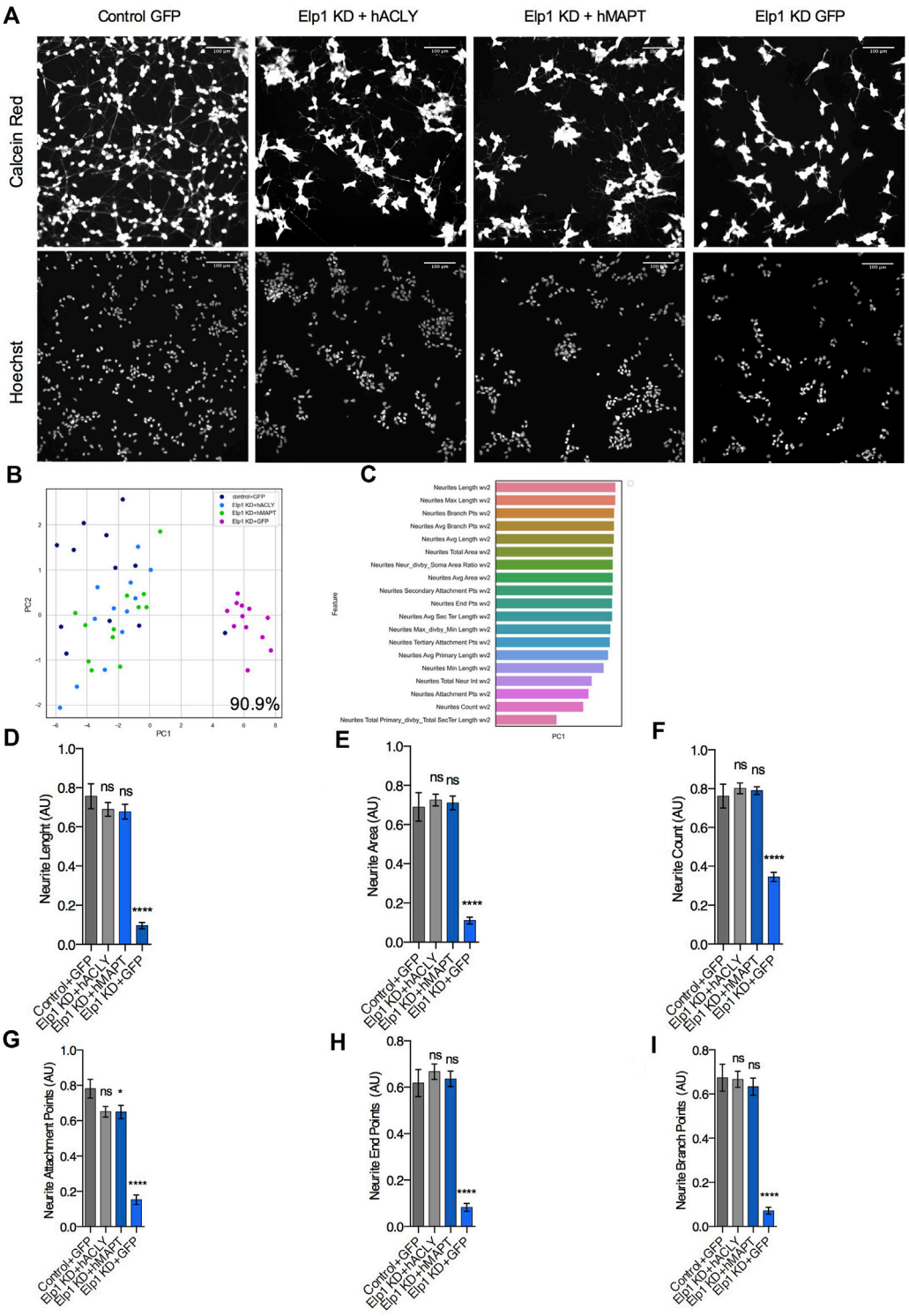

FIGURE 7
Expression of Acly or Tau rescues both Tau levels and neurites morphology defects in Elp1 KD cells. **(A)** Representative images of live fluorescence microscopy of differentiated SHSY5Y cells transfected with control GFP or MAPT or ACLY expressing plasmids stained with both Calcein AM (Red) and Hoechst (Blue); control (Control + GFP), Elp1 KD (Elp1KD + GFP), Elp1 KD expressing Tau (Elp1KD + hMAPT), Elp1 KD expressing acly (Elp1KD + hACLY) to visualize neurite morphology. Scale bar is 50 μm. **(B)** Two dimension principal component analysis (PCA) plot of stained cells based on morphological features. Symbols represent the control cells (dark blue); Elp1KD + hACLY cells (light blue), Elp1KD + GFP (pink), Elp1KD + hMAPT (green). each circle represent data extracted from 20 fields coming from one well, each field contain hundreds of cells. PCA Score
(*Continued*)

FIGURE 7 (Continued)
90.9% **(C)** Plot of features contribution to the separation in the PCA analysis **(D–I)** Quantification of the selected morphology features including Neurite Count **(D)**, Neurite Length **(E)**, Neurite Area **(F)**, Neurite Attachment Points **(G)**, Neurite End Points **(H)** and Neurite Branch Points **(I)**. All graphs show values of means ± SEM. Significance was determined by: e-j two-sided one-way analysis of variance (ANOVA), Specifically, [**(D)** $p < 0.0001$, F = 38.78; **(E)** $p < 0.0001$, F = 54.43; **(F)** $p < 0.0001$, F = 46.52; **(G)** $p < 0.0001$, F = 53.2; **(H)** $p < 0.0001$, F = 50.29; **(I)** $p < 0.0001$] In addition, the post hoc multiple comparisons, to analyze statistical difference of each condition compared to control for **(D–I)** by Dunnett test ****$p < 0.0001$. n = Number of wells (each well contains data from 20 fields, each field contains hundreds of cells): **(D–I)** Control + GFP n = 12; Elp1KD + GFP n = 12; Elp1KD + hACLY n = 12; Elp1KD + hMAPT n = 12.

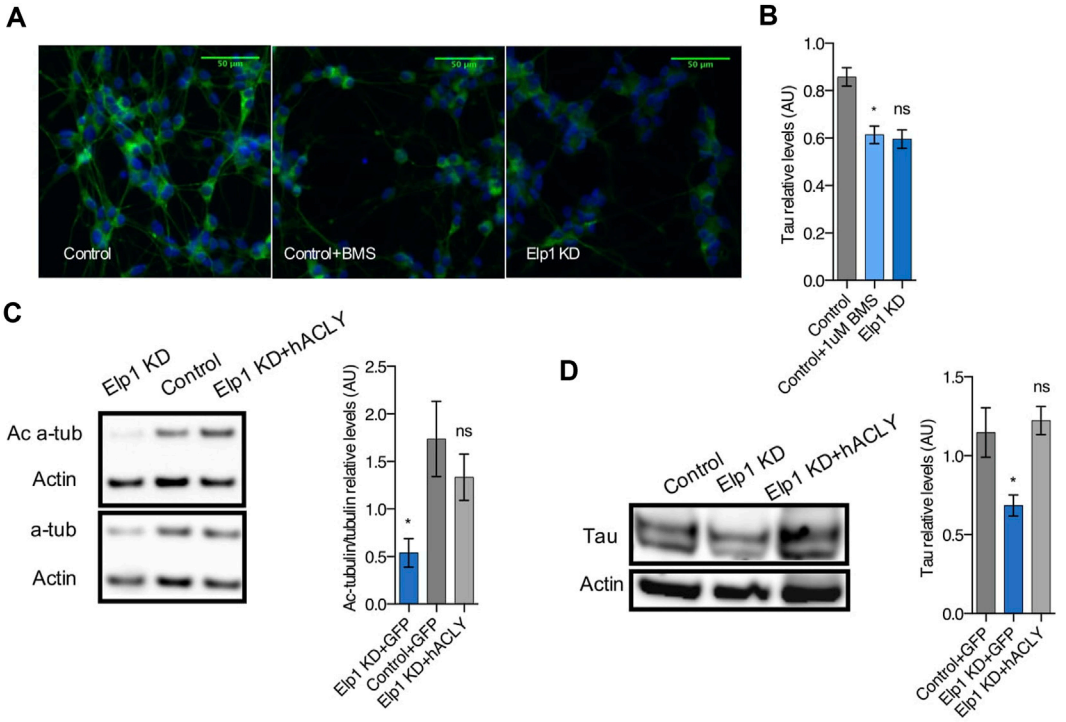

FIGURE 8
Inhibition of Acly interferes with Tau stability and Ac-α-tubulin levels establishing hierarchy involved in neurite morphology defects in Elp1 KD cells. **(A–B)** Immunolabeling and quantification of Tau levels in differentiated SHSY5Y extracts from Elp1KD cells and Control cells incubated with vehicle or BMS 303141 (BMS, 1 μM) for 72h. Scale bar is 50 μm. **(C–D)** Immunoblotting and quantification of Acetylated α-tubulin (Ac α-Tub), Total α-tubulin (t α-Tub) **(C)** and Tau **(D)** from differentiated SHSY5Y extracts from Control and Elp1 KD cells transfected with ACLY or GFP carrying constructs. All graphs show values of means ± SEM. Significance was determined by: **(B–D)** two-sided one-way analysis of variance (ANOVA), Specifically, [**(B)** $p = 0.0072$, F = 6.112; **(C)** $p = 0.0405$, F = 4.494; **(D)** $p = 0.0277$, F = 5.487;] In addition, the post hoc multiple comparisons, to analyze statistical difference of each condition compared to control for **(B–D)** by Dunnett test *$p < 0.05$. n = Number of wells (each well contains data from 20 fields, each field contains hundreds of cells): **(B)** Control n = 4; Control + BMS n = 7; Elp1KD n = 16; n = Number of experimental repeats: **(C)** Control + GFP n = 4; Elp1KD + GFP n = 4; Elp1KD + hACLY n = 5; **(D)** Control + GFP n = 4; Elp1KD + GFP n = 3; Elp1KD + hACLY n = 5.

to the Tau levels found in Elp1KD cells (Figures 8A,B) as judged by quantitative immunofluorescence analysis. This finding strongly suggests that Tau stability depends on Acly activity, establishing a regulatory relationship between the two in this system. Moreover, Acly overexpression in Elp1KD cells restores both the level of Tau and the level of ac α-tubulin (Figures 8C,D) confirming the dependence of Acly activity for Tau and MT integrity under Elongator deficiency background in these cells.

Altogether, these results, as depicted in the cartoon in Figure 9, suggest that reduction of Acly expression causes reduction of MTs acetylation and Tau protein levels which directly affect the neurite morphology phenotype in Elp1KD neuroblastoma FD cells.

Discussion

Here, we show that loss of Elongator activity impairs Tau stability *via* reduction of expression of Acly. This directly affects the neurite morphology, as exemplified in Elp1KD neuroblastoma cells. The neurite morphology defects observed in Elp1 KD are shared by Tau KD neuroblastoma

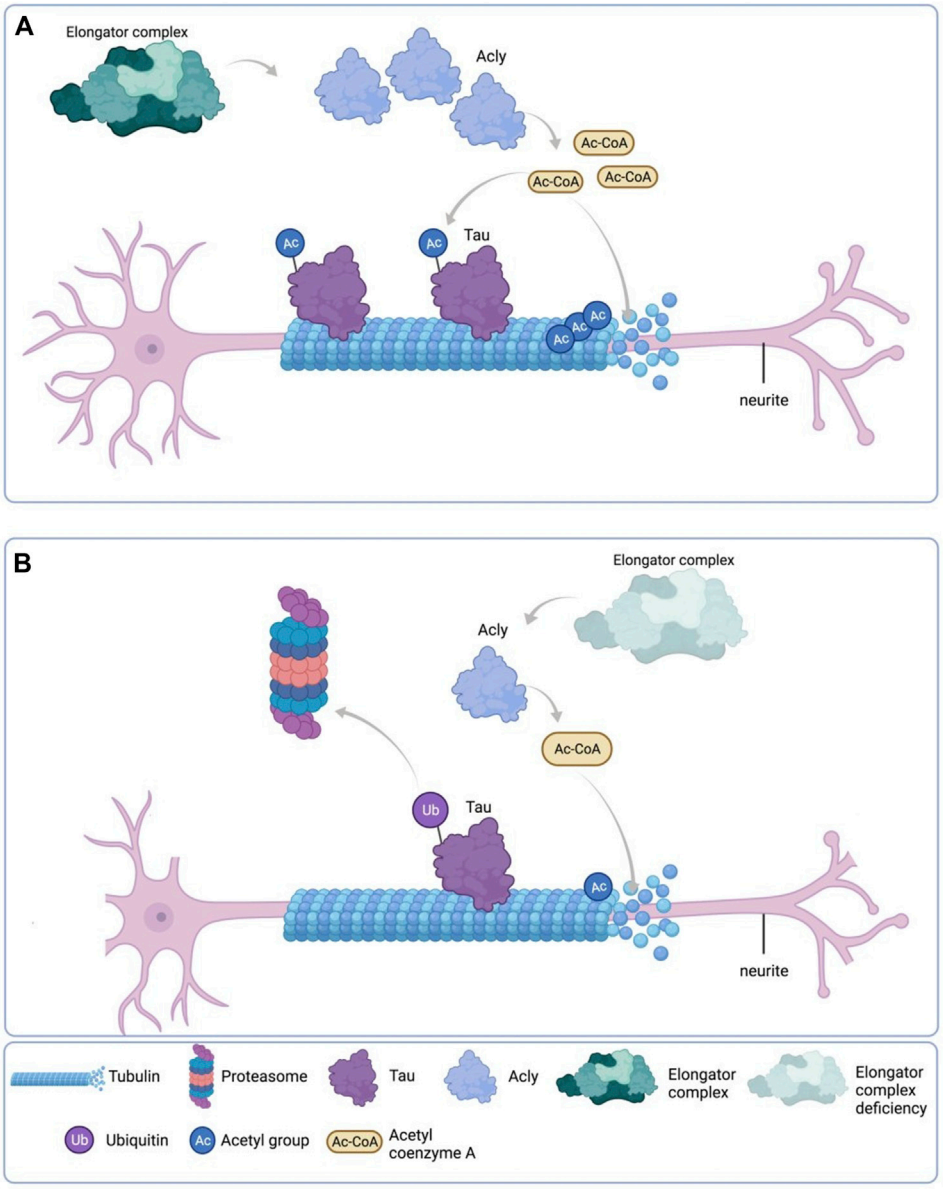

FIGURE 9
Schematic representation of the results. **(A)** Under normal Elongator complex activity, Acly's enzymatic activity in the cytoplasm of neurons produces sufficient Ac-CoA for maintenance of acetylation levels of both Tau and MT *via* their respective acetyltransferases, contributing to normal neurite morphology. **(B)** Under Elongator complex deficiency (hElp1-KD), Acly's enzymatic activity is compromised due to protein instability producing low Ac-CoA in the cytoplasm of neurons compromising acetylation levels required for maintenance of both Tau and MT causing polyubiquitylation and proteasomal degradation of Tau, contributing to MT instability and abnormal neurite morphology. Adapted from "Neuron Anatomy", by BioRender.com (September 2020). Retrieved from https://app.biorender.com/biorender-templates/t-5f5b7e6139954000b2bde860-neuron-anatomy Copyright 2022 by BioRender.

cells, including features that relate to neurite network organization and neurite outgrowth that are correlated with the Tau expression levels in these cells. Evidence from different Tau knockout and knockdown models has shown that this protein is required for neurite outgrowth, which resulted in reduced neurite number and length, suppression of axon elongation and progressive degeneration of neurons (Liu, Lee and Jay, 1999; Hana N. Dawson et al., 2001; Ke et al., 2012; Bolkan and Kretzschmar, 2014). This may imply that both Elp1 and Tau deficiencies share a common pathway that is involved in the neurite phenotype in the FD cells. It has been shown that Tau plays significant role in the peripheral nervous system; it increases the structural stability and contributes to the high rate of axonal transport observed in peripheral axons

(Tolkovsky and Brelstaff, 2018; Yi et al., 2019; Marquez et al., 2021) Peripheral neuropathy, like FD (Tourtellotte, 2016), results from neuronal dysfunction due in part to a loss of neurotrophic support (Sahenk, 2006), and since Tau plays an important role in stabilizing neuronal microtubules and regulating axonal transport, the malfunction of Tau may cause peripheral nerve dysfunction and degeneration (Marquez et al., 2021). The reduced levels of Tau observed upon Elongator depletion may contribute to FD peripheral nerve degeneration together with our previous findings of transport defects resulting from impaired α-tubulin acetylation (Noack, Leyk and Richter-Landsberg, 2014; Even et al., 2021). In addition, Tau malfunction has been associated with several neurodegenerative disorders, including frontotemporal dementia, Alzheimer, parkinsonism and other Tauopathies (Spillantini et al., 1998; Ludolph et al., 2009) triggering neurodegeneration. Although the deleterious effects of Tau pathology in those diseases are still highly debated, there is an assumption that Tauopathies are the consequence of loss of the ability of Tau to bind to and promote the assembly of microtubules (Lee and Leugers, 2012). Evidence of neurodegenerative diseases involving Tau downregulation are yet to be reported, but the connection between Tau misfunction and neurodegeneration is well described by others.

Moreover, we show that the reduced levels of Tau occur in other Elongator depleted models *in vitro* and *in vivo*. Therefore, we hypothesize that Elongator indirectly regulates Tau expression. Our results show in differentiated Elp1 KD neuroblastoma cells that Tau instability results from its hypoacetylation, which in turn increases its UPS degradation. This phenotype could be reversed by treatment with either or both Hdac6 and proteasomal degradation inhibitors treatment (Figure 4D, Figure 6A). It is already known that the hypoacetylation of Tau causes its reduced stability through UPS (Min et al., 2010). Therefore, an imbalance between acetylation and ubiquitylation at Tau lysine residues causes the dramatic reduction of Tau in Elp1 KD cells, which results from impaired acetylation due to reduced activity of Acly (see Figure 5, Figure 6) under the Elongator depletion background. This is part of a global and conserved mechanism by the Elongator regulating cellular acetylation processes through Acly which so far we have found that it is involved in α-tubulin acetylation, MT stabilization and neuronal transport and now Tau stability that is compromised in Elongator depleted models (Even et al., 2021).

Therefore, it is possible that under such hypoacetylation conditions increased proteasomal degradation of multiple proteins takes place in FD cells by default which might have a profound impact in neuronal function and survival. Ibrahim and others' work on FD human olfactory ectomesenchymal stem cells (hOE-MSCs) supports this assumption (Hervé and Chérif, 2017) where Elp1 deficiency could induce proteasome alterations and that Elongator dysfunction in FD disturbs proteasome activity. Together with it, transcriptome and proteome analyses that have been done on DRG of mice in which Elp1 is conditionally ablated in the peripheral nervous system (PNS) suggest that the translational defects observed in Elongator loss are affecting downstream misregulation of numerous genes that function in ubiquitination, resulting in polyubiquitylation and proteasomal degradation of proteins (Goffena et al., 2018).

We propose that Elongator indirectly contributes to global cell levels of Ac-CoA *via* stabilization of Acly, which is regulating Tau stability *via* a fine balance between its lysine acetylation/ubiquitylation. This process is key to allowing proper neuritogenesis in differentiating neuroblastoma cells. Under Elongator deficiency in Elp1KD neuroblastoma cells, due to Acly instability, the reduced amount of available acetyl-CoA, that donates the acetate group needed for proteins acetylation, results in hypoacetylation of alpha-tubulin and Tau (which might affect also other protein targets) and their concomitant instability which has a direct profound impact in neurite morphology and vesicular transport as described previously (Even et al., 2021) (see Figure 9). Interestingly, overexpression of Tau and Acly recovers neurite morphology but apparently not the known cell-cell adhesion Contactin-1 dependent phenotype in Elp1 KD cells (Cohen-kupiec et al., 2010), as judged by the similar nuclei density and cell clusters observed in the images of the different groups (see Figure 7A). This suggests that the distinct Elp1 KD neuritogenesis Tau-dependent phenotype might be regulated separately from the Contactin-1 dependent one.

In conclusion, loss of Elongator activity might contribute to FD neuropathy by interfering with Acly expression, thereby MT-dependent transport and Tau levels. Altogether these results suggest that boosting Acly expression/activity should be investigated to implement future therapy for FD as well as to prevent the progression of other neurodegenerative disorders characterized by poor axonal transport, an impairment of tubulin acetylation or malfunction of Tau.

Data availability statement

The raw data supporting the conclusions of this article will be made available by the authors, without undue reservation.

Author contributions

MS, AE, MW, and LN, designed the study. MS, performed and interpreted most experiments. AE and HG, contributed to molecular work. AE, provided guidance and help for experiments. MW and LN, contributed to data interpretation;

and MS, MW, and LN, wrote the manuscript with input from all coauthors.

Funding

This work is supported by the Israel Science Foundation, ISF Grant No. 1688/16 and ISF Grant No. 1513/20. LN. is Research Director of the F.R.S- F.N.R.S. The work performed in the Nguyen laboratory is supported by ULiège (Crédit Classique), the F.R.S.-F.N.R.S. (PDR T.0185.20; EOS 0019118F-RG36), WELBIO (CR-2022A-12), the Fonds Leon Fredericq, the Fondation Médicale Reine Elisabeth, the Fondation Simone et Pierre Clerdent, the Belgian Science Policy (IAP-VII network P7/20), the ERANET Neuron (STEM-MCD and NeuroTalk), and the Win2Wal (ChipOmics; #2010126).

Conflict of interest

The authors declare that the research was conducted in the absence of any commercial or financial relationships that could be construed as a potential conflict of interest.

Publisher's note

All claims expressed in this article are solely those of the authors and do not necessarily represent those of their affiliated organizations, or those of the publisher, the editors and the reviewers. Any product that may be evaluated in this article, or claim that may be made by its manufacturer, is not guaranteed or endorsed by the publisher.

Supplementary material

The Supplementary Material for this article can be found online at: https://www.frontiersin.org/articles/10.3389/fcell.2022.1015125/full#supplementary-material

SUPPLEMENTARY FIGURE 1
Elongator depletion leads to reduction in Tau protein expression **(A,B)** Western blotting to detect and quantify Tau, and ß-Actin in cortical extracts from newborn WT and Elp3 cKO mice. **(B)** Histogram of proportion of Tau expression to ß-Actin. **(C,D)** Western blotting to detect and quantify Tau, and ß-Actin in adult fly head extracts following neuronal (elav-driven) expression of wt and Elp3 KD. **(D)** Histogram of proportion of Tau expression to ß-Actin. All graphs show values of means ± SEM. Significance was determined by: b,d two-sided t test, Specifically, [**(B)** p = 0.0161; **(D)** p = 0.0216; **(B)** n = Number of mice: Control n = 4; Elp3 cKO n = 4; **(D)** n = Number of experimental repeats: Control n = 5; Elp3 KD n = 5.

SUPPLEMENTARY FIGURE 2
Tau is hypoacetylated, a result of impaired production of acetyl-CoA upon Elongator depletion. **(A)** Western blotting to detect and quantify acetylated alpha tubulin, and ß-Actin in differentiated SHSY5Y extracts from Control and Elp1 KD cells. Histogram of proportion of acetylated alpha tubulin expression to ß-Actin. **(B)** In vitro acetylation assay of non-acetylated MTs from HeLa cells incubated for 2 hours with extracts of differentiated SHSY5Y Control and Elp1 KD cells. All graphs show values of means ± SEM. Significance was determined by: b two-sided t test, Specifically, [p = 0.0106] **(D)** one-way analysis of variance (ANOVA), Specifically, [p < 0.0001, F = 1059]. n = Number of experimental repeats: **(B)** Control n = 5; Elp1 KD n = 5; **(D)** Control n = 6; WT n = 3 Elp1 KD n = 3.

References

Abashidze, A., Gold, V., Anavi, Y., Greenspan, H., and Weil, M. (2014). Involvement of IKAP in peripheral target innervation and in specific JNK and NGF signaling in developing PNS neurons. *PLoS ONE* 9 (11), e113428. doi:10.1371/journal.pone.0113428

Anderson, S. L., Coli, R., Daly, I. W., Kichula, E. A., Rork, M. J., Volpi, S. A., et al. (2001). Familial dysautonomia is caused by mutations of the IKAP gene. *Am. J. Hum. Genet.* 68 (3), 753–758. doi:10.1086/318808

Bar-Aluma, B. E. (2003). "Familial dysautonomia," in *GeneReviews*. Seattle (WA): University of Washington.

Bento-Abreu, A., Jager, G., Swinnen, B., Rue, L., Hendrickx, S., Jones, A., et al. (2018). Elongator subunit 3 (ELP3) modifies ALS through tRNA modification. *Hum. Mol. Genet.* 27 (7), 1276–1289. doi:10.1093/hmg/ddy043

Bolkan, B. J., and Kretzschmar, D. (2014). Loss of tau results in defects in photoreceptor development and progressive neuronal degeneration in Drosophila. *Dev. Neurobiol.* 74, 1210–1225. doi:10.1002/dneu.22199

Caceres, A., Potrebic, S., and Kosik, K. S. (1991). The effect of tau antisense oligonucleotides on neurite formation of cultured cerebellar macroneurons. *J. Neurosci.* 11 (6), 1515–1523. doi:10.1523/jneurosci.11-06-01515.1991

Cheishvili, D., Maayan, C., Cohen-Kupiec, R., Lefler, S., Weil, M., Ast, G., et al. (2011). IKAP/Elp1 involvement in cytoskeleton regulation and implication for familial dysautonomia. *Hum. Mol. Genet.* 20 (8), 1585–1594. doi:10.1093/hmg/ddr036

Close, P., Hawkes, N., Cornez, I., Creppe, C., Lambert, C. A., Rogister, B., et al. (2006). Transcription impairment and cell migration defects in elongator-depleted cells: Implication for familial dysautonomia. *Mol. Cell.* 22 (4), 521–531. doi:10.1016/j.molcel.2006.04.017

Cohen-Kupiec, R., Pasmanik-Chor, M., Oron-Karni, V., and Weil, M. (2011). Effects of IKAP/hELP1 deficiency on gene expression in differentiating Neuroblastoma cells: Implications for familial Dysautonomia. *PLoS ONE* 6 (4), e19147. doi:10.1371/journal.pone.0019147

Cohen-kupiec, R., Weinstein, S., Kantor, G., Peer, D., and Weil, M. (2010). IKAP/hELP1 downregulation in neuroblastoma cells causes enhanced cell adhesion mediated by contactin overexpression. *Cell. adh. Migr.* 4, 541–550. doi:10.4161/cam.4.4.12923

Cook, C., Stankowski, Jeannette N., Carlomagno, Y., Stetler, C., and Petrucelli, L. (2014). Acetylation: A new key to unlock tau's role in neurodegeneration. *Alzheimers Res. Ther.* 6 (3), 29–38. doi:10.1186/alzrt259

Creppe, C., Malinouskaya, L., Volvert, M. L., Gillard, M., Close, P., Malaise, O., et al. (2009)., Elongator controls the migration and differentiation of cortical neurons through acetylation of alpha-tubulin. *Cell.*136. 3. Cell, 551–564. doi:10.1016/j.cell.2008.11.043

David, D. C., Layfield, R., Serpell, L., Narain, Y., Goedert, M., and Spillantini, M. G. (2002). Proteasomal degradation of tau protein. *J. Neurochem.* 83 (1), 176–185. doi:10.1046/j.1471-4159.2002.01137.x

Dawson, Hana N., FerreirA, A., Eyster, M. V., GhoshalN.Binder, L. I., and Vitek, M. P. (2001). Inhibition of neuronal maturation in primary hippocampal neurons from tau deficient mice. *J. Cell. Sci.* 114 (6), 1179–1187. doi:10.1242/jcs.114.6.1179

Esberg, A., Huang, B., Johansson, M. J. O., and Bystrom, A. S. (2006). Elevated levels of two tRNA species bypass the requirement for elongator complex in transcription and exocytosis. *Mol. Cell.* 24 (1), 139–148. doi:10.1016/j.molcel.2006.07.031

Esmaeli-azad, B., Mccarty, J. H., and Feinstein, S. C. (1994). Sense and antisense transfection analysis of tau function : Tau influences net microtubule assembly. *neurite outgrowth neuritic stability*' 879, 869–879.

Even, A., Morelli, G., Turchetto, S., Shilian, M., Bail, R. L., Laguesse, S., et al. (2021). ATP-citrate lyase promotes axonal transport across species. *Nat. Commun.* 12 (1), 5878–5914. doi:10.1038/s41467-021-25786-y

Even, A., Morelli, G., Broix, L., Scaramuzzino, C., Turchetto, S., Gladwyn-Ng, I., et al. (2019). ATAT1-enriched vesicles promote microtubule acetylation via axonal transport. *Sci. Adv.* 5 (12), eaax2705. doi:10.1126/sciadv.aax2705

Froelich, S., Lendon, C. L., Rizzu, P., BakerM., Houlden, H., et al. (1998). Association of missense and 5'-splice-site mutations in tau with the inherited dementia FTDP-17. *Nature* 393, 702–705. doi:10.1038/31508

Goffena, J., Lefcort, F., Zhang, Y., Lehrmann, E., Chaverra, M., Felig, J., et al. (2018). Elongator and codon bias regulate protein levels in mammalian peripheral neurons. *Nat. Commun.* 9 (1), 889. doi:10.1038/s41467-018-03221-z

Hermand, D. (2020). Anticodon wobble uridine modification by elongator at the crossroad of cell signaling, differentiation, and diseases. *Epigenomes* 4 (2), 7. doi:10.3390/epigenomes4020007

Hervé, M., and Chérif, E. (2017). Proteasome inhibitors to alleviate aberrant IKBKAP mRNA splicing and low IKAP/hELP1 synthesis in familial dysautonomia. *Neurobiol. Dis.* 103, 113–122. doi:10.1016/j.nbd.2017.04.009

Hirokawa, N., Funakoshi, T., Sato-HaRada, R., and Kanai, Y. (1996). Selective stabilization of tau in axons and microtubule-associated protein 2C in cell bodies and dendrites contributes to polarized localization of cytoskeletal proteins in mature neurons. *J. Cell. Biol.* 132 (4), 667–679. doi:10.1083/jcb.132.4.667

Huang, B., Johansson, M. J. O., and Byström, A. S. (2005). An early step in wobble uridine tRNA modification requires the Elongator complex. *Rna* 11 (4), 424–436. doi:10.1261/rna.7247705

Kalebic, N., Sorrentino, S., Perlas, E., Bolasco, G., Martinez, C., and Heppenstall, P. A. (2013). αTAT1 is the major α-tubulin acetyltransferase in mice. *Nat. Commun.* 4, 1962. doi:10.1038/ncomms2962

Ke, Y. D., Suchowerska, A. K., van der Hoven, J., De Silva, D. M., Wu, C. W., van Eersel, J., et al. (2012). Lessons from tau-deficient mice. *Int. J. Alzheimers Dis.* 2012, 873270. doi:10.1155/2012/873270

Laguesse, S., Creppe, C., Nedialkova, D. D., Prevot, P. P., Borgs, L., Huysseune, S., et al. (2015). A dynamic unfolded protein response contributes to the control of cortical Neurogenesis. *Dev. Cell.* 35 (5), 553–567. doi:10.1016/j.devcel.2015.11.005

Lee, G., and Leugers, C. J. (2012). Tau and tauopathies. *Prog. Mol. Biol. Transl. Sci.* 107, 263–293. doi:10.1016/B978-0-12-385883-2.00004-7

Li, J. J., Wang, H., Tino, J. A., Robl, J. A., Herpin, T. F., Lawrence, R. M., et al. (2007). 2-Hydroxy-N-arylbenzenesulfonamides as ATP-citrate lyase inhibitors. *Bioorg. Med. Chem. Lett.* 17 (11), 3208–3211. doi:10.1016/j.bmcl.2007.03.017

Liu, C. W. A., Lee, G., and Jay, D. G. (1999). Tau is required for neurite outgrowth and growth cone motility of chick sensory neurons. *Cell. Motil. Cytoskelet.* 43 (3), 232–242. doi:10.1002/(SICI)1097-0169(1999)43:3<232::AID-CM6>3.0.CO;2-7

Ludolph, A. C., Kassubek, J., Landwehrmeyer, B. G., MandElkow, E., Mandelkow, E. M., Burn, D. J., et al. (2009). Tauopathies with parkinsonism: Clinical spectrum, neuropathologic basis, biological markers, and treatment options. *Eur. J. Neurol.* 16 (3), 297–309. doi:10.1111/j.1468-1331.2008.02513.x

Marquez, A., Guernsey, L. S., Frizzi, K. E., Cundiff, M., Constantino, I., Muttalib, N., et al. (2021). Tau associated peripheral and central neurodegeneration: Identification of an early imaging marker for tauopathy. *Neurobiol. Dis.* 151, 105273. doi:10.1016/j.nbd.2021.105273

Martin, L., Latypova, X., and Terro, F. (2011). Post-translational modifications of tau protein: Implications for alzheimer's disease. *Neurochem. Int.* 58 (4), 458–471. doi:10.1016/j.neuint.2010.12.023

Mietelska-Porowska, A., Wasik, U., Goras, M., Filipek, A., and Niewiadomska, G. (2014). Tau protein modifications and interactions: Their role in function and dysfunction. *Int. J. Mol. Sci.* 15 (3), 4671–4713. doi:10.3390/ijms15034671

Min, S., Cho, S-H., Zhou, Y., Schroeder, S., Haroutunian, V., Seeley, W. W., et al. (2010). Acetylation of tau inhibits its degradation and contributes to tauopathy. *Neuron* 67 (6), 953–966. doi:10.1016/j.neuron.2010.08.044

Miśkiewicz, K., Jose, L. E., Bento-Abreu, A., Fislage, M., Taes, I., Kasprowicz, J., et al. (2011). ELP3 controls active zone morphology by acetylating the ELKS family member bruchpilot. *Neuron* 72 (5), 776–788. doi:10.1016/j.neuron.2011.10.010

Noack, M., Leyk, J., and Richter-Landsberg, C. (2014). HDAC6 inhibition results in tau acetylation and modulates tau phosphorylation and degradation in oligodendrocytes. *Glia* 62 (4), 535–547. doi:10.1002/glia.22624

Petrakis, T. G., Wittschieben, B., and Svejstrup, J. Q. (2004). Molecular architecture, structure-function relationship, and importance of the Elp3 subunit for the RNA binding of holo-Elongator. *J. Biol. Chem.* 279 (31), 32087–32092. doi:10.1074/jbc.M403361200

Riley, C. M., Day, R. L., Greeley, D. M., and Langford, W. S. (1949). Central autonomic dysfunction with defective lacrimation; report of five cases. *Pediatrics* 3 (4), 468–478. doi:10.1542/peds.3.4.468

Sahenk, Z. (2006). Neurotrophins and peripheral neuropathies. *Brain Pathol.* 16 (4), 311–319. doi:10.1111/j.1750-3639.2006.00038.x

Singh, N., Lorbeck, M. T., Zervos, A., Zimmerman, J., and Elefant, F. (2010). The histone acetyltransferase Elp3 plays in active role in the control of synaptic bouton expansion and sleep in Drosophila. *J. Neurochem.* 115 (2), 493–504. doi:10.1111/j.1471-4159.2010.06892.x

Slaugenhaupt, S. A., Blumenfeld, A., Gill, S. P., LeyneM., Mull, J., Cuajungco, M. P., et al. (2001). Tissue-specific expression of a splicing mutation in the IKBKAP gene causes familial dysautonomia. *Am. J. Hum. Genet.* 68 (3), 598–605. doi:10.1086/318810

Sola, M., Magrin, C., Pedrioli, G., Pinton, S., Salvade, A., Papin, S., et al. (2020). Tau affects P53 function and cell fate during the DNA damage response. *Commun. Biol.* 3 (1), 245–315. doi:10.1038/s42003-020-0975-4

Solinger, J. A., Paolinelli, R., Kloss, H., Scorza, F. B., Marchesi, S., Sauder, U., et al. (2010). The *Caenorhabditis elegans* elongator complex regulates neuronal α-tubulin acetylation. *PLoS Genet.* 6 (1), e1000820. doi:10.1371/journal.pgen.1000820

Spillantini, M. G., Murrell, J. R., GoedertM., Farlow, M. R., Klug, A., and Ghetti, B. (1998). Mutation in the tau gene in familial multiple system tauopathy with presenile dementia. *Proc. Natl. Acad. Sci. U. S. A.* 95 (13), 7737–7741. doi:10.1073/pnas.95.13.7737

Tolkovsky, A. M., and Brelstaff, J. (2018). Sensory neurons from tau transgenic mice and their utility in drug screening. *Methods Mol. Biol.* 1727, 93–105. doi:10.1007/978-1-4939-7571-6_7

Tourtellotte, W. G. (2016). Axon transport and neuropathy: Relevant perspectives on the etiopathogenesis of familial dysautonomia', *American Journal of Pathology. Am. J. Pathol.* 186 (3), 489–499. doi:10.1016/j.ajpath.2015.10.022

Wellen, K. E., Hatzivassiliou, G., Sachdeva, U. M., Bui, T. V., Cross, J. R., and Thompson, C. B. (2009). ATP-citrate lyase links cellular metabolism to histone acetylation. *Science* 324 (5930), 1076–1080. doi:10.1126/science.1164097

Winkler, G. S., Kristjuhan, A., Erdjument-Bromage, H., Tempst, P., and Svejstrup, J. Q. (2002). Elongator is a histone H3 and H4 acetyltransferase important for normal histone acetylation levels *in vivo*. *Proc. Natl. Acad. Sci. U. S. A.* 99 (6), 3517–3522. doi:10.1073/pnas.022042899

Yi, S., Liu, Q., Wang, X., Qian, T., Wang, H., Zha, G., et al. (2019). Tau modulates Schwann cell proliferation, migration and differentiation following peripheral nerve injury. *J. Cell. Sci.* 132 (6), jcs222059. doi:10.1242/jcs.222059

frontiers | Frontiers in Cell and Developmental Biology

TYPE Brief Research Report
PUBLISHED 05 December 2022
DOI 10.3389/fcell.2022.1014798

OPEN ACCESS

EDITED BY
Suneel Kateriya,
Jawaharlal Nehru University, India

REVIEWED BY
Mariafrancesca Scalise,
University of Calabria, Italy
José Ignacio Ruiz-Sanz,
University of the Basque Country, Spain

*CORRESPONDENCE
Sara Eyal,
sarae@ekmd.huji.ac.il
Or Kakhlon,
ork@hadassah.org.il

SPECIALTY SECTION
This article was submitted to Cellular Biochemistry,
a section of the journal
Frontiers in Cell and Developmental Biology

RECEIVED 09 August 2022
ACCEPTED 31 October 2022
PUBLISHED 05 December 2022

CITATION
Granit A, Mishra K, Barasch D, Peretz-Yablonsky T, Eyal S and Kakhlon O (2022), Metabolomic profiling of triple negative breast cancer cells suggests that valproic acid can enhance the anticancer effect of cisplatin.
Front. Cell Dev. Biol. 10:1014798.
doi: 10.3389/fcell.2022.1014798

Metabolomic profiling of triple negative breast cancer cells suggests that valproic acid can enhance the anticancer effect of cisplatin

Avital Granit[1,2], Kumudesh Mishra[3,4], Dinorah Barasch[5], Tamar Peretz-Yablonsky[1,4], Sara Eyal[2,6]* and Or Kakhlon[3,4]*

[1]Sharett Institute of Oncology, Hadassah-Hebrew University Medical Center, Jerusalem, Israel, [2]Institute for Drug Research School of Pharmacy, The Hebrew University of Jerusalem, Jerusalem, Israel, [3]Department of Neurology, Hadassah-Hebrew University Medical Center, Jerusalem, Israel, [4]Faculty of Medicine, Hebrew University of Jerusalem, Jerusalem, Israel, [5]Mass Spectrometry Unit, Institute for Drug Research, School of Pharmacy, The Hebrew University of Jerusalem, Jerusalem, Israel, [6]The Dame Susan Garth Chair of Cancer Research, The David R. Bloom Centre for Pharmacy and Dr. Adolf and Klara Brettler Centre for Research in Molecular Pharmacology and Therapeutics at The Hebrew University of Jerusalem, Jerusalem, Israel

Cisplatin is an effective chemotherapeutic agent for treating triple negative breast cancer (TNBC). Nevertheless, cisplatin-resistance might develop during the course of treatment, allegedly by metabolic reprograming, which might influence epigenetic regulation. We hypothesized that the histone deacetylase inhibitor (HDACi) valproic acid (VPA) can counter the cisplatin-induced metabolic changes leading to its resistance. We performed targeted metabolomic and real time PCR analyses on MDA-MB-231 TNBC cells treated with cisplatin, VPA or their combination. 22 (88%) out of the 25 metabolites most significantly modified by the treatments, were acylcarnitines (AC) and three (12%) were phosphatidylcholines (PCs). The most discernible effects were up-modulation of AC by cisplatin and, contrarily, their down-modulation by VPA, which was partial in the VPA-cisplatin combination. Furthermore, the VPA-cisplatin combination increased PCs, sphingomyelins (SM) and hexose levels, as compared to the other treatments. These changes predicted modulation of different metabolic pathways, notably fatty acid degradation, by VPA. Lastly, we also show that the VPA-cisplatin combination increased mRNA levels of the fatty acid oxidation (FAO) promoting enzymes acyl-CoA synthetase long chain family member 1 (ACSL1) and decreased mRNA levels of fatty acid synthase (FASN), which is the rate limiting enzyme of long-chain fatty acid synthesis. In conclusion, VPA supplementation altered lipid metabolism, especially fatty acid oxidation and lipid synthesis, in cisplatin-treated MDA-MB-231 TNBC cells. This metabolic reprogramming might reduce cisplatin resistance. This finding may lead to the discovery of new therapeutic targets, which might reduce side effects and counter drug tolerance in TNBC patients.

KEYWORDS
valproic acid, metabolomics, metabolism, cisplatin, triple negative breast cancer

Introduction

Breast cancer is the most common cancer and the second death-causing cancer in women worldwide (Siegel et al., 2021). Breast cancer is subdivided into three main molecular subtypes according to the expression pattern of estrogen receptor (ER), progesterone receptor (PR), human epidermal growth factor receptor 2 (HER2), or none of them (triple negative breast cancer, TNBC). TNBC is an aggressive subtype of breast cancer and accounts for 15% of all breast cancer cases (Yin et al., 2020). The main treatment regime for TNBC is chemotherapy. One therapeutic option is cis-diamminedichloroplatinum (II) (cisplatin). Cisplatin was first approved in 1978 for the treatment of bladder and testicular cancer (Prestayko et al., 1979) and has since been used for many different solid malignancies.

The mechanism of action of cisplatin is linked to its ability to crosslink purine bases in the DNA, causing DNA damage and resulting in cell division blockage and apoptotic cell death.

Valproic acid (VPA) is approved as an antiepileptic drug since 1967 (Mattson et al., 1978). VPA possesses an anti-cancer capacity, notably against breast cancer (Wawruszak et al., 2021), which is related to its ability to inhibit histone deacetylase. As histone acetylation enables the interaction of transcription factors and RNA polymerase with DNA, deacetylation of histones and non-histone proteins can modify gene expression and cellular pathways, regulating different functions in cancer cells, such as apoptosis, cell cycle and DNA repair (Brancolini et al., 2022).

Due to the ability of VPA to alter chromatin condensation and transcription and the ability of cisplatin to alkylate DNA, combining both drugs demonstrated a synergistic antitumor activity *in vitro* in different breast cancer cell lines. However, the combination generated a sub-additive (antagonistic) anti-cancer effect when applied in a 1:1 ratio in the TNBC cell line, MDA-MB-231 (Wawruszak et al., 2015). To gain a better understanding of the joint influence of cisplatin and VPA on TNBC cells, we decided to investigate their effect on the intracellular metabolism of MDA-MB-231 cells. To that end, we used targeted metabolomics. Metabolomics is a fast advancing field of research aimed at identifying and quantifying the small molecules (together known as metabolome) involved in attaining metabolic homeostasis (Liesenfeld et al., 2013). Previous metabolomic studies in MDA-MB-231 cells, assessing cisplatin or VPA individually, showed that cisplatin can alter phospholipid biosynthesis (Resendiz-Acevedo et al., 2021) and that VPA can alter the beta-alanine, taurine, and hypotaurine pathways (Zhou et al., 2020). Although these studies demonstrated dramatic metabolic changes in the MDA-MB-231 cells following cisplatin or VPA treatment, there has been no study to date, which compared the metabolomic profile of TNBC cells treated with the VPA-cisplatin combination to cells treated with each drug separately. As HDAC inhibition and cisplatin are key strategies for TNBC therapy, it is important to understand their mutual interaction so as to improve the efficacy of this co-therapy strategy. In the present study, we provide evidence that VPA and cisplatin alone or together can change the levels of carnitine, AC, amino acids (AA), biogenic amines, lipids, and hexose, and the pathways in which they are implicated. Thus our work provides a new perspective on the effect of the VPA and cisplatin combination therapy on TNBC tumors.

Materials and methods

Reagents

Sodium valproate was purchased from Merck (KGaA, Darmstadt, Germany). VPA was freshly dissolved in double distilled water (DDW) to a stock concentration of 1 M. Cisplatin was from Pharmachemie B.V. (Haarlem, Netherlands). 3.3 mM stock cisplatin solution in DDW was stored at room temperature. All cell culturing reagents were from Biological Industries Ltd. (Beit HaEmek, Israel). All reagents, internal and calibration standards, quality controls, test mixes, UHPLC column, and a patented 96-well filter plate required for the AbsoluteIDQ®p180 analysis were included in the kit or provided by Biocrates Life Science AG (Innsbruck, Austria). The RNeasy Mini-Isolation Kit was from Qiagen (Hilden, Germany). High-Capacity cDNA Reverse Transcription Kit was from Thermo Fisher scientific (MA, United States). Xpert Fast SYBR was from Grisp (Porto, Portugal). PCR primers used were: CPT1A (forward TCCAGT TGGCTTATCGTGGTG, reverse CTAACGAGGGGTCGATCT TGG); ACSL1 (forward CTTCTGGTACGCCACGAGAC, reverse GTCGCTGTCAAGTAGTGCG); FASN (forward CTT CCGAGATTCCATCCTACGC, reverse TGGCAGTCAGGC TCACAAACG); SLC22A5 (forward GACCATATCAGTGGG CTATTT, reverse CTGCATGAAGAGAAGGACAC); SLC25A20 (forward GGGGTCACTCCCATGTTTG, reverse TGTGGTGAATACGCCAGATAAC); and TBP (forward CGG TTTGCTGCGGTAATC, reverse TCTGGACTGTTCTTCACT CTTG).

Cell lines and cell culture

MDA-MB-231 cells were kindly provided by Prof. Michael Elkin (Hadassah-Hebrew University Medical Center, Jerusalem,

Israel) and maintained in Dulbecco's modified Eagle medium (DMEM) supplemented with 10% fetal calf serum, 1% penicillin, 1% streptomycin, and 1% glutamine. Cells were maintained at 37°C in 5% CO_2. For treatment, 10^6 cells were seeded in 10 cm plates, 5 replicate plates per treatment. After 24 h, cells were treated with 10 μM cisplatin alone [the IC50 of cisplatin in MDA-MB-231 cell viability assay was 12 μM (Wawruszak et al., 2015)], with 1 mM VPA [the concentration used for inhibition of HDAC and proliferation in MDA-MB-231 cells (Granit et al., 2018)], or with their combination for 72 h.

Metabolite extraction

Cells were washed twice with cold saline (0.9% NaCl solution) and detached using a cell scraper. The samples were centrifuged at 1,200 rpm for 3 min at 4°C. The supernatant was removed and ice cold 90% methanol in H_2O was added to each cell pellet. Three cycles of 3 min sonication at 4°C, snap freeze in liquid nitrogen for 3 min, and thawing were performed. The samples were then centrifuged at 18,000 rpm for 5 min at 4°C. The supernatants were transferred to new tubes and stored at liquid nitrogen until analysis.

Targeted metabolomics

To capture a broad spectrum of metabolites, we used the AbsoluteIDQ® p180 kit (Biocrates Life Sciences AG, Innsbruck, Austria), targeting 40 AC, 42 AA/biogenic amines, 90 phospholipids, 15 sphingolipids, and hexose, following the manufacturer's instructions. Briefly, 10 μL of calibration standards, quality controls, and samples were added to the respective wells of the 96-well-based Biocrates sample preparation plate containing a mix of internal standards. After drying the samples under nitrogen, 50 μL of 5% phenyl-isothiocyanate solution were added to each well for derivatization. After incubation for 25 min and subsequent evaporation to dryness under nitrogen, 300 μL of 5 mM ammonium acetate in methanol were added for metabolite extraction, stirred for 30 min and centrifuged. The extracts were diluted with 250 μl of 40% methanol/water. The extracts were analyzed by liquid chromatography with tandem mass spectrometry (LC-MS/MS). This system comprised Nexera UHPLC system (Shimadzu, Kyoto, Japan) coupled to a Triple Quad™ 5500 mass spectrometer (Sciex, Framingham, MA, United States) in electrospray ionization (ESI) mode. AA and biogenic amines were analyzed *via* LC-MS in a positive mode. 5 μL of the sample extract were injected to Biocrates AbsoluteIDQ® p180 kit UHPLC column, 2.1 × 50 mm, protected by a VanGuard® pre-column (Waters, Milford, MA, United States) at 50°C using a 5.8 min solvent gradient employing 0.2% formic acid in water and 0.2% formic acid in acetonitrile. 20 μl of the sample extracts were used in the flow injection analysis (FIA) in the positive mode to capture AC, glycerophospholipids, sphingolipids and hexoses. All FIA injections were carried out using the Biocrates FIA Solvent. All metabolites were identified and quantified using isotopically-labeled internal standards and multiple reaction monitoring (MRM).

Analysis of mRNA expression

Total RNA was isolated from one million cells using the RNeasy Mini-Isolation Kit according to the manufacturer instructions. The cDNA was synthesized in a 20 μl reverse transcriptase reaction mix containing 1 μg of total RNA. An aliquot of 1 μl reverse-transcribed cDNA was used in each 10 μl PCR reaction, containing Xpert Fast SYBR, and reactions were run on an ABI StepOnePlus PCR system (Thermo Fisher Scientific, MA, United States).

Data processing and statistical analysis

The LC-MS raw data were quantified using the Analyst 1.6.3 software (Sciex) and exported to the Biocrates MetIDQ™ software. FIA raw data from the AbsoluteIDQ® assay were exported and quantified using the MetIDQ™ software. Quality control samples-based data normalization was performed to minimize the variation of analyses. Initial data cleaning was performed by excluding metabolites with > 20% missing values or values below the limit of detection (LOD) in all experimental groups. Thus, all metabolites with > 80% of the concentration values above the LOD in at least one of the four experimental groups were included for statistical analysis. Remaining missing values were replaced by 1/5 of the minimum positive value of each variable. Data were log-transformed to confirm normal distribution before comprehensive downstream analysis using the web-based tool MetaboAnalyst 5.0 (https://www.metaboanalyst.ca) (Pang et al., 2021). Fold changes (FCs) were calculated to evaluate differences between metabolites in treated samples compared to control samples. FCs >1.5 were considered significant. To correct for multiple comparisons and thus to minimize false positives, false discovery rates (FDRs) were calculated based on the Benjamini–Hochberg procedure (Benjamini and Hochberg, 1995). FDR-corrected p-values < 0.05 were considered statistically significant. Both unsupervised principal component analysis (PCA) and supervised partial least squares-discriminant analysis PLS-DA were performed whenever necessary to determine the metabolic signature contributing to group separation. PLS-DA decreases intergroup variability and improves separation. However, PLS-DA is prone to data overfitting. Thus, the quality of the model was assessed by cross-validation (calculation of Q2, R2, and

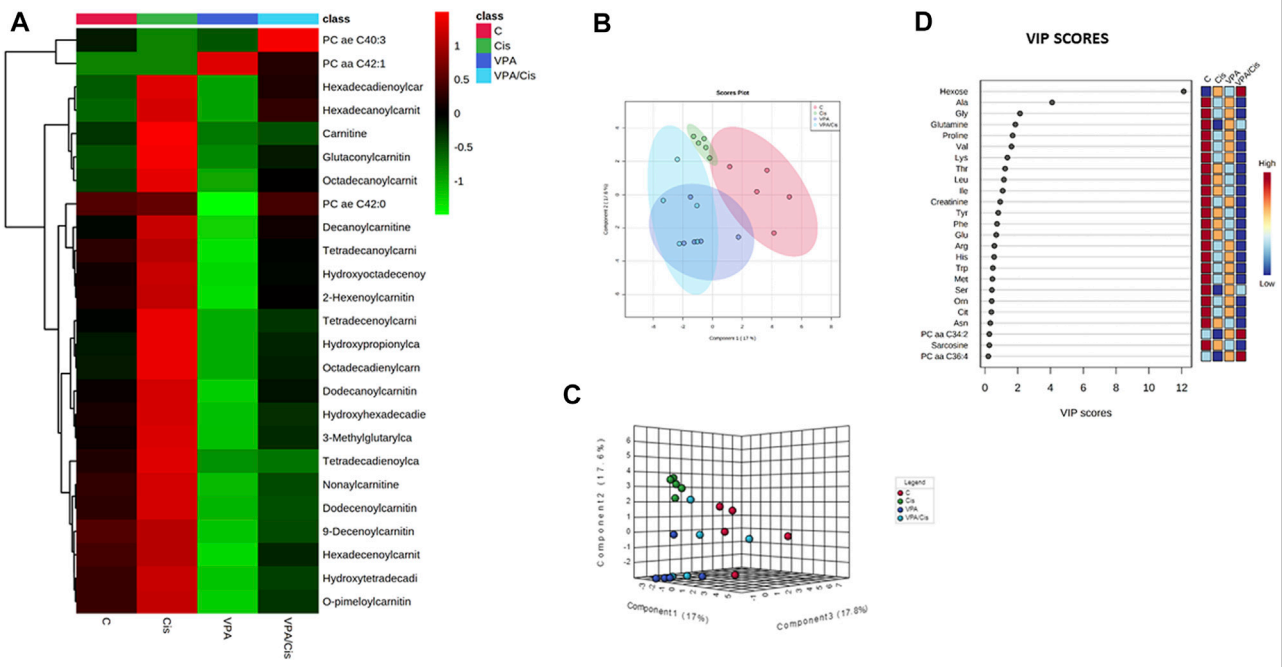

FIGURE 1
Metabolic analysis of VPA, Cisplatin, their combination and control (untreated) MDA-MB-231 cells after 72 h of treatment. **(A)** Heatmap showing the 25 metabolites most influenced by the treatments. **(B)** PLS-DA supervised score plot. **(C)** 3D supervised PLS-DA score plot. **(D)** VIP score plot. From each condition, n = 5 replicates were analyzed.

accuracy values) and the overfitting tendency of the model, or the significance of class separations, was tested using permutations. The PLS-DA Variable Importance in Projection (VIP-score) was calculated and metabolites with a VIP score >1 were considered important for group separation. Thus, for Metabolomic Pathway Analysis (MetPA) we only considered metabolites that overlapped between the two different statistical approaches (FDR-corrected p-value < 0.05 and VIP score >1 or FDR-corrected p-value < 0.05 and FC > 1.5). The Homo sapiens KEGG pathway libraries were used as references for the MetPA. Heatmaps were created using MetaboAnalyst 5.0.

For analysis of mRNA expression and metabolites subgroups concentrations, the Kruskal-Wallis test followed by Dunn's post-hoc test (Prism ver. 9; Graph Pad, La Jolla, CA, United States (were used to determine the statistical significance of the differences between experimental groups. Data are presented as mean and standard deviation. A p-value <0.05 was considered significant.

Cell viability

We determined the extent of metabolically viable cells by the overall cellular ATP levels using the CellTiter Glo kit (Promega, Madison, WI, United States) according to manufacturer instructions.

NAD^+/NADH

NAD^+/NADH ratio was determined by Promega's NAD/NADH-Glo kit according to manufacturer instructions.

Results

Hierarchical clustering, principal component and VIP analyses

The hierarchical clustering metabolomic analysis, represented by a heatmap, shows the 25 hits most significantly modified by the treatments when all experimental groups are considered (Figure 1A). Notably, 22 (88%) out of these hits are acylcarnitines (and carnitine itself) and 3 are PCs. Importantly, the most discernible effects were up-modulation of the levels of these AC by cisplatin and, contrarily, their down-modulation by VPA. When cisplatin and VPA were combined, these changes in AC levels were partially abolished. Because only three PCs were significantly modulated by the treatments, a pattern could not be easily detected for PCs. Our partial least squares-discriminant analysis (PLS-DA, Figures 1B,C) suggests that cisplatin and cisplatin-VPA treated cells were most affected by the treatment (their ellipsoid center of gravity was most distant from that of control) and that cisplatin rendered the

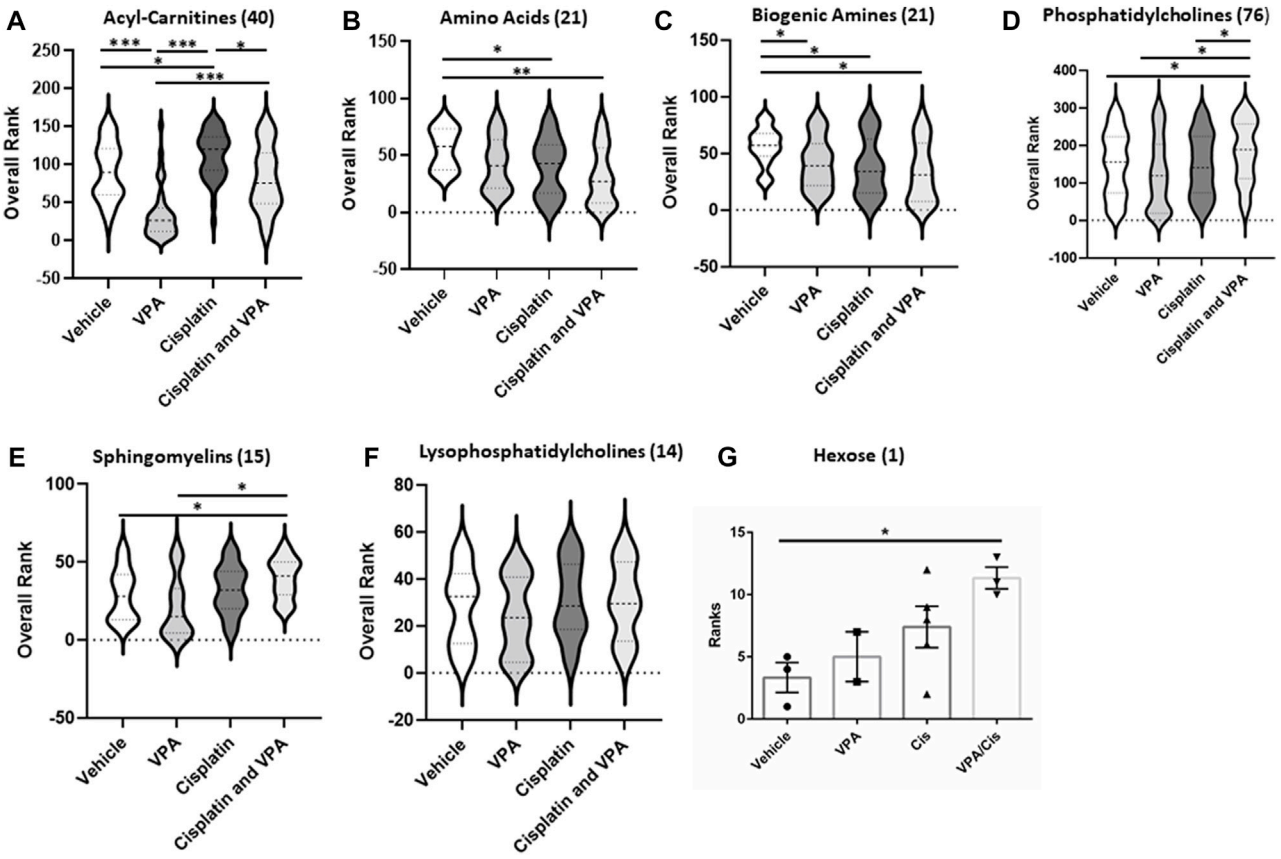

FIGURE 2
Metabolic subclass analysis of vehicle, VPA, Cisplatin and their combination treated MDA-MB-231 cells after 72 h. Profiling data of overall rank: **(A)** Acyl-Carnitines, **(B)** Amino, **(C)** Biogenic Amides **(D)** Phosphatidylcholines, **(E)** sphingomyelins, **(F)** Lysophosphatidylcholines and **(G)** Hexose; n = 5. The number in the brackets represent the number of metabolites. The middle line in the violin is the mean rank. *$p < 0.05$, **$p < 0.001$, ***$p < 0.0001$.

cells the most homogenous in terms of metabolite variety as compared to the other groups (represented by larger ellipsoids). The PLS-DA VIP score, which ranks metabolites according to their importance for intergroup separation, revealed 25 metabolites with a VIP-score >0. Hexose received VIP score of 12, followed by the AA alanine (VIP = 4), glutamine, and glycine (VIP = 2). The rest of the list included all the AA-related metabolites except aspartate and two biogenic amines [creatinine and sarcosine (Figure 1D)]. These results are in agreement with the often observed high discriminatory power of these metabolites, where even relatively small quantitative changes can have substantial implications on metabolic heterogeneity.

Metabolite subgroup profiling

To further investigate the treatment effects on the metabolome signature, we classified the targeted metabolites analyzed into six groups: AC, AA, biogenic amines, phosphatidylcholines, sphingomyelins, lysophosphatidylcholines and hexose. The concentration rank distribution of the metabolites is displayed as violin plots, where the concentration mean rank is the middle line (Figure 2). As demonstrated for the most affected AC (Figure 1A), VPA also significantly reduced the mean concentration rank of total AC, as compared to vehicle control ($p < 0.0001$), cisplatin ($p < 0.0001$), and the VPA/cisplatin combination ($p < 0.0001$) (Figure 2A, for individual AC, see Supplementary Figure S1A). Cisplatin treatment, on the other hand, increased the AC mean concentration rank as compared to control ($p < 0.05$) and VPA/cisplatin ($p < 0.05$). In the AA group, both cisplatin and VPA/cisplatin treatments reduced the mean concentration rank as compared to control ($p < 0.03$ and $p < 0.001$, respectively, Figure 2B), while VPA also reduced it but only with $p < 0.06$. For two AA, however, glutamate and aspartate, these reductions by cisplatin and VPA/cisplatin were not statistically significant (Supplementary Figure S1B). As opposed to the AC and AA,

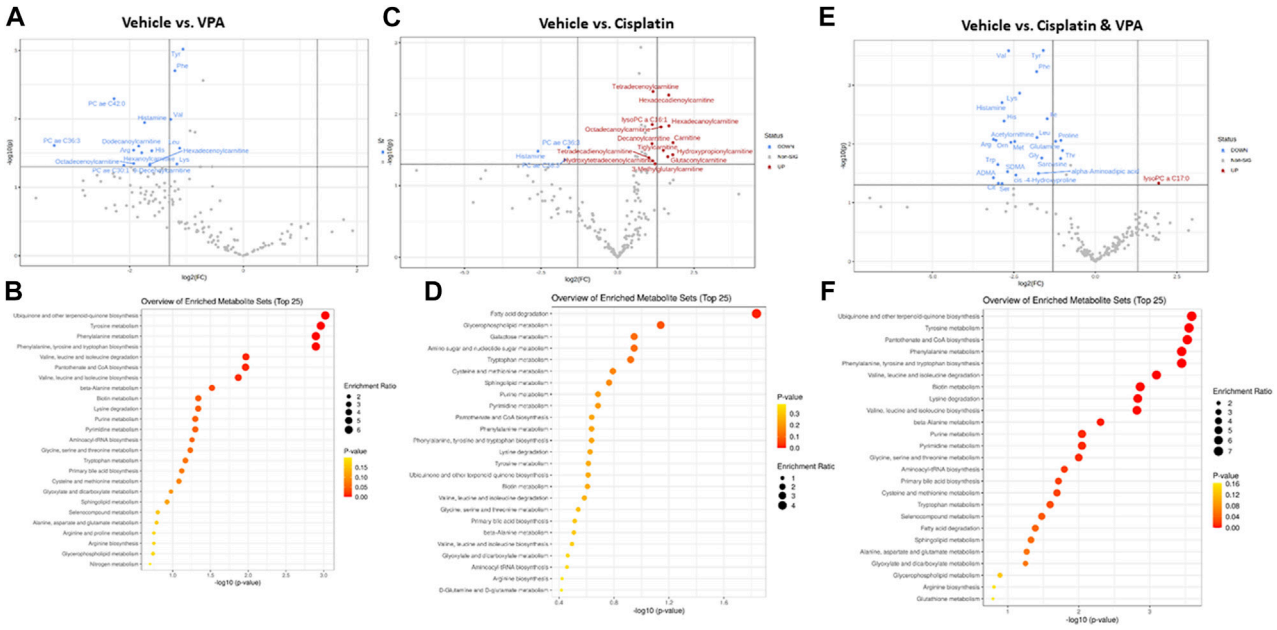

FIGURE 3
Specific metabolite alterations and metabolic set enrichment analyses (MSEA). Volcano plots with annotated metabolites that were significantly altered in MDA-MB-231 cells following 72 h treatment with **(A)** VPA, **(B)** Cisplatin, **(C)** Cisplatin & VPA, all compared to controls. The red dots represent metabolites above the threshold. The blue dots represent metabolites below the threshold. The further the metabolite's position away from the (0, 0) coordinate, the more influenced it is by the treatment. Volcano plots show the −log10 FDR-adjusted *p*-values and log2 fold-changes. Metabolites with adjusted *p*-values less than 0.05 and a fold-change greater than 2-fold or less than ½-fold are highlighted and labeled. MSEA show significant metabolic pathway enrichments caused by **(D)** VPA, **(E)** Cisplatin, **(F)** Cisplatin/VPA all compared to controls. The pathways are arranged by *p*-values from pathway enrichment annotation values (X-axis). Node color and radius are based on the *p*-value and enrichment value, respectively.

in the biogenic amines group, all treatments reduced the mean concentration rank as compared to control ($p < 0.05$). The biogenic amines not affected by the treatments were putrescine, spermidine, spermine and taurine (Supplementary Figure S1C). In the lipid groups, mixed trends were observed: While in both the PC and sphingomyelin groups, VPA/cisplatin significantly increased the mean concentration rank over control ($p < 0.05$, Figures 2D,E), no significant difference among treatments was observed in the lysophosphatidylcholines group (Figure 2F). In the hexose group (~90% D-glucose), the VPA/cisplatin combination was the only treatment which increased ($p < 0.07$) the concentration mean rank (Figure 2G), possibly suggesting glucose accumulation and inhibition of glycolysis by the combination.

Specific metabolites and major metabolic pathways modified by the different treatments are presented in volcano plots (Figures 3A,C,E), and metabolite set enrichment analysis (MSEA, Figures 3B,D,F), respectively. Volcano plots highlight the most important [(fold change>2, $p < 0.05$, false discovery rate (FDR) < 0.1] metabolites modified by the different treatments. Metabolite set enrichment analysis (MSEA), on the other hand, was used to demonstrate the effect of these treatments on metabolic pathway enrichment.

VPA (Figure 3A) reduced the abundance of several key AA (tyrosine, phenylalanine, histidine, and lysine), as well as the branched chain AA valine and leucine, all of which are critical for key intracellular biosynthesis and energy transformation pathways. The AC dodecanoylcarnitine, hexadecenoylcarnitine, octadecenoylcarnitine and decenoylcarnitine were also lowered by VPA. In addition, VPA significantly lowered the level of the PCs PC ae C36:3 (PC with acyl-alkyl residue sum C44:5), PC ae C42:0 (PC with acyl-alkyl residue sum C42:0), and PC ae C30:1 (PC with acyl-alkyl residue sum C30:1) and of histamine. The major metabolic pathways influenced by VPA involved ubiquinone biosynthesis, and tyrosine and phenylalanine metabolism and biosynthesis (Figure 3B). The main effect of cisplatin treatment, on the other hand, was the notable increase of 12 different AC (including free carnitine) suggesting inhibition of β-oxidation. Two PCs and histamine were also inhibited by cisplatin (Figure 3C). In agreement with this exclusive effect on AC, cisplatin also exclusively affected the fatty acid degradation pathway (Figure 3D). While significantly increasing a single metabolite, lysoPC C17:0, the combined VPA/cisplatin treatment mainly decreased the levels of different AA (more than VPA alone (Figure 3E, cf Figure 3A) and biogenic amines, such as asymmetric dimethylarginine ADMA. Our MSEA analysis

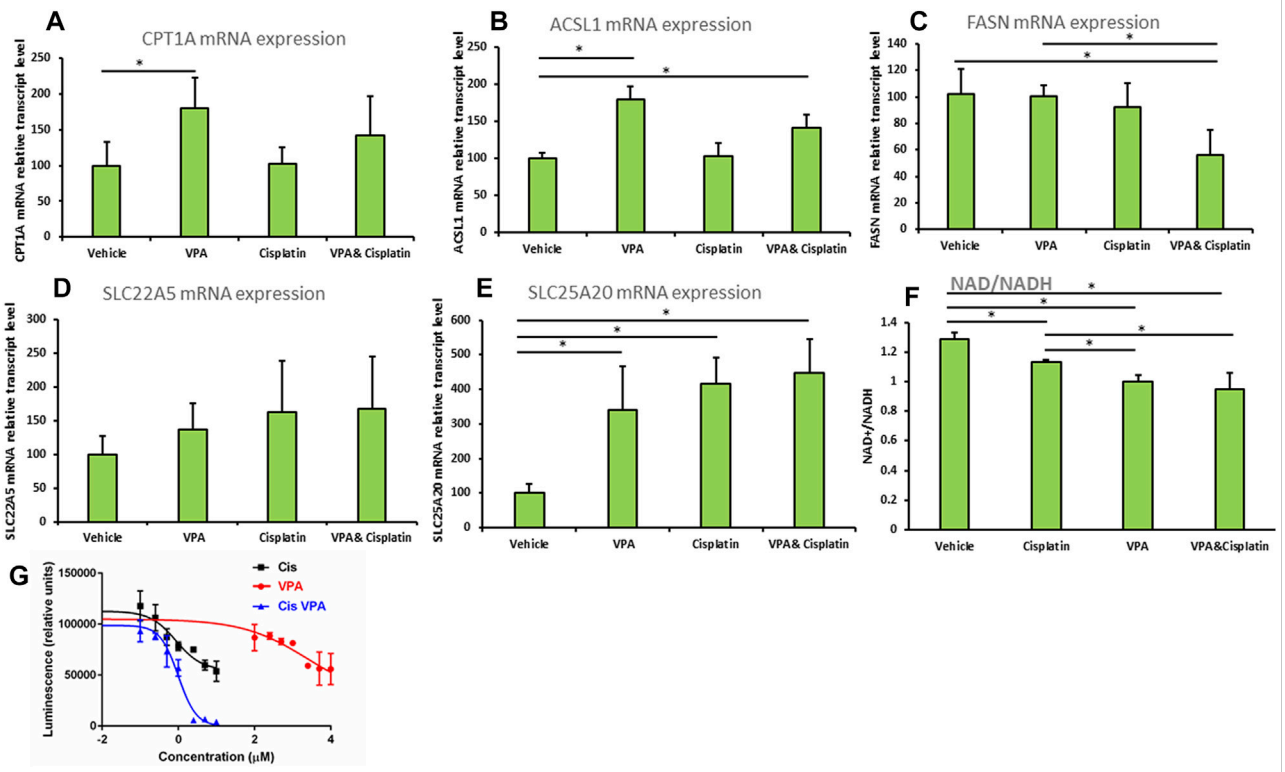

FIGURE 4
(A–E) Expression of beta oxidation genes in MDA-MB-231 cells treated with VPA, cisplatin and their combination. Cells were incubated with 1 mM VPA, 10 μM cisplatin, or their combination for 72 h mRNA expressions of **(A)** CPT1A, **(B)** ASCL1, **(C)** FASN, **(D)** SLC22A5, **(E)** SLC25A20 (by RT-PCR). Results are presented as percent of control (mean ± SD); n = 3 replicates/treatment. **(F)** NAD^+/NADH was determined in MDA-MB-231 cells treated as indicated. Results shown are means ± SD; n = 3 replicates/treatment. **(G)** ATP-based cell viability was determined in MDA-MB-231 cells treated as indicated. X-axis is presented as log of μg/mL concentration and curves were fitted by a non-linear variable slopes (four parameters) regression. We used 10(−8) μg/ml instead of the zero concentration to avoid the undefined log (0). Please note that VPA effects on cell viability are comparable to cisplatin's at molar concentrations which are 2 orders of magnitude higher (Wawruszak et al. (2015) PLoS One 10: e0143013). *, significant difference according to Dunnett's test, where each treatment was compared to vehicle **(A–E)**, or to Tukey tes, where each treatment was compared with every other treatment **(F)**.

demonstrates that, in contradistinction to cisplatin, the same main metabolic pathways, involving ubiquinone, tyrosine, and phenylalanine, were affected by both VPA and the VPA/cisplatin combination (Figure 3F), suggesting a stronger effect of VPA. Another pathway uniquely enriched by VPA/cisplatin is pantothenate and CoA biosynthesis (Figure 3F).

The effects of the treatments on fatty acid metabolism and cell viability

The mRNA expression of carnitine palmitoytransferase 1(CPT1), a rate limiting enzyme in FAO (Qu et al., 2016), was significantly increased 1.8-fold ($p < 0.01$) in cells treated with VPA, as compared to control cells (Figure 4A). The mRNA level of the Acyl-CoA synthetase long chain family member 1 (ASCL1), which esterifies long chain fatty acids into acyl-CoA, further metabolized by FAO (Li et al., 2010), was significantly elevated relative to control by both VPA and VPA/cisplatin treatments ($p < 0.01$ in both, Figure 4B). Carnitine transporters across the plasma membrane (SLC22A5, Figure 4C), or mitochondrial inner membrane (SLC25A20, Figure 4D), were respectively not affected, or equally increased by all treatments. Thus VPA (and to a lesser extent VPA/cisplatin) putatively affected FAO by up-modulation of its committed biochemical steps—acyl-CoA and subsequent acylcarnitine synthesis—and not by affecting carnitine transport. In contrast, the mRNA expression of fatty acid synthase (FASN), committed to synthesis, rather than degradation, of fatty acids was reduced by half in VPA/cisplatin treated cells as compared to control ($p < 0.01$) or VPA treated cells ($p < 0.01$) (Figure 4E).

We predicted that by reducing the FAO precursor carnitine, supplementation of VPA to cisplatin would reduce both FAO and cell viability. We thus indirectly estimated the extent of FAO by the NAD^+/NADH ratio (Akie et al., 2015), which correlates

with OxPhos that is significantly driven by FAO in MDA-MB-231 and most other cell lines. Indeed we show that the order of NAD^+/NADH-estimated FAO rate is vehicle > cisplatin > VPA > VPA/cisplatin (Figure 4F) and, importantly, that supplementation of VPA to cisplatin significantly decreases FAO. Correspondingly, our ATP-based dose-response cell viability curves show that supplementation of VPA to cisplatin-treated MDA-MB-231 significantly reduces their viability (Figure 4G). Please note that the Area Under the Curve, or bottom of the VPA/cisplatin curve, is significantly lowered as compared to cisplatin alone [from 54777 to −627 (arbitrary units) according to the non-linear regression] and so the insignificant change in IC50 (from 0.262 μg/ml in cisplatin to 0.300 in μg/mL in VPA/cisplatin) cannot be used to estimate the change in viability.

Discussion

Cisplatin is one of the most efficient anticancer drugs currently used for treating many types of cancer, including TNBC (Tchounwou et al., 2021). However, tumor cells may acquire resistance to cisplatin. One suggested mechanism of resistance is the ability to reprogram the cellular metabolism (Wang et al., 2021), as demonstrated, for instance, by cisplatin resistant gastric cancer cells, which manifested higher rate of glycolysis (Qian et al., 2017). In addition, metabolic reprogramming often involves epigenetic modulation (Sun et al., 2021a). For example, acetyl-CoA is a central metabolite and functions as a carbon source for histone acetylation (Cai et al., 2011). The aim of this work was to compare the metabolomic landscapes of cisplatin, HDACi (VPA) and the HDACi/cisplatin combination in order to gain insight into how metabolic reprogramming by these treatments can modulate therapy resistance and possibly improve it.

Our metabolomic analysis demonstrated that the most distinct metabolic shift caused by the treatments was in AC (Figure 1A and Figure 2A). VPA reduced and cisplatin increased AC levels. On the other hand, the VPA/cisplatin combination reinstated AC to control levels, apparently suggesting that the VPA/cisplatin combination might contribute to therapy resistance by mitigating cisplatin's anti-cancer effect caused by AC accumulation and inhibition of FAO. However, increasing cisplatin tumor resistance by VPA would require stimulation, rather than inhibition, of FAO. The alleged enhancement of cisplatin's anticancer effect by VPA (or VPA/cisplatin) can thus be ascribed to their reduction of free carnitine as a FAO precursor (Supplementary Figure S1A). Free carnitine reduction is expected to inhibit, rather than stimulate, FAO and thus VPA is expected to enhance, rather than limit, the anti-cancer effect of cisplatin:

Carnitine is a small, polar molecule *de novo* synthesized from two AA, lysine and methionine. Carnitine facilitates fatty acids transport into the mitochondria to generate FAO substrates for mitochondrial FAO (Reuter and Evans, 2012). Cisplatin inhibits mitochondrial FAO (Li et al., 2020) by inducing oxidative stress, DNA damage and mitochondrial dysfunction (Marullo et al., 2013). In kidney cells, it was discovered that cisplatin can inhibit the plasma membrane carnitine transporter organic cation/carnitine transporter 2 (SLC22A5) (Lancaster et al., 2010), in agreement with the increase in plasma carnitine levels observed in cancer patients upon cisplatin treatment (Heuberger et al., 1998). However, in our hands in TNBC cells, cisplatin increased, rather than decreased, intracellular free carnitine levels (Figure 1A and Figure 3C) with no significant (Figure 4C) or specific (Figure 4D) effects on carnitine transporters. On the other hand, similar to other FAO inhibitors, cisplatin treatment led to AC accumulation. This phenotype of increased free carnitine and AC is atypical of FAO blockade characterized by relatively low free carnitine and increased AC (Semba et al., 2017). Thus we surmise that cisplatin had an intermediate inhibitory effect on FAO. VPA, on the other hand, reduced both free carnitine and AC (Figure 1A and Supplementary Figure S1A), purportedly causing a more pronounced FAO inhibition than cisplatin, which necessitated compensatory up-modulation of the FAO enzymes CPT1 and ASCL1 (Figure 4). The reductions in AC and subsequent FAO are probably attributed to the free carnitine substrate reduction and agree with the documented VPA-mediated FAO inhibition: VPA is a short-chain fatty acid, which requires carnitine for its mitochondrial β-oxidation. VPA combines with carnitine in the mitochondrial inner membrane *via* carnitine acyltransferases (CPT1), acting as the carnitine sink valproylcarnitine, which is eliminated in the urine (Lheureux and Hantson, 2009). However, valproylcarnitine makes only a minor contribution to carnitine sequestration by VPA (Lheureux and Hantson, 2009). VPA also inhibits carnitine biosynthesis by lowering the levels of α-ketoglutarate, a cofactor of the carnitine biosynthesizing enzyme butyrobetaine hydroxylase (Farkas et al., 1996), by restricting restoration of carnitine from AC *via* CPT2 (Lheureux and Hantson, 2009), and by inhibiting SLC22A5-mediated uptake of serum carnitine (Sun et al., 2021b). Limiting the levels of carnitine as an AC substrate resulted in FAO mitochondrial dysfunction (Lheureux and Hantson, 2009; Choi et al., 2015).

It is well established that FAO is the major source for electrons in mitochondrial electron transport chain (ETC) in cancer cells and that fatty acids, rather than glycolysis, are a major source of electrons for ATP production (Lee et al., 2020). The lack of ATP as a substrate for AA synthesis, for instance in the urea cycle, might reduce the levels of AA and biogenic amines in the VPA or cisplatin treatments, and especially in the VPA/cisplatin treatment (Figures 2B,C).

In summary, our main argument is that VPA counters cisplatin tolerance by further inhibiting FAO (Figure 4F), so that when supplemented to cisplatin it can enhance its cancer cell killing capacity (Figure 4G). While cisplatin causes AC

accumulation, suggesting lack of degradation of the AC-generated acyl-CoA, it also decreases the levels of carnitine as the ultimate FAO precursor and so its FAO inhibition is limited. VPA, on the other hand, decreases carnitine and also, probably as a consequence, AC, thus further inhibiting FAO and cell viability.

While total biogenic amines were down-modulated by all treatments by a still unknown mechanism (Figure 2C), the biogenic amines putrescine, spermidine, spermine and taurine were not modified by any treatment (Supplementary Figure S1C). Putrescine, spermidine and spermine are cationic molecules that are sequentially synthesized from ornithine and are essential for eukaryotic cell growth and differentiation (Agostinelli et al., 2010). As opposed to our observations, cisplatin has been elsewhere reported to reduce putrescine levels, without changing the level of spermidine and spermine, through modulation of ornithine decarboxylase (ODC) (Geck et al., 2020). These differences might be attributed to the different TNBC cell lines, cisplatin concentration and exposure time used. For VPA, however, it is still not known how it affects putrescine, spermidine and spermine and it is also not known how cisplatin and VPA affect taurine.

Finally, an increase in hexose levels was observed only following treatment with the VPA/cisplatin combination (Figure 2G). This result is also in support of a possible relief of cisplatin resistance brought about by combining cisplatin with VPA. The hexose (90% D-glucose) accumulation caused by the combination suggests inhibition of glycolysis, which could be cytotoxic to TNBC cells.

We also tested the effects of the different treatments on metabolic pathways enrichment. The VPA (Figure 3B) and VPA/cisplatin (Figure 3F) treatments are associated with ubiquinone, tyrosine, and phenylalanine metabolism (Figure 3B). Ubiquinone is an electron-shuttle in the mitochondrial respiratory chain (Lester and Crane, 1959). Ubiquinone's head group is derived from the essential AA phenylalanine, which is converted into tyrosine (Olson et al., 1963). VPA could interfere with the respiratory chain by inhibiting cytochrome c oxidase (COX), an ETC rate limiting enzyme (Salsaa et al., 2020), FAO, as shown above [Figure 4F and (Silva et al., 2008)], or the TCA cycle (El Hage et al., 2012), thus affecting ubiquinone and its chemical equilibrium. The cellular pathway most affected by cisplatin is the fatty acid degradation pathway (Figure 3D), or FAO as explained above (Figure 4F).

In our study, only VPA increased the mRNA expression of CPT1 and ACSL1 (Figures 4A,B). This finding is in contrast with the observed inhibition of CPT1A by VPA in hepatocytes (Aires et al., 2010) and might subserve a compensatory up-modulation of FAO, which was inhibited by VPA more than cisplatin (Figure 4F). *De novo* synthesis of fatty acids relies on a key rate limiting enzyme, fatty acid synthase (FASN) (Kuhajda, 2006). Many cancer cells depended on FASN for proliferation and survival, which, in turn, are dependent on the synthesis of biological membranes (Currie et al., 2013). According to our results, the VPA/cisplatin combination decreased the mRNA expression of FASN (Figure 4E). The apparent discrepancy between the VPA/cisplatin-mediated increase in PC levels and decrease in FASN mRNA expression suggests negative feedback compensation between the two.

Lastly, our study has some limitations. Firstly, while MDA-MB-231 is commonly accepted as a representative TNBC cell line, it is still only 1 cell line. As this is a proof-of-concept short study, we opted to first determine whether at all cisplatin and VPA can significantly modify the metabolomic landscape before embarking on more comprehensive studies including several cell lines, chemotherapies and HDACi's. Secondly, we used targeted metabolomics with defined metabolites. Some metabolites were not analyzed in this method, thus additional, possibly untargeted, metabolomic analysis should be performed to obtain a wider view of the metabolomic changes. Thirdly, to confirm our results, it would be interesting to investigate the metabolome in primary cells derived from breast cancer patients receiving cisplatin, VPA or VPA/cisplatin in clinical settings.

In summary, our results, schematically summarized in Supplementary Figure S2, showed that treatment with VPA, cisplatin, or both alters the metabolome of MBA-MB-231 TNBC cells. Especially AC, which are enhanced by cisplatin, were influenced, but also AA, lipids and biogenic amines. Separately, cisplatin and VPA might lead to mitochondrial ETC and FAO dysfunction. However, the VPA/cisplatin combination also presents additional effects, such as further FAO inhibition, and further reductions in AA or biogenic amines levels, by which it could modify cisplatin monotherapy (VPA is often not used as a monotherapy for TNBC) and enhance its anticancer effect. The exact underlying mechanism of these modifications remains to be further explored. Therefore, novel treatments targeting the reprogramed metabolism might diminish the resistance of current therapies and increase the overall survival of TNBC patients.

Data availability statement

The raw data supporting the conclusion of this article will be made available by the authors, without undue reservation.

Author contributions

AG, SE, and TP-Y conceived and designed the experiments. AG, KM, and DB preformed the experiments. AG and OK wrote the paper. SE, OK, and TP-Y reviewed/

edited the manuscript. All authors read and approved the final version of the manuscript.

Funding

This study was supported by the Israel cancer association (Grant No. 301103091).

Conflict of interest

The authors declare that the research was conducted in the absence of any commercial or financial relationships that could be construed as a potential conflict of interest.

Publisher's note

All claims expressed in this article are solely those of the authors and do not necessarily represent those of their affiliated organizations, or those of the publisher, the editors and the reviewers. Any product that may be evaluated in this article, or claim that may be made by its manufacturer, is not guaranteed or endorsed by the publisher.

Supplementary material

The Supplementary Material for this article can be found online at: https://www.frontiersin.org/articles/10.3389/fcell.2022.1014798/full#supplementary-material

References

Agostinelli, E., Marques, M. P., Calheiros, R., Gil, F. P., Tempera, G., Viceconte, N., et al. (2010). Polyamines: Fundamental characters in chemistry and biology. *Amino Acids* 38 (2), 393–403. doi:10.1007/s00726-009-0396-7

Aires, C. C., Ijlst, L., Stet, F., Prip-Buus, C., de Almeida, I. T., Duran, M., et al. (2010). Inhibition of hepatic carnitine palmitoyl-transferase I (CPT IA) by valproyl-CoA as a possible mechanism of valproate-induced steatosis. *Biochem. Pharmacol.* 79 (5), 792–799. doi:10.1016/j.bcp.2009.10.011

Akie, T. E., Liu, L., Nam, M., Lei, S., and Cooper, M. P. (2015). OXPHOS-mediated induction of NAD+ promotes complete oxidation of fatty acids and interdicts non-alcoholic fatty liver disease. *PLoS One* 10 (5), e0125617. doi:10.1371/journal.pone.0125617

Benjamini, Y., and Hochberg, Y. (1995). Controlling the false discovery rate: A practical and powerful approach to multiple testing. *J. R. Stat. Soc. Ser. B Methodol.* 57 (1), 289–300. doi:10.1111/j.2517-6161.1995.tb02031.x

Brancolini, C., Gagliano, T., and Minisini, M. (2022). HDACs and the epigenetic plasticity of cancer cells: Target the complexity. *Pharmacol. Ther.* 238, 108190. doi:10.1016/j.pharmthera.2022.108190

Cai, L., Sutter, B. M., Li, B., and Tu, B. P. (2011). Acetyl-CoA induces cell growth and proliferation by promoting the acetylation of histones at growth genes. *Mol. Cell* 42 (4), 426–437. doi:10.1016/j.molcel.2011.05.004

Choi, Y. M., Kim, H. K., Shim, W., Anwar, M. A., Kwon, J. W., Kwon, H. K., et al. (2015). Mechanism of cisplatin-induced cytotoxicity is correlated to impaired metabolism due to mitochondrial ROS generation. *PLoS One* 10 (8), e0135083. doi:10.1371/journal.pone.0135083

Currie, E., Schulze, A., Zechner, R., Walther, T. C., and Farese, R. V., Jr. (2013). Cellular fatty acid metabolism and cancer. *Cell Metab.* 18 (2), 153–161. doi:10.1016/j.cmet.2013.05.017

El Hage, M., Baverel, G., and Martin, G. (2012). Effects of valproate on glutamate metabolism in rat brain slices: A (13)C NMR study. *Epilepsy Res.* 99 (1-2), 94–100. doi:10.1016/j.eplepsyres.2011.10.028

Farkas, V., Bock, I., Cseko, J., and Sandor, A. (1996). Inhibition of carnitine biosynthesis by valproic acid in rats--the biochemical mechanism of inhibition. *Biochem. Pharmacol.* 52 (9), 1429–1433. doi:10.1016/s0006-2952(96)00507-2

Geck, R. C., Foley, J. R., Murray Stewart, T., Asara, J. M., Casero, R. A., Jr., and Toker, A. (2020). Inhibition of the polyamine synthesis enzyme ornithine decarboxylase sensitizes triple-negative breast cancer cells to cytotoxic chemotherapy. *J. Biol. Chem.* 295 (19), 6263–6277. doi:10.1074/jbc.RA119.012376

Granit, A., Tetro, N., Shmuel, M., Peretz, T., and Eyal, S. (2018). Lacosamide at therapeutic concentrations induces histone hyperacetylation *in vitro*. *Epilepsia Open* 3 (4), 535–539. doi:10.1002/epi4.12269

Heuberger, W., Berardi, S., Jacky, E., Pey, P., and Krahenbuhl, S. (1998). Increased urinary excretion of carnitine in patients treated with cisplatin. *Eur. J. Clin. Pharmacol.* 54 (7), 503–508. doi:10.1007/s002280050504

Kuhajda, F. P. (2006). Fatty acid synthase and cancer: New application of an old pathway. *Cancer Res.* 66 (12), 5977–5980. doi:10.1158/0008-5472.CAN-05-4673

Lancaster, C. S., Hu, C., Franke, R. M., Filipski, K. K., Orwick, S. J., Chen, Z., et al. (2010). Cisplatin-induced downregulation of OCTN2 affects carnitine wasting. *Clin. Cancer Res.* 16 (19), 4789–4799. doi:10.1158/1078-0432.CCR-10-1239

Lee, J. S., Oh, S. J., Choi, H. J., Kang, J. H., Lee, S. H., Ha, J. S., et al. (2020). ATP production relies on fatty acid oxidation rather than glycolysis in pancreatic ductal adenocarcinoma. *Cancers* 12 (9), E2477. doi:10.3390/cancers12092477

Lester, R. L., and Crane, F. L. (1959). The natural occurrence of coenzyme Q and related compounds. *J. Biol. Chem.* 234 (8), 2169–2175. doi:10.1016/s0021-9258(18)69886-2

Lheureux, P. E., and Hantson, P. (2009). Carnitine in the treatment of valproic acid-induced toxicity. *Clin. Toxicol.* 47 (2), 101–111. doi:10.1080/15563650902752376

Li, L. O., Klett, E. L., and Coleman, R. A. (2010). Acyl-CoA synthesis, lipid metabolism and lipotoxicity. *Biochim. Biophys. Acta* 1801 (3), 246–251. doi:10.1016/j.bbalip.2009.09.024

Li, M., Li, C. M., Ye, Z. C., Huang, J., Li, Y., Lai, W., et al. (2020). Sirt3 modulates fatty acid oxidation and attenuates cisplatin-induced AKI in mice. *J. Cell. Mol. Med.* 24 (9), 5109–5121. doi:10.1111/jcmm.15148

Liesenfeld, D. B., Habermann, N., Owen, R. W., Scalbert, A., and Ulrich, C. M. (2013). Review of mass spectrometry-based metabolomics in cancer research. *Cancer Epidemiol. Biomarkers Prev.* 22 (12), 2182–2201. doi:10.1158/1055-9965.EPI-13-0584

Marullo, R., Werner, E., Degtyareva, N., Moore, B., Altavilla, G., Ramalingam, S. S., et al. (2013). Cisplatin induces a mitochondrial-ROS response that contributes to cytotoxicity depending on mitochondrial redox status and bioenergetic functions. *PLoS One* 8 (11), e81162. doi:10.1371/journal.pone.0081162

Mattson, R. H., Cramer, J. A., Williamson, P. D., and Novelly, R. A. (1978). Valproic acid in epilepsy: Clinical and pharmacological effects. *Ann. Neurol.* 3 (1), 20–25. doi:10.1002/ana.410030105

Olson, R. E., Bentley, R., Aiyar, A. S., Dialameh, G. H., Gold, P. H., Ramsey, V. G., et al. (1963). Benzoate derivatives as intermediates in the biosynthesis of coenzyme Q in the rat. *J. Biol. Chem.* 238, 3146–3148. doi:10.1016/s0021-9258(18)51887-1

Pang, Z., Chong, J., Zhou, G., de Lima Morais, D. A., Chang, L., Barrette, M., et al. (2021). MetaboAnalyst 5.0: Narrowing the gap between raw spectra and functional insights. *Nucleic Acids Res.* 49 (W1), W388–W396. doi:10.1093/nar/gkab382

Prestayko, A. W., D'Aoust, J. C., Issell, B. F., and Crooke, S. T. (1979). Cisplatin (cis-diamminedichloroplatinum II). *Cancer Treat. Rev.* 6 (1), 17–39. doi:10.1016/s0305-7372(79)80057-2

Qian, X., Xu, W., Xu, J., Shi, Q., Li, J., Weng, Y., et al. (2017). Enolase 1 stimulates glycolysis to promote chemoresistance in gastric cancer. *Oncotarget* 8 (29), 47691–47708. doi:10.18632/oncotarget.17868

Qu, Q., Zeng, F., Liu, X., Wang, Q. J., and Deng, F. (2016). Fatty acid oxidation and carnitine palmitoyltransferase I: Emerging therapeutic targets in cancer. *Cell Death Dis.* 7, e2226. doi:10.1038/cddis.2016.132

Resendiz-Acevedo, K., Garcia-Aguilera, M. E., Esturau-Escofet, N., and Ruiz-Azuara, L. (2021). (1)H -nmr metabolomics study of the effect of cisplatin and

casiopeina IIgly on MDA-MB-231 breast tumor cells. *Front. Mol. Biosci.* 8, 742859. doi:10.3389/fmolb.2021.742859

Reuter, S. E., and Evans, A. M. (2012). Carnitine and acylcarnitines: Pharmacokinetic, pharmacological and clinical aspects. *Clin. Pharmacokinet.* 51 (9), 553–572. doi:10.1007/BF03261931

Salsaa, M., Pereira, B., Liu, J., Yu, W., Jadhav, S., Huttemann, M., et al. (2020). Valproate inhibits mitochondrial bioenergetics and increases glycolysis in *Saccharomyces cerevisiae*. *Sci. Rep.* 10 (1), 11785. doi:10.1038/s41598-020-68725-5

Semba, R. D., Trehan, I., Li, X., Moaddel, R., Ordiz, M. I., Maleta, K. M., et al. (2017). Environmental enteric dysfunction is associated with carnitine deficiency and altered fatty acid oxidation. *EBioMedicine* 17, 57–66. doi:10.1016/j.ebiom.2017.01.026

Siegel, R. L., Miller, K. D., Fuchs, H. E., and Jemal, A. (2021). Cancer statistics, 2017. *Ca. Cancer J. Clin.* 71 (1), 7–30. doi:10.3322/caac.21387

Silva, M. F., Aires, C. C., Luis, P. B., Ruiter, J. P., Ijlst, L., Duran, M., et al. (2008). Valproic acid metabolism and its effects on mitochondrial fatty acid oxidation: A review. *J. Inherit. Metab. Dis.* 31 (2), 205–216. doi:10.1007/s10545-008-0841-x

Sun, D., Chen, Q., Gai, Z., Zhang, F., Yang, X., Hu, W., et al. (2021). The role of the carnitine/organic cation transporter novel 2 in the clinical outcome of patients with locally advanced esophageal carcinoma treated with oxaliplatin. *Front. Pharmacol.* 12, 684545. doi:10.3389/fphar.2021.684545

Sun, L., Zhang, H., and Gao, P. (2021). Metabolic reprogramming and epigenetic modifications on the path to cancer. *Protein Cell* 13, 877–919. doi:10.1007/s13238-021-00846-7

Tchounwou, P. B., Dasari, S., Noubissi, F. K., Ray, P., and Kumar, S. (2021). Advances in our understanding of the molecular mechanisms of action of cisplatin in cancer therapy. *J. Exp. Pharmacol.* 13, 303–328. doi:10.2147/JEP.S267383

Wang, L., Zhao, X., Fu, J., Xu, W., and Yuan, J. (2021). The role of tumour metabolism in cisplatin resistance. *Front. Mol. Biosci.* 8, 691795. doi:10.3389/fmolb.2021.691795

Wawruszak, A., Halasa, M., Okon, E., Kukula-Koch, W., and Stepulak, A. (2021). Valproic acid and breast cancer: State of the art in 2021. *Cancers (Basel)* 13 (14), 3409. doi:10.3390/cancers13143409

Wawruszak, A., Luszczki, J. J., Grabarska, A., Gumbarewicz, E., Dmoszynska-Graniczka, M., Polberg, K., et al. (2015). Assessment of interactions between cisplatin and two histone deacetylase inhibitors in MCF7, T47D and MDA-MB-231 human breast cancer cell lines - an isobolographic analysis. *PLoS One* 10 (11), e0143013. doi:10.1371/journal.pone.0143013

Yin, L., Duan, J. J., Bian, X. W., and Yu, S. C. (2020). Triple-negative breast cancer molecular subtyping and treatment progress. *Breast Cancer Res.* 22 (1), 61. doi:10.1186/s13058-020-01296-5

Zhou, X., Li, Z., Wang, X., Jiang, G., Shan, C., and Liu, S. (2020). Metabolomics reveals the effect of valproic acid on MCF-7 and MDA-MB-231 cells. *Xenobiotica.* 50 (3), 252–260. doi:10.1080/00498254.2019.1618510

frontiers | Frontiers in Cell and Developmental Biology

TYPE Original Research
PUBLISHED 18 January 2023
DOI 10.3389/fcell.2023.1013721

OPEN ACCESS

EDITED BY
Ann Saada,
Hebrew University of Jerusalem, Israel

REVIEWED BY
Miguel Sánchez-Álvarez,
Spanish National Centre for Cardiovascular Research, Spain
Pablo Vicente Escriba,
University of the Balearic Islands, Spain

*CORRESPONDENCE
Miguel Weil,
miguelw@tauex.tau.ac.il
Haguy Wolfenson,
haguyw@technion.ac.il

SPECIALTY SECTION
This article was submitted to Cellular Biochemistry, a section of the journal Frontiers in Cell and Developmental Biology

RECEIVED 07 August 2022
ACCEPTED 03 January 2023
PUBLISHED 18 January 2023

CITATION
Gharaba S, Paz O, Feld L, Abashidze A, Weinrab M, Muchtar N, Baransi A, Shalem A, Sprecher U, Wolf L, Wolfenson H and Weil M (2023), Perturbed actin cap as a new personalized biomarker in primary fibroblasts of Huntington's disease patients.
Front. Cell Dev. Biol. 11:1013721.
doi: 10.3389/fcell.2023.1013721

Perturbed actin cap as a new personalized biomarker in primary fibroblasts of Huntington's disease patients

Saja Gharaba[1], Omri Paz[1], Lea Feld[2], Anastasia Abashidze[3], Maydan Weinrab[1], Noam Muchtar[1], Adam Baransi[1], Aviv Shalem[1,4,5], Uri Sprecher[1], Lior Wolf[4], Haguy Wolfenson[2]* and Miguel Weil[1]*

[1]Laboratory for Personalized Medicine and Neurodegenerative Diseases, The Shmunis School of Biomedicine and Cancer Research, The George S. Wise Faculty for Life Sciences, Sagol School of Neurosciences, Tel Aviv University, Tel Aviv, Israel, [2]Department of Genetics and Developmental Biology, The Rappaport Faculty of Medicine and Research Institute, Technion—Israel Institute of Technology, Haifa, Israel, [3]The Blavatnik Center for Drug Discovery, Tel Aviv University, Tel Aviv, Israel, [4]The Blavatnik School of Computer Sciences, Tel Aviv University, Tel Aviv, Israel, [5]School of Electrical Engineering, Faculty of Engineering, Tel Aviv University, Tel Aviv, Israel

Primary fibroblasts from patient's skin biopsies are directly isolated without any alteration in the genome, retaining in culture conditions their endogenous cellular characteristics and biochemical properties. The aim of this study was to identify a distinctive cell phenotype for potential drug evaluation in fibroblasts from Huntington's Disease (HD) patients, using image-based high content analysis. We show that HD fibroblasts have a distinctive nuclear morphology associated with a nuclear actin cap deficiency. This in turn affects cell motility in a similar manner to fibroblasts from Hutchinson-Gilford progeria syndrome (HGPS) patients used as known actin cap deficient cells. Moreover, treatment of the HD cells with either Latrunculin B, used to disrupt actin cap formation, or the antioxidant agent Mitoquinone, used to improve mitochondrial activity, show expected opposite effects on actin cap associated morphological features and cell motility. Deep data analysis allows strong cluster classification within HD cells according to patients' disease severity score which is distinct from HGPS and matching controls supporting that actin cap is a biomarker in HD patients' cells correlated with HD severity status that could be modulated by pharmacological agents as tool for personalized drug evaluation.

KEYWORDS

huntington's disease, actin cap, nuclear morphology, primary skin fibroblast, personalized drug screening, image-based high content analysis, disease marker

Introduction

Huntington's disease (HD) is a fatal rare inherited disorder with a broad impact on a person's functional abilities characterized by unwanted choreatic movements, behavioral and psychiatric disturbances, and dementia (Kirkwood et al., 2001; Walker, 2007). HD is an autosomal dominant disease caused by elongated CAG repeats on the short arm of chromosome 4p16.3 in the huntingtin gene (HTT). Normally, the CAG segment is repeated 10–35 times within the gene, but in people with HD, the CAG segment is repeated 36 to more than 120 times, causing a mutated translated protein with long Poly glutamine (Poly-Q) repeats called mutant Huntingtin protein (mHtt). The Huntingtin

protein is expressed in all human and mammalian cells (Strong et al., 1993; Dé Ric Saudou and Humbert, 2016). The role of the Htt protein in humans is unclear. It interacts with over 100 other proteins that are involved in a number of biological functions like transcription, cell signaling, and intracellular transport (Harjes and Wanker, 2003). Although the mutated protein function is poorly understood, it is toxic to certain cell types due to Poly-Q mediated protein aggregation, particularly in the brain (Moily et al., 2017). Notably, it has become clear from different studies that HD is not only a brain disorder, but a multisystem disease that affects numerous cell types (Sathasivam et al., 1999; Mielcarek, 2015). It is therefore appealing to use easily accessible cells from patients for phenotype characterization and *in vitro* studies.

Human primary skin fibroblast cells from patient's skin biopsies were used previously as a model to study different neurodegenerative diseases (Connolly, 1998; Huang et al., 2006), including HD (Marchina et al., 2014; Gardiner et al., 2018). These cells are directly isolated from the patient's tissue without any alteration in the genome (Alge et al., 2006), retaining in culture conditions their endogenous cellular characteristics and biochemical properties, as well as their cellular proliferation capacity for several passages. This allows performing multiple experiments in a reproducible manner from a single patient's sample and identify distinctive cellular phenotypes and potential disease biomarkers also expressed in more disease-relevant tissues *in vivo*, as previously described for Amyotrophic Lateral Sclerosis patients' bone marrow mesenchymal stem cells (Wald-Altman et al., 2017). Here we adopted image-based high content analysis (HCA) cell phenotyping (Solmesky and Weil, 2014) as an unbiased approach for screening of robust and distinctive subcellular morphological features in primary skin fibroblasts of HD patients. We found altered nuclear morphology as a significant phenotypic feature of HD cells. Detailed confocal and deep morphometric image analyses of the nuclei, combined with cell migration assays, revealed that this abnormal morphology is due to a nuclear actin cap deficiency in HD patients' fibroblasts. The nuclear actin cap is an organized apical dome that covers the nucleus and is composed of thick, parallel, and highly contractile actin and myosin filament bundles (Khatau et al., 2009). Actin cap formation is functionally related to cell migration, intranuclear shaping, chromosomal organization (Kim et al., 2014), and cellular mechanoregulation (Kim et al., 2013). The actin cap is present in a wide range of adherent eukaryotic cells, but it is disrupted in several human diseases such as cancer (Zink et al., 2004) and muscular dystrophy (Booth-Gauthier et al., 2013). It is a distinctive biomarker in Hutchinson–Gilford syndrome (HGPS), the accelerated nuclear laminopathy aging syndrome also known as progeria, caused by a dominant mutation in LMNA gene affecting Lamin A/C levels (Khatau et al., 2009; Kim et al., 2017). Our results demonstrate that actin cap deficiency is a robust biomarker in HD primary skin fibroblast cells that could be used as a powerful functional measure in drug screening assays as well as for future personalized drug test validations for treatment of HD patients.

Materials and methods

Most of the reagents used in this study (otherwise stated) were purchased from Thermo Fischer Scientific, United States of America.

Primary skin fibroblasts samples and cell culture handling

Primary skin fibroblasts (see Table 1, Table 2) used in this study were obtained from different cell and tissue repositories as mentioned by the ethical declaration of this manuscript. The cells from 28 HD patients and 19 matched healthy controls (age 23–68), and from 6 HGPS and 4 young healthy controls (age 1–11) were grown in culture media DMEM supplemented with 1% MEM Sodium Pyruvate, 1% PSA (Biological industries, Israel), 10% heat inactivated FBS, and 1% NEAA in polystyrene plastic 75-cm2 culture flasks (Corning, NY) at 37°C with 5% CO2. Cell passages and expansion of human skin fibroblasts were performed when cells were at 80%–100% confluency. Cells passaging and re-plating was accomplished using .25% Trypsin-EDTA (Biological industries, Israel) for 2 min, followed by addition of twice the volume of a complete culture media to neutralize the enzyme. Cells were subsequently centrifuged at 1200 rpm for 5 min before their pellets being resuspended in 1 ml medium for cell counting using TC10 automated cell counter (BioRad United State) before re-plating. All experiments were performed between passages 7–15.

Image based cell HCA live phenotyping experiments

For live image microscopy experiments, 1500 cells in 100 µL of complete medium per well were automatically plated in 96-well plates (Grenier, Austria) using Tecan Freedom EVO 200 robot equipped with a 96 MultiChannel Arm (MCA). The plates accommodated serially and in columns, alternating 5 cell samples from each group HD and HC. All steps of the seeding, washing, staining, replacing media protocols were programmed for running automatically with optimized pipetting parameters for each task. After 24 h incubation at 37°C and 5% CO2, culture media was removed and replaced, after one wash with DPBS, with fluorescent dyes mix diluted in HBSS. After 30 min incubation at 37°C, and 5% CO2 the plate was transferred to the IN Cell Analyzer 2200 (GE Healthcare) for image acquisition under cell culture environmental conditions. The fluorescent vital dyes mix used contain Hoechst 33,342 (Merck-Sigma, Unite State) 1:10,000, CellTrace™ Calcein Green AM (Invitrogen, Unite State) 1:5000, mitochondria TMRE red (Invitrogen, Unite State) 1:2500 and MitoTracker™ Deep Red (Invitrogen, Unite State) 1:5000. Twenty images per fluorescent channel (fixed spacing fields) for each well were acquired in four different channels in less than 60 min. All images under a 20x magnification were taken using the same acquisition protocol with constant exposures for each fluorescent channel for each of the four fluorescent dyes used to stain the cells. Image acquisition has been done in a horizontal serpentine pattern. The multiple cell images were subsequently segmented and high content analyzed using IN Cell Developer software (GE Healthcare).

Actin F and nuclear staining assay for fluorescent microscopy

Cells from HC and HD samples were seeded and culture in 96 well plates as described above, then fixed in 4% v/v Paraformaldehyde

TABLE 1 List of skin fibroblasts samples of HD individuals.

HD individual	Age	Gender	CAG Repeats	CAP Score- Fneur	Disease Severity	Figure Number
GM02165	57 YR	Male	46[a]	140.5239	Severe	4
GM05031	60 YR	Male	45[a]	138.6749	Severe	4
GM04476	57 YR	Male	45[b]	131.7411	Severe	1,2,3,4
GM04200	53 YR	Male	46[a]	130.6626	Severe	4
GM00305	56 YR	Female	45[a]	129.4299	Severe	4
GM04285	40 YR	Male	51[b]	129.4299	Severe	4
GM06274	56 YR	Female	45[a]	129.4299	Severe	1,4
GM04807	41 YR	Male	50[b]	126.3482	Severe	4
GM04287	43 YR	Male	49[b]	125.886	Severe	1,2,4,5
GM02147	55 YR	Male	44[a]	118.6441	Severe	4
GM04691	31 YR	Male	54[b]	114.6379	Severe	4
GM04687	37 YR	Female	50[b]	114.0216	Severe	4
GM04709	38 YR	Female	49[b]	111.2481	Mild	1,2,3,4,5
GM04715	40 YR	Male	48[b]	110.9399	Mild	3,4,5
GM04887	48 YR	Female	45[b]	110.9399	Mild	1,2,3,4
GM04196	51 YR	Female	44[a]	110.0154	Mild	1,2,4
GM04767	43 YR	Female	46[b]	106.0092	Mild	4
GM04849	28 YR	Female	54[a]	103.5439	Mild	4
GM04212	50 YR	Female	43[a]	100.1541	Mild	1,2,4,5
GM04819	48 YR	Male	43[b]	96.14792	Mild	1,2,4,5
GM04799	47 YR	Male	43[b]	94.14484	Mild	1,2,4
GM04721	37 YR	Female	46[b]	91.21726	Mild	1,2,3,4
GM04719	39 YR	Female	44[b]	84.12943	Premanifest	1,2,4
GM04847	31 YR	Male	46[b]	76.42527	Premanifest	4
GM04693	33 YR	Male	45[b]	76.27119	Premanifest	4
GM04717	44 YR	Female	41[b]	74.57627	Premanifest	1,2,3,4
GM04689	30 YR	Female	45[b]	69.33744	Premanifest	4
GM04837	23 YR	Male	47[b]	60.24653	Premanifest	4

[a]CAG repeat number of the HD sample was obtained using AmplideX® PCR/CE HTT Kit following the manufacturers protocol guidelines.
[b]CAG repeat number of the HD sample was provided by Coriell Institute Cell Repository.

(Electron Microscopy Sciences, Unite State) in PBS for 10 min, and washed 3 times with DPBS. Cells were then permeabilized with .1% Triton X-100 (Merk-Sigma, Unite State) in PBS for 10 min at room temperature. Then Blocking solution 5% w/v BSA (Chem-Impex, Unite State) in TBST was added to the cells for 1 h. After 1 h. After 1 h, the sample was washed 3 times with .05% Triton X-100 for 5 min. After the removal of the 5% BSA solution.

The cells were washed with PBS and the nuclei and actin filaments were stained at room temperature for 1 h in the dark with a mix of 30 µL Hoechst 33,342 1:10,000 and Phalloidin (Merk-Sigma, Unite State) 1:400 in 5% BSA (in TBST) respectively. The stained cells were washed three times with DPBS and image acquisition and analysis of the plate was performed similarly as described above.

Confocal microscopy, image and data analysis

Confocal microscopy of actin and nuclei labeled cells for actin cap validation experiments was performed under a Leica SP8 LIGHTNING (Leica Microsystems, Germany) confocal microscope with a 40x 1.2 N.A objective using 561 nm and 405 nm laser wavelengths for actin fibers and nucleus, respectively. The analysis of the actin cap fibers at the at the apical and basal focal planes was done using the LAS X software (Leica Microsystems, Germany). To determine different morphological clusters of actin cap in the HD skin fibroblast confocal microscopy analysis was performed using a Zeiss LSM800 confocal microscope with a 63x

TABLE 2 List of skin fibroblasts control samples (Adult HC, Young HC, and HGPS).

HC individual	Age	Gender	Figure Number	HGPS individuals	Age	Gender	Figure Number
0205C	68 YR	Female	1,2,4	HGADFN367	3 YR 0 mos	Female	2,4
0495C	53 YR	Female	4	HGADFN188	2 YR 3 mos	Female	2,4
0951C	61 YR	Female	4	HGADFN169	8 YR 6 mos	Male	2,4,5
0025C	48 YR	Male	1,2,3,4	HGADFN122	5 YR `0 mos	Female	2,4,5
0553C	49 YR	Male	1,2,4	HGADFN127	3 YR 9 mos	Female	2,4
0795C	50 YR	Male	1,2,4	HGADFN271	1 YR 3 mos	Male	2,4
0971C	56 YR	Male	4				
1170C	43 YR	Male	1,2,3,4,5	**Young HC individuals**			
0143C	42 YR	Male	1,2,4,5	GM2036	11 YR	Female	2,4
0981C	50 YR	Male	1,2,4	07525C	4 YR	Male	2,4
0561C	48 YR	Male	1,2,4	0015C	1 YR 6 mos	Male	2,4
GM00726	26 YR	Female	4	0044C	2 YR	Male	2,4
GM01650	37 YR	Female	4				
GM01653	37 YR	Male	4				
1016C	62 YR	Male	4				
0848C	48 YR	Female	1,2,3,4,5				
0730C	51 YR	Male	4				
0633C	50 YR	Male	4				
0579C	40 YR	Male	1,2,4				
0233C	61 YR	Female	1,2,4				

1.4NA objective and Airyscan module. A region of interest of 40.6 μm by 40.6 μm and scan zoom of 2.5 was acquired using 561 nm and 405 nm laser wavelengths for actin fibers and nucleus, respectively. Images were processed using the Airyscan algorithm in the ZEN blue software (Zeiss). Actin cap fibers were identified using Trainable Weka segmentation plugin for FIJI (Arganda-Carreras et al., 2017), and thresholding was used to define the nucleus region. Fiber orientation analysis was done using the Ridge Detection and Orientation J plugins for FIJI.

Cell migration time lapse microscopy assay

The primary fibroblasts were plated in a 96-well plate at low density (800 cells/well) and then incubated overnight at 37°C and 5% CO2. Time lapse microscopy imaging of these plated cells was performed using an IN Cell Analyzer 2200 equipped with a long working distance 4× objective, phase contrast capability and controlled environmental chamber. The image acquisition frequency was set every 10 min for 21 h for 30 wells. The analysis of the time lapse images was performed by CellTracker program using semi-automated cell tracking function which allows a quantitative determination of cell motion parameters, including cell total travel length, net displacement and velocity. The cells paths were plotted and analyzed through The Chemotaxis and Migration Tool (ImageJ plug-in) to create the sun plots shown in the results.

Custom image analysis tool for actin cap like morphological features

The image analysis tool was fully programmed and validated in our lab using python 3.7 programming language https://gitlab.com/maydanw/CellDoctor.

The image analysis script can be found under: https://gitlab.com/maydanw/CellDoctor/-/blob/master/Notebooks/Run_Image_Analysis.ipynb. The image analysis script is divided into two parts. The first part is for linking between the image channel specification (e.g., DAPI - DAPI) to the logical channel (e.g., NucliChannel). The second part is for extracting different morphological features of a particular object (in DataExtractors). The overall process of the image analysis tool is described in the "Protocol" section. The images were mostly processed by different functions of the OpenCV library.

The first step in image pre-processing is applying image binarization using binary thresholding which turns the raw image into a grayscale. Followed by noise reduction using image thresholding. Various techniques for object detection and segmentation were used according to the label and to the object morphology. For example, on the nuclei image a Simple Binary Thresholding was applied where for every pixel the same threshold value is applied. If the pixel value is smaller than the threshold, it is set to 0, otherwise it is set to a maximum value = 255. On the Binary Thresholding different morphological operations like Erosion,

Dilation, Opening and Closing etc. was applied through the Morphological Transformation which is one of the Image Processing applications in OpenCV.

Microscopy images of skin fibroblast cells were processed through the tool, extracting the following actin cap like parameters: The nucleus circularity.

The standard deviation of actin fibres' slope in each cell–slopes of all actin fibers were calculated per cell followed by a calculation of the standard deviation of the slopes per cell.

$$\textbf{Circularity} = (4 * \textbf{pi} * \textbf{Area}) / \textbf{Perimeter}\hat{}2$$

$$slope = \frac{y_1 - y_2}{x_1 - x_2} \quad STD = \sqrt{\left(\frac{1}{N}\sum_{i=1}^{N}\left(slope_i - \overline{slope}\right)\right)^2}$$

Statistical analysis

The raw data obtained from the image analysis in this study was further statistically analyzed using the imaging assay development notebook script at https://github.com/disc04/simplydrug site, found under HTS notebook, under imaging-based assays development script being adapted to our data. For checking if the two groups were significantly different from each other, the Mann-Whitney U test was used on the medians of different parameters comparing between two groups using GraphPad 8, and the results were presented in box plots using Tableau 2020.3. For graph generations. The stars presented on the different graphs indicate different significance levels (*) p-value <.05 (**) p-value <.01 (***) p-value <.001.

Data sharing

The data that support the findings of this study are available on request from the corresponding author. The data are not publicly available due to privacy or ethical restrictions.

Results

Primary skin fibroblasts from HD patients display distinct morphological features

To determine phenotypic differences by image-based HCA of primary HD fibroblasts, we analyzed 12 HD and matching human control (HC) cell samples. The primary cells from five individuals from each group were plated using a robotic liquid handling unit in 96 well plates in DMEM and 10% FBS and incubated for 24 h at 37°C, 5% CO_2, washed, and finally stained with a mix of fluorescent dyes, Hoechst 33,342 (blue), calcein-AM (green), mitotracker (far red), and TMRE (red) in HBSS to label the nuclei, cell cytoplasm, mitochondria, and functional mitochondria, respectively. Automated imaging with a 20x objective of thousands of fluorescently stained cells per sample at the four fluorescence channels was performed under environmental controlled conditions using an IN Cell 2200 Analyzer, and image HCA was performed using this system software as described in the Materials and Methods. Figure 1 shows the results from these experiments. Representative micrographs of the labeled cells for image analysis are shown in Figure 1A. Quantitative analysis of these experiments showed clear segregation of the phenotype between the HD and HC cell samples by principal component analysis (PCA) that gave a 64% variance ratio (Figure 1B). The feature histogram distribution by PC dimension indicates a clear difference between the groups (Figure 1C). Detailed analysis of all significant features from HC and HD fibroblasts samples is shown in Supplementary Figure S1. Together with this we performed a cell by cell analysis to verify the nature of the data distribution (see Supplementary Figure S2) which showed similar results as in Figures 1B, C. As shown in Figure 1D, the most relevant HD phenotypic characteristics were mitochondria features and cell morphology, consistent with previous studies (Costa and Scorrano, 2012). Notably, besides these features, we found that nuclear morphological features are distinctive in the HD cell populations, indicating an HD nuclear phenotype which, to the best of our knowledge, has not been described before.

Lack of actin cap in skin fibroblast samples from HD patients is correlated with deficient cell motility and low lamin A/C levels

To investigate this phenotype further, we analyzed all the nuclei images obtained from the above experiment together with newly and similarly acquired nuclear images of primary fibroblasts from five HGPS patients and respective matching controls. The HGPS cells were used as a known reference for disease nuclear morphology (Hale et al., 2008). Results from these experiments (Figures 2A, B) show significant qualitative and quantitative differences in nuclear morphological features (form factor and major axis of the nucleus) between HD and HGPS and their respective adult and young HC groups. Compared to controls, the HD and HGPS cells show significantly higher roundness, which is expressed here as median nucleus form factor. In contrast, the healthy controls show a significant difference in median nucleus major axis, indicating a more oval nuclear morphology than both HD and HGPS cells.

Previous studies showed that nuclear morphological changes are linked to changes in the assembly or absence of a nuclear actin cap (Khatau et al., 2009). To investigate the possibility that the different nuclear morphology in HD cells is linked to an actin cap deficiency, we performed similar experiments as described above but stained the cells after 4% PFA/PBS fixation with Hoechst and phalloidin to label the nuclei and actin filaments respectively. Confocal imaging was applied to measure the phalloidin-labelled actin filaments within the stained nuclear area at three different optical z-section levels – basal, middle, and apical, taken from HD (n = 2), matching HC (n = 2), and HGPS (n = 2) (Figure 2C). Representative images of these cells at the three different z confocal planes, along with linescan analyses of phalloidin fluorescence intensity at the apical level of the cells for three arbitrary nuclei for each group, are shown in Figure 2C upper and lower panels, respectively. Quantitative analysis of the phalloidin mean fluorescence intensity in all apical z-sections analyzed (~50 nuclei per sample) in each group show significantly higher values in HC compared to HD and HGPS (Figure 2D). These results strongly indicate that actin filaments at the apical side of the nucleus (actin cap fibers) are more readily assembled in HC compared to HD and HGPS cells, although HD cells displayed higher levels than HGPS cells. The significantly low F-actin levels in HGPS cells are in line with their known severe actin cap deficiency (Hale et al., 2008; Khatau et al., 2009).

10.3389/fcell.2023.1013721

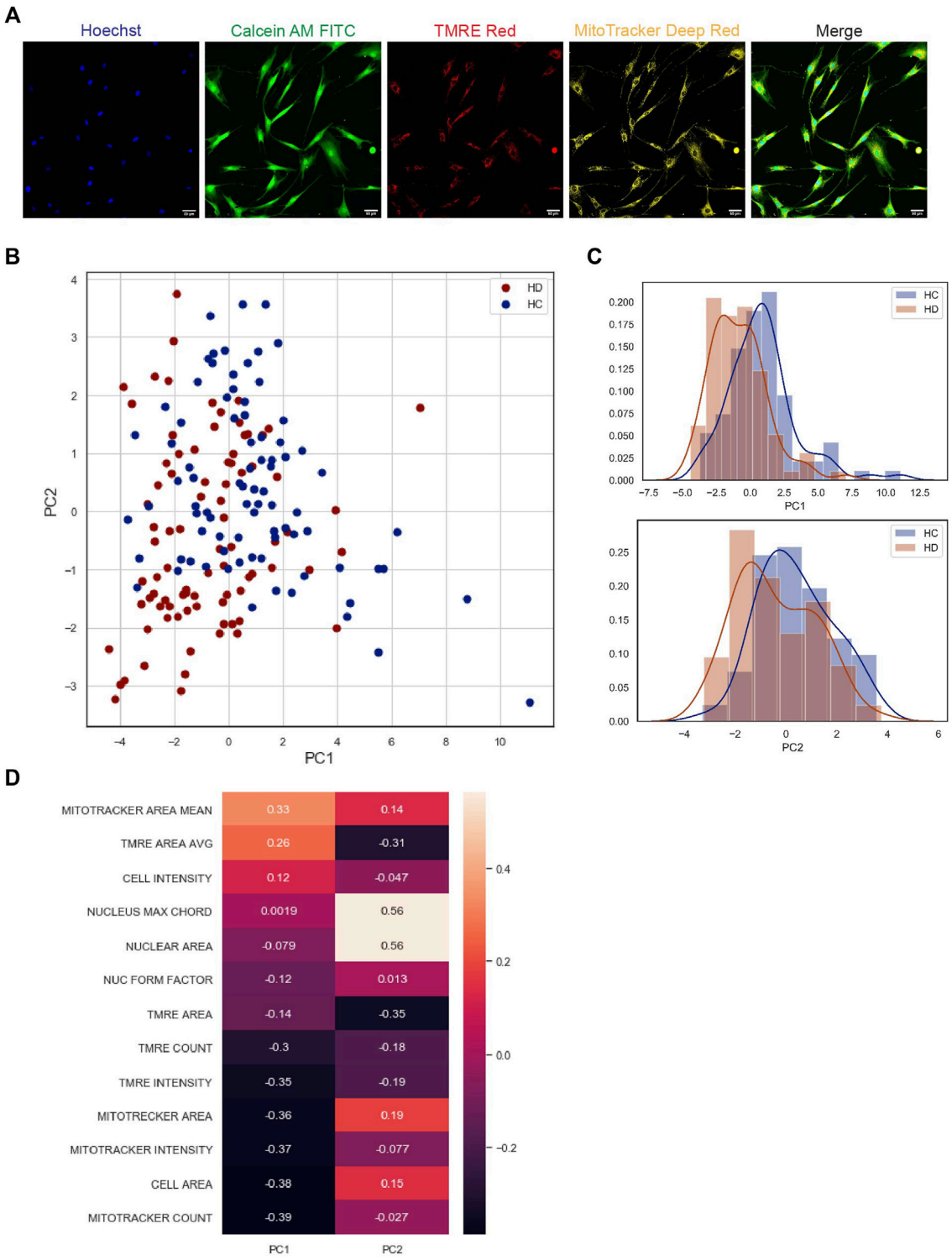

FIGURE 1
High content image based analysis of primary skin fibroblast samples of HD patients compared to HC **(A)** Representative images of skin fibroblast cells stained with 4 different fluorescent vital dyes (Hoechst 22,342 to label the cell nuclei, Calcein AM to label cytoplasm of living cells, TMRE to label functional mitochondria, and Mitotracker far-red to label mitochondria). The images were acquired by 20x magnification using INCell 2200 image analyzer. Scale bar = 50 µm. **(B)** Principal component analysis of 12HD vs. 11HC phenotypic data (PCA graph on the right) The analysis shows a separation between the two groups. Each sample is represented by 6 circles each circle is the median of phenotypic data extracted from 20 fields coming from one well, each field contain 10–40 cells, blue circles represent HC samples, red circles represent HD samples. **(C)** (Histogram graphs on the right) represent the distribution of the analyzed PCA data of the two populations in the two dimensions (PC1, PC2), blue histogram represents HC and red histogram represents HD. **(D)** Plot of feature importance in the two PCA dimensions PC1 & PC2, organized from the most important (orange) to the least important feature (black) to the significant difference between the two populations in the PCA analysis.

10.3389/fcell.2023.1013721

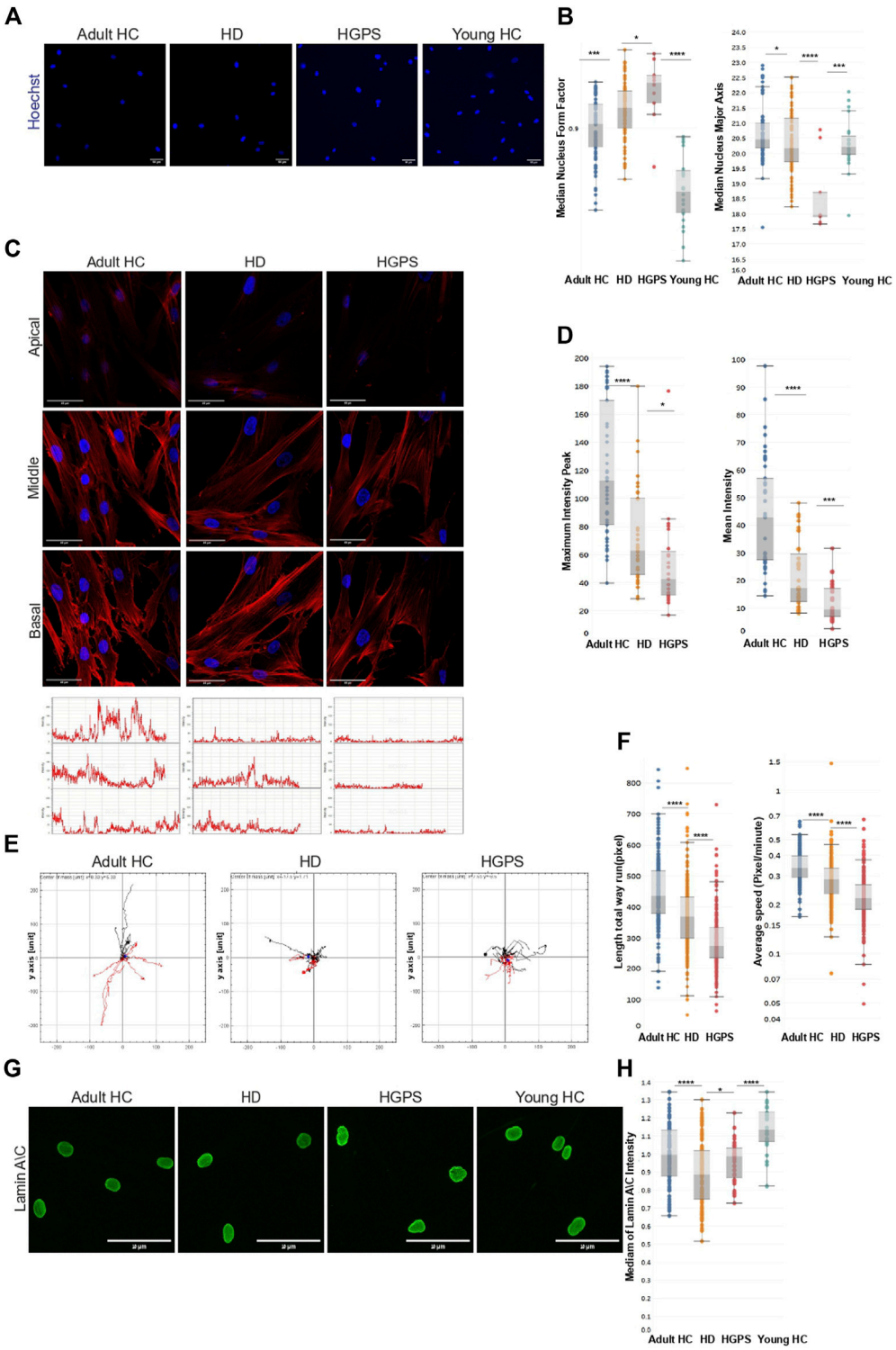

FIGURE 2
Actin Cap in HD skin fibroblast cells **(A)** Representative images of fixed primary skin fibroblast cells of Adult HC, HD, HGPS, and young HC cells stained with Hoechst to label the cell nuclei and phalloidin to label F-actin, acquired with a 20x magnification using INCell 2200 image analyzer. Scale bar = 50 μm. Cells of indicated groups were segmented automatically using the INCell Developer toolbox software. **(B)** Mann-Whitney's U test was performed on the medians of the nuclear form factor and nuclear major axis per well (11 HC, 12 HD, 5 HGPS, 4 young HC), ~500 cells from each skin fibroblast sample using GraphPad 8; the results are presented in box plots using Tableau 2020.3. **(C)** On the upper panel representative confocal immunofluorescence staining images of HD, HC, and HGPS skin fibroblast cells of 3 z-stacks (Basal, Middle, Apical) showing less actin filaments in the apical surface of the HD and the HGPS fibroblast cells. Skin fibroblast cell images were acquired with a 40x magnification using Leica SP8 confocal microscope. Scale bar = 50 μm. Cells were stained with Hoechst to label the cell nuclei and phalloidin to label F-actin of fixed cells. On the lower panel representative intensity graphs of actin in the apical z-stack, each graph represents one nucleus, Y-axis represents intensity levels (0–250), X-axis represents pixels. **(D)** Mann-Whitney's U test was performed on the medians of the mean intensity of actin fibers, and of the maximum peak of different actin intensity graphs in the apical z-stack of ~20 cells from each skin fibroblast sample (2 HC, 2 HD, 2 HGPS) showing significant lower measurements in the two parameters in HD and HGPS samples. **(E)** Single-cell random
(*Continued*)

FIGURE 2 (Continued)
migration analysis of HD and HC skin fibroblast cells shows significant lower motility parameters in HD and HGPS cells compared to HC. Cell tracking analysis was carried out for 21 h at a rate of 1 frame per 10 min. Several parameters of random motility were quantified on (N = 2) of each HD and HC and HGPS skin fibroblast cells. Time-lapse images were acquired in brightfield with a 4x magnification using INCell 2200 image analyzer. Cells of indicated groups were tracked semi-automatically by CellTracker analysis software. After cell tracking, the cells' paths were plotted and analyzed through The Chemotaxis and Migration Tool (ImageJ plug-in) to create the sun plots. Sun plots show the cell path for representative 15 cells from each population. **(F)** Mann-Whitney's U test was performed on the medians of different parameters of random motility in HC fibroblast cells compared to the HD and HGPS per cell (2HC, 2HD, 2HGPS), ~150 cells from each skin fibroblast sample using GraphPad 8, the results are presented in box plots using Tableau 2020.3. **(G)** Representative merged fluorescence images of fixed primary skin fibroblast cells of Adult HC, HD, HGPS, and Young HC cells stained with Hoechst to label the cell nuclei and phalloidin to label F-actin, and Anti-mouse secondary antibody 488 to label Lamin A\C acquired with a 20x magnification using Operetta-high-content screening system, Perkin Elmer. Scale bar = 100 μm. Cells of indicated groups were segmented automatically using the Harmony software for image analysis. **(H)** Mann-Whitney's U test was performed on the medians of Lamin A\C intensity levels (normalized to HC adult) per well (7 HC- 108 wells, 12 HD- 128 wells, Young HC- 24 wells, 3 HGPS- 36 wells) using GraphPad 8; the results are presented in box plots using Tableau 2020.3.

Based on these findings, we next tested whether the actin cap had an effect on cell motility, as shown in previous studies (Kim et al., 2014). To this end, we performed cell motility analyses on HD (n = 3), HC (n = 3) and HGPS (n = 3) fibroblasts samples using phase contrast time lapse microscopy and image acquisition every 10 min for 21 h (see Supplementary Figure S3 for representative cell migration videos) (tracking of ~150 cells per sample was performed). As shown by the sunplot cell migration graphs in Figure 2E, both HD and HGPS cells display significantly lower migratory capacity compared to HC cells. Measurements of track distance and average speed of all tracked cells (Figure 2F) confirm the observed migration phenotypes and the differences between HD and HGPS as compared to HC. Together with this we measured the Lamin A\C protein levels by immunofluorescence analysis in the HD and HGPS skin fibroblast samples to investigate apparent phenotype resemblance. Results from these experiments (Figures 2G, H) show significant difference in the intensity levels of Lamin A\C protein between HD and HGPS and their respective adult and young 0HC groups. Compared to their controls, the HD and HGPS cells show significantly lower intensity levels of Lamin A\C. Altogether, these results confirm that aberrant cell motility and Lamin A/C levels of HD cells is correlated with the newly described actin cap deficiency in these cells.

Classification of different actin cap morphologies in HD skin fibroblast population

To further investigate the actin cap phenotype in HD cells and better classify it compared to HGPS cells, which are known for their actin cap deficiency, we developed a machine learning tool for actin cap segmentation using the Trainable Weka segmentation plugin for FIJI (Arganda-Carreras et al., 2017). To this end we performed similar experiments as shown above (see Figure 2C) but images were acquired using higher resolution confocal imaging (63x 1.4NA objective and Airyscan processing) to obtain better description and higher number of the actin cap morphological features (Figure 3A). Phalloidin-labeled actin filaments within the stained nuclear area were analyzed at the apical and basal optical z-section levels from images of 120 cells in total taken from HD (n = 9), matching HC (n = 6), and HGPS (n = 2) samples. Image analysis of HGPS cells produced no segmentation of the actin cap, as expected (see Supplementary Figure S4), and therefore were not included for further analyses. The data obtained from the image segmentation analysis from HC and HD cells in these experiments was analyzed using the script available at https://github.com/disc04/simplydrug. To get a better resolution in actin cap morphology in HD cells, we extracted different morphological features of the actin cap and the nucleus from the images. Detailed analysis of all significant features from HC and HD fibroblasts samples is shown in Supplementary Figure S6. This enabled us to obtain classification within each group, as shown in Figure 3. PCA analysis of these features gave a 55% variance ratio showing a significant difference between the two populations (Figure 3B). The feature histogram distribution by PC dimension indicates a clear difference between the groups (Figure 3C). K-means clustering analysis of three clusters was performed, and results are shown as a heat map (Figure 3D). Cluster 0, which is composed of 23.6% HD cells and 76.4% HC cells, is identified by moderate size and oval nuclei, with the highest actin cap area and highly parallel actin cap fibers with high F-actin intensity levels. Cluster 1, which is composed of 89.3% HD cells and 10.7% of HC cells, is characterized by the largest, more circular nuclei, together with the smallest actin cap area in combination with highly parallel actin cap fibers and low F-actin intensity levels. Cluster 2, which is composed of 70.3% HD cells and 29.7% HC cells, is characterized by the smallest and most circular nuclei, together with a larger actin cap area, compared to those in cluster 1, with non-parallel actin cap fibers and moderate F-actin intensity levels. Overall, these results show that the HD cell population is represented in two different clusters, strongly indicating that the HD actin cap phenotype is heterogeneous, although most of the HD cells analyzed were found in cluster 2. To better understand the different HD actin cap clusters, we analyzed six features describing the actin fiber network at the apical side of the nucleus. These analyses show high correlation between the features (Supplementary Figures S5A, B) which enabled us to reduce the features into one representative feature of the actin cap, namely, actin network complexity. As shown in Supplementary Figure S5C, this feature manages to segregate HD from HC groups, by medium and high values in 11.4% of the HD data and 15.9% of the HC data, respectively. Moreover, low values of actin network complexity are represented in 88.6% of the HD data and 84.1% of the HC data, respectively. These results suggest that the actin network complexity of HD cell population is lower than that of the HC group.

Altogether, these results strongly support the notion that actin cap deficiency in HD is a novel representative cellular phenotype of HD primary fibroblasts, which is characterized differently within the HD sample population as compared to control.

Image-based high content analysis algorithm for extraction of actin cap like features from 2D images

The above results demonstrate a characteristic actin cap deficiency in HD cells. We therefore wished to test whether this phenotype is

10.3389/fcell.2023.1013721

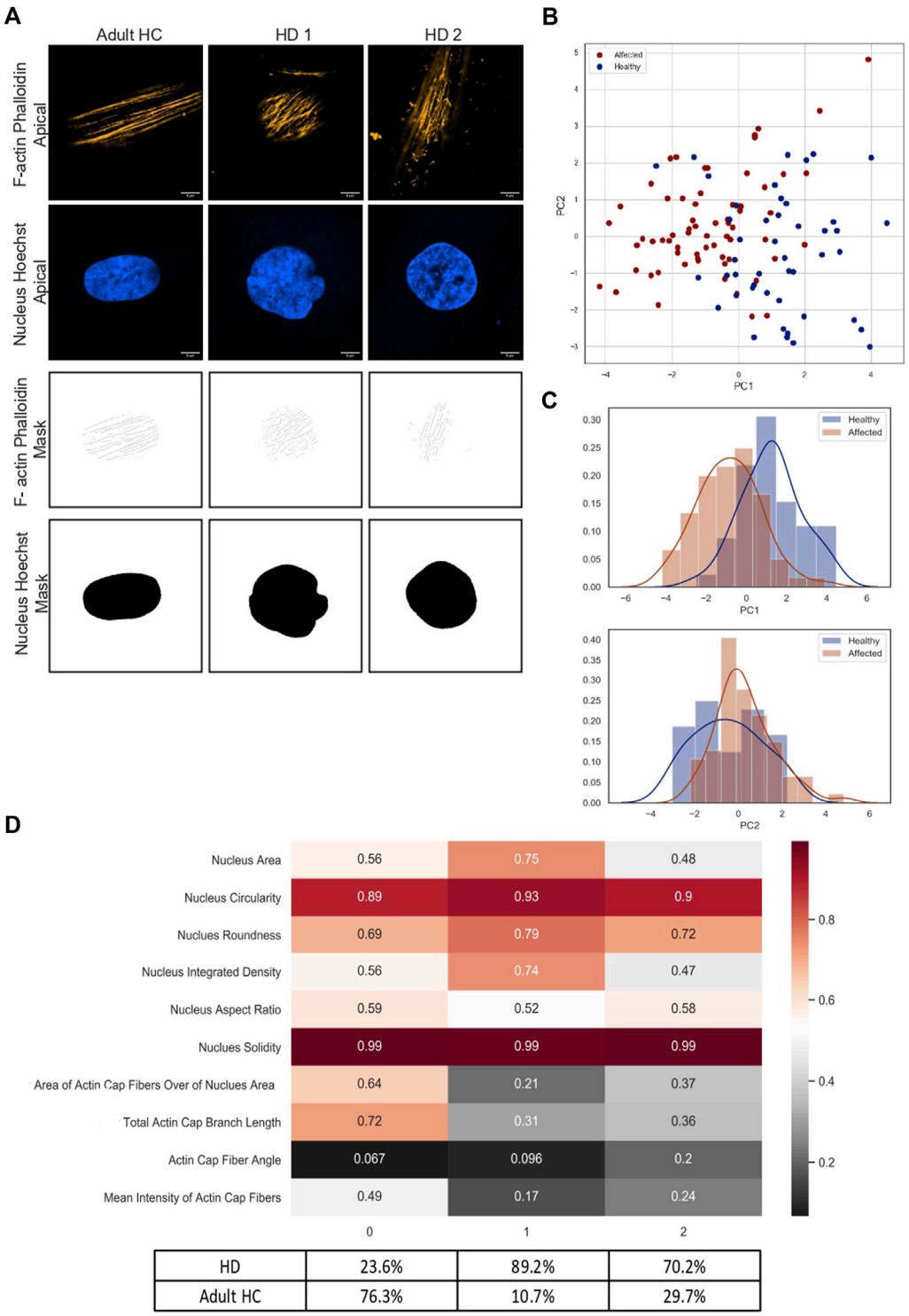

HD	23.6%	89.2%	70.2%
Adult HC	76.3%	10.7%	29.7%

FIGURE 3
Deeper analysis for the different actin cap morphologies in HD skin fibroblast cells **(A)** Representative confocal immunofluorescence staining images of data acquired under 63x magnification 1.4NA objective and Airyscan module. Cells were stained with Hoechst to label the cell nuclei and phalloidin to label actin filaments of fixed cells. Scale bar = 5 µm For analysis of different morphological clusters of actin cap, for each skin fibroblast cell 3 images were acquired – basal nucleus, apical nucleus, and apical actin. Representative Images of the segmented actin cap fibers and nucleus generated by the WEKA trainable segmentation tool. **(B)** PCA analysis of 8 HD vs. 8 HC actin cap and nucleus morphological features. The analysis shows a significant separation between the two groups. Each sample is represented by 10 morphological features extracted from 1 cell, in total ~50 cells from each population, blue circles represent HC samples, red circles represent HD samples **(C)** Histogram graphs represent the distribution of the analyzed PCA data of the two populations in the two dimensions (PC1, PC2), blue histogram represents HC and red histogram represents HD **(D)** K-means analysis of three clusters of the same data analyzed by PCA in **(B)**. The values in the plot are the average of the different values of one measurement in specific cluster. Cluster 0 accumulated mainly by HC (Class0: 76.3% HC, 23.6% HD) and Cluster 1, and 2 accumulated mainly by HD cells (Cluster 1: 89.2% HD, 10.7% HC; Cluster 2: 70.2% HD, 29.7% HC).

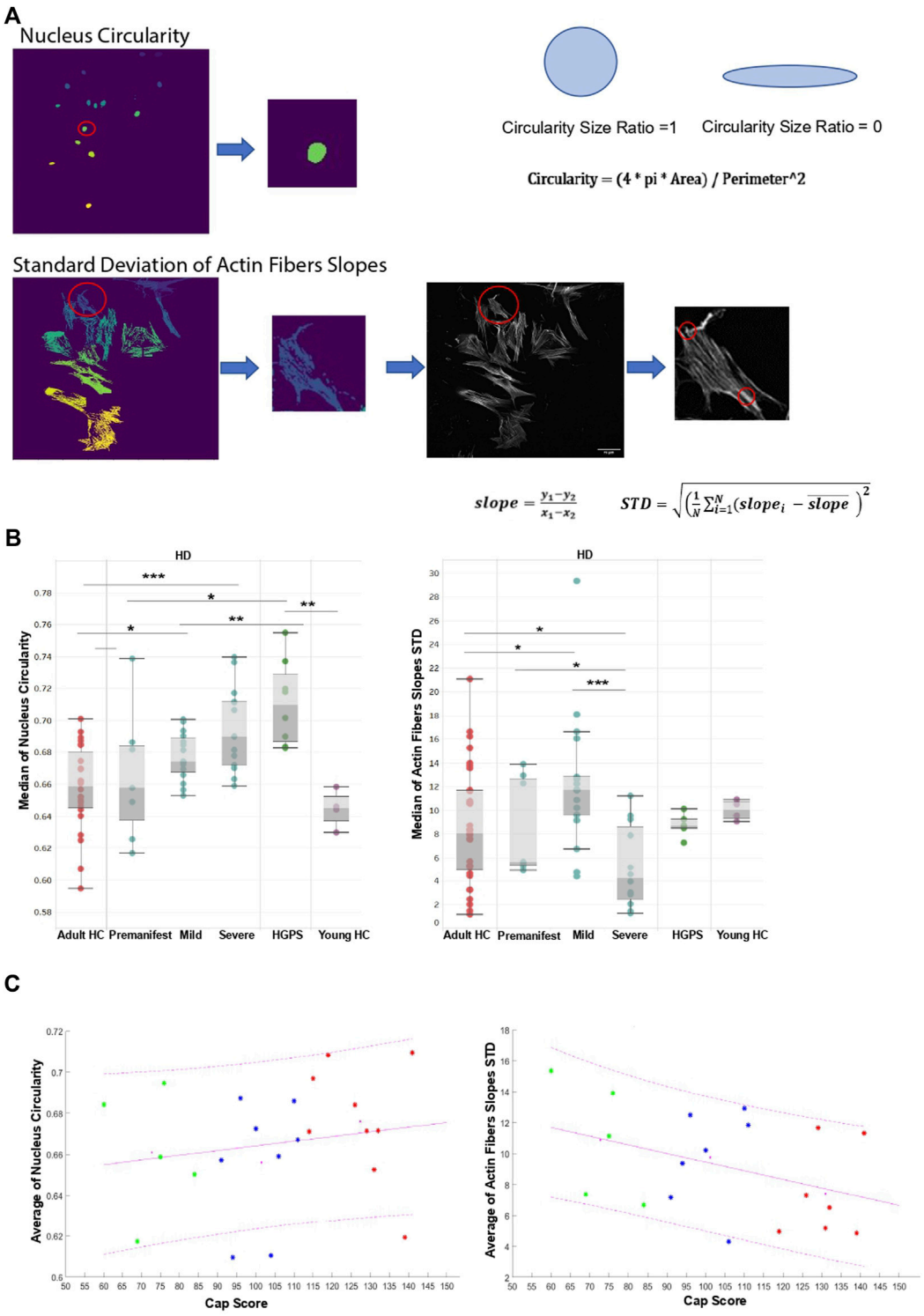

FIGURE 4
An automatic image based high content analysis algorithm for actin cap like features **(A)** Schematic Representation of the segmentation steps for each feature. For the "Nucleus Circularity" feature the algorithm counts the total number of pixels constructing each nucleus segment over the nucleus image. A binary mask of each nuclear segment is generated and then used to measure the circularity. For the "Standard Deviation of Actin Fibers Slopes" feature, the algorithm segments the cell body (cytoplasm), and a binary mask is applied over the actin fibers image to receive an output image of actin fibers that overlap the specific cell's cytoplasm. Then, an algorithm for line detection was applied on the output image in order to detect edge points couples of each actin fiber over the cytoplasm. For each actin fiber ("line") over the cytoplasm, a linear slope was calculated, and a standard deviation value of all slopes was determined to assess the level of actin fibers parallelization over the cytoplasm **(B)** Mann-Whitney's U test was performed on the medians of different actin cap like features generated from the image analysis tool mentioned above in HC fibroblast cells compared to the HD and HGPS per patient (20 HC, 6 Premanifest HD, 10 Mild HD, 12 Severe HD, 6 HGPS, 4 young HC), ~500 cells from each skin fibroblast sample using GraphPad 8, the results are presented in box plots using Tableau 2020.3 **(C)** Trend analysis was performed on the average of different actin cap like features in relation to Cap Score of different HD samples divided into three groups (Premanifest in green, Mild in blue, and Severe in red). Magenta lines are represented as least squares lines (solid line - for the average of the data, dashed lines - for the maximum and the minimum of the data) Magenta points are an average point of each group presented in a plot using MATLAB R2021a.

linked to global actin cell organization and nuclear morphology in the cells, which could be used as a high throughput drug screening assay for HD. To this end we developed a 2D image analysis tool to extract separate features that describe the nuclear morphology and the total actin fiber organization in the cells. Since nuclear elongation and actin cap organization were highly linked (e.g., cluster 0 in Figure 3D), we focused on nuclear circularity and the standard deviation (STD) of actin fibers slopes (see the schematic representation of the image analysis tool in Figure 4A; the image analysis tool is available at https://gitlab.com/maydanw/CellDoctor). This HCA method allowed us to increase the number of fibroblasts samples (a total of 15 HD and 9 HC samples were added to the sample cohort) for analysis as well as the number of cells tested in each sample per experiment. The experiments were performed as described above (see Figure 2). Image analysis using this tool was performed on ~500 cells per sample of 28 HD, 20 HC, 6 HGPS and 3 young HC fibroblasts (see Table 1; Table 2). The HD samples were analyzed according to their respective CAP score (Abreu et al., 2021) which divides the total number of patients into 3 subgroups: 6 premanifest, 10 mild, 12 severe). Box plot results of the image analysis data representing each of these features is shown in Figure 4B. Using this tool, we found that within the HD cells only mild and severe subgroups show significantly higher values of nuclear circularity compared to matching HC. This is consistent with the levels of HGPS cells that are higher as compared to their matching HC in a similar way as shown above (see Figure 2B). Moreover, HD cells from mild and severe subgroups show higher STD of actin fiber slopes which represent a more disorganized actin fiber arrangement in the cells as compared to matching HC. This is in accordance with what is shown in Figure 3D regarding clustering of the actin cap content and nuclei morphology. Together with this, HGPS cells show higher organization of the actin fibers in the cells, confirming the above detailed confocal data analysis (see cluster one in Figure 3D), which shows that the fewer the number of actin cap fibers, the more organized they are. Therefore, in a similar way here in Figure 4B, the standard deviation of the actin fiber slopes is lower in the matching HC compared to mild and severe HD subgroups. Interestingly, within the HD group data there is a significant difference between premanifest, mild and severe subgroups while the premanifest subgroup of HD cells show no significant difference if compared to HC cells. Figure 4C show the trend analysis of the two nuclear circularity and actin fibers slope STD features in relationship with the cap score of each of the 28 HD samples (premanifest subgroup in green; mild subgroup in blue; severe subgroup in red). The least square lines in both plots indicate the data tendency in relationship with the HD sample cap score. While the nuclear circularity feature increases with the HD cap score the actin fibers slope STD feature decreases. Altogether, these results validate the use of our image HCA tool for actin content and organization in primary skin fibroblasts of HD patients to identify actin cap related phenotype in these cells according to the patients' disease severity score.

To strengthen the morphological differences coming from the extracted features of the 2D image analysis algorithm with a biological evidence a Lamin A\C immunofluorescence analysis was done on the different HD subgroups (4 Premanifest, 4 Mild, 4 Severe) compared to 7 healthy controls and to 3 HGPS samples see Supplementary Figure S7. Showing significant difference between the HD subgroups.

These results prompted us to test the robustness of the distinctive actin cap HD phenotype as a new predictive tool by treating the cells with two different pharmacological agents, latrunculin B that blocks actin cap formation at low concentrations (Kim et al., 2014), and Mitoquinone mesylate (MitoQ), an antioxidant agent targeted to mitochondria to protect from oxidative stress. For functional treatment effects we performed in parallel cell motility time lapse microscopy assays as described (see Figure 2E). We hypothesized that latrunculin B treatment of HD cells would lead to a phenotype similar to that of HGPS cells that lack an actin cap completely. In contrast, we hypothesized that MitoQ treatment might recover the actin cap phenotype in HD cells due to the potential improvement in the known mitochondrial distress in HD cells (Carmo et al., 2018). To this end we performed experiments similar to those described above, where HD cells from five patients were treated for 24 h with either 60 nM latrunculin B or with 1 μM MitoQ, or DMSO (1:1000 v/v) as control. Matching HC (n = 3) and HGPS (n = 2) fibroblasts were used as controls. The effects of latrunculin B and MitoQ treatments on actin and nuclei morphology features in HD fibroblast cells are shown in Figure 5A. Interestingly, these two different drugs exert an opposite effect on the cells, where Latrunculin B treatment resembles HGPS nuclear circularity and shows a significant difference from HD DMSO control cells. In contrast, MitoQ led to a significant effect on nuclei circularity in HD treated cells compared to DMSO and similar to those of HC cells. In addition, Latrunculin B decreased the actin fiber slope standard deviation of HD cells compared to the DMSO control, indicating more parallel actin fiber organization despite the decrease in intensity. This effect resembles the phenotype that defines cluster one in Figure 3D. MitoQ in these experiments also affected the actin fiber slope standard deviation of HD cells significantly, but in contrast the phenotype resembles cluster 0 in Figure 3D which is representative of the HC.

Altogether, from these results we conclude that Latrunculin B at low concentrations exacerbates the actin cap phenotype of the HD cells, making it more similar to the actin cap phenotype of HGPS cells. In contrast, MitoQ improves the actin cap phenotype significantly in HD cells, making it more similar to the actin cap phenotype of HC cells. Remarkably, MitoQ also restored the motility of HD cells in all the measured parameters whereas Latrunculin B did not (see Figure 5B). Moreover, the opposite effects of the two drugs on cell motility demonstrate the direct functional link between their respective effects on actin, actin cap, and nuclear morphologies and cell motility. Altogether, these results strongly support the use of the actin cap associated features and cell motility assay to screen and evaluate drugs on HD patient cells for potential personalized treatment of HD patients in the clinic.

Discussion

Although the HD mutation in the Htt gene is a well-characterized cause of disease, the mechanism of disease in the different tissues and organs remains to be elucidated. Brain pathology has become a hallmark of HD, but critical mass of new studies suggest that HD is a multi-system challenging disorder, contributing to the patient's individual disease progression and disease severity independently of the high number of CAG repeats in the mtHtt (Sathasivam et al., 1999; Mielcarek, 2015). Therefore, it is important to characterize the phenotypic implications of mtHtt expression in cells other than neurons, such as primary HD fibroblasts, and try to connect them with

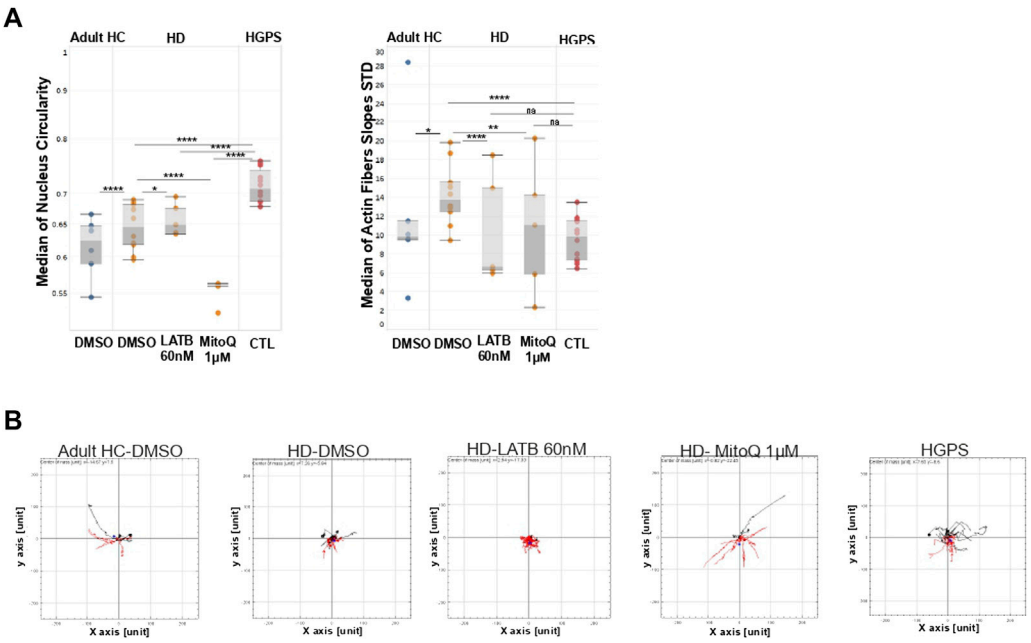

FIGURE 5
Effect of MitoQ and Latrunculin B on the actin cap in HD Fibroblast compared to HC and HGPS **(A)** Mann-Whitney's U test was performed on the medians of different actin cap like features generated from the image analysis tool mentioned above in HC fibroblast cells compared to the HD and HGPS per field (3 HC, 5 HD, 2 HGPS), ~200 cells from each skin fibroblast sample using GraphPad 8, the results are presented in box plots using Tableau 2020.3 **(B)** Cell tracking analysis was carried out in the same conditions mentioned in materials and methods section. Sun plots show the cell path for representative ~10 cells from each population. Graphs were generated by The Chemotaxis and Migration Tool (ImageJ plug-in).

specific cellular biological functions affected in the HD patients' cells. To this end we applied an unbiased high throughput cell-based image analysis approach to characterize an HD phenotype in these cells. Our results show that primary HD patients' fibroblasts exhibit a distinctive cellular phenotype that allows accurate classification from HC by image-based HCA tools. This analysis on 16 HD fibroblasts samples compared to 18 matching HC, strongly supports the robustness of such phenotypic classification. The HD cell phenotype is characterized by differences in cell morphology and mitochondrial features previously described in other HD models (Squitieri et al., 2010; Carmo et al., 2018). In addition, we found, for the first time, that significant nuclear morphological features are distinctive in the HD cell population (see Figure 1). A deeper analysis into the nuclear morphology of the cell by confocal microscopy allowed us to test the known link between nuclear roundness and the actin cap morphology (Figure 2) (Khatau et al., 2009). These experiments were performed using both HC fibroblasts as positive control and HGPS fibroblasts as reference for actin cap depletion control, since these patient cells are known to have a severe actin cap and concomitant nuclear morphology abnormalities (Booth-Gauthier et al., 2013). The confocal morphometric results strongly indicate that HD cells resemble more the HGPS nuclear morphology together with an associated actin cap deficient phenotype than the HC, suggesting that HD shares aspects associated with HGPS laminopathy. Further support for the HD phenotype comes from our mechanistic actin cap-related experiments, measuring cell migration for 24 h by time-lapse microscopy (Figure 2) (Kim et al., 2014). The migratory capacity of the HD cells confirms that their actin cap deficiency is correlated with their cell motility, which falls also in between the HC and HGPS control groups.

Studies show that mutant Htt interferes with actin dependent cellular remodeling. Mutant Htt fragments interact abnormally with actin binding proteins in HEK293 cells transfected with Htt Exon 1 (Munsie et al., 2011), and in mouse striatal neuron-derived cell line (STHdh) expressing full-length endogenous levels of either wild-type (STHdhQ7/Q7), or mutant (STHdhQ111/Q111) (Angeli et al., 2010). Different studies support the idea that Htt is involved in regulating adhesion and actin dependent functions including those involving α-actinin (Tousley et al., 2019) – an actin-binding protein and one of the components of the actin cap (Djinovic´ et al., 1999; Sjöblom et al., 2008). α-Actinin is recruited to focal complexes, where it provides a structural link between integrins and actin microfilaments (Sjöblom et al., 2008; Meacci et al., 2016). An interactome analysis of huntingtin in mouse brain models showed that Htt is associated with α-actinin-1, -2 and -4 both in wild type and Htt mutant huntingtin (Culver et al., 2012; Shirasaki et al., 2012). Follow up studies validated these results through immunoprecipitations using exogenously expressed proteins, immunofluorescence co-localization, and proximity ligation assay, showing a functional interaction of Huntingtin with isoforms of α-actinin in human primary fibroblasts and neurons (Tousley et al., 2019). This study, along with work of others (Greenwood et al., 2000; Guo et al., 2006; Kovac et al., 2013), proposed a model in which Huntingtin regulates α-actinin-1 localization and couples growth factor signaling with actin polymerization with bundling functions at new sites of adhesion. This evidence regarding htt and α-actinin subtypes strongly supports the possibility in HD patients' fibroblasts that actin cap might be aberrated due to abnormal binding between α-actinins and htt due to mt-htt expression.

Lamin B protein is one of the two subgroups that compose the lamin family which not only provide structural support to the nuclear

envelope membrane, but is also involved in a wide variety of cell functions and processes (Hozak et al., 1995). Lamin B is expressed in almost all cell types independently of their differentiation state (Verstraeten et al., 2007), suggesting its critical role in mammalian cell survival (Harborth et al., 2001). It is also known that lamin B binds directly to F-actin that forms the actin cap (Simon et al., 2010). Thus, altered levels of lamin B may have a direct effect on the formation, stabilization, and organization of the actin cap. Very recent work demonstrated a new pathogenic mechanism for HD by showing an increase in the Lamin B1 protein levels in HD brains in a neuron-type specific manner, which is correlated with alterations in nuclear morphology and nucleocytoplasmic transport (Alcalá-Vida et al., 2021).

We also show here that the actin cap phenotype in HD fibroblast cells is correlated with a distinctive nuclear morphology which allowed us to develop an image high throughput analysis tool of the actin content and organization in the nucleus area and nuclear morphology phenotype using 20X low power magnification. This tool allowed us to increase the amount of data for analysis which in turn gave us grading power to characterize and identify the morphological cell-based data with the respective HD sample's cap scoring. Moreover, these results support that actin cap morphological features are reliable HD cell biomarkers. Interestingly an important conclusion from the actin cap/cap scoring analyses of the data is that the actin cap phenotype in HD cells is acquired during the symptomatic phase of the disease. Following by the evidence that there is no actin cap alteration within the HD premanifest subgroup in relation with the other two HD symptomatic subgroups (mild and severe) which are significantly different from HC. Furthermore, the HD severe subgroup showed no significant difference from the HGPS group which is hallmark for actin cap defect.

The relative simplicity of this method should allow using this HD cell phenotype biomarker as reliable indicator to test or screen drug effects for patients with HD. This observation could allow us to classify/treat the patients in the future according to their cell phenotype severity level. The use of known pharmacological agents such as Latrunculin B and MitoQ to test their expected opposite effects on the HD actin content and organization in the nucleus area and nuclear morphology allowed us to test the drug screening potential of the assay. From these experiments, it becomes clear that while Latrunculin B exacerbates the HD cell phenotype by blocking actin polymerization, MitoQ, which reduces oxidative stress, improves significantly all the morphological features as well as cell migration parameters in the HD cells. Interestingly, these results strongly indicate that the mitochondrial function may regulate the actin cap/nuclear system and concomitant cell motility. Aberrant mitochondrial activity, possibly by increased reactive oxygen species (ROS) production, may be responsible for the actin cap phenotype in HD cells which can be reversed by MitoQ treatment that also recovers functional motility in HD patients' cells.

Our results strongly support the power of the image based phenotypic HCA assay in discovering new personalized biomarkers in HD. In addition, they also support the use of primary skin fibroblasts from HD patients as personalized model for disease phenotype classification based on linked actin cap/nuclear morphologies that functionally affect cell migration, which can be recovered by pharmacological agents. Altogether, our results and the HCA phenotypic tool used to describe the HD cell phenotype, together with application of machine learning approaches both for improving disease assessment, as well as exploration of novel parameters open the door for future drug testing or drug screening campaigns directly using the HD patient derived cells.

Data availability statement

The raw data supporting the conclusions of this article will be made available by the authors, without undue reservation.

Ethics statement

Ethical review and approval was not required for the study on human participants in accordance with the local legislation and institutional requirements. Written informed consent from the participants' legal guardian/next of kin was not required to participate in this study in accordance with the national legislation and the institutional requirements. HD and HC cells were purchased from the NIA and NIGMS Human Genetic Cell Repository at the Coriell Institute for Medical Research (USA). Some of the HC cell samples used in this study were obtained from the Neurology department at the University of Michigan Medical Center under a signed Material transfer agreement. The HGPS cells were purchased from The Progeria Research Foundation Cell and Tissue bank.

Author contributions

SG, MW designed the study SG performed and interpreted all experiments OP developed the algorithm for extraction of actin cap like features from 2D images and performed the relevant statistical analysis LF developed the machine learning tool for actin cap segmentation using the Trainable Weka segmentation plugin for FIJI. Maydan Weinrab developed the costumed image analysis tool found under: https://gitlab.com/maydanw/CellDoctor AA developed the imaging assay development notebook script at https://github.com/disc04/simplydrug. NM, AB performed the experiments of Figure 4 together with SG, AS performed the trend analysis shown in Figure 4C. HW provided guidance and help for the actin cap classification experiments. MW, and HW contributed to data interpretation; and SG, MW, HW contributed to reviewing and editing the manuscript.

Funding

This work was supported by the Taube-Koret Global Collaboration in Neurodegenerative Diseases Fund SG scholarship was partially supported by the Planning & Budgeting Committee of the Council for higher education AS Scholarship was partially funded by The Program for Data Science Research Centers Council for Higher Education Competitive grant 590957. HW acknowledges support from the Israel Science Foundation (1738/17) and from the Rappaport Family Foundation. HW is an incumbent of the David and Inez Myers Career Advancement Chair in Life Sciences.

Acknowledgments

We acknowledge the technical help of Itay Bosidan from The Future Scientists Center–Alpha Program at Tel Aviv Youth University, Tel Aviv 6997801, Israel.

Conflict of interest

The authors declare that the research was conducted in the absence of any commercial or financial relationships that could be construed as a potential conflict of interest.

Publisher's note

All claims expressed in this article are solely those of the authors and do not necessarily represent those of their affiliated organizations, or those of the publisher, the editors and the reviewers. Any product that may be evaluated in this article, or claim that may be made by its manufacturer, is not guaranteed or endorsed by the publisher.

Supplementary material

The Supplementary Material for this article can be found online at: https://www.frontiersin.org/articles/10.3389/fcell.2023.1013721/full#supplementary-material

References

Abreu, D., Ware, J., Georgiou-Karistianis, N., Leavitt, B. R., Fitzer-Attas, C. J., Lobo, R., et al. (2021). Utility of huntington's disease assessments by disease stage: Floor/ceiling effects. *Front. Neurol.* 12, 595679. doi:10.3389/fneur.2021.595679

Alcalá-Vida, R., Garcia-Forn, M., Castany-Pladevall, C., Creus-Muncunill, J., Ito, Y., Blanco, E., et al. (2021). Neuron type-specific increase in lamin B1 contributes to nuclear dysfunction in Huntington's disease. *EMBO Mol. Med.* 13, e12105. doi:10.15252/emmm.202012105

Alge, C. S., Hauck, S. M., Priglinger, S. G., Kampik, A., and Ueffing, M. (2006). Differential protein profiling of primary versus immortalized human RPE cells identifies expression patterns associated with cytoskeletal remodeling and cell survival. *J. Proteome. Res.* 5, 862–878. doi:10.1021/PR050420T

Angeli, S., Shao, J., and Diamond, M. I. (2010). F-actin binding regions on the androgen receptor and huntingtin increase aggregation and alter aggregate characteristics. *PLoS One* 5, e9053. doi:10.1371/journal.pone.0009053

Arganda-Carreras, I., Kaynig, V., Rueden, C., Eliceiri, K. W., Schindelin, J., Cardona, A., et al. (2017). Trainable Weka segmentation: A machine learning tool for microscopy pixel classification. *Bioinformatics* 33, 2424–2426. doi:10.1093/bioinformatics/btx180

Booth-Gauthier, E. A., Du, V., Ghibaudo, M., Rape, A. D., Dahl, K. N., and Ladoux, B. (2013). Hutchinson-Gilford progeria syndrome alters nuclear shape and reduces cell motility in three dimensional model substrates. *Integr. Biol. (United Kingdom)* 5, 569–577. doi:10.1039/c3ib20231c

Carmo, C., Naia, L., Lopes, C., and Rego, A. C. (2018). Mitochondrial dysfunction in huntington's disease. *Adv. Exp. Med. Biol.* 1049, 59–83. doi:10.1007/978-3-319-71779-1_3

Connolly, G. P. (1998). Fibroblast models of neurological disorders: Fluorescence measurement studies. *Trends Pharmacol. Sci.* 19, 171–177. doi:10.1016/s0165-6147(98)01202-4

Costa, V., and Scorrano, L. (2012). Shaping the role of mitochondria in the pathogenesis of Huntington's disease. *EMBO J.* 31, 1853–1864. doi:10.1038/emboj.2012.65

Culver, B. P., Savas, J. N., Park, S. K., Choi, J. H., Zheng, S., Zeitlin, S. O., et al. (2012). Proteomic analysis of wild-type and mutant huntingtin-associated proteins in mouse brains identifies unique interactions and involvement in protein synthesis. *J. Biol. Chem.* 287, 21599–21614. doi:10.1074/jbc.M112.359307

Dé Ric Saudou, F., and Humbert, S. (2016). The Biology of huntingtin. *Neuron* 89, 910–926. doi:10.1016/j.neuron.2016.02.003

Djinovic´, K. D., Carugo, D., Young, P., Gautel, M., and Saraste, M. (1999). Structure of the-Actinin Rod: Molecular Basis for Cross-Linking of Actin Filaments-Actinin is composed of an amino-terminal actin-binding region consisting of two calponin homology (CH) domains, a central rod containing four spectrin-like re. *Cell* 98, 537–546. doi:10.1016/S0092-8674(00)81981-9

Gardiner, S. L., Milanese, C., Boogaard, M. W., Buijsen, R. A. M., Hogenboom, M., Roos, R. A. C., et al. (2018). Bioenergetics in fibroblasts of patients with Huntington disease are associated with age at onset. *Neurol. Genet.* 4, 275. doi:10.1212/NXG.0000000000000275

Greenwood, J. A., Theibert, A. B., Prestwich, G. D., and Murphy-Ullrich, J. E. (2000). Restructuring of focal adhesion plaques by PI 3-kinase: Regulation by PtdIns (3, 4, 5)-P3 binding to α-actinin. *J. Cell Biol.* 150, 627–642. doi:10.1083/jcb.150.3.627

Guo, F., Debidda, M., Yang, L., Williams, D. A., and Zheng, Y. (2006). Genetic deletion of Rac1 GTPase reveals its critical role in actin stress fiber formation and focal adhesion complex assembly. *J. Biol. Chem.* 281, 18652–18659. doi:10.1074/jbc.M603508200

Hale, C. M., Shrestha, A. L., Khatau, S. B., Stewart-Hutchinson, P. J., Hernandez, L., Stewart, C. L., et al. (2008). Dysfunctional connections between the nucleus and the actin and microtubule networks in laminopathic models. *Biophys. J.* 95, 5462–5475. doi:10.1529/biophysj.108.139428

Harborth, J., Elbashir, S. M., Bechert, K., Tuschl, T., and Weber, K. (2001). Identification of essential genes in cultured mammalian cells using small interfering RNAs. *J. Cell Sci.* 114, 4557–4565. doi:10.1242/jcs.114.24.4557

Harjes, P., and Wanker, E. E. (2003). The hunt for huntingtin function: Interaction partners tell many different stories. *Trends biochem. Sci.* 28, 425–433. doi:10.1016/S0968-0004(03)00168-3

Hozak, P., Sasseville, A. M. J., Raymond, Y., and Cook, P. R. (1995). Lamin proteins form an internal nucleoskeleton as well as a peripheral lamina in human cells. *J. Cell Sci.* 108, 635–644. doi:10.1242/jcs.108.2.635

Huang, H.-M., Martins, R., Gandy, S., Etcheberrigaray, R., Ito, E., Alkon, D. L., et al. (2006). Use of cultured fibroblasts in elucidating the pathophysiology and diagnosis of alzheimer's diseasea. *Ann. N. Y. Acad. Sci.* 747, 225–244. doi:10.1111/j.1749-6632.1994.tb44412.x

Khatau, S. B., Hale, C. M., Stewart-Hutchinson, P. J., Patel, M. S., Stewart, C. L., Searson, P. C., et al. (2009). A perinuclear actin cap regulates nuclear shape. *Proc. Natl. Acad. Sci.* 106, 19017–19022. doi:10.1073/pnas.0908686106

Kim, D. H., Chambliss, A. B., and Wirtz, D. (2013). The multi-faceted role of the actin cap in cellular mechanosensation and mechanotransduction. *Soft Matter* 9, 5516–5523. doi:10.1039/C3SM50798J

Kim, D. H., Cho, S., and Wirtz, D. (2014). Tight coupling between nucleus and cell migration through the perinuclear actin cap. *J. Cell Sci.* 127, 2528–2541. doi:10.1242/jcs.144345

Kim, J. K., Louhghalam, A., Lee, G., Schafer, B. W., Wirtz, D., and Kim, D. H. (2017). Author Correction: Nuclear lamin A/C harnesses the perinuclear apical actin cables to protect nuclear morphology. *Nat. Commun.* 8, 1115–1213. doi:10.1038/s41467-018-03450-2

Kirkwood, S. C., Su, J. L., Conneally, P. M., and Foroud, T. (2001). Progression of symptoms in the early and middle stages of Huntington disease. *Arch. Neurol.* 58, 273–278. doi:10.1001/archneur.58.2.273

Kovac, B., Teo, J. L., Mäkelä, T. P., and Vallenius, T. (2013). Assembly of non-contractile dorsal stress fibers requires α-actinin-1 and Rac1 in migrating and spreading cells. *J. Cell Sci.* 126, 263–273. doi:10.1242/jcs.115063

Marchina, E., Misasi, S., Bozzato, A., Ferraboli, S., Agosti, C., Rozzini, L., et al. (2014). Gene expression profile in fibroblasts of Huntington's disease patients and controls. *J. Neurol. Sci.* 337, 42–46. doi:10.1016/j.jns.2013.11.014

Meacci, G., Wolfenson, H., Liu, S., Stachowiak, M. R., Iskratsch, T., Mathur, A., et al. (2016). α-Actinin links extracellular matrix rigidity-sensing contractile units with periodic cell-edge retractions. *Mol. Biol. Cell* 27, 3471–3479. doi:10.1091/mbc.E16-02-0107

Mielcarek, M. (2015). Huntington's disease is a multi-system disorder. *Rare Dis.* 3, e1058464. doi:10.1080/21675511.2015.1058464

Moily, N. S., Ormsby, A. R., Stojilovic, A., Ramdzan, Y. M., Diesch, J., Hannan, R. D., et al. (2017). Transcriptional profiles for distinct aggregation states of mutant Huntingtin exon 1 protein unmask new Huntington's disease pathways. *Mol. Cell. Neurosci.* 83, 103–112. doi:10.1016/j.mcn.2017.07.004

Munsie, L., Caron, N., Atwal, R. S., Marsden, I., Wild, E. J., Bamburg, J. R., et al. (2011). Mutant huntingtin causes defective actin remodeling during stress: Defining a new role for transglutaminase 2 in neurodegenerative disease. *Hum. Mol. Genet.* 20, 1937–1951. doi:10.1093/hmg/ddr075

Sathasivam, K., Hobbs, C., TurMaine, M.Mangiarini, L., MahAl, A., BertauxF., et al. (1999). Formation of polyglutamine inclusions in non-CNS tissue. *Hum. Mol. Genet.* 8, 813–822. doi:10.1093/hmg/8.5.813

Shirasaki, D. I., Greiner, E. R., Al-Ramahi, I., Gray, M., Boontheung, P., Geschwind, D. H., et al. (2012). Network organization of the huntingtin proteomic interactome in mammalian brain. *Neuron* 75, 41–57. doi:10.1016/j.neuron.2012.05.024

Simon, D. N., Zastrow, M. S., and Wilson, K. L. (2010). Direct actin binding to A- and B-type lamin tails and actin filament bundling by the lamin A tail. *Nucleus* 1, 264–272. doi:10.4161/nucl.1.3.11799

Sjöblom, B., Salmazo, A., and Djinović-Carugo, K. (2008). α-Actinin structure and regulation. *Cell. Mol. Life Sci.* 65, 2688–2701. doi:10.1007/s00018-008-8080-8

Solmesky, L., and Weil, M. (2014). Personalized drug discovery: HCA approach optimized for rare diseases at Tel Aviv university. *Comb. Chem. High. Throughput Screen* 17, 253–255. doi:10.2174/1386207317666140109123249

Squitieri, F., Falleni, A., Cannella, M., Orobello, S., Fulceri, F., Lenzi, P., et al. (2010). Abnormal morphology of peripheral cell tissues from patients with Huntington disease. *J. Neural. Transm.* 117, 77–83. doi:10.1007/s00702-009-0328-4

Strong, T. V., Tagle, D. A., Valdes, J. M., Elmer, L. W., Boehm, K., SwaroopM., et al. (1993). Widespread expression of the human and rat Huntington's disease gene in brain and nonneural tissues. *Nat. Genet.* 5, 259–265. doi:10.1038/ng1193-259

Tousley, A., Iuliano, M., Weisman, E., Sapp, E., Richardson, H., Vodicka, P., et al. (2019). Huntingtin associates with the actin cytoskeleton and α-actinin isoforms to influence stimulus dependent morphology changes. *PLoS One* 14, e0212337. doi:10.1371/journal.pone.0212337

Verstraeten, R. M., Broers, V., Ramaekers, J. S., and van Steensel, M. (2007). The nuclear envelope, a key structure in cellular integrity and gene expression. *Curr. Med. Chem.* 14, 1231–1248. doi:10.2174/092986707780598032

Wald-Altman, S., Pichinuk, E., Kakhlon, O., and Weil, M. (2017). A differential autophagy-dependent response to DNA doublestrand breaks in bone marrow mesenchymal stem cells from sporadic ALS patients. *DMM Dis. Model. Mech.* 10, 645–654. doi:10.1242/dmm.027938

Walker, F. O. (2007). Huntington's disease. *Lancet* 369, 218–228. doi:10.1016/S0140-6736(07)60111-1

Zink, D., Fischer, A. H., and Nickerson, J. A. (2004). Nuclear structure in cancer cells. *Nat. Rev. Cancer* 4, 677–687. doi:10.1038/nrc1430

frontiers | Frontiers in Cell and Developmental Biology

TYPE Review
PUBLISHED 17 May 2023
DOI 10.3389/fcell.2023.1184159

OPEN ACCESS

EDITED BY
Or Kakhlon,
Hadassah Medical Center, Israel

REVIEWED BY
Sarah Andres,
Oregon Health and Science University, United States
Feihong Deng,
Central South University, China

*CORRESPONDENCE
Yongyan Shi,
yyshi@cmu.edu.cn

RECEIVED 11 March 2023
ACCEPTED 09 May 2023
PUBLISHED 17 May 2023

CITATION
Yang J and Shi Y (2023), Paneth cell development in the neonatal gut: pathway regulation, development, and relevance to necrotizing enterocolitis. *Front. Cell Dev. Biol.* 11:1184159. doi: 10.3389/fcell.2023.1184159

Paneth cell development in the neonatal gut: pathway regulation, development, and relevance to necrotizing enterocolitis

Jiahui Yang and Yongyan Shi*

Department of Pediatrics, Shengjing Hospital of China Medical University, Shenyang, China

Paneth cells (PCs) are intestinal epithelial cells (IECs) that contain eosinophilic granules, which are located in Lieberkühn crypts. An increasing number of animal and human experiments have indicated that PCs are involved in the progression of a variety of intestinal as well as systemic inflammatory responses including necrotizing enterocolitis (NEC). NEC is an enteric acquired disease with high mortality that usually occurs in premature infants and neonates, however the underlying mechanisms remain unclear. In this review, we summarize the features of PCs, including their immune function, association with gut microbiota and intestinal stem cells, and their mechanism of regulating IEC death to explore the possible mechanisms by which PCs affect NEC.

KEYWORDS

neonatal necrotizing enterocolitis, Paneth cells, gut microbiota, intestinal stem cells, necroptosis, apoptosis, pyroptosis

1 Introduction

Necrotizing enterocolitis (NEC) is one of the most common acute intestinal necrotizing diseases (Blakely et al., 2021). In neonatal intensive care units, NEC has high morbidity and mortality rates, with 90%–95% of NEC cases occurring in premature infants and few in full-term infants (Horbar et al., 2012; Patel et al., 2015; Battersbyet al. 2018). After 30 years of intensive research, the exact cause of NEC is still unknown, but premature infants with immature intestinal development, imbalanced intestinal microbiota, and imbalanced inflammatory responses, as well as hypoxia, artificial feeding, and other factors, are associated with a high risk of developing NEC (Niño et al., 2016; Caplan et al., 2019; Masi et al., 2021). It is necessary to explore the pathogenesis and therapeutic targets of NEC to reduce neonatal mortality rate and improve the quality of life of premature infants.

One possible explanation may be suggested by Paneth cell (PC), a highly specific cell of the small intestinal, which have the function of coordinating the physiological environment of the small intestine. The history of this special type of intestinal columnar epithelial cell can

Abbreviations: NEC, necrotizing enterocolitis; PC, Paneth cell; Ig, immunoglobulin; TNF-α, tumor necrosis factor-α; IL-17, Interleukin-17; HD5, human defensin 5; ISCs, intestinal stem cells; NOD2, nucleotide-binding oligomerization domain protein 2; NF-κB, nuclear factor-κB; XIAP, X-linked inhibitor of apoptosis protein; RIPK2, receptor kinase 2; MLKL, mixed-lineage kinase domine-like protein; FADD, Fas-associated protein death domain; PERK, protein kinase RNA-like ER kinase; NEK7, NIMA-related kinase 7; NLRP3, NOD-like receptor pyrin domain-containing protein 3; GSDMD, gasdermin D.

be traced back to a century ago when it was first documented by Gustav Schwalbe and detailed in 1888 by Josef Paneth in Vienna (Paneth, 1887). The identity of the content of PC was still largely unknown. Not until 1967, lysozyme, as a constituent of the PC granules, was found in mouse intestinal mucosa (Deckx et al., 1967). A large number of antibacterial substances and proteins contained in PC play an important role in maintaining the host-microbial relationship, maintaining intestinal microbial balance, regulating intestinal stem cell development and immune protection (Clevers and Bevins, 2013) (Figure 1).

In this review, we explore the relationship between PCs and intestinal epithelial barrier, how PCs affect intestinal stem cell differentiation and gut microbiota ecological balance, and whether several modes of intestinal epithelial death contribute to NEC by affecting PCs function.

2 The characteristics and biological role of PC

PCs are highly specific cells of the small intestine, located within Lieberkühn crypts in a pyramidal shape (Paneth, 1887). Under normal conditions, PCs are located all along the entire length of the small intestine, but under disease conditions, they may also be found in the esophagus and colon (Chen et al., 2015; Singh et al., 2020; Gleizes et al., 2021). PCs first appear at 13.5 weeks of gestation, and at this point, their density is very low (Stanford et al., 2020). As gestational age increases, the number of PCs gradually increase until they reach maturity at term (Kandasamy et al., 2014). Preterm infants are prone to abnormal colonization of intestinal microorganisms and enrichment of special metabolites within a few weeks after birth (Korpela et al., 2018; Samara et al., 2022). During this period, PCs are not mature and anti-inflammatory factor levels are insufficient; hence, they cannot play a role in defending against pathogen invasion and protecting the intestinal barrier, increasing the susceptibility to NEC (Autran et al., 2018; Lueschow et al., 2018; Li et al., 2020).

Most of the functions of PCs are related to their secreted products. Specific antibacterial products, lysozyme, and a variety of antimicrobial peptides in PCs can form an immune barrier near the crypt epithelium to resist the invasion of pathogenic microorganisms (Yu S. et al., 2020; Azabdaftari and Uhlig, 2021). By secreting Wnt, Notch, EGF, and other signals, PCs form a "stem cell niche" with intestinal stem cells (ISCs) in the intestinal crypts, regulate the proliferation and differentiation of ISCs and self-renewal of intestinal epithelial cells (IECs), and maintain homeostasis of the mechanical barrier of the intestinal mucosa (Yu et al., 2018; van Es et al., 2019; Böttcher et al., 2021; Weis et al., 2021) (Figure 2).

3 PCs and immune regulation

The intestinal barrier is an important defense against harmful substances and pathogenic microorganisms found in the external environment. It is composed of four parts: the biological barrier composed of intestinal flora, the chemical barrier composed of the mucus layer, the mechanical barrier composed of epithelial cells, and the immune barrier composed of immune cells and immune factors (Atarashi et al., 2015; Moore et al., 2016; Sun et al., 2018; Doron et al., 2021). Intestinal homeostasis depends on the combined regulation of immune, mechanical, and biological barriers, which PCs play a major role in the maintenance of these three barriers.

PCs secrete antimicrobial peptides and proteins (AMPs), enzymes and growth factors, which form a biochemical barrier near the crypts, prevent bacterial invasion, and maintain stability of the intestinal environment (Brodrick et al., 2011; Gubatan et al., 2021; He et al., 2022). These defense proteins are released into the intestinal lumen as "degranulation" by cytoplasmic granules at the top of PC(Ayabe et al., 2000).

AMPs fall into two major classes in the human body: cathelicidins and defensins (Liang et al., 2022). During the neonatal period, cathelicidins play an important role in the maintenance of environmental homeostasis in epithelial cells (Chen et al., 2021; Gubatan et al., 2021). As time goes by, immature PCs are gradually replaced by mature PCs, while cathelicidins also gradually decrease and eventually disappear (Ménard et al., 2008). The protective effect of defensin in the intestinal barrier is dominant (Fusco et al., 2021). The transition of AMPs from one to the other is probably around the second trimester of human pregnancy (between 20 and 28 weeks) and 10–21 days after birth in mice, which highly coincides with the onset of NEC (Mallow et al., 1996; Hu et al., 2019).

The main defensin secreted by PCs is α-defensin (also known as cryptdins in mice) (Ayabe et al., 2002). The human defensin (HD)5 and HD6 have indirect antiviral effects owing to their similarity to viral coats and their ability to affect DNA and RNA replication (Bevins, 2013; Ehmann et al., 2019). HD5 can also be used as an effective marker to identify PCs (Heida et al., 2016). Before 28 weeks of gestation, HD5 expression is correlated with the number of PCs and gradually increases. Between weeks 29 and 37, the number of PCs and the level of HD5 rapidly increase until the expression of HD5 is no longer correlated with the number of PCs (McElroy et al., 2013). The clinical peak of NEC incidence occurs at 29–33 weeks of corrected gestational age, which coincides with the rapid growth of PCs and expression of HD5 (Ehmann et al., 2019). The defense proteins secreted by PCs are overactivated in the immature immune system, resulting in the occurrence of inflammation and colonization by pathogenic bacteria in the immature intestinal tract, ultimately leading to the occurrence of NEC (González-Rivera et al., 2011; McElroy et al., 2013).

Lysozyme is considered to be an indicator of PC localization (Peeters and Vantrappen, 1975). Lysozyme can destroy microbial cell membranes and regulate immune function (Bel and Hooper, 2018). Lysozyme achieves bactericidal action by processing the bacterial cell wall and destroying the permeability of the bacterial cell membrane (Bel et al., 2017). In the absence of PCs, the secretion of specific antibacterial substances, such as defensins and lysozyme, is reduced, leading to the inability to resist the invasion by foreign pathogens and microorganisms (Schaart et al., 2009). When the intestinal barrier is destroyed, more pathogens enter the intestine, and break the serious imbalance of the intestinal environment (Bergmann et al., 2013). This suggests that the relative PC deficiency was the key to the intestinal inflammation.

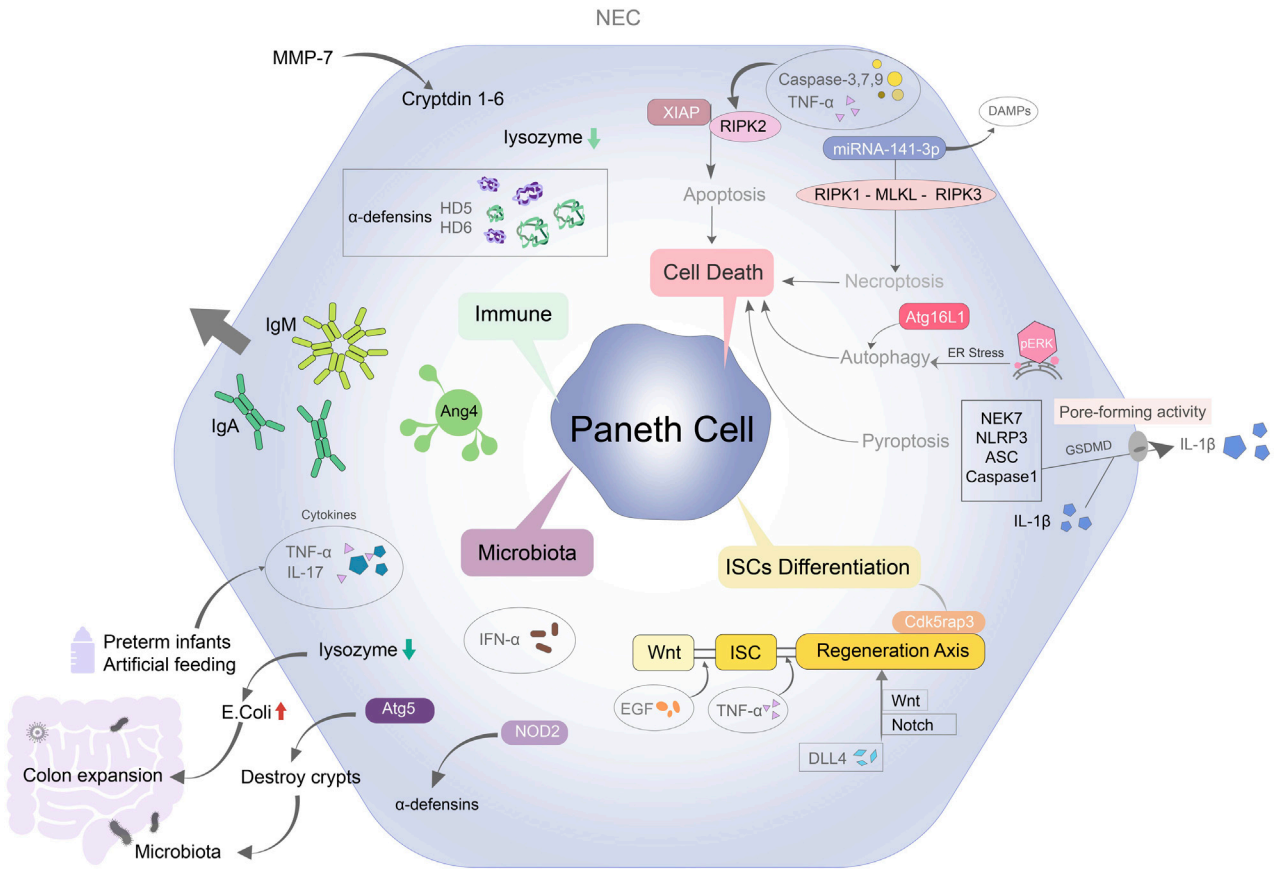

FIGURE 1
Overview of mechanisms regulating Paneth cell leads to NEC. PC can contribute to NEC through immune system, microbiota, cell deaths and intestinal stem cells differentiation. PC protects immune barrier function by secreting specific antimicrobial peptides such as lysozyme and defensins. The inflammatory factors in the preterm infants and artificial feeding infants with NEC are increased. Lysozyme secreted by PCs is decreased, the structure of intestinal crypts is destroyed, and a large number of *Escherichia coli* colonize in the intestinal tract, which aggravates the degree of colon expansion. Disruption of the functional structure of PCs also affects Wnt and Notch signaling mediated intestinal stem cell differentiation. PC-mediated apoptosis, autophagy, necroptosis and pyroptosis are also closely related to NEC.

The immunological changes of NEC include the deficiency of anti-inflammatory mediators and the increase of pro-inflammatory mediators, most of which are produced by PCs. Secretory immunoglobulin (Ig)A and M are produced at the apex of PCs. Secretory IgA is released through hydrolysis of the apical part of the PC membrane, which inhibits the adhesion and adsorption of pathogens (viruses and bacteria) in the intestinal mucosa that form the biofilm, thereby protecting the mucosal barrier (Wang et al., 2017). PCs are also an important source of cathepsin G, which sterilizes the intestinal epithelium, regulates the immune response, and destroys pathogens (Zamolodchikova et al., 2020). When intestinal mucosal inflammation occurs, PCs are stimulated by microorganisms to release a large amount of lysozyme and cathepsin G, which kill harmful pathogens and mediate homeostasis of the intestinal flora and intestinal biological barrier (Burclaff et al., 2022).

PCs also produce the pro-inflammatory tumor necrosis factor-α (TNF-α), which accumulates in secretory granules and enhances systemic inflammation (Tan et al., 1993). When PCs are destroyed, TNF-α is released, resulting in increased diffusion of IECs (Bykov, 2014). Interleukin-17 (IL-17) is another anti-inflammatory factor secreted by PCs, which co-reacts with TNF-α in acute inflammation to participate in the rapid response to systemic inflammatory factors (Gyongyosi et al., 2019). IL-17A is normally produced by activated T lymphocytes (Park et al., 2005). However, production of IL-17A in PCs is induced in contrast to TNF-α secretion, and increases when the intestinal is infected (Bykov, 2014). Therefore, the content of anti-inflammatory mediators in PCs decreases, and the increase in the content of pro-inflammatory mediators can be used as one of the evaluation indicators of NEC.

4 PCs and impaired differentiation of ISCs

ISCs, as an important component of environmental homeostasis in the gut, are characterized by the expression of the stem cell marker Lgr5^{+}(Tian et al., 2011). Differentiated cells migrate from the base of the crypt to the villus, whereas PCs remain at the base of the crypt and are distributed between Lgr5+ stem cells, providing ligands such

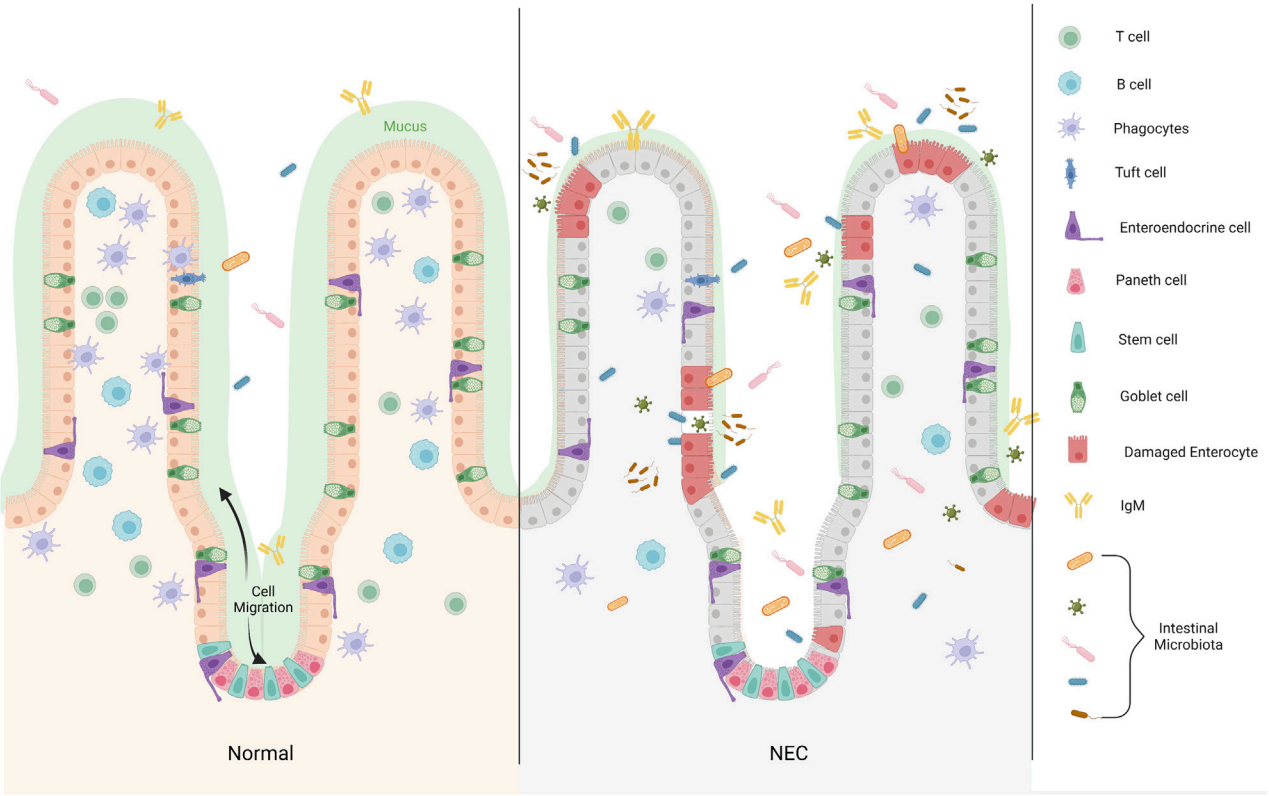

FIGURE 2
The distribution of Paneth cell in epithelium of the small intestine. Differentiated cells migrate from the base of the crypt to the villus, whereas PCs remain at the base of the crypt and are distributed between Lgr5+ stem cells. In the development of NEC, the microbial dysbiosis decrease binding of bacteria by IgA, and the mucosal layer becomes thinner. Increased inflammatory infiltration reduce the secretion of immune cells in the intestinal lumen, which is not enough to resist the invasion of pathogenic microorganisms. Large numbers of microbiota pass through the disrupted intestinal barrier (Created with BioRender.com).

as Wnt, Notch, epidermal growth factor (EGF), TGF-α to ISCs(Sato et al., 2011).

As an important factor in ISC differentiation, Wnt signaling regulates ISC lineage differentiation by activating the β-catenin/Tcf transcription program and regulating the activity of mitogen-activated protein kinase (Zha et al., 2019; Wang et al., 2020; Wang et al., 2021; Li et al., 2023). Cell-specific knockout of PC *in vivo* resulted in the loss of Lgr5+ stem cells (Pentinmikko et al., 2019). In both mouse NEC models and clinical NEC children, ISC expression, Wnt activity and intestinal cell differentiation were downregulated (Li et al., 2019). Notch is an inhibitor of Wnt: when the Wnt level increases or the Notch level decreases, the signal is transmitted to ISCs and stimulates the continuous renewal of PCs(Pentinmikko et al., 2019). The expression of Notch signaling is very low under normal conditions (Sancho et al., 2015). When the intestine is injured, Notch signaling is activated to stimulate the release of ISCs ligands from PCs which plays a role in maintaining the intestinal homeostasis (Yu et al., 2018; Jones et al., 2019). Notch ligand DLL4 binds to Notch1 and Notch2 to promote the homeostasis of the ISC microenvironment as well as the growth and development of ISCs (Dominguez-Brauer et al., 2016).

ISCs are essential for maintaining intestinal homeostasis and protecting the neonatal intestine (Hua et al., 2012; Zou et al., 2018). Intestinal epithelial cell lineages are damaged by stressors such as ischemia, hypoxia, and low temperature, and ISCs are responsible for promoting the repair and regeneration of IEC lineages damaged by these stressors (Lee C. et al., 2018; Holmberg et al., 2018; Sittipo et al., 2021). The loss of Cdk5 regulatory subunit-related protein 3, which is secreted by PCs, can affect the cell cycle progression of ISCs, cause differentiation of ISCs into PCs and the proliferation of IECs (Quintero et al., 2021). Many studies have found that the number of PCs and ISCs is significantly reduced in NEC mice. When NEC and other inflammatory reactions occur, the amount of IL-22 (secreted by CD4+T cells) decreases, which can affect the differentiation and maturation of PCs (Lindemans et al., 2015). The secretion of Wnt and Notch signals in PCs is inhibited, which prevent the differentiation and maturation of ISC (Zha et al., 2019; Gaudino et al., 2021). These studies highlight the critical link between ISC function, PC-secreted ISC ligands, and intestinal barrier disruption in NEC.

5 PCs and imbalance of intestinal flora

The intestinal microbiota is important for regulating physiology, metabolism, and the host immune response. Intestinal homeostasis depends on the co-regulation of symbiotic bacteria, IECs, and

mucosal immune cells. Maintaining the balance of intestinal microbiota is crucial for sustaining the host nutritional metabolism and immune system (Lee Y.-S. et al., 2018). Intestinal dysbiosis have been associated with a variety of diseases, including inflammatory bowel disease, NEC, sepsis, diabetes, and obesity (Wellman et al., 2017).

PC-derived α-defensin is the main bactericidal protein in the intestinal epithelium. α-defensin promotes homeostasis by establishing and maintaining the intestinal microbiota (Kamioka et al., 2022). A reduction in the levels of α-defensin leads to alterations in the composition of the intestinal microbiota, which leads to the occurrence of various diseases (Hayase et al., 2017; Takakuwa et al., 2019). α-defensin level is significantly reduced in patients with coding mutations in the nucleotide-binding oligomerization domain protein 2 (NOD2). These mutations are the basis of genetic susceptibility to a variety of intestinal diseases; therefore, the reduced expression of α-defensin in PCs may change the composition of the intestinal microbiota and lead to a series of related intestinal inflammatory reactions (Fakhoury et al., 2020).

The loss of PCs results in decreased levels of lysozymes, altered intestinal bacterial composition, increased abundance of *E. coli*, hypersensitivity of the viscera, the epithelial proliferation and anti-inflammatory macrophages in the intestinal (Yu T.-X. et al., 2020; Nakamura et al., 2021; Chiang et al., 2022). Oral lysozyme can prevent the excessive growth of *E. coli* and visceral hypersensitivity induced by maternal isolation, thus achieving the prevention and treatment of NEC (Riba et al., 2017). There are a variety of bacteria in the gut that interact during the development and progression of NEC. Intestinal bacterial infection causes massive bacterial replication and increased activity of specific organisms, leading to an imbalance in the metabolites of the intestinal environment and ultimately causing NEC (Morowitz et al., 2010). However, increased levels of NEC-related metabolites, such as some small bactericidal peptides, bacteriocin, firmicide (produced by *Clostridium perfringens* and *C. difficile*), encoded polypeptides, and butylactones, result in cell lysis and the release of immune-stimulating compounds, increasing the severity of NEC (Olm et al., 2019).

The developmental pattern of PCs causes exposure of premature infants to various external pathogenic factors before the developing PCs can reach their full potential (Kandasamy et al., 2014). Additionally, the disruption of the normal intestinal tract can induce NEC (White et al., 2017; Lueschow et al., 2018; Lueschow et al., 2020). Exogenous factors also affect the gut microbiota. Murine norovirus causes increased interferon (IFN)-γ expression, intestinal microbiome-mediated inflammation, the loss of PCs, and bacterial dysregulation in mouse intestinal immunopathology (Farin et al., 2014; Rocha-Pereira et al., 2018). Loss of the specific autophagy protein ATG5 in PCs destroys intestinal crypts and causes excessive intestinal inflammation (Burger et al., 2018). When premature exposure to exogenous antigens occurs (for example, during formula feeding), the levels of inflammatory cytokines increase, and the resulting anti-inflammatory environment results in the formation of fewer PCs with compromised functional capacity (Qi-Xiang et al., 2022). This environment leads to reduced levels of adenosine phosphate, affecting the differentiation process of stem cells. The loss of intestinal epithelial cells makes the intestinal barrier unable to resist the invasion of inflammatory factors and intestinal microorganisms, which ultimately contributes to NEC (Autran et al., 2018; Battistini et al., 2020; Lueschow et al., 2020; Nolan et al., 2020).

6 PCs and IEC death

The death modes of intestinal cells include apoptosis, autophagy, necrosis, necroptosis, and pyroptosis. The main pathological change that occurs during NEC is intestinal tissue necrosis, and many different cell death pathways are related to the pathogenesis of NEC. PCs may participate in the pathogenesis of NEC by regulating multiple types of intestinal cell death.

6.1 Apoptosis

Apoptosis is a common mode of death in normal cells that manifests as cell pseudopodia contraction, cell pyknosis, fragmentation, dissolution, and plasma membrane blistering (Günther et al., 2013). Some genes and protein products related to cell proliferation and apoptosis are related to the development of PCs and NEC.

Although apoptosis is not an extremely important mechanism for maintaining intestinal homeostasis, maladjusted or excessive apoptosis can seriously impair intestinal physiology. In mice with an elevated apoptosis phenotype of the IECs, spontaneous intestinal inflammation or increased sensitivity to intestinal inflammation occurs (Li et al., 2018). Specific deletion of the gene *NEMO* (nuclear factor-κB (NF-κB) basic regulator) in IECs leads to intraepithelial TNF-dependent apoptosis, followed by intestinal barrier rupture and bacterial translocation into the intestinal wall, triggering a cellular inflammatory response (Nenci et al., 2007).

The occurrence of intestinal inflammation is related to the disappearance of antibiotics and the destruction of intestinal barrier. X-linked inhibitor of apoptosis protein (XIAP), which is a key component of the NOD1 and NOD2 complex, is a necessary ubiquitin ligase for NOD2 signaling (Wang et al., 2017). It is recruited into the NOD complex via receptor kinase 2 (RIPK2), ubiquitinated RIPK2, and the recruitment of linear ubiquitin chain assembly complexes linking NOD-mediated bacterial recognition with NF-κB activation and IL secretion (Larabi et al., 2020). Additionally, XIAP is an inhibitor of non-immunogenic apoptotic cell death pathways; it directly binds and inhibits caspase-3, -7, and -9, thus limiting apoptotic cell death (Damgaard et al., 2012; Damgaard et al., 2013). XIAP does not influence the intestinal microbiota but is essential for maintaining homeostasis. The levels of bactericidal substances, such as defensin and lysozyme, were significantly reduced in the ileum of XIAP-knockout mice, which suggests a deficiency of PCs(Wahida et al., 2021). XIAP reduces levels of inflammatory cytokines such as IL-1 and TNF-α; thus, the loss of XIAP may contribute to the loss of TNF receptor-1-dependent PCs (Azabdaftari and Uhlig, 2021; Strigli et al., 2021). Furthermore, loss of XIAP reduces toll-like receptor 5 and TNF signaling in myeloid cells, resulting in defects or disorders in the PCs and myeloid cells, contributing to IEC apoptosis (Wahida et al., 2021). The significantly increased

inflammatory IL, TNF-α and caspase-3 in intestinal epithelial cells during autophagy can cause mucosal injury by increasing intestinal mucosal permeability, which is also important in NEC (Zhou et al., 2017).

6.2 Necroptosis

Necroptosis is a special mode of death that exhibits similarities with both apoptosis and necrosis. The cytological morphology of necroptosis is similar to that of traditional necrosis, which is a highly inflammatory cell death. During necroptosis, RIPK1 recruits and activates RIPK3, which phosphorylates mixed-lineage kinase domine-like protein (MLKL), leading to MLKL oligomerization and transfer to the cell membrane; MLKL then depolarizes the cell membrane, leading to cell rupture (Liu et al., 2021). RIPK1 is a major regulator of IEC survival, homeostasis, and inflammation. Specific knockdown of the RIPK1 in IECs can contribute to apoptosis, villus atrophy, and loss of PCs (Dannappel et al., 2014).

Necroptosis may be an important form of NEC-related IEC death. The expression of RIPK1, RIPK3, and MLKL in the intestinal mucosa of children with NEC was significantly upregulated, and this upregulation correlated with the severity of NEC (Werts et al., 2020). Intestinal epithelial cell-specific caspase-8-deficient mice have significantly increased necroptosis levels, resulting in a decrease in the number of PCs, showing progressive ileocecal inflammatory lesions and a high susceptibility to colitis, indicating that PC necroptosis is involved in the occurrence of intestinal inflammation (Sanders, 2005; Nenci et al., 2007; Schwarzer et al., 2020). When programmed necroptosis occurs, injury-related molecular patterns in cells are released, resulting in persistent inflammation and secondary tissue damage, which reduces the secretion of antimicrobial peptides and lysozyme and weakens the defense function against pathogens (Bertheloot et al., 2021). The high expression level of RIPK1/RIPK3 in human and mouse PCs suggests that PCs have a unique sensitivity to necroptosis (Duan et al., 2022). PC necroptosis-induced intestinal inflammation is consistent with the clinical characteristics of NEC in preterm infants, severe intestinal mucosal necrosis, and severe systemic inflammatory response, suggesting that PC necroptosis may be an important event in the pathogenesis of NEC.

Previous studies have reported necroptosis of IECs in NEC mice and that inhibiting necroptosis of IECs could reduce inflammation in these mice. We further found necroptosis of PCs in the intestinal crypts in NEC mice (Shi et al., 2018; Liu et al., 2022). When PCs experience programmed necrosis, resistance to pathogens is weakened, proliferation and differentiation of ISCs is impaired, repair of the intestinal epithelial barrier is weakened, and a large number of inflammatory factors are released. The "triple injury" pattern of intestinal mucosal inflammation is consistent with the clinical characteristics of acute onset, severe intestinal mucosal necrosis, and severe systemic inflammatory response in children with NEC. The occurrence of PC necroptosis is spatially and temporally consistent with NEC events. Therefore, we speculate that necroptosis of PCs is an important event in the pathogenesis of NEC. The dysfunction of PC function and number can lead to the dysfunction of the programmed necrosis pathway "RIPK1-RIPK3-MLKL", which ultimately contributes to the occurrence of NEC.

6.3 Autophagy

Autophagy refers to the isolation of cytoplasmic substances into autophagosomes, which are then fused with lysozyme, resulting in content degradation that can help remove misfolded or aggregated proteins or resolve other intracellular damage (Günther et al., 2013). Similar to apoptosis, autophagy tends to prevent inflammation because the degradation of dead cells occurs in another cell. Autophagy is essential for the development, maintenance, and functioning of PCs (van Es and Clevers, 2014). Since PCs tend to live longer than most other cells in the gut and contain excessive amounts of accumulated proteins that can be recycled by other neighboring cells, autophagy is activated when PCs are damaged or stressed (Günther et al., 2013).

The autophagic gene *Atg16L1* is expressed in IECs (Cadwell et al., 2008). Mice with *Atg16L1* deletion in the intestinal epithelium showed significant defects in the PC granular exocytosis pathway, resulting in reduced antimicrobial peptide secretion. In mice infected with norovirus, *Atg16L1* has a germline gene-trapping mutation, which can further induce morphological and functional defects in PCs (Matsuzawa-Ishimoto et al., 2017; Larabi et al., 2020). Both clinical samples and animal models have suggested that autophagy gene ATG16L1 can promote the severity of NEC by promoting intestinal microbiota-related inflammation and affecting intestinal immune function (Sampath et al., 2017).

Secretory autophagy can also occur in PCs when endoplasmic reticulum (ER) stress leads to phosphorylation of protein kinase RNA-like ER kinase (PERK) (Adolph et al., 2013). p-PERK affects the phosphorylation of initiation factor 2α (ELF2A), and DC MyD88 is specifically activated by dendritic cells at the TLR signal transduction junction to inactivate Paneth cells, resulting in PC-lysozyme secretory autophagy (Deuring et al., 2014; Yu S. et al., 2020). Stem cells can restore intestinal epithelial tight junction and permeability by regulating ER stress in NEC. (Li et al., 2021).

In conclusion, the specific autophagy that occurs during PC homeostasis is dependent on the microbiome and the proinflammatory cytokine IFN-γ. *Atg16L1* and upstream autophagic *Atg5* have a compensatory role in ER stress as they control the autophagy pathway and help to maintain IEC homeostasis. The disruption of mitochondrial homeostasis in PCs is caused by the synergism of *Atg16L1* deletion and ER stress (Cray et al., 2021).

6.4 Pyroptosis

Under stress conditions (such as intestinal ischemia-reperfusion injury) or lipopolysaccharide stimulation, another inflammatory mode of cell death called pyroptosis can occur (Jia et al., 2020). Stress can induce TLR4/NF-κB activation of the NIMA-related kinase 7 (NEK7) promoter region and increase NEK7 expression (Chen et al., 2019). NEK7 interacts with NOD-like receptor pyrin domain-containing protein 3 (NLRP3) and regulates the activation of the NLRP3 inflammasome. These

inflammatory bodies act on caspase-8 and convert pro-caspase-1 to cleaved caspase-1 (Fritsch et al., 2019; Patankar and Becker, 2020). Gasdermin D (GSDMD) is cleaved by active caspase-1/4/5/11 and caspase-3 through an intermediate linker, resulting in cytoplasmic swelling and "pore-making activity" (Gaidt et al., 2016; Kovacs and Miao, 2017; Tan et al., 2020). The release of N-terminal fragments of GSDMD, along with inflammatory factors, such as IL-β and IL-18, induces pyroptosis (Huang et al., 2019). Recent studies have shown that the NLRP3 inflammasome is involved in a variety of adaptive immune diseases and that NLRP3 mutations could lead to chronic autoinflammatory syndrome (Yu et al., 2019). The expression of NLRP3 in NEC is significantly upregulated and could stimulate the production of pro-inflammatory cytokines such as IL-1β, IL-6, and IL-18, leading to pyroptosis (Grishin et al., 2016). Intracellular IFN-γ in murine PCs, an important mediator of intestinal inflammation, alters mitochondrial integrity and membrane potential of PCs, leading to a TORC1-dependent pyroptosis distinct from the classical cell death pathway (Araujo et al., 2021). However, the relationship between pyroptosis and NEC remains unclear, which may be a new direction for future research.

Summary

PCs are a type of IECs that play an important role in maintaining intestinal microbiota homeostasis, ISC growth, and IEC death. Various growth factors secreted by PCs are important for maintaining the intestinal barrier as a defense against pathogens. The loss of PCs causes loss of α-defensin, immunoglobulins, and other products, followed by disruption of the intestinal barrier, thereby leading to NEC. Disruptions of PCs can also reduce the production of lysozyme and other factors that maintain intestinal microbiota homeostasis, resulting in intestinal microbiota disorders and NEC. PCs secrete Wnt3, Notch, and other signaling factors to maintain the function of ISCs and prevent the occurrence of NEC. Autophagy, necroptosis, and apoptosis are also closely related to PCs. Reduced production of antimicrobial peptides by PCs makes the intestine hypersensitive and highly prone to NEC. The development of PCs, intestinal flora homeostasis, and pathogenesis of NEC are closely related; however, only few studies have investigated the possible mechanism of this relationship. Therefore, further exploration of the mechanism affecting the number and function of PCs is of great significance for the prevention, early diagnosis, and treatment of NEC.

Author contributions

JY collected the literatures, conceptualized the idea, wrote a first draft, and revised the manuscript according to YS's comments, modifications, and suggestions. All authors listed have made a substantial, direct, and intellectual contribution to the work and approved it for publication. All authors contributed to the article and approved the submitted version.

Funding

This work was supported by the National Natural Science Foundation of China (82171709 and 81801500), the 345 Talent Project of Shengjing Hospital (M1392 and M1415), and Key R&D Guidance Plan Project in Liaoning Province (2020JH1/10300001).

Conflict of interest

The authors declare that the research was conducted in the absence of any commercial or financial relationships that could be construed as a potential conflict of interest.

Publisher's note

References

Adolph, T. E., Tomczak, M. F., Niederreiter, L., Ko, H.-J., Böck, J., Martinez-Naves, E., et al. (2013). Paneth cells as a site of origin for intestinal inflammation. *Nature* 503 (7475), 272–276.

Araujo, A., Safronova, A., Burger, E., López-Yglesias, A., Giri, S., Camanzo, E. T., et al. (2021). IFN-γ mediates Paneth cell death via suppression of mTOR. *ELife* 10.

Atarashi, K., Tanoue, T., Ando, M., Kamada, N., Nagano, Y., Narushima, S., et al. (2015). Th17 cell induction by adhesion of microbes to intestinal epithelial cells. *Cell* 163 (2), 367–380. doi:10.1016/j.cell.2015.08.058

Autran, C. A., Kellman, B. P., Kim, J. H., Asztalos, E., Blood, A. B., Spence, E. C. H., et al. (2018). Human milk oligosaccharide composition predicts risk of necrotising enterocolitis in preterm infants. *Gut* 67 (6), 1064–1070. doi:10.1136/gutjnl-2016-312819

Ayabe, T., Satchell, D. P., Pesendorfer, P., Tanabe, H., Wilson, C. L., Hagen, S. J., et al. (2002). Activation of Paneth cell alpha-defensins in mouse small intestine. *J. Biol. Chem.* 277 (7), 5219–5228. doi:10.1074/jbc.M109410200

Ayabe, T., Satchell, D. P., Wilson, C. L., Parks, W. C., Selsted, M. E., and Ouellette, A. J. (2000). Secretion of microbicidal alpha-defensins by intestinal Paneth cells in response to bacteria. *Nat. Immunol.* 1 (2), 113–118. doi:10.1038/77783

Azabdaftari, A., and Uhlig, H. H. (2021). Paneth cell dysfunction and the intestinal microbiome in XIAP deficiency. *Sci. Immunol.* 6 (65), eabm0293. doi:10.1126/sciimmunol.abm0293

Battersby, C., Santhalingam, T., Costeloe, K., and Modi, N. (2018). Incidence of neonatal necrotising enterocolitis in high-income countries: A systematic review. *Archives Dis. Child. Fetal Neonatal Ed.* 103 (2), F182–F189. doi:10.1136/archdischild-2017-313880

Battistini, C., Ballan, R., Herkenhoff, M. E., Saad, S. M. I., and Sun, J. (2020). Vitamin D modulates intestinal microbiota in inflammatory bowel diseases. *Int. J. Mol. Sci.* 22 (1), 362. doi:10.3390/ijms22010362

Bel, S., and Hooper, L. V. (2018). Secretory autophagy of lysozyme in Paneth cells. *Autophagy* 14 (4), 719–721. doi:10.1080/15548627.2018.1430462

Bel, S., Pendse, M., Wang, Y., Li, Y., Ruhn, K. A., Hassell, B., et al. (2017). Paneth cells secrete lysozyme via secretory autophagy during bacterial infection of the intestine. *Sci. (New York, N.Y.)* 357 (6355), 1047–1052. doi:10.1126/science.aal4677

Bergmann, K. R., Liu, S. X. L., Tian, R., Kushnir, A., Turner, J. R., Li, H.-L., et al. (2013). Bifidobacteria stabilize claudins at tight junctions and prevent intestinal barrier

dysfunction in mouse necrotizing enterocolitis. *Am. J. Pathology* 182 (5), 1595–1606. doi:10.1016/j.ajpath.2013.01.013

Bertheloot, D., Latz, E., and Franklin, B. S. (2021). Necroptosis, pyroptosis and apoptosis: An intricate game of cell death. *Cell. Mol. Immunol.* 18 (5), 1106–1121. doi:10.1038/s41423-020-00630-3

Bevins, C. L. (2013). Innate immune functions of α-defensins in the small intestine. *Dig. Dis. (Basel, Switz.* 31 (3-4), 299–304. doi:10.1159/000354681

Blakely, M. L., Tyson, J. E., Lally, K. P., Hintz, S. R., Eggleston, B., Stevenson, D. K., et al. (2021). Initial laparotomy versus peritoneal drainage in extremely low birthweight infants with surgical necrotizing enterocolitis or isolated intestinal perforation: A multicenter randomized clinical trial. *Ann. Surg.* 274 (4), e370–e380. doi:10.1097/SLA.0000000000005099

Böttcher, A., Büttner, M., Tritschler, S., Sterr, M., Aliluev, A., Oppenländer, L., et al. (2021). Non-canonical Wnt/PCP signalling regulates intestinal stem cell lineage priming towards enteroendocrine and Paneth cell fates. *Nat. Cell Biol.* 23 (1), 23–31. doi:10.1038/s41556-020-00617-2

Brodrick, B., Vidrich, A., Porter, E., Bradley, L., Buzan, J. M., and Cohn, S. M. (2011). Fibroblast growth factor receptor-3 (FGFR-3) regulates expression of paneth cell lineage-specific genes in intestinal epithelial cells through both TCF4/beta-catenin-dependent and -independent signaling pathways. *J. Biol. Chem.* 286 (21), 18515–18525. doi:10.1074/jbc.M111.229252

Burclaff, J., Bliton, R. J., Breau, K. A., Ok, M. T., Gomez-Martinez, I., Ranek, J. S., et al. (2022). A proximal-to-distal survey of healthy adult human small intestine and colon epithelium by single-cell transcriptomics. *Cell. Mol. Gastroenterology Hepatology* 13 (5), 1554–1589. doi:10.1016/j.jcmgh.2022.02.007

Burger, E., Araujo, A., López-Yglesias, A., Rajala, M. W., Geng, L., Levine, B., et al. (2018). Loss of paneth cell autophagy causes acute susceptibility to toxoplasma gondii-mediated inflammation. *Cell host microbe* 23 (2), 177–190. doi:10.1016/j.chom.2018.01.001

Bykov, V. L. (2014). Paneth cells: History of discovery, structural and functional characteristics and the role in the maintenance of homeostasis in the small intestine. *Morfol. St. Petersbg. Russ.* 145 (1), 67–80.

Cadwell, K., Liu, J. Y., Brown, S. L., Miyoshi, H., Loh, J., Lennerz, J. K., et al. (2008). A key role for autophagy and the autophagy gene Atg16l1 in mouse and human intestinal Paneth cells. *Nature* 456 (7219), 259–263. doi:10.1038/nature07416

Caplan, M. S., Underwood, M. A., Modi, N., Patel, R., Gordon, P. V., Sylvester, K. G., et al. (2019). Necrotizing enterocolitis: Using regulatory science and drug development to improve outcomes. *J. Pediatr.* 212, 208–215.e1. doi:10.1016/j.jpeds.2019.05.032

Chen, K., Yoshimura, T., Yao, X., Gong, W., Huang, J., Dzutsev, A. K., et al. (2021). Distinct contributions of cathelin-related antimicrobial peptide (CRAMP) derived from epithelial cells and macrophages to colon mucosal homeostasis. *J. Pathology* 253 (3), 339–350. doi:10.1002/path.5572

Chen, W., Frankel, W. L., Cronley, K. M., Yu, L., Zhou, X., and Yearsley, M. M. (2015). Significance of paneth cell metaplasia in barrett esophagus: A morphologic and clinicopathologic study. *Am. J. Clin. Pathology* 143 (5), 665–671. doi:10.1309/AJCPVUJMCVBC9PKM

Chen, X., Liu, G., Yuan, Y., Wu, G., Wang, S., and Yuan, L. (2019). NEK7 interacts with NLRP3 to modulate the pyroptosis in inflammatory bowel disease via NF-κB signaling. *Cell Death Dis.* 10 (12), 906. doi:10.1038/s41419-019-2157-1

Chiang, H.-Y., Lu, H.-H., Sudhakar, J. N., Chen, Y.-W., Shih, N.-S., Weng, Y.-T., et al. (2022). IL-22 initiates an IL-18-dependent epithelial response circuit to enforce intestinal host defence. *Nat. Commun.* 13 (1), 874. doi:10.1038/s41467-022-28478-3

Clevers, H. C., and Bevins, C. L. (2013). Paneth cells: Maestros of the small intestinal crypts. *Annu. Rev. Physiology* 75, 289–311. doi:10.1146/annurev-physiol-030212-183744

Cray, P., Sheahan, B. J., and Dekaney, C. M. (2021). Secretory sorcery: Paneth cell control of intestinal repair and homeostasis. *Cell. Mol. gastroenterology hepatology* 12 (4), 1239–1250. doi:10.1016/j.jcmgh.2021.06.006

Damgaard, R. B., Fiil, B. K., Speckmann, C., Yabal, M., zur Stadt, U., Bekker-Jensen, S., et al. (2013). Disease-causing mutations in the XIAP BIR2 domain impair NOD2-dependent immune signalling. *EMBO Mol. Med.* 5 (8), 1278–1295. doi:10.1002/emmm.201303090

Damgaard, R. B., Nachbur, U., Yabal, M., Wong, W. W.-L., Fiil, B. K., Kastirr, M., et al. (2012). The ubiquitin ligase XIAP recruits LUBAC for NOD2 signaling in inflammation and innate immunity. *Mol. Cell* 46 (6), 746–758. doi:10.1016/j.molcel.2012.04.014

Dannappel, M., Vlantis, K., Kumari, S., Polykratis, A., Kim, C., Wachsmuth, L., et al. (2014). RIPK1 maintains epithelial homeostasis by inhibiting apoptosis and necroptosis. *Nature* 513 (7516), 90–94. doi:10.1038/nature13608

Deckx, R. J., Vantrappen, G. R., and Parein, M. M. (1967). Localization of lysozyme activity in a Paneth cell granule fraction. *Biochimica Biophysica Acta* 139 (1), 204–207. doi:10.1016/0005-2744(67)90136-2

Deuring, J. J., Fuhler, G. M., Konstantinov, S. R., Peppelenbosch, M. P., Kuipers, E. J., de Haar, C., et al. (2014). Genomic ATG16L1 risk allele-restricted Paneth cell ER stress in quiescent Crohn's disease. *Gut* 63 (7), 1081–1091. doi:10.1136/gutjnl-2012-303527

Dominguez-Brauer, C., Hao, Z., Elia, A. J., Fortin, J. M., Nechanitzky, R., Brauer, P. M., et al. (2016). Mule regulates the intestinal stem cell niche via the Wnt pathway and targets EphB3 for proteasomal and lysosomal degradation. *Cell stem Cell* 19 (2), 205–216. doi:10.1016/j.stem.2016.04.002

Doron, I., Mesko, M., Li, X. V., Kusakabe, T., Leonardi, I., Shaw, D. G., et al. (2021). Mycobiota-induced IgA antibodies regulate fungal commensalism in the gut and are dysregulated in Crohn's disease. *Nat. Microbiol.* 6 (12), 1493–1504. doi:10.1038/s41564-021-00983-z

Duan, C., Xu, X., Lu, X., Wang, L., and Lu, Z. (2022). RIP3 knockdown inhibits necroptosis of human intestinal epithelial cells via TLR4/MyD88/NF-κB signaling and ameliorates murine colitis. *BMC Gastroenterol.* 22 (1), 137. doi:10.1186/s12876-022-02208-x

Ehmann, D., Wendler, J., Koeninger, L., Larsen, I. S., Klag, T., Berger, J., et al. (2019). Paneth cell α-defensins HD-5 and HD-6 display differential degradation into active antimicrobial fragments. *Proc. Natl. Acad. Sci. U. S. A.* 116 (9), 3746–3751. doi:10.1073/pnas.1817376116

Fakhoury, H. M. A., Kvietys, P. R., AlKattan, W., Anouti, F. A., Elahi, M. A., Karras, S. N., et al. (2020). Vitamin D and intestinal homeostasis: Barrier, microbiota, and immune modulation. *J. steroid Biochem. Mol. Biol.* 200, 105663. doi:10.1016/j.jsbmb.2020.105663

Farin, H. F., Karthaus, W. R., Kujala, P., Rakhshandehroo, M., Schwank, G., Vries, R. G. J., et al. (2014). Paneth cell extrusion and release of antimicrobial products is directly controlled by immune cell-derived IFN-γ. *J. Exp. Med.* 211 (7), 1393–1405. doi:10.1084/jem.20130753

Fritsch, M., Günther, S. D., Schwarzer, R., Albert, M.-C., Schorn, F., Werthenbach, J. P., et al. (2019). Caspase-8 is the molecular switch for apoptosis, necroptosis and pyroptosis. *Nature* 575 (7784), 683–687. doi:10.1038/s41586-019-1770-6

Fusco, A., Savio, V., Donniacuo, M., Perfetto, B., and Donnarumma, G. (2021). Antimicrobial peptides human beta-defensin-2 and -3 protect the gut during Candida albicans infections enhancing the intestinal barrier integrity: *In vitro* study. *Front. Cell. Infect. Microbiol.* 11, 666900. doi:10.3389/fcimb.2021.666900

Gaidt, M. M., Ebert, T. S., Chauhan, D., Schmidt, T., Schmid-Burgk, J. L., Rapino, F., et al. (2016). Human monocytes engage an alternative inflammasome pathway. *Immunity* 44 (4), 833–846. doi:10.1016/j.immuni.2016.01.012

Gaudino, S. J., Beaupre, M., Lin, X., Joshi, P., Rathi, S., McLaughlin, P. A., et al. (2021). IL-22 receptor signaling in Paneth cells is critical for their maturation, microbiota colonization, Th17-related immune responses, and anti-Salmonella immunity. *Mucosal Immunol.* 14 (2), 389–401. doi:10.1038/s41385-020-00348-5

Gleizes, A., Triki, M., Bonnet, S., Baccari, N., Jimenez-Dominguez, G., Covinhes, A., et al. (2021). RIP140 represses intestinal paneth cell differentiation and interplays with SOX9 signaling in colorectal cancer. *Cancers* 13 (13), 3192. doi:10.3390/cancers13133192

González-Rivera, R., Culverhouse, R. C., Hamvas, A., Tarr, P. I., and Warner, B. B. (2011). The age of necrotizing enterocolitis onset: An application of sartwell's incubation period model. *J. perinatology official J. Calif. Perinat. Assoc.* 31 (8), 519–523. doi:10.1038/jp.2010.193

Grishin, A., Bowling, J., Bell, B., Wang, J., and Ford, H. R. (2016). Roles of nitric oxide and intestinal microbiota in the pathogenesis of necrotizing enterocolitis. *J. Pediatr. Surg.* 51 (1), 13–17. doi:10.1016/j.jpedsurg.2015.10.006

Gubatan, J., Holman, D. R., Puntasecca, C. J., Polevoi, D., Rubin, S. J., and Rogalla, S. (2021). Antimicrobial peptides and the gut microbiome in inflammatory bowel disease. *World J. Gastroenterology* 27 (43), 7402–7422. doi:10.3748/wjg.v27.i43.7402

Günther, C., Neumann, H., Neurath, M. F., and Becker, C. (2013). Apoptosis, necrosis and necroptosis: Cell death regulation in the intestinal epithelium. *Gut* 62 (7), 1062–1071. doi:10.1136/gutjnl-2011-301364

Gyongyosi, B., Cho, Y., Lowe, P., Calenda, C. D., Iracheta-Vellve, A., Satishchandran, A., et al. (2019). Alcohol-induced IL-17A production in Paneth cells amplifies endoplasmic reticulum stress, apoptosis, and inflammasome-IL-18 activation in the proximal small intestine in mice. *Mucosal Immunol.* 12 (4), 930–944. doi:10.1038/s41385-019-0170-4

Hayase, E., Hashimoto, D., Nakamura, K., Noizat, C., Ogasawara, R., Takahashi, S., et al. (2017). R-Spondin1 expands Paneth cells and prevents dysbiosis induced by graft-versus-host disease. *J. Exp. Med.* 214 (12), 3507–3518. doi:10.1084/jem.20170418

He, G.-W., Lin, L., DeMartino, J., Zheng, X., Staliarova, N., Dayton, T., et al. (2022). Optimized human intestinal organoid model reveals interleukin-22-dependency of paneth cell formation. *Cell Stem Cell* 29 (9), 1718–1720. doi:10.1016/j.stem.2022.11.001

Heida, F. H., Beyduz, G., Bulthuis, M. L. C., Kooi, E. M. W., Bos, A. F., Timmer, A., et al. (2016). Paneth cells in the developing gut: When do they arise and when are they immune competent? *Pediatr. Res.* 80 (2), 306–310. doi:10.1038/pr.2016.67

Holmberg, F. E. O., Pedersen, J., Jørgensen, P., Soendergaard, C., Jensen, K. B., and Nielsen, O. H. (2018). Intestinal barrier integrity and inflammatory bowel disease: Stem cell-based approaches to regenerate the barrier. *J. Tissue Eng. Regen. Med.* 12 (4), 923–935. doi:10.1002/term.2506

Horbar, J. D., Carpenter, J. H., Badger, G. J., Kenny, M. J., Soll, R. F., Morrow, K. A., et al. (2012). Mortality and neonatal morbidity among infants 501 to 1500 grams from 2000 to 2009. *Pediatrics* 129 (6), 1019–1026. doi:10.1542/peds.2011-3028

Hu, X., Deng, J., Yu, T., Chen, S., Ge, Y., Zhou, Z., et al. (2019). ATF4 deficiency promotes intestinal inflammation in mice by reducing uptake of glutamine and expression of antimicrobial peptides. *Gastroenterology* 156 (4), 1098–1111. doi:10.1053/j.gastro.2018.11.033

Hua, G., Thin, T. H., Feldman, R., Haimovitz-Friedman, A., Clevers, H., Fuks, Z., et al. (2012). Crypt base columnar stem cells in small intestines of mice are radioresistant. *Gastroenterology* 143 (5), 1266–1276. doi:10.1053/j.gastro.2012.07.106

Huang, X., Feng, Z., Jiang, Y., Li, J., Xiang, Q., Guo, S., et al. (2019). VSIG4 mediates transcriptional inhibition of Nlrp3 and Il-1β in macrophages. *Sci. Adv.* 5 (1), eaau7426. doi:10.1126/sciadv.aau7426

Jia, Y., Cui, R., Wang, C., Feng, Y., Li, Z., Tong, Y., et al. (2020). Metformin protects against intestinal ischemia-reperfusion injury and cell pyroptosis via TXNIP-NLRP3-GSDMD pathway. *Redox Biol.* 32, 101534. doi:10.1016/j.redox.2020.101534

Jones, J. C., Brindley, C. D., Elder, N. H., Myers, M. G., Rajala, M. W., Dekaney, C. M., et al. (2019). Cellular plasticity of Defa4Cre-expressing paneth cells in response to Notch activation and intestinal injury. *Cell. Mol. Gastroenterology Hepatology* 7 (3), 533–554. doi:10.1016/j.jcmgh.2018.11.004

Kamioka, M., Goto, Y., Nakamura, K., Yokoi, Y., Sugimoto, R., Ohira, S., et al. (2022). Intestinal commensal microbiota and cytokines regulate Fut2+ Paneth cells for gut defense. *Proc. Natl. Acad. Sci. U. S. A.* 119 (3), e2115230119. doi:10.1073/pnas.2115230119

Kandasamy, J., Huda, S., Ambalavanan, N., and Jilling, T. (2014). Inflammatory signals that regulate intestinal epithelial renewal, differentiation, migration and cell death: Implications for necrotizing enterocolitis. *Pathophysiol. Official J. Int. Soc. For Pathophysiol.* 21 (1), 67–80. doi:10.1016/j.pathophys.2014.01.001

Korpela, K., Blakstad, E. W., Moltu, S. J., Strømmen, K., Nakstad, B., Rønnestad, A. E., et al. (2018). Intestinal microbiota development and gestational age in preterm neonates. *Sci. Rep.* 8 (1), 2453. doi:10.1038/s41598-018-20827-x

Kovacs, S. B., and Miao, E. A. (2017). Gasdermins: Effectors of pyroptosis. *Trends Cell Biol.* 27 (9), 673–684. doi:10.1016/j.tcb.2017.05.005

Larabi, A., Barnich, N., and Nguyen, H. T. T. (2020). New insights into the interplay between autophagy, gut microbiota and inflammatory responses in IBD. *Autophagy* 16 (1), 38–51. doi:10.1080/15548627.2019.1635384

Lee, C., Minich, A., Li, B., Miyake, H., Seo, S., and Pierro, A. (2018a). Influence of stress factors on intestinal epithelial injury and regeneration. *Pediatr. Surg. Int.* 34 (2), 155–160. doi:10.1007/s00383-017-4183-3

Lee, Y.-S., Kim, T.-Y., Kim, Y., Lee, S.-H., Kim, S., Kang, S. W., et al. (2018b). Microbiota-derived lactate accelerates intestinal stem-cell-mediated epithelial development. *Cell Host Microbe* 24 (6), 833–846.e6. doi:10.1016/j.chom.2018.11.002

Li, B., Lee, C., Cadete, M., Zhu, H., Koike, Y., Hock, A., et al. (2019). Impaired Wnt/β-catenin pathway leads to dysfunction of intestinal regeneration during necrotizing enterocolitis. *Cell Death Dis.* 10 (10), 743. doi:10.1038/s41419-019-1987-1

Li, B., Lee, C., Chuslip, S., Lee, D., Biouss, G., Wu, R., et al. (2021). Intestinal epithelial tight junctions and permeability can be rescued through the regulation of endoplasmic reticulum stress by amniotic fluid stem cells during necrotizing enterocolitis. *FASEB J. Official Publ. Fed. Am. Soc. For Exp. Biol.* 35 (1), e21265. doi:10.1096/fj.202001426R

Li, B., Wu, R. Y., Horne, R. G., Ahmed, A., Lee, D., Robinson, S. C., et al. (2020). Human milk oligosaccharides protect against necrotizing enterocolitis by activating intestinal cell differentiation. *Mol. Nutr. Food Res.* 64 (21), e2000519. doi:10.1002/mnfr.202000519

Li, C., Zhou, Y., Wei, R., Napier, D. L., Sengoku, T., Alstott, M. C., et al. (2023). Glycolytic regulation of intestinal stem cell self-renewal and differentiation. *Cell. Mol. Gastroenterology Hepatology* 15 (4), 931–947. doi:10.1016/j.jcmgh.2022.12.012

Li, L., Wan, G., Han, B., and Zhang, Z. (2018). Echinacoside alleviated LPS-induced cell apoptosis and inflammation in rat intestine epithelial cells by inhibiting the mTOR/STAT3 pathway. *Biomed. Pharmacother. = Biomedecine Pharmacother.* 104, 622–628. doi:10.1016/j.biopha.2018.05.072

Liang, W., Enée, E., Andre-Vallee, C., Falcone, M., Sun, J., and Diana, J. (2022). Intestinal cathelicidin antimicrobial peptide shapes a protective neonatal gut microbiota against pancreatic autoimmunity. *Gastroenterology* 162 (4), 1288–1302.e16. doi:10.1053/j.gastro.2021.12.272

Lindemans, C. A., Calafiore, M., Mertelsmann, A. M., O'Connor, M. H., Dudakov, J. A., Jenq, R. R., et al. (2015). Interleukin-22 promotes intestinal-stem-cell-mediated epithelial regeneration. *Nature* 528 (7583), 560–564. doi:10.1038/nature16460

Liu, T., Zong, H., Chen, X., Li, S., Liu, Z., Cui, X., et al. (2022). Toll-like receptor 4-mediated necroptosis in the development of necrotizing enterocolitis. *Pediatr. Res.* 91 (1), 73–82. doi:10.1038/s41390-021-01457-y

Liu, Y., Xu, Q., Wang, Y., Liang, T., Li, X., Wang, D., et al. (2021). Necroptosis is active and contributes to intestinal injury in a piglet model with lipopolysaccharide challenge. *Cell death Dis.* 12 (1), 62. doi:10.1038/s41419-020-03365-1

Lueschow, S. R., Kern, S. L., Gong, H., Grobe, J. L., Segar, J. L., Carlson, S. J., et al. (2020). Feeding formula eliminates the necessity of bacterial dysbiosis and induces inflammation and injury in the paneth cell disruption murine NEC model in an osmolality-dependent manner. *Nutrients* 12 (4), 900. doi:10.3390/nu12040900

Lueschow, S. R., Stumphy, J., Gong, H., Kern, S. L., Elgin, T. G., Underwood, M. A., et al. (2018). Loss of murine Paneth cell function alters the immature intestinal microbiome and mimics changes seen in neonatal necrotizing enterocolitis. *PloS One* 13 (10), e0204967. doi:10.1371/journal.pone.0204967

Mallow, E. B., Harris, A., Salzman, N., Russell, J. P., DeBerardinis, R. J., Ruchelli, E., et al. (1996). Human enteric defensins. Gene structure and developmental expression. *J. Biol. Chem.* 271 (8), 4038–4045. doi:10.1074/jbc.271.8.4038

Masi, A. C., Embleton, N. D., Lamb, C. A., Young, G., Granger, C. L., Najera, J., et al. (2021). Human milk oligosaccharide DSLNT and gut microbiome in preterm infants predicts necrotising enterocolitis. *Gut* 70 (12), 2273–2282. doi:10.1136/gutjnl-2020-322771

Matsuzawa-Ishimoto, Y., Shono, Y., Gomez, L. E., Hubbard-Lucey, V. M., Cammer, M., Neil, J., et al. (2017). Autophagy protein ATG16L1 prevents necroptosis in the intestinal epithelium. *J. Exp. Med.* 214 (12), 3687–3705. doi:10.1084/jem.20170558

McElroy, S. J., Underwood, M. A., and Sherman, M. P. (2013). Paneth cells and necrotizing enterocolitis: A novel hypothesis for disease pathogenesis. *Neonatology* 103 (1), 10–20. doi:10.1159/000342340

Ménard, S., Förster, V., Lotz, M., Gütle, D., Duerr, C. U., Gallo, R. L., et al. (2008). Developmental switch of intestinal antimicrobial peptide expression. *J. Exp. Med.* 205 (1), 183–193. doi:10.1084/jem.20071022

Moore, S. A., Nighot, P., Reyes, C., Rawat, M., McKee, J., Lemon, D., et al. (2016). Intestinal barrier dysfunction in human necrotizing enterocolitis. *J. Pediatr. Surg.* 51 (12), 1907–1913. doi:10.1016/j.jpedsurg.2016.09.011

Morowitz, M. J., Poroyko, V., Caplan, M., Alverdy, J., and Liu, D. C. (2010). Redefining the role of intestinal microbes in the pathogenesis of necrotizing enterocolitis. *Pediatrics* 125 (4), 777–785. doi:10.1542/peds.2009-3149

Nakamura, A., Kurihara, S., Takahashi, D., Ohashi, W., Nakamura, Y., Kimura, S., et al. (2021). Symbiotic polyamine metabolism regulates epithelial proliferation and macrophage differentiation in the colon. *Nat. Commun.* 12 (1), 2105. doi:10.1038/s41467-021-22212-1

Nenci, A., Becker, C., Wullaert, A., Gareus, R., van Loo, G., Danese, S., et al. (2007). Epithelial NEMO links innate immunity to chronic intestinal inflammation. *Nature* 446 (7135), 557–561. doi:10.1038/nature05698

Niño, D. F., Sodhi, C. P., and Hackam, D. J. (2016). Necrotizing enterocolitis: New insights into pathogenesis and mechanisms. *Nat. Rev. Gastroenterology hepatology* 13 (10), 590–600. doi:10.1038/nrgastro.2016.119

Nolan, L. S., Rimer, J. M., and Good, M. (2020). The role of human milk oligosaccharides and probiotics on the neonatal microbiome and risk of necrotizing enterocolitis: A narrative review. *Nutrients* 12 (10), 3052. doi:10.3390/nu12103052

Olm, M. R., Bhattacharya, N., Crits-Christoph, A., Firek, B. A., Baker, R., Song, Y. S., et al. (2019). Necrotizing enterocolitis is preceded by increased gut bacterial replication, Klebsiella, and fimbriae-encoding bacteria. *Sci. Adv.* 5 (12), eaax5727. doi:10.1126/sciadv.aax5727

Paneth, J. (1887). Ueber die secernirenden Zellen des Dünndarm-Epithels. *Arch. für Mikrosk. Anat.* 31 (1), 113–191. doi:10.1007/bf02955706

Park, H., Li, Z., Yang, X. O., Chang, S. H., Nurieva, R., Wang, Y.-H., et al. (2005). A distinct lineage of CD4 T cells regulates tissue inflammation by producing interleukin 17. *Nat. Immunol.* 6 (11), 1133–1141. doi:10.1038/ni1261

Patankar, J. V., and Becker, C. (2020). Cell death in the gut epithelium and implications for chronic inflammation. *Nat. Rev. Gastroenterology Hepatology* 17 (9), 543–556. doi:10.1038/s41575-020-0326-4

Patel, R. M., Kandefer, S., Walsh, M. C., Bell, E. F., Carlo, W. A., Laptook, A. R., et al. (2015). Causes and timing of death in extremely premature infants from 2000 through 2011. *N. Engl. J. Med.* 372 (4), 331–340. doi:10.1056/NEJMoa1403489

Peeters, T., and Vantrappen, G. (1975). The paneth cell: A source of intestinal lysozyme. *Gut* 16 (7), 553–558. doi:10.1136/gut.16.7.553

Pentinmikko, N., Iqbal, S., Mana, M., Andersson, S., Cognetta, A. B., Suciu, R. M., et al. (2019). Notum produced by Paneth cells attenuates regeneration of aged intestinal epithelium. *Nature* 571 (7765), 398–402. doi:10.1038/s41586-019-1383-0

Qi-Xiang, M., Yang, F., Ze-Hua, H., Nuo-Ming, Y., Rui-Long, W., Bin-Qiang, X., et al. (2022). Intestinal TLR4 deletion exacerbates acute pancreatitis through gut microbiota dysbiosis and Paneth cells deficiency. *Gut Microbes* 14 (1), 2112882. doi:10.1080/19490976.2022.2112882

Quintero, M., Liu, S., Xia, Y., Huang, Y., Zou, Y., Li, G., et al. (2021). Cdk5rap3 is essential for intestinal Paneth cell development and maintenance. *Cell Death Dis.* 12 (1), 131. doi:10.1038/s41419-021-03401-8

Riba, A., Olier, M., Lacroix-Lamandé, S., Lencina, C., Bacquié, V., Harkat, C., et al. (2017). Paneth cell defects induce microbiota dysbiosis in mice and promote visceral hypersensitivity. *Gastroenterology* 153 (6), 1594–1606. doi:10.1053/j.gastro.2017.08.044

Rocha-Pereira, J., Jacobs, S., Noppen, S., Verbeken, E., Michiels, T., and Neyts, J. (2018). Interferon lambda (IFN-λ) efficiently blocks norovirus transmission in a mouse model. *Antivir. Res.* 149, 7–15. doi:10.1016/j.antiviral.2017.10.017

Samara, J., Moossavi, S., Alshaikh, B., Ortega, V. A., Pettersen, V. K., Ferdous, T., et al. (2022). Supplementation with a probiotic mixture accelerates gut microbiome maturation and reduces intestinal inflammation in extremely preterm infants. *Cell Host Microbe* 30 (5), 696–711.e5. doi:10.1016/j.chom.2022.04.005

Sampath, V., Bhandari, V., Berger, J., Merchant, D., Zhang, L., Ladd, M., et al. (2017). A functional ATG16L1 (T300A) variant is associated with necrotizing enterocolitis in premature infants. *Pediatr. Res.* 81 (4), 582–588. doi:10.1038/pr.2016.260

Sancho, R., Cremona, C. A., and Behrens, A. (2015). Stem cell and progenitor fate in the mammalian intestine: Notch and lateral inhibition in homeostasis and disease. *EMBO Rep.* 16 (5), 571–581. doi:10.15252/embr.201540188

Sanders, D. S. A. (2005). Mucosal integrity and barrier function in the pathogenesis of early lesions in Crohn's disease. *J. Clin. pathology* 58 (6), 568–572. doi:10.1136/jcp.2004.021840

Sato, T., van Es, J. H., Snippert, H. J., Stange, D. E., Vries, R. G., van den Born, M., et al. (2011). Paneth cells constitute the niche for Lgr5 stem cells in intestinal crypts. *Nature* 469 (7330), 415–418. doi:10.1038/nature09637

Schaart, M. W., de Bruijn, A. C. J. M., Bouwman, D. M., de Krijger, R. R., van Goudoever, J. B., Tibboel, D., et al. (2009). Epithelial functions of the residual bowel after surgery for necrotising enterocolitis in human infants. *J. Pediatr. Gastroenterology Nutr.* 49 (1), 31–41. doi:10.1097/MPG.0b013e318186d341

Schwarzer, R., Jiao, H., Wachsmuth, L., Tresch, A., and Pasparakis, M. (2020). FADD and caspase-8 regulate gut homeostasis and inflammation by controlling MLKL- and GSDMD-mediated death of intestinal epithelial cells. *Immunity* 52 (6), 978–993. doi:10.1016/j.immuni.2020.04.002

Shi, Y., Liu, T., Zhao, X., Yao, L., Hou, A., Fu, J., et al. (2018). Vitamin D ameliorates neonatal necrotizing enterocolitis via suppressing TLR4 in a murine model. *Pediatr. Res.* 83 (5), 1024–1030. doi:10.1038/pr.2017.329

Singh, R., Balasubramanian, I., Zhang, L., and Gao, N. (2020). Metaplastic paneth cells in extra-intestinal mucosal niche indicate a link to microbiome and inflammation. *Front. Physiology* 11, 280. doi:10.3389/fphys.2020.00280

Sittipo, P., Kim, H. K., Han, J., Lee, M. R., and Lee, Y. K. (2021). Vitamin D3 suppresses intestinal epithelial stemness via ER stress induction in intestinal organoids. *Stem Cell Res. Ther.* 12 (1), 285. doi:10.1186/s13287-021-02361-2

Stanford, A. H., Gong, H., Noonan, M., Lewis, A. N., Gong, Q., Lanik, W. E., et al. (2020). A direct comparison of mouse and human intestinal development using epithelial gene expression patterns. *Pediatr. Res.* 88 (1), 66–76. doi:10.1038/s41390-019-0472-y

Strigli, A., Gopalakrishnan, S., Zeissig, Y., Basic, M., Wang, J., Schwerd, T., et al. (2021). Deficiency in X-linked inhibitor of apoptosis protein promotes susceptibility to microbial triggers of intestinal inflammation. *Sci. Immunol.* 6 (65), eabf7473. doi:10.1126/sciimmunol.abf7473

Sun, M., Wu, W., Chen, L., Yang, W., Huang, X., Ma, C., et al. (2018). Microbiota-derived short-chain fatty acids promote Th1 cell IL-10 production to maintain intestinal homeostasis. *Nat. Commun.* 9 (1), 3555. doi:10.1038/s41467-018-05901-2

Takakuwa, A., Nakamura, K., Kikuchi, M., Sugimoto, R., Ohira, S., Yokoi, Y., et al. (2019). Butyric acid and leucine induce α-defensin secretion from small intestinal paneth cells. *Nutrients* 11 (11), 2817. doi:10.3390/nu11112817

Tan, G., Huang, C., Chen, J., and Zhi, F. (2020). HMGB1 released from GSDME-mediated pyroptotic epithelial cells participates in the tumorigenesis of colitis-associated colorectal cancer through the ERK1/2 pathway. *J. Hematol. Oncol.* 13 (1), 149. doi:10.1186/s13045-020-00985-0

Tan, X., Hsueh, W., and Gonzalez-Crussi, F. (1993). Cellular localization of tumor necrosis factor (TNF)-alpha transcripts in normal bowel and in necrotizing enterocolitis. TNF gene expression by Paneth cells, intestinal eosinophils, and macrophages. *Am. J. Pathology* 142 (6), 1858–1865.

Tian, H., Biehs, B., Warming, S., Leong, K. G., Rangell, L., Klein, O. D., et al. (2011). A reserve stem cell population in small intestine renders Lgr5-positive cells dispensable. *Nature* 478 (7368), 255–259. doi:10.1038/nature10408

van Es, J. H., and Clevers, H. (2014). Paneth cells. *Curr. Biol. CB* 24 (12), R547–R548. doi:10.1016/j.cub.2014.04.049

van Es, J. H., Wiebrands, K., López-Iglesias, C., van de Wetering, M., Zeinstra, L., van den Born, M., et al. (2019). Enteroendocrine and tuft cells support Lgr5 stem cells on Paneth cell depletion. *Proc. Natl. Acad. Sci. U. S. A.* 116 (52), 26599–26605. doi:10.1073/pnas.1801888117

Wahida, A., Müller, M., Hiergeist, A., Popper, B., Steiger, K., Branca, C., et al. (2021). XIAP restrains TNF-driven intestinal inflammation and dysbiosis by promoting innate immune responses of Paneth and dendritic cells. *Sci. Immunol.* 6 (65), eabf7235. doi:10.1126/sciimmunol.abf7235

Wang, H., Zhang, X., Zuo, Z., Zhang, Q., Pan, Y., Zeng, B., et al. (2017). "Rip2 is required for nod2-mediated lysozyme sorting in paneth cells." *J. Immunol. Baltim. Md, 1950)* 198(9): 3729–3736. doi:10.4049/jimmunol.1601583

Wang, L. X., Zhu, F., Li, J. Z., Li, Y. L., Ding, X. Q., Yin, J., et al. (2020). Epidermal growth factor promotes intestinal secretory cell differentiation in weaning piglets via Wnt/β-catenin signalling. *Animal Int. J. Animal Biosci.* 14 (4), 790–798. doi:10.1017/S1751731119002581

Wang, Y., He, K., Sheng, B., Lei, X., Tao, W., Zhu, X., et al. (2021). The RNA helicase Dhx15 mediates Wnt-induced antimicrobial protein expression in Paneth cells. *Proc. Natl. Acad. Sci. U. S. A.* 118 (4), e2017432118. doi:10.1073/pnas.2017432118

Weis, V. G., Deal, A. C., Mekkey, G., Clouse, C., Gaffley, M., Whitaker, E., et al. (2021). Human placental-derived stem cell therapy ameliorates experimental necrotizing enterocolitis. *Am. J. Physiology. Gastrointest. Liver Physiology* 320 (4), G658–G674. doi:10.1152/ajpgi.00369.2020

Wellman, A. S., Metukuri, M. R., Kazgan, N., Xu, X., Xu, Q., Ren, N. S. X., et al. (2017). Intestinal epithelial sirtuin 1 regulates intestinal inflammation during aging in mice by altering the intestinal microbiota. *Gastroenterology* 153 (3), 772–786. doi:10.1053/j.gastro.2017.05.022

Werts, A. D., Fulton, W. B., Ladd, M. R., Saad-Eldin, A., Chen, Y. X., Kovler, M. L., et al. (2020). A novel role for necroptosis in the pathogenesis of necrotizing enterocolitis. *Cell. Mol. Gastroenterology Hepatology* 9 (3), 403–423. doi:10.1016/j.jcmgh.2019.11.002

White, J. R., Gong, H., Pope, B., Schlievert, P., and McElroy, S. J. (2017). Paneth-cell-disruption-induced necrotizing enterocolitis in mice requires live bacteria and occurs independently of TLR4 signaling. *Dis. models Mech.* 10 (6), 727–736. doi:10.1242/dmm.028589

Yu, R., Jiang, S., Tao, Y., Li, P., Yin, J., and Zhou, Q. (2019). Inhibition of HMGB1 improves necrotizing enterocolitis by inhibiting NLRP3 via TLR4 and NF-κB signaling pathways. *J. Cell. Physiology* 234 (8), 13431–13438. doi:10.1002/jcp.28022

Yu, S., Balasubramanian, I., Laubitz, D., Tong, K., Bandyopadhyay, S., Lin, X., et al. (2020a). Paneth cell-derived lysozyme defines the composition of mucolytic microbiota and the inflammatory tone of the intestine. *Immunity* 53 (2), 398–416. doi:10.1016/j.immuni.2020.07.010

Yu, S., Tong, K., Zhao, Y., Balasubramanian, I., Yap, G. S., Ferraris, R. P., et al. (2018). Paneth cell multipotency induced by Notch activation following injury. *Cell Stem Cell* 23 (1), 46–59. doi:10.1016/j.stem.2018.05.002

Yu, T.-X., Chung, H. K., Xiao, L., Piao, J.-J., Lan, S., Jaladanki, S. K., et al. (2020b). Long noncoding RNA H19 impairs the intestinal barrier by suppressing autophagy and lowering paneth and goblet cell function. *Cell. Mol. Gastroenterology Hepatology* 9 (4), 611–625. doi:10.1016/j.jcmgh.2019.12.002

Zamolodchikova, T. S., Tolpygo, S. M., and Svirshchevskaya, E. V. (2020). Cathepsin G-not only inflammation: The immune protease can regulate normal physiological processes. *Front. Immunol.* 11, 411. doi:10.3389/fimmu.2020.00411

Zha, J.-M., Li, H.-S., Lin, Q., Kuo, W.-T., Jiang, Z.-H., Tsai, P.-Y., et al. (2019). Interleukin 22 expands transit-amplifying cells while depleting Lgr5+ stem cells via inhibition of Wnt and Notch signaling. *Cell. Mol. Gastroenterology Hepatology* 7 (2), 255–274. doi:10.1016/j.jcmgh.2018.09.006

Zhou, Y., Li, Y., Zhou, B., Chen, K., Lyv, Z., Huang, D., et al. (2017). Inflammation and apoptosis: Dual mediator role for toll-like receptor 4 in the development of necrotizing enterocolitis. *Inflamm. Bowel Dis.* 23 (1), 44–56. doi:10.1097/MIB.0000000000000961

Zou, W. Y., Blutt, S. E., Zeng, X.-L., Chen, M.-S., Lo, Y.-H., Castillo-Azofeifa, D., et al. (2018). Epithelial WNT ligands are essential drivers of intestinal stem cell activation. *Cell Rep.* 22 (4), 1003–1015. doi:10.1016/j.celrep.2017.12.093

frontiers | Frontiers in Cell and Developmental Biology

TYPE Review
PUBLISHED 16 June 2023
DOI 10.3389/fcell.2023.1198794

OPEN ACCESS

EDITED BY
Or Kakhlon,
Hadassah Medical Center, Israel

REVIEWED BY
Kenji Nagao,
Ajinomoto, Japan
Ceereena Ubaida-Mohien,
National Institute on Aging (NIH),
United States

*CORRESPONDENCE
Xiuling Cao,
cxiuling@cau.edu.cn
Beidong Liu,
beidong.liu@cmb.gu.se

†These authors have contributed equally to this work

RECEIVED 02 April 2023
ACCEPTED 02 June 2023
PUBLISHED 16 June 2023

CITATION
Fang W, Chen S, Jin X, Liu S, Cao X and Liu B (2023), Metabolomics in aging research: aging markers from organs. *Front. Cell Dev. Biol.* 11:1198794. doi: 10.3389/fcell.2023.1198794

Metabolomics in aging research: aging markers from organs

Weicheng Fang[1†], Shuxin Chen[1†], Xuejiao Jin[1], Shenkui Liu[1], Xiuling Cao[1]* and Beidong Liu[1,2]*

[1]State Key Laboratory of Subtropical Silviculture, School of Forestry and Biotechnology, Zhejiang A&F University, Hangzhou, China, [2]Department of Chemistry and Molecular Biology, University of Gothenburg, Gothenburg, Sweden

Metabolism plays an important role in regulating aging at several levels, and metabolic reprogramming is the main driving force of aging. Due to the different metabolic needs of different tissues, the change trend of metabolites during aging in different organs and the influence of different levels of metabolites on organ function are also different, which makes the relationship between the change of metabolite level and aging more complex. However, not all of these changes lead to aging. The development of metabonomics research has opened a door for people to understand the overall changes in the metabolic level in the aging process of organisms. The omics-based "aging clock" of organisms has been established at the level of gene, protein and epigenetic modifications, but there is still no systematic summary at the level of metabolism. Here, we reviewed the relevant research published in the last decade on aging and organ metabolomic changes, discussed several metabolites with high repetition rate, and explained their role *in vivo*, hoping to find a group of metabolites that can be used as metabolic markers of aging. This information should provide valuable information for future diagnosis or clinical intervention of aging and age-related diseases.

KEYWORDS

aging, metabolomics, metabolite, biomarker, aging clock

Introduction

Human life expectancy has gradually increased with the development of human society. According to the World Health Organization report, the number and proportion of the population aged 60 and over is increasing. In 2019, there were 1 billion people aged 60 and over. By 2030, this number will increase to 1.4 billion, and will rise to 2.1 billion by 2050 (World Health Administration, 2020). This growth is unprecedented and will accelerate in the coming decades, especially in developing countries (Chao et al., 2021). Aging causes a decline in many bodily functions, such as decreased muscle strength, organ function, and bone density. These adverse effects make older people more susceptible to disease. The incidence of neurodegenerative diseases, such as Alzheimer's disease (AD) and Parkinson's disease, shows a strong correlation with age (Mattson and Arumugam, 2018). How to maintain health and physical function for longer periods of time to achieve "healthy aging" and ultimately extend "healthy lifespan" is a problem that has been pondered by humans for thousands of years. In the twentieth century, it was discovered that while the decline of cognitive and physical abilities may be an inevitable consequence of aging, changes in diet and metabolism could delay the onset of this consequence (Canevelli et al., 2016; Sanders et al., 2016). However, the exact mechanisms of aging are still unknown. Whether changes in several key pathways or substances in the body control the aging process, or whether aging is

the result of all the substances in the body beginning to deteriorate and working together at the same time, still needs to be confirmed by further research.

In recent years, an increasing number of researchers have begun to use omics technology to study normal aging because of its high-throughput characteristics, such as proteomics, genomics, transcriptomics, and metabolomics. Several "aging clocks" have been established to predict the onset of aging based on relevant omics research data, such as the proteome clock, the transcriptome clock, and the epigenetic clock (Fleischer et al., 2018; Horvath and Raj, 2018; Tanaka et al., 2018; Rutledge et al., 2022). Using metabolomics platforms, researchers can perform targeted or non-targeted tracking of large numbers of metabolites simultaneously, and compare metabolomic sample data from aging subjects, allowing them to understand changes in the aging process through changes in metabolite levels. Due to the functional differences between different organs, their respective metabolite compositions will also differ. In addition, the levels of metabolites in the same organ will be different in different age groups due to the different needs of the body's life activities. Understanding the mechanisms underlying such differences will give us the opportunity to understand the mysteries of aging.

Blood and urine samples are readily available, and the blood contains metabolites from various tissues and organs, so using blood or urine metabolites for research can reflect the overall situation of the body to some extent, and changes in the blood and urine metabolome during aging have been well described and summarized (Roberts et al., 2020; Clement et al., 2019; Johnson et al., 2019; Kondoh et al., 2020; Shao and Le, 2019; van den Akker et al., 2020; Robinson et al., 2020; Hertel et al., 2016; Adav and Wang, 2021). However, due to the fact that not all metabolites in tissues are completely excreted in blood or urine, and that changes in organ activity can have a significant impact on the metabolites in those organs, this advantage also brings with it the difficulty of determining which changes are truly reflected in the metabolomic data obtained from the blood and urine (Tryggvason and Wartiovaara, 2005; Rutledge et al., 2022). Therefore, the use of metabolomics data from specific tissues or organs can avoid the problem of metabolic signals being masked during the aging process (Schaum et al., 2020; Tabula Muris, 2020). In addition, appropriate *in vitro* cell model omics data can also represent the changes in organs during aging or disease to some extent (Chao et al., 2021).

Herein, we performed a detailed literature search for metabolic studies in multiple tissues and species related to aging (PubMed and Google Scholar search with the criteria "aging/ageing," "senescence," "metabolites," "metabolome"), which consulted over a thousand related articles in total. The manuscripts were then screened and reviewed, and the inclusion criteria for a manuscript included natural aging, metabolome results published on or after 2011, publications/authors provided list of significant/all metabolites, and choose those using nature aging mice, rats, human organs or *in vitro* aging cell models as research objects. Among the articles finally selected, eight articles described changes in the metabolome of aging cell models, eight described changes in the metabolome of aging muscle, four described changes in the metabolome of aging brain, four described changes in the metabolome of aging liver, two described changes in the metabolome of aging spleen. In addition, one article each described changes in the metabolome of the aging eye, skin, kidney, lung, and testes. Of these articles, eight focused on rats, seven on mice, and eight on human tissues or cell models. The measurements were performed using multiple platforms including but not limited to liquid chromatography-mass spectrometry-based metabolome and nuclear magnetic resonance-based metabolome. Using the authors' summary of the experimental data, we summarized more than 130 metabolites showed significant changes in the aging stage, and 47 metabolites appeared frequently (more than or equal to three articles) (Table 1). Among the 47 recurrent metabolites, 16 mostly decrease with aging in different organs, 7 mostly increase with aging. The remaining 24 metabolites showed different trends with aging in different species as well as in different tissues, and overall there did not seem to be a clear trend associated with aging. By collecting existing reports on the relationship between these metabolites and aging, we selected 14 metabolites with apparent changes in level and known to be closely related to the aging process for further discussion (Table 2). In this review, we describe the changes in metabolites during organ aging and discuss the analysis of changes in metabolites levels, as well as some metabolites that can serve as potential biomarkers of aging with apparent trends, providing potential references for future research.

Metabolites from carbohydrate metabolism is one of the extensively studied group as markers during aging

Carbohydrate metabolism refers to a series of complex chemical reactions of glucose (Glu), glycogen, etc. In the body. The major metabolic pathways of Glu *in vivo* include glycolysis, the tricarboxylic acid (TCA) cycle, and the pentose phosphate (PPP) pathway. The entire reaction process of glycolysis is completed in the cytoplasm, starting with the Glu, which is catalyzed by a series of enzymes to form the end-product pyruvate. Pyruvate is then reduced to lactate under anaerobic conditions. Under aerobic conditions, pyruvate enters the mitochondria and is further oxidized to produce acetyl coenzyme A (acetyl-CoA) for further oxidation in the TCA cycle, which is the primary pathway for energy production in the organism. In addition, the PPP is another important pathway for Glu oxidation and catabolism, and is designed to provide some of the raw materials needed for biosynthesis, rather than for cellular energy supply (Anastasiou et al., 2011; Gruning et al., 2011).

In the testis of aging rats, Glu levels are decreased (Jarak et al., 2018), and the masseter muscle showed lower levels of 3-phosphoglycerate, 2-phosphoglycerate, and phosphoenolpyruvate (PEP) (Kato et al., 2021). In aged mice, pyruvate levels are elevated in the eye, but fructose-1,6-bisphosphate (FBP) showed different changes in different parts of the eye (Wang et al., 2018). In cellular models, the trend in glycolysis consistent with the trend in rats and mice (Wu et al., 2017; Nagineni et al., 2021), suggesting that the degree of glycolysis is upregulated in senescent cells (Wu et al., 2017). In addition, the PPP also shows an increased trend (Garvey et al., 2014), while the TCA cycle shows the opposite trend. In the skeletal muscle of aging rats, the levels of fumaric acid and malic acid, intermediate metabolites of the TCA cycle, were decreased in older individuals. Levels of succinylcarnitine and flavin adenine

TABLE 1 Changes of metabolites in different aging organs.

Metabolite	Organ type										References
	Brain	Cell model	Eye	Liver	Muscle	Skin	Kidney	Lung	Spleen	Testes	
Carbohydrate metabolism											
2-Hydroxyglutaric acid			↓								Wang et al. (2018)
Acetyl-CoA		↓			↓						James et al. (2015), Hoshino et al. (2022)
Aconitic acid		↑									Wu et al. (2017)
Alpha-ketoglutaric acid		↑	↓								Wu et al. (2017), Wang et al. (2018)
Citric acid		↓↑			↑						James et al. (2015), Nagineni et al. (2021), Hoshino et al. (2022)
Fructose-1,6-bisphosphate		↓↓	↓		↑↓						Garvey et al. (2014), Wu et al. (2017), Wang et al. (2018), Nagineni et al. (2021)
Fructose-6-phosphate		↑↓			↓						James et al. (2015), Wu et al. (2017), Hoshino et al. (2022)
Fumaric acid		↓↓↑		↓	↓↓			↓	↓		Garvey et al. (2014), Wu et al. (2017), Yi et al. (2020), Nagineni et al. (2021), Zhang et al. (2021), Zhou et al. (2021)
Glucose				↓	↑↓↓↑				↑	↓	Houtkooper et al. (2011), Garvey et al. (2014), Tepp et al. (2017), Jarak et al. (2018), Zhou et al. (2021), Hoshino et al. (2022)
Glucose-1,6-bisphosphate					↑↓						Garvey et al. (2014)
Glucose-6-phosphate		↓↓↑			↓						James et al. (2015), Wu et al. (2017), Fernandez-Rebollo et al. (2020), Hoshino et al. (2022)
Glucose-1-phosphate		↓									Fernandez-Rebollo et al. (2020)
Glyceraldehyde-3-phosphate		↓									Nagineni et al. (2021)
Glycerate-1,3-bisphosphate		↓									Nagineni et al. (2021)
Glycerate-2-phosphate		↓↓			↓						Wu et al. (2017), Kato et al. (2021), Nagineni et al. (2021)
Glycerate-3-phosphate		↓↓↑			↑↓↓						Garvey et al. (2014), James et al. (2015), Wu et al. (2017), Kato et al. (2021), Nagineni et al. (2021)
Glycogen					↑						Zhou et al. (2021)

(Continued on following page)

TABLE 1 (*Continued*) **Changes of metabolites in different aging organs.**

Metabolite	Organ type										References
	Brain	Cell model	Eye	Liver	Muscle	Skin	Kidney	Lung	Spleen	Testes	
Isocitrate		↑									Nagineni et al. (2021)
Lactate	↓	↑↑↓		↓	↓↑↓				↑		Houtkooper et al. (2011), James et al. (2015), Tepp et al. (2017), Yi et al. (2020), Nagineni et al. (2021), Zhang et al. (2021), Zhou et al. (2021)
Malic acid		↓↑	↓		↓						Garvey et al. (2014), Wu et al. (2017), Wang et al. (2018), Nagineni et al. (2021)
Malonate		↑						↓			Yi et al. (2020), Zhang et al. (2021)
Maltose				↑	↑↑						Houtkooper et al. (2011), Garvey et al. (2014)
Oxaloacetate		↑	↓								Wu et al. (2017), Wang et al. (2018)
Phosphocreatine	↓				↓↑↓						Hunsberger et al. (2020), Wilkinson et al. (2020), Kato et al. (2021), Hoshino et al. (2022)
Phosphoenolpyruvate		↑↓			↑↓↓						Garvey et al. (2014), James et al. (2015), Wu et al. (2017), Kato et al. (2021)
Pyruvate		↑↑↑	↑		↑						James et al. (2015), Wang et al. (2018), Fernandez-Rebollo et al. (2020), Nagineni et al. (2021), Hoshino et al. (2022)
Succinic acid		↓↑			↓						Wu et al. (2017), Nagineni et al. (2021), Hoshino et al. (2022)
Succinyl							↓				Zhang et al. (2021)
Succinylcarnitine					↓						Garvey et al. (2014)
Amino Acid Metabolism											
3-Methylhistidine					↑						Garvey et al. (2014)
Alanine		↑↓↓		↑	↑↑↓↓↓	↑					Kuehne et al. (2017), Tepp et al. (2017), Wesley et al. (2019), Yi et al. (2020), Domingo-Orti et al. (2021), Nagineni et al. (2021), Zhou et al. (2021), Zhuang et al. (2021), Hoshino et al. (2022)
Acylamino base				↑							Son et al. (2012)
Acetylcysteine			↑								Wang et al. (2018)
Anserine					↓						Garvey et al. (2014)

(Continued on following page)

TABLE 1 (*Continued*) **Changes of metabolites in different aging organs.**

Metabolite	Organ type										References
	Brain	Cell model	Eye	Liver	Muscle	Skin	Kidney	Lung	Spleen	Testes	
Arginine	↑	↓			↑↓						Hunsberger et al. (2020), Nagineni et al. (2021), Zhou et al. (2021), Hoshino et al. (2022)
Aspartate					↓↑						Zhuang et al. (2021), Hoshino et al. (2022)
Betaine				↑	↓					↓	Son et al. (2012), Jarak et al. (2018), Zhuang et al. (2021)
Carnosine					↓↓						Garvey et al. (2014), Hoshino et al. (2022)
Creatine		↓			↑↑↓↓		↑			↓	Tepp et al. (2017), Jarak et al. (2018), Yi et al. (2020), Zhang et al. (2021), Zhou et al. (2021), Hoshino et al. (2022)
Cysteine			↑↓								Wang et al. (2018)
Cysteine-Glycine			↑								Wang et al. (2018)
Dimethylarginine		↑									James et al. (2015)
Dimethylglycine		↓			↓						Morrison et al. (2019), Zhuang et al. (2021)
Gamma-aminobutyric acid	↓				↓						Zheng et al. (2016b), Zhuang et al. (2021)
Glutamate	↓	↓↓			↑↓	↑					Zheng et al. (2016b), Kuehne et al. (2017), Tepp et al. (2017), Yi et al. (2020), Nagineni et al. (2021), Zhuang et al. (2021)
Glutamine		↑↑↓			↑↓	↑					Kuehne et al. (2017), Tepp et al. (2017), Morrison et al. (2019), Yi et al. (2020), Nagineni et al. (2021), Zhuang et al. (2021)
Glutathione	↓	↓↓			↓↓						Wesley et al. (2019), Yi et al. (2020), Nagineni et al. (2021), Zhuang et al. (2021), Hoshino et al. (2022)
Glycine		↓↓			↓↓↓						Yi et al. (2020), Nagineni et al. (2021), Zhou et al. (2021), Zhuang et al. (2021), Hoshino et al. (2022)
Glycyl leucine		↓									James et al. (2015)
Glycyl valine		↓									James et al. (2015)
Hydroxyproline					↑↓						Zhuang et al. (2021), Hoshino et al. (2022)
Hypotaurine		↓	↓								Wang et al. (2018), Fernandez-Rebollo et al. (2020)

(Continued on following page)

TABLE 1 (*Continued*) **Changes of metabolites in different aging organs.**

Metabolite	Organ type										References
	Brain	Cell model	Eye	Liver	Muscle	Skin	Kidney	Lung	Spleen	Testes	
Isoleucine	↑↑	↑↓			↑↓↑	↑	↓	↑		↑	Kuehne et al. (2017), Jarak et al. (2018), Wesley et al. (2019), Yi et al. (2020), Zhang et al. (2021), Zhou et al. (2021), Zhuang et al. (2021)
Isoleucyl-glycine		↓									James et al. (2015)
Leucine	↑				↑↓↑↓		↓	↑		↑	Jarak et al. (2018), Zhang et al. (2021), Zhou et al. (2021), Zhuang et al. (2021), Hoshino et al. (2022)
Lysin					↓						Hoshino et al. (2022)
Methionine	↑				↓↓		↓	↑	↓		Zhang et al. (2021), Zhuang et al. (2021), Hoshino et al. (2022)
Methyl-histidine	↓		↑								Hunsberger et al. (2020)
N6-Trimethyl-lysine					↑						Garvey et al. (2014)
Ornithine		↑↓			↓↓						James et al. (2015), Nagineni et al. (2021), Zhuang et al. (2021), Hoshino et al. (2022)
Phenylalanine	↑				↑↓↑		↓	↑	↓	↑	Jarak et al. (2018), Zhang et al. (2021), Zhou et al. (2021), Zhuang et al. (2021), Hoshino et al. (2022)
Proline		↑↓↓			↓	↑					Kuehne et al. (2017), Yi et al. (2020), Domingo-Orti et al. (2021), Nagineni et al. (2021), Zhuang et al. (2021)
S-Adenosylmethionine					↑						Kato et al. (2021)
Serine					↓↓						Zhuang et al. (2021), Hoshino et al. (2022)
Taurine	↓	↑↓	↓		↑↓	↑					Kuehne et al. (2017), Tepp et al. (2017), Wang et al. (2018), Wesley et al. (2019), Fernandez-Rebollo et al. (2020), Yi et al. (2020), Zhuang et al. (2021)
Trimethyllysine			↑								Wang et al. (2018)
Tryptophan					↓↓						Zhuang et al. (2021), Hoshino et al. (2022)
Tyrosine	↓↑				↑↓↑↓		↓	↑	↓	↑	Jarak et al. (2018), Wesley et al. (2019), Zhang et al. (2021), Zhou et al. (2021), Zhuang et al. (2021), Hoshino et al. (2022)

(Continued on following page)

TABLE 1 (*Continued*) **Changes of metabolites in different aging organs.**

Metabolite	Organ type										References
	Brain	Cell model	Eye	Liver	Muscle	Skin	Kidney	Lung	Spleen	Testes	
Valine	↑	↓			↑↓↓	↑	↓	↑		↑	Kuehne et al. (2017), Jarak et al. (2018), Yi et al. (2020), Zhang et al. (2021), Zhuang et al. (2021), Hoshino et al. (2022)
Valyl Aspartate		↓									James et al. (2015)
Valyl glycine		↓									James et al. (2015)
Lipid metabolism											
3-Ureidopropionate		↑									James et al. (2015)
Acetylcarnitine					↓						Zhuang et al. (2021)
Acylcarnitine	↓				↓						Garvey et al. (2014), Zheng et al. (2016b)
Carnitine				↑	↓↓						Son et al. (2012), Garvey et al. (2014)
Cholesterol			↓	↑							Son et al. (2012), Wang et al. (2018)
Choline					↑↓		↓			↑	Jarak et al. (2018), Kato et al. (2021), Zhang et al. (2021), Zhuang et al. (2021)
Dihomolinolenic acid					↓						Garvey et al. (2014)
Fatty acid			↓		↑↓↓						Garvey et al. (2014), Wang et al. (2018), Zhang et al. (2021)
Glycerol-3-phosphate				↑	↑↓						Son et al. (2012), Garvey et al. (2014), Hoshino et al. (2022)
Glycerin		↓		↓	↑						Garvey et al. (2014), James et al. (2015), Zhang et al. (2021)
Glycerophosphocholine					↑						Garvey et al. (2014)
Glycerophospholipids					↓						Garvey et al. (2014)
Inositol		↓									Yi et al. (2020)
Linoleic acid				↓	↓						Son et al. (2012), Garvey et al. (2014)
Lysophosphatidylcholine	↑				↑↓						Zheng et al. (2016b), Wilkinson et al. (2020), Zhang et al. (2021)
Oleic acid					↑						Garvey et al. (2014)
Palmitoleate					↑						Garvey et al. (2014)
Phospholipids			↓								Wang et al. (2018)
Stearic acid					↓						Garvey et al. (2014)
Steroid			↓								Wang et al. (2018)
Nucleotide metabolism											
7-Methylguanine		↑									James et al. (2015)

(Continued on following page)

TABLE 1 (*Continued*) **Changes of metabolites in different aging organs.**

Metabolite	Organ type										References
	Brain	Cell model	Eye	Liver	Muscle	Skin	Kidney	Lung	Spleen	Testes	
Adenine triphosphate ribonucleotide		↓↓↓			↓↓						Morrison et al. (2019), Yi et al. (2020), Kato et al. (2021), Nagineni et al. (2021), Hoshino et al. (2022)
Adenosine monophosphate					↓						Zhuang et al. (2021)
Allantoin	↓				↓		↑	↑	↑		Zhang et al. (2021), Zhuang et al. (2021)
Deoxyribose			↑								Wang et al. (2018)
Flavin adenine dinucleotide					↓						Garvey et al. (2014)
Guanine diphosphate ribonucleotide		↑		↑	↑↑						Morrison et al. (2019), Kato et al. (2021), Zhang et al. (2021), Hoshino et al. (2022)
Guanine monophosphate ribonucleotide					↑↑						Kato et al. (2021), Hoshino et al. (2022)
Hypoxanthine		↑↑		↑	↑↓						James et al. (2015), Morrison et al. (2019), Kato et al. (2021), Zhang et al. (2021), Zhuang et al. (2021)
Inosine	↓	↑		↓	↓↑↓		↓				Morrison et al. (2019), Zhang et al. (2021), Zhou et al. (2021), Hoshino et al. (2022)
Inosine monophosphate		↑		↑	↑↑						Morrison et al. (2019), Kato et al. (2021), Zhang et al. (2021), Hoshino et al. (2022)
Phosphoribosyl pyrophosphate		↓									Nagineni et al. (2021)
Ribose		↓			↓↑						Garvey et al. (2014), Nagineni et al. (2021)
Ribulose-5-phosphate					↓↑						Garvey et al. (2014)
Thymidine		↓									James et al. (2015)
Uracil	↑	↑			↑↑		↑				Morrison et al. (2019), Kato et al. (2021), Zhang et al. (2021)
Urate		↑									James et al. (2015)
Uridine	↓			↑↓	↓		↓				Son et al. (2012), Morrison et al. (2019), Zhang et al. (2021)
Xylulose-5-phosphate					↓↑						Garvey et al. (2014)
Polyamine and NAD⁺ metabolism											
Putrescine		↓			↓						Nagineni et al. (2021), Hoshino et al. (2022)
Spermidine					↑↓						Kato et al. (2021), Zhuang et al. (2021), Hoshino et al. (2022)
Spermine		↑			↑						Wilkinson et al. (2020), Nagineni et al. (2021)

(Continued on following page)

TABLE 1 (*Continued*) **Changes of metabolites in different aging organs.**

Metabolite	Organ type										References
	Brain	Cell model	Eye	Liver	Muscle	Skin	Kidney	Lung	Spleen	Testes	
Nicotinamide			↑	↓	↑		↓	↓			Wang et al. (2018), Zhang et al. (2021), Zhuang et al. (2021)
Nicotinamide adenine dinucleotide	↓	↓↓	↑	↓	↑↓↓						Garvey et al. (2014), Wang et al. (2018), Wesley et al. (2019), Yi et al. (2020), Nagineni et al. (2021), Zhuang et al. (2021), Hoshino et al. (2022)
Nicotinamide ribonucleotide		↓									Fernandez-Rebollo et al. (2020)
Nicotinamide riboside		↓									Fernandez-Rebollo et al. (2020)
Nicotinic acid	↑										Wesley et al. (2019)
Reduced nicotinamide adenine dinucleotide		↓↓↓	↓	↑							James et al. (2015), Wesley et al. (2019), Yi et al. (2020), Nagineni et al. (2021), Hoshino et al. (2022)
Reduced nicotinamide adenine dinucleotide phosphate		↓			↑						Wu et al. (2017), Hoshino et al. (2022)
Other											
Acetate	↑										Zhang et al. (2021)
Ethanolamine							↓				Zhang et al. (2021)
Fenugreek			↓								Wang et al. (2018)
Formate				↓							Wesley et al. (2019)
Glyceric acid			↑								Wang et al. (2018)
Indole-3-acetic acid			↓								Wang et al. (2018)
Methyl glutamate			↑								Wang et al. (2018)
Methyl-histamine	↓										Hunsberger et al. (2020)
Phosphocholine									↓		Wang et al. (2018)
Riboflavin			↑								Wang et al. (2018)
Sorbitol					↑↓						Garvey et al. (2014), Zhuang et al. (2021)
Thiamine			↓								Wang et al. (2018)

A single arrow is used to represent the research result of an article. Up arrows indicate the metabolite level increases in older organ samples compared to younger samples, and the down arrows indicate that it decreases. Red arrows represents rat tissue, green represents mouse tissue or cell model, and blue represents human tissue or cell model.

dinucleotide (FAD) were also reduced (Garvey et al., 2014). In addition, the liver, spleen, lungs, and eye of aging mice all have decreased levels of fumaric acid, oxaloacetate, malic acid, and α-ketoglutarate (Wang et al., 2018; Zhang et al., 2021). Studies at the cell level yielded similar results. Senescent cells showed a downward trend in malic acid, fumaric acid, and succinic acid levels, while isocitrate and citric acid levels were relatively elevated (Yi et al., 2020; Nagineni et al., 2021). In addition to the major metabolites listed above, other metabolic intermediates such as allantoin, acetate, ethanolamine, choline, phosphorylcholine, 2-hydroxyglutarate, succinyl, malonic acid, and citrate, also change with age (Table 1).

Because of the different functions of organs in different parts of the body, their metabolite level changes at the same time can be distinguished. For example, in rat gastrocnemius muscle, the levels of glycolytic intermediates such as FBP, and PEP are significantly increased, but in soleus muscle, FBP, PEP, glucose-6-phosphate (G6P), etc., showed the opposite changes in the same age group of rats (Garvey et al., 2014). Studies have shown that the aging process of the soleus muscle may be

TABLE 2 Changes in metabolite levels with apparent trends in different aging organs and cell models.

Metabolite	Organ type		References
	Up	Down	
Adenosine triphosphate		Mice master muscle; Human Colon cancer cells; Umbilical vein endothelial cells	Morrison et al. (2019), Yi et al. (2020), Kato et al. (2021), Nagineni et al. (2021)
Fatty acids	Rat Gastrocnemius	Mice heart; eye; Rat soleus	Garvey et al. (2014), Wang et al. (2018), Zhang et al. (2021)
Glucose	Mice spleen; Rat Gastrocnemius	Mice liver, muscle; Rat Soleus, Testis	Houtkooper et al. (2011), Garvey et al. (2014), Jarak et al. (2018), Zhou et al. (2021)
Glutamate	Rat heart; Human skin	Rat brain, muscle; Human Colon cancer cells; Umbilical vein endothelial cells	Kuehne et al. (2017), Tepp et al. (2017), Wesley et al. (2019), Yi et al. (2020), Nagineni et al. (2021), Zhuang et al. (2021)
Glutamine	Human Umbilical vein endothelial cells, skin; Rat heart	Rat muscle; Human Colon cancer cells	Kuehne et al. (2017), Tepp et al. (2017), Morrison et al. (2019), Yi et al. (2020), Nagineni et al. (2021), Zhuang et al. (2021)
Glutathione		Rat brain, muscle; Human Colon cancer cells; Umbilical vein endothelial cells	Morrison et al. (2019), Wesley et al. (2019), Yi et al. (2020), Nagineni et al. (2021), Zhuang et al. (2021), Hoshino et al. (2022)
Glycine		Rat muscle; Mice muscle; Human Colon cancer cells; Umbilical vein endothelial cells	Yi et al. (2020), Nagineni et al. (2021), Zhou et al. (2021), Zhuang et al. (2021), Hoshino et al. (2022)
Isoleucine	Mice Lung, brain, heart, muscle; Rat testis, brain; Human skin	Mice kidney; Rat muscle; Human Umbilical vein endothelial cells	Kuehne et al. (2017), Jarak et al. (2018), Wesley et al. (2019), Yi et al. (2020), Zhang et al. (2021), Zhou et al. (2021), Zhuang et al. (2021)
Lactate	Mice spleen; Rat heart; Human Colon cancer cells, Fibroblast	Mice muscle, liver, brain; Human Umbilical vein endothelial cells	Houtkooper et al. (2011), James et al. (2015), Tepp et al. (2017), Yi et al. (2020), Nagineni et al. (2021), Zhang et al. (2021), Zhou et al. (2021)
Lysophosphatidylcholine	Rat brain; Human Vastus lateralis	Mice heart	Wesley et al. (2019), Wilkinson et al. (2020), Zhang et al. (2021)
Nicotinamide adenine dinucleotide	Mice eye; Rat muscle	Rat brain, liver, muscle; Human colon cancer cells; Umbilical vein endothelial cells	Garvey et al. (2014), Wang et al. (2018), Wesley et al. (2019), Yi et al. (2020), Nagineni et al. (2021), Zhuang et al. (2021), Hoshino et al. (2022)
Pyruvate	Mice eye; Human Colon cancer cells, Mesenchymal cells		Wang et al. (2018), Fernandez-Rebollo et al. (2020), Nagineni et al. (2021)
Uracil	Mice brain, heart, kidney, red blood cells, master muscle		Morrison et al. (2019), Kato et al. (2021), Zhang et al. (2021)
Valine	Mice lung, brain, heart; Rat testis; Human skin	Mice kidney; Rat muscle; Human Umbilical vein endothelial cells	Kuehne et al. (2017), Jarak et al. (2018), Yi et al. (2020), Zhang et al. (2021), Zhuang et al. (2021), Hoshino et al. (2022)

later than that of the gastrocnemius muscle (Oliveira et al., 2019; Yanar et al., 2019), which may account for the different metabolic trends seen in these two muscles in rats of the same age. In addition, relatively high levels of the TCA cycle intermediate fumaric acid, malic acid, succinic acid, and α-ketoglutarate were detected in human breast cancer cells with a senescent phenotype induced by doxorubicin (Wu et al., 2017). These changes are different from the aforementioned changes in mitochondria-related metabolome in normal aging cells. The reason for this phenomenon may be that when the damage accumulation does not reach the threshold, cells can repair the damaged DNA by increasing the strength of the PPP and TCA pathways to synthesize nucleotides, thereby compensating for the cellular dysfunctions caused by DNA damage as soon as possible (Gewirtz, 1999; Thorn et al., 2011).

Pyruvate is the key metabolite linking glycolysis and the TCA cycle. Pyruvate has been shown to have antioxidant, anti-nitrite stress, and anti-inflammatory effects, among others (Flaherty et al., 2010; James et al., 2015). In addition, pyruvate can undergo transamination reactions with glutamate to produce alanine and α-ketoglutarate, which are used as reaction intermediates to participate in the remaining steps of the TCA cycle. A study has shown that the consumption priority of pyruvate is higher than that of glucose in isolated mouse skeletal muscle (Khattri et al., 2022). In addition, pyruvate can counteract hypoxic lactic acidosis and the Warburg effect by increasing the ratio of nicotinamide adenine dinucleotide to reduced nicotinamide adenine dinucleotide (NAD^+/NADH) (Hu et al., 2013). It also protects the structural integrity of the mitochondria and the function of the endoplasmic reticulum, thereby preventing cell apoptosis (Zhang et al., 2020a; Li et al., 2020). In addition, studies have shown that artificially elevated pyruvate can increase NAD^+ levels (Iannetti et al., 2018; Kim et al., 2018), and there are no reports of adverse effects, which has led researchers to consider the possibility of using pyruvate or pyruvate derivatives as drugs to treat certain diseases. Some scientists believe that pyruvate can be used instead of NAD^+ as an exogenous supplement to treat diabetes, but more research is needed to verify this hypothesis

10.3389/fcell.2023.1198794

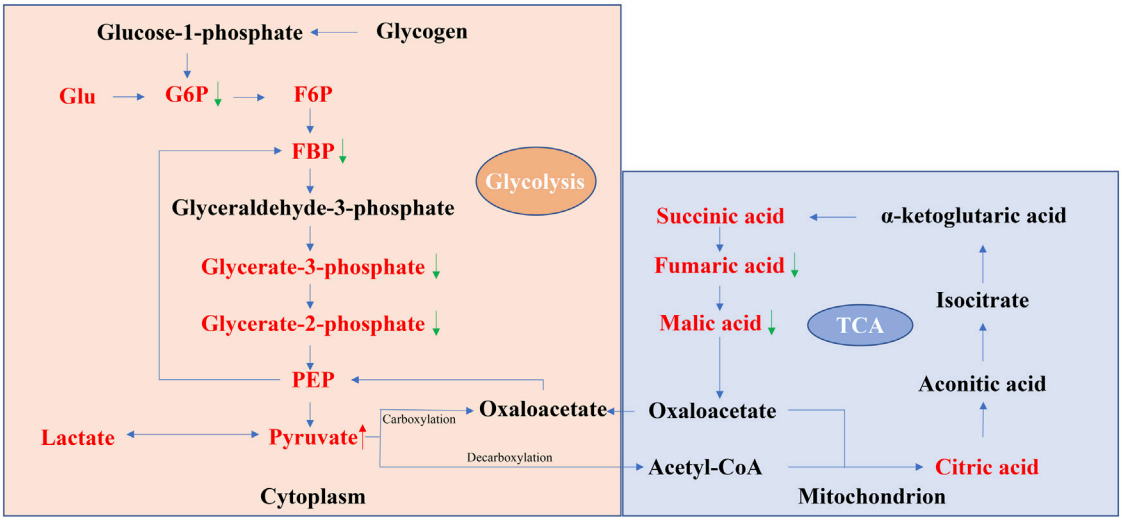

FIGURE 1
Schematic representation of glycolysis and the TCA cycle. The red font indicates the metabolites with significant changes in the level of aging organs found in most studies (data from Table 1). The red up arrow indicates that the changes of metabolites in different reports and tissues are mostly increasing, while the green down arrow indicates the opposite. In aging organs, the levels of the glycolytic intermediate products G6P, FBP, glycerate-3-phosphate, and glycerate-2-phosphate and the TCA intermediate products fumaric acid and malic acid are relatively low, while the levels of the glycolytic end product pyruvate are relatively high, reflecting that the glycolytic flux increased at the stage of organ aging, while the TCA cycle flux decreased.

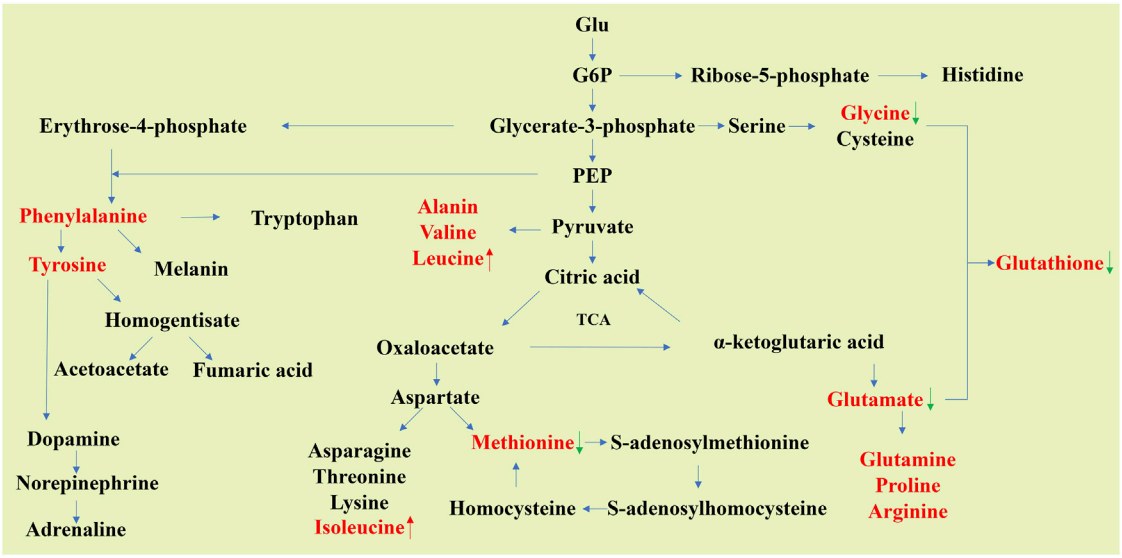

FIGURE 2
Schematic of carbon skeleton sources during nonessential amino acid synthesis. The metabolites reported in many articles that their levels in aging organs will change significantly are shown in red font (data from Table 1). The red up arrow indicates that the metabolites are increased in aging tissues, while the green down arrow indicates that they are decreased in aging tissues. The levels of glycine, glutamate, and methionine can be seen to decline in aging organs, while the opposite is true for leucine and isoleucine.

(Zhang et al., 2020b; Zhou, 2021). Thus, the elevated levels of pyruvate, a key central metabolite, during the aging phase, indicate that the downstream pathways it mediates are inhibited. Given the variety of stress conditions that occur during aging, inhibition of these pathways is likely to be a direct manifestation of aging. All of these results suggest that pyruvate can be used as an indicator of organ aging.

In addition to pyruvate, Glu is one of our first choices as a marker metabolite of aging, but Glu in different organs does not change consistently with age. Studies have shown that the Glu uptake capacity of high-energy-consuming organs such as the brain and skeletal muscle is reduced due to the decline in insulin signaling, insulin sensitivity, and Glu transporter levels that

occurs with aging (Muzumdar et al., 2004; Karakelides et al., 2010; dos Santos et al., 2012). The expression levels of phosphoenolpyruvate carboxykinase (PEPCK) and Glu-6-phosphatase (G6Pase) were increased in the livers of aging rats, which ultimately increased hepatic Glu production (Gaspar et al., 2020). These results suggest that different organs have different levels of Glu requirements, which means that Glu may not be a suitable aging marker for the whole-body. However, because of its high detection sensitivity, it is possible to combine changes in Glu levels with other metabolites in specific organs to provide a targeted indication of organ age.

Lactate is reduced from pyruvate under anaerobic conditions, and several studies in different organs have found that lactate levels change with age as well as in senescent cell models (Houtkooper et al., 2011; Tepp et al., 2017; Nagineni et al., 2021; Zhang et al., 2021), but the of change trends are different. Lactate has long been considered a metabolic waste product for a long time. However, studies have shown that most of the lactate produced by muscle contraction is taken up by other organs through the bloodstream and used as fuel for oxidation to produce energy, a phenomenon now known as the lactate shuttle (Brooks, 1986; Bergersen, 2007; Adeva-Andany et al., 2014). Central nervous system lactate increase as plasma lactate levels increase, with decreased Glu uptake, suggesting that the brain may prefer lactate to Glu as a raw material for energy production (Smith et al., 2003). Muscle cells can convert lactate to pyruvate, which can enter the TCA cycle directly, if oxygen is available, and the liver can also convert lactate to Glu through gluconeogenesis (Bergman et al., 2000; Meyer et al., 2002; Le et al., 2010; Emhoff et al., 2013). In fact, lactate can not only directly enter the mitochondria directly to complete the oxidation process to pyruvate, but it can also be converted to pyruvate in the cytoplasm and then transported to the mitochondria, and an increase in lactate intake can help cells generate more energy faster through the TCA process (Bouzat et al., 2014). In recent years, studies have shown that lactate can bind to GPR81 (also known as hydroxycarboxylic acid receptor HCAR1), a member of the members of the G protein-coupled receptor family (Lauritzen et al., 2014), shedding new light on how lactate is involved in more complex signaling processes (Bozzo et al., 2013). Overall, similar to Glu, the general changes in lactate levels in aging organs suggest that lactate is closely related to aging and could be a targeted indicator of organ age.

Taken together, these results suggest that the energy centers of the cell undergo a shift from the mitochondria to the cytoplasm during senescence. Changes in the levels of several metabolites reflect this age-related transition (Figure 1), such as the levels of fumaric acid and malic acid were relatively decreased in the aging stage, accompanied by a relative increase in the level of pyruvate, indicating an enhancement of the glycolytic pathway and the weaking of the TCA pathway during the aging phase. On the other hand, some modalities thought to prolong the lifespan, such as energy restriction (CR), can increase the metabolic level of the TCA cycle, which laterally reflects that the decrease in the TCA cycle may be a symbol of aging (Heilbronn and Ravussin, 2003; Mitchell et al., 2016). Based on studies summarized above, it seems that pyruvate can be used as a marker for carbohydrate metabolism changes during aging, while more research on Glu, lactate is needed to better understand their role in aging.

Amino acid metabolites showing different trends during aging

Amino acids and small-molecule peptides are also metabolites that appear frequently in many studies. Amino acids can be used to synthesize proteins necessary for life activities, and are associated with a number of other metabolites (Figure 2), and some important anti-stress substances in the body are also synthesized through amino acid metabolism, such as glutathione (GSH) and creatine (Hopkins, 1929; Kendall et al., 1930; Van Pilsum et al., 1972).

Most protein amino acids show different metabolic trends in different aging organs or cells. For example, in aged rats, glutamate level decreased while alanine, and glutamine levels increased (Table 1). In senescent human umbilical vein endothelial cells, the levels of glutamate and alanine decreased as the number of cell passages increased. In human skin samples, the level of glutamate was higher in older samples, as were the levels of glutamine and alanine (Kuehne et al., 2017). Some amino acids even show inconsistent metabolic trends in different parts of the same organ, such as cysteine. Cysteine levels increased with age in the retina and lens, but decreased in the cornea (Wang et al., 2018). The same is true for non-protein amino acids and modified amino acids, such as taurine, methylhistidine, and methylhistamine, as well as small molecular weight peptides, such as creatine (Table 1).

Glutamate is a free amino acid that is abundant in the human body and was originally known for its unique umami taste. Glutamate is an excitatory neurotransmitter (Burger et al., 1989; Watkins and Jane, 2006; Zhou and Danbolt, 2014), and because of the close link between glutamate recycling at synapses and energy metabolism (Sibson et al., 1998; Yu et al., 2018), maintaining of glutamate homeostasis at synaptic sites is of great importance for normal brain function. In addition, neurons actively take up glutamate and use it as a substrate for energy production (Sonnewald et al., 1996; Olstad et al., 2007). An increasing number of studies have shown that brain energy metabolism homeostasis is closely related to neurological diseases. Some neurological diseases are associated with abnormal glutamate levels, such as AD. Significantly lower glutamate levels have been found in patients with major depression and AD compared to healthy subjects (Rupsingh et al., 2011; Gueli and Taibi, 2013; Inoshita et al., 2018). This information raised the question of whether abnormal glutamate metabolism may be a major cause and an important manifestation of neurodegenerative diseases (Cunnane et al., 2020). Studies have shown that decreased expression of a key glutamate receptor, GLT-1, in both AD and Huntington's disease (HD) patients and related rodent disease models reduces the efficiency of glutamate uptake by astrocytes for release into the synaptic cleft (Andersen et al., 2021). Glutamate is also active in peripheral organs such as the digestive tract, pancreas, and bone (Julio-Pieper et al., 2011; Tremolizzo et al., 2012). It has been reported that approximately 35% of the total energy consumption of intestinal mucosal cells comes from dietary glutamate (Uneyama et al., 2017). Together with the decreasing trend of glutamate in the aging rat brain described above, these results together raise the possibility of using glutamate as a marker of brain aging.

Glutamine is listed as a non-essential amino acid because it can be synthesized *in vivo*, and it is involved in many metabolic

pathways as well as glutamate transfer processes in the nervous system. One article suggested that inhibiting the normal breakdown of glutamine may promote various age-related diseases by prolonging the survival time of senescent cells (Johmura et al., 2021). This is similar to the conclusion that timely removal of senescent cells in some age-related diseases can maintain overall organ or body health (Xu et al., 2018; Justice et al., 2019). Here, relatively high levels of glutamine were found in several aging organs and cell models (Table 1), as if glutamine degradation in inhibited during aging. However, not all aging organs show higher glutamine levels (Table 1). Recently, a study has shown that aging mesenchymal stem cells exhibit metabolic remodeling, characterized by reduced glucose uptake, which in turn compensates for energy generation gaps by degrading glutamine (Choudhury et al., 2022). Therefore, further studies on the metabolic changes in glutamine in aging are needed.

GSH is a tripeptide synthesized from three amino acids by the enzymatic system and is a common antioxidant in cells. Although its primary anabolic sites are the liver and kidney, GSH is present in almost all cells of the body (Jana et al., 2021). Previous studies have mentioned that its levels decrease during aging (Mitchell et al., 2000; Rebrin and Sohal, 2008; Cantor and Sabatini, 2012; Homma and Fujii, 2015; Verdin, 2015; DeBerardinis and Chandel, 2016; Pavlova and Thompson, 2016), which is consistent with the results of metabolomic studies in recent years (Table 2). The oxidized form of GSH is called GSSG. GSH is the major form that exerts its function, and GSSG must be reduced to obtain GSH before the next round of reaction. GSH has significant effects in enhancing immunity and detoxification, and it has been reported in recent years that the intracellular detoxification process involving GSH has a certain delaying effect on senile deafness (Escartin et al., 2011; Scire et al., 2019; Ferreira et al., 2021; Someya and Kim, 2021). Combined with its functions, especially its antioxidant capacity, proper supplementation of GSH may have unexpected effects on aging or some age-related diseases. However, the strong antioxidant capacity of GSH itself also indicates that it is easily oxidized and has poor stability. In addition, as a tripeptide, it cannot cross the cell membrane directly by itself. These factors make it difficult to preserve and directly replenish GSH. However, the nanodrug delivery system developed in recent years may provide a new direction for artificial GSH supplementation (Li et al., 2021). According to the metabolomic research literature discussed above, GSH levels or GSH/GSSG levels in aging organs were relatively decreased in the aging stage, which means that it may indicate the aging process and could be an aging marker.

Glycine levels showed a tendency to decrease with aging (Table 1). Glycine is one of the amino acids that synthesize GSH, and its level is affected to some extent by the level of GSH, then influence the progress of aging (Kumar et al., 2020; Kumar et al., 2021). Glycine is also simultaneously the input amino acid for one-carbon metabolism and is able to contribute single carbon units to the folate cycle to produce a variety of one-carbon bound tetrahydrofolates (THF) (Locasale, 2013). These act as coenzymes in methylation reactions, including the generation of methionine by methionine synthase (METR-1 in *C. elegans*) and the universal methyl donor S-adenosylmethionine (SAMe) by S-adenosylmethionine synthase (SAMS-1) in *C. elegans* (Locasale, 2013). These output metabolites of one carbon metabolism support a number of biological functions (Locasale, 2013). In *C. elegans*, mutations in the metabolic gene SAMS-1 and levels of SAMe and S-adenosylhomocysteine (SAH) have been implicated in the regulation of senescence (Hansen et al., 2005; Cabreiro et al., 2013). Another study in mouse pluripotent stem cells showed that threonine catabolism contributes one carbon to the same synthesis and histone methylation via the glycine cleavage pathway (Shyh-Chang et al., 2013). In recent years, glycine and N-acetylcysteine (GlyNAC) supplementation for 16 or 24 weeks has been shown to improve GSH deficiency, oxidative stress, mitochondrial dysfunction, inflammatory response, insulin resistance, muscle strength, and cognition in elderly subjects, whereas these beneficial effects were reduced 12 weeks after cessation of GlyNAC supplementation (Kumar et al., 2021; Kumar et al., 2023). A study in *C. elegans* showed that the addition of 5–500 μM glycine was able to increase the lifespan of nematode, whereas higher levels of glycine (5–10 mM) had no such effect (Liu et al., 2019). Taken together, these results suggest that glycine may serve as an aging marker.

Leucine, isoleucine, and valine all contain a branched chain structure, so they are collectively called branched-chain amino acids (BCAAs), and they are all essential amino acids. BCAAs have three main roles: as a raw material for protein synthesis, as a signaling molecule to stimulate protein synthesis, and to break down energy production during fasting (Le Couteur et al., 2020). Metabolism of BCAAs is concentrated in the muscle, and muscle tend to suffer from loss of quality and strength as the body ages. Reduced muscle anabolism and decreased response to insulin and amino acids in aging skeletal muscle, but still responsive to the administration of BCAAs, particularly leucine (Fujita and Volpi, 2006). Leucine can stimulate insulin secretion from beta cells in the pancreatic islets and work synergistically with glucose to regulate insulin secretion in response to dietary carbohydrate and protein intake (Neinast et al., 2019; Le Couteur et al., 2020). Studies have shown that a diet high in leucine can reverse the phenomenon of impaired muscle protein synthesis in the elderly, but the same diet had no significant effect on muscle protein synthesis in young adults (Katsanos et al., 2006). In addition, a study showed that skeletal muscle mass increased in the intervention group after dietary intervention with BCAA-rich supplements in patients with gait disorders, although there was no significant impact on daily activated (Moriwaki et al., 2019). However, it remains to be confirmed whether supplemental leucine can help older adults regain lost muscle mass. A systematic review and meta-analysis of leucine supplementation in older adults showed that leucine increased the rate of protein synthesis, but had no effect on lean body mass or lean leg mass in older adults (Xu et al., 2015). In addition, BCAAs levels tend to increase with age during the aging process (Table 1), and energy restriction, protein restriction, gastric bypass surgery, etc., which are thought to improve metabolism, will decrease plasma BCAA levels (Magkos et al., 2013; Zheng et al., 2016a; Fontana et al., 2016). A study examining the effect of a low-BCAAs diet on normal lifespan in mice found that starting a low-BCAAs diet midway through life increased lifespan and that this effect was associated with decreased mTORC1 signaling, while increased levels of BCAAs in the brain may increase mTORC1 signaling (Richardson et al.,

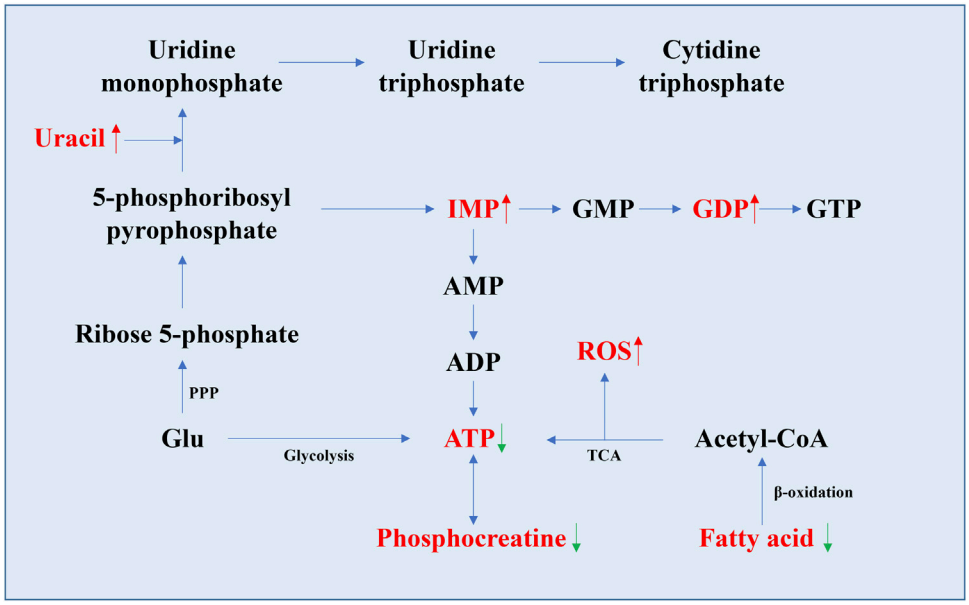

FIGURE 3
Schematic diagram of the nucleotide synthesis pathway and the pathway related to ATP generation. Metabolites with significant changes in their levels in aging organs are indicated in red font (data from Table 1). The rising trend is indicated by the red up arrow, and the decreasing trend is indicated by the green down arrow. The levels of IMP, GDP, and uracil were all relatively increased in aging organs, as well as ROS, while the levels of ATP, fatty acids, and phosphocreatine changed inversely.

2021). In addition to rodents and humans, studies of the effect of BCAAs on lifespan have been conducted in other biological models, such as *Saccharomyces cerevisiae*, *Caenorhabditis elegans*, and *Drosophila*, but the results have been inconsistent (Aris et al., 2013; Mansfeld et al., 2015; Juricic et al., 2020). In addition, BCAAs have been implicated in disease. Studies have shown that complete deprivation of BCAAs for a short period of time can improve insulin sensitivity in the liver (Xiao et al., 2011; Xiao et al., 2014). Experiments in mice and rats have shown that artificially increasing BCAA levels in the daily diet can induce obesity and insulin resistance (Newgard et al., 2009). These findings all indicate that low levels of BCAAs are beneficial for maintaining health and slowing down aging. However, plasma levels of BCAAs were lower in sarcopenic elderly subjects than in healthy elderly subjects, which means that sarcopenia is associated with reduced levels of BCAAs (Ottestad et al., 2018; Ter Borg et al., 2019). Taken together, differential changes in the levels of BCAAs in different age-related diseases suggest that BCAAs along may not be directly associated with the development of these diseases. Some scholars have noted that it may not be the right choice to group the three BCAAs into one category. The functions of leucine, valine, and isoleucine in the body are still different. For example, the blood level of isoleucine is positively correlated with human mortality, while valine and leucine show the opposite correlation (Deelen et al., 2019). Furthermore, leucine and isoleucine are insulinotropic in the postprandial phase, whereas valine and isoleucine are gluconeogenic in the fasting state (Le Couteur et al., 2020). Overall, although BCAAs may have an intriguing relationship with aging, more research is needed to further elucidate their role in aging and age-related diseases, as well as the differences between different species (Le Couteur et al., 2020; Babygirija and Lamming, 2021).

The involvement of amino acids and their derived metabolites in multiple metabolic pathways, combined with their diversity, makes it more difficult to delineate changes in their levels in aging organs from a holistic perspective. Significant changes in the levels of glutamate, glutamine, and BCAA have been reported in many publications, suggesting a close relationship between them and organ aging and making them important age-related metabolites. But their changing trends in different organs are not the same, more studies are needed to help better understand the role they may play in aging. Nevertheless, GSH or GSH/GSSG, as well as glycine levels, were decreased with aging in several organs, thus may serve as markers of aging.

ATP and uracil in nucleotide metabolites can be used as aging markers

Nucleotides, as the basic structural units of nucleic acids, are involved in almost all metabolic pathways in cells, such as coenzyme function, regulation, substrate activation, anabolism, and provision of nucleic acid subunits (Lane and Fan, 2015). Studies have shown that adenosine triphosphate (ATP) levels were significantly lower in the aging group in various organs of rats, mice, and human cell aging models (Table 1). The levels of inosine monophosphate (IMP), guanosine diphosphate (GDP), hypoxanthine, and uracil all increase with age (Figure 3). In the human fibroblast model, higher levels of purines (hypoxanthine,

7-methylguanine, and urate) and pyrimidine (3-ureidopropionate) and lower levels of thymidine were measured in normal and γ-ray-induced aging groups (James et al., 2015). In addition, the changes in inosine and uridine levels found in several studies varied. In the brain, heart, kidney, and liver of mice, the levels of inosine and uridine levels decreased with age (Zhang et al., 2021), whereas a study in rat showed an increase in uridine levels in the liver (Wesley et al., 2019). Increased levels of guanosine monophosphate (GMP) can be detected in the masseter muscle of aged rats (Morrison et al., 2019; Kato et al., 2021). Other substances with age-related changes in metabolite levels include deoxyribose and methylated nucleotides, which increase with age in the retina and optic nerve of aging mice, respectively (Wang et al., 2018).

The decrease in ATP is consistent with previous findings of decreased TCA cycle and OXPHOS flux in the mitochondria. Because of its important basic function in the body, it is difficult to confirm its role in the aging process. However, the total ATP level is detectable, so it is possible to make ATP a simple marker of aging with a perfect evaluation system. Hypoxanthine levels were positively correlated with age. Hypoxanthine is the product of the nucleotide degradation pathway and produces xanthine and uric acid under the action of xanthine oxidase (Lawal and Adeloju, 2012). Uracil is mentioned in several articles, and all point to a relative increase in uracil levels with age (Morrison et al., 2019; Kato et al., 2021; Zhang et al., 2021). It is a component of RNA in the form of uracil ribonucleotides, and appears in DNA in some special cases, such as abnormal cytosine deamination, and incorrect insertion of deoxy uracil dUTP during DNA synthesis (Fadda and Pomes, 2011; Lewis et al., 2016; Chakraborty and Stover, 2020). In general, uracil misincorporation into DNA is recognized and removed by DNA repair enzymes, but excess uracil mutations can cause DNA double-strand breaks, which in turn activate the p53-mediated apoptosis pathway (Yadav et al., 2016). From this perspective, the increase or accumulation of uracil that occurs during normal aging reflects the accumulation of DNA damage in organs and can be used as an aging marker.

Lysophosphatidylcholine (LPC) and fatty acids are possible aging markers in lipid metabolism

Lipids have important functions in living organisms, including energy storage, organ protection, and the formation of cell membrane systems in living organisms. In addition, many lipid metabolites and their derivatives play key roles in cell signaling, metabolic regulation, and other processes. In aged rats, studies have shown that the levels of several glycerophospholipids (GPLs) decreased in the soleus, while glycerol, 3-phosphoglycerol, and glycerophosphocholine increased in the gastrocnemius increased (Garvey et al., 2014). Fatty acids levels of in the soleus decrease with age but increase in the gastrocnemius muscle (Garvey et al., 2014). Lower levels of carnitine and low molecular weight acylcarnitine were found in the gastrocnemius and soleus (Garvey et al., 2014). Glycerol-3-phosphate and linolenic acid levels were reduced in the liver (Son et al., 2012). However, increased levels of cholesterol, betaine, carnitine, and acylamino bases were found in the liver (Son et al., 2012). An increase in total LPC and fatty acids was found in the brain (Zheng et al., 2016b), and the same occurred in the human vastus lateralis (Zheng et al., 2016b; Wilkinson et al., 2020; Zhang et al., 2021). In addition, except for alpha-linolenic acid, the levels of omega-3 and omega-6 fatty acids levels were significantly lower, whereas linoleic acid and arachidonic acid levels were higher in the rat brain (Zheng et al., 2016b). In aged mice, fatty acids accumulate in muscle, with increased levels of polyunsaturated fatty acids and decreased levels of phospholipids such as renal phospholipids and LPC in the heart (Houtkooper et al., 2011; Zhang et al., 2021). Relatively low levels of cholesterol are found in the cornea and optic nerve (Wang et al., 2018). Glycerol decreased in kidney and liver (Eum et al., 2020; Zhang et al., 2021), but increased in the retina (Wang et al., 2018). In addition, glycerol levels were decreased, and palmitic acid, oleic acid, myristic acid, stearic acid, and linoleic acid were increased after CR treatment (Mitchell et al., 2016).

Under normal conditions, the mitochondrial membrane is polyunsaturated, and its lipid composition is dominated by unsaturated lipids. Previous studies have shown that the unsaturation of the mitochondrial membrane decreases with age (Almaida-Pagan et al., 2012; Stanley et al., 2012), resulting in reduced mitochondrial production of energy production and increased levels of ROS, causing excessive oxidative stress that can damage organs during aging (Kubota et al., 2016; Wang et al., 2018). One study showed that individuals with higher levels of LPC had greater mitochondrial oxidative capacity (Semba et al., 2019), suggesting that LPC may affect mitochondrial oxidative capacity by participating in the formation of the normal mitochondrial membrane system. In addition, studies have shown that LPC levels can be significantly altered from normal conditions in several age-related diseases, including rheumatoid arthritis, atherosclerosis, cardiovascular disease, and AD (Newgard et al., 2009; Xiao et al., 2011; Xiao et al., 2014; Ottestad et al., 2018). Therefore, LPC, a substance involved in the composition of the mitochondrial membrane structure, can be used as a universal marker of aging. On this basis, if the effective level of LPC in the body can be artificially increased by external intervention, it may have unexpected effects on delaying the aging process.

Fatty acids showed a tendency to decrease with age in most studies. However, a significant accumulation of free fatty acids was observed in aged rat gastrocnemius muscle (Garvey et al., 2014). Considering that an important pathway for energy production from fatty acids is beta-oxidation which occurs in mitochondria (Kasumov et al., 2005; Lopaschuk et al., 2010; Houten et al., 2016), it is possible that the gastrocnemius muscle attempts to compensate for the gap in energy production through fatty acid β-oxidation capacity, but due to mitochondrial damage from aging, β-oxidation cannot proceed normally, resulting in the accumulation of free fatty acids (Garvey et al., 2014). Similar results have been found in rat livers (Son et al., 2012; Garvey et al., 2014). In the above research results, the level of carnitine, a substance that helps macromolecular fatty acids enter the mitochondrial membrane, was relatively lower in the aging stage (Table 1), which may reflect the inhibited β-oxidation pathway. In addition, fatty acids may also be involved in more complex regulatory processes, such as cognitive maintenance (Pifferi et al., 2010; Pifferi et al., 2015; Royo et al., 2018). However, some studies have shown that n-3 PUFAs

have an opposite regulatory effect in the human brain (Cunnane et al., 2009). Therefore, more research is needed to confirm the overall trend of changes in the levels of these substances with age.

Polyamine metabolism, NAD$^+$ and ROS

Polyamines (PAs) are ubiquitous low molecular weights biogenic amines and classically refer to three molecules: putrescine, spermidine, and spermine. Polyamines can interact with various cellular macromolecules, such as nucleic acids, ATP, proteins, and phospholipids, and thus play a critical role in many biological processes, including nucleic acids stabilization, protein synthesis, cell cycle progression, and cell proliferation (Bae et al., 2018; Igarashi and Kashiwagi, 2019). The changing trend of spermidine has different characteristics in different organs, with increasing levels in the masseter muscle of aging rats, but no significant changes levels in the colon cancer cell model (Kato et al., 2021). In contrast, spermine shows an increasing trend with aging in various organs (Wilkinson et al., 2020; Nagineni et al., 2021). Although rarely reported in the literature, polyamines may have unexpected anti-aging effects (Xu et al., 2020; Soda, 2022). One study showed that when rats were treated with spermine or spermidine, their cardiac creatine levels were reduced during aging, along with taurine, which were the same results as in CR-treated experiments (Mitchell et al., 2016; Zhang et al., 2017).

NAD$^+$, NADH, nicotinamide adenine dinucleotide phosphate (NADP) and reduced nicotinamide adenine dinucleotide phosphate (NADPH), as proton transfer carriers, are responsible for the function of transferring protons in various metabolic pathways. A study in rats showed that liver NAD$^+$/NADH levels decreased with age, and nicotinamide levels were also reduced (Son et al., 2012; Wesley et al., 2019). Correspondingly, NAD$^+$ levels in the gastrocnemius muscle decreased significantly, consistent with the concomitant observation of glycolysis (Garvey et al., 2014). In the brain, a relative decrease in NAD$^+$ levels was observed along with an increase in niacin levels (Wesley et al., 2019). Some studies have shown that lower levels of nicotinamide in the kidney, liver, and lungs of aging mice and relatively high levels of NAD$^+$, riboflavin, and nicotinamide in the choroid of the eye (Wang et al., 2018; Zhang et al., 2021). In cell models, relatively low levels of acetyl-CoA were detected in senescent breast cancer cells, and the amount of NADPH produced by the PPP pathway increased in the cells of the aging and apoptosis groups, but the total amount of NADPH in the cells decreased at the same time (Wu et al., 2017). Relative decreases in nicotinamide riboside and nicotinamide ribonucleotide levels were detected in the mesenchymal stromal cell model (Fernandez-Rebollo et al., 2020), and relatively low levels of NAD$^+$ and NADPH were detected in human umbilical vein endothelial cells and colon cancer cells, respectively (Yi et al., 2020; Nagineni et al., 2021). Overall, NAD$^+$ shows a relative decrease in levels in aging organs, and can be used as an aging marker. Research has shown that the decrease in tissue NAD$^+$ levels during aging is directly related to the increased expression of macrophage CD38$^+$, a transmembrane protein that can consume NAD$^+$ to form cyclic adenosine diphosphate (ADP)-ribose, ADP-ribose, and nicotinamide (Camacho-Pereira et al., 2016; Covarrubias et al., 2020).

As reported, ROS has been widely used as an aging marker. ROS are partially reduced or excited forms of oxygen, negative changes in the external environment can directly cause ROS accumulation. And cells also continue to generate endogenous ROS during normal metabolism (Sarniak et al., 2016). It is generally believed that the latter is the main reason for the marked increase in ROS levels in senescent cells. The level of intracellular ROS shows a trend of continuous accumulation throughout the life cycle of cells, and the levels of several antioxidant molecules, such as GSH, creatine, and fumarate, in senescent cells gradually decreased with increasing cell passage (Table 1), indicating that the cell's antioxidant defense system weakens as cells age. Although the metabolomic article selected here does not provide a direct examination of ROS levels, in the free radical theory of senescence established more than five decades ago, ROS are essential for senescence and a large number of experiments to date have demonstrated the role of ROS in inducing senescence (Baranov and Baranova, 2017). However, new experimental data and clinical studies in recent years suggest that ROS also play an important role in normal cellular life processes, a finding that transforms ROS change from harmful to common metabolites like other metabolites (Baranov and Baranova, 2017; Mittler, 2017). During the development of *C. elegans*, the gradually increasing levels of ROS enhance the nematode's ability to tolerate stress and thus have the effect of prolonging its lifespan (Bazopoulou et al., 2019). However, such findings rather emphasize the validity of ROS as a marker of senescence.

In general, the NAD$^+$ levels decreased relatively in aging organs, while ROS showed a trend of continuous accumulation. Since NADPH can be used to maintain the reduced state of GSH, it is believed that this may be due to the increase in the amount of intracellular ROS, which consumes a large amount of GSH and causes the reduction of senescent cells (Wu et al., 2017). Therefore, the close relationship between ROS, NAD$^+$ and aging, the fundamental role that ROS and NAD$^+$ play in the life activities of cell, and the relatively mature means of detecting their levels make ROS and NAD$^+$ good markers of aging.

Conclusion

Aging, as a common phenomenon in nature, has attracted the continuous research of people for thousands of years. The study of the aging metabolome has shown that the intensity of mitochondrial TCA cycle in organs decreases during the aging stage, and at the same time, the glycolytic flux increased increases. Dysregulation of lipid oxidation pathways in normal aging and similar energy production manifestations in some age-related diseases further suggest that disruption of energy production pathways during aging may be the key to initiating or accelerating aging.

On the other hand, we also found that changes in the levels of some metabolites with the aging process have different trends in different organs, and some have obvious anteroposterior sequences, such as the gastrocnemius and soleus of rats, while others have no clear pattern in terms of current data. There may be two reasons for

this phenomenon: first, the methods used were different, which in turn led to opposite results regarding changes in the levels of some metabolites. Second, it is true that different organs do not start to age at the same time. Because of their different functions, they are affected by aging to different degrees, which ultimately manifests itself as a difference in the progression of aging (Schaum et al., 2020; Tabula Muris, 2020). Since different organs often work together as a whole, combining data from multiple omics studies may be a better approach to understanding aging.

Finally, metabolomic studies directly on organs can reflect the metabolite status of these organs during aging, and the establishment of an aging organ metabolite clock may allow us to understand aging from a new perspective, provide more ways to treat aging-related diseases, and be beneficial to the health maintenance of elderly individuals. Recently, an article detailed the brains of aging and young mice, yielding a total of 1,547 different annotated metabolites (Ding et al., 2021). Through this work, the author presents a large-scale, comprehensive metabolomic map of the aging mouse brain that can inform and help researchers better understand previously established genome, transcriptome, and proteome maps (Ding et al., 2021).

Here, we use metabolomics data from aging tissues to summarize that pyruvate, GSH or GSH/GSSG levels, glycine, ATP, uracil, NAD^+, and ROS as global aging markers that have the same change trend in different organs, while Glu, lactate, glutamate, glutamine, BCAAs, LPC, and fatty acids as potential aging markers that need more research to confirm their role in aging. We hope that this will be useful for constructing metabolomic aging clocks based on organ metabolomic data. However, at the present stage, it is extremely difficult to sample and detect organs *in vivo* compared to blood or other body fluids. In addition, some low-abundance or structurally specific small-molecule metabolites may require multiple detection methods to be effectively detected. These factors have a certain hindering effect on the promotion of metabolomic research results in organs, which may be the reason why there is no clear and accurate aging clock based on organ metabolomics to date (Rutledge et al., 2022). In conclusion, metabolomics studies of aging organs using omics techniques can truly reflect the changes we go through with aging, and will expand our understanding of aging as well as age-related diseases.

Author contributions

WF and SC wrote the manuscript. WF, SC, and XC compiled the tables and created the figures. XJ and SL revised the manuscript. Both XC and BL designed and edited the manuscript. All authors contributed to the article and approved the submitted version.

Funding

This work was supported by grants from the National Natural Science Foundation of China (32000387) to XC, the Zhejiang Provincial Natural Science Foundation of China (LY23C060001) and the Scientific Research Foundation of Zhejiang A&F University (2021LFR053) to XJ, as well as the Swedish Cancer Fund (Cancerfonden) (19 0069) and the Swedish Research Council (Vetenskapsrådet) (VR 2019-03604) to BL.

Conflict of interest

The authors declare that the research was conducted in the absence of any commercial or financial relationships that could be construed as a potential conflict of interest.

Publisher's note

References

Adav, S. S., and Wang, Y. (2021). Metabolomics signatures of aging: Recent advances. *Aging Dis.* 12 (2), 646–661. doi:10.14336/AD.2020.0909

Adeva-Andany, M., Lopez-Ojen, M., Funcasta-Calderon, R., Ameneiros-Rodriguez, E., Donapetry-Garcia, C., Vila-Altesor, M., et al. (2014). Comprehensive review on lactate metabolism in human health. *Mitochondrion* 17, 76–100. doi:10.1016/j.mito.2014.05.007

Almaida-Pagan, P. F., de Costa, J., Mendiola, P., and Tocher, D. R. (2012). Changes in tissue and mitochondrial membrane composition during rapid growth, maturation and aging in rainbow trout, oncorhynchus mykiss. *Comp. Biochem. Physiol. B Biochem. Mol. Biol.* 161 (4), 404–412. doi:10.1016/j.cbpb.2012.01.006

Anastasiou, D., Poulogiannis, G., Asara, J. M., Boxer, M. B., Jiang, J. K., Shen, M., et al. (2011). Inhibition of pyruvate kinase M2 by reactive oxygen species contributes to cellular antioxidant responses. *Science* 334 (6060), 1278–1283. doi:10.1126/science.1211485

Andersen, J. V., Markussen, K. H., Jakobsen, E., Schousboe, A., Waagepetersen, H. S., Rosenberg, P. A., et al. (2021). Glutamate metabolism and recycling at the excitatory synapse in health and neurodegeneration. *Neuropharmacology* 196, 108719. doi:10.1016/j.neuropharm.2021.108719

Aris, J. P., Alvers, A. L., Ferraiuolo, R. A., Fishwick, L. K., Hanvivatpong, A., Hu, D., et al. (2013). Autophagy and leucine promote chronological longevity and respiration proficiency during calorie restriction in yeast. *Exp. Gerontol.* 48 (10), 1107–1119. doi:10.1016/j.exger.2013.01.006

Babygirija, R., and Lamming, D. W. (2021). The regulation of healthspan and lifespan by dietary amino acids. *Transl. Med. Aging* 5, 17–30. doi:10.1016/j.tma.2021.05.001

Bae, D. H., Lane, D. J. R., Jansson, P. J., and Richardson, D. R. (2018). The old and new biochemistry of polyamines. *Biochim. Biophys. Acta Gen. Subj.* 1862 (9), 2053–2068. doi:10.1016/j.bbagen.2018.06.004

Baranov, V. S., and Baranova, E. V. (2017). Aging and ambiguous ROS: System genetics analysis. *Curr. aging Sci.* 10 (1), 6–11. doi:10.2174/1874609809666160921114504

Bazopoulou, D., Knoefler, D., Zheng, Y., Ulrich, K., Oleson, B. J., Xie, L., et al. (2019). Developmental ROS individualizes organismal stress resistance and lifespan. *Nature* 576 (7786), 301–305. doi:10.1038/s41586-019-1814-y

Bergersen, L. H. (2007). Is lactate food for neurons? Comparison of monocarboxylate transporter subtypes in brain and muscle. *Neuroscience* 145 (1), 11–19. doi:10.1016/j.neuroscience.2006.11.062

Bergman, B. C., Horning, M. A., Casazza, G. A., Wolfel, E. E., Butterfield, G. E., and Brooks, G. A. (2000). Endurance training increases gluconeogenesis during rest and

exercise in men. *Am. J. Physiol. Endocrinol. Metab.* 278 (2), E244–E251. doi:10.1152/ajpendo.2000.278.2.E244

Bouzat, P., Sala, N., Suys, T., Zerlauth, J. B., Marques-Vidal, P., Feihl, F., et al. (2014). Cerebral metabolic effects of exogenous lactate supplementation on the injured human brain. *Intensive Care Med.* 40 (3), 412–421. doi:10.1007/s00134-013-3203-6

Bozzo, L., Puyal, J., and Chatton, J. Y. (2013). Lactate modulates the activity of primary cortical neurons through a receptor-mediated pathway. *PLoS One* 8 (8), e71721. doi:10.1371/journal.pone.0071721

Brooks, G. A. (1986). The lactate shuttle during exercise and recovery. *Med. Sci. Sports Exerc* 18 (3), 360–368. doi:10.1249/00005768-198606000-00019

Burger, P. M., Mehl, E., Cameron, P. L., Maycox, P. R., Baumert, M., Lottspeich, F., et al. (1989). Synaptic vesicles immunoisolated from rat cerebral cortex contain high levels of glutamate. *Neuron* 3 (6), 715–720. doi:10.1016/0896-6273(89)90240-7

Cabreiro, F., Au, C., Leung, K. Y., Vergara-Irigaray, N., Cochemé, H. M., Noori, T., et al. (2013). Metformin retards aging in *C. elegans* by altering microbial folate and methionine metabolism. *Cell* 153 (1), 228–239. doi:10.1016/j.cell.2013.02.035

Camacho-Pereira, J., Tarrago, M. G., Chini, C. C. S., Nin, V., Escande, C., Warner, G. M., et al. (2016). CD38 dictates age-related nad decline and mitochondrial dysfunction through an SIRT3-dependent mechanism. *Cell metab.* 23 (6), 1127–1139. doi:10.1016/j.cmet.2016.05.006

Canevelli, M., Lucchini, F., Quarata, F., Bruno, G., and Cesari, M. (2016). Nutrition and dementia: Evidence for preventive approaches? *Nutrients* 8 (3), 144. doi:10.3390/nu8030144

Cantor, J. R., and Sabatini, D. M. (2012). Cancer cell metabolism: One hallmark, many faces. *Cancer Discov.* 2 (10), 881–898. doi:10.1158/2159-8290.CD-12-0345

Chakraborty, J., and Stover, P. J. (2020). Deoxyuracil in DNA in health and disease. *Curr. Opin. Clin. Nutr. Metab. Care* 23 (4), 247–252. doi:10.1097/MCO.0000000000000660

Chao, C. C., Shen, P. W., Tzeng, T. Y., Kung, H. J., Tsai, T. F., and Wong, Y. H. (2021). Human iPSC-derived neurons as a platform for deciphering the mechanisms behind brain aging. *Biomedicines* 9 (11), 1635. doi:10.3390/biomedicines9111635

Choudhury, D., Rong, N., Ikhapoh, I., Rajabian, N., Tseropoulos, G., Wu, Y., et al. (2022). Inhibition of glutaminolysis restores mitochondrial function in senescent stem cells. *Cell Rep.* 41 (9), 111744. doi:10.1016/j.celrep.2022.111744

Clement, J., Wong, M., Poljak, A., Sachdev, P., and Braidy, N. (2019). The plasma NAD(+) metabolome is dysregulated in "normal" aging. *Rejuvenation Res.* 22 (2), 121–130. doi:10.1089/rej.2018.2077

Covarrubias, A. J., Kale, A., Perrone, R., Lopez-Dominguez, J. A., Pisco, A. O., Kasler, H. G., et al. (2020). Senescent cells promote tissue NAD(+) decline during ageing via the activation of CD38(+) macrophages. *Nat. Metab.* 2 (11), 1265–1283. doi:10.1038/s42255-020-00305-3

Cunnane, S. C., Plourde, M., Pifferi, F., Begin, M., Feart, C., and Barberger-Gateau, P. (2009). Fish, docosahexaenoic acid and Alzheimer's disease. *Prog. Lipid Res.* 48 (5), 239–256. doi:10.1016/j.plipres.2009.04.001

Cunnane, S. C., Trushina, E., Morland, C., Prigione, A., Casadesus, G., Andrews, Z. B., et al. (2020). Brain energy rescue: An emerging therapeutic concept for neurodegenerative disorders of ageing. *Nat. Rev. Drug Discov.* 19 (9), 609–633. doi:10.1038/s41573-020-0072-x

DeBerardinis, R. J., and Chandel, N. S. (2016). Fundamentals of cancer metabolism. *Sci. Adv.* 2 (5), e1600200. doi:10.1126/sciadv.1600200

Deelen, J., Kettunen, J., Fischer, K., van der Spek, A., Trompet, S., Kastenmuller, G., et al. (2019). A metabolic profile of all-cause mortality risk identified in an observational study of 44,168 individuals. *Nat. Commun.* 10 (1), 3346. doi:10.1038/s41467-019-11311-9

Ding, J., Ji, J., Rabow, Z., Shen, T., Folz, J., Brydges, C. R., et al. (2021). A metabolome atlas of the aging mouse brain. *Nat. Commun.* 12 (1), 6021. doi:10.1038/s41467-021-26310-y

Domingo-Orti, I., Lamas-Domingo, R., Ciudin, A., Hernandez, C., Herance, J. R., Palomino-Schatzlein, M., et al. (2021). Metabolic footprint of aging and obesity in red blood cells. *Aging (Albany NY)* 13 (4), 4850–4880. doi:10.18632/aging.202693

dos Santos, J. M., Benite-Ribeiro, S. A., Queiroz, G., and Duarte, J. A. (2012). The effect of age on glucose uptake and GLUT1 and GLUT4 expression in rat skeletal muscle. *Cell Biochem. Funct.* 30 (3), 191–197. doi:10.1002/cbf.1834

Emhoff, C. A., Messonnier, L. A., Horning, M. A., Fattor, J. A., Carlson, T. J., and Brooks, G. A. (2013). Gluconeogenesis and hepatic glycogenolysis during exercise at the lactate threshold. *J. Appl. Physiol.* 114 (3), 297–306. doi:10.1152/japplphysiol.01202.2012

Escartin, C., Won, S. J., Malgorn, C., Auregan, G., Berman, A. E., Chen, P. C., et al. (2011). Nuclear factor erythroid 2-related factor 2 facilitates neuronal glutathione synthesis by upregulating neuronal excitatory amino acid transporter 3 expression. *J. Neurosci.* 31 (20), 7392–7401. doi:10.1523/JNEUROSCI.6577-10.2011

Eum, J. Y., Lee, J. C., Yi, S. S., Kim, I. Y., Seong, J. K., and Moon, M. H. (2020). Aging-related lipidomic changes in mouse serum, kidney, and heart by nanoflow ultrahigh-performance liquid chromatography-tandem mass spectrometry. *J. Chromatogr. A* 1618, 460849. doi:10.1016/j.chroma.2020.460849

Fadda, E., and Pomes, R. (2011). On the molecular basis of uracil recognition in DNA: Comparative study of T-A versus U-A structure, dynamics and open base pair kinetics. *Nucleic Acids Res.* 39 (2), 767–780. doi:10.1093/nar/gkq812

Fernandez-Rebollo, E., Franzen, J., Goetzke, R., Hollmann, J., Ostrowska, A., Oliverio, M., et al. (2020). Senescence-associated metabolomic phenotype in primary and iPSC-derived mesenchymal stromal cells. *Stem Cell Rep.* 14 (2), 201–209. doi:10.1016/j.stemcr.2019.12.012

Ferreira, A. V., Koeken, V., Matzaraki, V., Kostidis, S., Alarcon-Barrera, J. C., de Bree, L. C. J., et al. (2021). Glutathione metabolism contributes to the induction of trained immunity. *Cells* 10 (5), 971. doi:10.3390/cells10050971

Flaherty, D. C., Hoxha, B., Sun, J., Gurji, H., Simecka, J. W., Mallet, R. T., et al. (2010). Pyruvate-fortified fluid resuscitation improves hemodynamic stability while suppressing systemic inflammation and myocardial oxidative stress after hemorrhagic shock. *Mil. Med.* 175 (3), 166–172. doi:10.7205/milmed-d-09-00161

Fleischer, J. G., Schulte, R., Tsai, H. H., Tyagi, S., Ibarra, A., Shokhirev, M. N., et al. (2018). Predicting age from the transcriptome of human dermal fibroblasts. *Genome Biol.* 19 (1), 221. doi:10.1186/s13059-018-1599-6

Fontana, L., Cummings, N. E., Arriola Apelo, S. I., Neuman, J. C., Kasza, I., Schmidt, B. A., et al. (2016). Decreased consumption of branched-chain amino acids improves metabolic health. *Cell Rep.* 16 (2), 520–530. doi:10.1016/j.celrep.2016.05.092

Fujita, S., and Volpi, E. (2006). Amino acids and muscle loss with aging. *J. Nutr.* 136, 277S–280S. doi:10.1093/jn/136.1.277S

Garvey, S. M., Dugle, J. E., Kennedy, A. D., McDunn, J. E., Kline, W., Guo, L., et al. (2014). Metabolomic profiling reveals severe skeletal muscle group-specific perturbations of metabolism in aged FBN rats. *Biogerontology* 15 (3), 217–232. doi:10.1007/s10522-014-9492-5

Gaspar, R. C., Munoz, V. R., Nakandakari, S., Vieira, R. F. L., da Conceicao, L. R., de Oliveira, F., et al. (2020). Aging is associated with increased TRB3, ER stress, and hepatic glucose production in the liver of rats. *Exp. Gerontol.* 139, 111021. doi:10.1016/j.exger.2020.111021

Gewirtz, D. A. (1999). A critical evaluation of the mechanisms of action proposed for the antitumor effects of the anthracycline antibiotics adriamycin and daunorubicin. *Biochem. Pharmacol.* 57 (7), 727–741. doi:10.1016/s0006-2952(98)00307-4

Gruning, N. M., Rinnerthaler, M., Bluemlein, K., Mulleder, M., Wamelink, M. M., Lehrach, H., et al. (2011). Pyruvate kinase triggers a metabolic feedback loop that controls redox metabolism in respiring cells. *Cell metab.* 14 (3), 415–427. doi:10.1016/j.cmet.2011.06.017

Gueli, M. C., and Taibi, G. (2013). Alzheimer's disease: Amino acid levels and brain metabolic status. *Neurol. Sci.* 34 (9), 1575–1579. doi:10.1007/s10072-013-1289-9

Hansen, M., Hsu, A. L., Dillin, A., and Kenyon, C. (2005). New genes tied to endocrine, metabolic, and dietary regulation of lifespan from a *Caenorhabditis elegans* genomic RNAi screen. *PLoS Genet.* 1 (1), 119–128. doi:10.1371/journal.pgen.0010017

Heilbronn, L. K., and Ravussin, E. (2003). Calorie restriction and aging: Review of the literature and implications for studies in humans. *Am. J. Clin. Nutr.* 78 (3), 361–369. doi:10.1093/ajcn/78.3.361

Hertel, J., Friedrich, N., Wittfeld, K., Pietzner, M., Budde, K., Van der Auwera, S., et al. (2016). Measuring biological age via metabonomics: The metabolic age score. *J. Proteome Res.* 15 (2), 400–410. doi:10.1021/acs.jproteome.5b00561

Homma, T., and Fujii, J. (2015). Application of glutathione as anti-oxidative and anti-aging drugs. *Curr. Drug Metab.* 16 (7), 560–571. doi:10.2174/1389200216666151015114515

Hopkins, F. G. (1929). On glutathione: A reinvestigation. *J. Biol. Chem.* 84 (1), 269–320. doi:10.1016/s0021-9258(18)77062-2

Horvath, S., and Raj, K. (2018). DNA methylation-based biomarkers and the epigenetic clock theory of ageing. *Nat. Rev. Genet.* 19 (6), 371–384. doi:10.1038/s41576-018-0004-3

Hoshino, T., Kato, Y., Sugahara, K., and Katakura, A. (2022). Aging-related metabolic changes in the extensor digitorum longus muscle of senescence-accelerated mouse-prone 8. *Geriatr. Gerontol. Int.* 22 (2), 160–167. doi:10.1111/ggi.14333

Houten, S. M., Violante, S., Ventura, F. V., and Wanders, R. J. (2016). The biochemistry and physiology of mitochondrial fatty acid beta-oxidation and its genetic disorders. *Annu. Rev. physiology* 78, 23–44. doi:10.1146/annurev-physiol-021115-105045

Houtkooper, R. H., Argmann, C., Houten, S. M., Canto, C., Jeninga, E. H., Andreux, P. A., et al. (2011). The metabolic footprint of aging in mice. *Sci. Rep.* 1, 134. doi:10.1038/srep00134

Hu, S., Bai, X. D., Liu, X. Q., Wang, H. B., Zhong, Y. X., Fang, T., et al. (2013). Pyruvate ringer's solution corrects lactic acidosis and prolongs survival during hemorrhagic shock in rats. *J. Emerg. Med.* 45 (6), 885–893. doi:10.1016/j.jemermed.2013.04.062

Hunsberger, H. C., Greenwood, B. P., Tolstikov, V., Narain, N. R., Kiebish, M. A., and Denny, C. A. (2020). Divergence in the metabolome between natural aging and Alzheimer's disease. *Sci. Rep.* 10 (1), 12171. doi:10.1038/s41598-020-68739-z

Iannetti, E. F., Smeitink, J. A. M., Willems, P., Beyrath, J., and Koopman, W. J. H. (2018). Rescue from galactose-induced death of leigh syndrome patient cells by pyruvate and NAD. *Cell Death Dis.* 9 (11), 1135. doi:10.1038/s41419-018-1179-4

Igarashi, K., and Kashiwagi, K. (2019). The functional role of polyamines in eukaryotic cells. *Int. J. Biochem. Cell Biol.* 107, 104–115. doi:10.1016/j.biocel.2018.12.012

Inoshita, M., Umehara, H., Watanabe, S. Y., Nakataki, M., Kinoshita, M., Tomioka, Y., et al. (2018). Elevated peripheral blood glutamate levels in major depressive disorder. *Neuropsychiatr. Dis. Treat.* 14, 945–953. doi:10.2147/NDT.S159855

James, E. L., Michalek, R. D., Pitiyage, G. N., de Castro, A. M., Vignola, K. S., Jones, J., et al. (2015). Senescent human fibroblasts show increased glycolysis and redox homeostasis with extracellular metabolomes that overlap with those of irreparable DNA damage, aging, and disease. *J. Proteome Res.* 14 (4), 1854–1871. doi:10.1021/pr501221g

Jana, A., Joseph, M. M., Munan, S., Maiti, K. K., and Samanta, A. (2021). A single benzene fluorescent probe for efficient formaldehyde sensing in living cells using glutathione as an amplifier. *J. Photochem Photobiol. B* 214, 112091. doi:10.1016/j.jphotobiol.2020.112091

Jarak, I., Almeida, S., Carvalho, R. A., Sousa, M., Barros, A., Alves, M. G., et al. (2018). Senescence and declining reproductive potential: Insight into molecular mechanisms through testicular metabolomics. *Biochim. Biophys. Acta Mol. Basis Dis.* 1864 (10), 3388–3396. doi:10.1016/j.bbadis.2018.07.028

Johmura, Y., Yamanaka, T., Omori, S., Wang, T. W., Sugiura, Y., Matsumoto, M., et al. (2021). Senolysis by glutaminolysis inhibition ameliorates various age-associated disorders. *Science* 371 (6526), 265–270. doi:10.1126/science.abb5916

Johnson, L. C., Parker, K., Aguirre, B. F., Nemkov, T. G., D'Alessandro, A., Johnson, S. A., et al. (2019). The plasma metabolome as a predictor of biological aging in humans. *Geroscience* 41 (6), 895–906. doi:10.1007/s11357-019-00123-w

Julio-Pieper, M., Flor, P. J., Dinan, T. G., and Cryan, J. F. (2011). Exciting times beyond the brain: Metabotropic glutamate receptors in peripheral and non-neural tissues. *Pharmacol. Rev.* 63 (1), 35–58. doi:10.1124/pr.110.004036

Juricic, P., Grönke, S., and Partridge, L. (2020). Branched-chain amino acids have equivalent effects to other essential amino acids on lifespan and aging-related traits in *Drosophila*. *journals gerontology Ser. A, Biol. Sci. Med. Sci.* 75 (1), 24–31. doi:10.1093/gerona/glz080

Justice, J. N., Nambiar, A. M., Tchkonia, T., LeBrasseur, N. K., Pascual, R., Hashmi, S. K., et al. (2019). Senolytics in idiopathic pulmonary fibrosis: Results from a first-in-human, open-label, pilot study. *EBioMedicine* 40, 554–563. doi:10.1016/j.ebiom.2018.12.052

Karakelides, H., Irving, B. A., Short, K. R., O'Brien, P., and Nair, K. S. (2010). Age, obesity, and sex effects on insulin sensitivity and skeletal muscle mitochondrial function. *Diabetes* 59 (1), 89–97. doi:10.2337/db09-0591

Kasumov, T., Adams, J. E., Bian, F., David, F., Thomas, K. R., Jobbins, K. A., et al. (2005). Probing peroxisomal beta-oxidation and the labelling of acetyl-coa proxies with [1-(13C)]octanoate and [3-(13C)]octanoate in the perfused rat liver. *Biochem. J.* 389 (2), 397–401. doi:10.1042/BJ20050144

Kato, Y., Hoshino, T., Ogawa, Y., Sugahara, K., and Katakura, A. (2021). Metabolome analysis of masseter muscle in senescence-accelerated mouse-prone 8 (SAMP8). *Resear Sq.* 2021. doi:10.21203/rs.3.rs-389321/v1

Katsanos, C. S., Kobayashi, H., Sheffield-Moore, M., Aarsland, A., and Wolfe, R. R. (2006). A high proportion of leucine is required for optimal stimulation of the rate of muscle protein synthesis by essential amino acids in the elderly. *Am. J. Physiol. Endocrinol. Metab.* 291 (2), E381–E387. doi:10.1152/ajpendo.00488.2005

Kendall, E. C., Mason, H. L., and McKenzie, B. F. (1930). A study of glutathione. The structure of glutathione. *J. Biol. Chem.* 87 (1), 55–79. doi:10.1016/s0021-9258(18)76892-0

Khattri, R. B., Puglise, J., Ryan, T. E., Walter, G. A., Merritt, M. E., and Barton, E. R. (2022). Isolated murine skeletal muscles utilize pyruvate over glucose for oxidation. *Metabolomics Official J. Metabolomic Soc.* 18 (12), 105. doi:10.1007/s11306-022-01948-x

Kim, J. Y., Lee, S. H., Bae, I. H., Shin, D. W., Min, D., Ham, M., et al. (2018). Pyruvate protects against cellular senescence through the control of mitochondrial and lysosomal function in dermal fibroblasts. *J. Invest. Dermatol* 138 (12), 2522–2530. doi:10.1016/j.jid.2018.05.033

Kondoh, H., Kameda, M., and Yanagida, M. (2020). Whole blood metabolomics in aging research. *Int. J. Mol. Sci.* 22 (1), 175. doi:10.3390/ijms22010175

Kubota, M., Shui, Y. B., Liu, M., Bai, F., Huang, A. J., Ma, N., et al. (2016). Mitochondrial oxygen metabolism in primary human lens epithelial cells: Association with age, diabetes and glaucoma. *Free Radic. Biol. Med.* 97, 513–519. doi:10.1016/j.freeradbiomed.2016.07.016

Kuehne, A., Hildebrand, J., Soehle, J., Wenck, H., Terstegen, L., Gallinat, S., et al. (2017). An integrative metabolomics and transcriptomics study to identify metabolic alterations in aged skin of humans *in vivo*. *BMC Genomics* 18 (1), 169. doi:10.1186/s12864-017-3547-3

Kumar, P., Liu, C., Hsu, J. W., Chacko, S., Minard, C., Jahoor, F., et al. (2021). Glycine and N-acetylcysteine (GLyNAC) supplementation in older adults improves glutathione deficiency, oxidative stress, mitochondrial dysfunction, inflammation, insulin resistance, endothelial dysfunction, genotoxicity, muscle strength, and cognition: Results of a pilot clinical trial. *Clin. Transl. Med.* 11 (3), e372. doi:10.1002/ctm2.372

Kumar, P., Liu, C., Suliburk, J., Hsu, J. W., Muthupillai, R., Jahoor, F., et al. (2023). Supplementing glycine and N-acetylcysteine (GLyNAC) in older adults improves glutathione deficiency, oxidative stress, mitochondrial dysfunction, inflammation, physical function, and aging hallmarks: A randomized clinical trial. *journals gerontology Ser. A, Biol. Sci. Med. Sci.* 78 (1), 75–89. doi:10.1093/gerona/glac135

Kumar, P., Liu, C., Suliburk, J. W., Minard, C. G., Muthupillai, R., Chacko, S., et al. (2020). Supplementing glycine and N-acetylcysteine (GLyNAC) in aging hiv patients improves oxidative stress, mitochondrial dysfunction, inflammation, endothelial dysfunction, insulin resistance, genotoxicity, strength, and cognition: Results of an open-label clinical trial. *Biomedicines* 8 (10), 390. doi:10.3390/biomedicines8100390

Lane, A. N., and Fan, T. W. (2015). Regulation of mammalian nucleotide metabolism and biosynthesis. *Nucleic Acids Res.* 43 (4), 2466–2485. doi:10.1093/nar/gkv047

Lauritzen, K. H., Morland, C., Puchades, M., Holm-Hansen, S., Hagelin, E. M., Lauritzen, F., et al. (2014). Lactate receptor sites link neurotransmission, neurovascular coupling, and brain energy metabolism. *Cereb. Cortex* 24 (10), 2784–2795. doi:10.1093/cercor/bht136

Lawal, A. T., and Adeloju, S. B. (2012). Progress and recent advances in fabrication and utilization of hypoxanthine biosensors for meat and fish quality assessment: A review. *Talanta* 100, 217–228. doi:10.1016/j.talanta.2012.07.085

Le, A., Cooper, C. R., Gouw, A. M., Dinavahi, R., Maitra, A., Deck, L. M., et al. (2010). Inhibition of lactate dehydrogenase a induces oxidative stress and inhibits tumor progression. *Proc. Natl. Acad. Sci. U. S. A.* 107 (5), 2037–2042. doi:10.1073/pnas.0914433107

Le Couteur, D. G., Solon-Biet, S. M., Cogger, V. C., Ribeiro, R., de Cabo, R., Raubenheimer, D., et al. (2020). Branched chain amino acids, aging and age-related health. *Ageing Res. Rev.* 64, 101198. doi:10.1016/j.arr.2020.101198

Lewis, C. A., Jr., Crayle, J., Zhou, S., Swanstrom, R., and Wolfenden, R. (2016). Cytosine deamination and the precipitous decline of spontaneous mutation during Earth's history. *Proc. Natl. Acad. Sci. U. S. A.* 113 (29), 8194–8199. doi:10.1073/pnas.1607580113

Li, M., Zhou, S., Chen, C., Ma, L., Luo, D., Tian, X., et al. (2020). Therapeutic potential of pyruvate therapy for patients with mitochondrial diseases: A systematic review. *Ther. Adv. Endocrinol. Metab.* 11, 2042018820938240. doi:10.1177/2042018820938240

Li, W., Li, M., and Qi, J. (2021). Nano-drug design based on the physiological properties of glutathione. *Molecules* 26 (18), 5567. doi:10.3390/molecules26185567

Liu, Y. J., Janssens, G. E., McIntyre, R. L., Molenaars, M., Kamble, R., Gao, A. W., et al. (2019). Glycine promotes longevity in *Caenorhabditis elegans* in a methionine cycle-dependent fashion. *PLoS Genet.* 15 (3), e1007633. doi:10.1371/journal.pgen.1007633

Locasale, J. W. (2013). Serine, glycine and one-carbon units: Cancer metabolism in full circle. *Nat. Rev. Cancer* 13 (8), 572–583. doi:10.1038/nrc3557

Lopaschuk, G. D., Ussher, J. R., Folmes, C. D., Jaswal, J. S., and Stanley, W. C. (2010). Myocardial fatty acid metabolism in health and disease. *Physiol. Rev.* 90 (1), 207–258. doi:10.1152/physrev.00015.2009

Magkos, F., Bradley, D., Schweitzer, G. G., Finck, B. N., Eagon, J. C., Ilkayeva, O., et al. (2013). Effect of Roux-en-Y gastric bypass and laparoscopic adjustable gastric banding on branched-chain amino acid metabolism. *Diabetes* 62 (8), 2757–2761. doi:10.2337/db13-0185

Mansfeld, J., Urban, N., Priebe, S., Groth, M., Frahm, C., Hartmann, N., et al. (2015). Branched-chain amino acid catabolism is a conserved regulator of physiological ageing. *Nat. Commun.* 6, 10043. doi:10.1038/ncomms10043

Mattson, M. P., and Arumugam, T. V. (2018). Hallmarks of brain aging: Adaptive and pathological modification by metabolic states. *Cell metab.* 27 (6), 1176–1199. doi:10.1016/j.cmet.2018.05.011

Meyer, C., Dostou, J. M., Welle, S. L., and Gerich, J. E. (2002). Role of human liver, kidney, and skeletal muscle in postprandial glucose homeostasis. *Am. J. Physiol. Endocrinol. Metab.* 282 (2), E419–E427. doi:10.1152/ajpendo.00032.2001

Mitchell, J. B., Russo, A., Kuppusamy, P., and Krishna, M. C. (2000). Radiation, radicals, and images. *Ann. N. Y. Acad. Sci.* 899, 28–43. doi:10.1111/j.1749-6632.2000.tb06174.x

Mitchell, S. J., Madrigal-Matute, J., Scheibye-Knudsen, M., Fang, E., Aon, M., Gonzalez-Reyes, J. A., et al. (2016). Effects of sex, strain, and energy intake on hallmarks of aging in mice. *Cell metab.* 23 (6), 1093–1112. doi:10.1016/j.cmet.2016.05.027

Mittler, R. (2017). ROS are good. *Trends Plant Sci.* 22 (1), 11–19. doi:10.1016/j.tplants.2016.08.002

Moriwaki, M., Wakabayashi, H., Sakata, K., and Domen, K. (2019). The effect of branched chain amino acids-enriched nutritional supplements on activities of daily living and muscle mass in inpatients with gait impairments: A randomized controlled trial. *J. Nutr. health & aging* 23 (4), 348–353. doi:10.1007/s12603-019-1172-3

Morrison, E. J., Champagne, D. P., Dzieciatkowska, M., Nemkov, T., Zimring, J. C., Hansen, K. C., et al. (2019). Parabiosis incompletely reverses aging-induced metabolic

changes and oxidant stress in mouse red blood cells. *Nutrients* 11 (6), 1337. doi:10.3390/nu11061337

Muzumdar, R., Ma, X., Atzmon, G., Vuguin, P., Yang, X., and Barzilai, N. (2004). Decrease in glucose-stimulated insulin secretion with aging is independent of insulin action. *Diabetes* 53 (2), 441–446. doi:10.2337/diabetes.53.2.441

Nagineni, C. N., Naz, S., Choudhuri, R., Chandramouli, G. V. R., Krishna, M. C., Brender, J. R., et al. (2021). Radiation-induced senescence reprograms secretory and metabolic pathways in colon cancer HCT-116 cells. *Int. J. Mol. Sci.* 22 (9), 4835. doi:10.3390/ijms22094835

Neinast, M., Murashige, D., and Arany, Z. (2019). Branched chain amino acids. *Annu. Rev. physiology* 81, 139–164. doi:10.1146/annurev-physiol-020518-114455

Newgard, C. B., An, J., Bain, J. R., Muehlbauer, M. J., Stevens, R. D., Lien, L. F., et al. (2009). A branched-chain amino acid-related metabolic signature that differentiates obese and lean humans and contributes to insulin resistance. *Cell metab.* 9 (4), 311–326. doi:10.1016/j.cmet.2009.02.002

Oliveira, J. R. S., Mohamed, J. S., Myers, M. J., Brooks, M. J., and Alway, S. E. (2019). Effects of hindlimb suspension and reloading on gastrocnemius and soleus muscle mass and function in geriatric mice. *Exp. Gerontol.* 115, 19–31. doi:10.1016/j.exger.2018.11.011

Olstad, E., Qu, H., and Sonnewald, U. (2007). Glutamate is preferred over glutamine for intermediary metabolism in cultured cerebellar neurons. *J. Cereb. Blood Flow. Metab.* 27 (4), 811–820. doi:10.1038/sj.jcbfm.9600400

Ottestad, I., Ulven, S. M., Oyri, L. K. L., Sandvei, K. S., Gjevestad, G. O., Bye, A., et al. (2018). Reduced plasma concentration of branched-chain amino acids in sarcopenic older subjects: A cross-sectional study. *Br. J. Nutr.* 120 (4), 445–453. doi:10.1017/S0007114518001307

Pavlova, N. N., and Thompson, C. B. (2016). The emerging hallmarks of cancer metabolism. *Cell metab.* 23 (1), 27–47. doi:10.1016/j.cmet.2015.12.006

Pifferi, F., Dorieux, O., Castellano, C. A., Croteau, E., Masson, M., Guillermier, M., et al. (2015). Long-chain n-3 PUFAs from fish oil enhance resting state brain glucose utilization and reduce anxiety in an adult nonhuman primate, the grey mouse lemur. *J. Lipid Res.* 56 (8), 1511–1518. doi:10.1194/jlr.M058933

Pifferi, F., Jouin, M., Alessandri, J. M., Roux, F., Perriere, N., Langelier, B., et al. (2010). N-3 long-chain fatty acids and regulation of glucose transport in two models of rat brain endothelial cells. *Neurochem. Int.* 56 (5), 703–710. doi:10.1016/j.neuint.2010.02.006

Rebrin, I., and Sohal, R. S. (2008). Pro-oxidant shift in glutathione redox state during aging. *Adv. Drug Deliv. Rev.* 60 (13-14), 1545–1552. doi:10.1016/j.addr.2008.06.001

Richardson, N. E., Konon, E. N., Schuster, H. S., Mitchell, A. T., Boyle, C., Rodgers, A. C., et al. (2021). Lifelong restriction of dietary branched-chain amino acids has sex-specific benefits for frailty and lifespan in mice. *Nat. Aging* 1 (1), 73–86. doi:10.1038/s43587-020-00006-2

Roberts, J. A., Varma, V. R., Huang, C. W., An, Y., Oommen, A., Tanaka, T., et al. (2020). Blood metabolite signature of metabolic syndrome implicates alterations in amino acid metabolism: Findings from the baltimore longitudinal study of aging (BLSA) and the tsuruoka metabolomics cohort study (TMCS). *Int. J. Mol. Sci.* 21 (4), 1249. doi:10.3390/ijms21041249

Robinson, O., Chadeau Hyam, M., Karaman, I., Climaco Pinto, R., Ala-Korpela, M., Handakas, E., et al. (2020). Determinants of accelerated metabolomic and epigenetic aging in a UK cohort. *Aging Cell* 19 (6), e13149. doi:10.1111/acel.13149

Royo, J., Villain, N., Champeval, D., Del Gallo, F., Bertini, G., Aujard, F., et al. (2018). Effects of n-3 polyunsaturated fatty acid supplementation on cognitive functions, electrocortical activity and neurogenesis in a non-human primate, the grey mouse lemur (*Microcebus murinus*). *Behav. Brain Res.* 347, 394–407. doi:10.1016/j.bbr.2018.02.029

Rupsingh, R., Borrie, M., Smith, M., Wells, J. L., and Bartha, R. (2011). Reduced hippocampal glutamate in Alzheimer disease. *Neurobiol. Aging* 32 (5), 802–810. doi:10.1016/j.neurobiolaging.2009.05.002

Rutledge, J., Oh, H., and Wyss-Coray, T. (2022). Measuring biological age using omics data. *Nat. Rev. Genet.* 23 (12), 715–727. doi:10.1038/s41576-022-00511-7

Sanders, C., Behrens, S., Schwartz, S., Wengreen, H., Corcoran, C. D., Lyketsos, C. G., et al. (2016). Nutritional status is associated with faster cognitive decline and worse functional impairment in the progression of dementia: The cache county dementia progression study1. *J. Alzheimers Dis.* 52 (1), 33–42. doi:10.3233/JAD-150528

Sarniak, A., Lipinska, J., Tytman, K., and Lipinska, S. (2016). Endogenous mechanisms of reactive oxygen species (ROS) generation. *Postepy Hig. Med. Dosw (Online).* 70 (0), 1150–1165. doi:10.5604/17322693.1224259

Schaum, N., Lehallier, B., Hahn, O., Palovics, R., Hosseinzadeh, S., Lee, S. E., et al. (2020). Ageing hallmarks exhibit organ-specific temporal signatures. *Nature* 583 (7817), 596–602. doi:10.1038/s41586-020-2499-y

Scire, A., Cianfruglia, L., Minnelli, C., Bartolini, D., Torquato, P., Principato, G., et al. (2019). Glutathione compartmentalization and its role in glutathionylation and other regulatory processes of cellular pathways. *Biofactors* 45 (2), 152–168. doi:10.1002/biof.1476

Semba, R. D., Zhang, P., Adelnia, F., Sun, K., Gonzalez-Freire, M., Salem, N., Jr., et al. (2019). Low plasma lysophosphatidylcholines are associated with impaired mitochondrial oxidative capacity in adults in the baltimore longitudinal study of aging. *Aging Cell* 18 (2), e12915. doi:10.1111/acel.12915

Shao, Y., and Le, W. (2019). Recent advances and perspectives of metabolomics-based investigations in Parkinson's disease. *Mol. Neurodegener.* 14 (1), 3. doi:10.1186/s13024-018-0304-2

Shyh-Chang, N., Locasale, J. W., Lyssiotis, C. A., Zheng, Y., Teo, R. Y., Ratanasirintrawoot, S., et al. (2013). Influence of threonine metabolism on S-adenosylmethionine and histone methylation. *Sci. (New York, NY)* 339 (6116), 222–226. doi:10.1126/science.1226603

Sibson, N. R., Dhankhar, A., Mason, G. F., Rothman, D. L., Behar, K. L., and Shulman, R. G. (1998). Stoichiometric coupling of brain glucose metabolism and glutamatergic neuronal activity. *Proc. Natl. Acad. Sci. U. S. A.* 95 (1), 316–321. doi:10.1073/pnas.95.1.316

Smith, D., Pernet, A., Hallett, W. A., Bingham, E., Marsden, P. K., and Amiel, S. A. (2003). Lactate: A preferred fuel for human brain metabolism *in vivo*. *J. Cereb. Blood Flow. Metab.* 23 (6), 658–664. doi:10.1097/01.WCB.0000063991.19746.11

Soda, K. (2022). Overview of polyamines as nutrients for human healthy long life and effect of increased polyamine intake on DNA methylation. *Cells* 11 (1), 164. doi:10.3390/cells11010164

Someya, S., and Kim, M. J. (2021). Cochlear detoxification: Role of alpha class glutathione transferases in protection against oxidative lipid damage, ototoxicity, and cochlear aging. *Hear Res.* 402, 108002. doi:10.1016/j.heares.2020.108002

Son, N., Hur, H. J., Sung, M. J., Kim, M. S., Hwang, J. T., Park, J. H., et al. (2012). Liquid chromatography-mass spectrometry-based metabolomic analysis of livers from aged rats. *J. Proteome Res.* 11 (4), 2551–2558. doi:10.1021/pr201263q

Sonnewald, U., White, L. R., Odegard, E., Westergaard, N., Bakken, I. J., Aasly, J., et al. (1996). MRS study of glutamate metabolism in cultured neurons/glia. *Neurochem. Res.* 21 (9), 987–993. doi:10.1007/BF02532408

Stanley, W. C., Khairallah, R. J., and Dabkowski, E. R. (2012). Update on lipids and mitochondrial function: Impact of dietary n-3 polyunsaturated fatty acids. *Curr. Opin. Clin. Nutr. Metab. Care* 15 (2), 122–126. doi:10.1097/MCO.0b013e32834fdaf7

Tabula Muris, C. (2020). A single-cell transcriptomic atlas characterizes ageing tissues in the mouse. *Nature* 583 (7817), 590–595. doi:10.1038/s41586-020-2496-1

Tanaka, T., Biancotto, A., Moaddel, R., Moore, A. Z., Gonzalez-Freire, M., Aon, M. A., et al. (2018). Plasma proteomic signature of age in healthy humans. *Aging Cell* 17 (5), e12799. doi:10.1111/acel.12799

Tepp, K., Puurand, M., Timohhina, N., Adamson, J., Klepinin, A., Truu, L., et al. (2017). Changes in the mitochondrial function and in the efficiency of energy transfer pathways during cardiomyocyte aging. *Mol. Cell Biochem.* 432 (1-2), 141–158. doi:10.1007/s11010-017-3005-1

Ter Borg, S., Luiking, Y. C., van Helvoort, A., Boirie, Y., Schols, J., and de Groot, C. (2019). Low levels of branched chain amino acids, eicosapentaenoic acid and micronutrients are associated with low muscle mass, strength and function in community-dwelling older adults. *J. Nutr. health & aging* 23 (1), 27–34. doi:10.1007/s12603-018-1108-3

Thorn, C. F., Oshiro, C., Marsh, S., Hernandez-Boussard, T., McLeod, H., Klein, T. E., et al. (2011). Doxorubicin pathways: Pharmacodynamics and adverse effects. *Pharmacogenet Genomics* 21 (7), 440–446. doi:10.1097/FPC.0b013e32833ffb56

Tremolizzo, L., Sala, G., Zoia, C. P., and Ferrarese, C. (2012). Assessing glutamatergic function and dysfunction in peripheral tissues. *Curr. Med. Chem.* 19 (9), 1310–1315. doi:10.2174/092986712799462702

Tryggvason, K., and Wartiovaara, J. (2005). How does the kidney filter plasma? *Physiol. (Bethesda)* 20 (2), 96–101. doi:10.1152/physiol.00045.2004

Uneyama, H., Kobayashi, H., and Tonouchi, N. (2017). New functions and potential applications of amino acids. *Adv. Biochem. Eng. Biotechnol.* 159, 273–287. doi:10.1007/10_2016_35

van den Akker, E. B., Trompet, S., Wolf Jjh, B., Beekman, M., Suchiman, H. E. D., Deelen, J., et al. (2020). Metabolic age based on the BBMRI-NL ^{1}H-NMR metabolomics repository as biomarker of age-related disease. *Circ. Genom Precis. Med.* 13 (5), 541–547. doi:10.1161/CIRCGEN.119.002610

Van Pilsum, J. F., Stephens, G. C., and Taylor, D. (1972). Distribution of creatine, guanidinoacetate and the enzymes for their biosynthesis in the animal kingdom. Implications for phylogeny. *Biochem. J.* 126 (2), 325–345. doi:10.1042/bj1260325

Verdin, E. (2015). NAD^{+} in aging, metabolism, and neurodegeneration. *Science* 350 (6265), 1208–1213. doi:10.1126/science.aac4854

Wang, Y., Grenell, A., Zhong, F., Yam, M., Hauer, A., Gregor, E., et al. (2018). Metabolic signature of the aging eye in mice. *Neurobiol. Aging* 71, 223–233. doi:10.1016/j.neurobiolaging.2018.07.024

Watkins, J. C., and Jane, D. E. (2006). The glutamate story. *Br. J. Pharmacol.* 147, S100–S108. doi:10.1038/sj.bjp.0706444

Wesley, U. V., Bhute, V. J., Hatcher, J. F., Palecek, S. P., and Dempsey, R. J. (2019). Local and systemic metabolic alterations in brain, plasma, and liver of rats in response to aging and ischemic stroke, as detected by nuclear magnetic resonance (NMR) spectroscopy. *Neurochem. Int.* 127, 113–124. doi:10.1016/j.neuint.2019.01.025

Wilkinson, D. J., Rodriguez-Blanco, G., Dunn, W. B., Phillips, B. E., Williams, J. P., Greenhaff, P. L., et al. (2020). Untargeted metabolomics for uncovering biological markers of human skeletal muscle ageing. *Aging (Albany NY)* 12 (13), 12517–12533. doi:10.18632/aging.103513

World Health Administration (2020). *Decade of healthy ageing: The global strategy and action plan on ageing and health 2016–2020: Towards a world in which everyone can live a long and healthy life: Report by the director-general*. Geneva: World Health Organization.

Wu, M., Ye, H., Shao, C., Zheng, X., Li, Q., Wang, L., et al. (2017). Metabolomics-proteomics combined approach identifies differential metabolism-associated molecular events between senescence and apoptosis. *J. Proteome Res.* 16 (6), 2250–2261. doi:10.1021/acs.jproteome.7b00111

Xiao, F., Huang, Z., Li, H., Yu, J., Wang, C., Chen, S., et al. (2011). Leucine deprivation increases hepatic insulin sensitivity via GCN2/mTOR/S6K1 and AMPK pathways. *Diabetes* 60 (3), 746–756. doi:10.2337/db10-1246

Xiao, F., Yu, J., Guo, Y., Deng, J., Li, K., Du, Y., et al. (2014). Effects of individual branched-chain amino acids deprivation on insulin sensitivity and glucose metabolism in mice. *Metabolism* 63 (6), 841–850. doi:10.1016/j.metabol.2014.03.006

Xu, M., Pirtskhalava, T., Farr, J. N., Weigand, B. M., Palmer, A. K., Weivoda, M. M., et al. (2018). Senolytics improve physical function and increase lifespan in old age. *Nat. Med.* 24 (8), 1246–1256. doi:10.1038/s41591-018-0092-9

Xu, T. T., Li, H., Dai, Z., Lau, G. K., Li, B. Y., Zhu, W. L., et al. (2020). Spermidine and spermine delay brain aging by inducing autophagy in SAMP8 mice. *Aging (Albany NY)* 12 (7), 6401–6414. doi:10.18632/aging.103035

Xu, Z. R., Tan, Z. J., Zhang, Q., Gui, Q. F., and Yang, Y. M. (2015). The effectiveness of leucine on muscle protein synthesis, lean body mass and leg lean mass accretion in older people: A systematic review and meta-analysis. *Br. J. Nutr.* 113 (1), 25–34. doi:10.1017/S0007114514002475

Yadav, M. K., Manoli, N. M., and Madhunapantula, S. V. (2016). Comparative assessment of vitamin-B12, folic acid and homocysteine levels in relation to p53 expression in megaloblastic anemia. *PLoS One* 11 (10), e0164559. doi:10.1371/journal.pone.0164559

Yanar, K., Simsek, B., Atukeren, P., Aydin, S., and Cakatay, U. (2019). Is D-galactose a useful agent for accelerated aging model of gastrocnemius and soleus muscle of sprague-dawley rats? *Rejuvenation Res.* 22 (6), 521–528. doi:10.1089/rej.2019.2185

Yi, S., Lin, K., Jiang, T., Shao, W., Huang, C., Jiang, B., et al. (2020). NMR-based metabonomic analysis of HUVEC cells during replicative senescence. *Aging (Albany NY)* 12 (4), 3626–3646. doi:10.18632/aging.102834

Yu, Y., Herman, P., Rothman, D. L., Agarwal, D., and Hyder, F. (2018). Evaluating the gray and white matter energy budgets of human brain function. *J. Cereb. Blood Flow. Metab.* 38 (8), 1339–1353. doi:10.1177/0271678X17708691

Zhang, F., Kerbl-Knapp, J., Akhmetshina, A., Korbelius, M., Kuentzel, K. B., Vujic, N., et al. (2021). Tissue-specific landscape of metabolic dysregulation during ageing. *Biomolecules* 11 (2), 235. doi:10.3390/biom11020235

Zhang, H., Wang, J., Li, L., Chai, N., Chen, Y., Wu, F., et al. (2017). Spermine and spermidine reversed age-related cardiac deterioration in rats. *Oncotarget* 8 (39), 64793–64808. doi:10.18632/oncotarget.18334

Zhang, X. M., Deng, H., Tong, J. D., Wang, Y. Z., Ning, X. C., Yang, X. H., et al. (2020b). Pyruvate-enriched oral rehydration solution improves glucometabolic disorders in the kidneys of diabetic db/db mice. *J. Diabetes Res.* 2020, 2817972. doi:10.1155/2020/2817972

Zhang, X. M., Wang, Y. Z., Tong, J. D., Ning, X. C., Zhou, F. Q., Yang, X. H., et al. (2020a). Pyruvate alleviates high glucose-induced endoplasmic reticulum stress and apoptosis in HK-2 cells. *FEBS Open Bio* 10 (5), 827–834. doi:10.1002/2211-5463.12834

Zheng, X., Chen, T., Zhao, A., Wang, X., Xie, G., Huang, F., et al. (2016b). The brain metabolome of male rats across the lifespan. *Sci. Rep.* 6, 24125. doi:10.1038/srep24125

Zheng, Y., Ceglarek, U., Huang, T., Li, L., Rood, J., Ryan, D. H., et al. (2016a). Weight-loss diets and 2-y changes in circulating amino acids in 2 randomized intervention trials. *Am. J. Clin. Nutr.* 103 (2), 505–511. doi:10.3945/ajcn.115.117689

Zhou, F. Q. (2021). NAD(+), senolytics, or pyruvate for healthy aging? *Nutr. metabolic insights* 2021, 117863882110534. doi:10.1177/11786388211053407

Zhou, Q., Kerbl-Knapp, J., Zhang, F., Korbelius, M., Kuentzel, K. B., Vujic, N., et al. (2021). Metabolomic profiles of mouse tissues reveal an interplay between aging and energy metabolism. *Metabolites* 12 (1), 17. doi:10.3390/metabo12010017

Zhou, Y., and Danbolt, N. C. (2014). Glutamate as a neurotransmitter in the healthy brain. *J. Neural Transm. (Vienna)* 121 (8), 799–817. doi:10.1007/s00702-014-1180-8

Zhuang, H., Karvinen, S., Tormakangas, T., Zhang, X., Ojanen, X., Velagapudi, V., et al. (2021). Interactive effects of aging and aerobic capacity on energy metabolism-related metabolites of serum, skeletal muscle, and white adipose tissue. *Geroscience* 43 (6), 2679–2691. doi:10.1007/s11357-021-00387-1

frontiers | Frontiers in Cell and Developmental Biology

TYPE Original Research
PUBLISHED 03 July 2023
DOI 10.3389/fcell.2023.1212375

OPEN ACCESS

EDITED BY
Ann Saada,
Hebrew University of Jerusalem, Israel

REVIEWED BY
Vaibhav Deshmukh,
Washington University in St. Louis, United States
Irene Zohn,
Children's National Hospital, United States

*CORRESPONDENCE
Daisuke Sakai,
dsakai@kanazawa-med.ac.jp

RECEIVED 26 April 2023
ACCEPTED 22 June 2023
PUBLISHED 03 July 2023

CITATION
Sakai D, Murakami Y, Shigeta D, Tomosugi M, Sakata-Haga H, Hatta T and Shoji H (2023), Glycolytic activity is required for the onset of neural plate folding during neural tube closure in mouse embryos.
Front. Cell Dev. Biol. 11:1212375.
doi: 10.3389/fcell.2023.1212375

Glycolytic activity is required for the onset of neural plate folding during neural tube closure in mouse embryos

Daisuke Sakai[1]*, Yuki Murakami[2], Daichi Shigeta[3], Mitsuhiro Tomosugi[3], Hiromi Sakata-Haga[3], Toshihisa Hatta[3] and Hiroki Shoji[1]

[1]Department of Biology, Kanazawa Medical University, Uchinada, Ishikawa, Japan, [2]Department of Hygiene and Public Health, Kansai Medical University, Osaka, Japan, [3]Department of Anatomy, Kanazawa Medical University, Uchinada, Ishikawa, Japan

Physiological hypoxia is critical for placental mammalian development. However, the underlying mechanisms by which hypoxia regulates embryonic development remain unclear. We discovered that the expression of glycolytic genes partially depends on hypoxia in neuroepithelial cells of E8.25 mouse embryos. Consistent with this finding, inhibiting glycolysis during the early phase of neural tube closure (E8.0–8.5) resulted in a neural tube closure defect. In contrast, inhibiting the electron transport chain did not affect neural tube formation. Furthermore, inhibiting glycolysis affected cell proliferation, but not differentiation and survival. Inhibiting glycolysis repressed the phosphorylation of myosin light chain 2, and consequent neural plate folding. Our findings revealed that anaerobic glycolysis regulates neuroepithelial cell proliferation and apical constriction during the early phase of neural tube closure.

KEYWORDS

hypoxia, neural tube closure, metabolism, glycolysis, mouse

Introduction

Placental mammalian embryos are exposed to rapid changes in environmental oxygen and nutrient availability during development (Fischer and Bavister, 1993; Leese, 1995; Dunwoodie, 2009; Ufer and Wang, 2011). The oxygen concentration is relatively high in the oviduct (~8%) where fertilization and pre-implantation development occur, but ~3%–5% in the uterus where blastocyst implantation occurs. Furthermore, post-implantation embryos encounter hypoxic conditions as they become embedded in the endometrium (Ufer and Wang, 2011). Therefore, mammalian embryos are considered to acquire and develop an adaptive system for extreme changes in oxygen concentration. The conventional ablation of hypoxia-inducible factor 1 α (*Hif1α*), an oxygen-dependent transcriptional activator, causes defective cardiovascular formation, somitogenesis, and neural tube closure, resulting in embryonic lethality (Iyer et al., 1998; Ryan et al., 1998; Kotch et al., 1999; Lee et al., 2001; Compernolle et al., 2003; Ream et al., 2008). Furthermore, hypoxia is necessary for normal early post-implantation development in rodent embryos cultured *ex utero* (Morriss and New, 1979). These findings suggest that post-implantation embryos express hypoxia-inducible genes that regulate the metabolism, angiogenesis, and other cellular functions necessary for gastrulation and organogenesis.

Several types of mammalian cells under normoxia rely on aerobic respiration *via* the tricarboxylic acid (TCA) cycle and electron transport chain (ETC) to generate ATP. In contrast, cells alter their metabolic dependence to anaerobic glycolysis *via* Hif1α-dependent hypoxia signaling under hypoxic conditions (Semenza, 2003). To increase anaerobic glycolysis, Hif1α activates its target glycolytic genes, glucose transporter 1 (*Glut1*), hexokinase 2 (*HKII*), lactate dehydrogenase A (*Ldha*), aldolase A (*Aldoa*), and 6-phosphofructo-2-kinase/fructose-2,6-biphosphatase 3 (*Pfkfb3*). In early mammalian development, energy metabolism is rewired for developmental progression in embryos at the stage of neural tube closure (NTC), depending on the increased oxygen supplied by maternal blood (Miyazawa et al., 2017; Miyazawa et al., 2018; Fame et al., 2019; Fame and Lehtinen, 2021). Mouse embryos exhibit metabolic plasticity in response to the changes in oxygen concentration during the early phase of the NTC stage at embryonic day (E) 8.5 but not E7.5 (Miyazawa et al., 2018). Thus, anaerobic glycolysis appears to be exclusively activated in mouse embryos before E8.5, and glucose metabolism is gradually shifted to the TCA cycle, ETC, from E8.5, depending on increases in environmental oxygen concentrations (Miyazawa et al., 2017; Miyazawa et al., 2018). In addition, the activation of glycolysis regulates neural crest cell delamination under physiological conditions (Bhattacharya et al., 2020). Collectively, these findings suggest the essential roles of glucose metabolic shift in embryogenesis.

Mouse embryos at E8.5 cultured with Carbonyl cyanide p-trifluoro-methoxyphenyl hydrazine (FCCP), an uncoupler of the ETC, that disrupts ATP synthesis, causes NTC defect (Miyazawa et al., 2018). This finding suggests that glucose metabolism functions in NTC. Furthermore, inhibiting glycolytic enzyme activity leads to severe defective neural tube formation (Hunter and Tugman, 1995). However, the cellular mechanisms by which glycolytic enzymes regulate NTC remain poorly understood.

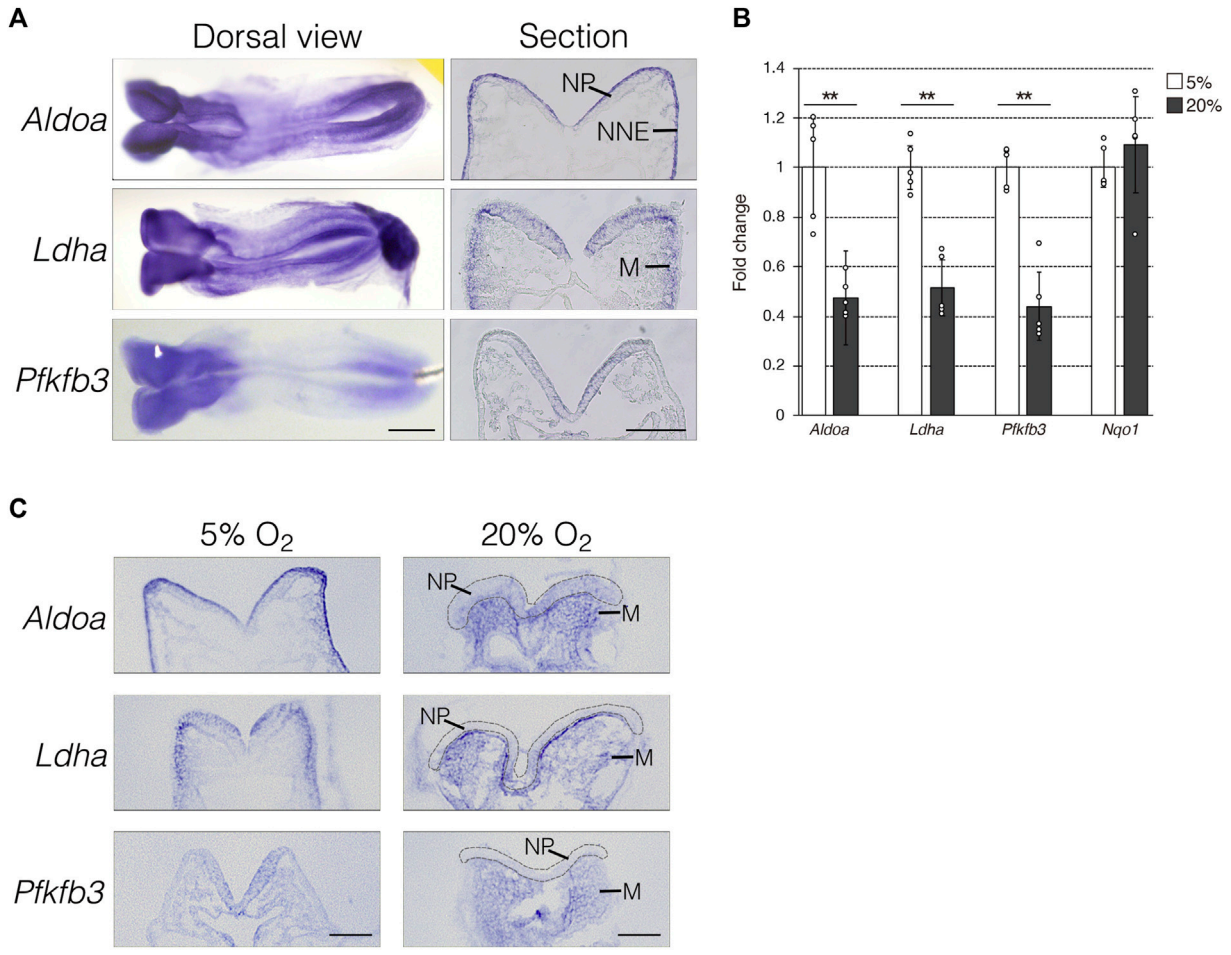

FIGURE 1
Hypoxia-dependent expression of glycolytic genes in the mouse embryo. **(A)** Expression of *Aldoa, Ldha,* and *Pfkfb3* mRNA was detected in whole-mount (Dorsal view) and cryosection (Section) *in situ* hybridization of E8.25 (six to eight somite stage) embryos. Scale bars, 500 μm (Dorsal view) and 100 μm (Section). Data are representative of six independent experiments. NP, neural plate; NNE, non-neural ectoderm; M, cranial mesenchyme. **(B)** Expression of *Aldoa, Ldha, Pfkfb3,* and *Nqo1* after the whole-embryo culture with 5% or 20% O_2 determined by RT-qPCR. Messenger RNA levels of genes were normalized to that of *Gapdh*, and the relative values are presented as white (5% O_2) and gray (20% O_2) bars. Data are shown as means ± S.E.M of five embryos. Statistical differences were assessed using Student's *t*-tests, $^{**}p < 0.001$. **(C)** Embryos were cultured under hypoxia (5% O_2) or normoxia (20% O_2) from E8.0 (three to five somite stage) to E8.25 (six to eight somite stage). Expression of *Aldoa, Ldha,* and *Pfkfb3* mRNA was detected by *in situ* hybridization. Neural plates are indicated by gray dotted lines. Scale bars, 100 μm. Data are representative of four independent experiments. NP, neural plate; M, cranial mesenchyme.

This study discovered that glycolytic genes are expressed in the neural plate (NP) and induced by hypoxia in mouse embryos. Furthermore, glycolytic activity is required for the apical constriction of neuroepithelial cells. This is essential for NP folding, which is an early step in NTC. Inhibiting glycolysis moderately reduced neuroepithelial cell proliferation. Our findings showed that glycolytic enzymes localized at the apical surface. Thus, anaerobic glycolysis might be required for local ATP production to promote NP folding and cell proliferation during NTC in mouse embryos.

Results

Glycolytic genes are expressed in neural plates of mouse embryos

To determine the role of anaerobic glycolysis in NTC, we initially confirmed the mRNA expression of the hypoxia-inducible glycolytic genes *Aldoa*, *Ldha*, and *Pfkfb3* using whole-mount *in situ* hybridization. The expression of *Aldoa*, *Ldha*, and *Pfkfb3* was abundant in the anterior and posterior NP of E8.0 (three to five somite stage) mouse embryos (Figure 1A, dorsal view). Next, we analyzed the mRNA expression profiles using transverse sectioning. We found that *Aldoa* mRNA localized to the apical surface of neuroepithelial and non-neural ectodermal cells, *Ldha* mRNA was expressed in neuroepithelial and mesenchymal cells adjacent to the non-neural ectoderm, and *Pfkfb3* mRNA was detected in neuroepithelial cells (Figure 1A, section). Thus, our finding revealed that NP expression was common among these three genes. We examined whether the expression of glycolytic genes is dependent on hypoxia. We developed E8.0 (3-5 somite stage) mouse embryos under normoxia (20% O_2) or hypoxia (5% O_2) and then isolated RNA at E8.5 (9–11 somite stage). The results of RT-qPCR revealed that glycolytic gene expression decreased by ~ 50% under normoxia compared with hypoxia (Figure 1B). The expression of NAD(P)H dehydrogenase (quinone) 1 (*Nqo1*) that encodes the electron respiratory chain enzyme is independent of, and was not altered by hypoxia. These results indicated that glycolytic genes are expressed in NP and that this part depends on hypoxia. Furthermore, we determined whether hypoxia-

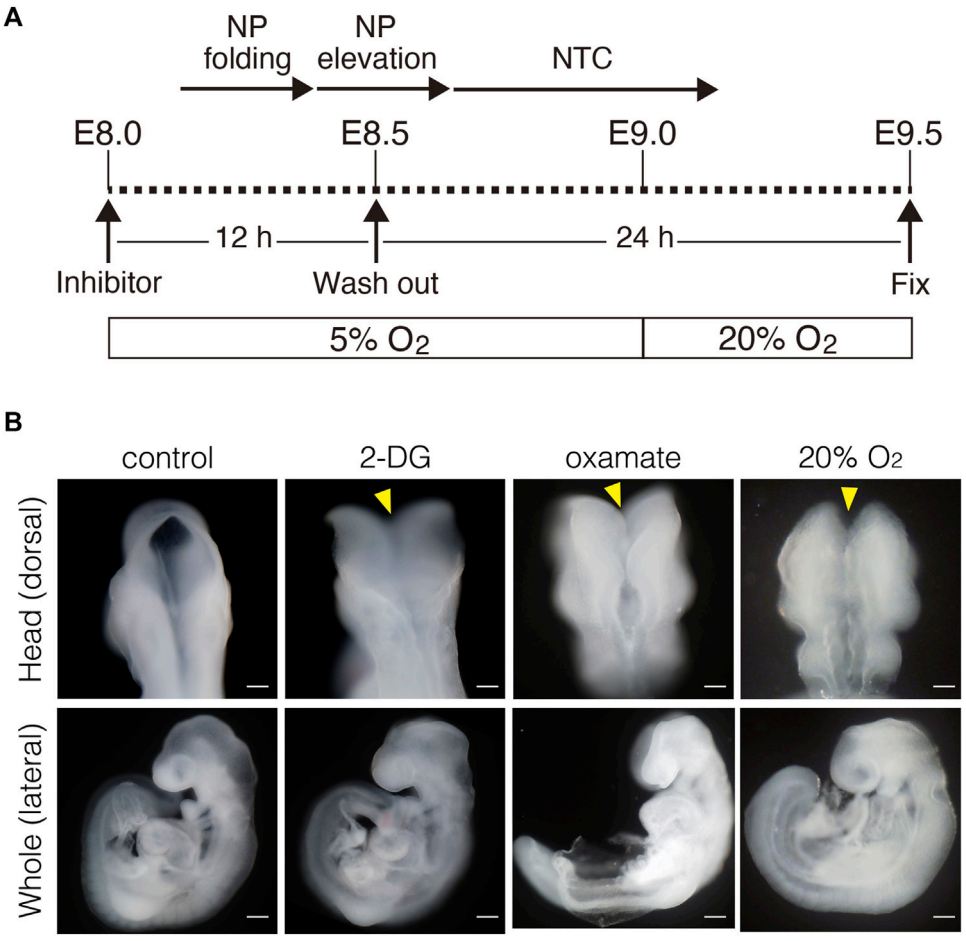

FIGURE 2
Inhibition of glycolytic activity results in neural tube closure defects. **(A)** Schema of *exo utero* whole-embryo culture with glycolysis inhibitors. Cellular events occurring during the neural tube closure process are shown above. NP, neural plate; NTC, neural tube closure. **(B)** Morphology of head and whole body of embryos incubated with PBS (control), 0.1 mM 2-DG (2-DG), 28 mM oxamate (oxamate), and normoxia (20% O_2). Yellow arrowheads, defective neural tube closure. Scale bars, 100 μm (head), 500 μm (whole). Images are representative of 33 (control), 21 (2-DG), 15 (oxamate), and 8 (20% O_2) embryos after *exo utero* whole-embryo cultur.

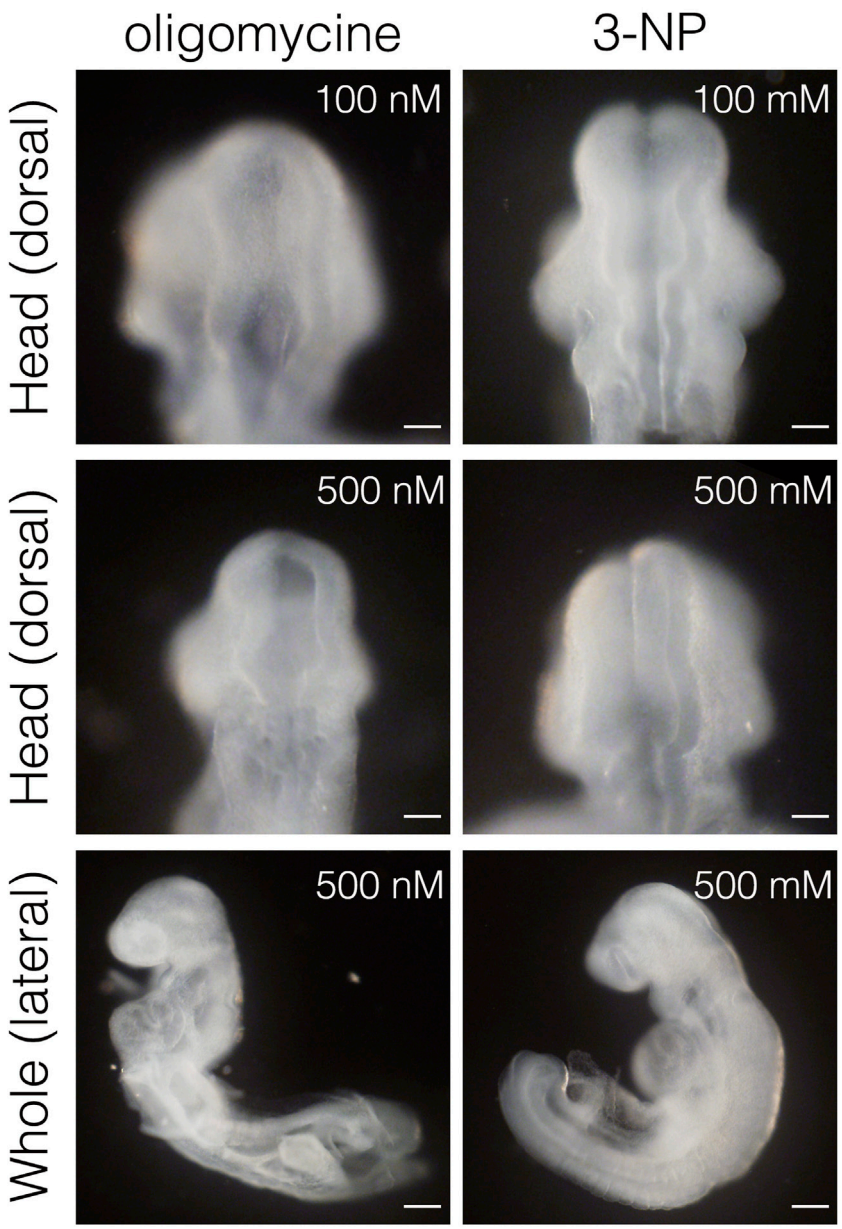

FIGURE 3
Inhibition of ETC, results in severe growth retardation, but not neural tube closure defect. Head and whole body morphology of embryos incubated with oligomycin and 3-NP. Scale bars, 100 μm (head), 500 μm (whole). Images are representative of 23 (oligomycin) and 20 (3-NP) embryos after *exo utero* whole-embryo culture.

dependent glycolytic gene expression is tissue-specific. To address this, we performed *in situ* hybridization (Figure 1C). *Aldoa* mRNA expression was diminished in the apical surface of neuroepithelial and non-neural ectodermal cells by normoxia. Unexpectedly, *Aldoa* mRNA turned out to be expressed in cranial mesenchyme of embryos cultured under normoxia. *Ldha* mRNA expression was significantly reduced in neuroepithelial cells, but slightly increased in cranial mesenchyme by normoxia. Furthermore, *Ldha* mRNA was highly expressed in cranial mesenchymal cells localized near the basal side of NP. *Pfkfb3* mRNA expression was observed in embryonic cranial mesenchyme, but not in neuroepithelial cells under normoxia (Figure 1C). Collectively, these findings demonstrated that glycolytic gene expression is dependent on hypoxia in neuroepithelial cells of early stage embryos.

Glycolytic enzyme activity is essential for the early phase of NTC

Inhibiting glycolysis using the glucose analog 2-deoxy-D-glucose (2-DG) prevents NTC (Hunter and Tugman, 1995). Therefore, we reevaluated the role of glycolytic enzyme activity in NTC. First, we confirmed that inhibiting glycolysis prevented NTC in our *ex utero*

whole-embryo culture system. E8.0 (3-5 somite stage) embryos were cultured with 2-DG for 24 h, then the gross morphology of the embryos was analyzed. We found that NTC was completely impaired by 2-DG, whereas untreated embryos formed normal NTs (data not shown). Next, we incubated E8.0 (3-5 somite stage) embryos with 2-DG or the lactate dehydrogenase inhibitor sodium oxamate (oxamate) for 12 h, then removed the inhibitors by changing the culture medium. The embryos were cultured for a further 24 h (Figure 2A). Figure 2A also shows the developmental events that occurred during *exo utero* whole-embryo culture. Neural tubes formed normally in control cultures (81.2%, 27/33 embryos). In contrast, NTC was completely prevented by the glycolytic inhibitors (2-DG; 100%, 21/21 embryos. Oxamate; 100%, 15/15 embryos), whereas developmental defects were not found in other tissues (Figure 2B, yellow arrowheads). Incubation with glycolytic inhibitors for 12 h (E8.0-8.5, 3–11 somite stage) was sufficient to prevent NTC, suggesting that glycolytic activity is required for the early phase of NTC process. Moreover, NTC is prevented by *exo utero* whole-embryo culture under normoxia (Figure 2B, 20% O_2) (75.0%, 6/8 embryos). This result shows that a hypoxic condition is required for glycolytic gene expression during embryogenesis. The TCA cycle and ETC, are the major metabolic pathway for ATP production after E8.5. Hence, incubating E8.5 embryos with FCCP causes NTC defects (Miyazawa et al., 2018), indicating that the ETC, is involved in the late phase of the NTC. We examined if incubation with an ETC, inhibitor for 12 h (E8.0–8.5) affects NTC progression. To examine this, E8.0 embryos (3-5 somite stage) were incubated with the ATP synthase inhibitor oligomycin, or the electron transport chain complex II inhibitor 3-nitropropionic acid (3-NP). Oligomycin and 3-NP obviously retarded embryonic growth and caused abnormal gross morphology, whereas NTC was not impaired in oligomycin-treated (74.0%, 17/23 embryos) and 3-NP-treated embryos (80.0%, 16/20 embryos) (Figure 3). These results indicated that the ETC, is not required during the early phase of NTC progression, at least during E8.0-8.5.

Glycolytic activity is required for the onset of NP folding

During NTC in mouse embryos, NP undergoes a dynamic morphological transformation comprising the following four spatially and temporally overlapping stages: (1) NP shaping (transverse view of NP is M-shaped), (2) NP folding (V-shaped), (3) NP elevation (U-shaped), and (4) neural fold fusion (O-shaped) (Figure 4A) (Colas and Schoenwolf, 2001). Next, we examined the stage at which the NTC is compromised by glycolytic inhibition using *exo utero* whole-embryo culture. We initially confirmed that the NTC process was precisely simulated through the appropriate steps in control cultures (Figure 4B, control) (6 h: 100%, 8/8 embryos; 12 h: 100%, 9/9 embryos; 24 h: 87.5%, 7/8 embryos). Notably, the NP retained the M shape in embryos incubated with 2-DG for 24 h (Figure 4B, 2-DG) (6 h: 100%, 10/10 embryos; 12 h: 100%, 10/10 embryos; 24 h: 100%, 10/10 embryos), suggesting that glycolytic activity is required for the onset of NP folding. The NP transformed from the M to the V shape during the first 6h in control cultures. Hence, somite segmentation is controlled by a segmentation clock with a 2-h cycles (Pourquie, 2022), when E8.0 embryos at the 3-5 somite stage develop into the 6-8 somite stage during 6 h of culture. This indicated that NP folding is sensitive to glycolytic inhibition during the 3-5 somite stage. To examine the time window of sensitivity for 2-DG exposure on NP folding, we incubated embryos with 2-DG at the 4, 5, 6, and 7 somite stages for 12, 10, 8, and 6 h, respectively. After the exposure to inhibitors, removed the inhibitors by changing the culture medium. The embryos were cultured for a further 24 h. As a result of glycolytic inhibition, 93.8% (15/16 embryos), 100% (26/26 embryos), and 71.4% (10/14 embryos) of the 4, 5, and 6 somite stage embryos, respectively, had defective NTC. Importantly, 2-DG did not affect the NTC of 7 somite stage embryos (0/13 embryos) (Figure 4C). Taken together, these results suggest that anaerobic glycolysis functions within a short time frame during neural tube development.

Glycolytic inhibition affects cell proliferation, but not cell survival and differentiation

We investigated whether defective NTC in 2-DG-treated embryos was associated with cell proliferation, viability, and differentiation. Proliferating and apoptotic cells were detected by immunofluorescent staining using anti-phospho-histone H3 and anti-cleaved caspase3 antibodies, respectively. The number of phospho-histone H3+ mitotic cells moderately decreased in neuroepithelial cells incubated with 2-DG (Figure 5). The numbers of apoptotic cells did not significantly differ between neuroepithelial cells incubated with or without 2-DG-treated (Supplementary Figure S1A). Cell differentiation, including dorso-ventral patterning of the NP and cranial mesenchyme formation, plays crucial roles in NTC (Yamaguchi and Miura, 2013). The expression of *Wnt1* mRNA, a marker of the dorsal edge of the NP, and *Twist1* mRNA, a marker of cranial mesenchymal cells, was not altered by 2-DG (Supplementary Figure S1B). These findings suggested that glycolysis regulates NTC through the proliferation of neuroepithelial cells.

Glycolytic inhibition prevents apical constriction of neuroepithelial cells

Neuroepithelial cells undergo dynamic morphological changes during the early phase of NP folding. The thickness of the NP is initially increased by the elongation of neuroepithelial cells along the apico-basal polarity, accompanied by microtubule extension. Thereafter, the apical F-actin ring constricts dependently on the activation of myosin *via* the phosphorylation of myosin light chain 2 (Suzuki et al., 2012). We investigated whether morphological changes in neuroepithelial cells are impaired by inhibiting glycolysis. Microtubule extension was comparable between NPs incubated with and without 2-DG (Figure 6A, tubulin). The F-actin ring also formed normally in NPs incubated with 2-DG (Figure 6A, F-actin). In contrast, the amount of phosphorylated myosin light chain 2 (pMLC2) was significantly reduced at the apical surface of neuroepithelial cells in 2-DG-treated embryos, suggesting impaired apical F-actin constriction (Figure 6A, pMLC2, and Figure 6B). The amount of pMLC2 was also reduced at the apical surface of neuroepithelial cells in embryos cultured under

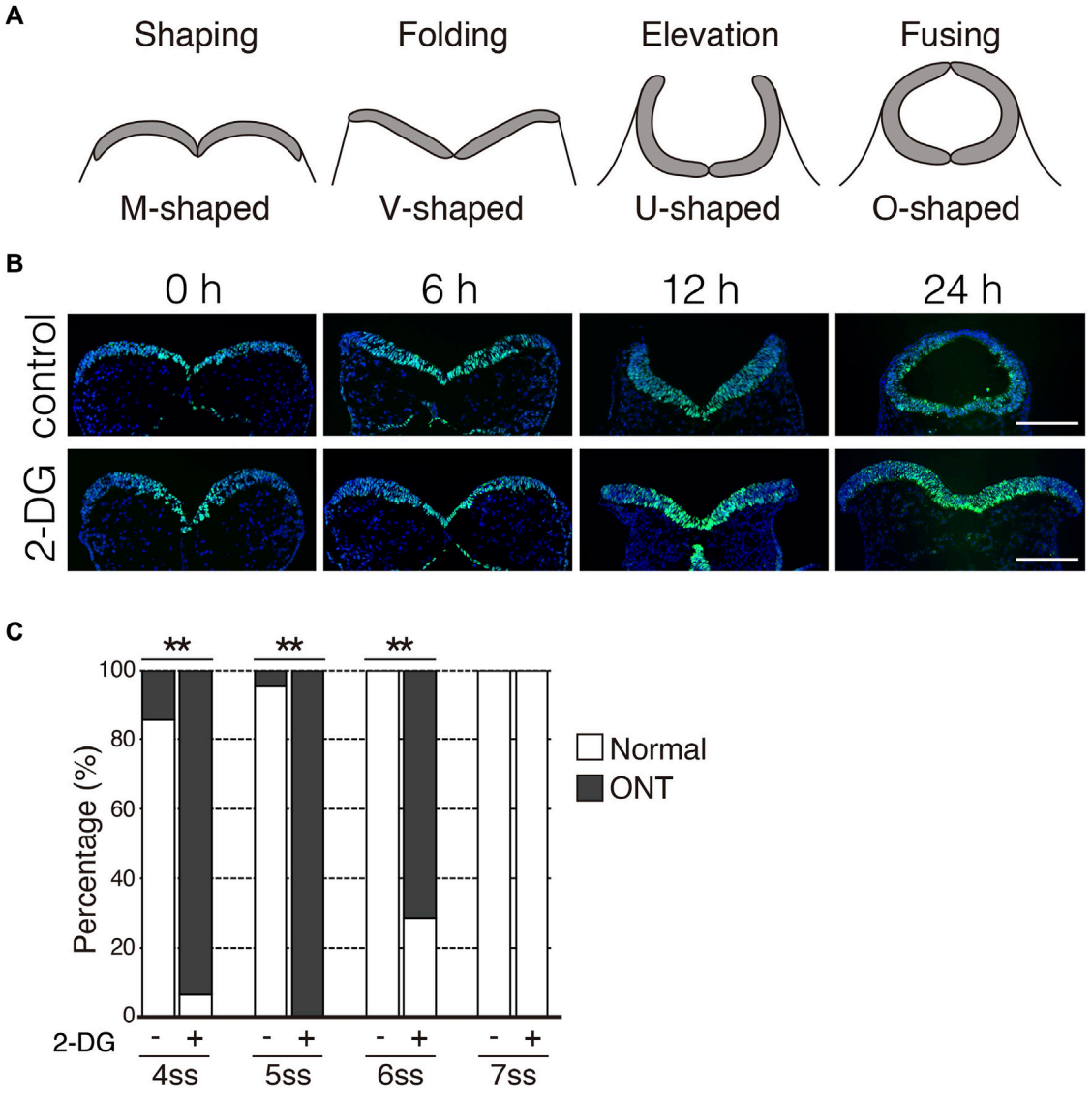

FIGURE 4
Inhibition of glycolytic activity prevents neural plate folding. **(A)** Schematic transverse sections of four stages of neural tube closure. **(B)** Neuroepithelial cells were detected by immunofluorescence staining Sox2 (green) at indicated times after incubation without (control) or with 2-DG. Scale bars, 100 μm. Images are representative of 8 (6 h in control), 9 (12 h in control), 8 (24 h in control), and 10 (6, 12, and 24 h in 2-DG) independent experiments. **(C)** Ratios (%) of embryos with normal morphology (white bar) and open neural tube (ONT, Gy bar) after incubation without (–) or with 2-DG (+) at indicated somite stage (ss). Data are shown of 14 (control, 4 somite stage), 16 (2-DG, 4 somite stage), 22 (control, 5 somite stage), 26 (2-DG, 5 somite stage), 10 (control, 6 somite stage), 14 (2-DG, 6 somite stage), 13 (control. Seven somite stage) and, 13 (2-DG 7 somite stage) embryos after incubation. Statistical differences were assessed using Chi-Square tests, $^{**}p < 0.001$.

normoxia (Figure 6C). This defect is probably due to the downregulation of glycolytic gene expression in NP by normoxia (Figure 1C). We evaluated the size of the F-actin ring on the apical side of dissected phalloidin-labeled NPs using confocal microscopy. The size of the apical F-actin ring was substantially reduced in NPs incubated with 2-DG compared to NPs not incubated with 2-DG (Figure 6D). The apical area of individual cells was quantified, and its distribution was quantified. The results showed that the proportion of cells with large apical areas was significantly increased in embryos incubated with, than without 2-DG (Figure 6E). These findings indicated that glycolysis regulates myosin light chain 2 phosphorylation and subsequent apical constriction.

Glycolytic enzymes localize at apical surfaces of neuroepithelial cells

Local ATP synthesis contributes to the dynamic rearrangement of F-actin at the leading edge of migrating cells (De Bock et al., 2013; Cruys et al., 2016; Cunniff et al., 2016). Furthermore, some glycolytic enzymes, such as Aldoa, and Pfkfb3 protein, directly bind to F-actin, and this interaction is required for the local activation of glycolysis (Roberts and Somero, 1987; 1989; De Bock et al., 2013; Hu et al., 2016). Therefore, we examined the cellular localization of Aldoa, Ldha, and Pfkfb3 protein in neuroepithelial cells at E8.25 (six to eight somite stage). These glycolytic enzymes were localized at the apical surface of the neuroepithelial cells,

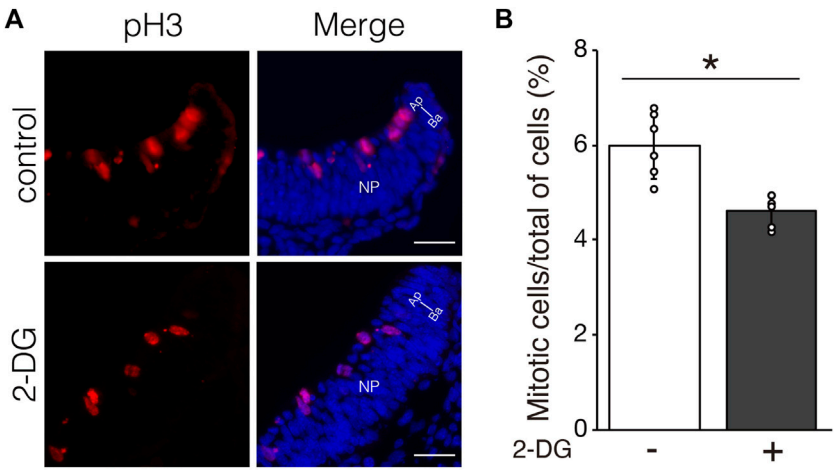

FIGURE 5
Effect of glycolytic inhibition on mitosis. **(A)** Mitotic cells detected by immunofluorescence staining phospho-histone H3 (Red) in transverse sections of the neural plate (unilateral) at E8.25 (six to eight somite stage). Directional planes are shown (Ap; apical, Ba; basal). **(B)** Percentage of phospho-histone H3$^+$ mitotic cells among all neuroepithelial cells after incubation without (−) or with 2-DG (+). Data are shown as means ± S.E.M of six histological sections from three embryos. Statistical differences were assessed using Student's *t*-tests, $*p < 0.05$.

where pMLC2 was also localized. Both Ldha and Pfkfb3 proteins were detected in the cytosol as well (Figure 7). Notably, Aldoa, Ldha, and Pfkfb3 proteins formed punctate structures and resided in close proximity to pMLC2; however, most of these were not colocalized (Figure 7). These results implied that ATP is locally produced to regulate apical constriction.

Discussion

The inhibition of glycolysis by 2-DG causes NTC defects in mouse embryos (Hunter and Tugman, 1995). Similarly, the ablation of *Hif1α*, a key transcription factor for the induction of glycolytic genes under hypoxia, impairs morphogenesis in mouse embryos, including the NTC (Iyer et al., 1998; Ryan et al., 1998; Kotch et al., 1999; Compernolle et al., 2003). These findings suggest that anaerobic glycolysis is essential for NTC; however, its function in the NTC process is unknown. We investigated the role of glycolysis in detailed E8.0-E8.5 (3–11 somite stage) embryos and uncovered a critical early developmental window for NTC. We found that glycolytic activity is required for neural plate folding at a very early stage of NTC, at least until the 6 somite stage. In contrast, 7 somite stage embryos were not vulnerable to glycolysis inhibition. It has been known that embryos do not exhibit glucose metabolic plasticity before E8.5, thus anaerobic glycolysis is activated even under high oxygen concentrations (Miyazawa et al., 2017). Furthermore, glucose metabolism is rewired at E8.5; that is, glycolysis becomes coupled to the TCA cycle, and the ETC, is activated to respond to the increase in extraembryonic oxygen concentration, which is required for NP elevation (Miyazawa et al., 2018). Taking these findings into consideration, we propose that NTC can be divided according to dependence on glucose metabolism activity as NP shaping and folding that depend on anaerobic glycolysis activity (-E8.25), and subsequent NTC which depends on TCA cycle activity (E8.5-). Enhanced glycolysis plays an essential role in epithelial-mesenchymal transition during neural crest development in chick embryos (Bhattacharya et al., 2020). In mouse embryos, neural crest cells start to delaminate from NP at E8.5 (Weston et al., 2004). Thus, high levels of glycolytic activity in neuroepithelial cells may be involved in both NTC and neural crest development in mouse embryos.

Previous studies have shown that ATP is generated through anaerobic glycolysis at implantation (Zhou et al., 2012; Takashima et al., 2014; Sperber et al., 2015). The production of ATP in neuroepithelial cells relies on anaerobic glycolysis before NTC, and then the primary source of ATP switches from anaerobic glycolysis to the TCA cycle and the ETC during NTC (Miyazawa et al., 2017; Miyazawa et al., 2018; Fame et al., 2019). Taken together, these findings suggest that ATP produced by anaerobic glycolysis is involved in the early stages of NTC. What is the use of ATP during NTC? It is generally accepted that ATP provides energy to drive many cellular processes, including cell proliferation. In this study, we discovered that 2-DG reduced neuroepithelial cell proliferation (Figure 5), but had no effect on cell survival or differentiation (Supplementary Figure S1). These results indicated that anaerobic glycolysis produces ATP for neuroepithelial cell proliferation, therefore defective NTC would be partially due to impaired cell proliferation. Consistent with our findings, *Pfkfb3* promotes cell cycle progression (Jia et al., 2018). In contrast, *miR-302* ablated embryos exhibit NTC defects owing to the increased proliferation of neuroepithelial cells through upregulated glycolytic genes, including *Pfkfb3* (Keuls et al., 2020). These paradoxical findings could account for the tight control of neuroepithelial cell proliferation in normal NTC. We further demonstrated that MLC2 phosphorylation and subsequent apical constriction were substantially suppressed by glycolytic inhibition in neuroepithelial cells (Figure 6). Phosphorylation of MLC2 by Rho-associated kinase (ROCK) increases the ATPase activity of the myosin light chain (Quintin et al., 2008), and generates a contractile force for the apical constriction of neuroepithelial cells (Lee and Nagele, 1985; Rolo et al., 2009). Apical constriction reduces the sizes of the cell apices and causes morphological changes in neuroepithelial cells from rectangular to wedge-like shapes, generating a physical force for NP folding (Suzuki et al., 2012). Moreover, glycolytic enzymes have been shown in endothelial cells to regulate F-actin remodeling in filopodia and lamellipodia *via* ATP

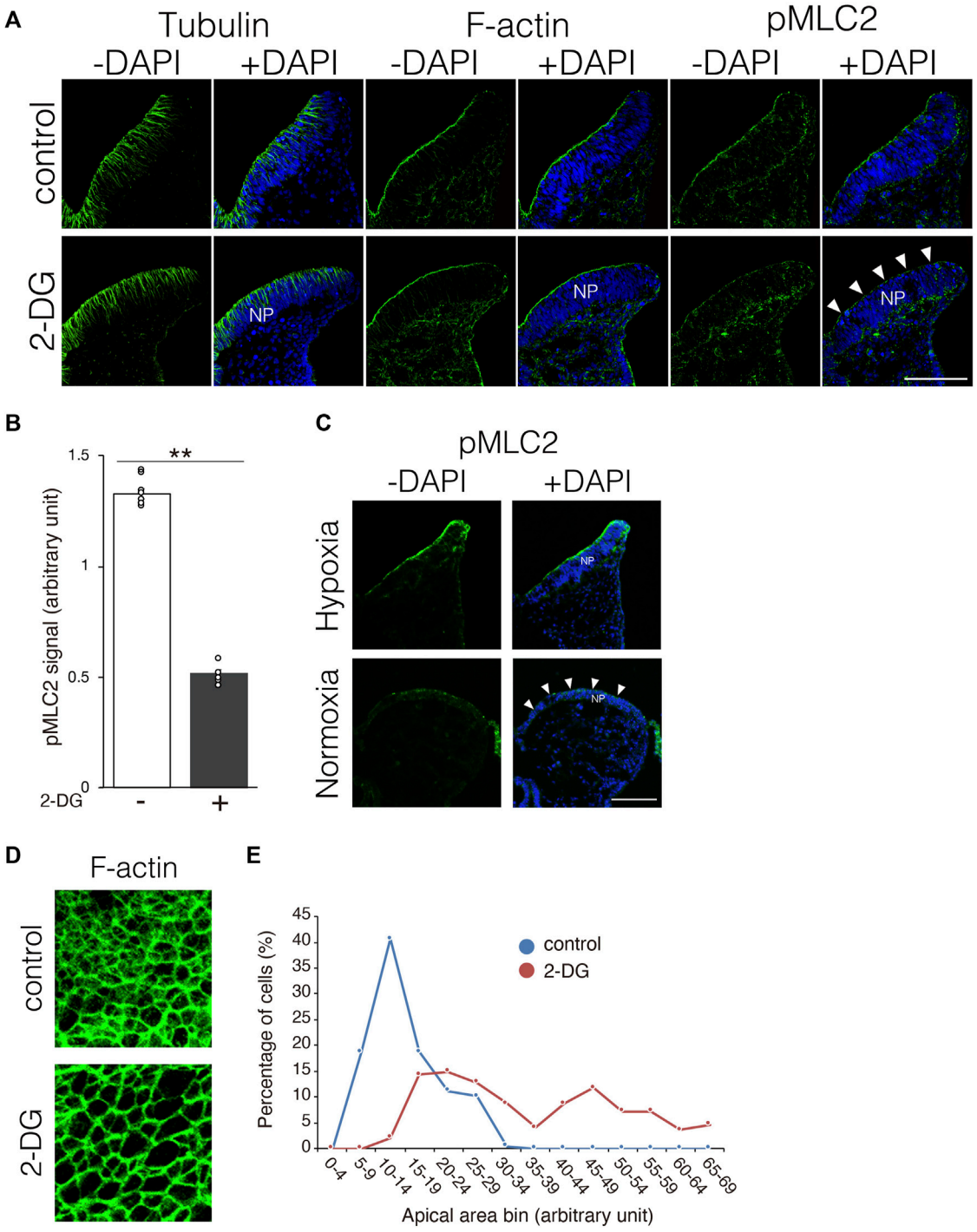

FIGURE 6
Substantially reduced pMLC2, and consequent failure of apical constriction of neuroepithelial cells caused by 2-DG. **(A)** Localization of tubulin, F-actin, and pMLC2 in transverse sections of the neural plate at E8.25 (six to eight somite stage). White arrowheads indicate reduced pMLC2 in embryos incubated with 2-DG. Scale bars, 50 μm. Images are representative of three independent experiments. White arrowheads reduced pMLC2. NP, neural plate. **(B)** Fluorescence intensity of pMLC2 in neural plate after incubation without (–) or with 2-DG (+). Data are shown as means ± S.E.M of eight histological sections from four embryos. Statistical differences were assessed using Student's *t*-tests, $^{**}p < 0.001$. **(C)** Localization of pMLC2 in transverse sections of the neural plate at E8.25 (6-8 somite stage) cultured under normoxia and hypoxia. Scale bars, 50 μm. Images are representative of eight independent experiments from four embryos. White arrowheads indicate reduced pMLC2. NP, neural plate. **(D)** F-actin rings at the apical side of NP visualized by staining with Phalloidin-488 at E8.5 (9–11 somite stage). **(E)** Graph shows numbers of neuroepithelial cells with different apical areas. Cells were counted in five histological sections from five embryos. The total cell number was 197 in control, and 195 in 2-DG, respectively. Blue, control; Red, 2-DG.

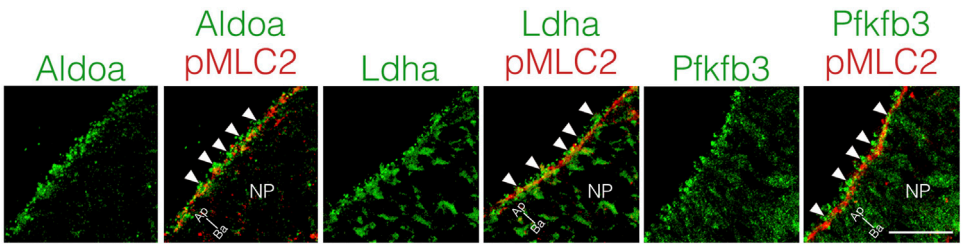

FIGURE 7
Apical localization of glycolytic enzymes in neuroepithelial cells.Localization of Aldoa, Ldha, and Pfkfb3 in transverse sections of the neural plate at E8.25 (six to eight somite stage). Apical surface visualized by pMLC2 staining. Scale bars, 20 μm. Images are representative of five independent experiments. Directional planes were shown (Ap; apical, Ba; basal). White arrowheads, punctate structures. NP, neural plate.

production (De Bock et al., 2013; Cruys et al., 2016). Based on our results, we believe that anaerobic glycolysis contributes to the production of ATP, which is utilized to generate physical force for NP folding. Anaerobic glycolysis is considered a less efficient metabolic process for ATP generation than the TCA cycle and the ETC Glycolytic enzymes are compartmentalized with F-actin in lamellipodia for local ATP production in endothelial cells to cope with high and rapidly changing ATP demands to maintain motor activity (De Bock et al., 2013). We found that Aldoa, Ldha, and Pfkfb3 proteins were localized at the apical surface of the neuroepithelial cells in dot-like structures located near pMLC2 (Figure 7). Thus, glycolytic enzymes might supply ATP not only for cell proliferation, but also for apical constriction, and the apical localization of enzymes might be important for the efficient supply of ATP for MLC2 phosphorylation. Whether ATP is locally generated at the apical surface of neuroepithelial cells remains unknown. Further studies are necessary to confirm local ATP generation at the apical surface by ATP imaging using an ATP biosensor.

Our principal findings were related to glycolytic inhibition by 2-DG and oxamate. Therefore, the study needs to be extended to include genetic analysis. In fact, we created neuroepithelial cell-specific *Ldha* knockout mice using *Sox1-cre* driver. These mice had normal NTC, probably due to genetic redundancy (data not shown). We also attempted to knock down *Ldha*, *Aldo*a, and *Pfkfb3* in neuroepithelial cells using a combination of siRNA electroporation and *exo utero* whole-embryo culture. However, a combination of siRNA electroporation and *exo utero* whole-embryo culture frequently induces abnormal NT development, even when an empty vector is electroporated as the control. Thus, knock down efficiency is difficult to evaluate. Further genetic studies are needed to determine the mechanism through which glycolysis regulates NTC.

Materials and methods

Mice

All animal experiments were performed following the Guidelines for the Care and Use of Laboratory Animals of Kanazawa Medical University. A minimum sample size of five individuals was used in each assay unless otherwise stated. ICR mice were obtained from Sankyo Lab Service. For embryonic staging, the morning on which the vaginal plug was observed was designated as E0.5.

Exo utero whole-embryo culture and pharmacological inhibition of glucose metabolism

Exo utero whole-embryo culture was performed as previously described (Takahashi et al., 2008; Sakai et al., 2016; Ogoh et al., 2017). Figure 2A shows a schema of pharmacological inhibition. Briefly, E8.0 (three to five somite stage) embryos were dissected and cultured under a 5% O_2; 5% CO_2; 90% N2, 37°C atm in DR50 (50% rat serum; 50% DMEM/F-12, 2% glucose) with or without 0.1 mM 2-deoxy-D-glucose (2-DG), 28 mM oxamate, 0.1 and 0.5 mM oligomycin, or 0.1 and 0.5 mM 3-nitropropionic acid (3-NP). After 12 h of culture (corresponding to E8.5), the culture medium was changed to remove inhibitors and the cells were cultured for 24 h (corresponding to E9.5).

RT-qPCR

We analyzed gene expression using RT-qPCR as described (Sakai et al., 2022). Briefly, total RNA extracted from E8.5 (9–11 somite stage) embryos was reverse-transcribed into cDNA, which was then amplified by qPCR using SYBR Green on a LightCycler Nano System (Roche). Gene expression was normalized to that of *Gapdh*. All samples were analyzed at least in triplicate. Relative fold change was calculated using the $2^{-\Delta\Delta CT}$ method. The expression of *Aldoa, Ldha, Pfkfb3, Nqo1,* and *Gapdh* was detected using the following primers: *Aldoa* FW: TGGGAA GAAGGAGAACCTGA and *Aldoa* RV: GACAAGCGAGGCTGT TGG; *Ldha* FW: GGCACTGACGCAGACAAG and *Ldha* RV: TGA TCACCTCGTAGGCACTG; *Pfkfb3* FW: AACAGCTTTGAGGAG CGTGT and *Pfkfb3* RV: CGGGAGCTCTTCATGTTTTG; *Nqo1* FW: AGCGTTCGGTATTACGATCC and *Nqo1* RV: AGTACAATC AGGGCTCTTCTCG; *Gapdh* FW: CATGTTCCAGTATGACTCCAC TC and *Gapdh* RV: GGCCTCACCCCATTTGATGT.

In situ hybridization

Some mouse *Aldoa, Ldha, and Pfkfb3* sequences were amplified by PCR using the following primers: FW-*Aldoa*: TCTGACATCGCT CACCGCATT and RV- *Aldoa*: AAGAGAGATTCACTGGCTGCG, FW-*Ldha*: TGAAGAACCTTAGGCGGGTG and RV- *Ldha*: TGT GTCTCAGAGACAGTGGG, FW-*Pfkfb3*: TCACCAGGCTGTTCT

ACGCT and RV- *Pfkfb3*: GTTGTCTTTGCCACCCCAAC. The PCR products were cloned into the pGEM-T Easy vector (Promega) to synthesize the cRNA probes. Plasmids for the synthesis of cRNA probes against *Wnt1* and *Twist1* were gifts from Dr. Paul Trainor (Stowers Institute for Medical Research, USA).

Whole-mount *in situ* hybridization proceeded as described (Sakai et al., 2012).

Immunofluorescence

Mouse embryos were fixed with 4% paraformaldehyde (PFA) in phosphate-buffered saline (PBS) for 3 h at 4°C and cryopreserved in 30% sucrose in PBS. Brains were embedded in optimal cutting temperature compound (OCT) and stored at −80°C until further use. The cryostat sections (10 μm thick) were adhered to glass slides and washed with PBS. Antigens were retrieved by incubation with 10 mM citric acid (pH 6.0) for 30 min at 80°C. After a brief wash with PBS, the sections were incubated with 0.5% Triton X-100 in PBS for 15 min at room temperature. Non-specific antigen binding was blocked by incubation with a blocking buffer (3% BSA in TBST) for 30 min at room temperature. The sections were then incubated at 4°C overnight with primary antibodies against phospho-histone H3 (ser28) (06-570, Upstate; 1/500), cleaved caspase 3 (9661, Cell Signaling; 1/200), Sox2 (AF 2018, R&D systems; 1/200), acetylated α-tubulin (6-11B-1)(T6793, Sigma; 1/2000), phospho-MLC2 (3671, Cell Signaling; 1/100), Aldoa (sc-12059, Santa Cruz; 1/200), Ldha (sc-27230, Santa Cruz; 1/200), and Pfkfb3 (60,241-1, Protein Tech; 1/500).

The sections were washed three times with TBST for 10 min and then incubated with the appropriate secondary antibodies conjugated with Alexa 488 or 546 (A11001, A21208, Invitrogen; 1/300) for 1 h at room temperature. Nuclei were stained with DAPI. Sections were assessed using a BX51 fluorescence microscope equipped with a DP30BW CCD camera (Olympus) and 10× and 20× objective lenses. Images were acquired using the DP controller software (Olympus).

Apical surface area calculations

We outlined apical membranes by staining the F-actin ring with Alexa Fluor-488 phalloidin (A12379, Thermo Fisher; 1/1000). Sections were assessed using a LSM PASCAL confocal fluorescence microscope (Carl Zeiss) and a 40× objective lens. Confocal optical slices were collected, and maximum-intensity projections of 0.3 mm stacks were generated using Zeiss LSM5 software. The apical surface area was calculated using ImageJ software.

Statistics

Data were statistically analyzed using two-tailed Student's *t*-tests and Chi-square test. Values with $p < 0.05$ indicated statistically significant differences.

Data availability statement

The datasets generated during current study are available in the Figshare, at 10.6084/m9.figshare.23577999.

Ethics statement

The animal study was reviewed and approved by the Ethics Committee on Animal Experiments of the Kanazawa Medical University.

Author contributions

DS and HS designed the study. DS and YM conducted and interpreted most of the experiments. MT contributed to the RT-qPCR and DSH assisted with image analysis. HS-H, TH, and HS interpreted the data and edited the manuscript, and DS wrote the manuscript. All authors have read and approved the final version of this manuscript.

Funding

This study was supported by JSPS KAKENHI grant-in-aid for scientific research (Nos 19K06680 and 17H05965) to DS.

Acknowledgments

We thank Dr. Yoshio Wakamatsu (Tohoku University) for his valuable help and advice. *Wnt1*-and *Twist1*-pBluescriptII plasmids were kindly provided by Dr. Paul Trainor (Stowers Institute for Medical Research, United States). We would like to thank Editage (www.editage.com) for English language editing.

Conflict of interest

The authors declare that the research was conducted in the absence of any commercial or financial relationships that could be construed as a potential conflict of interest.

Publisher's note

Supplementary material

The Supplementary Material for this article can be found online at: https://www.frontiersin.org/articles/10.3389/fcell.2023.1212375/full#supplementary-material

SUPPLEMENTARY FIGURE S1
Effect of glycolytic inhibition on apoptosis and differentiation. **(B)** Percentage of cleaved caspase3$^+$ apoptotic cells among all neuroepithelial cells after incubation without (-) or with 2-DG (+). Data are shown as means ± S.E.M of six histological sections from three

embryos. Statistical differences were assessed using Student's *t*-tests. **(C)** Expression of *Wnt1,* and *Twist1* mRNA was detected by cryosection *in situ* hybridization of E8.25 embryos. Scale bars, 100 μm. Image is representative of four independent experiments.

References

Bhattacharya, D., Azambuja, A. P., and Simoes-Costa, M. (2020). Metabolic reprogramming promotes neural crest migration via yap/tead signaling. *Dev. Cell* 53 (2), 199–211.e6. doi:10.1016/j.devcel.2020.03.005

Colas, J. F., and Schoenwolf, G. C. (2001). Towards a cellular and molecular understanding of neurulation. *Dev. Dyn.* 221 (2), 117–145. doi:10.1002/dvdy.1144

Compernolle, V., Brusselmans, K., Franco, D., Moorman, A., Dewerchin, M., Collen, D., et al. (2003). Cardia bifida, defective heart development and abnormal neural crest migration in embryos lacking hypoxia-inducible factor-1alpha. *Cardiovasc Res.* 60 (3), 569–579. doi:10.1016/j.cardiores.2003.07.003

Cruys, B., Wong, B. W., Kuchnio, A., Verdegem, D., Cantelmo, A. R., Conradi, L. C., et al. (2016). Glycolytic regulation of cell rearrangement in angiogenesis. *Nat. Commun.* 7, 12240. doi:10.1038/ncomms12240

Cunniff, B., McKenzie, A. J., Heintz, N. H., and Howe, A. K. (2016). AMPK activity regulates trafficking of mitochondria to the leading edge during cell migration and matrix invasion. *Mol. Biol. Cell* 27 (17), 2662–2674. doi:10.1091/mbc.E16-05-0286

De Bock, K., Georgiadou, M., Schoors, S., Kuchnio, A., Wong, B. W., Cantelmo, A. R., et al. (2013). Role of PFKFB3-driven glycolysis in vessel sprouting. *Cell* 154 (3), 651–663. doi:10.1016/j.cell.2013.06.037

Dunwoodie, S. L. (2009). The role of hypoxia in development of the Mammalian embryo. *Dev. Cell* 17 (6), 755–773. doi:10.1016/j.devcel.2009.11.008

Fame, R. M., and Lehtinen, M. K. (2021). Mitochondria in early forebrain development: From neurulation to mid-corticogenesis. *Front. Cell Dev. Biol.* 9, 780207. doi:10.3389/fcell.2021.780207

Fame, R. M., Shannon, M. L., Chau, K. F., Head, J. P., and Lehtinen, M. K. (2019). A concerted metabolic shift in early forebrain alters the CSF proteome and depends on MYC downregulation for mitochondrial maturation. *Development* 146 (20), dev182857. doi:10.1242/dev.182857

Fischer, B., and Bavister, B. D. (1993). Oxygen tension in the oviduct and uterus of rhesus monkeys, hamsters and rabbits. *J. Reprod. Fertil.* 99 (2), 673–679. doi:10.1530/jrf.0.0990673

Hu, H., Juvekar, A., Lyssiotis, C. A., Lien, E. C., Albeck, J. G., Oh, D., et al. (2016). Phosphoinositide 3-kinase regulates glycolysis through mobilization of aldolase from the actin cytoskeleton. *Cell* 164 (3), 433–446. doi:10.1016/j.cell.2015.12.042

Hunter, E. S., 3rd, and Tugman, J. A. (1995). Inhibitors of glycolytic metabolism affect neurulation-staged mouse conceptuses *in vitro*. *Teratology* 52 (6), 317–323. doi:10.1002/tera.1420520602

Iyer, N. V., Kotch, L. E., Agani, F., Leung, S. W., Laughner, E., Wenger, R. H., et al. (1998). Cellular and developmental control of O2 homeostasis by hypoxia-inducible factor 1 alpha. *Genes Dev.* 12 (2), 149–162. doi:10.1101/gad.12.2.149

Jia, W., Zhao, X., Zhao, L., Yan, H., Li, J., Yang, H., et al. (2018). Non-canonical roles of PFKFB3 in regulation of cell cycle through binding to CDK4. *Oncogene* 37 (13), 1685–1698. doi:10.1038/s41388-017-0072-4

Keuls, R. A., Kojima, K., Lozzi, B., Steele, J. W., Chen, Q., Gross, S. S., et al. (2020). MiR-302 regulates glycolysis to control cell-cycle during neural tube closure. *Int. J. Mol. Sci.* 21 (20), 7534. doi:10.3390/ijms21207534

Kotch, L. E., Iyer, N. V., Laughner, E., and Semenza, G. L. (1999). Defective vascularization of HIF-1alpha-null embryos is not associated with VEGF deficiency but with mesenchymal cell death. *Dev. Biol.* 209 (2), 254–267. doi:10.1006/dbio.1999.9253

Lee, H., and Nagele, R. G. (1985). Neural tube defects caused by local anesthetics in early chick embryos. *Teratology* 31 (1), 119–127. doi:10.1002/tera.1420310114

Lee, Y. M., Jeong, C. H., Koo, S. Y., Son, M. J., Song, H. S., Bae, S. K., et al. (2001). Determination of hypoxic region by hypoxia marker in developing mouse embryos *in vivo*: A possible signal for vessel development. *Dev. Dyn.* 220 (2), 175–186. doi:10.1002/1097-0177(20010201)220:2<175:AID-DVDY1101>3.0.CO;2-F

Leese, H. J. (1995). Metabolic control during preimplantation mammalian development. *Hum. Reprod. Update* 1 (1), 63–72. doi:10.1093/humupd/1.1.63

Miyazawa, H., Yamaguchi, Y., Sugiura, Y., Honda, K., Kondo, K., Matsuda, F., et al. (2017). Rewiring of embryonic glucose metabolism via suppression of PFK-1 and aldolase during mouse chorioallantoic branching. *Development* 144 (1), 63–73. doi:10.1242/dev.138545

Miyazawa, H., Yamamoto, M., Yamaguchi, Y., and Miura, M. (2018). Mammalian embryos show metabolic plasticity toward the surrounding environment during neural tube closure. *Genes* 23 (9), 794–802. doi:10.1111/gtc.12626

Morriss, G. M., and New, D. A. (1979). Effect of oxygen concentration on morphogenesis of cranial neural folds and neural crest in cultured rat embryos. *J. Embryol. Exp. Morphol.* 54, 17–35. doi:10.1242/dev.54.1.17

Ogoh, H., Yamagata, K., Nakao, T., Sandell, L. L., Yamamoto, A., Yamashita, A., et al. (2017). Mllt10 knockout mouse model reveals critical role of Af10-dependent H3K79 methylation in midfacial development. *Sci. Rep.* 7 (1), 11922. doi:10.1038/s41598-017-11745-5

Pourquie, O. (2022). A brief history of the segmentation clock. *Dev. Biol.* 485, 24–36. doi:10.1016/j.ydbio.2022.02.011

Quintin, S., Gally, C., and Labouesse, M. (2008). Epithelial morphogenesis in embryos: Asymmetries, motors and brakes. *Trends Genet.* 24 (5), 221–230. doi:10.1016/j.tig.2008.02.005

Ream, M., Ray, A. M., Chandra, R., and Chikaraishi, D. M. (2008). Early fetal hypoxia leads to growth restriction and myocardial thinning. *Am. J. Physiol. Regul. Integr. Comp. Physiol.* 295 (2), R583–R595. doi:10.1152/ajpregu.00771.2007

Roberts, S. J., and Somero, G. N. (1987). Binding of phosphofructokinase to filamentous actin. *Biochemistry* 26 (12), 3437–3442. doi:10.1021/bi00386a028

Roberts, S. J., and Somero, G. N. (1989). Properties of the interaction between phosphofructokinase and actin. *Arch. Biochem. Biophys.* 269 (1), 284–294. doi:10.1016/0003-9861(89)90110-0

Rolo, A., Skoglund, P., and Keller, R. (2009). Morphogenetic movements driving neural tube closure in Xenopus require myosin IIB. *Dev. Biol.* 327 (2), 327–338. doi:10.1016/j.ydbio.2008.12.009

Ryan, H. E., Lo, J., and Johnson, R. S. (1998). HIF-1 alpha is required for solid tumor formation and embryonic vascularization. *EMBO J.* 17 (11), 3005–3015. doi:10.1093/emboj/17.11.3005

Sakai, D., Dixon, J., Achilleos, A., Dixon, M., and Trainor, P. A. (2016). Prevention of Treacher Collins syndrome craniofacial anomalies in mouse models via maternal antioxidant supplementation. *Nat. Commun.* 7, 10328. doi:10.1038/ncomms10328

Sakai, D., Dixon, J., Dixon, M. J., and Trainor, P. A. (2012). Mammalian neurogenesis requires Treacle-Plk1 for precise control of spindle orientation, mitotic progression, and maintenance of neural progenitor cells. *PLoS Genet.* 8 (3), e1002566. doi:10.1371/journal.pgen.1002566

Sakai, D., Sugawara, T., Kurokawa, T., Murakami, Y., Tomosugi, M., Masuta, H., et al. (2022). Hif1α-dependent hypoxia signaling contributes to the survival of deep-layer neurons and cortex formation in a mouse model. *Mol. Brain* 15 (1), 28. doi:10.1186/s13041-022-00911-0

Semenza, G. L. (2003). Targeting HIF-1 for cancer therapy. *Nat. Rev. Cancer* 3 (10), 721–732. doi:10.1038/nrc1187

Sperber, H., Mathieu, J., Wang, Y., Ferreccio, A., Hesson, J., Xu, Z., et al. (2015). The metabolome regulates the epigenetic landscape during naive-to-primed human embryonic stem cell transition. *Nat. Cell Biol.* 17 (12), 1523–1535. doi:10.1038/ncb3264

Suzuki, M., Morita, H., and Ueno, N. (2012). Molecular mechanisms of cell shape changes that contribute to vertebrate neural tube closure. *Dev. Growth Differ.* 54 (3), 266–276. doi:10.1111/j.1440-169X.2012.01346.x

Takahashi, M., Nomura, T., and Osumi, N. (2008). Transferring genes into cultured mammalian embryos by electroporation. *Dev. Growth Differ.* 50 (6), 485–497. doi:10.1111/j.1440-169X.2008.01046.x

Takashima, Y., Guo, G., Loos, R., Nichols, J., Ficz, G., Krueger, F., et al. (2014). Resetting transcription factor control circuitry toward ground-state pluripotency in human. *Cell* 158 (6), 1254–1269. doi:10.1016/j.cell.2014.08.029

Ufer, C., and Wang, C. C. (2011). The roles of glutathione peroxidases during embryo development. *Front. Mol. Neurosci.* 4, 12. doi:10.3389/fnmol.2011.00012

Weston, J. A., Yoshida, H., Robinson, V., Nishikawa, S., Fraser, S. T., and Nishikawa, S. (2004). Neural crest and the origin of ectomesenchyme: neural fold heterogeneity suggests an alternative hypothesis. *Dev. Dyn.* 229 (1), 118–130. doi:10.1002/dvdy.10478

Yamaguchi, Y., and Miura, M. (2013). How to form and close the brain: Insight into the mechanism of cranial neural tube closure in mammals. *Cell Mol. Life Sci.* 70 (17), 3171–3186. doi:10.1007/s00018-012-1227-7

Zhou, W., Choi, M., Margineantu, D., Margaretha, L., Hesson, J., Cavanaugh, C., et al. (2012). HIF1α induced switch from bivalent to exclusively glycolytic metabolism during ESC-to-EpiSC/hESC transition. *EMBO J.* 31 (9), 2103–2116. doi:10.1038/emboj.2012.71

frontiers | Frontiers in Molecular Biosciences

TYPE Review
PUBLISHED 13 July 2023
DOI 10.3389/fmolb.2023.1229760

OPEN ACCESS

EDITED BY
Ann Saada,
Hebrew University of Jerusalem, Israel

REVIEWED BY
Sovannarith Korm,
Marine Biological Laboratory (MBL), United States
Xiuling Cao,
Zhejiang Agriculture and Forestry University, China

*CORRESPONDENCE
Susana Fiorentino,
susana.fiorentino@javeriana.edu.co

RECEIVED 27 May 2023
ACCEPTED 30 June 2023
PUBLISHED 13 July 2023

CITATION
Arévalo CM, Cruz-Rodriguez N, Quijano S and Fiorentino S (2023), Plant-derived extracts and metabolic modulation in leukemia: a promising approach to overcome treatment resistance. *Front. Mol. Biosci.* 10:1229760. doi: 10.3389/fmolb.2023.1229760

Plant-derived extracts and metabolic modulation in leukemia: a promising approach to overcome treatment resistance

Cindy Mayerli Arévalo[1], Nataly Cruz-Rodriguez[2], Sandra Quijano[1] and Susana Fiorentino[1]*

[1]Grupo de Inmunobiología y Biología Celular, Facultad de Ciencias, Pontificia Universidad Javeriana, Bogotá, Colombia, [2]Versiti Blood Research Institute, Milwaukee, WI, United States

Leukemic cells acquire complex and often multifactorial mechanisms of resistance to treatment, including various metabolic alterations. Although the use of metabolic modulators has been proposed for several decades, their use in clinical practice has not been established. Natural products, the so-called botanical drugs, are capable of regulating tumor metabolism, particularly in hematopoietic tumors, which could partly explain the biological activity attributed to them for a long time. This review addresses the most recent findings relating to metabolic reprogramming—Mainly in the glycolytic pathway and mitochondrial activity—Of leukemic cells and its role in the generation of resistance to conventional treatments, the modulation of the tumor microenvironment, and the evasion of immune response. In turn, it describes how the modulation of metabolism by plant-derived extracts can counteract resistance to chemotherapy in this tumor model and contribute to the activation of the antitumor immune system.

KEYWORDS

resistance, acute leukemias, metabolism, natural products, botanical drugs

1 Introduction

Acute leukemias (ALs) are a group of malignant diseases of the hematopoietic system characterized by disordered proliferation and clonal expansion of immature precursors, resulting in bone marrow failure with blockage in cell differentiation processes (Swerdlow et al., 2017). ALs are classified, considering their morphological, immunophenotypic, cytogenetic, and molecular characteristics, into two large groups: acute myeloid leukemia (AML) and acute lymphoblastic leukemia (ALL). AML is characterized by the accumulation and blocked differentiation of progenitors of myeloid, monocytic, erythroid, or megakaryocytic lineage, and ALL instead arises from the transformation of B-cell (B-ALL) or T-cell progenitors (T-ALL) (Arber et al., 2016).

Although the use of various chemotherapy schemes for the treatment of ALs has achieved a high percentage of survival in developed countries, in Colombia its implementation has shown discouraging results, with complete remission rates of 45% in AML and 61% in ALL in the adult population (Combariza et al., 2007; Ballesteros-Ramírez et al., 2020a; Sossa et al., 2021). Treatment options for patients who do not achieve a complete remission are limited, as even with salvage therapy followed by allogeneic stem cell transplantation (HSCT), outcomes remain poor (Thol, 2018). For four decades, the

mortality rates of patients with ALs have been the highest when compared to the rates of other groups of leukemias (Shallis et al., 2019).

The lack of response to current chemotherapeutics has been attributed to different resistance mechanisms, among them: 1) the acquisition of new mutations or genetic alterations (clonal evolution) (Hackl et al., 2017); 2) the presence of leukemia-initiating cells (LICs) remaining after chemotherapy (Yeung and Radich, 2017); 3) the autophagy as a cooperative mechanism for the stability of oncoproteins or as a cytoprotective against the cytotoxic effects induced by drugs (Auberger and Puissant, 2017); 4) the overexpression of ATP-binding cassette transporters (ABC transporters) that allow drug efflux (Marin et al., 2016); 5) the microbiota affecting the metabolism, toxicity, and efficacy of certain drugs (Wilkinson et al., 2018); 6) inherent patient factors such as body mass index and age (Li et al., 2017), 7) the microenvironment through soluble factors or direct interaction between leukemic blasts and mesenchymal or stromal cells (Shafat et al., 2017); and 8) which has recently been recognized as one of the hallmarks of cancer, can also contribute to the evasion of the antitumor immune response (Desbats et al., 2020).

Reprogrammed metabolic activities of tumor cells that support survival, maintenance, and drug response are related to altered bioenergetic pathways, enhanced macromolecule biosynthesis, and maintenance of the redox balance (DeBerardinis and Chandel, 2016; Vander Heiden and Deberardinis, 2017). The addition of therapies that modulate tumor metabolism to conventional chemotherapy has been emerging, (Luppi et al., 2018; Winer and Stone, 2019), and more therapeutic strategies are needed that achieve tumor metabolic modulation that can lead to the activation of the immune system and an accentuated anti-neoplastic effect. Then, our group focused on seeking anti-leukemic therapies based on plant-derived extracts that serve as the basis for the preparation of botanical drugs or phytomedicines (Urueña et al., 2008; Castañeda et al., 2012; Sandoval et al., 2016; Ballesteros-Ramírez et al., 2020b). The use of plant-derived extracts, due to their multiple active components, offers a multi-target mechanism of action, unlike many current therapies that follow the classic "one drug, one target" pharmacological dogma and have fewer toxic side effects, so they are more tolerable (Herranz-López et al., 2018). In addition, its main components can be combined with conventional chemotherapy to reduce the development of chemoresistance through the modulation of metabolism (Kumar and Jaitak, 2019).

In this review, we describe the intrinsic and extrinsic mechanisms that have been associated with alterations in glycolytic metabolism and mitochondrial function in chemoresistant leukemic cells and how natural products could reverse resistance with a metabolic and immunomodulatory approach.

2 Reprogramming glycolytic metabolism induces chemoresistance in ALs

The final product of glucose oxidation can be lactate or carbon dioxide (CO_2) (via mitochondrial respiration). Tumor cells, regardless of oxygen availability, increase glucose consumption and produce large amounts of lactate, which is known as the Warburg effect (Icard et al., 2018; Liu et al., 2021; Marcucci and Cristiano, 2021). The increase in the glycolytic pathway is advantageous for tumor cells because: first, it promotes uncontrolled proliferation due to biomass generation; second, it is a fast way to produce adenosine triphosphate (ATP), even more than oxidative phosphorylation (OxPhos); and third, it prevents damage from oxidative stress, directly by reducing mitochondrial respiration and therefore the generation of reactive oxygen species (ROS), and indirectly by the production of nicotinamide adenine reduced dinucleotide phosphate (NADPH) through the pentose pathway (PPP), which maintains glutathione (GSH) in a reduced state, the main non-protein thiol that acts as an intracellular redox regulator (Marcucci and Cristiano, 2021). Some intrinsic and extrinsic factors related to increased glycolysis described below are associated with chemoresistance mechanisms in various tumor models, including ALs (Supplementary Table S1).

2.1 ALL and AML cells resistant to chemotherapy and increase glycolysis

Most of the studies in cell lines and primary samples derived from myeloid and lymphoid leukemias demonstrate a relationship between the increase in the glycolytic pathway and resistance to different types of drugs, such as anthracyclines (daunorubicin, -DNR-, doxorubicin, -DOX-, and idarubicin, -IDA-), some glucocorticoids such as prednisolone, and tyrosine kinase inhibitors (TKIs) such as imatinib, among others.

In DNR-resistant cell lines such as HL60/DNR and CEM/R2, of myeloid and T-lymphoid origin, respectively, a higher glucose demand has been described together with a lower glutamine dependence and a lower rate of fatty acid oxidation compared with their non-resistant counterparts (Stäubert et al., 2015). Similarly, myeloid cell lines (K562-r and LAMA84-r) with aberrant expression of Breakpoint Cluster Region-Breakpoints in the Abelson (ABL)1 fusion (BCR-ABL1) and resistance to imatinib maintain a highly glycolytic metabolic phenotype with elevated lactate production (Kominsky et al., 2009). On the other hand, the TEX cell line, which mimics the characteristics of AML and LICs, is resistant to tigecycline (an antibiotic that induces an antitumor effect by inhibiting the translation of mitochondrial proteins) (Xu et al., 2016), and it has an increased glycolytic rate (Jhas et al., 2013). Importantly, in some B-ALL and T-ALL cell lines and cells derived from patients with B-ALL, reduction of the glycolytic rate using 2-deoxy-D-glucose (2-DG), lonidamine (LND), or 3-bromopyruvate (3-BrPA), can restore the sensitivity of these cells to glucocorticoids (Hulleman et al., 2009; Gu et al., 2017); and the combined treatment of a glycolytic inhibitor in conjunction with the silencing of anti-apoptotic proteins such as myeloid cell leukemia sequence 1 protein (MCL-1) can enhance the antitumor activity in cells resistant to prednisolone (Ariës et al., 2013).

In contrast to the above, a single publication by Herst et al. (2011) using primary AML cells describes that patients with highly glycolytic blasts had higher overall survival rates and longer rates of first complete remission compared to patients who had blasts with moderate glycolytic rate. Likewise, leukemic blasts that had a high

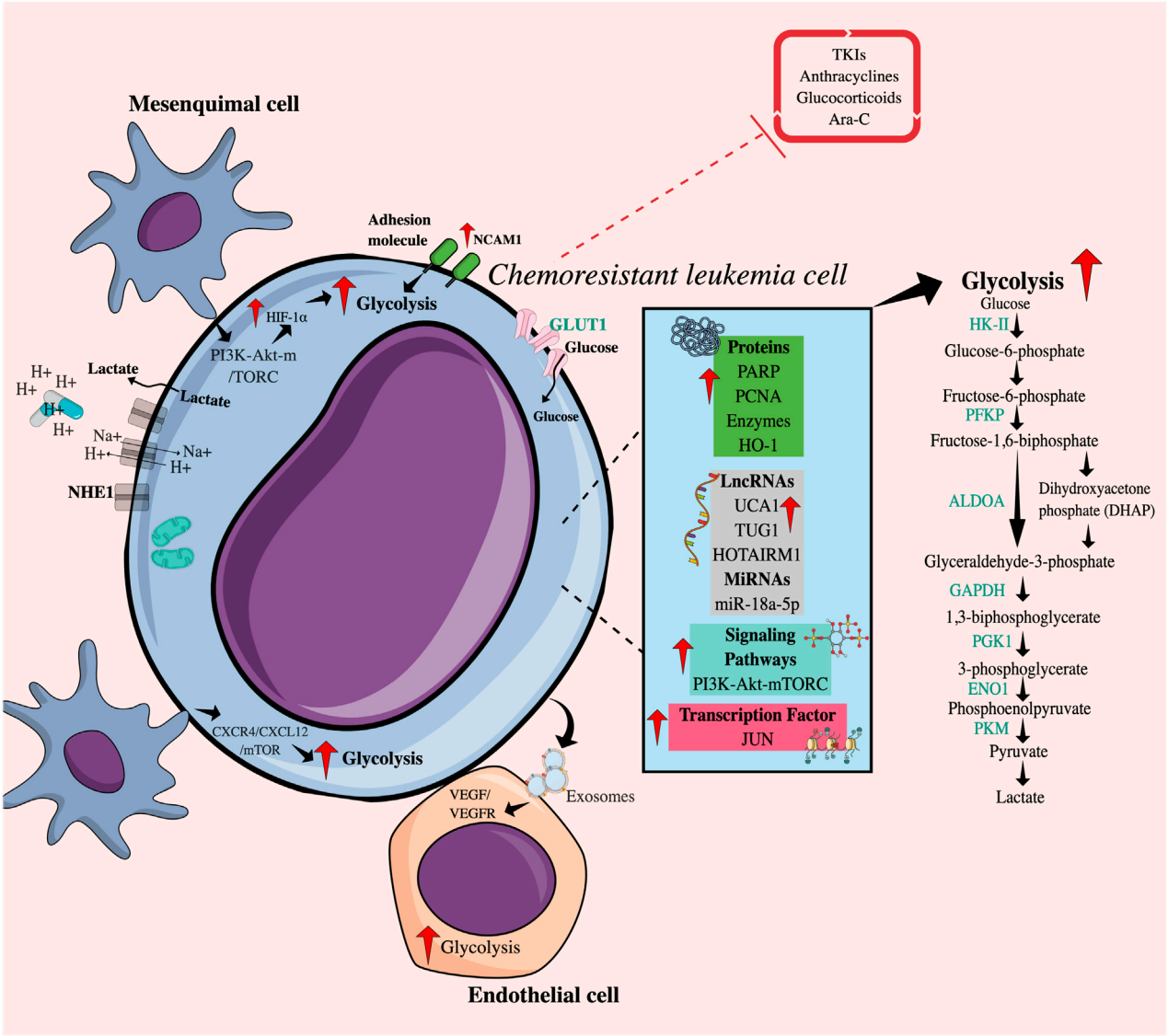

FIGURE 1
Intrinsic and extrinsic mechanisms related to increased glycolytic flux in chemoresistant leukemia cells. Intrinsically, chemoresistant leukemia cells overexpress cytoplasmic proteins, enzymes, RNA molecules, transcription factors, and receptors and present alterations in signaling pathways that favor an increase in glycolytic flow. Additionally, the direct or indirect interaction between chemoresistant leukemia cells and various cell populations of the tumor microenvironment, such as mesenchymal and endothelial cells, promotes glucose uptake achieved by tumor cells through the PI3K-mTORC pathway or the CXCR4/CXCL12 axis. The release of exosomes containing VEGF-RVEFG can also increase glycolysis in endothelial cells. Taken together, all these factors may regulate resistance to drugs including TKIs, anthracyclines, Ara-C, and glucocorticoids. TKIs, Tyrosine kinase inhibitors; Ara-C, Cytarabine; HIF-1, Hypoxia-induced factor; GLUT1, Glucose transporter 1; NCAM1, Neural cell adhesion molecule 1; NHE1, Na (+)/H (+) antiporter; HK-II, Hexokinase II; PFKP, Phosphofructokinase; GPI, Glucose phosphate isomerase; ALDOA, Aldolase A; GAPDH, Glyceraldehyde-3-phosphate dehydrogenase; PGK1, Phosphoglycerate kinase; ENO1, Enolase 1; LDHA, Lactate dehydrogenase A; PKM, Pyruvate kinase 2; HO-1, Heme oxygenase-1; PARP, Poly (ADP-ribose) polymerases; PCNA, Proliferating cell nuclear antigen; LncRNAs, Long non-coding RNAs; microRNAs, Short non-coding RNAs; UCA1, Associated with urothelial carcinoma; TUG1, Taurine upregulated gene 1; HOTAIRM1, Myeloid-specific antisense intergenic RNA HOX transcript 1.

glycolytic level were more susceptible to the anti-tumor activity of all-trans retinoic acid (ATRA) and arsenic trioxide (ATO). These data show us that tumor cells require homeostatic mechanisms to avoid scenarios of accumulation or depletion of secondary metabolites that can be toxic and that an excessive glycolytic flux can represent an unfavorable event for their survival and adaptation to different stress conditions. However, the direct relationship between the increase in glycolysis and chemoresistance in leukemic cells must be studied in depth at the mechanistic level.

2.2 Regulation of increased glycolytic flux: intrinsic mechanistic factors

Different intrinsic factors have been established that influence an improvement in the glycolytic pathway in chemoresistant leukemia cells (Figure 1). Genetic alterations that involve mutations in oncogenes and/or tumor suppressor genes lead to deregulated signaling pathways and consequently to the aberrant expression of transcription factors, enzymes, transporters, proteins

(nuclear and cytoplasmic), and regulatory molecules of glucose metabolism (Lo Presti et al., 2020; Di Martino et al., 2021).

The phosphoinositide 3-kinase-Akt-mammalian target of rapamycin (PI3K-Akt-mTOR) signaling pathway, commonly activated in cancer, including AML, contributes to the maintenance of glycolysis by translational and post-translational regulation of metabolic enzymes (Hoxhaj and Manning, 2020; Nepstad et al., 2020). Ryu et al. (2019) established that AKT activation by phosphatidylinositol 3,4,5-trisphosphate 3-phosphatase and dual-specificity protein phosphatase (PTEN) deficiency, a direct PI3K antagonist, maintained a refractory state of cells to treatment with cytarabine (Ara-C) and IDA through the improvement of glycolysis in the myeloid lines HL60 and KG1α.

A master transcription factor in the regulation of glycolysis is hypoxia-inducible factor 1 α (HIF-1α) because it promotes the transcription of glucose transporters, such as glucose transporter 1 (GLUT1), and glycolytic enzymes, such as hexokinase II (HK-II), and pyruvate kinase M2 (PKM2) (Yu et al., 2017). An increase in the expression levels of GLUT1, HIF1-α, and HK-II mRNA has been reported in primary AML cells from non-responders and HL60/DNR cells (Jhas et al., 2013; Song et al., 2014; Song et al., 2016). Also, recently, Valin et al. (2022) reported JUN, an oncogenic transcription factor, as a regulator of glycolytic metabolism in AML, since it increases the expression of hexokinase I (HKI) and HKII, glucose phosphate isomerase (GPI), phosphofructo-1-kinase (PFKP), aldolase A (ALDOA), glyceraldehyde-3-phosphate dehydrogenase (GAPDH), phosphoglycerate kinase (PGK1), enolase 1 (ENO1), and PKM. Similarly, in breast cancer, the c-JUN family of proteins has been associated with resistance to cisplatin (Xia et al., 2013).

Another molecule that promotes glycolysis is the proliferating cell nuclear antigen (PCNA), which is a nuclear protein synthesized in the early G1 phase and in the S phase of the cell cycle and is considered a marker of the proliferation index in some neoplasms (Cardano et al., 2020). It has been shown that the interaction between PCNA and nicotinamide phosphoribosyl transferase (NAMPT), an enzyme that participates in the rescue pathway for the generation of the nicotinamide adenine dinucleotide (NAD+) cofactor, can coordinate the increase in glycolysis, favoring the survival of DNR-resistant HL60 cells (Ohayon et al., 2016).

On the other hand, the enzyme heme oxygenase-1 (HO-1) catalyzes the degradation of the heme group, causing carbon monoxide (CO), biliverdin, and iron, where the heme group is a critical component of multiple hemoproteins involved in glucose metabolism and of lipids and proteins. Interestingly, elevated levels of HO-1 have been described in primary myeloid cells and HL60 cells resistant to Ara-C and DNR. HO-1 inhibition abrogates the expression of HIF-1α, and GLUT1, improving the sensitivity to the two drugs, apparently by decreasing the glycolysis (Zhe et al., 2015). Furthermore, HO-1 is involved in the generation of a resistant profile in patients with myelodysplastic syndrome (MDS) who can progress to AML (He et al., 2019). Also, the increased expression of the adhesion protein NCAM1 (Neural Cell Adhesion Molecule 1) in K562 BCR-ABL$^+$ myeloid cells increases the IC_{50} for dasatinib (Sasca et al., 2019). Knockdown of NCAM1 decreases the expression of genes involved in glucose metabolism, and the reduction in their expression sensitizes NOMO shNCAM_3 leukemic cells to treatment with Ara-C in a murine NSG (NOD *scid* gamma mouse) model.

Poly (ADP-ribose) polymerases (PARP) family of polymerases is made up of proteins involved in many cellular processes, including DNA repair and apoptosis. Particularly, PARP14 can promote glycolysis in different tumor models, such as human hepatocellular carcinoma (HCC), by maintaining reduced PKM2 activity (Iansante et al., 2015); on the other hand, a close relationship between c-myc and AKT has been reported in B lymphomas (Cho et al., 2011) and AML through the NF-κB/HIF-1α axis (Zhu et al., 2022). Interestingly, the use of Niraparib, a PARP1/2 inhibitor, decreases resistance to ATO and hypomethylating agents (azacytidine and decitabine) in tumor promyelocytes (Giansanti et al., 2021).

Deregulation of LncRNAs and microRNAs (long and short non-coding RNAs, respectively), considered epigenetic regulators, contributes to therapeutic resistance through the regulation of energy metabolism (Agbu and Carthew, 2021; Taghvimi et al., 2022). The LncRNA associated with urothelial carcinoma (UCA1) is overexpressed in AML cells from patients who did not respond to DOX treatment and in the HL60/DNR cell line (Liu et al., 2014). UCA1 promotes glycolysis by inhibiting the action of mRNA125a, which usually functions as a tumor suppressor but also appears to be involved in blocking HK-II (Sun et al., 2017), which in turn could participate in the stabilization of HIF1-α (Zhang et al., 2018). Also, thanks to its oncogenic role, the increase in the expression of the LncRNA TUG1 (taurine-upregulated gene 1) is accompanied by the increase in the expression of the mRNAs of HK-II and PKM2 in HL60 cells resistant to doxorubicin (HL60/DOX) (Chen L. et al., 2019a). Another LncRNA, HOTAIRM1 (HOX transcript antisense intergenic RNA myeloid-specific 1), involved in myeloid lineage maturation and overexpressed in AML, has been compromised by resistance to Ara-C. Its deletion has been reported to improve drug activity and decrease glucose consumption and therefore lactate production, mainly mediated by the reduction of PFKP in HL60/WT and THP-1/WT cells (Chen et al., 2020).

Particularly in K562 cells, the expression level of miR-18a-5p in DOX-resistant cells is lower compared to K562 cells and normal lymphocytes, and strikingly, miR-18a-5p can inhibit the expression of HIF-1α and, in turn, induce a reduction in the production of pyruvate, ATP and affect the expression of GLUT1, HK-II, PKM2, and lactate dehydrogenase A (LDHA) (Wu et al., 2021).

2.3 Regulation of increased glycolytic flux: extrinsic mechanistic factors

In the bone marrow microenvironment, there are cellular and non-cellular components that influence the metabolic reprogramming of leukemia cells and can be considered external factors (Jiang and Nakada, 2016). Contact between mesenchymal cells (MSC) and/or endothelial cells (EC) and leukemic cells improves tumor survival in the presence of different chemotherapeutic agents (Boutin et al., 2020; Okamoto et al., 2022). Culturing primary B-ALL cells or Reh lymphoid cell line with bone marrow-derived MSCs under hypoxic conditions induces a higher expression of HIF-1α and therefore an acquisition of the glycolytic phenotype of leukemic cells, which in part is due to signaling-regulated by the AKT/mTOR pathway induced by stromal cells. Inhibition of mTOR using everolimus, an

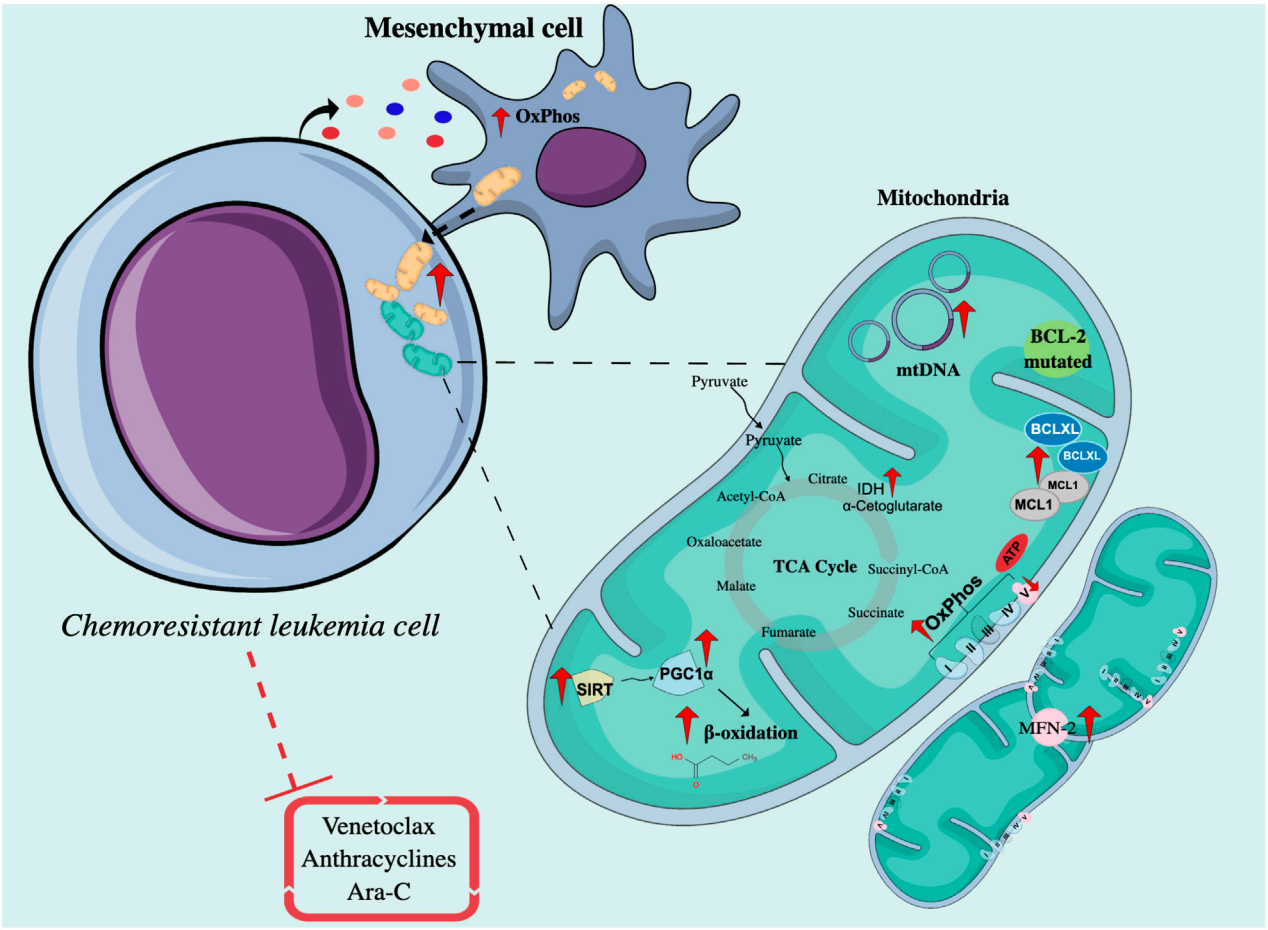

FIGURE 2
Intrinsic and extrinsic mechanisms related to mitochondrial function in chemoresistant leukemia cells. Chemoresistant leukemia cells exposed to drugs such as Venetoclax, Ara-C, and anthracyclines interact with mesenchymal cells through mitochondrial transfer to increase OxPhos and ATP production. On the other hand, the mitochondria of resistant cells are characterized by the upregulation of proteins involved in the regulation of apoptosis, mitochondrial biogenesis, and fatty acid metabolism, and present a higher number of mtDNA copies. OxPhos, Oxidative phosphorylation; Ara-C, Cytarabine; TCA cycle, Cycle of tricarboxylic acids; MFN-2, Mitofusin 2; SIRT, Sirtuins; PGC1α, PPARγ coactivator-1α; IDH, Isocitrate dehydrogenase; mtDNA, Mitochondrial DNA; BCL-2, B-Cell Leukemia/Lymphoma 2; Bax, Bcl-2-associated X protein; Bak, Bcl-2 homologous antagonist/killer; MCL1, Myeloid cell leukemia sequence 1 protein.

antiproliferative agent, reduces the expression of HIF-1α, decreases the glycolytic rate, and partially restores the sensitivity of ALL cells to vincristine under co-culture and hypoxic conditions (Frolova et al., 2012). Also, the interaction with stromal cells increases the glycolytic flux of AML cells from patients through the CXCR4/CXCL12/mTOR axis (Braun et al., 2016), and the use of selective inhibitors of this axis represents an opportunity to block MSC-mediated chemoresistance (Braun et al., 2016). In AML, leukemic cells have been reported to secrete VEGF/VEGFR-containing exosomes that induce glycolysis in endothelial cells -HUVECs-, leading to vascular remodeling and the acquisition of chemoresistance (Wang et al., 2019).

On the other hand, the Warburg effect implies an increase in the production of lactic acid and, therefore, an acidic microenvironment. Tumor cells express several families of pH regulators in the plasma membrane to protect themselves, such as NHE1 (Sodium-hydrogen antiporter 1), which exports H^+ and contributes to the decrease in extracellular pH. Acidification in the microenvironment plays an immunosuppressive role and mediates the protonation of drugs, affecting their cell permeability (Altaf et al., 2017; de la Cruz-López et al., 2019). In T-ALL, increased NHE1 activity may promote resistance to DOX and imatinib (Man et al., 2014).

2.4 Association between increased glycolysis with clinical response and survival rates in ALs

Despite the strong evidence that glycolytic metabolism can promote chemoresistance in primary leukemic cells from non-responders and/or multiresistant cell lines, recent advances in metabolomics platforms have allowed further investigation into tumor metabolism at the systemic level in patients with acute leukemia (Grønningsæter et al., 2019; Kim et al., 2021), however, only a few studies have focused on the impact of glycolytic

alterations on response to chemotherapy treatment, with mixed results. An increase in circulating serum glucose (α-glucose and β-glucose) in patients with different subtypes of AML—Including leukemias with monocytic differentiation characterized by having a poor prognosis—In comparison with healthy controls has been reported (Duan et al., 2022). In contrast, in plasma samples of bone marrow from pediatric ALL patients with positive minimal residual disease (MRD), a decrease in glucose and a higher concentration of other metabolites related to glycolysis, the PPP pathway, and the tricarboxylic acid (TCA) cycle were observed (Schraw et al., 2019). These results demonstrate the functional compartmentalization of glucose and the ability of tumor cells to influence systemic glucose regulation (Ye et al., 2018). Likewise, Chen et al. (2014) managed to identify a serum metabolic signature related mainly to the glycolysis pathway, where the decrease in glycerol-3-phosphate (glycerol-3P) and lactate, together with the increase in 2-hydroxyglutarate (2-HG), 2-oxoglutarate, and pyruvate, would be negatively related to the overall survival of patients with AML with a normal karyotype; while decreased citrate levels would positively impact, evidencing the clinical utility of the identification of energetic metabolic biomarkers. However, taking into account that the global metabolome of a patient is a complex, specialized metabolic network at different levels (Schmidt et al., 2021) and that it is not only influenced by the glycolytic metabolism of tumor cells, but the focus of metabolism studies in cancer with clinical utility must also have a comprehensive vision.

3 Chemoresistance-induced mitochondrial function in ALs

Mitochondria allow metabolic adaptation to various stress conditions as they are an integrating center of important cellular processes that include energy production through OxPhos, redox signaling, anabolic and catabolic reactions, epigenetic regulation, cell self-renewal and differentiation, initiation, and run-time programmed cell death (PCD) (Basak and Banerjee, 2015; Guerra et al., 2017; Bokil and Sancho, 2019; Grasso et al., 2020); and particularly in leukemias, they have emerged as a determinant for the progression and development of cancer as well as the response to chemotherapeutics (Basak and Banerjee, 2015). Interestingly, several studies have shown that AML and B-ALL cells have increased respiratory activity, increased mitochondrial mass, and significantly higher mitochondrial DNA (mtDNA) content than normal $CD34^+$ cells and peripheral blood mononuclear cells (PBMCs) (Panina et al., 2019; Jain et al., 2022). However, they show a lower energy reserve capacity and reduced activity of complexes III, IV, and V, which could explain why they are more sensitive to mitochondrial damage than normal cells or other tumor models, such as ovarian cancer (Panina et al., 2019). In addition, synergistic and selective cytotoxicity has been reported in AML cell lines by combining components that target mitochondria (mitocans) with glycolytic inhibitors, TKIs, or microtubule destabilizers (Panina et al., 2020). Added to the above, cells with low levels of ROS, within which LICs could be, are unable to use glucose when mitochondrial respiration is inhibited (Lagadinou et al., 2013). For all the above, mitochondrial function is essential for the survival of leukemic cells and is currently a highly explored therapeutic target.

3.1 Mitochondria as a promoter of chemoresistant AML and ALL cells

Various publications have described the role of mitochondrial activity in resistance or sensitivity to chemotherapy treatment in ALs. Most of the reports currently described show that resistant leukemic cells have enhanced mitochondrial activity, while other works suggest that impaired or stable mitochondrial activity could be related to resistance. The association between mitochondrial activity and low sensitivity to anthracyclines, Ara-C, and Venetoclax has been documented in cell lines and primary leukemia cells and confirmed using *in vivo* models (Farge et al., 2017) (Figure 2).

Regarding improved mitochondrial activity, AML cells persistent to treatment with Ara-C in an NSG mouse model presented a higher rate and a genetic signature associated with OxPhos, accompanied by an increase in mitochondrial mass, membrane potential, and ROS production (Farge et al., 2017). Through the use of metabolic sensors, in B-ALL, it was shown that cells resistant to Ara-C had greater mitochondrial respiration capacity (Chen et al., 2021). Several reports have shown that by inhibiting mitochondrial processes such as the oxidation of fatty acids, the activity of the electron transport chain (ETC), the replication of mtDNA, or the synthesis of mitochondrial proteins, the sensitivity to Ara-C increases *in vitro* and *in vivo* (Farge et al., 2017), and the proliferation of primary AML cells have slightly decreased (Vitkevičienė et al., 2019).

On the other hand, regarding stable or impaired mitochondrial activity, in Jurkat rho zero (ρ0) T lymphoid cells (cells without mitochondria), there is greater resistance to treatment with bleomycin, an antineoplastic antibiotic, compared to Jurkat cells with mitochondria (Yeung et al., 2015), reflecting a susceptibility to mitochondrial damage in these cells. And also, interestingly, Henkenius et al. (2017) reported that resistant HL60 and MV4-11 cells maintain stable mitochondrial activity after exposure to different concentrations of Ara-C and sorafenib, compared to sensitive HL60 cells, in which their mitochondrial activity is affected.

3.2 Intrinsic and extrinsic mechanistic factors of mitochondrial function mediating chemoresistance in ALs cells

There are also intrinsic and extrinsic factors that affect mitochondrial function and, therefore, mediate therapeutic sensitivity. Among the intrinsic factors are the sirtuins (SIRTs), a family of NAD^+-dependent lysine deacetylases, some of which are exclusively expressed in mitochondria (SIRTs 3, 4, and 5) (Jaiswal et al., 2022). These enzymes mediate the response to cellular stress, inducing metabolic changes by regulating the activity of proteins such as PGC1α (PPARγ coactivator-1α) (Chalkiadaki and Guarente, 2015), which is a master in the regulation of mitochondrial metabolism and an activator of genes associated with the

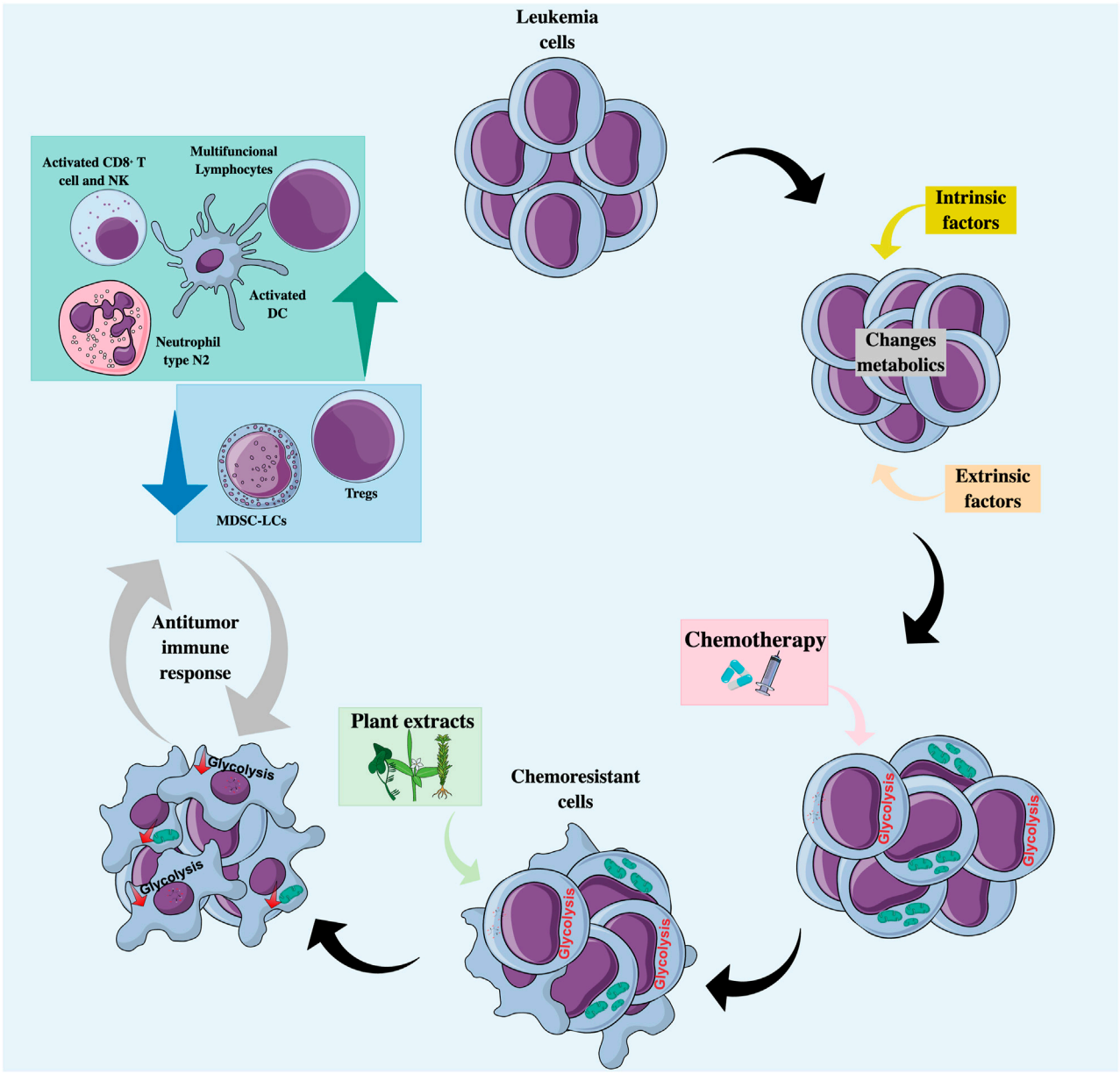

FIGURE 3
Natural products as co-adjuvant therapy in acute leukemia with a metabolic and immunomodulatory approach. Treatment with chemotherapeutic agents may favor the selection of chemoresistant clones characterized by an increase in glycolytic flux or an increase in mitochondrial activity. Combined treatment with natural products can lead to the regulation of tumor metabolism by decreasing glycolysis and/or altering mitochondrial function, making cells more sensitive to cell death, and promoting the recognition and elimination of tumor cells by cells of the immune system. DC, Dendritic cells; MDSC-LCs, Myeloid-derived suppressor-like cells; N2 neutrophils, Anti-tumor phenotype; NK, Natural killer; Tregs, Regulators T cells.

oxidation of fatty acids (Mattes et al., 2019). In AML, SIRT3 activity has been implicated in chemoresistance to Ara-C by regulating OxPhos in the myeloid cell line MV4-11 (Ma et al., 2019). In addition, it has been described that many AML patient samples are highly dependent on SIRT5. Genetic or pharmacological SIRT5 inhibition impairs *in vitro* transformation of mouse hematopoietic cells by several myeloid oncogenes, including MLL-AF9, and attenuates *in vivo* leukemogenesis. SIRT5 knockdown or pharmacological inhibition with NRD167 is associated with reduced OXPHOS, reduced GSH levels, and increased mitochondrial superoxide, suggesting that AML cells depend on SIRT5 to maintain redox homeostasis (Yan et al., 2021).

Another important enzyme in mitochondrial function is ATP synthase, a transmembrane enzyme that catalyzes the synthesis of ATP from ADP, a phosphate group, and the energy supplied by the flow of H^+ supplied by the coenzymes NADH and reduced flavin adenine dinucleotide ($FADH_2$). It is made up of two subunits: the Fo subunit, a component that crosses the inner mitochondrial membrane, and the F1 subunit, which protrudes into the mitochondrial matrix. The decrease in the expression of the

ATP-F1-β subunit, probably due to epigenetic changes related to hypermethylation of the gene, has been reported in cells from refractory or relapsed AML patients and has been confirmed in DOX-resistant HL60 myeloid lines and DNR (Xiao et al., 2013; Song et al., 2016; Yang et al., 2016).

Mitochondrial fusion and fission are two opposite processes that go according to cellular metabolic requirements. Fusion allows mitochondria to connect with each other to form networks or fragments and is commonly associated with increased ATP production and protection against autophagy; on the contrary, fission allows mitochondria to constantly divide and is mainly related to apoptosis, facilitating the segregation of mtDNA in mitosis and eliminating defective mitochondria (Genovese et al., 2021). The survival of T-ALL cells after DOX treatment was correlated with the expression of Mitofusin-2 (MFN-2)—A GTPase protein that mediates mitochondrial fusion—With an increase in the expression of CTE complexes as well as a proportional increase in oxygen consumption rate (OCR), and increased sensitivity to DOX was evident upon inactivating MFN-2 by CRISPR (Decker et al., 2020).

The anti-apoptotic protein Bcl-2 homologous antagonist/killer (BCL-2), overexpressed in some subtypes of B-cell lymphomas, regulates mitochondrial function and mediates therapeutic resistance by inhibiting the oligomerization of the pro-apoptotic Bcl-2 homologous antagonist/killer (Bak) and Bcl-2-associated X protein (Bax) proteins and by facilitating the import of GSH and complex IV subunits to mitochondria (Mattes et al., 2019). The dependence of BCL-2 activity has been demonstrated in both chemosensitive and chemoresistant myeloblasts but not in normal hematopoietic stem cells (HSCs) (Vo et al., 2012); therefore, the use of BCL-2 inhibitors has recently emerged, especially the use of venetoclax in the treatment of AML (Griffioen et al., 2022). Despite its potential *in vivo*, factors such as the upregulation of fatty acid oxidation (FAO) (Stevens et al., 2020), mutations in BCL-2, overexpression of the anti-apoptotic proteins MCL1 or B-cell lymphoma extra-large (Bcl-xL) (Saliba et al., 2021), or the OPA1 (Mitochondrial Dynamin Like GTPase) fusion protein have been described as mediators of resistance to venetoclax (Chen X. et al., 2019b).

The enzymes isocitrate dehydrogenases (IDH) produce NADPH by metabolizing isocitrate to α-ketoglutarate (α-KG), which is an important factor in the TCA cycle. In AML, IDH mutations lead to the consumption of NADPH by converting isocitrate to 2-HG, considered an oncometabolite. The accumulation of 2-HG triggers the inhibition of α-KG-dependent enzymes, such as TET2 (Tet methylcytosine dioxygenase 2) demethylase, and consequently alters gene expression by favoring DNA hypermethylation (Raimondi et al., 2022). The improvement in mitochondrial oxidative metabolism has been associated with resistance to the use of IDH inhibitors and the concomitant use of OxPhos inhibitors improves the efficacy of treatment against IDH mutated *in vivo* in AML (Stuani et al., 2021).

Regarding external factors, microenvironment-induced tumor reprogramming also affects mitochondrial function. In AL, the transfer of mitochondria between leukemic cells and MSCs as a mechanism of tumor protection has been reported (Polak et al., 2015; Moschoi et al., 2016; Wang et al., 2018). Transfer inhibition using metformin improves the chemosensitivity of AML cells cocultured with MSCs to Ara-C (You et al., 2022). In fact, Ara-C increases mitochondrial transfer from MSCs to AML cells triggered by OxPhos inhibition, favoring tumor progression (Saito et al., 2021). Zhang et al. (2022) described that OCI-AML3 myeloid cells induce adipogenic differentiation in MSCs and reduce osteoblastic differentiation (Figure 2). This alteration is accompanied by a metabolic change from glycolysis to a more oxidative form given by a decrease in phosphoglycerate mutase 1 (PGAM1), ALDOA, LDHA/B, and an increase in succinate dehydrogenase (SDH) A/B/C/D from the ADP-forming beta subunit of succinate-CoA ligase (SUCLA2), aconitase 2 (ACO2), PDK, and pyruvate dehydrogenase phosphatase (PDP), among others.

3.3 Association between mitochondrial function and clinical response and survival rates in ALs

In AML, patients with lower rates of remission and overall survival have a proteogenomic profile characterized by high expression of mitochondrial proteins and a more complex I-dependent respiration (Jayavelu et al., 2022). Additionally, Nan et al. (2022) in a group with high-risk AML identified an increased mitochondrial gene signature: electron transfer flavoprotein subunit beta (ETFB), carnitine palmitoyl transferase 1A (CPT1A), 4-Hydroxyphenylpyruvate Dioxygenase Like (HPDL), and isocitrate Dehydrogenase NAD^+ 3 Catalytic Subunit Alpha (IDH3A) (Jiang et al., 2022). Likewise, patients with mutations in CTE complexes have worse overall survival compared to those without mutations (Silkjaer et al., 2013). Also, a proteomic study on primary AML cells derived from patients in their first relapse shows enrichment of mitochondrial ribosomal proteins (Mitochondrial Ribosomal Protein L21 -MRPL21-, Mitochondrial Ribosomal Protein S33 -MRPS3-), and CTE proteins: Translocase of Inner Mitochondrial Membrane Domain Containing 1 (TIMMDC1), a chaperone protein involved in the assembly of Complex I, and Mitochondrial Import Inner Membrane Translocase subunit (Tim8B TIMM8B), a chaperone that participates in the import and insertion of some transmembrane proteins in the inner mitochondrial membrane (Aasebø et al., 2020). In addition, patients treated with chemotherapy show lasting changes in the expression of genes involved with OxPhos activation, which can be explained because tumor cells, after chemotherapy-induced damage, increase their demand for ATP for repair processes (Vellinga et al., 2015). Therefore, these studies in patients support the idea that enhanced mitochondrial metabolism is associated with a poor prognosis; however, further studies are needed to elucidate the role of mitochondria in chemoresistance in acute leukemia.

4 Relationship between altered energy metabolism and the immune system

Malignant transformation is accompanied by changes in cell metabolism that have an impact on immune system function, reducing the control of cancer cells (O'Sullivan et al., 2019; Patel et al., 2019). These alterations include competition for substrates, the

abundant release of bioactive metabolites, and microenvironmental metabolic remodeling that favors the induction or survival of subsets of tolerogenic cells (Mougiakakos, 2019). Modulation of tumor metabolism can improve immune cell activation, allowing an efficacious antitumor response, which achieves an effective therapeutic approach against ALs.

Increased glycolysis has been associated with inflammatory effector phenotypes in a variety of activated immune cells. In contrast, mitochondrial oxidation programs are associated with memory, suppressor, or wound-healing immune cell phenotypes. Each subset of immune cells has been shown to have distinct metabolic requirements. Thus, although T cells, macrophages, and dendritic cells (DC) each have significant plasticity to engage in other metabolic pathways for energy generation, survival, and proliferation, these changes alter or impair immune function. These alterations in cell function are due to the needs of each immunological subset for specific metabolites, signaling intermediates, or epigenetic modifications mediated by metabolite levels. As metabolic intermediaries change, cell differentiation is not adequately induced, or stress response pathways feedback to restrict or alter the ultimate fate of cells (Andrejeva and Rathmell, 2017).

4.1 Tumor glycolytic metabolism and immune response

The metabolites and waste products excreted by tumor cells (lactate, CO_2, H^+, $NH4^+$, nitric oxide, butyrate, polyamines, and ROS, among others) establish acidification of the microenvironment, that is, compatible with cell proliferation and dissemination, promoting several processes such as decreased cell adhesion, angiogenesis, and mesenchyme-epithelial transition (MET) in other tumor models.

Tumor cells can evade the surveillance of the immune system by secreting lactate. This extracellular metabolite generates acidification of the medium that reduces the pH inside immune cells, affecting various signaling pathways and inhibiting the activation and proliferation of $CD4^+$, $CD8^+$ T cells, NK cells, and DCs. In models of solid tumors, it has been described that the increase in lactate stimulates the polarization of resident macrophages to M2-type macrophages (immunosuppressants), promotes angiogenesis, and stimulates the production of hyaluronic acid by fibroblasts that can contribute to tumor invasion (Hirschhaeuser et al., 2011; Pavlova and Thompson, 2016; de la Cruz-López et al., 2019). It has been described that ROS and HIF can promote a "reverse Warburg effect" in cancer-associated fibroblasts (CAFs), which release lactate through the MCT4 (proton-linked monocarboxylate transporter) receptor, which is captured by tumor cells through MCT1, to be converted to pyruvate and metabolized at the mitochondrial level (Icard et al., 2018). In AML, it has been described that lactate could contribute to the induction of regulatory T lymphocytes and suppressor myeloid cells. (Mougiakakos, 2019). Cancer cells' greed for glucose inactivates effector T cells and DCs, whereas programmed cell death ligand-1 (PD-L1) expressed by tumor cells stimulates glycolysis and the Akt pathway in cancer cells, thereby helping maintain its proliferation (Jayavelu et al., 2022).

4.2 Mitochondrial function and immune response

Mitochondria influence immunosurveillance through intrinsic and extrinsic mechanisms in cancer cells. On the one hand, mitochondria are the source of many danger signals released by dying cancer cells, and these signals are crucial for the DCs activation (Porporato et al., 2018) and tumor-associated macrophages (TAMs) (Icard et al., 2018), as well as the concentrations of succinate and citrate. M1 macrophages, which have a proinflammatory and anticancer role, are dependent on glycolysis and an abnormal TCA cycle that leads to citrate and succinate accumulation. Citrate accumulation increases the production of the main mediators of acute inflammation (nitric oxide, ROS, and prostaglandins), while succinate induces the production of IL-1β, a central molecule in inflammation (Icard et al., 2018).

Furthermore, mitochondrial metabolism is involved in many functions linked to cancer immunity, including (but not limited to) the activation of inflammasomes, the establishment of protective immunological memory, tumor subset differentiation, and macrophage-specific activity (Porporato et al., 2018). Mitochondria serve as sources of molecules that activate inflammatory pathways as well as signaling platforms to propagate these signals (Giampazolias and Tait, 2016).

2-HG has also been implicated in tumor immune evasion. 2-HG transport into T cells is facilitated by the sodium-dependent dicarboxylate transporter (SLC13A3), altering its effector function and cell proliferation. In addition, it interferes with the activation of activated T-cell nuclear factor 1 (NFATC1), a key transcription factor for activated T-cell function, which is linked to ATP deficiency. This oncometabolite also acts at the biochemical level in T cells by inhibiting ornithine decarboxylase, an enzyme that participates in the biosynthesis of polyamines (such as putrescine), molecules necessary for the proper functioning of T cells. This represents a self-perpetuating effect since putrescine can antagonize 2-HG, suppressing cell proliferation. 2-HG has also been shown to inhibit CD12 expression on DC and inhibit CXCL-10 secretion, thus preventing T-cell recruitment. In naive T cells, 2-HG is associated with the destabilization of HIF-1α, preservation of OxPhos, and increased differentiation of $CD4^+$/$CD25^+$/$FOXP3^+$ regulatory T cells. This proceeds at the expense of differentiation into Th17 cells. Finally, 2-HG, through the stimulation of NF-kB, induces cell proliferation in a stromal niche for AML cells and, at relatively low concentrations, promotes fibroblast proliferation (Ježek, 2020).

5 Modulation of energy metabolism and activation of the immune system as targets of natural products

Substantial studies highlight the antineoplastic effect of natural products in addition to their use in the development of new drugs (Newman and Cragg, 2016; Sarwar et al., 2018), suggesting their great potential to become a coadjuvant alternative for the ALs treatment. According to their chemical composition, natural

TABLE 1 Summary of plant-derived extracts or compounds that target tumor metabolism or are proven immunomodulators in acute leukemias.

Extracts or compound	Activity		Mechanism	Model	Reference
	Changes metabolism	Immuno-modulation			
Wheat germ extract	X		Inhibits the enzymes G6PDH and transketolase	Jurkat cell line	Comi-Anduix et al. (2022)
Lipid B	X		CPT1-mediated accumulation within mitochondria and inhibition of fatty acid oxidation	Primary AML cells	Lee et al. (2015)
Berberine		X	Favors a change in the pro-tumor neutrophil phenotype towards an anti-tumor phenotype	HL60 cell line	Zhang et al. (2020)
Chrysophanol		X	Decreased PD-L1	Jurkat cell line	Yin et al. (2020)
Resveratrol		X	Improve T lymphocyte proliferation and NK cell activity	Mouse leukemia model (L1210)	Li et al. (2007)

CPT1, Carnitine palmitoyl transferase 1; G6PDH, Glucose-6-phosphate dehydrogenase; NK, natural killer; PD-L1, Programmed cell death ligand-1.

TABLE 2 Summary of some plant-derived extracts or compounds that target tumor metabolism or are proven immunomodulators in different cancer models.

Extracts or compound	Activity		Mechanism	Model	Reference
	Changes metabolism	Immuno-modulation			
Curcumin	X		Decreases the level and activity of the HK II protein, has little influence on other glycolytic enzymes (PFKP, LDH), and decreases GLUT1	Colon cancer	Vaughan et al. (2013), Wang et al. (2017)
Scutellarein	X		Decreases extracellular acidification rate and oxygen consumption rate	Breast cancer	Chen et al. (2012)
Chrysin	X		Inhibits HK-II binding to VDAC1, resulting in extensive apoptosis	Hepatocelular carcinoma	Xu et al. (2017)
Grape seed extract	X		Target ETC, complex III, deplete levels of glutathione	Head and neck cancer	Shrotriya et al. (2015)
Amorfrutin C	X		mPTP opening, mitochondrial oxygen consumption and extracellular acidification increased	Colorectal adenocarcinoma	Jacobsen et al. (2018)
P2Et	X	X	Decreases ROS, induces immunogenic cell death, depolarizes mitochondria, and increases multifunctional lymphocytes	Breast cancer Melanoma	Gomez-Cadena et al. (2016), Lasso et al. (2018), Prieto et al. (2019), Lasso et al. (2022)
P. nigrum extract	X	X	Decrease in intracellular glucose uptake, increases ROS, increasing the frequency of DC and activated $CD8^+$ T cells and decreases MDSC-LCs and Tregs	Melanoma Breast cancer	Unpublished data
T. usneoides extract	X	X	Decreases intracellular glucose uptake, increases ROS, increases the frequency of DC, and activated $CD8^+$ T lymphocytes, and decreases MDSC-LC and Tregs	Melanoma Breast cancer	Lasso et al. (2022)

DC, dendritic cells; ETC, electron transport chain; GLUT1, Glucose transporter 1; HK-II, Hexokinase-II; LDH, lactate dehydrogenase; MDSC-LCs, Myeloid-derived suppressor-like cells; mPTP, mitochondrial permeability transition pore; PFKP, phosphofructokinase; Tregs, Regulators T cells; VDAC1, Voltage-dependent anion-selective channel 1.

products can be subclassified into: alkaloids, carotenoids, nitrogen-containing compounds, organosulfur compounds, and phenolic compounds, the latter being the group that has the greatest *in vitro* effect on AML cells, perhaps because they are one of the substances more widespread among plants (Hwang et al., 2019).

Currently, there are natural products that have been used in the treatment of ALL and AML, such as vincristine, an alkaloid derived from *Catharanthus roseus*, and etoposide, a semisynthetic derivative of podophyllin obtained from *Podophyllum* (Lucas et al., 2010). In *in vitro* assays, there are various plants that show a cytotoxic effect on AML cells through different mechanisms (Hwang et al., 2019). Interestingly, the potentiation of the antineoplastic effect has been published when natural products and conventional chemotherapeutics are used

in combination. In AML, there is a synergy between Ara-C and resveratrol. The latter can act by inhibiting the CTE complex III, affecting the pool of dNTPs, and reducing the proliferation of leukemic cells (Horvath et al., 2005).

In addition to the role of natural products in PCD, they may also prevent resistance by tumor cells to conventional chemotherapeutics (Yuan et al., 2017), thanks to their intervention in tumor metabolism (Figure 3). Plant-derived components can modulate energy metabolism at both the glycolytic (Hasanpourghadi et al., 2017) and mitochondrial (Tao et al., 2019) levels in different cancer models.

Focusing on the modulation of metabolism, fermented wheat germ extract is a complex mixture of biologically active molecules with an antimetastatic activity that inhibits the enzymes glucose-6-phosphate dehydrogenase (G6PDH) and transketolase, which regulate carbon flux in glycolysis and the pathway of the pentoses in Jurkat line cell (Comi-Anduix et al., 2022). Phenolic phytometabolites such as curcumin, apigenin, resveratrol, or some alkaloids such as alkeberberine or capsaicin target HIF-1, GLUTs, or some enzymes of the glycolytic pathway such as HK-II, PFKP, and PK, among others (Hasanpourghadi et al., 2017). However, in ALs, the role of natural compounds on glycolytic metabolic regulation has been poorly evaluated.

On the other hand, phenolic compounds can act as mitocans through different mechanisms that include inhibition of HK-II, BCL-2, electron transport chain complexes, induction of oxidative stress, voltage-gated anion channel (VDAC)/adenine nucleotide translocase (ANT) complex dysregulation, or as lipophilic cations targeting the inner mitochondrial membrane, some intermediates of the TCA cycle, or mitochondrial DNA (Guerra et al., 2018). One of the widely studied anti-tumor effects of phenolic compounds is the neutralization of ROS because of its integral role in carcinogenesis and mitochondria as its main source. The antioxidant effect is attributed to the modulating capacity of intracellular antioxidant enzymes, direct elimination of ROS by donation of electrons or hydrogens, chelation of transition metals, or induction of antioxidant pathways such as Kelch-like ECH-associated protein 1- Nuclear factor erythroid 2 related factor 2 (Keap1-Nrf2) (Stevens et al., 2018). Interestingly, phenolic compounds can also exert a prooxidant role that depends on the total number of hydroxyl groups and their substitution patterns. The dual effects of some compounds are promising in combination therapies.

An example of the modulation of mitochondrial metabolism in primary AML cells is the action of lipid B extracted from avocado, which can exert a selective cytotoxic effect on leukemic cells. This specificity can be attributed to increased mitochondrial mass and altered mitochondrial metabolism. Lipid B can enter the mitochondria through carnitine palmitoyl transferase I (CPT1), an enzyme that facilitates the transport of mitochondrial lipids, favoring their accumulation and consequently the inhibition of fatty acid oxidation and reduction in NADPH levels, leading to cell death (Lee et al., 2015).

Regarding the immunomodulatory potential of natural products in ALs, in *in vitro* assays, continuous treatment of HL60 cells with DOX induces a differentiation towards type N1 neutrophils (pro-tumor phenotype); however, the addition of berberine, an alkaloid, favors a change towards type N2 neutrophils (anti-tumor phenotype) (Zhang et al., 2020). Also, chrysophanol, one of the most important anthraquinone components isolated from plants of the genus *Rheum*, was proposed as an immunomodulator by Zhong et al. (2022), since they suggested that its antitumor effects against acute leukemia T cells were due to thorough regulation of the immunosuppressive molecule PD-L1 (Yin et al., 2020). In turn, resveratrol improved T lymphocyte proliferation and NK cell activity in a mouse leukemia model (L1210) (Li et al., 2007). Further studies of natural products as immunomodulators in AL could help discover promising compounds against immune checkpoints.

The central research area of our group is the study and development of phytomedicines from Colombian plants, among them Petiveria alliacea (P. alliacea), Caesalpinia spinosa (C. spinosa), Tillandsia usneoides (T. usneoides), and Piper nigrum (P. nigrum) (Lasso et al., 2018; Urueña et al., 2020; Lasso et al., 2022; Urueña et al., 2022). Each one of the extracts of these plants has been characterized from a chemical point of view, and the main compounds have been isolated and studied. The extracts are standardized to be developed as botanical drugs due to their interesting antitumor and immunomodulatory activity in animal models (Lasso et al., 2018; Urueña et al., 2020). C. spinosa has also been studied in normal individuals to assess its safety and in coronavirus disease 2019 (COVID-19) patients, where significant biological activity has been demonstrated (Duran et al., 2022; Urueña et al., 2022).

P. alliacea is a plant used in Central and South America as traditional medicine due to its antispasmodic, antirheumatic, anti-inflammatory, and analgesic activities. Regarding its activity on metabolism, traditional knowledge attributes hypoglycemic properties to it (Fiorentino and Urueña, 2018). We have found cytotoxic activity in tumor cell lines of murine and human origin for melanoma, breast cancer, and acute leukemia (Sandoval et al., 2016; Prieto et al., 2019; Ballesteros-Ramírez et al., 2020b). The proteomic analysis of tumor cells treated with aqueous extract of *P. alliacea* revealed an alteration of proteins that participate in cell proliferation and energy metabolism, as well as a decrease in glucose uptake and lactate production. This suggests that the extract uses multiple biological mechanisms to regulate tumor growth (Hernández et al., 2014). In the *in vivo* model, the extract slows the progression of murine mammary tumors after orthotopic transplantation with 4T1 cells (Hernández et al., 2014).

More recently, it has been observed that the activity of *P. alliacea* extract is specific to tumor cells, inducing a reduction in the expression of the enzyme β-F1-ATPase, the concentration of intracellular ATP, and mitochondrial respiration (Hernández et al., 2017). Like other compounds obtained from plants, *P. alliacea* can act on DCs, inducing their partial activation, which is evidenced by morphological and phenotypic changes, associated with a differential profile of secreted cytokines (Santander et al., 2012). Our group is currently delving into the tumor context of acute leukemias.

On the other hand, in traditional medicine, the seeds and pods of *C. spinosa* are used to treat tonsillitis, gastric ulcers, and skin infections due to their high content of hydrolyzable tannins

(derived from gallic acid) and their antibacterial, antitumor, astringent, anti-inflammatory, and healing properties. They are also known for their high antioxidant capacity (Fiorentino and Urueña, 2018). It is distributed throughout Latin America, and in Colombia, it occurs naturally. The extract obtained from *C. spinosa* was called P2Et. This extract can induce apoptosis through depolarization of mitochondria, activation of caspase 3, chromatin condensation, and decreased clonogenic capacity in K562 leukemia cells and 4T1 breast cancer cells. In addition, when used in combination with DOX at sublethal concentrations, a reduction in IC_{50} is observed, representing an increase in the net antitumor activity of the drug (Castañeda et al., 2012; Urueña et al., 2013). Interestingly, *in vitro*, P2Et is cytotoxic both in resistant lines with the expression of Pgp^+ and in Pgp-lines in 2D and 3D cultures (Sandoval et al., 2016). It has been possible to show that the marked antioxidant activity of *C. spinosa* may participate in the regulation of ROS production inside and outside the tumor mass in some cancer models, which would confer great antitumor potential (Prieto et al., 2019). An immunomodulatory effect has been attributed to P2Et since it can induce the expression of immunogenic cell death markers such as calreticulin and High Mobility Group-Box superfamily 1 (HMGB1) and the release of ATP. In the *in vivo* model, mice transplanted with 4T1 cells treated *in vitro* with P2Et showed reduced tumor growth, and *ex vivo* analysis revealed multifunctional $CD4^+$ and $CD8^+$ T lymphocytes (Urueña et al., 2013; Gomez-Cadena et al., 2016).

Focusing on ALs, cells isolated from patients with ALL or AML have been shown to be less sensitive to P2Et and more sensitive to *P. alliacea*. In addition, the treatment of leukemic blasts with each of the two extracts combined with some drugs increases the sensitivity to death even in tumor cells that, in some cases, do not respond to conventional therapies. These data show that, at least *in vitro*, the extracts of *P. alliacea* and *C. spinosa* are capable of acting on human primary tumors, improving the response to chemotherapy (Ballesteros-Ramírez et al., 2020b).

Other plants with emerging anti-leukemic activity in our group are the extracts of T. usneoides and P. nigrum. In a mouse model transplanted with DA-3/ER-GM murine acute myeloid leukemia cells, both P2Et and T. usneoides-derived extracts were found to decrease the tumor load in peripheral blood with respect to the control group (unpublished data). Furthermore, in the 4T1 murine breast cancer model, extracts derived from *T. usneoides* and *P. nigrum* modulate the immune response by increasing the frequency of DC and activated $CD8^+$ T cells and decreasing myeloid-derived suppressor-like cells (MDSC-LCs) and regulators T cells (Tregs) in the tumor microenvironment, thus favoring control of tumor growth (Lasso et al., 2022). At the metabolic level, *T. usneoides* and *P. nigrum* extracts behave as prooxidants in both B16-F10 melanoma cells and 4T1 breast cancer cells (Lasso et al., 2022). Regarding glucose consumption, *T. usneoides* does not induce significant changes in glucose uptake in 4T1 cells; however, it induces an evident increase at 12 h in B16-F10 cells (Lasso et al., 2022). *P. nigrum* induces a dose-dependent decrease in intracellular glucose uptake, in contrast to a small increase in intracellular glucose uptake in B16-F10 cells (unpublished data). The mechanisms related to the intrinsic sensitivity of the different tumor cells to each of these extracts could be related to differences in their metabolic plasticity, so immunomodulation and involvement in metabolic changes are being studied in the acute leukemia model. Some extracts or isolated compounds derived from plants with the capacity to induce metabolic changes and/or with immunomodulatory potential evaluated in leukemias are summarized in Table 1 and in other tumor models in Table 2.

6 Conclusion

Both an increase in glycolytic activity and mitochondrial changes may underlie tumor cell resistance to many types of drugs. Although mechanistic evidence has been mainly in tumor cell lines, there is evidence of increased glycolytic metabolism in patients with ALs related to poor response to treatment. However, Recent *in vivo* and systemic studies in cancer patients support the notion that mitochondria, through their role in metabolic adaptation, also play a pivotal role in chemoresistance in ALs rather than the glycolytic phenotype. These findings suggest that both ways can be implicated, and possibly other factors such as population differences (genetics, lifestyle, microbiome nutrition, co-infections, oncogenic mutations, etc.) could influence this modulation and resistance to chemotherapy. Therapeutic intervention using extracts derived from plants developed as botanical medicines to induce metabolic changes by altering glycolysis or mitochondrial function in resistant leukemic cells can sensitize the tumor cell, potentiating the action of conventional chemotherapeutics and resulting in an immunomodulatory effect that allows the activation of an antitumor immune response.

Author contributions

CA, SQ, and SF gave the idea and drafted the manuscript. CA performed the literature search and drafted figures. CA, NC-R, SQ, and SF edited the manuscript and supervised the whole study. All authors contributed to the article and approved the submitted version.

Funding

Ministerio de Ciencia, Tecnología e Innovación (Colciencias), Ministerio de Educación Nacional, Ministerio de Industria, Comercio y Turismo e ICETEX (792–2017 2a Convocatoria Ecosistema Científico—Colombia Científica para la Financiación de Proyectos de I + D + i), and Vicerrectoría de Investigaciones, Pontificia Universidad Javeriana, Bogotá D.C., Colombia (Contract no. FP44842-221-2018).

Acknowledgments

The authors would like to thank Pontificia Universidad Javeriana, the Grupo de Inmunobiología y Biología Celular, Bogotá D.C., Colombia, and the Programa de Colombia Científica (GAT), contract no. FP44842-221-2018.

Conflict of interest

The authors declare that the research was conducted in the absence of any commercial or financial relationships that could be construed as a potential conflict of interest.

Publisher's note

All claims expressed in this article are solely those of the authors and do not necessarily represent those of their affiliated organizations, or those of the publisher, the editors and the reviewers. Any product that may be evaluated in this article, or claim that may be made by its manufacturer, is not guaranteed or endorsed by the publisher.

Supplementary material

The Supplementary Material for this article can be found online at: https://www.frontiersin.org/articles/10.3389/fmolb.2023.1229760/full#supplementary-material

References

Aasebø, E., Berven, F. S., Hovland, R., Døskeland, S. O., Øystein, B., Selheim, F., et al. (2020). The progression of acute myeloid leukemia from first diagnosis to chemoresistant relapse: A comparison of proteomic and phosphoproteomic profiles. *Cancers (Basel)* 12 (6), 1466. doi:10.3390/cancers12061466

Agbu, P., and Carthew, R. W. (2021). MicroRNA-mediated regulation of glucose and lipid metabolism. *Nat. Rev. Mol. Cell Biol.* 22 (6), 425–438. doi:10.1038/s41580-021-00354-w

Altaf, E., Huang, X., Xiong, J., Yang, X., Deng, X., Xiong, M., et al. (2017). NHE1 has a notable role in metastasis and drug resistance of T-cell acute lymphoblastic leukemia. *Oncol. Lett.* 14 (4), 4256–4262. doi:10.3892/ol.2017.6716

Andrejeva, G., and Rathmell, J. C. (2017). Similarities and distinctions of cancer and immune metabolism in inflammation and tumors. *Cell Metab.* 26 (1), 49–70. doi:10.1016/j.cmet.2017.06.004

Arber, D., Orazi, A., Hasserjian, R., Thiele, J., Borowitz, M., Le Beau, M., et al. (2016). The 2016 revision to the World Health Organization classification of myeloid neoplasms and acute leukemia. *Blood* 127 (20), 2391–2405. doi:10.1182/blood-2016-03-643544

Ariës, I. M., Hansen, B. R., Koch, T., Van Den Dungen, R., Evans, W. E., Pieters, R., et al. (2013). The synergism of MCL1 and glycolysis on pediatric acute lymphoblastic leukemia cell survival and prednisolone resistance. *Haematologica* 98 (12), 1905–1911. doi:10.3324/haematol.2013.093823

Auberger, P., and Puissant, A. (2017). Autophagy, a key mechanism of oncogenesis and resistance in leukemia. *Blood* 129 (5), 547–552. doi:10.1182/blood-2016-07-692707

Ballesteros-Ramírez, R., Aldana, E., Herrera, M. V., Urueña, C., Rojas, L. Y., Echeverri, L. F., et al. (2020b). Preferential activity of *Petiveria alliacea* extract on primary myeloid leukemic blast. *Evid. Based Complement. Altern. Med.* 2020, 4736206. doi:10.1155/2020/4736206

Ballesteros-Ramírez, R., Quijano, S., Solano, J., Ordoñez-Reyes, C., Herrera, M. V., Murillo, R., et al. (2020a). Influence of dose intensity in consolidation with HIDAC and other clinical and biological parameters in the survival of AML. *J. Cancer Epidemiol.* 2020, 8021095. doi:10.1155/2020/8021095

Basak, N. P., and Banerjee, S. (2015). Mitochondrial dependency in progression of acute myeloid leukemia. *Mitochondrion* 21, 41–48. doi:10.1016/j.mito.2015.01.006

Bokil, A., and Sancho, P. (2019). Mitochondrial determinants of chemoresistance. *Cancer Drug Resist* 2 (3), 634–646. doi:10.20517/cdr.2019.46

Boutin, L., Arnautou, P., Trignol, A., Ségot, A., Farge, T., Desterke, C., et al. (2020). Mesenchymal stromal cells confer chemoresistance to myeloid leukemia blasts through Side Population functionality and ABC transporter activation. *Haematologica* 105 (4), 987–9998. doi:10.3324/haematol.2018.214379

Braun, M., Qorraj, M., Büttner, M., Klein, F. A., Saul, D., Aigner, M., et al. (2016). CXCL12 promotes glycolytic reprogramming in acute myeloid leukemia cells via the CXCR4/mTOR axis. *Leukemia* 30 (8), 1788–1792. doi:10.1038/leu.2016.58

Cardano, M., Tribioli, C., and Prosperi, E. (2020). Targeting proliferating cell nuclear antigen (PCNA) as an effective strategy to inhibit tumor cell proliferation. *Curr. Cancer Drug Targets* 20 (4), 240–252. doi:10.2174/1568009620666200115162814

Castañeda, D. M., Pombo, L. M., Urueña, C. P., Hernandez, J. F., and Fiorentino, S. (2012). A gallotannin-rich fraction from *Caesalpinia spinosa* (Molina) Kuntze displays cytotoxic activity and raises sensitivity to doxorubicin in a leukemia cell line. *BMC Complement. Altern. Med.* 12, 38. doi:10.1186/1472-6882-12-38

Chalkiadaki, A., and Guarente, L. (2015). The multifaceted functions of sirtuins in cancer. *Nat. Rev. Cancer* 15 (10), 608–624. doi:10.1038/nrc3985

Chen, C., Hao, X., Lai, X., Liu, L., Zhu, J., Shao, H., et al. (2021). Oxidative phosphorylation enhances the leukemogenic capacity and resistance to chemotherapy of B cell acute lymphoblastic leukemia. *Sci. Adv.* 7 (11), eabd6280. doi:10.1126/sciadv.abd6280

Chen, L., Hu, N., Wang, C., and Zhao, H. (2020). HOTAIRM1 knockdown enhances cytarabine-induced cytotoxicity by suppression of glycolysis through the Wnt/β-catenin/PFKP pathway in acute myeloid leukemia cells. *Arch. Biochem. Biophys.* 680, 108244. doi:10.1016/j.abb.2019.108244

Chen, L., Zhao, H., Wang, C., and Hu, N. (2019a). TUG1 knockdown enhances adriamycin cytotoxicity by inhibiting glycolysis in adriamycin-resistant acute myeloid leukemia HL60/ADR cells. *RSC Adv.* 9 (19), 10897–10904. doi:10.1039/c9ra00306a

Chen, V., Staub, R. E., Baggett, S., Chimmani, R., Tagliaferri, M., Cohen, I., et al. (2012). Identification and analysis of the active phytochemicals from the anti-cancer botanical extract Bezielle. *PLoS One* 7 (1), e30107. doi:10.1371/journal.pone.0030107

Chen, W. L., Wang, J. H., Zhao, A. H., Xu, X., Wang, Y. H., Chen, T. L., et al. (2014). A distinct glucose metabolism signature of acute myeloid leukemia with prognostic value. *Blood* 124 (10), 1645–1654. doi:10.1182/blood-2014-02-554204

Chen, X., Glytsou, C., Zhou, H., Narang, S., Reyna, D. E., Lopez, A., et al. (2019b). Targeting mitochondrial structure sensitizes acute myeloid leukemia to venetoclax treatment. *Cancer Discov.* 9 (7), 890–909. doi:10.1158/2159-8290.CD-19-0117

Cho, S. H., Ahn, A. K., Bhargava, P., Lee, C-H., Eischen, C. M., Mcguinness, O., et al. (2011). Glycolytic rate and lymphomagenesis depend on PARP14, an ADP ribosyltransferase of the B aggressive lymphoma (BAL) family. *Proc. Natl. Acad. Sci. U. S. A.* 108 (38), 15972–15977. doi:10.1073/pnas.1017082108

Combariza, J. F., Casas, C. P., Rodríguez, M., Cardona, A. F., Ospina, É., and Grajales, M. (2007). Supervivencia en adultos con leucemia linfoide aguda de novo tratados con el esquema HyperCVAD en el Instituto Nacional de Cancerología (Colombia), entre enero de 2001 y junio de 2005. *Rev. Colomb. Cancerol.* 11, 92–100.

Comi-Anduix, B., Boros, L. G., Marin, S., Boren, J., Callol-Massot, C., Centelles, J. J., et al. (2022). Fermented wheat germ extract inhibits glycolysis/pentose cycle enzymes and induces apoptosis through poly(ADP-ribose) polymerase activation in Jurkat T-cell leukemia tumor cells. *J. Biol. Chem.* 277 (48), 46408. doi:10.1074/jbc.M206150200

de la Cruz-López, K. G., Castro-Muñoz, L. J., Reyes-Hernández, D. O., García-Carrancá, A., and Manzo-Merino, J. (2019). Lactate in the regulation of tumor microenvironment and therapeutic approaches. *Front. Oncol.* 9, 1143. doi:10.3389/fonc.2019.01143

DeBerardinis, R. J., and Chandel, N. S. (2016). Fundamentals of cancer metabolism. *Sci. Adv.* 2 (5), e1600200. doi:10.1126/sciadv.1600200

Decker, C. W., Garcia, J., Gatchalian, K., Arceneaux, D., Choi, C., Han, D., et al. (2020). Mitofusin-2 mediates doxorubicin sensitivity and acute resistance in Jurkat leukemia cells. *Biochem. Biophys. Rep.* 24, 100824. doi:10.1016/j.bbrep.2020.100824

Desbats, M. A., Giacomini, I., Prayer-Galetti, T., and Montopoli, M. (2020). Metabolic plasticity in chemotherapy resistance. *Front. Oncol.* 10, 281. doi:10.3389/fonc.2020.00281

Di Martino, L., Tosello, V., Peroni, E., and Piovan, E. (2021). Insights on metabolic reprogramming and its therapeutic potential in acute leukemia. *Int. J. Mol. Sci.* 22 (16), 8738. doi:10.3390/ijms22168738

Duan, Z., Chen, Y., Ye, M., Xiao, L., Chen, Y., Cao, Y., et al. (2022). Differentiation and prognostic stratification of acute myeloid leukemia by serum-based spectroscopy coupling with metabolic fingerprints. *FASEB J.* 36 (7), e22416. doi:10.1096/fj.202200487R

Duran, M. I., Ballesteros-Ramírez, R., Tellez, A., Torregrosa, L., Olejua, P. A., Galvis, S., et al. (2022). Safety evaluation in healthy Colombian volunteers of P2Et extract obtained from *Caesalpinia spinosa*: Design 3+3 phase I clinical trial. *Evid. Based Complement. Altern. Med.* 2022, 7943001. doi:10.1155/2022/7943001

Farge, T., Saland, E., de Toni, F., Aroua, N., Hosseini, M., Perry, R., et al. (2017). Chemotherapy-resistant human acute myeloid leukemia cells are not enriched for leukemic stem cells but require oxidative metabolism. *Cancer Discov.* 7 (7), 716–735. doi:10.1158/2159-8290.CD-16-0441

Fiorentino, S., and Urueña, C. (2018). La fitoterapia como fuente de medicamentos reguladores del metabolismo tumoral y activadores de la respuesta inmunitaria. *Rev. Acad. Colomb. Cienc. Exact. Fis. Nat.* 42 (163), 132. doi:10.18257/raccefyn.542

Frolova, O., Samudio, I., Benito, J. M., Jacamo, R., Kornblau, S. M., Markovic, A., et al. (2012). Regulation of HIF-1α signaling and chemoresistance in acute lymphocytic leukemia under hypoxic conditions of the bone marrow microenvironment. *Cancer Biol. Ther.* 13 (10), 858–870. doi:10.4161/cbt.20838

Genovese, I., Carinci, M., Modesti, L., Aguiari, G., Pinton, P., and Giorgi, C. (2021). Mitochondria: Insights into crucial features to overcome cancer chemoresistance. *Int. J. Mol. Sci.* 22 (9), 4770. doi:10.3390/ijms22094770

Giampazolias, E., and Tait, S. W. G. (2016). Mitochondria and the hallmarks of cancer. *FEBS J.* 283 (5), 803–814. doi:10.1111/febs.13603

Giansanti, M., De Gabrieli, A., Prete, S. P., Ottone, T., Divona, M. D., Karimi, T., et al. (2021). Poly(ADP-Ribose) polymerase inhibitors for arsenic trioxide–resistant acute promyelocytic leukemia: Synergistic *in vitro* antitumor effects with hypomethylating agents or high-dose vitamin C. *J. Pharmacol. Exp. Ther.* 377 (3), 385–397. doi:10.1124/jpet.121.000537

Gomez-Cadena, A., Uruenã, C., Prieto, K., Martinez-Usatorre, A., Donda, A., Barreto, A., et al. (2016). Immune-system-dependent anti-tumor activity of a plant-derived polyphenol rich fraction in a melanoma mouse model. *Cell Death Dis.* 7 (6), e2243. doi:10.1038/cddis.2016.134

Grasso, D., Zampieri, L., Capelôa, T., Van de Velde, J., and Sonveaux, P. (2020). Mitochondria in cancer. *Cell Stress* 4 (6), 114–146. doi:10.15698/cst2020.06.221

Griffioen, M. S., De Leeuw, D. C., Janssen, J. J. W. M., and Smit, L. (2022). Targeting acute myeloid leukemia with venetoclax; biomarkers for sensitivity and rationale for venetoclax-based combination therapies. *Cancers (Basel).* 14 (14), 3456. doi:10.3390/cancers14143456

Grønningsæter, I. S., Fredly, H. K., Gjertsen, B. T., Hatfield, K. J., and Øystein, B. (2019). Systemic metabolomic profiling of acute myeloid leukemia patients before and during disease-stabilizing treatment based on all-trans retinoic acid, valproic acid, and low-dose chemotherapy. *Cells* 8 (10), 1229. doi:10.3390/cells8101229

Gu, L., Yi, Z., Zhang, Y., Ma, Z., Zhu, Y., and Gao, J. (2017). Low dose of 2-deoxy-D-glucose kills acute lymphoblastic leukemia cells and reverses glucocorticoid resistance via N-linked glycosylation inhibition under normoxia. *Oncotarget* 8 (19), 30978–30991. doi:10.18632/oncotarget.16046

Guerra, A. R., Duarte, M. F., and Duarte, I. F. (2018). Targeting tumor metabolism with plant-derived natural products: Emerging trends in cancer therapy. *J. Agric. Food Chem.* 66 (41), 10663–10685. doi:10.1021/acs.jafc.8b04104

Guerra, F., Arbini, A. A., and Moro, L. (2017). Mitochondria and cancer chemoresistance. *Biochim. Biophys. Acta Bioenerg.* 1858 (8), 686–699. doi:10.1016/j.bbabio.2017.01.012

Hackl, H., Astanina, K., and Wieser, R. (2017). Molecular and genetic alterations associated with therapy resistance and relapse of acute myeloid leukemia. *J. Hematol. Oncol.* 10 (1), 51. doi:10.1186/s13045-017-0416-0

Hasanpourghadi, M., Yeng Looi, C., Kumar Pandurangan, A., Sethi, G., Fen Wong, W., and Rais Mustafa, M. (2017). Phytometabolites targeting the Warburg effect in cancer cells: A mechanistic review. *Curr. Drug Targets* 18 (9), 1086–1094. doi:10.2174/1389450117666160401124842

He, Z., Zhang, S., Ma, D., Fang, Q., Yang, L., Shen, S., et al. (2019). HO-1 promotes resistance to an EZH2 inhibitor through the pRB-E2F pathway: Correlation with the progression of myelodysplastic syndrome into acute myeloid leukemia. *J. Transl. Med.* 17 (1), 366. doi:10.1186/s12967-019-2115-9

Henkenius, K., Greene, B. H., Barckhausen, C., Hartmann, R., Märken, M., Kaiser, T., et al. (2017). Maintenance of cellular respiration indicates drug resistance in acute myeloid leukemia. *Leuk. Res.* 62, 56–63. doi:10.1016/j.leukres.2017.09.021

Hernández, J. F., Urueña, C. P., Cifuentes, M. C., Sandoval, T. A., Pombo, L. M., Castañeda, D., et al. (2014). A *Petiveria alliacea* standardized fraction induces breast adenocarcinoma cell death by modulating glycolytic metabolism. *J. Ethnopharmacol.* 153 (3), 641–649. doi:10.1016/j.jep.2014.03.013

Hernández, J. F., Urueña, C. P., Sandoval, T. A., Cifuentes, M. C., Formentini, L., Cuezva, J. M., et al. (2017). A cytotoxic *Petiveria alliacea* dry extract induces ATP depletion and decreases β-F1-ATPase expression in breast cancer cells and promotes survival in tumor-bearing mice. *Braz. J. Pharmacogn.* 27 (3), 306–314. doi:10.1016/j.bjp.2016.09.008

Herranz-López, M., Losada-Echeberría, M., and Barrajón-Catalán, E. (2018). The multitarget activity of natural extracts on cancer: Synergy and xenohormesis. *Med. (Basel)* 6 (1), 6. doi:10.3390/medicines6010006

Herst, P. M., Howman, R. A., Neeson, P. J., Berridge, M. V., and Ritchie, D. S. (2011). The level of glycolytic metabolism in acute myeloid leukemia blasts at diagnosis is prognostic for clinical outcome. *J. Leukoc. Biol.* 89 (1), 51–55. doi:10.1189/jlb.0710417

Hirschhaeuser, F., Sattler, U. G. A., and Mueller-Klieser, W. (2011). Lactate: A metabolic key player in cancer. *Cancer Res.* 71 (22), 6921–6925. doi:10.1158/0008-5472.CAN-11-1457

Horvath, Z., Saiko, P., Illmer, C., Madlener, S., Hoechtl, T., Bauer, W., et al. (2005). Synergistic action of resveratrol, an ingredient of wine, with Ara-C and tiazofurin in HL-60 human promyelocytic leukemia cells. *Exp. Hematol.* 33 (3), 329–335. doi:10.1016/j.exphem.2004.11.009

Hoxhaj, G., and Manning, B. D. (2020). The PI3K–AKT network at the interface of oncogenic signalling and cancer metabolism. *Nat. Rev. Cancer* 20 (2), 74–88. doi:10.1038/s41568-019-0216-7

Hulleman, E., Kazemier, K. M., Holleman, A., VanderWeele, D. J., Rudin, C. M., Broekhuis, M. J., et al. (2009). Inhibition of glycolysis modulates prednisolone resistance in acute lymphoblastic leukemia cells. *Blood* 113 (9), 2014–2021. doi:10.1182/blood-2008-05-157842

Hwang, D., Kim, M., Park, H., Jeong, M. I., Jung, W., and Kim, B. (2019). Natural products and acute myeloid leukemia: A review highlighting mechanisms of action. *Nutrients* 11 (5), 1010. doi:10.3390/nu11051010

Iansante, V., Choy, P. M., Fung, S. W., Liu, Y., Chai, J-G., Dyson, J., et al. (2015). PARP14 promotes the Warburg effect in hepatocellular carcinoma by inhibiting JNK1-dependent PKM2 phosphorylation and activation. *Nat. Commun.* 6, 7882. doi:10.1038/ncomms8882

Icard, P. S., Shulman, S., Farhat, D., Steyaert, J. M., Alifano, M., and Lincet, H. (2018). How the Warburg effect supports aggressiveness and drug resistance of cancer cells? *Drug Resist Updat* 38, 1–11. doi:10.1016/j.drup.2018.03.001

Jacobsen, K. M., Villadsen, N. L., Torring, T., Nielsen, C. B., Salomon, T., Nielsen, M. M., et al. (2018). APD-containing cyclolipodepsipeptides target mitochondrial function in hypoxic cancer cells. *Cell Chem. Biol.* 25, 1337–1349.e12. doi:10.1016/j.chembiol.2018.07.010

Jain, A., Katiyar, A., Singh, R., Bakhshi, S., Singh, H., Palanichamy, J. K., et al. (2022). Implications of mitochondrial DNA variants in pediatric B-cell acute lymphoblastic leukemia. *Egypt J. Med. Hum. Genet.* 23 (1), 133. doi:10.1186/s43042-022-00347-0

Jaiswal, A., Xudong, Z., Zhenyu, J., and Saretzki, G. (2022). Mitochondrial sirtuins in stem cells and cancer. *FEBS J.* 289 (12), 3393–3415. doi:10.1111/febs.15879

Jayavelu, A. K., Wolf, S., Buettner, F., Alexe, G., Häupl, B., Comoglio, F., et al. (2022). The proteogenomic subtypes of acute myeloid leukemia. *Cancer Cell* 40 (3), 301–317.e12. doi:10.1016/j.ccell.2022.02.006

Ježek, P. (2020). 2-Hydroxyglutarate in cancer cells. *Antioxid. Redox Signal* 33 (13), 903–926. doi:10.1089/ars.2019.7902

Jhas, B., Sriskanthadevan, S., Skrtic, M., Sukhai, M. A., Voisin, V., Jitkova, Y., et al. (2013). Metabolic adaptation to chronic inhibition of mitochondrial protein synthesis in acute myeloid leukemia cells. *PLoS One* 8 (3), e58367. doi:10.1371/journal.pone.0058367

Jiang, N., Zhang, X., Chen, Q., Kantawong, F., Wan, S., Liu, J., et al. (2022). Identification of a mitochondria-related gene signature to predict the prognosis in AML. *Front. Oncol.* 12, 823831. doi:10.3389/fonc.2022.823831

Jiang, Y., and Nakada, D. (2016). Cell intrinsic and extrinsic regulation of leukemia cell metabolism. *Int. J. Hematol.* 103 (6), 607–616. doi:10.1007/s12185-016-1958-6

Kim, H. K., Son, S. Y., Oh, J. S., Song, Y. N., Byun, J. M., Koh, Y., et al. (2021). Metabolic profiling during acute myeloid leukemia progression using paired clinical bone marrow serum samples. *Metabolites* 11 (9), 586. doi:10.3390/metabo11090586

Kominsky, D. J., Klawitter, J., Brown, J. L., Boros, L. G., Melo, J. V., Eckhardt, S. G., et al. (2009). Abnormalities in glucose uptake and metabolism in imatinib-resistant human BCR-ABL-positive cells. *Clin. Cancer Res.* 15 (10), 3442–3450. doi:10.1158/1078-0432.CCR-08-3291

Kumar, A., and Jaitak, V. (2019). Natural products as multidrug resistance modulators in cancer. *Eur. J. Med. Chem.* 176, 268–291. doi:10.1016/j.ejmech.2019.05.027

Lagadinou, E. D., Sach, A., Callahan, K., Rossi, R. M., Neering, S. J., Minhajuddin, M., et al. (2013). BCL-2 inhibition targets oxidative phosphorylation and selectively eradicates quiescent human leukemia stem cells. *Cell Stem Cell* 12 (3), 329–341. doi:10.1016/j.stem.2012.12.013

Lasso, P., Gomez-Cadena, A., Urueña, C., Donda, A., Martinez-Usatorre, A., Barreto, A., et al. (2018). Prophylactic vs. therapeutic treatment with P2Et polyphenol-rich extract has opposite effects on tumor growth. *Front. Oncol.* 8, 356. doi:10.3389/fonc.2018.00356

Lasso, P., Rojas, L., Arévalo, C., Urueña, C., Murillo, N., Barreto, A., et al. (2022). *Tillandsia usneoides* extract decreases the primary tumor in a murine breast cancer model but not in melanoma. *Cancers (Basel)* 14 (21), 5383. doi:10.3390/cancers14215383

Lee, E. A., Angka, L., Rota, S. G., Hanlon, T., Mitchell, A., Hurren, R., et al. (2015). Targeting mitochondria with avocatin B induces selective leukemia cell death. *Cancer Res.* 75 (12), 2478–2488. doi:10.1158/0008-5472.CAN-14-2676

Li, S., Chen, L., Jin, W., Ma, X., Ma, Y., Dong, F., et al. (2017). Influence of body mass index on incidence and prognosis of acute myeloid leukemia and acute promyelocytic leukemia: A meta-analysis. *Sci. Rep.* 7 (1), 17998. doi:10.1038/s41598-017-18278-x

Li, T., Fan, G. X., Wang, W., Li, T., and Yuan, Y. K. (2007). Resveratrol induces apoptosis, influences IL-6 and exerts immunomodulatory effect on mouse lymphocytic leukemia both *in vitro* and *in vivo*. *Int. Immunopharmacol.* 7 (9), 1221–1231. doi:10.1016/j.intimp.2007.05.008

Liu, C. J., Jin, Y., and Fan, Z. (2021). The mechanism of Warburg effect-induced chemoresistance in cancer. *Front. Oncol.* 11, 698023. doi:10.3389/fonc.2021.698023

Liu, S. M., Chen, W., and Wang, J. (2014). Distinguishing between cancer cell differentiation and resistance induced by all-trans retinoic acid using transcriptional profiles and functional pathway analysis. *Sci. Rep.* 4, 5577. doi:10.1038/srep05577

Lo Presti, C., Fauvelle, F., Mondet, J., and Mossuz, P. (2020). The differential activation of metabolic pathways in leukemic cells depending on their genotype and micro-environmental stress. *Metabolomics* 16 (1), 13. doi:10.1007/s11306-020-1633-z

Lucas, D. M., Still, P. C., Bueno Perez, L., Grever, M. R., and Douglas Kinghorn, A. (2010). Potential of plant-derived natural products in the treatment of leukemia and lymphoma. *Curr. Drug Targets* 11 (7), 812–822. doi:10.2174/138945010791320809

Luppi, M., Fabbiano, F., Visani, G., Martinelli, G., and Venditti, A. (2018). Novel agents for acute myeloid leukemia. *Cancers (Basel)* 10 (11), 429. doi:10.3390/cancers10110429

Ma, J., Liu, B., Yu, D., Zuo, Y., Cai, R., Yang, J., et al. (2019). SIRT3 deacetylase activity confers chemoresistance in AML via regulation of mitochondrial oxidative phosphorylation. *Br. J. Haematol.* 187 (1), 49–64. doi:10.1111/bjh.16044

Man, C. L., Sun, S. S., Chow, M. K., Gill, H. C., Kwong, H., Leung, Y. L. A. Y., et al. (2014). A novel tescalcin-sodium/hydrogen exchange axis underlying sorafenib resistance in FLT3-ITD+ AML. *Blood* 123 (16), 2530–2539. doi:10.1182/blood-2013-07-512194

Marcucci, F. R., and Cristiano, R. (2021). Glycolysis-induced drug resistance in tumors-A response to danger signals? *Neoplasia* 23 (2), 234–245. doi:10.1016/j.neo.2020.12.009

Marin, J. J. G., Briz, O., Rodríguez-Macias, G., Díez-Martín, J. L., and Macias, R. I. R. (2016). Role of drug transport and metabolism in the chemoresistance of acute myeloid leukemia. *Blood Rev.* 30 (1), 55–64. doi:10.1016/j.blre.2015.08.001

Mattes, K., Vellenga, E., and Schepers, H. (2019). Differential redox-regulation and mitochondrial dynamics in normal and leukemic hematopoietic stem cells: A potential window for leukemia therapy. *Crit. Rev. Oncol./Hematol.* 144, 102814. doi:10.1016/j.critrevonc.2019.102814

Moschoi, R., Imbert, V., Nebout, M., Chiche, J., Mary, D., Prebet, T., et al. (2016). Protective mitochondrial transfer from bone marrow stromal cells to acute myeloid leukemic cells during chemotherapy. *Blood* 128 (2), 253–264. doi:10.1182/blood-2015-07-655860

Mougiakakos, D. (2019). The induction of a permissive environment to promote T cell immune evasion in acute myeloid leukemia: The metabolic perspective. *Front. Oncol.* 9, 1166. doi:10.3389/fonc.2019.01166

Nepstad, I., Hatfield, K. J., Grønningsæter, I. S., and Reikvam, H. (2020). The PI3K-Akt-mTOR signaling pathway in human acute myeloid leukemia (AML) cells. *Int. J. Mol. Sci.* 21 (8), 2907. doi:10.3390/ijms21082907

Newman, D. J., and Cragg, G. M. (2016). Natural products as sources of new drugs from 1981 to 2014. *J. Nat. Prod.* 79 (3), 629–661. doi:10.1021/acs.jnatprod.5b01055

Ohayon, D., De Chiara, A., Chapuis, N., Candalh, C., Mocek, J., Ribeil, J. A., et al. (2016). Cytoplasmic proliferating cell nuclear antigen connects glycolysis and cell survival in acute myeloid leukemia. *Sci. Rep.* 6, 35561. doi:10.1038/srep35561

Okamoto, S., Miyano, K., Kitakaze, K., Kato, H., Yamauchi, A., Kajikawa, M., et al. (2022). Coculture *in vitro* with endothelial cells induces cytarabine resistance of acute myeloid leukemia cells in a VEGF-A/VEGFR-2 signaling-independent manner. *Biochem. Biophys. Res. Commun.* 587, 78–84. doi:10.1016/j.bbrc.2021.11.090

O'Sullivan, D., Sanin, D. E., Pearce, E. J., and Pearce, E. L. (2019). Metabolic interventions in the immune response to cancer. *Nat. Rev. Immunol.* 19 (5), 324–335. doi:10.1038/s41577-019-0140-9

Panina, S. B., Baran, N., Brasil da Costa, F. H., Konopleva, M., and Kirienko, N. V. (2019). A mechanism for increased sensitivity of acute myeloid leukemia to mitotoxic drugs. *Cell Death Dis.* 10 (8), 617. doi:10.1038/s41419-019-1851-3

Panina, S. B., Pei, J., Baran, N., Konopleva, M., and Kirienko, N. V. (2020). Utilizing synergistic potential of mitochondria-targeting drugs for leukemia therapy. *Front. Oncol.* 10, 435. doi:10.3389/fonc.2020.00435

Patel, C. H., Leone, R. D., Horton, M. R., and Powell, J. D. (2019). Targeting metabolism to regulate immune responses in autoimmunity and cancer. *Nat. Rev. Drug Discov.* 18 (9), 669–688. doi:10.1038/s41573-019-0032-5

Pavlova, N. N., and Thompson, C. B. (2016). The emerging hallmarks of cancer metabolism. *Cell Metab.* 23 (1), 27–47. doi:10.1016/j.cmet.2015.12.006

Polak, R., de Rooij, B., Pieters, R., and den Boer, M. L. (2015). B-cell precursor acute lymphoblastic leukemia cells use tunneling nanotubes to orchestrate their microenvironment. *Blood* 126 (21), 2404–2414. doi:10.1182/blood-2015-03-634238

Porporato, P. E., Filigheddu, N., Pedro, J. M. B. S., Kroemer, G., and Galluzzi, L. (2018). Mitochondrial metabolism and cancer. *Cell Res.* 28 (3), 265–280. doi:10.1038/cr.2017.155

Prieto, K., Cao, Y., Mohamed, E., Trillo-Tinoco, J., Sierra, R. A., Urueña, C., et al. (2019). Polyphenol-rich extract induces apoptosis with immunogenic markers in melanoma cells through the ER stress-associated kinase PERK. *Cell Death Discov.* 5, 134. doi:10.1038/s41420-019-0214-2

Raimondi, V., Ciotti, G., Gottardi, M., and Ciccarese, F. (2022). 2-Hydroxyglutarate in acute myeloid leukemia: A journey from pathogenesis to therapies. *Biomedicines* 10 (6), 1359. doi:10.3390/biomedicines10061359

Ryu, M. J., Han, J., Kim, S. J., Lee, M. J., Ju, X., Lee, Y. L., et al. (2019). PTEN/AKT signaling mediates chemoresistance in refractory acute myeloid leukemia through enhanced glycolysis. *Oncol. Rep.* 42 (5), 2149–2158. doi:10.3892/or.2019.7308

Saito, K., Zhang, Q., Yang, H., Yamatani, K., Ai, T., Ruvolo, V., et al. (2021). Exogenous mitochondrial transfer and endogenous mitochondrial fission facilitate AML resistance to OxPhos inhibition. *Blood Adv.* 5 (20), 4233–4255. doi:10.1182/bloodadvances.2020003661

Saliba, A. N., John, A., and Kaufmann, S. H. (2021). Resistance to venetoclax and hypomethylating agents in acute myeloid leukemia. *Cancer Drug Resist* 4 (1), 125–142. doi:10.20517/cdr.2020.95

Sandoval, T. A., Urueña, C. P., Llano, M., Gómez-Cadena, A., Hernández, J. F., Sequeda, L. G., et al. (2016). Standardized extract from *Caesalpinia spinosa* is cytotoxic over cancer stem cells and enhance anticancer activity of doxorubicin. *Am. J. Chin. Med.* 44 (8), 1693–1717. doi:10.1142/S0192415X16500956

Santander, S. P., Hernández, J. F., Cifuentes, B. C., Aoki, M., Moins-Teisserenc, H., and Fiorentino, S. (2012). Immunomodulatory effects of Aqueous and organic fractions from *Petiveria alliacea* on human dendritic cells. *Am. J. Chin. Med.* 40 (4), 833–844. doi:10.1142/S0192415X12500620

Sarwar, M. S., Zhang, H-J., and Tsang, S. W. (2018). Perspectives of plant natural products in inhibition of cancer invasion and metastasis by regulating multiple signaling pathways. *Curr. Med. Chem.* 25 (38), 5057–5087. doi:10.2174/0929867324666170918123413

Sasca, D., Szybinski, J., Schüler, A., Shah, V., Heidelberger, J., Haehnel, P. S., et al. (2019). NCAM1 (CD56) promotes leukemogenesis and confers drug resistance in AML. *Blood* 133 (21), 2305–2319. doi:10.1182/blood-2018-12-889725

Schmidt, D. R., Patel, R., Kirsch, D. G., Lewis, C. A., Vander Heiden, M. G., and Locasale, J. W. (2021). Metabolomics in cancer research and emerging applications in clinical oncology. *CA Cancer J. Clin.* 71 (4), 333–358. doi:10.3322/caac.21670

Schraw, J. M., Junco, J. J., Brown, A. L., Scheurer, M. E., Rabin, K. R., and Lupo, P. J. (2019). Metabolomic profiling identifies pathways associated with minimal residual disease in childhood acute lymphoblastic leukaemia. *EBioMedicine* 48, 49–57. doi:10.1016/j.ebiom.2019.09.033

Shafat, M. S., Gnaneswaran, B., Bowles, K. M., and Rushworth, S. A. (2017). The bone marrow microenvironment – home of the leukemic blasts. *Blood Rev.* 31 (5), 277–286. doi:10.1016/j.blre.2017.03.004

Shallis, R. M., Wang, R., Davidoff, A., Ma, X., and Zeidan, A. M. (2019). Epidemiology of acute myeloid leukemia: Recent progress and enduring challenges. *Blood Rev.* 36, 70–87. doi:10.1016/j.blre.2019.04.005

Shrotriya, S., Deep, G., Lopert, P., Patel, M., Agarwal, R., and Agarwal, C. (2015). Grape seed extract targets mitochondrial electron transport chain complex III and induces oxidative and metabolic stress leading to cytoprotective autophagy and apoptotic death in human head and neck cancer cells. *Mol. Carcinog.* 54 (12), 1734–1747. doi:10.1002/mc.22246

Silkjaer, T., Nørgaard, J. M., Aggerholm, A., Ebbesen, L. H., Kjeldsen, E., Hokland, P., et al. (2013). Characterization and prognostic significance of mitochondrial DNA variations in acute myeloid leukemia. *Eur. J. Haematol.* 90 (5), 385–396. doi:10.1111/ejh.12090

Song, K., Li, M., Xu, X., Xuan, L., Huang, G., and Liu, Q. (2016). Resistance to chemotherapy is associated with altered glucose metabolism in acute myeloid leukemia. *Oncol. Lett.* 12 (1), 334–342. doi:10.3892/ol.2016.4600

Song, K., Li, M., Xu, X. J., Xuan, L., Huang, G. N., Song, X. L., et al. (2014). HIF-1α and GLUT1 gene expression is associated with chemoresistance of acute myeloid leukemia. *Asian Pac J. Cancer Prev.* 15 (4), 1823–1829. doi:10.7314/apjcp.2014.15.4.1823

Sossa, C. A., Abello, V., Salazar, L., Rosales, M., Idrobo, H., Reyes-Castellanos, J., et al. (2021). AML-425: Acute myeloid leukemia: A multicenter experience in Colombia. *Clin. Lymphoma Myeloma Leuk.* 21, 2. doi:10.1016/S2152-2650(21)01735-3

Stäubert, C., Bhuiyan, H., Lindahl, A., Broom, O. J., Zhu, Y., Islam, S., et al. (2015). Rewired metabolism in drug-resistant leukemia cells: A metabolic switch hallmarked by reduced dependence on exogenous glutamine. *J. Biol. Chem.* 290 (13), 8348–8359. doi:10.1074/jbc.M114.618769

Stevens, B. M., Jones, C. L., Pollyea, D. A., Culp-Hill, R., D'Alessandro, A., Winters, A., et al. (2020). Fatty acid metabolism underlies venetoclax resistance in acute myeloid leukemia stem cells. *Nat. Cancer* 1 (12), 1176–1187. doi:10.1038/s43018-020-00126-z

Stevens, J. F., Revel, J. S., and Maier, C. S. (2018). Mitochondria-centric review of polyphenol bioactivity in cancer models. *Antioxid. Redox Signal* 29 (16), 1589–1611. doi:10.1089/ars.2017.7404

Stuani, L., Sabatier, M., Saland, E., Cognet, G., Poupin, N., Bosc, C., et al. (2021). Mitochondrial metabolism supports resistance to IDH mutant inhibitors in acute myeloid leukemia. *J. Exp. Med.* 218 (5), e20200924. doi:10.1084/jem.20200924

Sun, Z., Zhang, W., and Li, Q. (2017). miR-125a suppresses viability and glycolysis and induces apoptosis by targeting Hexokinase 2 in laryngeal squamous cell carcinoma. *Cell Biosci.* 7, 51. doi:10.1186/s13578-017-0178-y

Swerdlow, S. H., Campo, E., Harris, N. L., Jaffe, E. S., Pileri, S. A., Stein, H., et al. (2017). *WHO Classification of tumors for haematopoietic and lymphoid tissues*. Lyon, France: International Agency for Research on Cancer (IARC).

Taghvimi, S., Abbaszadeh, S., Banan, F. B., Fard, E. S., Jamali, Z., Najafabadi, M. A., et al. (2022). LncRNAs roles in chemoresistance of cancer cells. *Curr. Mol. Med.* 22 (8), 691–702. doi:10.2174/1566524021666211027090515

Tao, F., Zhang, Y., and Zhang, Z. (2019). The role of herbal bioactive components in mitochondria function and cancer therapy. *Evid. Based Complement. Altern. Med.* 2019, 3868354. doi:10.1155/2019/3868354

Thol, F. (2018). Can we forecast induction failure in acute myeloid leukemia? *Haematologica* 103 (3), 375–377. doi:10.3324/haematol.2018.187575

Urueña, C., Ballesteros-Ramírez, R., Gomez-Cadena, A., Barreto, A., Prieto, K., Quijano, S., et al. (2022). Randomized double-blind clinical study in patients with COVID-19 to evaluate the safety and efficacy of a phytomedicine (P2Et). *Front. Med.* 9, 991873. doi:10.3389/fmed.2022.991873

Urueña, C., Cifuentes, C., Castañeda, D., Arango, A., Kaur, P., Asea, A., et al. (2008). *Petiveria alliacea* extracts uses multiple mechanisms to inhibit growth of human and mouse tumoral cells. *BMC Complement. Altern. Med.* 8, 60. doi:10.1186/1472-6882-8-60

Urueña, C., Mancipe, J., Hernandez, J., Castañeda, D., Pombo, L., Gomez, A., et al. (2013). Gallotannin-rich *Caesalpinia spinosa* fraction decreases the primary tumor and factors associated with poor prognosis in a murine breast cancer model. *BMC Complement. Altern. Med.* 13, 74. doi:10.1186/1472-6882-13-74

Urueña, C., Sandoval, T. A., Lasso, P., Tawil, M., Barreto, A., Torregrosa, L., et al. (2020). Evaluation of chemotherapy and P2Et extract combination in *ex-vivo* derived tumor mammospheres from breast cancer patients. *Sci. Rep.* 10 (1), 19639. doi:10.1038/s41598-020-76619-9

Valin, J., Martinez, E., Huhn, J., Di, M., Orsola, S., Stephen, J., et al. (2022). Acute myeloid leukemia cells rely on the glycolytic enzyme PGK1 to support energy production and amino acid metabolism. *Blood* 140, 8694–8695. doi:10.1182/blood-2022-166659

Vander Heiden, M. G., and Deberardinis, R. J. (2017). Understanding the intersections between metabolism and cancer biology. *Cell* 168 (4), 657–669. doi:10.1016/j.cell.2016.12.039

Vaughan, R. A., Garcia-Smith, R., Dorsey, J., Griffith, J. K., Bisoffi, M., and Trujillo, K. A. (2013). Tumor necrosis factor alpha induces Warburg-like metabolism and is reversed by anti-inflammatory curcumin in breast epithelial cells. *Int. J. Cancer* 133 (10), 2504–2510. doi:10.1002/ijc.28264

Vellinga, T. T., De Boer, V. C. J., Fatrai, S., Van Schelven, S., Trumpi, K., Verheem, A., et al. (2015). SIRT1/PGC1a-Dependent increase in oxidative phosphorylation supports chemotherapy resistance of colon cancer. *Clin. Cancer Res.* 21 (12), 2870–2879. doi:10.1158/1078-0432.CCR-14-2290

Vitkevičienė, A., Janulis, V., Žučenka, A., Borutinskaitė, V., Kaupinis, A., Valius, M., et al. (2019). Oxidative phosphorylation inhibition induces anticancerous changes in therapy-resistant–acute myeloid leukemia patient cells. *Mol. Carcinog.* 58 (11), 2008–2016. doi:10.1002/mc.23092

Vo, T. T., Ryan, J., Carrasco, R., Neuberg, D., Rossi, D. J., Stone, R. M., et al. (2012). Relative mitochondrial priming of myeloblasts and normal HSCs determines chemotherapeutic success in AML. *Cell* 151 (2), 344–355. doi:10.1016/j.cell.2012.08.038

Wang, B., Wang, X., Hou, D., Huang, Q., Zhan, W., Chen, C., et al. (2019). Exosomes derived from acute myeloid leukemia cells promote chemoresistance by enhancing glycolysis-mediated vascular remodeling. *J. Cell Physiol.* 234 (7), 10602–10614. doi:10.1002/jcp.27735

Wang, G., Wang, J. J., Guan, R., Du, L., Gao, J., and Fu, X. L. (2017). Strategies to target glucose metabolism in tumor microenvironment on cancer by flavonoids. *Nutr. Cancer* 69 (4), 534–554. doi:10.1080/01635581.2017.1295090

Wang, J., Liu, X., Qiu, Y., Shi, Y., Cai, J., Wang, B., et al. (2018). Cell adhesion-mediated mitochondria transfer contributes to mesenchymal stem cell-induced chemoresistance on T cell acute lymphoblastic leukemia cells. *Hematol. Oncol.* 11 (1), 11. doi:10.1186/s13045-018-0554-z

Wilkinson, E. M., Ilhan, Z. E., and Herbst-Kralovetz, M. M. (2018). Microbiota–drug interactions: Impact on metabolism and efficacy of therapeutics. *Maturitas* 112, 53–63. doi:10.1016/j.maturitas.2018.03.012

Winer, E. S., and Stone, R. M. (2019). Novel therapy in acute myeloid leukemia (AML): Moving toward targeted approaches. *Ther. Adv. Hematol.* 10, 2040620719860645. doi:10.1177/2040620719860645

Wu, K., Guo, C., Li, Y., Yang, J., Zhou, Q., Cheng, S., et al. (2021). MicroRNA-18a-5p regulates the Warburg effect by targeting hypoxia-inducible factor 1α in the K562/ADM cell line. *Exp. Ther. Med.* 22 (4), 1069. doi:10.3892/etm.2021.10503

Xia, Y., Yang, W., Bu, W., Ji, H., Zhao, X., Zheng, Y., et al. (2013). Differential regulation of c-jun protein plays an instrumental role in chemoresistance of cancer cells. *J. Biol. Chem.* 288 (27), 19321–19329. doi:10.1074/jbc.M113.475442

Xiao, X., Yang, J., Li, R., Liu, S., Xu, Y., Zheng, W., et al. (2013). Deregulation of mitochondrial ATPsyn-β in acute myeloid leukemia cells and with increased drug resistance. *PLoS One* 8 (12), e83610. doi:10.1371/journal.pone.0083610

Xu, D., Jin, J., Yu, H., Zhao, Z., Ma, D., Zhang, C., et al. (2017). Chrysin inhibited tumor glycolysis and induced apoptosis in hepatocellular carcinoma by targeting hexokinase-2. *J. Exp. Clin. Cancer Res.* 36 (1), 44. doi:10.1186/s13046-017-0514-4

Xu, Z., Yan, Y., Li, Z., Qian, L., and Gong, Z. (2016). The antibiotic drug tigecycline: A focus on its promising anticancer properties. *Front. Pharmacol.* 7, 473. doi:10.3389/fphar.2016.00473

Yan, D., Franzini, A., Pomicter, A. D., Halverson, B. J., Antelope, O., Mason, C. C., et al. (2021). SIRT5 is a druggable metabolic vulnerability in acute myeloid leukemia. *Blood cancer Discov.* 2 (3), 266–287. doi:10.1158/2643-3230.BCD-20-0168

Yang, J., Xiao, X., Li, R., Li, Z., Deng, M., and Zhang, G. (2016). Hypermethylation of CpG sites at the promoter region is associated with deregulation of mitochondrial ATPsyn-β and chemoresistance in acute myeloid leukemia. *Cancer Biomark.* 16 (1), 81–88. doi:10.3233/CBM-150543

Ye, H., Adane, B., Khan, N., Alexeev, E., Nusbacher, N., Minhajuddin, M., et al. (2018). Subversion of systemic glucose metabolism as a mechanism to support the growth of leukemia cells. *Cancer Cell* 34 (4), 659–673.e6. doi:10.1016/j.ccell.2018.08.016

Yeung, C. C. S., and Radich, J. (2017). Predicting chemotherapy resistance in AML. *Curr. Hematol. Malig. Rep.* 12 (6), 530–536. doi:10.1007/s11899-017-0378-x

Yeung, M., Hurren, R., Nemr, C., Wang, X., Hershenfeld, S., Gronda, M., et al. (2015). Mitochondrial DNA damage by bleomycin induces AML cell death. *Apoptosis* 20 (6), 811–820. doi:10.1007/s10495-015-1119-z

Yin, J., Yin, Q., Liang, B., Mi, R., Ai, H., Chen, L., et al. (2020). Chrysophanol suppresses growth and metastasis of T cell acute lymphoblastic leukemia via miR-9/PD-L1 axis. *Naunyn-Schmiedeberg's archives Pharmacol.* 393 (2), 273–286. doi:10.1007/s00210-019-01778-0

You, R., Wang, B., Chen, P., Zheng, X., Hou, D., Wang, X., et al. (2022). Metformin sensitizes AML cells to chemotherapy through blocking mitochondrial transfer from stromal cells to AML cells. *Cancer Lett.* 532, 215582. doi:10.1016/j.canlet.2022.215582

Yu, L., Chen, X., Sun, X., Wang, L., and Chen, S. (2017). The glycolytic switch in tumors: How many players are involved? *J. Cancer* 8 (17), 3430–3440. doi:10.7150/jca.21125

Yuan, R., Hou, Y., Sun, W., Yu, J., Liu, X., Niu, Y., et al. (2017). Natural products to prevent drug resistance in cancer chemotherapy: A review. *Ann. N. Y. Acad. Sci.* 1401 (1), 19–27. doi:10.1111/nyas.13387

Zhang, L., Zhao, Q., Cang, H., Wang, Z., Hu, X., Pan, R., et al. (2022). Acute myeloid leukemia cells educate mesenchymal stromal cells toward an adipogenic differentiation propensity with leukemia promotion capabilities. *Adv. Sci. (Weinh).* 9 (16), 2105811. doi:10.1002/advs.202105811

Zhang, S., Zhou, L., Zhang, M., Wang, Y., Wang, M., Du, J., et al. (2020). Berberine maintains the neutrophil N1 phenotype to reverse cancer cell resistance to doxorubicin. *Front. Pharmacol.* 10, 1658. doi:10.3389/fphar.2019.01658

Zhang, Y., Liu, Y., and Xu, X. (2018). Knockdown of LncRNA-UCA1 suppresses chemoresistance of pediatric AML by inhibiting glycolysis through the microRNA-125a/hexokinase 2 pathway. *J. Cell Biochem.* 119 (7), 6296–6308. doi:10.1002/jcb.26899

Zhe, N., Wang, J., Chen, S., Lin, X., Chai, Q., Zhang, Y., et al. (2015). Heme oxygenase-1 plays a crucial role in chemoresistance in acute myeloid leukemia. *Hematology* 20 (7), 384–391. doi:10.1179/1607845414Y.0000000212

Zhu, Y., Liu, Z., Wan, Y., Zou, L., Liu, L., Ding, S., et al. (2022). PARP14 promotes the growth and glycolysis of acute myeloid leukemia cells by regulating HIF-1α expression. *Clin. Immunol.* 242, 109094. doi:10.1016/j.clim.2022.109094

Glossary

α-KG	α-ketoglutarate
2-DG	2-deoxy-D-glucose
2-HG	2-Hidroxiglutarate
3-BrPA	3-bromopyruvate;
ABC transporters	ATP-binding cassette transporters
ACO2	Aconitase 2
ALs	Acute leukemias
ALDOA	Aldolase A
ALL	Acute lymphoid leukemia
AML	Acute myeloid leukemia
Ara-C	Cytarabine
ATO	Arsenic trioxide
ATP	Adenosine triphosphate
ATRA	All-trans retinoic acid
B-ALL	B-acute lymphoid leukemia; Bak: Bcl-2 homologous antagonist/killer; Bax: Bcl-2-associated X protein
BCR-ABL1	Breakpoint Cluster Region-Breakpoints in the Abelson (ABL) 1 fusion
BCL-2	B-Cell Leukemia/Lymphoma 2
CAFs	cancer-associated fibroblasts
CE	Endothelial cells
CO2	Carbon dioxide
COVID-19	Coronavirus disease 2019
CPT1A	Carnitine palmitoyl transferase 1A
CRISPR	Clustered Regularly Interspaced Short Palindromic Repeats
DC	Dendritic cells
DNR	Daunorubicin
DOX	Doxorubicin
ENO1	Enolase 1
ETC	electron transport chain
ETFB	Electron transfer flavoprotein subunit beta
FADH2	Reduced flavin adenine dinucleotide
FAO	Fatty acid oxidation
GAPDH	Glyceraldehyde-3-phosphate dehydrogenase
GLUT1	Glucose transporter 1
GPI	Glucose phosphate isomerase
GSH	Glutathione
H+	Hydrogen (proton)
HCC	Human hepatocellular carcinoma
HGMB-1	High mobility group box 1 protein
HIF-1	Hypoxia-induced factor 1
HK-II	Hexokinase II

HMGB1	High Mobility Group-Box superfamily 1
HO-1	Heme oxygenase-1
HOTAIRM1	Myeloid-specific antisense intergenic RNA - HOX transcript 1
HPDL	4-Hydroxyphenylpyruvate Dioxygenase Like
HSC	Hematopoietic stem cell
HSCT	Allogeneic stem cell transplantation
hTERT	Human telomerase reverse transcriptase
IDA	Idarubicin
IDH3A	(Isocitrate Dehydrogenase NAD+) 3 Catalytic Subunit Alpha
IDH	Isocitrate dehydrogenase
Keap1	Kelch-like ECH-associated protein 1
LDHA	Lactate dehydrogenase A
LICs	Leukemia-initiating cells
LncRNAs	Long non-coding RNAs
LND	Lonidamine
MCL1	Myeloid cell leukemia sequence 1 protein
MCT	proton-linked monocarboxylate transporter
microRNAs	Short non-coding RNAs
MDSC-LCs	Myeloid-derived suppressor-like cells
MFN-2	Mitofusin 2
MRC	Programmed cell death
MRD	Minimal residual disease
MRPL21	Mitochondrial Ribosomal Protein L21; Mitochondrial Ribosomal Protein S33
MSC	Mesenchymal cells
mtDNA	Mitochondrial DNA
NAD+	Oxidized nicotinamide adenine dinucleotide cofactor
NADPH	Reduced nicotinamide adenine dinucleotide phosphate
NCAM1	Neural cell adhesion molecule 1
NH4+	Ammonium ion
NHE1	Na (+)/H (+) antiporter
NFATC1	T-cell nuclear factor 1
Nrf2	Nuclear factor erythroid 2–related factor 2
NSG	NOD scid gamma mouse
OCR	Oxygen consumption rate
OPA1	Mitochondrial Dynamin Like GTPase
OxPhos	Oxidative phosphorylation
PARP	poly (ADP-ribose) polymerases
PBMCs	Peripheral blood mononuclear cells
PCD	Programmed cell death
PCNA	Proliferating cell nuclear antigen
PD-L1	Programmed cell death ligand-1
PDP	Pyruvate dehydrogenase phosphatase

PFKP	Phosphofructokinase
PGC1α	PPARγ coactivator-1α
PGK1	Phosphoglycerate kinase
PGMA1	Phosphoglycerate mutase 1
PKM	Pyruvate kinase 2
PPP	Pentose pathway
PTEN	Phosphatidylinositol 3,4,5-trisphosphate 3-phosphatase and dual-specificity protein phosphatase
ROS	Reactive oxygen species
SDH	Succinate dehydrogenase
SIRT	Sirtuins
SLC12A3	Sodium-dependent dicarboxylate transporter
SUCLA	Succinate-CoA ligase
T-ALL	T-acute lymphoid leukemia
TAMs	Tumor associated macrophages
TCA cycle	Cycle of tricarboxylic acids
TET2	Tet methylcytosine dioxygenase 2
TIMM8B	Mitochondrial Import Inner Membrane Translocase subunit Tim8B
TIMMDC1	Translocase of Inner Mitochondrial Membrane Domain Containing 1
TKIs	Tyrosine kinase inhibitors
Tregs	Regulatory T cells
TUG1	Taurine upregulated gene 1
UCA1	Associated with urothelial carcinoma
VDAC/ANT	Voltage-gated anion channel adenine nucleotide

frontiers | Frontiers in Cell and Developmental Biology

TYPE Brief Research Report
PUBLISHED 26 October 2023
DOI 10.3389/fcell.2023.1217149

OPEN ACCESS

EDITED BY
Pablo Vicente Escriba,
University of the Balearic Islands, Spain

REVIEWED BY
Giulia Pinton,
University of Eastern Piedmont, Italy
Kin Man Suen,
University of Leeds, United Kingdom

*CORRESPONDENCE
Sara Eyal,
sara.eyal@mail.huji.ac.il

†These authors have contributed equally to this work

RECEIVED 04 May 2023
ACCEPTED 02 October 2023
PUBLISHED 26 October 2023

CITATION
Granit Mizrahi A, Gugenheim A, Hamad H, Hamed R, Tetro N, Maimon O, Khutsurauli S, Nechushtan H, Nisman B, Duran D, Samman W, Birimberg-Schwartz L, Grunewald M, Eyal S and Peretz T (2023), Valproic acid reprograms the metabolic aberration of cisplatin treatment via ALDH modulation in triple-negative breast cancer cells. *Front. Cell Dev. Biol.* 11:1217149. doi: 10.3389/fcell.2023.1217149

Valproic acid reprograms the metabolic aberration of cisplatin treatment via ALDH modulation in triple-negative breast cancer cells

Avital Granit Mizrahi[1,2], Ahinoam Gugenheim[1], Haneen Hamad[1], Roa'a Hamed[2], Nino Tetro[2], Ofra Maimon[1], Salome Khutsurauli[1], Hovav Nechushtan[1], Benjamin Nisman[1], Deborah Duran[3,4], Widad Samman[3,4], Liron Birimberg-Schwartz[3,4,5], Myriam Grunewald[3,4], Sara Eyal[2*†] and Tamar Peretz[1,3†]

[1]Oncology Laboratory, Sharett Institute of Oncology, Hadassah-Hebrew University Medical Center, Jerusalem, Israel, [2]School of Pharmacy, Institute for Drug Research, The Hebrew University, Jerusalem, Israel, [3]Faculty of Medicine, Hebrew University, Jerusalem, Israel, [4]Hadassah Organoid Center, The Hadassah Medical Organization, Jerusalem, Israel, [5]Department of Pediatric Gastroenterology, The Hadassah Medical Organization, Jerusalem, Israel

We recently demonstrated that the histone deacetylase inhibitor valproic acid (VPA) reprograms the cisplatin-induced metabolome of triple-negative breast cancer (TNBC) cells, including a shift in hexose levels. Accordingly, here, we tested the hypothesis that VPA alters glucose metabolism in correlation with cisplatin sensitivity. Two TNBC cell lines, MDA-MB-231 (a cisplatin-resistant line) and MDA-MB-436 (a cisplatin-sensitive line), were analyzed. The glycolysis and oxidative metabolism were measured using the Glycolysis Stress Test kit. The expression of aldehyde dehydrogenases (ALDHs), enzymes linked to drug resistance, was investigated by Western blot and real-time PCR analyses. We additionally studied the influence of ALDH inhibition by disulfiram on the viability of MDA-MB-231 cells and on a TNBC patient-derived organoid system. Cisplatin treatment reduced the extracellular acidification rate in MDA-MB-436 cells but not MDA-MB-231 cells, whereas VPA addition increased the extracellular acidification rate in both cell lines. VPA further reduced the oxygen consumption rate of cisplatin-treated MDA-MB-436 cells, which correlated with cell cycle alterations. However, in MDA-MB-231 cells, the cell cycle distribution did not change between cisplatin/VPA–cisplatin treatments. In both cell lines, VPA increased the expression of ALDH isoform and ALDH1A1 expression. However, only in MDA-MB-231 cells, VPA synergized with cisplatin to augment this effect. Disulfiram sensitized the cells to the cytotoxic effects of the VPA–cisplatin combination. Furthermore, the disulfiram–VPA–chemotherapy combination was most effective in TNBC organoids. Our results show that ALDH overexpression may act as one mechanism of cellular resistance to VPA in TNBC and that its inhibition may enhance the therapeutic efficacy of VPA–chemotherapeutic drug combinations.

KEYWORDS

valproic acid, cisplatin, disulfiram, glucose, metabolism, aldehyde dehydrogenase, ALDH, GLUT1

Introduction

Triple-negative breast cancer (TNBC) represents 15% of breast carcinomas and is defined by the absence of the three main breast cancer biomarkers—estrogen receptors, progesterone receptors, and HER2 (also known as ERBB2) (Denkert et al., 2017). Treatment regimens include taxanes, anthracyclines, platinum compounds, topoisomerase inhibitors (e.g., topotecan), and therapeutic proteins (Marra et al., 2020; Loibl et al., 2021). Despite advances in pharmacotherapy, TNBC has relatively poor outcomes with a peak risk of disease recurrence at ~3 years after treatment (von Minckwitz et al., 2012). Among the causes of treatment failure are altered drug uptake, drug efflux, remodeling of DNA repair pathways, and metabolic reprograming (Ranasinghe et al., 2022).

Metabolic reprogramming is a key characteristic of cancer cells that distinguishes them from normal cells. One feature is the Warburg effect, in which tumor cells produce energy through high rate of glycolysis rather than mitochondrial oxidative phosphorylation (OXPHOS), even in the presence of oxygen (Warburg, 1956). The altered glucose metabolism contributes to cancer progression and metastasis and is being utilized in diagnostic imaging with [^{18}F] fluorodeoxyglucose ([^{18}F]FDG) (Mankoff et al., 2007).

Innovative treatments of TNBC include histone deacetylase (HDAC) inhibitors, which have shown efficacy against TNBC in combination with chemotherapeutic agents (Luu et al., 2008; Yardley et al., 2013; Bilen et al., 2015; Wawruszak et al., 2021). Recently, we have shown that exposure of MDA-MD-231 cells to the HDAC inhibitors, valproic acid (VPA), generates profound changes in their metabolites profile and shifted the cisplatin-induced metabolic profile to higher levels of hexose and phosphatidylcholine, indicative of alteration in glucose and lipid metabolism (Granit et al., 2022). VPA-induced metabolic reprogramming has previously been observed in breast cancer stem cells (Debeb et al., 2016) and in a Fanconi anemia cell model (Bertola et al., 2023). This phenomenon has been linked to the ability of VPA to increase the activity of aldehyde dehydrogenase (ALDH). HDAC inhibitors have demonstrated the ability to epigenetically modify the ALDH isotype, specifically the ALDH1A1 expression, via interaction with the bromodomain and extraterminal (BET) family of proteins, which recognize acetylated lysine on histones through their bromodomains (Yokoyama et al., 2016). ALDHs may play an important role in the chemo-resistance ability, clonogenicity, and spherogenesis of the cancer stem cell (Ginestier et al., 2007; Wang et al., 2020), and the ALDH1A1 expression was correlated with poorer overall survival in breast cancer patients (Morimoto et al., 2009). In addition, ALDH overexpression was associated with poor prognostic features, including an increased tumor grade, extensive lymph node metastasis, and a greater extent of luminal B and triple-negative subtypes of breast cancer (Althobiti et al., 2020). The precise mechanism through which ALDHs regulate stemness remains partially understood. ALDH1A1 has also been shown to exhibit metabolic activity and contribute to the promotion of DNA repair, thereby affecting cancer progression. (Yue et al., 2022).

ALDH enzymes are involved in the detoxification of aldehydes in an NAD(P)+-dependent manner, thus reducing oxidative stress (Pors and Moreb, 2014). Chemotherapeutics and radiation therapy induce heightened levels of reactive oxygen species (ROS), resulting in oxidative stress within cancer cells, which contributes to their therapeutic efficacy (Marullo et al., 2013). Elevated ALDH expression potentially serves as a safeguard for cancer cells against these treatments, by maintaining ROS at low levels (Lawenda et al., 2008; Singh et al., 2013). In breast cancer cells, knockdown of ALDH1A1 increased the sensitivity to chemotherapy and radiotherapy (Croker et al., 2017). Additionally, VPA-treated breast cancer stem cells with ALDH activity are shown to be more resistant to chemotherapy (Debeb et al., 2012). ALDHs also participate in retinoic acid (RA) synthesis and can modulate the binding of the transcription factors retinoic acid receptor α (RAR), retinoic X receptor (RXR), and estrogen receptor α (ERα) to DNA, thus promoting cell proliferation, drug resistance, and inhibition of apoptosis (Zanoni et al., 2022).

In the current study, we focused on the effects of the following treatment on glucose metabolism of TNBC cells. Our aims were 1) assessing the effects of VPA, cisplatin, and their combination on glucose metabolism; 2) evaluating the expression of ALDH isoforms upon cisplatin and VPA treatment; and 3) evaluating the potential of the non-specific ALDH inhibitor disulfiram, which inhibits ALDHs, ALDH1A1, and ALDH2 (Koppaka et al., 2012), to reverse untoward effects of VPA–cisplatin. To address these aims, we used representative TNBC cell lines, cisplatin-sensitive cells (MDA-MB-436) and cells intrinsically resistant to cisplatin (MDA-MB-231) (Dominguez-Gomez et al., 2015; Dunne et al., 2018), and a TNBC patient-derived organoid model.

Materials and methods

Sodium valproate, propidium iodide (PI), and red blood cell lysis buffer were purchased from Merck (KGaA, Darmstadt, Germany). Cisplatin was from Pharmachemie B.V (Haarlem, Netherlands). Disulfiram and the fluorescent 2-deoxyglucose analog 2-[N-(7-nitrobenz-2-oxa-1,3-diazol-4-yl)amino]-2-deoxy-D-glucose (2-NBDG) were from Cayman chemical (MI, USA). Paclitaxel was from Teva (Tel Aviv, Israel). GFR Matrigel was purchased from Corning (AZ, USA). All cell culturing reagents and the 2,3-bis(2-methoxy-4-nitro-5-sulfophenyl)-2H-tetrazolium-5-carboxanilide (XTT) Assay Kit were from Sartorius (Biological Industries Ltd., Beit Haemek, Israel). The Protease Inhibitor Cocktail Kit, the High-Capacity cDNA Reverse Transcription Kit, and RnaseA were purchased from Thermo Fisher Scientific (Waltham, MA, USA). The RNeasy Mini-Isolation Kit was from QIAGEN (Hilden, Germany). Xpert Fast SYBR was from Grisp (Porto, Portugal). Anti-ALDH1A1 was from R&D Systems (Minneapolis, MN, USA). Anti-H4, anti-AcH4, and anti-β-actin were purchased from Abcam (Cambridge, UK). The horseradish peroxidase (HRP)-conjugated goat anti-mouse secondary antibody was from Jackson ImmunoResearch (West Grove, PA, USA). The Bicinchoninic Acid (BCA) Protein Assay Kit was from Pierce (Rockford, IL, USA). The Glycolysis Stress Test kit was from Agilent (Santa Clara, CA, USA).

Cell lines and cell culture

The MDA-MB-436 cells were from the American Type Culture Collection. The MDA-MB-231 cells were kindly provided by Prof.

Michael Elkin (Hadassah Medical Center) and maintained in Dulbecco's Modified Eagle Medium (DMEM) supplemented with 10% fetal calf serum, 1% penicillin, 1% streptomycin, and 1% glutamine. The cells were maintained at 37°C in an atmosphere of 5% CO_2. For assessing treatment effects, they were incubated in a culture medium with 1 mM VPA (representing plasma concentrations in the order of magnitude which has been achieved in patients with solid tumors) (Atmaca et al., 2007), 10 μM cisplatin, 20 μM disulfiram, their combination, or the vehicle (0.1% DMSO).

TBNC-derived organoid culture

The patient's pleural effusion was obtained during thoracic drainage after obtaining written informed consent according to the protocol (#HMO-0921-20) approved by the Hadassah Medical Organization ethics committee and the Israeli Ministry of Health. The pleural effusion was collected in a 50 mL sterile tube, transported to the laboratory on ice and processed within 30 min as previously reported (Pan et al., 2021). In brief, the pleural effusion was strained through a 100 μm cell strainer and centrifuged at 250 g for 5 min. Red blood cells were lysed with red blood cell lysis buffer and washed with advanced DMEM-F12. The cell pellet was resuspended in GFR Matrigel (1.6×10^6 cells/mL). Cell suspension droplets were deposited on a pre-heated 24-well culture plate which was inverted and placed at 37°C for 30 min to allow gelation. Then, 500 μl of complete medium (Advanced DMEM-F12, 1% penicillin, 1% streptomycin, 1% HEPES 1 M solution, 1% glutamine, 1 x B27, 5 ng/mL human neuregulin-1, 1.25 mM *N*-acetyl-L-cysteine, 5 mM nicotinamide, 5 ng/mL recombinant human epidermal growth factor (EGF), 20 ng/mL recombinant human fibroblast growth factor (FGF)-1, 5 ng/mL recombinant human FGF-7, 100 ng/mL recombinant human Noggin, 250 ng/mL recombinant human r-spondin-1, 500 nM SB202190, 10 μM Y-27632, 20 ng/mL human insulin-like growth factor-I, 10 nM 17β-estradiol, 50 nM hydrocortisone, and 1 x insulin-transferrin-selenium) was added in each well. Three-dimensional organoids were typically formed during the first 4 days of culture in a 37°C, 5% CO_2 incubator. The medium was refreshed every 5 days, and confluent cultures were passaged at a ratio of 1–2 by mechanical disruption.

Metabolic assays

Ten thousand cells were seeded per well in XF 96-well microplates and incubated for 24 h with the medium and then for an additional 72 h with the aforementioned treatments. Basal oxygen consumption rate (OCR) and extracellular acidification rate (ECAR) measurements were performed by the Seahorse XFe96 Analyzer (Agilent Technologies Inc., Santa Clara, CA, USA) using the Glycolysis Stress Test kit. Following completion of the measurements, cell viability was analyzed using the sodium 3′-[1-[(phenylamino)-carbony]-3,4-tetrazolium]-bis(4-methoxy-6-nitro)benzene-sulfonic acid hydrate (XTT) assay.

Cell cycle analysis

For fluorescence-activated cell sorting (FACS) analysis, the cells were fixed overnight at 4°C in 70% ethanol and stained with PI for 1 h. The cells were analyzed using the CytoFLEX Platform flow cytometer (Beckman Coulter Life Sciences, Indianapolis, IN, USA).

Immunoblotting

Approximately 10 million cells were harvested by trypsinization, washed in ice-cold phosphate-buffered saline (PBS), and lysed in 1 x radioimmunoprecipitation assay (RIPA) lysis buffer with the Halt™ Protease Inhibitor Cocktail Kit. Protein concentrations were determined by the BCA Protein Assay Kit. Thirty microgram protein underwent electrophoresis on 15% gradient sodium dodecyl sulfate (SDS)-polyacrylamide gels. Membranes were incubated with primary antibodies—anti-ALDH1A1 (1:450), anti-acetyl-H4 (1:10,000), anti-H4 (1:1,000), or anti-β-actin (1:1,000)—overnight at 4°C. The blots were then incubated for 1 h with a HRP-conjugated goat anti-mouse secondary antibody (1:5,000) and developed by enhanced chemiluminescence.

Analyses of mRNA expression

Total RNA was isolated from one million cells using the RNeasy Mini-Isolation Kit according to the manufacturer's instructions. The cDNA was synthesized by using the High-Capacity cDNA Reverse Transcription Kit in a 20 μL reaction containing 1 μg of total RNA. An aliquot of 1 μL cDNA was used in each 10 μL PCR reaction, using Xpert Fast SYBR, and reactions were run on an ABI StepOnePlus PCR system (Thermo Fisher Scientific). The primers used for PCR are listed in Supplementary Table S1.

Viability assays

Cell and organoid viability were analyzed using the XTT Assay Kit, according to the manufacturer's instructions. In brief, 10,000 cells were seeded in 96-well plates at 37°C, incubated for 24 h, and treated with the indicated concentrations of cisplatin alone or with 1 mM VPA, 20 μM disulfiram, or their combinations for 72 h. Organoids were harvested, washed, and resuspended in a complete medium. About 100 organoids were transferred to 96 wells that were pre-coated with a layer of 35 μl of Matrigel. Organoids were allowed to settle down on the Matrigel overnight in a 37°C, 5% CO_2 incubator. Paclitaxel alone (7 μM) or with 1 mM VPA, 20 μM disulfiram, or their combinations were added to the growth medium. Organoids were exposed to the drug combinations for 5 days. To quantify the drug effect on cell or organoid viability, 50 μl of the XTT reagent was added to the medium, and the cells were further incubated for 2–4 h. The plate was analyzed by using a plate reader (Sunrise™, Tecan, Männedorf, Switzerland) at 450 nm.

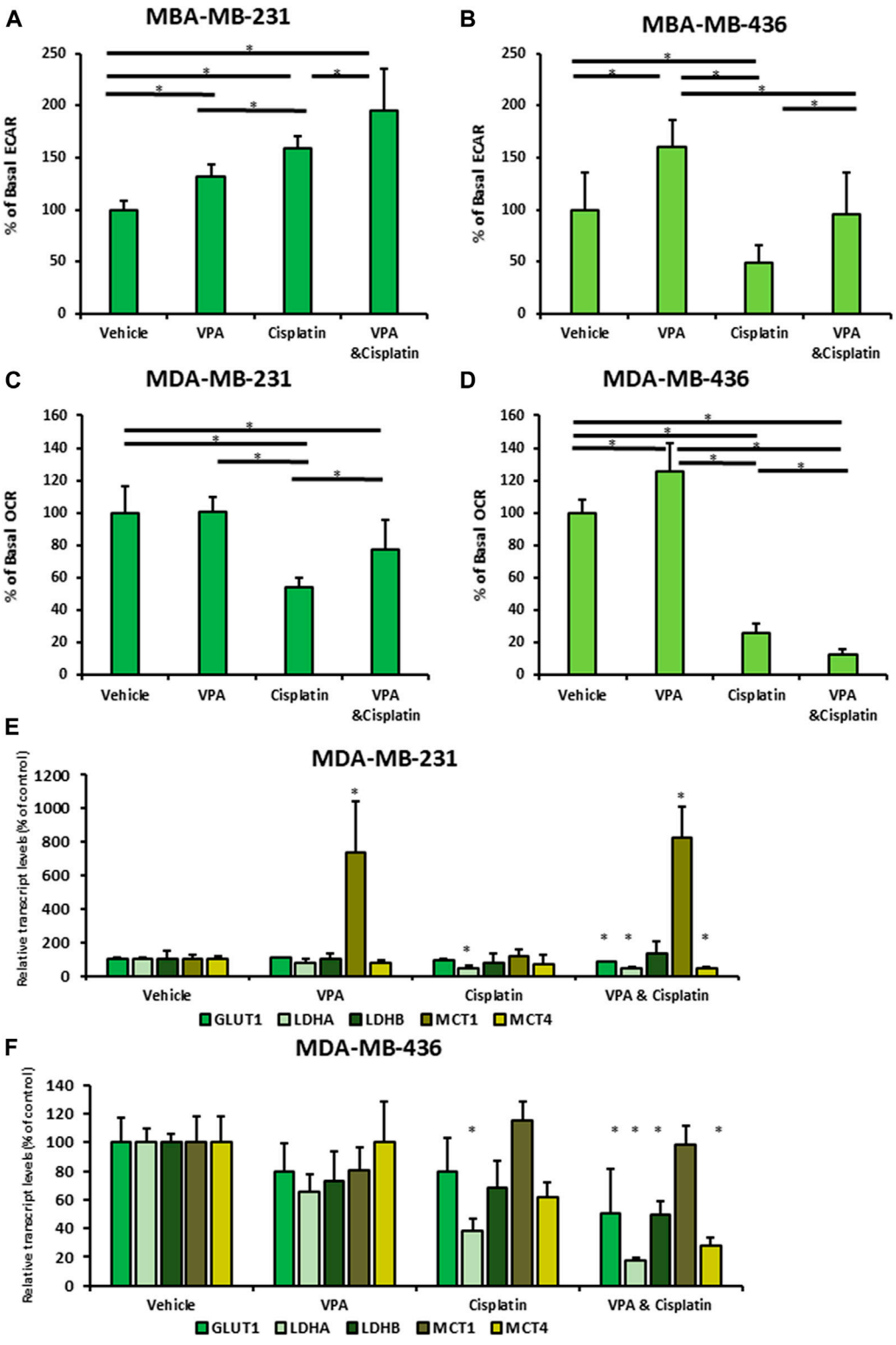

FIGURE 1
Vaplroic acid (VPA) effect on glucose and mitochondrial metabolism in MDA-MB-231 and MDA-MB-436 cells in the presence of cisplatin. MDA-MB-231 and MBA-MB-436 cells were exposed for 72 h to 1 mM VPA, 5 μM cisplatin (for MDA-MB-436), 10 μM cisplatin (for MDA-MB-231), or their combination. The cells were evaluated using a Seahorse XFe Extracellular Flux Analyzer. **(A,B)** Basal ECAR assessment of the glycolytic capacity of MBA-MB-231 **(A)** and MDA-MB-436 cells **(B)**. **(C,D)** OCR assessment of basal respiration for MDA-MB-231 **(C)** and MDA-MB-436 cells **(D)**. Results are presented as the percent of control (mean ± standard deviation [SD]); N = 5/group. **(E)** Real-time PCR of GLUT1, LDH A, LDH B, MCT1, and MCT4. MDA-MB-231 cells were treated with VPA, cisplatin, or both, for 72 h. **(F)** The same as mentioned above for MDA-MB-436 cells. Results are presented as the percent of control (mean ± standard deviation [SD]); *$p < 0.05$; N = 6/group.

Uptake assays

Treated cells ($1*10^6$) were cultured for 72 h and then washed with a glucose-free medium. The medium was replaced with glucose-free DMEM, and the cells were incubated for 1 hr at 37°C. 2-NBDG was added to the cells in glucose-free DMEM (final concentration 10 μM), and the cells were incubated for an additional 2 h at 37°C. The incubation medium was then removed, and the cells were washed twice with cold PBS. The cells were then trypsinized and resuspended in cold PBS with 4′,6-diamidino-2-phenylindole (DAPI; final concentration 1 μg/mL). The plate was read using the CytoFLEX Platform flow cytometer (Beckman Coulter Life Sciences, Indianapolis, IN, USA) at 525/540 nm.

Data analysis

The OCR and ECAR values were normalized by the results of the XTT viability analysis. The flow cytometry data (10,000 cells/assay) were analyzed using the CytExpert software (Beckman Coulter). ImageLab (ChemiDocTMXRS+, Bio-Rad, USA) was used to quantify the densities of the target bands obtained by Western blotting. The results are expressed as the relative intensity ratio of the ALDH1A1 and β-actin bands or the relative intensity of AchH4 and H4 bands. The RT-PCR data were analyzed using StepOnePlus software v2.3 (Thermo Fisher Scientific, Waltham, MA, USA). Relative cell viability was calculated with the values of vehicle-treated cells set as 100%. Unless otherwise stated, studies were conducted in triplicate, on two different days (n = 6 per treatment group).

Statistical analysis

The Kruskal–Wallis test followed by Dunn's post-test was used to determine the statistical significance of the differences between experimental groups. Data are presented as mean and standard deviation. A p-value <0.05 was considered significant. The final inhibitory concentration $(IC)_{50}$ value was determined by using the dose-response data with a linear regression model. Statistical analyses were performed using GraphPad Prism, version 8 (San Diego, CA, USA).

Results

VPA shifts the effects of cisplatin on the energy metabolism of breast cancer cells

For the ECAR analysis, cisplatin served as a positive control because cisplatin-resistant tumor cell lines are characterized by enhanced glycolysis (Qian et al., 2017). Cisplatin and VPA each increased the basal ECAR in MDA-MB-231 cells (cisplatin resistant; 1.6-fold and 1.3-fold, respectively; $p < 0.05$; Figure 1A) indicating higher glycolysis rate. The VPA–cisplatin combination further increased this effect (1.95-fold as compared to control, $p < 0.05$). Similarly, VPA increased the ECAR levels by 1.6-fold in MDA-MB-436 cells (cisplatin-sensitive; $p < 0.05$). However, in these cells, cisplatin reduced the ECAR level by one half ($p < 0.05$; Figure 1B), and VPA rescued the cells from the cisplatin effect. In MDA-MB-231 cells, cisplatin reduced the basal OCR level (indicating mitochondrial respiration) by half ($p < 0.05$), whereas VPA did not significantly affect it and partially rescued the cells from the cisplatin effect (Figure 1C). A 70% decrease ($p < 0.05$) in the basal OCR level was detected in MDA-MB-436 cells following cisplatin treatment. In contrast to MDA-MB-231 cells, VPA increased it by 1.25-fold ($p < 0.05$) as compared to control (Figure 1D). The VPA–cisplatin combination further decreased the OCR level ($p < 0.05$) as compared to cisplatin alone.

Next, to investigate the mechanism of the energy metabolism after VPA–cisplatin treatment, we examined the mRNA expression of glucose transporter 1 (GLUT1), lactate dehydrogenase (LDH) A and B, and monocarboxylate transporters 1 and 4 (MCT 1 and 4). The level of GLUT1, LDH A, and MCT4 mRNA expression was decreased after VPA–cisplatin treatment in both cell lines (Figures 1E, F). MCT1 levels were significantly higher in the presence of VPA in MDA-MB-231 cells but not in MDA-MB-436 cells.

VPA affects cell cycle distribution in cisplatin-treated cells

To further understand the phenotype of the metabolism shift in VPA–cisplatin-treated cells, we studied their cell cycle distribution using flow cytometry. In both cell lines, treatment with cisplatin resulted in increased proportion of the cells in the S and G2/M phases (Figures 2A–C). VPA-treated cells exhibited the same cell cycle distribution as the vehicle-treated controls. The addition of VPA to cisplatin did not alter the effect of cisplatin in MDA-MB-231 cells, but in MDA-MB-436 cells, the VPA–cisplatin treatment reduced the percentage of cells in the G2/M phase and increased early cell cycle arrest at the S phase by approximately 14% ($p < 0.05$) as compared to cisplatin-treated cells.

VPA–cisplatin combination increases ALDH1A1 expression in an additive manner

We next addressed the question of whether VPA, cisplatin, and their combination affect the expression of the representative ALDH and ALDH1A1 in TNBC cells. Western blot analysis showed that ALDH1A1 was expressed at significantly higher levels in VPA–cisplatin-treated MDA-MB-231 cells and in VPA-treated MDA-MB-436 cells (Figures 3A–D). An analysis confirmed the effect of the drug combination on the ALDH1A1 expression also at the mRNA level in MDA-MB-231 cells (but not MDA-MB-436 cells). It additionally demonstrated a significant increase in ALDH1A1 transcript levels following treatment with VPA only (Figures 3E, F). However, only in the presence of cisplatin, higher ROS level was detected, and VPA addition did not modulate their amount (Supplementary Figure S2).

Next, we examined whether the H4 acetylation of MDA-MB-231- and MDA-MB-436-treated cells is associated with ALDH1A1 expression. The H4 acetylation levels VPA-treated MDA-MB-231 and MDA-MB-436 cells exhibited significant change in the H4 acetylation level. In addition, H4 acetylation

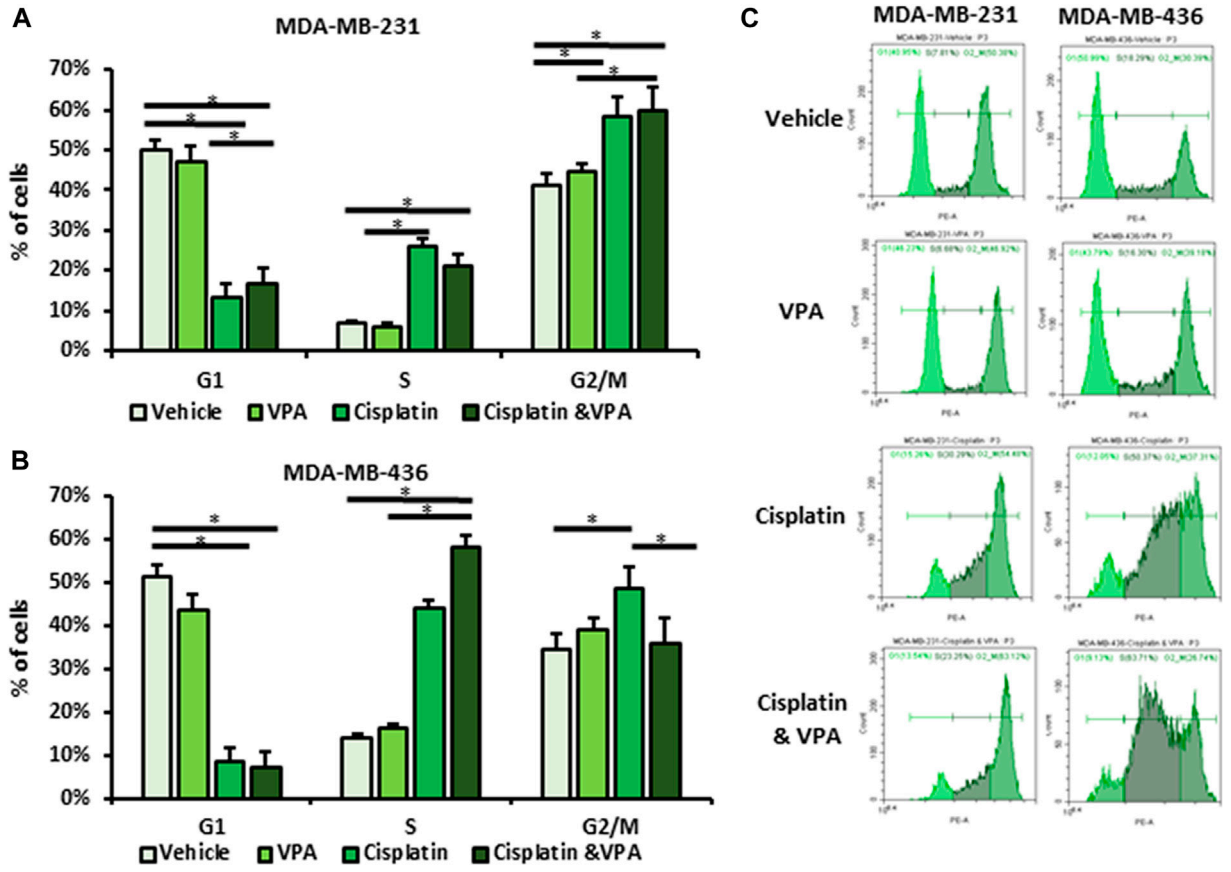

FIGURE 2
Effect of Valproic acid (VPA), cisplatin, and their combination on cell cycle distribution of MDA-MB-231 and MDA-MB-436 cells. The cells were treated with 1 mM of VPA, 5 μM cisplatin (for MDA-MB-436), 10 μM cisplatin (for MDA-MB-231), or their combination for 72 h. The cell cycle phases were analyzed by flow cytometry and propidium iodide (PI) labeling. **(A,B)** Cell cycle analysis of MBA-MB-231 **(A)** and MBA-MB-436 cells **(B)**. Results are presented as the percent of control (mean ± standard deviation [SD]); *$p < 0.05$; N = 6/group. **(C)** Representative flow cytometry histograms.

was enhanced in MDA-MB-436 cells following treatment with VPA and VPA–cisplatin ($p < 0.05$) (Figures 3G–J).

ALDH inhibition by disulfiram sensitizes MDA-MB-231 cells to VPA-cisplatin treatment

We sought to investigate whether non-specific ALDH inhibition can enhance the sensitivity of MDA-MB-231 to cisplatin and VPA treatment. Disulfiram, an anti-alcoholism medication, is an irreversible inhibitor of ALDH (Koppaka et al., 2012) with anti-cancer effect (Nechushtan et al., 2015). Indeed, the addition of disulfiram to the other treatments enhanced their cytotoxicity, producing the largest reduction in cell viability (Figure 4A). The IC50 value of cisplatin alone was 17.1 ± 4.5 μM. The addition of VPA, disulfiram, and a VPA–disulfiram combination to cisplatin reduced the IC50 values to 12.9 ± 1.7, 5.3 ± 0.7, and 3.5 ± 0.8 μM, respectively (Figure 4B).

We also measured the uptake of 2-NBDG, a fluorescent tracer used for monitoring glucose uptake into live cells. Disulfiram and VPA treatments did not affect the cellular uptake of 2-NBDG. As predicted, the uptake was 1.7-fold higher in the cisplatin-treated cells as compared to controls (Figure 4C) and remained elevated when cisplatin was combined with VPA or disulfiram. Interestingly, the disulfiram–VPA–cisplatin combination did not increase the 2-NBDG uptake in comparison with the control, suggesting an effect on glucose metabolism.

Finally, we examined the cytotoxic effect of the disulfiram–VPA–chemotherapy combination on pleural effusion-derived organoids from TNBC patients. Because cisplatin had no effect on cell viability (Supplementary Figure S3), we continued with another ROS inducing chemotherapy, paclitaxel (Samanta et al., 2014). In correlation with the results obtained for the MDA-MB-231 cells, the addition of disulfiram reduced the viability of VPA-chemotherapy-treated organoids (Figure 4D).

Discussion

In recent years, there has been a growing interest in cancer metabolism and the impact of anti-cancer therapies on glucose utilization. This study aimed to characterize the metabolic response of TNBC cells to the addition of VPA to chemotherapy and identify its association with their sensitivity to treatment. A different response to VPA–cisplatin combination has been observed in

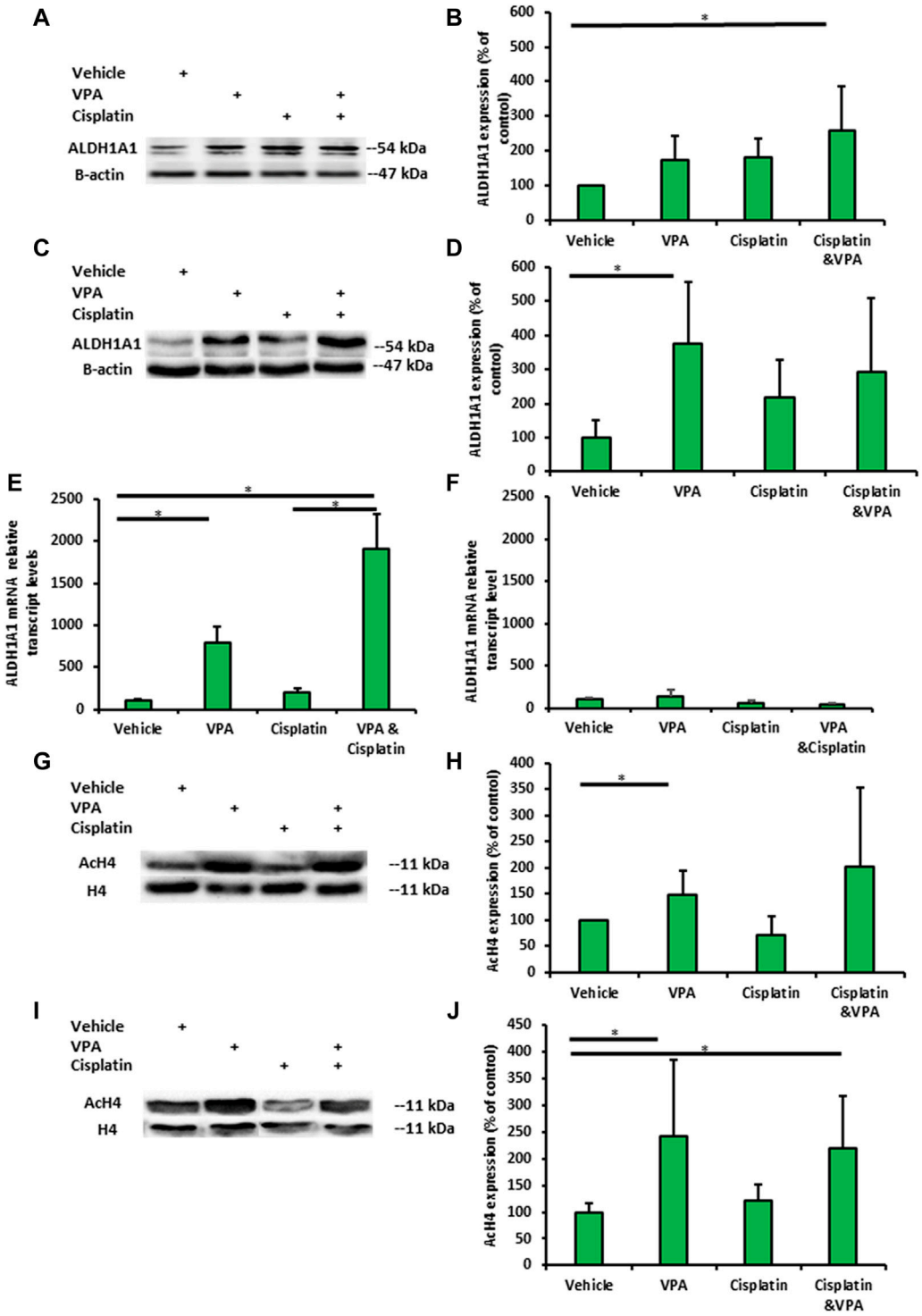

FIGURE 3
Valproic acid (VPA) and cisplatin exert an additive effect on ALDH1A1 expression in MDA-MB-231 cells but not on MDA-MB-436 cells. The cells were incubated with 1 mM VPA, 5 μM cisplatin (for MDA-MB-436), 10 μM cisplatin (MDA-NB-231), or their combination for 72 h. **(A)** Representative images of ALDH1A1 protein expression in MDA-MB-231 cells by Western blotting. **(B)** Quantification of the optic density. Results are presented as the percent of control (mean ± standard deviation [SD]); N = 6/group. **(C,D)** The same as mentioned above for MDA-MB-436 cells. **(E)** ALDH1A1 mRNA expression in MDA-MB-231 cells (by RT-PCR). Results are presented as the percent of control (mean ± standard deviation [SD]); N = 6/group. **(F)** The same as mentioned above for MDA-MB-436 cells. **(G)** Representative images of histone 4 acetylation in MDA-MB-231 cells. **(H)** Quantification of the optic density. Results are presented as the percent of control (mean ± standard deviation [SD]); N = 6/group. **(I,J)** The same as mentioned above for MDA-MB-436 cells. *$p < 0.05$.

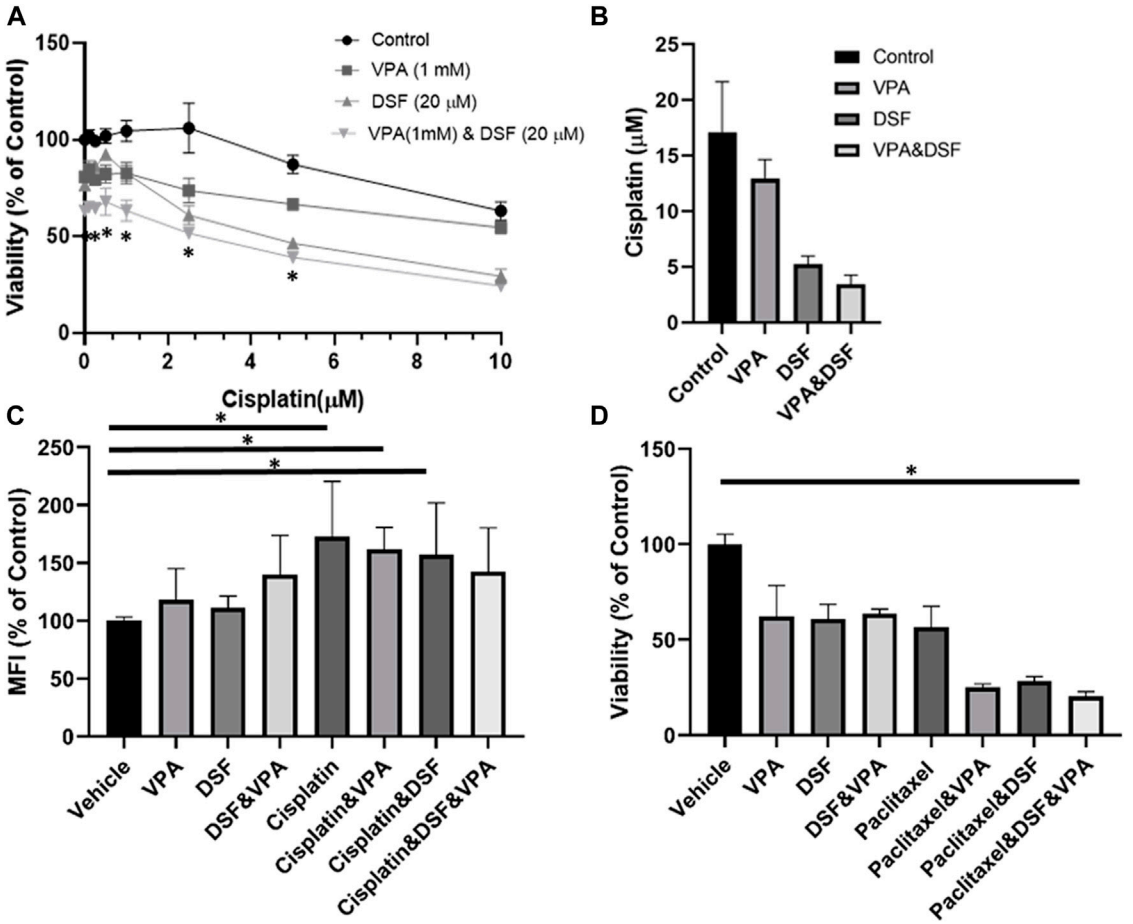

FIGURE 4
Disulfiram sensitizes MDA-MB-231 cells to the effects of VPA and chemotherapy. **(A)** MDA-MB-231 cells were treated with increasing concentration of cisplatin alone or with 1 mM Valproic acid (VPA), 20 μM disulfiram (DSF), or their combination for 72 h, followed by the XTT analysis of cellular viability. *$p < 0.05$ **(B)** Half-maximal inhibitory concentration (IC50) plotted from the cell viability analysis. **(C)** 2-NBDG uptake by MDA-MB-231 treated for 72 h with 1 mM VPA, 20 μM DSF, 10 μM of cisplatin, or their combination. 2-NBDG cellular accumulation was analyzed by flow cytometry. Results are presented as the percent of control (mean ± standard deviation [SD]); N = 6/group. **(D)** Effect of disulfiram on cell viability in VPA- and paclitaxel-treated organoids. TNBC pleural effusion-derived tumor organoids were treated with 1 mM VPA, 7 μM paclitaxel, 20 μM DSF, or their combination for 5 days, followed by the XTT assay for cellular viability. Results are presented as the percent of control (mean ± standard deviation [SD]); N = 4/group. *$p < 0.05$.

breast cancer cell lines, and MDA-MB-231 cells were particularly resistant to this combination (Wawruszak et al., 2015). In addition, different responses of TNBC cells to drugs have been shown in metabolic rates and principle metabolic components, demonstrating the ability MDA-MB-231 cells to undergo metabolic adaption (Lanning et al., 2017). These findings are consistent with our previous metabolomics analyses, in which MDA-MB-231 cells also exhibited alterations in their metabolite profile after VPA–cisplatin treatment (Granit et al., 2022). Therefore, the different metabolic response between the TNBC cell lines in our present work extends these observations. Our findings not only revealed common patterns between TNBC cells but also identified cell line-specific responses. VPA addition to cisplatin treatment had a similar trend in the glycolysis pathway, increasing the ECAR in both cell lines compared to cisplatin alone (Figures 1A, B). In contrast to the reduced GLUT1, LDH A, and MCT4 transcript expression, MCT1 expression increased in MDA-MB-231 cells (Figures 1E, F). Furthermore, a diverse response was observed in the oxidative phosphorylation pathway represented by the OCR. VPA combined with cisplatin increased the OCR compared to cisplatin only in MDA-MB-231 cells but had the opposite effect in MDA-MB-436 cells (Figures 1C, D). MDA-MB-436 cells also exhibit early-phase cell cycle arrest, indicating an increased sensitivity to the VPA–cisplatin combination (Figure 2B). The difference in ECAR and OCR response to the VPA–cisplatin combination, together with the cell cycle alterations, help understand the common pathways and differences between these TNBC cell lines in a wider metabolic context. For example, our previous work demonstrated that the VPA–cisplatin combination increased the hexose level in MDA-MB-231 cells. Here, we showed a correlation with the ECAR for that observation. In addition, the metabolomic analysis assumed that VPA increased cisplatin sensitivity, which was the case for MDA-MB-436 but not MDA-MB-231 cells. Therefore, metabolite analysis combined with metabolic rates and cell cycle analysis can provide a deeper conception of drug-induced changes in metabolic profiles of TNBC cells.

VPA has been described as a potential anti-breast cancer treatment as monotherapy or combined with chemotherapy, such as cisplatin (Wawruszak et al., 2021). Cisplatin can cause DNA damage and metabolic reprogramming by inducing oxidative stress, as demonstrated for head and neck squamous cell carcinoma (HNSCC) (Yu et al., 2018). One mechanism by which tumor cells survive cisplatin treatment is the overexpression of ALDHs. ALDHs mediate the oxidation of a wide range of aldehydes to acids (Koppaka et al., 2012), and they are closely associated to drug resistance during conventional cancer chemotherapy (Liu et al., 2021). In breast cancer cell lines, ALDH activity also altered the metabolic phenotype by increasing the oxidative phosphorylation activity (Lee et al., 2017). In addition, HDAC inhibitors increased ALDH1A1 expression through the transcription factor BRD4 in ovarian cancer cells (Yokoyama et al., 2016). ALDH1A2 played a role in conferring resistance to 13-cis-retinoic acid (13-cis-RA) in neuroblastoma cells (Hartomo et al., 2015). Also, the knockdown of ALDH1A3 markedly enhanced the sensitivity of lung adenocarcinoma to cisplatin (Yun et al., 2018). Together, these findings led us to investigate the expression of ALDHs as a metabolic resistance indicator. In this study, we found that the cisplatin-induced upregulation of ALDH1A1 was markedly enhanced by VPA in MDA-MB-231 cells but not in MDA-MB-436 cells (Figures 3A–F). As expected, this additivity was not seen in the H4 acetylation analysis (because cisplatin is not an HDAC inhibitor), implying different mechanisms involving the ALDH1A1 overexpression (Figures 3G–J). High ALDH1A1 levels further suggest that MDA-MB-231 cells could have acquired metabolic resistance. Based on these observations, we used the non-specific ALDH inhibitor, disulfiram, in our viability experiments, revealing that a combination treatment with disulfiram and VPA has significantly sensitized MDA-MB-231 cells to cisplatin, as compared with the other treatments (cisplatin, VPA-cisplatin, or disulfiram-cisplatin) (Figures 4A, B). Similar results were obtained in TNBC organoids (Figure 4D). In addition, we found that disulfiram combined with VPA–cisplatin can reprogram cellular metabolism by reducing the uptake of glucose, as compared to cisplatin with the other combinations (Figure 3C). Although disulfiram is a non-specific ALDH inhibitor, our findings provide support to the assumption that ALDH1A1 overexpression is associated with metabolic resistance and may represent an effective target for sensitizing cancer cells to cisplatin.

This study has limitations. First, we studied the drug effect on glucose metabolism *in vitro*, in only two TNBC cell lines (and an organoid model from a TNBC patient). Other cell lines representing different types of breast cancer, and *in vivo* studies, might be used for confirming our current findings. Second, we focused on cisplatin, with one paclitaxel study. It would be interesting to investigate the effect of VPA and disulfiram treatment on reprograming glucose metabolism in breast cancer cells following other chemotherapeutic treatments. Third, we did not specifically knockdown ALDH1A1 expression. Therefore, our results may indicate the effects of other ALDHs. An ALDH1A1 knockdown cell line should be constructed in future studies to investigate whether VPA treatment could result in cisplatin resistance in breast cancer cells; this might verify our present data in other aspects.

In summary, we demonstrated that VPA-cisplatin combination could differently reprogram the glucose metabolism of TNBC cells. The cisplatin-resistant MDA-MB-231 cells showed higher metabolic activity under VPA–cisplatin treatment. On the contrary, VPA had further decreased the oxidative phosphorylation rate that resulted in an early cell cycle of cisplatin-sensitive MDA-MB-436 cells. This effect might be attributed to the elevation of ALDH1A1 expression. Given the association of ALDH1A1 expression with the chemotherapeutic response in MDA-MB-231 TNBC cells, ALDH inhibitors which are capable of inhibiting ALDH1A1 may be a potential novel strategy for improving the chemotherapy response in TNBC patients, especially for the patients who are co-treated with VPA.

Data availability statement

The raw data supporting the conclusion of this article will be made available by the authors, without undue reservation.

Ethics statement

The studies involving humans were approved by the Hadassah Medical Organization 124 ethics committee and the Israeli Ministry of Health. The studies were conducted in accordance with the local legislation and institutional requirements. Written informed consent for participation in this study was provided by the participants' legal guardians/next of kin.

Author contributions

AGM, SE, OM, BN, LBN and TP contributed to the conception and design of the study. AGM, AG, NT, RH and HH performed the experiments and organized the database. DD, MG and WS performed the experiments depicted in Figure 4D. AGM preformed the statistical analysis. AGM wrote the first draft of the manuscript. SE wrote section, edit and reviewed the manuscript. TP, SK, and HN reviewed the manuscript. All authors contributed to the article and approved the submitted version.

Funding

This study was kindly supported by the Israel Cancer Association, Grant #20211181 and the David R. Bloom Centre for Pharmacy. HN was kindly supported by a grant from the Sasson Naor Foundation.

Acknowledgments

The authors thank Avraham Naim (Cytotoxic unit, Hadassah Medical Center, Jerusalem, Israel) for providing the cytotoxic drugs and Prof. Michael Elkin for providing the MDA-MB-231 cells. SE is affiliated with the David R. Bloom Centre for Pharmacy and Dr. Adolf and Klara Brettler Center for Research in Molecular Pharmacology and Therapeutics at the Hebrew University of Jerusalem, Israel, and is holding a Dame Susan Garth Chair of Cancer Research.

Conflict of interest

SE has served as a consultant for Biopass and TrueMed, Israel.

The remaining authors declare that the research was conducted in the absence of any commercial or financial relationships that could be construed as a potential conflict of interest.

Publisher's note

All claims expressed in this article are solely those of the authors and do not necessarily represent those of their affiliated organizations, or those of the publisher, the editors, and the reviewers. Any product that may be evaluated in this article, or claim that may be made by its manufacturer, is not guaranteed or endorsed by the publisher.

Supplementary material

The Supplementary Material for this article can be found online at: https://www.frontiersin.org/articles/10.3389/fcell.2023.1217149/full#supplementary-material

References

Althobiti, M., El Ansari, R., Aleskandarany, M., Joseph, C., Toss, M. S., Green, A. R., et al. (2020). The prognostic significance of ALDH1A1 expression in early invasive breast cancer. *Histopathology* 77 (3), 437–448. doi:10.1111/his.14129

Atmaca, A., Al-Batran, S. E., Maurer, A., Neumann, A., Heinzel, T., Hentsch, B., et al. (2007). Valproic acid (VPA) in patients with refractory advanced cancer: a dose escalating phase I clinical trial. *Br. J. Cancer* 97 (2), 177–182. doi:10.1038/sj.bjc.6603851

Bertola, N., Regis, S., Bruno, S., Mazzarello, A. N., Serra, M., Lupia, M., et al. (2023). Effects of deacetylase inhibition on the activation of the antioxidant response and aerobic metabolism in cellular models of Fanconi anemia. *Antioxidants (Basel)* 12 (5), 1100. doi:10.3390/antiox12051100

Bilen, M. A., Fu, S., Falchook, G. S., Ng, C. S., Wheler, J. J., Abdelrahim, M., et al. (2015). Phase I trial of valproic acid and lenalidomide in patients with advanced cancer. *Cancer Chemother. Pharmacol.* 75 (4), 869–874. doi:10.1007/s00280-015-2695-x

Croker, A. K., Rodriguez-Torres, M., Xia, Y., Pardhan, S., Leong, H. S., Lewis, J. D., et al. (2017). Differential functional roles of ALDH1A1 and ALDH1A3 in mediating metastatic behavior and therapy resistance of human breast cancer cells. *Int. J. Mol. Sci.* 18 (10), 2039. doi:10.3390/ijms18102039

Debeb, B. G., Lacerda, L., Larson, R., Wolfe, A. R., Krishnamurthy, S., Reuben, J. M., et al. (2016). Histone deacetylase inhibitor-induced cancer stem cells exhibit high pentose phosphate pathway metabolism. *Oncotarget* 7 (19), 28329–28339. doi:10.18632/oncotarget.8631

Debeb, B. G., Lacerda, L., Xu, W., Larson, R., Solley, T., Atkinson, R., et al. (2012). Histone deacetylase inhibitors stimulate dedifferentiation of human breast cancer cells through WNT/β-catenin signaling. *Stem Cells* 30 (11), 2366–2377. doi:10.1002/stem.1219

Denkert, C., Liedtke, C., Tutt, A., and von Minckwitz, G. (2017). Molecular alterations in triple-negative breast cancer-the road to new treatment strategies. *Lancet* 389 (10087), 2430–2442. doi:10.1016/S0140-6736(16)32454-0

Dominguez-Gomez, G., Diaz-Chavez, J., Chavez-Blanco, A., Gonzalez-Fierro, A., Jimenez-Salazar, J. E., Damian-Matsumura, P., et al. (2015). Nicotinamide sensitizes human breast cancer cells to the cytotoxic effects of radiation and cisplatin. *Oncol. Rep.* 33 (2), 721–728. doi:10.3892/or.2014.3661

Dunne, M., Dou, Y. N., Drake, D. M., Spence, T., Gontijo, S. M. L., Wells, P. G., et al. (2018). Hyperthermia-mediated drug delivery induces biological effects at the tumor and molecular levels that improve cisplatin efficacy in triple negative breast cancer. *J. Control Release* 282, 35–45. doi:10.1016/j.jconrel.2018.04.029

Ginestier, C., Hur, M. H., Charafe-Jauffret, E., Monville, F., Dutcher, J., Brown, M., et al. (2007). ALDH1 is a marker of normal and malignant human mammary stem cells and a predictor of poor clinical outcome. *Cell Stem Cell* 1 (5), 555–567. doi:10.1016/j.stem.2007.08.014

Granit, A., Mishra, K., Barasch, D., Peretz-Yablonsky, T., Eyal, S., and Kakhlon, O. (2022). Metabolomic profiling of triple negative breast cancer cells suggests that valproic acid can enhance the anticancer effect of cisplatin. *Front. Cell Dev. Biol.* 10, 1014798. doi:10.3389/fcell.2022.1014798

Hartomo, T. B., Van Huyen Pham, T., Yamamoto, N., Hirase, S., Hasegawa, D., Kosaka, Y., et al. (2015). Involvement of aldehyde dehydrogenase 1A2 in the regulation of cancer stem cell properties in neuroblastoma. *Int. J. Oncol.* 46 (3), 1089–1098. doi:10.3892/ijo.2014.2801

Koppaka, V., Thompson, D. C., Chen, Y., Ellermann, M., Nicolaou, K. C., Juvonen, R. O., et al. (2012). Aldehyde dehydrogenase inhibitors: a comprehensive review of the pharmacology, mechanism of action, substrate specificity, and clinical application. *Pharmacol. Rev.* 64 (3), 520–539. doi:10.1124/pr.111.005538

Lanning, N. J., Castle, J. P., Singh, S. J., Leon, A. N., Tovar, E. A., Sanghera, A., et al. (2017). Metabolic profiling of triple-negative breast cancer cells reveals metabolic vulnerabilities. *Cancer Metab.* 5, 6. doi:10.1186/s40170-017-0168-x

Lawenda, B. D., Kelly, K. M., Ladas, E. J., Sagar, S. M., Vickers, A., and Blumberg, J. B. (2008). Should supplemental antioxidant administration be avoided during chemotherapy and radiation therapy? *J. Natl. Cancer Inst.* 100 (11), 773–783. doi:10.1093/jnci/djn148

Lee, K. M., Giltnane, J. M., Balko, J. M., Schwarz, L. J., Guerrero-Zotano, A. L., Hutchinson, K. E., et al. (2017). MYC and MCL1 cooperatively promote chemotherapy-resistant breast cancer stem cells via regulation of mitochondrial oxidative phosphorylation. *Cell Metab.* 26 (4), 633–647. doi:10.1016/j.cmet.2017.09.009

Liu, C., Qiang, J., Deng, Q., Xia, J., Deng, L., Zhou, L., et al. (2021). ALDH1A1 activity in tumor-initiating cells remodels myeloid-derived suppressor cells to promote breast cancer progression. *Cancer Res.* 81 (23), 5919–5934. doi:10.1158/0008-5472.CAN-21-1337

Loibl, S., Poortmans, P., Morrow, M., Denkert, C., and Curigliano, G. (2021). Breast cancer. *Lancet* 397 (10286), 1750–1769. doi:10.1016/s0140-6736(20)32381-3

Luu, T. H., Morgan, R. J., Leong, L., Lim, D., McNamara, M., Portnow, J., et al. (2008). A phase II trial of vorinostat (suberoylanilide hydroxamic acid) in metastatic breast cancer: a California Cancer Consortium study. *Clin. Cancer Res.* 14 (21), 7138–7142. doi:10.1158/1078-0432.CCR-08-0122

Mankoff, D. A., Eary, J. F., Link, J. M., Muzi, M., Rajendran, J. G., Spence, A. M., et al. (2007). Tumor-specific positron emission tomography imaging in patients: [18F] fluorodeoxyglucose and beyond. *Clin. Cancer Res.* 13 (12), 3460–3469. doi:10.1158/1078-0432.CCR-07-0074

Marra, A., Trapani, D., Viale, G., Criscitiello, C., and Curigliano, G. (2020). Practical classification of triple-negative breast cancer: intratumoral heterogeneity, mechanisms of drug resistance, and novel therapies. *npj Breast Cancer* 6 (1), 54. doi:10.1038/s41523-020-00197-2

Marullo, R., Werner, E., Degtyareva, N., Moore, B., Altavilla, G., Ramalingam, S. S., et al. (2013). Cisplatin induces a mitochondrial-ROS response that contributes to cytotoxicity depending on mitochondrial redox status and bioenergetic functions. *PLoS One* 8 (11), e81162. doi:10.1371/journal.pone.0081162

Morimoto, K., Kim, S. J., Tanei, T., Shimazu, K., Tanji, Y., Taguchi, T., et al. (2009). Stem cell marker aldehyde dehydrogenase 1-positive breast cancers are characterized by negative estrogen receptor, positive human epidermal growth factor receptor type 2, and high Ki67 expression. *Cancer Sci.* 100 (6), 1062–1068. doi:10.1111/j.1349-7006.2009.01151.x

Nechushtan, H., Hamamreh, Y., Nidal, S., Gotfried, M., Baron, A., Shalev, Y. I., et al. (2015). A phase IIb trial assessing the addition of disulfiram to chemotherapy for the treatment of metastatic non-small cell lung cancer. *Oncologist* 20 (4), 366–367. doi:10.1634/theoncologist.2014-0424

Pan, B., Zhao, D., Liu, Y., Li, N., Song, C., Li, N., et al. (2021). Breast cancer organoids from malignant pleural effusion-derived tumor cells as an individualized medicine platform. *Vitro Cell Dev. Biol. Anim.* 57 (5), 510–518. doi:10.1007/s11626-021-00563-9

Pors, K., and Moreb, J. S. (2014). Aldehyde dehydrogenases in cancer: an opportunity for biomarker and drug development? *Drug Discov. Today* 19 (12), 1953–1963. doi:10.1016/j.drudis.2014.09.009

Qian, X., Xu, W., Xu, J., Shi, Q., Li, J., Weng, Y., et al. (2017). Enolase 1 stimulates glycolysis to promote chemoresistance in gastric cancer. *Oncotarget* 8 (29), 47691–47708. doi:10.18632/oncotarget.17868

Ranasinghe, R., Mathai, M. L., and Zulli, A. (2022). Cisplatin for cancer therapy and overcoming chemoresistance. *Heliyon* 8 (9), e10608. doi:10.1016/j.heliyon.2022.e10608

Samanta, D., Gilkes, D. M., Chaturvedi, P., Xiang, L., and Semenza, G. L. (2014). Hypoxia-inducible factors are required for chemotherapy resistance of breast cancer stem cells. *Proc. Natl. Acad. Sci. U. S. A.* 111 (50), E5429–E5438. doi:10.1073/pnas.1421438111

Singh, S., Brocker, C., Koppaka, V., Chen, Y., Jackson, B. C., Matsumoto, A., et al. (2013). Aldehyde dehydrogenases in cellular responses to oxidative/electrophilic stress. *Free Radic. Biol. Med.* 56, 89–101. doi:10.1016/j.freeradbiomed.2012.11.010

von Minckwitz, G., Untch, M., Blohmer, J. U., Costa, S. D., Eidtmann, H., Fasching, P. A., et al. (2012). Definition and impact of pathologic complete response on prognosis after neoadjuvant chemotherapy in various intrinsic breast cancer subtypes. *J. Clin. Oncol.* 30 (15), 1796–1804. doi:10.1200/JCO.2011.38.8595

Wang, W., He, S., Zhang, R., Peng, J., Guo, D., Zhang, J., et al. (2020). ALDH1A1 maintains the cancer stem-like cells properties of esophageal squamous cell carcinoma by activating the AKT signal pathway and interacting with beta-catenin. *Biomed. Pharmacother.* 125, 109940. doi:10.1016/j.biopha.2020.109940

Warburg, O. (1956). On the origin of cancer cells. *Science* 123 (3191), 309–314. doi:10.1126/science.123.3191.309

Wawruszak, A., Halasa, M., Okon, E., Kukula-Koch, W., and Stepulak, A. (2021). Valproic acid and breast cancer: state of the art in 2021. *Cancers (Basel)* 13 (14), 3409. doi:10.3390/cancers13143409

Wawruszak, A., Luszczki, J. J., Grabarska, A., Gumbarewicz, E., Dmoszynska-Graniczka, M., Polberg, K., et al. (2015). Assessment of interactions between cisplatin and two histone deacetylase inhibitors in MCF7, T47D and MDA-MB-231 human breast cancer cell lines - an isobolographic analysis. *PLoS One* 10 (11), e0143013. doi:10.1371/journal.pone.0143013

Yardley, D. A., Ismail-Khan, R. R., Melichar, B., Lichinitser, M., Munster, P. N., Klein, P. M., et al. (2013). Randomized phase II, double-blind, placebo-controlled study of exemestane with or without entinostat in postmenopausal women with locally recurrent or metastatic estrogen receptor-positive breast cancer progressing on treatment with a nonsteroidal aromatase inhibitor. *J. Clin. Oncol.* 31 (17), 2128–2135. doi:10.1200/JCO.2012.43.7251

Yokoyama, Y., Zhu, H., Lee, J. H., Kossenkov, A. V., Wu, S. Y., Wickramasinghe, J. M., et al. (2016). BET inhibitors suppress ALDH activity by targeting ALDH1A1 super-enhancer in ovarian cancer. *Cancer Res.* 76 (21), 6320–6330. doi:10.1158/0008-5472.CAN-16-0854

Yu, W., Chen, Y., Dubrulle, J., Stossi, F., Putluri, V., Sreekumar, A., et al. (2018). Cisplatin generates oxidative stress which is accompanied by rapid shifts in central carbon metabolism. *Sci. Rep.* 8 (1), 4306. doi:10.1038/s41598-018-22640-y

Yue, H., Hu, Z., Hu, R., Guo, Z., Zheng, Y., Wang, Y., et al. (2022). ALDH1A1 in cancers: bidirectional function, drug resistance, and regulatory mechanism. *Front. Oncol.* 12, 918778. doi:10.3389/fonc.2022.918778

Yun, X., Zhang, K., Wang, J., Pangeni, R. P., Yang, L., Bonner, M., et al. (2018). Targeting USP22 suppresses tumorigenicity and enhances cisplatin sensitivity through ALDH1A3 downregulation in cancer-initiating cells from lung adenocarcinoma. *Mol. Cancer Res.* 16 (7), 1161–1171. doi:10.1158/1541-7786.MCR-18-0042

Zanoni, M., Bravaccini, S., Fabbri, F., and Arienti, C. (2022). Emerging roles of aldehyde dehydrogenase isoforms in anti-cancer therapy resistance. *Front. Med. (Lausanne)* 9, 795762. doi:10.3389/fmed.2022.795762

frontiers | Frontiers in Molecular Biosciences

TYPE Perspective
PUBLISHED 20 November 2023
DOI 10.3389/fmolb.2023.1274221

OPEN ACCESS

EDITED BY
Or Kakhlon,
Hadassah Medical Center, Israel

REVIEWED BY
Shen Chen,
Sun Yat-sen University, China

*CORRESPONDENCE
Shihori Tanabe,
stanabe@nihs.go.jp

RECEIVED 08 August 2023
ACCEPTED 08 November 2023
PUBLISHED 20 November 2023

CITATION
Esterhuizen M, Park C-B, Kim YJ, Kim T-Y, Yoon H, Andres F, Rodriguez-Rodriguez R and Tanabe S (2023), A perspective on the role of physiological stresses in cancer, diabetes and cognitive disease as environmental diseases.
Front. Mol. Biosci. 10:1274221.
doi: 10.3389/fmolb.2023.1274221

A perspective on the role of physiological stresses in cancer, diabetes and cognitive disease as environmental diseases

Maranda Esterhuizen[1], Chang-Beom Park[2], Young Jun Kim[3], Tae-Young Kim[4], Hakwon Yoon[2], Frederic Andres[5], Rosalia Rodriguez-Rodriguez[6,7] and Shihori Tanabe[8]*

[1]Ecosystems and Environment Research Programme, Faculty of Biological and Environmental Sciences, University of Helsinki, Lahti, Finland, [2]Environmental Exposure and Toxicology Research Center, Korea Institute Toxicology (KIT), Jinju, Republic of Korea, [3]Korean Institute of Science and Technology Europe (KIST Europe), Saarbrücken, Germany, [4]School of Earth Sciences and Environmental Engineering, Gwangju Institute of Science and Technology (GIST), Gwangju, Republic of Korea, [5]Digital Content and Media Sciences Research Division, National Institute of Informatics, Tokyo, Japan, [6]Department of Basic Sciences, Faculty of Medicine and Health Sciences, Universitat Internacional de Catalunya (UIC Barcelona), Barcelona, Spain, [7]Centro de Investigación Biomédica en Red de Fisiopatología de la Obesidad y la Nutrición (CIBEROBN), Instituto de Salud Carlos III, Madrid, Spain, [8]Division of Risk Assessment, Center for Biological Safety and Research, National Institute of Health Sciences, Kawasaki, Japan

With rapid industrialization, urbanization, and climate change, the impact of environmental factors on human health is becoming increasingly evident and understanding the complex mechanisms involved is vital from a healthcare perspective. Nevertheless, the relationship between physiological stress resulting from environmental stressors and environmental disease is complex and not well understood. Chronic exposure to environmental stressors, such as air and water contaminants, pesticides, and toxic metals, has been recognized as a potent elicitor of physiological responses ranging from systemic inflammation to immune system dysregulation causing or progressing environmental diseases. Conversely, physiological stress can exacerbate susceptibility to environmental diseases. Stress-induced alterations in immune function and hormonal balance may impair the ability to detoxify harmful substances and combat pathogens. Additionally, prolonged stress can impact lifestyle choices, leading to harmful behaviors. Understanding the link between physiological stress and environmental disease requires a systematic, multidisciplinary approach. Addressing this complex relationship necessitates the establishment of a global research network. This perspective discusses the intricate interplay between physiological stress and environmental disease, focusing on common environmental diseases, cancer, diabetes, and cognitive degeneration. Furthermore, we highlight the intricate and reciprocal nature of the connection between physiological stress and these environmental diseases giving a perspective on the current state of knowledge as well as identifying where further information is necessary. Recognizing the role of physiological stress in environmental health outcomes will aid in the development of comprehensive strategies to safeguard public health and promote ecological balance.

KEYWORDS

environmental stressors, reactive oxygen species, environmental disease, human health, cancer, cognitive function, diabetes

1 Introduction

Failure of an organism to respond adequately to stimuli, whether originating internally or externally, resulting in the disruption of cellular homeostasis can be classified as stress. Stress may stem from physical, physiological, and psychological sources. Physiological stress primarily occurs when the body faces environmental challenges, which alter normal physiological functionality, which is the focus of this perspective. Environmental stresses encompass a wide range of factors, including exposure to extreme temperatures, radiation, toxins, and pollution, including inadequate access to clean water and sanitation. These stressors can lead to oxidative stress which may result in lipid peroxidation, DNA mutations or damage, and protein oxidation, as well as weaken the immune system, cause inflammation, contributing to environmental diseases (Lovallo, 2005; Thanan et al., 2014) as depicted in Figure 1. For example, Thanan et al. (2014) reviewed the role of oxidative stress stemming from exposure to environmental factors in the development and progression of cancer and neurodegenerative disease. Furthermore, collection of Adverse Outcome Pathways (AOPs) dedicated to understanding the effects of reactive oxygen species (ROS) originating from environmental stressor exposure, related to disease development and progression, has been established with several hundreds of AOPs registered (Tanabe et al., 2022; Tanabe et al., 2023). Thus, the environment is central to human health in terms of disease development and progression.

At a cellular level, responses to stress are mediated by multifaceted interactions, including the nervous, endocrine, and immune systems and are adaptive to counteract acute instances effectively. However, repetitive or prolonged, chronic exposure to stress may cause maladapted responses and impact cellular physiology, resulting in the development and exacerbation of many diseases (Yang et al., 2014; Ketchesin et al., 2017). Furthermore, stress responses primarily mediated by the release of stress hormones like cortisol, can have profound effects on immune, metabolic and cognitive functions, as well as cardiovascular health, and neurological function (Russell and Lightman, 2019). Moreover, a weakened immune system could contribute to susceptibility to infections and diseases (Pedersen et al., 2011).

Individuals with compromised immune systems are more susceptible to developing respiratory issues, allergies, and autoimmune disorders related to environmental stresses (Glaser and Kiecolt-Glaser, 2005). Excessive inflammation has been associated with cardiovascular problems, respiratory disorders, and specific types of cancer (Steptoe et al., 2007; Manisalidis et al., 2020). Environmental pollutants can also induce oxidative stress, accelerating cell damage and increasing the risk of cancer, neurodegenerative disorders, and respiratory conditions (Halliwell and Gutteridge, 2015). Furthermore, hormonal disruption, caused by endocrine disruptors like pesticides and plasticizers, can impact reproductive health and raise the likelihood of hormone-related cancers (Zoeller et al., 2012). Moreover, neurotoxic substances such as heavy metals and organophosphates can impair neuronal development, leading to behavioral disorders and neurodegenerative diseases (Grandjean and Landrigan, 2006).

Many of the toxic effects induced by environmental stressors have been found to be mediated by the regulation or induction of apoptosis and redox signaling (West, 2000; Abdollahi et al., 2004; Assefa et al., 2005; Ryter et al., 2007; Valko et al., 2007), and their

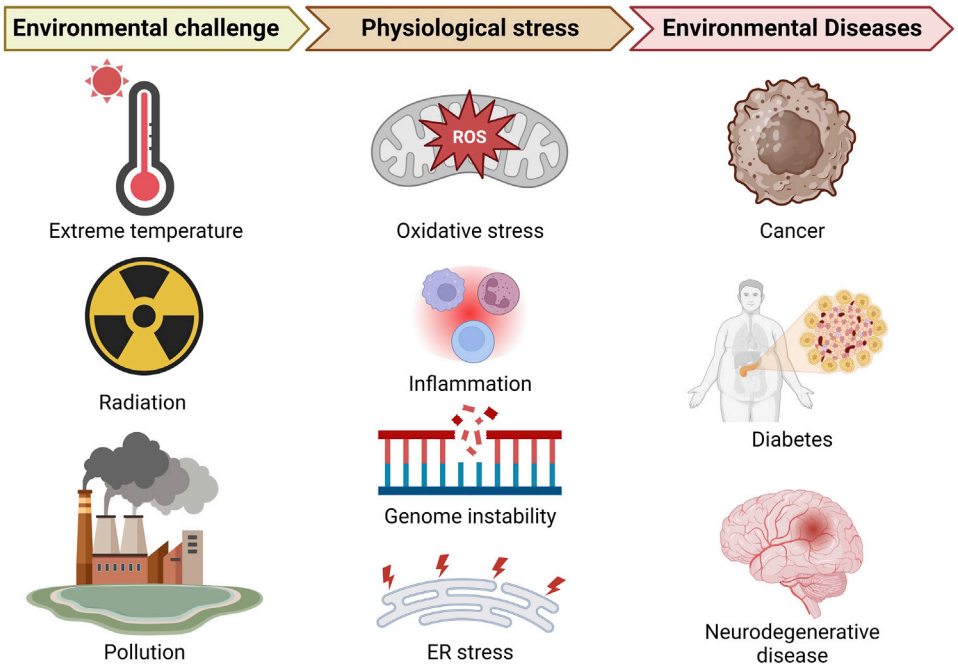

FIGURE 1
Compact depiction of physiological stress linking selected environmental stressors and the environmental diseases discussed in this perspective (created with the aid of BioRender.com).

deregulation associated to the etiology of many environmental diseases (Fadeel and Orrenius, 2005). Although redox signaling has been primarily linked to activating distinct apoptotic pathways in response to environmental stress, the direct molecular mechanisms involved remain elusive. In other words, although many toxicological studies have investigated cellular responses to environmental stress and the implication of oxidative stress in disease [reviewed by Kruk et al. (2019)], a clear understanding of the mechanistic events related to disease onset and progression is still lacking. The involvement of oxidative stress in the development of selected environmental diseases will be dealt with in more detail in the following sections.

As research towards understanding how environmental risk factors influence the development and progression of environmental diseases will lead to improved public health, understanding the underlying mechanisms in physiological stress related to disease becomes evident. In this perspective article, the current state of knowledge on the implication of physiological stress in environmental disease will be concisely assessed, especially concerning cancer, diabetes, and cognitive diseases, highlighting the knowledge gaps in understanding the mechanisms relating to physiological stress, and particularly oxidative stress, to disease etiology. We highlight existing and identify knowledge gaps that require further investigation to comprehend the underlying mechanisms involved in developing environmental diseases.

2 Cancer

Environmental risk factors, such as exposure to carcinogens and pollutants, contribute to the onset and progression of cancer. Petrinović et al. (2023) reviewed inflammation as a link between stress and cancer. Furthermore, physiological stress has been implicated in the activation of tumor progression genes (Zweitzig et al., 2007). By contrast, oxidative stress is considered a driver of cancer dormancy; however, disease recurrence after prolonged dormancy is a significant cause of cancer-associated mortality (Payne, 2022). The balance of the microenvironment is thought to be involved in cancer development (Chipurupalli et al., 2019). Hypoxic microenvironment condition induces adaptive responses such as endoplasmic reticulum (ER) stress response, unfolded protein response, anti-oxidative responses, and autophagy in cancer, which allows the adaption to a stressful microenvironment of cancer (Chipurupalli et al., 2019). Autophagy is a catabolic intracellular nutrient scavenging pathway triggered by nutrient deprivation and stress, which is upregulated in many cancers and in response to cancer therapy to confer treatment resistance (White et al., 2021). Genome instability, which is the consequence of DNA lesions that can result from errors in DNA replication, from the action of genotoxic compounds, including cellular metabolites or from ultraviolet (UV) and ionizing radiation, is a hallmark of cancer (Gaillard et al., 2015). DNA replication stress is a feature present in most cancers, which is induced by oncogenes inducing sustained proliferation and induces other cancer hallmarks, escape from apoptosis and genomic instability (Macheret and Halazonetis, 2015).

A recent review has proposed that ROS contribute to gastric cancer vascularization (Biagioni et al., 2023). Chronic ROS and oxidative stress can consequently suppress the antioxidant system and induce several signaling pathways such as interleukin-6 receptor (IL-6R)/gp130/STAT3 signaling pathway, leading to radiotherapy-resistant gastric cancer (Gu et al., 2018). Despite the already advanced insights into cancer development and progression, the complete mechanisms that link chronic stress to cancer remain incompletely understood. Nevertheless, physiological stresses clearly play central roles in cancer etiology and elucidation of this link is vital for the advancement of cancer therapeutics.

3 Diabetes

The acute activation of stress-related neuroendocrine systems contributes to maintain homeostasis; however, chronic and excessive stress can play a decisive role in the onset and progression of metabolic diseases such as type 2 diabetes (Hackett and Steptoe, 2017; Kautzky et al., 2022; Kivimäki et al., 2023). In response to stress, rapid alterations in central and peripheral metabolism and hormone trafficking occur by several biological pathways contributing to diabetes etiology: i) upregulation of the hypothalamic-pituitary-adrenal (HPA) axis with cortisol release, ii) activation of the sympathetic nervous system, and iii) inflammatory processes and oxidative stress. Under chronic stress, release of the corticotropin-releasing hormone from the hypothalamus leads to HPA axis activation, finally target adrenal cortex and promote the release of glucocorticoid cortisol, with relevant functions, many of them related to glucose homeostasis and mobilization of energy stores (Kagias et al., 2012; Kuo et al., 2015; Li and Cummins, 2022). Glucocorticoids stimulate hepatic gluconeogenesis and glycogen depletion, attenuate glucose update in muscle and adipose tissue, and antagonize insulin metabolic actions, promoting hyperglycemia and insulin resistance (Kuo et al., 2015; Li and Cummins, 2022). Cortisol-related stress pathways can also gradually induce visceral fat accumulation and pancreatic β-cell production and secretion of insulin. Activation of the immune system and chronic inflammatory processes is also a crucial mechanism by which stress influences the risk of developing diabetes (Donath and Shoelson, 2011). Chronic hyperglycemia is also leading to cellular disruption with mitochondrial dysfunction, ROS production, ER stress, and alterations of autophagy (Burgos-Morón et al., 2019). Cortisol release in response to stress, increases blood pressure and heart rate via sympathetic system activation (Brotman et al., 2007; Ulrich-Lai and Herman, 2009), thanks to the release of adrenaline, which also induces energy mobilization and the release of pro-inflammatory cytokines and insulin resistance (Emdin et al., 2005; Brotman et al., 2007; Ulrich-Lai and Herman, 2009).

Altogether, chronic changes in several stress-responsive biological systems influence glucose homeostasis and insulin metabolic actions and subsequently increase the risk of diabetes. Interventions based on stress management seem to alleviate stress symptoms and glycemia in patients with type 2 diabetes, but the impact of this intervention on disease progression has not been clearly established yet. Also, whether glucose and insulin levels can

be directly disrupted by chronic stress or indirectly affected through these pathways is a matter of debate.

4 Cognitive function and neurodegradation

The interplay between environmental risk factors and their impact on cognitive function and neurological disorders has become an increasingly significant area of concern in recent years. While stress is well-documented for its capacity to induce structural alterations in the brain, thereby influencing cognition and memory (Lupien et al., 2009), a broader spectrum of environmental stressors is now being recognized for their potential role in this complex relationship.

Beyond psychological stress, which is known to affect cognitive function, environmental stressors such as extreme temperature conditions (Taylor et al., 2016; Martin et al., 2019) and exposure to pollutants have been found to significantly impact cognitive performance. For example, Kishore et al. (2013) demonstrated that the ingestion of tyrosine can enhance the preservation of cognitive function during passive heat stress, correlated with increased levels of dopamine and epinephrine. Despite this indication of the importance of tyrosine, the underlying mechanism remains elusive.

Furthermore, it is crucial to acknowledge that other environmental stressors have firmly established their negative influence on cognitive health. Air pollution (Lopuszanska and Samardakiewicz, 2020; Gao et al., 2021) and heavy metal exposure (Wang and Matsushita, 2021) have both been associated with cognitive impairments. In a comprehensive review by Singh et al. (2019), it was highlighted that ROS, stemming from exposure to environmental stressors such as ultraviolet and ionizing radiation, as well as chemical pollution, play a central role in neurodegeneration and neurological disorders.

In addition to environmental stressors, inflammation has emerged as a central contributor to cognitive impairment (Leonardo and Fregni, 2023). The central nervous system's susceptibility to oxidative damage caused by radicals (Cui et al., 2004) emphasizes the significant role of oxidative stress in the onset and progression of neurodegenerative disorders (Angelova and Abramov, 2018; Singh et al., 2019). This sensitivity arises from the abundance of unsaturated fatty acids and oxygen, making lipid peroxidation a critical process (Cobley et al., 2018). Furthermore, an elevated oxidative stress status, coupled with increased apoptosis, has been shown to contribute to the pathogenesis of neurodegeneration (Bhat et al., 2015). Moreover, free radicals have been implicated in the development and progression of cognitive deficits through their disruptive effects on synaptic transmission, mitochondrial function, neuroinflammation, and axonal transport (Cui et al., 2004; Angelova and Abramov, 2018; Cobley et al., 2018).

While it is evident that oxidative stress and inflammation play pivotal roles, the precise cellular and molecular mechanisms by which stress impairs cognitive function remain incompletely understood. Additionally, our knowledge concerning the impact of diverse environmental stressors on cognitive function and neurodegeneration remains limited. It is imperative to comprehend the link between physiological stress and cognitive function to develop interventions aimed at mitigating the adverse effects of stress on the brain, thus optimizing cognitive performance and overall wellbeing.

Significant strides have been taken in understanding how stress affects cognitive function, yet there exist numerous gaps in our understanding that necessitate further research. These gaps encompass the factors of individual variability, such as age, sex, predisposition, resilience, and more, as well as the timing and duration of stress exposure and the interactions with other contributing factors. The relationship between neurological disorders and environmental influences is intricate and multifaceted, requiring ongoing exploration to uncover the intricate mechanisms, variations among individuals, and the potential for interventions to ameliorate the detrimental effects of stress on cognition.

5 Discussion

The link between physiological stress and environmental disease is a complex and significant aspect of public health. The One-Health concept acknowledges the interconnectedness of human health, animal health, and environmental health. It underscores the significance of considering the health of humans, animals, and the environment in an integrated manner to achieve optimal health outcomes. Concerning environmental diseases, the One-Health approach recognizes that environmental factors exert a substantial influence on human health (Lippi et al., 2022). This includes understanding how emerging pollutants such as air particulate matter or emerging pollutants contribute to the development or exacerbation of various diseases in both humans and animals (Flies et al., 2019). By adopting this approach, a better understanding of the intricate interactions between the environment and human health can be achieved, thereby enabling the formulation of more effective strategies for preventing and managing environmental diseases.

This perspective aimed to deliver a concise overview of how physiological stresses can significantly impact human health and increase the risk of developing various environmental diseases. In most cases, the link between chronic physiological stress and disease etiology, primarily occurs via causing oxidative stress, disrupting the body's stress response system, leading to hormonal imbalances, increased inflammation, and impaired immune function. Thus, prolonged physiological stress can contribute to developing environmental diseases such as cardiovascular disorders, gastrointestinal problems, immune system dysfunction, and mental health disorders.

The relationship between environmental risk factors and environmental diseases has not been clearly elucidated to date, particularly pertaining to molecular mechanisms. To accurately determine the increased disease risk resulting from stress responses, further scientific evidence is required regarding the effects of different stressors, their severity, and the duration of stress (acute or chronic) on the physiological and metabolic responses in the body. In particular, the complex nature of chemical toxicants, such as non-linear dose-response relationships and mixture effects, hinders the attainment of consistent results in toxicological studies (Lee, 2012). Therefore, it is essential to establish a systematic pre- and post-management system for effectively addressing environmental disease studies. This system should encompass the categorization of environmental

disease occurrence based on exposure to exogenous risk factors, as well as hazard and risk assessment considering exposure scenarios, symptoms, and induction pathways. Moreover, considering the actual environmental conditions characterized by chronic exposure to low concentrations, future research should be discussed revolving around epigenome-based biomarkers, exposomes, and intergenerational effects (Wild, 2005). Furthermore, since environmental diseases arise from chronic exposure to environmental stressors, it is crucial to demonstrate the risk and persistence of these diseases under various conditions such as age, gender, and health status. A noteworthy consideration for future investigation is individual susceptibility to these stresses which can vary based on genetic factors, lifestyle choices, and overall health status (Rea, 2017; Mancinelli et al., 2021). Furthermore, prolonged exposure may not necessarily directly cause environmental diseases but can significantly increase the risk or exacerbate pre-existing conditions (Li et al., 2023). Thus, understanding the underlying mechanism involved in disease development and progression regulated by environmental factors is essential. To this end, the establishment of a global research network through collaborative efforts with specialized research institutes and researchers worldwide is necessary.

By taking a holistic approach to healthcare, addressing both physiological and environmental stresses, healthcare providers can improve their patient's overall health and quality of life. It emphasizes the importance of early intervention and promoting a healthy lifestyle to mitigate the impact of stressors on health. Understanding the role of physiological stresses in diseases is crucial for healthcare professionals in terms of prevention, diagnosis, and treatment. Understanding and addressing the connection between physiological stress and environmental disease is crucial for formulating effective public health strategies to protect and promote the wellbeing of individuals in an increasingly polluted and stress-inducing world. By identifying and addressing these stresses, healthcare providers can develop strategies to mitigate their impact on health and improve patient outcomes. This may involve lifestyle modifications, stress management techniques, environmental interventions, and targeted medical interventions. Overall, physiological stresses play a complex and multifaceted role in the development and progression of diseases. By recognizing and managing these stresses, healthcare professionals can help individuals sustain optimal health and wellbeing and ultimately, this knowledge will contribute to improved advanced methodologies aimed at mitigating the impact of environmental risk factors on human health.

Data availability statement

The original contributions presented in the study are included in the article/Supplementary Material, further inquiries can be directed to the corresponding author.

Author contributions

ME: Conceptualization, Writing–original draft, Writing–review and editing. C-BP: Conceptualization, Writing–original draft, Writing–review and editing. YK: Conceptualization, Writing–original draft, Writing–review and editing. T-YK: Conceptualization, Visualization, Writing–original draft, Writing–review and editing. HY: Conceptualization, Writing–original draft, Writing–review and editing. FA: Writing–review and editing. RR-R: Conceptualization, Writing–original draft, Writing–review and editing. ST: Conceptualization, Funding acquisition, Project administration, Writing–original draft, Writing–review and editing.

Funding

The author(s) declare financial support was received for the research, authorship, and/or publication of this article. This work was funded by Japan Agency for Medical Research and Development (AMED), Grant Number JP21mk0101216 (ST), JP22mk0101216 (ST), JP23mk0101216 (ST), and JSPS KAKENHI Grant Number 21K12133 (ST). This work is partially supported by the strategies for establishing global research networks in the National Research Council of Science and Technology (NST) grant (SK-2113).

Acknowledgments

The authors would like to acknowledge the members of the National Institutes of Health Sciences, Japan. We wish to thank Jonghyun Kim (GIST) for assistance with the graphical illustration.

Conflict of interest

The authors declare that the research was conducted in the absence of any commercial or financial relationships that could be construed as a potential conflict of interest.

The authors declared that they were an editorial board member of Frontiers, at the time of submission. This had no impact on the peer review process and the final decision.

Publisher's note

References

Abdollahi, M., Ranjbar, A., Shadnia, S., Nikfar, S., and Rezaie, A. (2004). Pesticides and oxidative stress: a review. *Med. Sci. Monit.* 10, RA141–147.

Angelova, P. R., and Abramov, A. Y. (2018). Role of mitochondrial ROS in the brain: from physiology to neurodegeneration. *FEBS Lett.* 592 (5), 692–702. doi:10.1002/1873-3468.12964

Assefa, Z., Van Laethem, A., Garmyn, M., and Agostinis, P. (2005). Ultraviolet radiation-induced apoptosis in keratinocytes: on the role of cytosolic factors. *Biochim. Biophys. Acta* 1755, 90–106. doi:10.1016/j.bbcan.2005.04.001

Bhat, A. H., Dar, K. B., Anees, S., Zargar, M. A., Masood, A., Sofi, M. A., et al. (2015). Oxidative stress, mitochondrial dysfunction and neurodegenerative diseases; a mechanistic insight. *Biomed. Pharmacother.* 74, 101–110. doi:10.1016/j.biopha.2015.07.025

Biagioni, A., Peri, S., Versienti, G., Fiorillo, C., Becatti, M., Magnelli, L., et al. (2023). Gastric cancer vascularization and the contribution of reactive oxygen species. *Biomolecules* 13 (6), 886. doi:10.3390/biom13060886

Brotman, D. J., Golden, S. H., and Wittstein, I. S. (2007). The cardiovascular toll of stress. *Lancet* 370, 1089–1100. doi:10.1016/S0140-6736(07)61305-1

Burgos-Morón, E., Abad-Jiménez, Z., de Marañón, A. M., Iannantuoni, F., Escribano-López, I., López-Domènech, S., et al. (2019). Relationship between oxidative stress, ER stress, and inflammation in type 2 diabetes: the battle continues. *J. Clin. Med.* 8, 1385. doi:10.3390/jcm8091385

Chipurupalli, S., Kannan, E., Tergaonkar, V., D'Andrea, R., and Robinson, N. (2019). Hypoxia induced ER stress response as an adaptive mechanism in cancer. *Int. J. Mol. Sci.* 20 (3), 749. doi:10.3390/ijms20030749

Cobley, J. N., Fiorello, M. L., and Bailey, D. M. (2018). 13 reasons why the brain is susceptible to oxidative stress. *Redox Biol.* 15, 490–503. doi:10.1016/j.redox.2018.01.008

Cui, K., Luo, X., Xu, K., and Murthy, M. V. (2004). Role of oxidative stress in neurodegeneration: recent developments in assay methods for oxidative stress and nutraceutical antioxidants. *Prog. Neuro-Psychopharmacol. Biol. Psychiatry* 28 (5), 771–799. doi:10.1016/j.pnpbp.2004.05.023

Donath, M. Y., and Shoelson, S. E. (2011). Type 2 diabetes as an inflammatory disease. *Nat. Rev. Immunol.* 11, 98–107. doi:10.1038/nri2925

Emdin, C. A., Anderson, S. G., Woodward, M., and Rahimi, K. (2005). Usual blood pressure and risk of new-onset diabetes: evidence from 4.1 million adults and a meta-analysis of prospective studies. *J. Am. Coll. Cardiol.* 66, 1552–1562. doi:10.1016/J.JACC.2015.07.059

Fadeel, B., and Orrenius, S. (2005). Apoptosis: a basic biological phenomenon with wide-ranging implications in human disease. *J. Intern. Med.* 258, 479–517. doi:10.1111/j.1365-2796.2005.01570.x

Flies, E. J., Mavoa, S., Zosky, G. R., Mantzioris, E., Williams, C., Eri, R., et al. (2019). Urban-associated diseases: candidate diseases, environmental risk factors, and a path forward. *Environ. Int.* 133, 105187. doi:10.1016/j.envint.2019.105187

Gaillard, H., García-Muse, T., and Aguilera, A. (2015). Replication stress and cancer. *Nat. Rev. Cancer.* 15, 276–289. doi:10.1038/nrc3916

Gao, H., Shi, J., Cheng, H., Zhang, Y., and Zhang, Y. (2021). The impact of long-and short-term exposure to different ambient air pollutants on cognitive function in China. *Environ. Int.* 151, 106416. doi:10.1016/j.envint.2021.106416

Glaser, R., and Kiecolt-Glaser, J. K. (2005). Stress-induced immune dysfunction: implications for health. *Nat. Rev. Immunol.* 5 (3), 243–251. doi:10.1038/nri1571

Grandjean, P., and Landrigan, P. J. (2006). Developmental neurotoxicity of industrial chemicals. *Lancet* 368 (9553), 2167–2178. doi:10.1016/S0140-6736(06)69665-7

Gu, H., Huang, T., Shen, Y., Liu, Y., Zhou, F., Jin, Y., et al. (2018). Reactive oxygen species-mediated tumor microenvironment transformation: the mechanism of radioresistant gastric cancer. *Oxid. Med. Cell* 2018, 5801209. doi:10.1155/2018/5801209

Hackett, R. A., and Steptoe, A. (2017). Type 2 diabetes mellitus and psychological stress-A modifiable risk factor. *Nat. Rev. Endocrinol.* 13, 547–560. doi:10.1038/nrendo.2017.64

Halliwell, B., and Gutteridge, J. M. C. (2015). *Free radicals in biology and medicine*. 5th ed. Oxford: Oxford Academic. doi:10.1093/acprof:oso/9780198717478.001.0001

Kagias, K., Nehammer, C., and Pocock, R. (2012). Neuronal responses to physiological stress. *Front. Genet.* 3, 222. doi:10.3389/fgene.2012.00222

Kautzky, A., Heneis, K., Stengg, K., Fröhlich, S., and Kautzky-Willer, A. (2022). Biological and psychological stress correlates are linked to glucose metabolism, obesity, and gender roles in women. *Neuroendocrinology* 112, 130–142. doi:10.1159/000514484

Ketchesin, K. D., Stinnett, G. S., and Seasholtz, A. F. (2017). Corticotropin-releasing hormone-binding protein and stress: from invertebrates to humans. *Stress* 20 (5), 449–464. doi:10.1080/10253890.2017.1322575

Kishore, K., Ray, K., Anand, J. P., Thakur, L., Kumar, S., and Panjwani, U. (2013). Tyrosine ameliorates heat induced delay in event related potential P300 and contingent negative variation. *Brain Cogn.* 83 (3), 324–329. doi:10.1016/j.bandc.2013.09.005

Kivimäki, M., Bartolomucci, A., and Kawachi, I. (2023). The multiple roles of life stress in metabolic disorders. *Nat. Rev. Endocrinol.* 19, 10–27. doi:10.1038/s41574-022-00746-8

Kruk, J., Aboul-Enein, H. Y., Kładna, A., and Bowser, J. E. (2019). Oxidative stress in biological systems and its relation with pathophysiological functions: the effect of physical activity on cellular redox homeostasis. *Free Radic. Res.* 53 (5), 497–521. doi:10.1080/10715762.2019.1612059

Kuo, T., McQueen, A., Chen, T. C., and Wang, J. C. (2015). Regulation of glucose homeostasis by glucocorticoids. *Adv. Exp. Med. Biol.* 872, 99–126. doi:10.1007/978-1-4939-2895-8_5

Lee, D. H. (2012). Endocrine disrupting chemicals and environmental diseases. *J. Korean Med. Assoc.* 55 (3), 243–249. doi:10.5124/jkma.2012.55.3.243

Leonardo, S., and Fregni, F. (2023). Association of inflammation and cognition in the elderly: a systematic review and meta-analysis. *Front. Aging Neurosci.* 15, 1069439. doi:10.3389/fnagi.2023.1069439

Li, A., Toll, M., Martino, E., Wiesel, I., Botha, F., and Bentley, R. (2023). Vulnerability and recovery: long-term mental and physical health trajectories following climate-related disasters. *Soc. Sci. Med.* 320, 115681. doi:10.1016/j.socscimed.2023.115681

Li, J. X., and Cummins, C. L. (2022). Fresh insights into glucocorticoid-induced diabetes mellitus and new therapeutic directions. *Nat. Rev. Endocrinol.* 18, 540–557. doi:10.1038/s41574-022-00683-6

Lippi, L., Sire, A. D., Folli, A., Turco, A., Moalli, S., Ammendolia, A., et al. (2022). Environmental factors in the rehabilitation framework: role of the one health approach to improve the complex management of disability. *Int. J. Environ. Res. Public Health.* 19, 155186. doi:10.3390/ijerph192215186

Lopuszanska, U., and Samardakiewicz, M. (2020). The relationship between air pollution and cognitive functions in children and adolescents: a systematic review. *Cogn. Behav. Neurol.* 33 (3), 157–178. doi:10.1097/WNN.0000000000000235

Lovallo, W. R. (2005). *Stress & health: biological and psychological interactions*. United States: SAGE Publications Inc. doi:10.4135/9781452233543

Lupien, S. J., McEwen, B. S., Gunnar, M. R., and Heim, C. (2009). Effects of stress throughout the lifespan on the brain, behaviour and cognition. *Nat. Rev. Neurosci.* 10 (6), 434–445. doi:10.1038/nrn2639

Macheret, M., and Halazonetis, T. D. (2015). DNA replication stress as a hallmark of cancer. *Annu. Rev. Pathol.* 10, 425–448. doi:10.1146/annurev-pathol-012414-040424

Mancinelli, R., Checcaglini, F., Coscia, F., Gigliotti, P., Fulle, S., and Fanò-Illic, G. (2021). Biological aspects of selected myokines in skeletal muscle: focus on aging. *Int. J. Mol. Sci.* 22, 8520. doi:10.3390/ijms22168520

Manisalidis, I., Stavropoulou, E., Stavropoulos, A., and Bezirtzoglou, E. (2020). Environmental and health impacts of air pollution: a review. *Front. Public Health* 8, 14. doi:10.3389/fpubh.2020.00014

Martin, K., McLeod, E., Périard, J., Rattray, B., Keegan, R., and Pyne, D. B. (2019). The impact of environmental stress on cognitive performance: a systematic review. *Hum. Factors* 61 (8), 1205–1246. doi:10.1177/0018720819839817

Payne, K. K. (2022). Cellular stress responses and metabolic reprogramming in cancer progression and dormancy. *Semin. Cancer Biol.* 78, 45–48. doi:10.1016/j.semcancer.2021.06.004

Pedersen, A. F., Bovbjerg, D. H., and Zachariae, R. (2011). "Stress and susceptibility to infectious disease," in *The handbook of stress science: biology, psychology, and health* (Berlin, Germany: Springer), 425–445.

Petrinović, S. V., Milošević, M. S., Marković, D., and Momčilović, S. (2023). Interplay between stress and cancer—a focus on inflammation. *Front. Physiol.* 14, 1119095. doi:10.3389/fphys.2023.1119095

Rea, I. M. (2017). Towards ageing well: use it or lose it: exercise, epigenetics and cognition. *Biogerontology* 18 (4), 679–691. doi:10.1007/s10522-017-9719-3

Russell, G., and Lightman, S. (2019). The human stress response. *Nat. Rev. Endocrinol.* 15, 525–534. doi:10.1038/s41574-019-0228-0

Ryter, S. W., Kim, H. P., Hoetzel, A., Park, J. W., Nakahira, K., Wang, X., et al. (2007). Mechanisms of cell death in oxidative stress. *Antioxid. Redox Signal* 9, 49–89. doi:10.1089/ars.2007.9.49

Singh, A., Kukreti, R., Saso, L., and Kukreti, S. (2019). Oxidative stress: a key modulator in neurodegenerative diseases. *Molecules* 24 (8), 1583. doi:10.3390/molecules24081583

Steptoe, A., Hamer, M., and Chida, Y. (2007). The effects of acute psychological stress on circulating inflammatory factors in humans: a review and meta-analysis. *Brain Behav. Immun.* 21 (7), 901–912. doi:10.1016/j.bbi.2007.03.011

Tanabe, S., Beaton, D., Chauhan, V., Choi, I., Choi, J., Clerbaux, L.-A., et al. (2023). Report of the 3rd and 4th mystery of reactive oxygen species conference. *ALTEX - Altern. animal Exp.* 40 (4), 689–693. doi:10.14573/altex.2307041

Tanabe, S., O'Brien, J., Tollefsen, K. E., Kim, Y., Chauhan, V., Yauk, C., et al. (2022). Reactive oxygen species in the adverse outcome pathway framework: toward creation of harmonized consensus key events. *Front. Toxicol.* 4, 887135. doi:10.3389/ftox.2022.887135

Taylor, L., Watkins, S. L., Marshall, H., Dascombe, B. J., and Foster, J. (2016). The impact of different environmental conditions on cognitive function: a focused review. *Front. Physiol.* 6, 372. doi:10.3389/fphys.2015.00372

Thanan, R., Oikawa, S., Hiraku, Y., Ohnishi, S., Ma, N., Pinlaor, S., et al. (2014). Oxidative stress and its significant roles in neurodegenerative diseases and cancer. *Int. J. Mol. Sci.* 16 (1), 193–217. doi:10.3390/ijms16010193

Ulrich-Lai, Y. M., and Herman, J. P. (2009). Neural regulation of endocrine and autonomic stress responses. *Nat. Rev. Neurosci.* 10, 397–409. doi:10.1038/nrn2647

Valko, M., Leibfritz, D., Moncol, J., Cronin, M. T., Mazur, M., and Telser, J. (2007). Free radicals and antioxidants in normal physiological functions and human disease. *Int. J. Biochem. Cell Biol.* 39, 44–84. doi:10.1016/j.biocel.2006.07.001

Wang, H., and Matsushita, M. T. (2021). Heavy metals and adult neurogenesis. *Curr. Opin. Toxicol.* 26, 14–21. doi:10.1016/j.cotox.2021.03.006

West, I. C. (2000). Radicals and oxidative stress in diabetes. *Diabet. Med.* 17, 171–180. doi:10.1046/j.1464-5491.2000.00259.x

White, E., Lattime, E. C., and Guo, J. Y. (2021). Autophagy regulates stress responses, metabolism, and anticancer immunity. *Trends Cancer* 7 (8), 778–789. doi:10.1016/j.trecan.2021.05.003

Wild, C. (2005). Complementing the genome with an "exposome": the outstanding challenge of environmental exposure measurement in molecular epidemiology. *Cancer Epidemiol. Biomarkers Prev.* 14 (8), 1847–1850. doi:10.1158/1055-9965.EPI-05-0456

Yang, C., Guo, X., Wang, G. H., Wang, H. L., Liu, Z. C., Liu, H., et al. (2014). Changes in tau phosphorylation levels in the hippocampus and frontal cortex following chronic stress. *Braz. J. Med. Biol. Res.* 47, 237–244. doi:10.1590/1414-431X20133275

Zoeller, R. T., Brown, T. R., Doan, L. L., Gore, A. C., Skakkebaek, N. E., Soto, A. M., et al. (2012). Endocrine-disrupting chemicals and public health protection: a statement of principles from the Endocrine Society. *Endocrinology* 153 (9), 4097–4110. doi:10.1210/en.2012-1422

Zweitzig, D. R., Smirnov, D. A., Connelly, M. C., Terstappen, L. W., O'Hara, S. M., and Moran, E. (2007). Physiological stress induces the metastasis marker AGR2 in breast cancer cells. *Mol. Cell. Biochem.* 306, 255–260. doi:10.1007/s11010-007-9562-y

frontiers | Frontiers in Cell and Developmental Biology

TYPE Review
PUBLISHED 20 November 2023
DOI 10.3389/fcell.2023.1276217

OPEN ACCESS

EDITED BY
Ann Saada,
Hebrew University of Jerusalem, Israel

REVIEWED BY
Jacopo Di Gregorio,
University of L'Aquila, Italy
Or Kakhlon,
Hadassah Medical Center, Israel

*CORRESPONDENCE
Xiaoshuang Zhou,
xiaoshuangzhou66@163.com

RECEIVED 11 August 2023
ACCEPTED 08 November 2023
PUBLISHED 20 November 2023

CITATION
Zhao L, Hao Y, Tang S, Han X, Li R and Zhou X (2023), Energy metabolic reprogramming regulates programmed cell death of renal tubular epithelial cells and might serve as a new therapeutic target for acute kidney injury.
Front. Cell Dev. Biol. 11:1276217.
doi: 10.3389/fcell.2023.1276217

Energy metabolic reprogramming regulates programmed cell death of renal tubular epithelial cells and might serve as a new therapeutic target for acute kidney injury

Limei Zhao[1], Yajie Hao[1], Shuqin Tang[1], Xiutao Han[2], Rongshan Li[3] and Xiaoshuang Zhou[3]*

[1]The Fifth Clinical Medical College of Shanxi Medical University, Taiyuan, Shanxi, China, [2]The Third Clinical College, Shanxi University of Chinese Medicine, Jinzhong, Shanxi, China, [3]Department of Nephrology, Shanxi Provincial People's Hospital, The Fifth Clinical Medical College of Shanxi Medical University, Taiyuan, Shanxi, China

Acute kidney injury (AKI) induces significant energy metabolic reprogramming in renal tubular epithelial cells (TECs), thereby altering lipid, glucose, and amino acid metabolism. The changes in lipid metabolism encompass not only the downregulation of fatty acid oxidation (FAO) but also changes in cell membrane lipids and triglycerides metabolism. Regarding glucose metabolism, AKI leads to increased glycolysis, activation of the pentose phosphate pathway (PPP), inhibition of gluconeogenesis, and upregulation of the polyol pathway. Research indicates that inhibiting glycolysis, promoting the PPP, and blocking the polyol pathway exhibit a protective effect on AKI-affected kidneys. Additionally, changes in amino acid metabolism, including branched-chain amino acids, glutamine, arginine, and tryptophan, play an important role in AKI progression. These metabolic changes are closely related to the programmed cell death of renal TECs, involving autophagy, apoptosis, necroptosis, pyroptosis, and ferroptosis. Notably, abnormal intracellular lipid accumulation can impede autophagic clearance, further exacerbating lipid accumulation and compromising autophagic function, forming a vicious cycle. Recent studies have demonstrated the potential of ameliorating AKI-induced kidney damage through calorie and dietary restriction. Consequently, modifying the energy metabolism of renal TECs and dietary patterns may be an effective strategy for AKI treatment.

KEYWORDS

acute kidney injury, renal tubular epithelial cells, energy metabolism, programmed cell death, therapeutic

1 Introduction

Acute kidney injury (AKI) is a pressing global health issue characterized by a swift decline in renal function, leading to elevated mortality and prevalence rates (Liu et al., 2020). AKI can be triggered by various factors such as trauma, sepsis, surgery, or drug toxicity, with ischemia-reperfusion injury (IRI) being the primary cause. IRI disrupts the cellular redox balance and triggers excessive generation of reactive oxygen species (ROS) in the kidneys during reperfusion, leading to a series of events, including mitochondrial damage, energy

consumption, apoptosis, and necrosis of renal tubular cells (Han et al., 2017). Furthermore, incomplete recovery from AKI may lead to renal fibrosis, increasing the risk of chronic kidney disease (CKD) and end-stage renal disease (ESRD) (Lee et al., 2022). Presently, no specific treatment exists for the prevention of AKI, enhancing recovery, or improving the long-term prognosis of AKI, including CKD, ESRD, or death (Yang et al., 2006). Therefore, there is an urgent need to identify novel therapeutic targets for AKI treatment.

The kidney is the second largest metabolic organ in the human body with abundant mitochondria, second only to the heart (O'Connor, 2006; Pagliarini et al., 2008). Under normal physiological conditions, the kidney requires a large amount of energy to maintain its functions. Tubular epithelial cells (TECs) are one of the primary sites of AKI injury, and under pathological conditions, their mitochondria suffer severe damage, leading to disruptions in oxidative phosphorylation and energy metabolism disorders (Bhargava and Schnellmann, 2017). Consequently, the utilization of metabolic substrates (such as glucose, amino acids, fatty acids (FAs), ketone bodies, citric acid, and lactate) in TECs undergoes alterations to adapt to the pathological environment during AKI (Bhargava and Schnellmann, 2017). It should be noted that this metabolic reprogramming in TECs during AKI serves as a double-edged sword. Current evidence suggests that this reprogramming may represent a protective mechanism for surviving TECs to adapt to the pathological environment. However, prolonged inhibition of FAO and increased glycolysis can influence kidney outcomes and promote the transition of AKI to CKD through multiple molecular mechanisms (Simon and Hertig, 2015). Additionally, numerous studies have found that changes in energy metabolism can also regulate programmed cell death (Fougeray et al., 2012; Wu et al., 2021). Therefore, this article presents a comprehensive summary of the changes in the energy metabolism of TECs and the interplay between these energy metabolism alterations and programmed cell death, offering insights into the diagnosis and treatment of AKI.

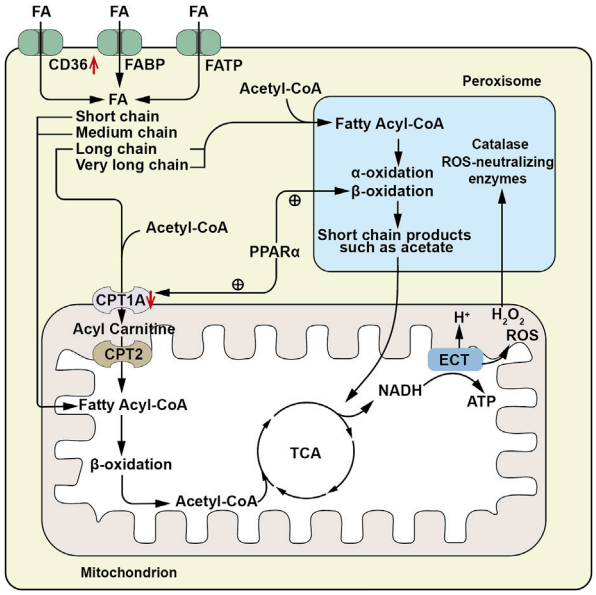

FIGURE 1
Schematic diagram of fatty acid metabolism pathway. FAs are absorbed by renal tubules via the CD36 receptor, fatty acid binding protein (FABP), and fatty acid transport protein (FATP). Long chain and very long chain FAs are acylated to acyl-CoA by very long chain acyl-CoA synthetase located on the peroxisomal membrane, then enter peroxisomes for beta-oxidation, generating short chain products such as acetic acid. The short chain products enter the mitochondrial TCA cycle for complete oxidation. Short -, medium - and long-chain FAs (FA) are conjugated to CoA by acyl- CoA synthetase on the outer mitochondrial membrane to form fatty acyl-CoA. Long chain acyl-CoA is converted to long chain acylcarnitine by carnitine palmitoyltransferase 1 A(CPT1A) located on the outer mitochondrial membrane, enters the mitochondrial matrix, and is then converted to acyl-CoA by carnitine palmitoyltransferase-2 (CPT2), releasing carnitine. Acyl-CoA undergoes β-oxidation in the mitochondria, producing acetyl-CoA which enters the tricarboxylic acid (TCA) cycle for complete oxidation. The resulting nicotinamide adenine dinucleotide (NADH) and flavin adenine dinucleotide (FADH) enter the electron transport chain (ETC) to provide electrons for generating an electrochemical gradient, leading to ATP production. The ROS and H2O2 generated during this process can enter peroxisomes for metabolism by peroxisomal catalase and other ROS neutralizing enzymes. ↑, Up-regulation of the substance or metabolic pathway in AKI; ↓, Down-regulation of the substance or metabolic pathway in AKI. ⊕, Positive regulatory effect.

2 Energy metabolism of renal tubular epithelial cells in healthy kidneys and acute kidney injury

2.1 Lipid metabolism

2.1.1 Lipid metabolism in healthy renal tubular epithelial cells

The kidney performs a complex reabsorption function, and TECs are the key players responsible for the reabsorption processes involving sodium, water, glucose, and other substances. Similar to the metabolically active cardiomyocyte, TECs relies on fatty acid oxidation (FAO), because per 1 molecule of 16-carbon saturated fatty acids provides 106 ATP units compared to 36 from one molecule of glucose metabolism (Simon and Hertig, 2015). Renal tubules absorb FAs through the cluster of differentiation 36 (CD36) receptor, fatty acid binding protein (FABP), and fatty acid transport protein (FATP) expressed on the plasma membrane (Trimble, 1982; Susztak et al., 2005). Additionally, FAs can be produced through fatty acid synthase in the cytosol or through the metabolism of phospholipids via phospholipase A2 (Simon and Hertig, 2015). Long-chain FAs, such as palmitic acid esters, are the preferred substrates for ATP generation by proximal renal tubular epithelial cells (PTECs). This transportation is facilitated by carnitine palmitoyltransferase 1 (CPT1), located on the outer mitochondrial membrane. CPT1 converts fatty acyl-coenzyme A into long-chain acylcarnitine, allowing it to enter the mitochondrial matrix, where it is converted back to acyl-coenzyme A (acyl-CoA) by CPT2, releasing carnitine. Acyl-CoA undergoes β-oxidation in the mitochondria, and the resulting acetyl-CoA is completely oxidized in the tricarboxylic acid (TCA) cycle. The resulting nicotinamide adenine dinucleotide hydrogen (NADH) and flavin adenine dinucleotide hydrogen (FADH) enter the electron transfer chain (ETC) generating an electrochemical gradient that promotes ATP production (Houten et al., 2016; Gewin, 2021) (Figure 1). Among

the three different gene-encoded subtypes of CPT1(a,b and c), CPT1A is most highly expressed in renal PTECs and is crucial for FAO initiation, as it catalyzes the rate-limiting step of the process, making its expression and activity key determinants of proximal renal tubular ATP production (Szeto, 2017).

In the proximal tubules, long-chain FAO occurs not only in the mitochondria but also in the peroxisomes. Peroxisomal FAO operates independently of carnitine and employs very long-chain acyl-CoA synthetase situated on the peroxisomal membrane to catalyze the esterification of very long-chain fatty acids with coenzyme A to generate very long chain acyl-CoAs. However, within peroxisomes, acyl-CoA oxidase (ACOX) remains inactive when presented with substrates containing an acyl group composed of eight or fewer carbon atoms. This restriction impedes the shortening of the carbon chain. Unlike the mitochondria, peroxisomes lack respiratory chain enzymes, and therefore, peroxisomal FAO is not directly coupled with ATP production. However, they metabolize long-chain FAs into acetic acid and other short-chain products with higher hydrophilicity, allowing them to cross the membrane to exit the cell or enter the mitochondria for complete oxidation (Hashimoto, 1996). Additionally, peroxisomes contain abundant catalase and other ROS-scavenging enzymes, protecting PTECS from the toxic accumulation of long-chain FAs and serving as a sink for ROS generated in mitochondria (Vasko, 2016) (Figure 1). Hashimoto (1996) discovered that ACOX dysfunction leads to peroxisomal dysfunction and subsequent accumulation of long chain FAs, confirming the role of peroxisomes. Furthermore, peroxisomal activity varies with different physiological conditions, and peroxisomal proliferation significantly increases the activity of peroxisomal oxidase (Hashimoto, 1996). These findings indicate a cooperative relationship between peroxisomes and mitochondria, supported by observed physical interactions between the two, and the secondary effect of peroxisome function ablation on mitochondrial function (Peeters et al., 2015).

The metabolic pathways of FAO are regulated by reversible post-translational modifications (PTMs) (Rardin et al., 2013), particularly lysine acylation, and the sirtuin deacetylase that removes these PTMs. Among the sirtuins, nuclear/cytosolic sirtuin1 (Sirt1) has been shown to prevent AKI by restoring the number and function of peroxisomes, upregulating catalase, and eliminating renal ROS (Hasegawa et al., 2010). Mitochondrial sirtuin3 (Sirt3) also exerts a renal protective effect by improving mitochondrial dynamics (Morigi et al., 2015). Sirtuin5 (Sirt5) has a unique substrate preference for succinyl-lysine, propionyl-lysine, and glutaryl-lysine among sirtuins. Studies have demonstrated that Sirt5 promotes FAO in mitochondria but inhibits FAO in peroxisomes. Notably, after ischemia- or cisplatin-induced AKI, Sirt5−/− mice showed higher peroxisomal FAO than mitochondrial FAO in PTECs, leading to significantly improved function with reduced tissue damage (Chiba et al., 2019).

2.1.2 Lipid metabolism in renal tubular epithelial cells during acute kidney injury

2.1.2.1 Fatty acid metabolism

Mitochondrial damage in PTECs is a common feature of AKI caused by various etiologies, and individual metabolic pathways are also dysregulated. Studies have shown that FAO is significantly downregulated in all types of AKI, primarily due to the lack of expression of CPT1A, which prevents medium-chain and long-chain FAs from entering the mitochondrial matrix. Overexpression of CPT1A and its activators has been found to alleviate AKI (Idrovo et al., 2012). CPT1A expression is regulated by various factors, including peroxisome proliferator-activated receptor coactivator (PGC)-1 alpha (PGC1α), as well as nuclear receptor family members such as the peroxisome proliferator-activated receptor-alpha (PPARα), PPARγ, estrogen-related receptor alpha (ESRRα), pregnane X receptor (PXR), and farnesoid X receptor (FXR). In AKI, alterations in the expression of these factors affect FAO metabolism. For example, the Kruppel-like factor (KLF15) positively regulates CPT1A transcription and controls FAO metabolism by binding to PPARα, but it is down-regulated in AKI (Piret et al., 2021a). Additionally, ESRRα inhibitors can inhibit the expression of PPARα and CPT1A (Dhillon et al., 2021). PXR-deficient rats exhibit reduced gene expression of CPT1A and medium-chain acyl-CoA dehydrogenase (MCAD) (Yu et al., 2020). Recent studies have also identified a co-regulation between FXR and PPARγ in PTEC FAO. In cisplatin-induced AKI, PPARγ in PTEC is down-regulated, and treating cisplatin-damage PTEC with FXR agonists restores PPARγ expression. PPARγ-specific knockdown mice experience aggravated renal TEC injury and increased lipid droplet formation after cisplatin treatment, with reduced expression of PGC1α, leading to a decrease in CPT1A expression (Fontecha-Barriuso et al., 2020; Fontecha-Barriuso et al., 2022; Xu et al., 2022). PGC1α, a key co-activator factor for peroxisomes, plays crucial roles in peroxisome remodeling and abundance. These discoveries imply a mutual interaction among these factors. Their up-regulation can enhance CPT1A expression, consequently improving mitochondrial FAO and ameliorating acute kidney injury (Hu et al., 2012; Wang et al., 2021). Furthermore, Chiba et al. (2019). upregulated peroxisomal FAO in mice by deleting the lysine deacetylase Sirt5, leading to the preservation and improvement of renal function after cisplatin and IRI. This indicates that upregulating peroxisomal FAO may serve as a novel therapeutic target for AKI. PPAR agonists have been shown to upregulate mRNA expression of peroxisomal FAO enzymes, as well as their metabolic activity and proliferation rate. Therefore, dual improvement of AKI TEC injury may be achieved by upregulating both CPT1A and peroxisomal FAO through PPAR agonists or overexpression of PPAR (Figure 1). However, considering that PPAR regulates many physiological processes in the kidney, its effects on AKI are multifaceted. In addition to their role in protecting the kidneys by regulating energy metabolism, synthetic PPARγ agonists as well as PGC1α agonists may have diverse adverse effects such as fluid retention or blood volume expansion, obesity, heart disease, and liver toxicity (Sauer, 2015; Fontecha-Barriuso et al., 2022). Studies have found that the use of endogenous and natural PPAR agonists can avoid the side effects of excessive activation of PPAR induced by synthetic PPAR agonists (Sharma and Patial, 2022). Therefore, it is crucial to select appropriate PGC1α and PPAR activators and establish the optimal therapeutic time window for PGC1α and PPAR activation.

After IRI, TECs show changes in other genes related to FAs metabolism, in addition to downregulation of the key gene CPT1A associated with FAO. Genes related to FAs transport or storage, such as CD36 and Perilipin 2, exhibit significant upregulation. Similarly,

genes involved in FAs synthesis, including fatty acid synthase (FASN), sterol regulatory element-binding transcription factor 1 (SREBF1), and elongation of very long chain fatty acids like protein 1 (ELOVL 1), show a trend of upregulation after IRI. Additionally, genes associated with lipoprotein intakes, such as low-density lipoprotein receptor-related protein 2(LRP2) and very low-density lipoprotein receptor (VLDLR), are increased (Zhang et al., 2018). These results indicate that TECs not only decrease the utilization of FAs but also significantly increase the uptake or storage of FAs during the progression of AKI. This leads to FA accumulation, and evidence shows that the storage of free lipids in lipid droplets can prevent the adverse effects of lipid peroxidation and mitochondrial membrane potential damage caused by the accumulation of free lipids (Zhang et al., 2018; Farmer et al., 2019). The formation of lipid droplets is regulated by the intracellular super transcription factor forkhead box protein O1(FOXO1), which is significantly upregulated in TECs during AKI, along with miR-21-3p, which regulates FOXO1 (Lin et al., 2019). This suggests that the increase in fatty acid synthesis, absorption, and transport in TECs during AKI also contributes to the accumulation of FAs, while the synthesis of lipid droplets is also increasing.

2.1.2.2 Cellular membrane lipid metabolism

The cell membrane lipids encompass various types, including phospholipids, sphingomyelin, glycerolipids, and cholesterol. Among these, phospholipids and sphingomyelin constitute the major components and predominate the cell membrane lipids. Metabolites of phospholipids play an important role in cellular stress response. Lysophosphatidylcholine acyltransferase (LPCAT) catalyzes the conversion of lysophosphatidylcholine (LPC) to phosphatidylcholine (PC) and participates in phospholipid metabolism. LPCAT enzymes include LPCAT1, LPCAT2, LPCAT3, and LPCAT4. Among them, LPCAT3 is widely expressed in various tissues, including the testis, kidney, liver, and small intestine, exhibiting the widest distribution (Yamazaki et al., 2012). In lipopolysaccharide-induced AKI, the expression of miR-124-3p.1 targeting LPCAT3 is decreased, leading to an increase in LPCAT3 activity and, subsequently, an elevation in phosphatidylcholine content in TECs, inducing cellular lipid peroxidation and ferroptosis (Zhang et al., 2022). Another study by Zager et al. (1999) reported an increased percentage of phosphatidylcholine in the renal cortex after 18 h of ischemia, supporting these findings.

Sphingomyelin, as a platform for receptor proteins and lipids, are strategically distributed to specific microdomains of the cell membrane, thereby promoting transmembrane signal transduction. Elevated levels of sphingomyelin have been observed in ischemic kidneys, which may alter the distribution and formation of cytomembrane microdomains in renal TECs, thereby affecting signal pathways and second messenger production. Sphingomyelin can be hydrolyzed by the sphingomyelinase (SMase) family to generate ceramide, a central lipid in the sphingolipid pathway that plays an important role in intracellular processes such as cell proliferation, differentiation, and cell cycle arrest, and is an effective regulator of cell fate and metabolism (Scantlebery et al., 2021). Numerous studies have consistently demonstrated that the upregulation of ceramide synthesis is a

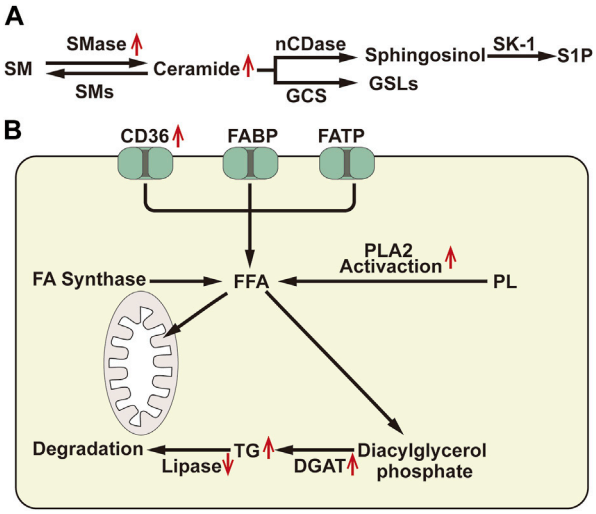

FIGURE 2
(A) Diagram of sphingomyelin metabolism: SM, Sphingomyelin; SMase, Sphingomyelinase; SMs, Sphingomyelin synthase; nCDase, Neutral Ceramidase; GCS, Glucosylceramide Synthase; SK-1, Sphingosine Kinase-1; S1P, Sphingosine-1-Phosphate; GSLs, GlycoSphingomyelin. **(B)** Diagram of fatty acid metabolism: FABP: atty acid binding protein; FATP, fatty acid transport protein; FA, Fatty Acid; FFA, Free Fatty Acid; PLA2, Phospholipase A2; TG, Triglyceride; DGAT, Diacylglycerol Acyltransferase. ↑, Up-regulation of the substance or metabolic pathway in AKI; ↓, Down-regulation of the substance or metabolic pathway in AKI.

common feature in several AKI causes (Laviad et al., 2008; Dahdouh et al., 2014; Valdés et al., 2021; Ma et al., 2022). Inhibiting the accumulation of ceramide by inhibiting SMase can potentially improve renal outcomes across several AKI models (Dupre et al., 2017; Nicholson et al., 2022). Ceramide can be enzymatically converted to sphingosine by neutral ceramidase (nCDase). Subsequently, sphingosine is phosphorylated by sphingosine kinase 1 (SK-1) to generate sphingosine-1-phosphate (S1P) (Figure 2A. A). S1P is a natural sphingolipid ligand of the 5 G protein-coupled receptor (S1P1-S1P5Rs) family, responsible for regulating cell survival and lymphocyte circulation (Bajwa et al., 2015). Several studies propose that S1P1 can stabilize mitochondrial function and alleviate renal TEC injury during IRI (Dupre et al., 2017). Promoting SK-1 synthesis and S1P1 production can prevent ischemia-reperfusion AKI (Park et al., 2012). Moreover, ceramide can also be enzymatically converted to glucosylceramide by glucosylceramide synthase. Inhibitors of glucosylceramide synthase have been shown to increase ceramide levels and decrease glucosylceramide in the renal cortex, rendering mice more susceptible to cisplatin-induced AKI (Nicholson et al., 2022). This indicates that the metabolism of ceramide to glucosylceramide could act as a buffer for renal ceramide and potentially alleviate renal injury. Therefore, reducing neuro amides or inducing S1P generation may represent a promising novel therapeutic strategy for AKI.

Arachidonic acid (AA) is a major component of cell membrane lipids and is mainly metabolized by three active enzymes: cyclooxygenase (COX), lipoxygenase (LOX), and cytochrome P450 (CYP450) enzymes. In the proximal tubules of the kidney,

the CYP450 pathway is the primary route for AA metabolism, leading to the formation of 20-hydroxyeicosatetraenoic acid (20-HETE) and 19-hydroxyeicosatetraenoic acid (19-HETE) by ω-19 hydroxylation (Quigley et al., 2000; Wang et al., 2019). Following renal ischemia/reperfusion (I/R), the production of 20-HETE increases, which can activate PPARs and participate in regulating lipid metabolism (Roman et al., 2011; Tanaka et al., 2011). Additionally, 20-HETE has been implicated in prolonging post-reperfusion vasoconstriction and exacerbating IRI in the kidney (Nilakantan et al., 2008). However, in certain instances, 20-HETE can mitigate the effects of IRI by increasing medullary oxygenation (Regner et al., 2009; Roman et al., 2011). Researchers have demonstrated that administration of 20-HETE agonists can prevent the secondary decrease in medullary blood flow and medullary hypoxia after bilateral renal ischemia, thereby reducing the severity of IRI (Regner et al., 2009). On the contrary, some studies have suggested that inhibiting 20-HETE can prevent IRI in acutely uninephrectomized rats (Hoff et al., 2011). Hence, the effect of 20-HETE on AKI may be closely related to the severity of the renal injury.

2.1.2.3 Metabolism of cholesterol and triglycerides

The accumulation of cholesterol in the renal cortex is a delayed consequence observed in various forms of renal damage. After ischemic, toxic, obstructive, or immune-related renal injuries for 18–24 h, the levels of free cholesterol, cholesterol esters, and triglycerides in the proximal renal tubules significantly increase (Zager et al., 1999). Triglyceride level regulation mainly involves the synthesis of free fatty acids (FFAs), diacylglycerol acyltransferase (DGAT)-mediated triglyceride assembly, and the catabolism of triglycerides (Figure 2B). Glycerol and ischemia/reperfusion-induced renal injury can lead to a 20%–35% decrease in lipase activity in the renal cortex, resulting in the accumulation of triglycerides in HK-2 cells. Moreover, HK2 cell injury induced by hypoxia/reoxygenation and lipopolysaccharide (LPS) can activate phospholipase A2 (PLA2), increase the expression of DGAT, and cause mobilization of FAs from the phospholipid pool, consequently increasing triglyceride formation (Johnson et al., 2005). Furthermore, after AKI, cells increase their uptake of FAs, while the consumption of FAs by mitochondria decreases, leading to an increase in substrate for triglycerides and ultimately resulting in triglycerides accumulation.

2.2 Glucose metabolism

2.2.1 Glucose metabolism in healthy renal tubular epithelial cells

The kidneys play an important role in the production and metabolism of glucose, with approximately 25% of all glucose released into circulation being produced by the human kidneys (Stumvoll et al., 1995). Glucose has two main sources: one is produced through glycogen breakdown, and the other is through gluconeogenesis. Given the limited glycogen reserves in the kidneys, it is probable that gluconeogenesis serves as the primary mechanism for glucose production. Both insulin signaling and glucose reabsorption by proximal tubular cells play a role in regulating gluconeogenesis. In HK-2 cells, these processes act to inhibit the expression of gluconeogenic genes by deactivating FOXO-1 and PGC1α, respectively (Akhtar et al., 2021). In gluconeogenesis, substrates such as lactate, glycerol, alanine, and glutamine can ultimately produce glucose through the process of glucose-6-phosphate. The primary precursor of renal gluconeogenesis is lactate, which is freely filtered by the glomerulus and subsequently reabsorbed by the renal TECs through the monocarboxylate transporters (MCTs) (Becker et al., 2010). Lactate is then converted to pyruvate by lactate dehydrogenase (LDH). Pyruvate enters the mitochondria and is sequentially converted to oxaloacetate and citrate, which is then exported from the mitochondria as citrate. Finally, citrate is converted back to oxaloacetate by phosphoenolpyruvate carboxykinase (PEPCK), and, ultimately, to glucose. However, although lactate is the predominant substrate for TECs gluconeogenesis, glutamine also makes a significant contribution.

Under normal physiological conditions, renal gluconeogenesis occurs mainly in the proximal tubules, expressing key enzymes required for this process (glucose-6-phosphatase, PEPCK, and fructose-1,6-bisphosphatase). On the other hand, glycolysis is predominant in the distal tubules, which express high levels of glycolytic enzymes (hexokinase (HK), phosphofructokinase (PFK), and pyruvate kinase (PK)) (Legouis et al., 2022). Glucose can be metabolized to pyruvate via glycolysis, and then further oxidized in the TCA cycle or metabolized to lactate. Studies have found that even under aerobic conditions, the distal tubules can also metabolize glucose to lactate (Bagnasco et al., 1985), and it has been discovered that glucose oxidation and ATP generation in the proximal tubules are significantly lower than in the distal tubule segments in rats (Klein et al., 1981). This indicates that glucose is produced by renal gluconeogenesis in the proximal tubule and metabolized by renal glycolysis in the distal renal unit segments.

2.2.2 Glucose metabolism in renal tubular epithelial cells in acute kidney injury

2.2.2.1 Glycolysis and the pentose phosphate pathway

Recent investigations have elucidated the consequences of impaired FAO in PTECs, resulting in compromised energy production, accumulation of lipids, cellular injury, and eventual fibrosis (Emma et al., 2016). Although under normal physiological conditions, PTEC does not primarily use glucose as fuel, the surviving PTECs during AKI can adapt to FAO defects by increasing glycolysis. Several studies have shown the upregulation of glycolytic enzymes (such as HK, PFK, and PK) at both mRNA and protein levels in sepsis, IRI, and aristolochic acid I (AAI)-induced AKI (Lan et al., 2016; Li et al., 2020). In addition, glucose-6-phosphate, the first metabolite of glycolysis, is produced from glucose under that catalysis of hexokinase, and can also enter the PPP pathway through a series of enzymatic reactions to produce NADPH and 5-phosphoribose (Figure 3), which can be used as substrates for the synthesis of purine and pyrimidine nucleic acids. In AKI, the mRNA expression of several genes encoding PPP enzyme is upregulated (Scantlebery et al., 2021), and the PPP pathway is activated, which in turn provides reducing capacity to antioxidant enzymes (such as glutathione (GSH) reductase) by increasing NADPH level to maintain REDOX homeostasis and reduce oxidative damage (Kim et al., 2009). Elsewhere, Smith et al. (2014) found that LPS-induced HK activation was

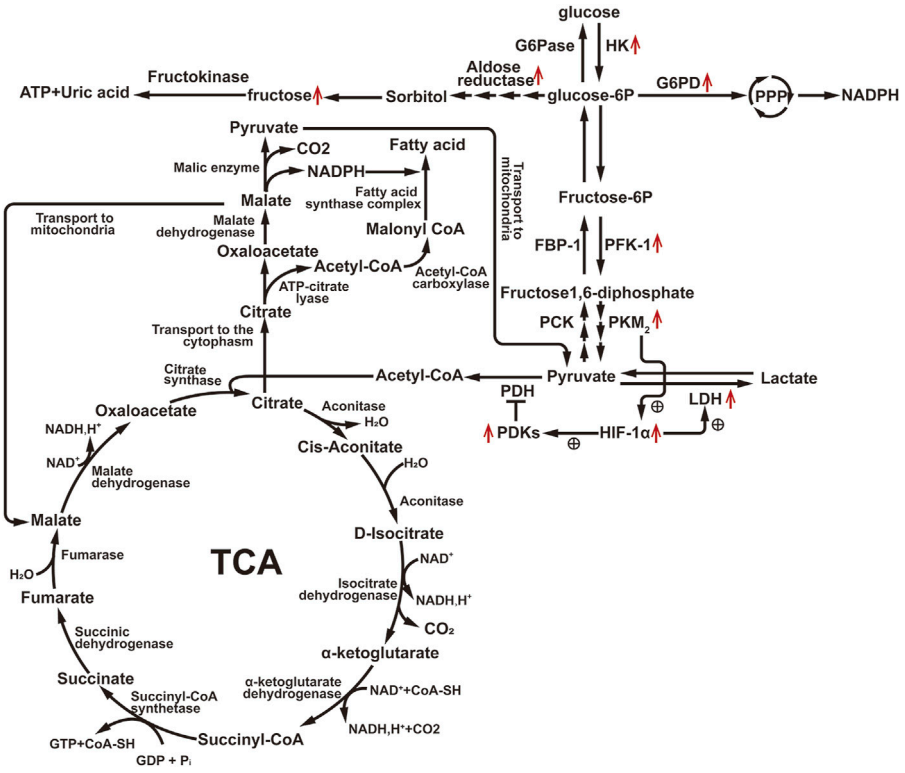

FIGURE 3
Diagram of glucose metabolism pathway. Illustration: G6Pase, Glucose-6-phosphatase; HK, Hexokinase; G6PD, Glucose-6-phosphate dehydrogenase; FBP-1, Fructose-1, 6-bisphosphatase; PFK-1, Phosphofructokinase-1; PCK, Phosphoenolpyruvate Carboxykinase; PKM2, Pyruvate Kinase M2; PDH, Pyruvate Dehydrogenase Complex; PDKs, Pyruvate Dehydrogenase Kinases; LDH, Lactate Dehydrogenase; HIF-1α, Hypoxia-Inducible Factor-1 alpha. ↑, Up-regulation of the substance or metabolic pathway in AKI; ↓, Down-regulation of the substance or metabolic pathway in AKI. ⊕, Positive regulatory effect.

associated with increased glucose-6-phosphate dehydrogenase activity in the pentose phosphate pathway. The above evidence suggests that both glycolysis and pentose phosphate pathways are upregulated in AKI.

Glycolysis generates only two ATP molecules in the cytoplasm. To produce more ATP, pyruvate, the final product of glycolysis, must enter the mitochondria and be transformed into acetyl-CoA by pyruvate dehydrogenase (PDH), which then enters the tricarboxylic acid cycle to form citric acid. PDH activity can be inhibited by phosphorylation at sites S232, S293, and S300 by pyruvate dehydrogenase kinases (PDKs). Additionally, pyruvate can be converted to lactate by LDH. Hypoxia/reoxygenation-induced elevation of hypoxia-inducible factor-1α (HIF-1α) can upregulate both PDKs and LDH (Eleftheriadis et al., 2022), leading to increased lactate production. In LPS-induced AKI, the expression of pyruvate kinase muscle isoform 2 (PKM2), a critical enzyme responsible for catalyzing the last step of glycolysis, is significantly increased, and PKM2 can directly stimulate HIF-1α transactivation (Luo et al., 2011), indicating that PKM2 can regulate PDKs and LDH to promote lactate generation by activating HIF-1α. Elevated lactate levels and decreased pyruvate levels were also observed in IRI mouse kidney tissues (Wei et al., 2007) (Figure 3). Inhibiting PKM2 to prevent IRI-induced kidney injury may be related to the increase in the pentose phosphate pathway (PPP) flux due to PKM2 inhibition, resulting in increased nicotinamide adenine dinucleotide phosphate (NADPH) generation, thus enhancing GSH and antioxidant enzyme levels (Zhou et al., 2019). This was confirmed by Kim et al. (2015), who demonstrated that activation of p53 during AKI could target TP53-induced glycolysis and apoptosis regulator (TIGAR). They also found that transient activation of TIGAR could suppress PFK-1 activity and the activity of glucose-6-phosphate dehydrogenase (G6PD). In cases of mild ischemic injury, G6PD can quickly recover, and TIGAR can reduce the sensitivity of TECs to injury by inhibiting glycolysis and redirecting glycolysis intermediates to the oxidative branch of the PPP to produce NADPH. However, in severe IRI, TIGAR only inhibits glycolysis and, since PPP and NADPH are not increased due to severe suppression of G6PD, cannot overcome the loss of renal function and histological damage. As a result, under mild ischemic conditions, inhibiting TIGAR may protect mouse TECs by promoting the PPP pathway. Therefore, simply inhibiting glycolysis may not be sufficient to improve AKI, it may require a combination of inhibiting glycolysis and promoting glycolysis intermediates toward the PPP pathway metabolism.

2.2.2.2 Gluconeogenesis

In conditions of fasting and stress, the kidney plays an important role in glucose production, accounting for 40% of the body's glucose through lactate gluconeogenesis in PTECs (Gerich et al., 2001). During the acute ischemia phase of AKI, gluconeogenic enzyme levels (such as fructose-1,6-bisphosphatase (FBP1), phosphoenolpyruvate

carboxykinase (PCK1), PCK2) are decreased, while mRNA levels of glycolytic enzymes (such as HK1, PKM, PFK) are relatively increased, leading to impaired glucose production and lactate clearance (Legouis et al., 2020) (Figure 3). In the early reperfusion phase of AKI, lactate levels are generally lower, possibly due to rapid lactate efflux, as the levels of PDH are decreased, limiting the conversion of pyruvate to acetyl-CoA and promoting its conversion to lactate. However, during the late reperfusion phase of AKI, the depletion of pyruvate is associated with an increase in gluconeogenesis. This observation is further confirmed by experiments where exogenous administration of pyruvate increases the renal cortex glucose content in AKI but not in normal kidneys (Zager et al., 2014). Thus, gluconeogenesis undergoes dynamic changes during the process of ischemia-reperfusion-induced AKI. Changes in gluconeogenesis are regulated by insulin. Studies have found that there is impaired insulin response and insulin resistance in the occurrence of acute kidney injury (Clark and Mitch, 1983; Portilla et al., 2006). The mechanism may be that the up-regulation of FOXO1 expression in renal TECs leads to the block of insulin signaling. Glucose-insulin infusion can reduce renal injury induced by severe I/R in mouse experimental models (Melo et al., 2010), and clinical studies have shown that insulin sensitizing agents can improve AKI (Hu et al., 2012), and intensive insulin therapy for tight control of blood glucose can reduce the incidence of AKI in diabetic patients and critically ill patients (Schetz et al., 2008). This further suggests that AKI is accompanied by an impaired insulin response. Improving insulin response can regulate gluconeogenesis and improve AKI renal function.

2.2.2.3 Polyol metabolism

Glucose metabolism can also generate some polyols, such as sorbitol and xylitol, through a pathway known as the polyol pathway. Under the influence of aldose reductase, glucose is reduced to sorbitol with the supply of NADPH, which can then be further converted to fructose (Figure 3). Normally, aldose reductase expression is rarely detected or absent in the PTECs (Lanaspa et al., 2014), but after AKI, its expression is significantly upregulated within 24 h, leading to the production of fructose in a time-dependent manner (Andres-Hernando et al., 2017). Elevated urine fructose levels have also been observed in AKI patients (Andres-Hernando et al., 2017). Fructose can be metabolized by fructokinase, leading to ATP consumption and uric acid generation (Johnson et al., 2010). Inhibiting fructokinase has been shown to increase ATP levels in the kidneys of AKI mice, reduce local uric acid generation and oxidative stress, and exert a protective effect against AKI. Notably, aldose reductase-deficient mice are unable to produce sorbitol and consequently, exhibit impaired urine concentration mechanisms, leading to polyuria (Andres-Hernando et al., 2017). Thus, targeting fructokinase, either alone or in combination with therapies that reduce renal uric acid production, could represent important treatment strategies for preventing kidney disease or expediting kidney recovery.

2.3 Metabolism of amino acids

2.3.1 Metabolism of amino acids in healthy renal tubular epithelial cells

The human kidney plays a major role in maintaining the body's amino acid pools' homeostasis. Approximately 50–70 g of amino acids are filtered daily, and the proximal tubules reabsorb almost all of them (97%–98%) (Garibotto et al., 2010). These reabsorbed amino acids can serve as substrates for gluconeogenesis and, after undergoing metabolism, enter the TCA cycle for oxidation. Branched-chain amino acids (BCAAs), including leucine, valine, and isoleucine, are important energy sources for the kidneys. They are metabolized by branched-chain aminotransferase (BCAT) to generate branched-chain α-keto acids, which are then oxidatively decarboxylated by the branched-chain α-keto acid dehydrogenase (BCKDH) complex, producing acyl-CoA. The resulting acetyl-CoA enters the TCA cycle for oxidation (Suryawan et al., 1998). Glutamine metabolism is also important for maintaining acid-base balance, in addition to energy production. Glutamine is metabolized by the proximal tubules to form glutamate, which can be converted to α-ketoglutarate (αKG), an intermediate in the TCA cycle. Ammonium ions resulting from this process are mainly excreted in the urine, serving as a disposable cation to promote acid excretion. The resulting αKG is transported into the mitochondria and converted to succinyl-CoA by the α-ketoglutarate dehydrogenase complex. This succinyl-CoA is further transformed into succinate through the action of succinyl-CoA synthetase. Succinate is then dehydrogenated into fumaric acid, which undergoes hydration to yield malic acid. Malic acid is subsequently transported out of the mitochondria into the cytoplasm, where it is further dehydrogenated to form oxaloacetate. This oxaloacetate is metabolized by phosphoenolpyruvate carboxylase to generate phosphoenolpyruvate (Reshef et al., 2022), a compound that is subsequently converted into glucose or carbon dioxide. This metabolic process generates bicarbonate ions, which are selectively transported into the venous bloodstream, thus partially compensating for metabolic acidosis (Scholz et al., 2021). Moreover, the kidneys play a major role in arginine synthesis and metabolism. Arginine can be metabolized through various pathways, such as generating citrulline and NO via nitric oxide synthase (NOS) in the cytoplasm. It can also produce creatine via mitochondrial arginine-glycine amidinotransferase, guanidinobutyrate via mitochondrial arginase; and urea and ornithine via both cytoplasmic and mitochondrial arginases (Bellinghieri et al., 2006). Ornithine, in turn, serves as a precursor for polyamine synthesis through ornithine decarboxylase. Additionally, tryptophan undergoes extensive metabolism via the kynurenine (KYN) pathway in the proximal tubules, ultimately leading to the *de novo* synthesis of nicotinamide adenine dinucleotide (NAD+). NAD+ is an important cofactor for many enzymes involved in FAO and the TCA cycle, making it essential for overall renal TEC metabolism. Furthermore, phenylalanine, glycine, tyrosine, and serine are also metabolized in the kidney (van de Poll et al., 2004). Taken together, while glucose and FAs are important energy sources for a healthy kidney, amino acid metabolism is undeniably indispensable for maintaining organismal homeostasis.

2.3.2 Amino acid metabolism in renal tubular epithelial cells in acute kidney injury

2.3.2.1 Glutamine

The kidney normally takes up only a small amount of glutamine. However, during the metabolic acidosis phase of AKI, about one-third of plasma glutamine is taken up and metabolized by the kidney. The increased utilization of glutamine occurs primarily in the proximal convoluted tubules, where a significant increase in

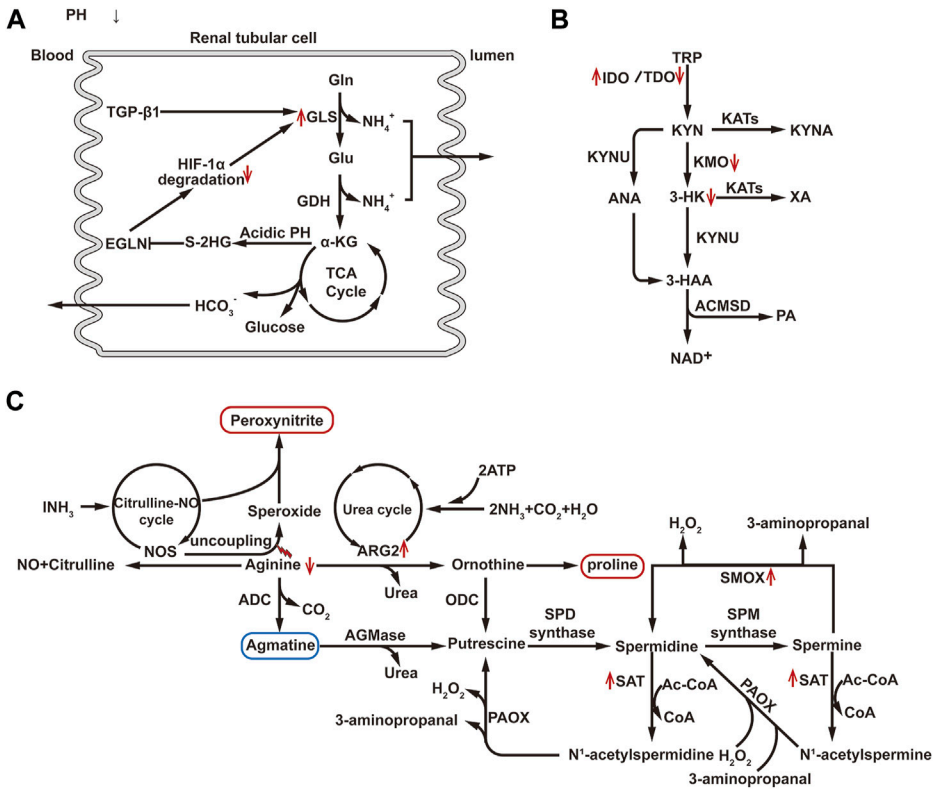

FIGURE 4
(A) Diagram of glutamine metabolism pathway. Gln, Glutamine; Glu, Glutamate; GLS, Glutaminase; GDH, Glutamate Dehydrogenase; HIF-1α, Hypoxia-Inducible Factor-1 alpha; TGF-β1, Transforming Growth Factor beta 1; αKG, Alpha Ketoglutarate; S-2-HG, S-2-hydroxyglutaric acid; EGLN, egg-laying defective nine homolog. **(B)** Diagram of tryptophan metabolism pathway: TRP, Tryptophan; IDO, Indoleamine 2, 3-dioxygenase; TDO, Tryptophan 2, 3-dioxygenase; KYN, Kynurenine; KYUN, Kynurenic Acid; KYNA, Kynurenine Acid; KAT, Kynurenine Aminotransferase; KMO, Kynurenine 3-Monooxygenase; XA, Xanthurenic Acid; 3-HK, 3-Hydroxykynurenine; ANA, Anthranilic Acid; ACMSD, 2-Amino-3-carboxymuconate semialdehyde decarboxylase; PA, Picolinic Acid. **(C)** Diagram of arginine and polyamine metabolism pathway: NOS, Nitric Oxide Synthase; ADC, Arginine Decarboxylase; ARG2, Arginase 2; ODC, Ornithine Decarboxylase; PAOX, Polyamine Oxidase; SSAT, Spermidine/Spermine N^1-acetyltransferase; SPD synthase, Spermidine Synthase; SPM synthase, Spermine Synthase; SMOX, Spermine oxidase; AGMase, Agmatinase; AC-CoA, Acetyl-CoA. ↑, Up-regulation of the substance or metabolic pathway in AKI; ↓, Down-regulation of the substance or metabolic pathway in AKI.

glutaminase activity has been observed (Anderson et al., 1982). The mechanism underlying this phenomenon may be related to z-crystal protein, which, under acidic conditions, enhances the binding with glutaminase mRNA sequence, inhibiting ribonuclease recruitment, and stabilizing glutaminase mRNA, resulting in increased glutaminase expression (Curthoys, 2001). Elevated glutaminase promotes glutamine metabolism thereby increase the production of metabolites, such as ammonium and bicarbonate ions, which help compensate for metabolic acidosis during AKI. Additionally, αKG generated from glutamine can supplement the TCA cycle. It has been observed that in IRI, the enhanced expression of transforming growth factor (TGF)-β1 in renal TECs leads to increased expression of glutaminase 1(GLS1), which promotes glutamine decomposition and αKG production (Spurgeon et al., 2005). However, under hypoxia conditions, an acidic PH will promotes the conversion of αKG to 2-hydroxyglutaric acid (2-HG), in which S-2HG constitutes the majority of the 2HG pool and has the effect of inhibiting the egg-laying defective nine homolog (EGLN). Under normoxic conditions, prolyl-4-hydroxylase of EGLN family can label HIF-1α subunits for degradation in an oxygen-dependent manner (Burr et al., 2016). Under hypoxic conditions, the lack of oxygen and the inhibitory effect of S-2HG on EGLN causes HIF-1α accumulation and sustained activation (Cienfuegos-Pecina et al., 2020; Hewitson and Smith, 2021). Activation of HIF-1α, in turn, can regulate the transcription of GLS1 (Stegen et al., 2016). Thus, there appears to be a potential vicious cycle, where the upregulation of HIF-1α leads to an increase in GLS1 expression, resulting in glutamine breakdown and αKG production. and the metabolite s-2-HG of αKG can inhibit prolyl hydroxylase and thus lead to the accumulation of HIF-1α (Figure 4A). HIF-1α, as a key regulatory factor of glycolysis, can induce the shift in cellular energy metabolism towards glycolysis by controlling the expression of several key enzymes involved in glycolysis. As the end product of glycolysis, most of the pyruvate is metabolized into lactate and does not enter the TCA cycle. Therefore, the αKG produced from glutamine metabolism may be essential for supplementing the TCA cycle. Studies in pulmonary fibroblasts using carbon tracing have demonstrated this flux change (Hewitson and Smith, 2021). Bernard et al. (2018) experimentally demonstrated that the primary function of glutamine metabolism in fibroblasts is to supply biosynthetic pathways rather than ATP generation. Elsewhere, Lu et al. (2021) through single-cell sequencing, found that renal TECs undergo

phenotype conversion during the repair and proliferation process. Newly generated PTEC circular cells can differentiate into PTEC-S1-new cells, and some of them may subsequently transform into PTEC damage and fibroblasts. In this process, energy metabolism plays an important role. Therefore, it is hypothesized that changes in glutamine metabolism pathways may affect this process, suggesting that intervening in glutamine metabolism could potentially improve kidney injury by regulating the phenotype conversion of newly generated renal TECs.

2.3.2.2 Tryptophan

Tryptophan is an essential amino acid in humans, with 95% of it being metabolized through the kynurenine pathway (KP). The key enzymes in KP include indoleamine 2,3-dioxygenase (IDO) and tryptophan 2,3-dioxygenase (TDO). Both IDO and TDO can be activated by inflammatory factors to degrade tryptophan into KYN. Under normal physiological conditions, tryptophan is mainly metabolized by TDO. However, during inflammation or stress, liver TDO activity is inhibited, and extrahepatic IDO is rapidly activated, leading to a shift in tryptophan metabolism from TDO-dominated to extrahepatic IDO-dominated pathways (Zheng et al., 2019). Subsequently, KYN undergoes further metabolism through three pathways: the NAD branch, converting KYN into 3-hydroxykynurenine (3-HK) and anthranilic acid (ANA), 3-hydroxy anthranilic acid (3-HAA), quinolinic acid (QUIN), and ultimately to NAD, the preferred end product of KP; the picolinic acid (PA) branch, producing PA as the second pathway of KYN metabolism in the kidney and liver. This branch also generates acetyl-CoA, which is further metabolized in the tricarboxylic acid cycle, providing CO_2 and ATP. The enzyme aminocarboxymuconate semialdehyde decarboxylase (ACMSD) is responsible for shifting KP metabolism from NAD + synthesis to PA production. The third branch of the KYN pathway is the kynurenic acid (KYNA) branch, which produces KYNA and xanthurenic acid (XA) through the mediation of kynurenine aminotransferases (KATs). KYNA exhibits protective effects against inflammation, clears ROS, and demonstrates antioxidant activity. This branch is a minor pathway under physiological conditions, and kynurenine hydroxylase (KYNU) also plays an important role in this pathway (Wee et al., 2021) (Figure 4B). The key enzyme kynurenine-3-monooxygenase (KMO), responsible for converting KYN to 3-HK in human kidneys, is located on the outer membrane of PTECs (Zheng et al., 2019). After AKI, the activity of the IDO enzyme increases in renal TECs leading to an increase in KP decomposition (Krupa et al., 2022). Studies have shown that the expression of KMO in renal TECs decreases in a dose-dependent manner after treatment with cisplatin, resulting in an increase in KYN entering the KYNA and NAD branch (Tan et al., 2021). A longitudinal study has demonstrated that the decrease in 3-HK and the increase in KYNA in AKI patients further support this point (Wee et al., 2021). Furthermore, research has indicated that administering KYNA externally or inhibiting KMO to elevate KYNA levels can alleviate AKI (Arora et al., 2014; Zheng et al., 2019). Inhibition of ACMSD to increase NAD production also showed a protective effect (Katsyuba et al., 2018). In addition, overexpression of PGC1α in the kidney, an important transcriptional co-regulation factor in tryptophan metabolism via KP, can restore mRNA expression of various KP enzymes in AKI mice, increase NAD + levels after IRI, and protect against kidney injury (Tran et al., 2016). These findings suggest that targeting the tryptophan KP pathway may improve AKI.

2.3.2.3 Arginine

The kidney is the primary site of arginine synthesis, responsible for maintaining arginine's steady state throughout the body. Arginine plays a key role in the urea cycle, acting as a precursor for urea, creatine, and nitric oxide. Under the influence of inflammatory cytokines, arginine metabolism is upregulated, leading to the synthesis of urea, creatine, and proline. In the urea cycle, arginase hydrolyzes arginine into urea and ornithine, facilitating the elimination of toxic ammonium ions (Bellinghieri et al., 2006). Mammals express two subtypes of arginase enzymes: arginase 1 (ARG1, cytosolic) and arginase 2 (ARG2, mitochondrial) (Oates et al., 2019). ARG1 is predominantly expressed in the liver, while ARG2 is primarily expressed in the cortical tubules of the kidney. ARG2 competes with NOS for the same substrate arginine, leading to reduced availability of arginine for NOS. This results in NOS uncoupling, characterized by the generation of superoxide rather than NO, inducing the formation of peroxynitrite. Peroxynitrite acts on proteins or DNA, ultimately leading to cell death or apoptosis. 3-nitrotyrosine (3-NT) is one of the major proteins nitrated by peroxynitrite and is widely used as a marker of nitrosative stress. Studies have shown that from hypoxia to reoxygenation, ARG2 expression is upregulated, and the accumulation of 3-NT gradually increases in HK-2 cells. Inhibition of ARG2 or supplementation with arginine can reduce nitrosative stress after hypoxia/reoxygenation injury to renal TECs, improve renal histological damage, and reduce renal tubular cell apoptosis (Hara et al., 2020; Tanuseputero et al., 2020). Furthermore, the upregulation of ARG2 can also lead to an increase in ornithine levels, and the production of proline from ornithine can promote pathological fibrosis (Hara et al., 2020). These results indicate that the upregulation of ARG2 mediates AKI induced by I/R, and targeting ARG2 may serve as a new therapeutic target for AKI. Furthermore, arginine can also generate guanidinoacetate via mitochondrial arginine decarboxylase, and numerous studies have shown that guanidinoacetate has a protective effect on AKI. Therefore, adjusting arginine metabolism pathways may be a promising strategy for improving AKI. Additionally, Jouret et al. (2016) have demonstrated through metabolomic analysis that arginine metabolism is crucial in the kidney following RI for 48 h.

2.3.2.4 Polyamine

Polyamine biosynthesis relies on the conversion of arginine to ornithine. Ornithine decarboxylase catalyzes the decarboxylation of ornithine, resulting in the production of putrescine. Subsequently, spermidine synthase and spermine synthase add the aminopropyl group to putrescine and spermidine, respectively, ultimately forming spermidine and spermine (Casero and Pegg, 2009). The process involves the acetylation of the N1 position of spermine or spermidine by spermine/spermidine N1-acetylation and N1-acetylpolyamine oxidase (SAT1). Following acetylation, these compounds can be either transported outside the cell or undergo oxidative reversion mediated by polyamine oxidase (PAOX). Additionally, spermine can be directly transformed

into spermidine through the action of spermine oxidase (SMOX). During these processes, hydrogen peroxide (H_2O_2) and reactive aldehydes are generated (Figure 4C). H_2O_2 can cause DNA damage by generating hydroxyl radicals, while reactive aldehydes can damage the integrity of lysosomal and mitochondrial membranes, leading to cell injury through the activation of cell death and apoptosis pathways (Wood et al., 2006). In AKI, activation of p53 enhances the expression and activity of key enzymes involved in polyamine degradation, such as SAT1 and SMOX, thereby enhancing polyamine degradation. Inhibition or ablation of SMOX and SAT1, as well as neutralization of metabolic products (such as H_2O_2 and reactive aldehydes), can reduce oxidative stress, inflammation/innate immune responses, and endoplasmic reticulum stress/unfolded protein response, thereby ameliorating renal tubular injury induced by endotoxins, I/R, and cisplatin-induced AKI (Zahedi et al., 2010; Zahedi et al., 2017). However, long-term use of polyamine catabolism inhibitors or ablation of the SAT1 gene has been reported to cause lung injury and induce changes in lipid metabolism (Jain et al., 2018; Yuan et al., 2018). Therefore, additional research is required to confirm the specific effects of improving AKI by inhibiting polyamine metabolism.

2.3.2.5 Branch chain amino acid

Recent studies have revealed a reduction in the activity of BCAA decomposition metabolism enzymes in mice treated with AAI and in cases of septic AKI, leading to decreased decomposition metabolism (Piret et al., 2021b; Standage et al., 2021). This downregulation may hold significant implications for ATP production in the AKI environment when FAO has been impaired, as BCAA decomposition metabolism may promote the TCA cycle through acetyl-CoA and succinyl-CoA. Piret et al. (2021a). discovered that increased expression of Klf6 in AKI injury inhibits the expression of BCAA decomposition metabolism enzymes in HK-2 cells, resulting in decreased mitochondrial ATP production. However, further research is required to confirm whether improving AKI can be achieved by upregulating branch-chain amino acid metabolism.

3 Relationship between energy metabolism and programmed cell death in renal tubular epithelial cells of acute kidney injury

3.1 Metabolism and autophagy

Autophagy can be categorized into three types based on the process of occurrence: macroautophagy, microautophagy, and chaperone-mediated autophagy (CMA). People commonly refer to macroautophagy as autophagy. Autophagy is an evolutionarily conserved lysosomal-dependent catabolic process and serves as an important mechanism for cell homeostasis and survival under pathological stress conditions in the kidney (Decuypere et al., 2015). Many studies have shown that autophagy is triggered in renal TECs during AKI. Inhibiting autophagy, either through pharmacological means or genetic intervention, has been found to exacerbate AKI. Conversely, promoting autophagy can alleviate kidney injury (Jiang et al., 2012). However, some studies have also found that autophagy can exacerbate IR-induced kidney injury (Wu et al., 2009), indicating a dual role of autophagy in AKI. Recently, increasing evidence suggests that autophagy regulates or controls metabolism, and changes in metabolism can also affect autophagy (Yang et al., 2019).

In AKI patients, lactate generated via glycolysis downregulated the levels of phosphorylated adenosine monophosphate-activated protein kinase (p-AMPK) and SIRT3 in LPS-treated HK-2 cells. This nullified the augmented impact of 2-DG on LC2II/I in LPS-treated HK-2 cells. The hindrance of glycolysis demonstrates a capacity to enhance autophagy through the decrease of lactate production and the up-regulation of p-AMPK and SIRT3 expression. This, in turn, contributes to averting sepsis-induced AKI (Tan et al., 2021). Gatticchi et al. (2015) reported that down-regulation of FAO in PTECs during AKI can also activate autophagy, while enhancing FAO reduces the need for autophagy. Transcription factor EB (TFEB) is a key regulator of lysosomal biogenesis and autophagy and can induce lipid metabolism by regulating transcription genes involved in lipophagy and lipolysis (Nakamura et al., 2020). Gene knockout of PGC1α exacerbates the inhibitory effect of cisplatin on TFEB in mouse kidneys (Lynch et al., 2019). Mice lacking TFEB experience lipid droplet accumulation (Settembre et al., 2013). Excessive lipid levels can stimulate autophagy activity in TECs (Settembre and Ballabio, 2014). However, prolonged lipid overload can lead to lysosomal dysfunction and impairment of autophagic flux, resulting in the accumulation of phospholipids in lysosomes (Yamamoto et al., 2017). The uncoupling protein (UCP) superfamily, a critical gene for lipid degradation, is significantly downregulated in AKI mice, and levels decrease with the severity of the renal injury. Upregulation of UCP1 can alleviate lipid accumulation in AKI and significantly inhibit the progression of AKI by promoting the AMPK/unc-51 like autophagy activating kinase 1 (ULK1)/autophagy pathway (Xiong et al., 2021). Additionally, Dany and Ogretmen. (2015) have found that upregulation of the metabolite of sphingomyelin, ceramide, can induce cell death-related autophagy. On the other hand, amino acid deprivation has been shown to induce autophagy (Eleftheriadis et al., 2017). Following AKI onset, the levels of amino acids in renal tubular cells significantly decrease (Zhang et al., 2017). Up-regulation of IDO enzyme-induced tryptophan depletion can increase the autophagic flux in human renal TECs by activating eukaryotic initiation factor 2 (eIF2α) kinase general control non-derepressible 2 (GCN2) (Fougeray et al., 2012; Krupa et al., 2022). Chaudhary et al. (2015) found that increasing renal IDO1 activity or inducing autophagy with GCN2 agonists can protect mice from renal inflammatory injury. These results suggest that the up-regulation of glycolysis reduces autophagy in TECs after AKI, while the down-regulation of fatty acid oxidation, lipid accumulation, amino acid deprivation, and up-regulation of ceramide synthesis, a sphingomyelin metabolite, promote autophagy. However, abnormal accumulation of intracellular lipids can impair autophagic clearance, while the reduction of autophagic clearance further promotes lipid accumulation, exacerbating autophagy dysfunction and forming a vicious cycle. In conclusion, changes in energy metabolism of renal TECs have dual and complex effects on autophagy during AKI. Hence, it is prudent to approach the modulation of cell autophagy through the regulation of energy metabolism with caution, aiming to enhance outcomes in cases of AKI.

TABLE 1 Summary of energy metabolism changes in renal tubular epithelial cells in acute kidney injury.

Energy metabolism substances and metabolic pathways			Key enzymes and products
Lipid metabolism	Fatty acid metabolism	Fatty acids oxidation↓	CPT1A↓
		The synthesis, intake, and storage of fatty acids↑	CD36↑, Perilipin 2↑, FASN↑, SREBF1↑, ELOVL1↑
	Cellular membrane lipid metabolism	Synthesis of phosphatidylcholine↑	LPCAT↑
		Hydrolysis of sphingomyelin↑	SMase↑, ceramide↑
		Arachidonic acid metabolism:CYP450↑	20-HETE↑
	Metabolism of triglycerides	Synthesis of triglycerides↑	DGAT↑
		Breakdown of triglycerides↓	lipase↓
Glucose metabolism		Glycolysis↑	HK↑, PFK↑, PKM2↑, PDKs↑, LDH↑, lactic acid↑
		The pentose phosphate pathway↑	G6PD↑
		Gluconeogenesis↓ (the acute ischemia phase of AKI)	FBP1↓, PCK1↓, PCK2↓ (the acute ischemia phase of AKI)
		Gluconeogenesis↑ (the late reperfusion phase of AKI)	
		Polyol metabolism↑	Aldose reductase↑, Fructose↑
Metabolism of amino acids	Glutamine metabolism	Glutaminolysis↑	GLS↑
	Tryptophan metabolism	Kynurenine pathway↑:the NAD branch↑, the picolinic acid branch, the KYNA branch↑	IDO↑, KMO↓, 3-HK↓
	Arginine metabolism	Hydrolysis of arginine↑	ARG2↑
	Polyamine metabolism	Polyamine degradation↑	SAT1↑, SMOX↑
	Branch chain amino acid metabolism	Decomposition metabolism of Branch chain amino acid↓	Branch chain amino acid decomposition metabolism enzymes↓

CPT1A, Carnitine palmitoyltransferase 1 A; CD36, Cluster of differentiation 36; FASN, fatty acid synthase; SREBF1, Sterol regulatory element-binding transcription factor 1; ELOVL, 1, Elongation of very long chain fatty acids like protein 1; LPCAT, lysophosphatidylcholine acyltransferase; CYP450, Cytochrome P450; SMase, Sphingomyelinase; 20-HETE, 20-hydroxyeicosatetraenoic acid; DGAT, diacylglycerol acyltransferase; PLA2, Phospholipase A2; HK, hexokinase; FBP-1, Fructose-1, 6-bisphosphatase; PFK-1, Phosphofructokinase-1; G6PD, Glucose-6-phosphate dehydrogenase; PCK, phosphoenolpyruvate carboxykinase; PKM2, Pyruvate Kinase M2; PDH, pyruvate dehydrogenase; PDKs, Pyruvate dehydrogenase kinases; LDH, lactate dehydrogenase; GLS, glutaminase; NAD, nicotinamide adenine dinucleotide; IDO, Indoleamine 2, 3-dioxygenase; TDO, Tryptophan 2, 3-dioxygenase; KYNA, kynurenine acid; KAT, kynurenine aminotransferase; KMO, Kynurenine 3-monooxygenase; 3-HK, 3-hydroxykynurenine; ARG, arginase; SAT1/PAOX, Spermidine/spermine and by N1-acetylation and N1-acetylpolyamine oxidase; SMOX, Spermine oxidase.↑, Up-regulation of the substance or metabolic pathway in AKI; ↓, Down-regulation of the substance or metabolic pathway in AKI.

3.2 Metabolism and apoptosis

Apoptosis represents the most extensively studied form of programmed cell death in various forms of AKI. This process relies heavily on the activation of effector cysteine aspartic proteases (namely, caspase-3, caspase-6, and caspase-7) (Van Opdenbosch Lamkanfi, 2019). PK, a key enzyme in the final step of glycolysis, exists in four isoforms: PKM1, PKM2, pyruvate kinase liver isoform (PKL), and pyruvate kinase red blood cell isoform (PKR). PKM2 is significantly upregulated in the LPS-induced AKI model, and its inhibition was found to significantly suppress the expression of HIF-1α and apoptosis-related factors, such as B-cell lymphoma 2/adenovirus E1B 19 kDa interacting protein 3(BNIP3), B-cell lymphoma 2-associated X protein (Bax), and caspase-3. Moreover, it improved the pathological symptoms of LPS-induced AKI tissue, indicating that PKM2 can potentially play a role in the regulation of cell apoptosis in AKI (Wu et al., 2021). IDO upregulation leads to the depletion of tryptophan (TRP), which can activate the general control non-derepressible 2 kinases (GCN2K) pathway and inhibit the mammalian target of rapamycin (mTOR) signaling, thereby promoting renal TEC's apoptosis. Increased IDO activity can also regulate cysteine aspartic protease-8 activation and TECs apoptosis via the Fas/Fas ligand (FasL) -dependent mechanism (Krupa et al., 2022). The metabolism of polyamines produces ROS and reactive aldehyde, which are important inducing factors for DNA damage, mitochondrial damage, endoplasmic reticulum stress/unfolded protein response, and can trigger TEC's apoptosis and AKI renal tubular injury (Zahedi et al., 2019). Therefore, all these factors may contribute to apoptosis in AKI.

3.3 Metabolism and necroptosis

Necroptosis is a form of programmed cell death mediated by the phosphorylation of mixed lineage kinase domain-like protein (MLKL) by receptor-interacting protein kinase 3 (RIPK3), leading to subsequent plasma membrane rupture. In many AKI models, MLKL stands out as one of the most upregulated genes. In a clamp ischemia model, mice with defects in RIPK3 and MLKL are protected from IRI (Maremonti et al., 2022). Studies have reported elevated levels of RIPK3 in the plasma and urine of sepsis-induced AKI patients, and RIPK3 expression is also higher in AKI kidneys with tubular injury in human biopsy samples (Uni and Choi, 2022). Elevated RIPK3 can influence metabolic

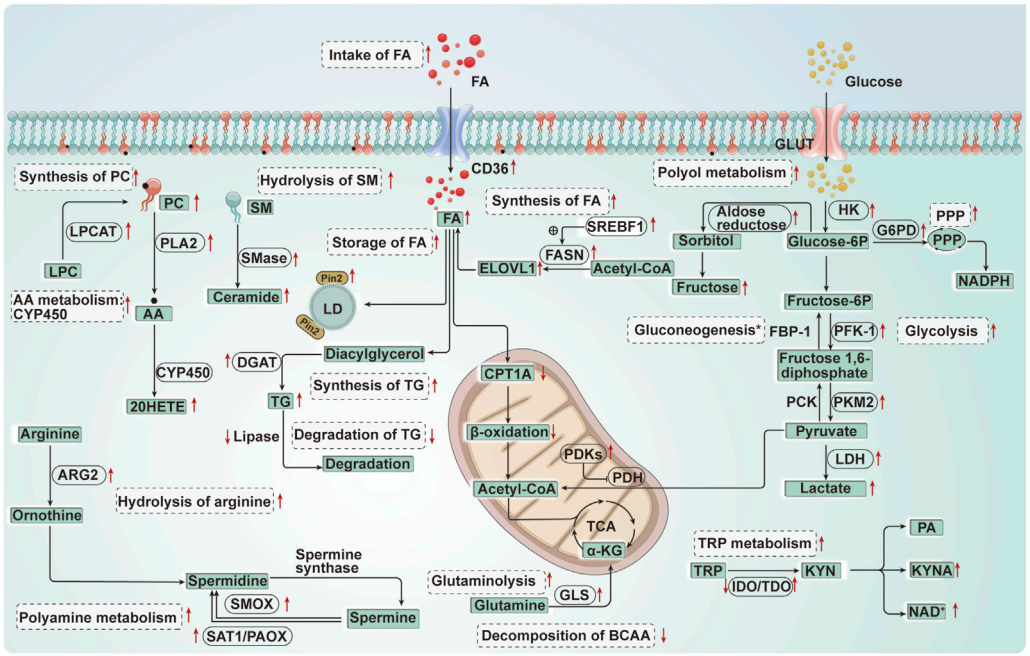

FIGURE 5
Diagram of energy metabolism changes in renal tubular epithelial cells in acute kidney injury. FA, Fatty acid; CPT1A, Carnitine palmitoyltransferase 1 A; CD36, Cluster of differentiation 36; FASN, Fatty acid synthase; SREBF1, Sterol regulatory element-binding transcription factor 1; ELOVL 1, Elongation of very long chain fatty acids like protein 1; PC, Phosphatidylcholine; LPC, Lysophosphatidylcholine; LPCAT, Lysophosphatidylcholine acyltransferase; AA, Arachidonic acid; CYP450, Cytochrome P450; 20-HETE, 20-hydroxyeicosatetraenoic acid; SM, Sphingomyelin; SMase, Sphingomyelinase; TG, Triglycerides; DGAT, Diacylglycerol acyltransferase; PLA2, Phospholipase A2; Plin2, Perilipin 2; LD, Lipid droplet; GLUT, Glucose transporters; HK, Hexokinase; FBP-1, Fructose-1, 6-bisphosphatase; PFK-1, Phosphofructokinase-1; G6PD, Glucose-6-phosphate dehydrogenase; PCK, Phosphoenolpyruvate carboxykinase; PKM2, Pyruvate Kinase M2; PDH, Pyruvate dehydrogenase; PDKs, Pyruvate dehydrogenase kinases; LDH, Lactate dehydrogenase; GLS, Glutaminase; TRP, Tryptophan; NAD, Nicotinamide adenine dinucleotide; IDO, Indoleamine 2, 3-dioxygenase; TDO, Tryptophan 2, 3-dioxygenase; KYNA, Kynurenine acid; PA, Picolinic Acid; ARG, Arginase; SAT1/PAOX, Spermidine/spermine and by N1-acetylation and N1-acetylpolyamine oxidase; SMOX, Spermine oxidase; BCAA, Branched-chain amino acid. *, Gluconeogenesis↓(FBP-1↓, PCK↓) (the acute ischemia phase of AKI); Gluconeogenesis↑ (the late reperfusion phase of AKI).↑:Up-regulation of the substance or metabolic pathway in AKI; ↓:Down-regulation of the substance or metabolic pathway in AKI. Progress of the relationship between energy metabolism reprogramming and programmed cell death in renal tubular epithelial cells of acute kidney injury.

enzymes in the mitochondrial matrix through the RIPK1/RIPK3/MLKL necrotic body, promoting the production of mitochondrial reactive oxygen species (mtROS) that can act on glutamate dehydrogenase (GDH) and catalyze the generation of αKG from glutamate. αKG, as an energy substrate, actively participates in the respiratory chain, promotes mtROS production, and induces necroptosis (Zhao et al., 2021; Maremonti et al., 2022; Tian et al., 2022). However, Li et al. (2021) found that glycolytic metabolism inhibits RIPK-dependent necroptosis by suppressing mtROS in renal TEC injury. Therefore, further research is needed to validate the relationship between the alterations in energy metabolism of renal TECs and necroptosis.

3.4 Metabolism and pyroptosis

Pyroptosis is an inflammatory form of programmed cell death that primarily occurs in macrophages and dendritic cells, but it can also happen in other cell types, including hepatocytes and renal TECs. In the kidney, cellular pyroptosis can be induced by various factors, such as cadmium, contrast agents, renal ischemia-reperfusion, and unilateral ureteral obstruction, characterized by the activation of inflammatory caspase cysteine-dependent aspartate proteases and the release of interleukin-1 beta (IL-1β) (Liu et al., 2022). Studies have demonstrated that the metabolite αKG induces pyroptosis in tumor cells through death receptor6 (DR6) and gasdermin-C (GSDMC) -dependent pathways. Additionally, treatment with the end product of glycolysis, lactate, to establish acidic environments, can make cancer cells more susceptible to α-KG induced pyroptosis (Zhang et al., 2021). Hao et al. (2017) found that microRNA-17-5p (miR-17-5p) may inhibit DR-6 to promote renal TEC survival during hypoxic/ischemic renal injury, suggesting that energy metabolism in renal TECs is closely related to pyroptosis. Given the scant research in this domain, additional studies are required to substantiate these discoveries.

3.5 Metabolism and ferroptosis

Ferroptosis is a form of cell death regulated by iron-dependent lipid peroxidation. After hypoxia-reoxygenation, metabolites such as KYN and KYNA produced from tryptophan metabolism via the KYN pathway, along with the IDO1 enzyme from the metabolism of indoleamine, can activate aryl hydrocarbon receptor (AhR) and trigger ROS generation, leading to AhR-mediated ferroptosis of

TABLE 2 Summary of the literature on the regulation of energy metabolic reprogramming to improve AKI.

Energy metabolism substances	Targeted energy metabolic pathways	Targets	Interventions	Injury model	References
Lipid metabolism	Fatty acids oxidation↑	CPT1A↑	C75	I/R	Idrovo et al. (2012)
			PPARγ agonist	I/R	Hu et al. (2012)
			PGC1α agonist	I/R	Wang et al. (2021)
			PXR agonist	I/R	Yu et al. (2020)
	Synthesis of S1P↑	S1P↑, SK-1↑	Selective A1AR agonist (CCPA)	I/R	Park et al. (2012)
	Synthesis of ceramides↓	Sphingomyelinase↓	Myriocin, amitriptyline	Cisplatin	Dupre et al. (2017)
	Arachidonic acid metabolism: CYP450	20-HETE↑	20-HETE agonists	I/R	Regner et al. (2009)
		20-HETE↓	20-HETE Inhibitors	I/R	Hoff et al. (2011)
Glucose metabolism	Glycolysis↓, pentose phosphate pathway↑	PKM2↓	Shikonin, S-nitroso-CoA	Lipopolysaccharide, I/R	Wu et al. (2021); Zhou et al. (2019)
	Gluconeogenesis↓	Reduction in insulin resistance	Insulin	I/R	Melo et al. (2010)
			Glipizidone	I/R	Hu et al. (2012)
	Polyol metabolism↓	Fructokinase↓	luteolin	I/R	Andres-Hernando et al. (2017)
Amino acid metabolism	Tryptophan metabolism: Kynurenine pathway↑:the NAD branch↑, the picolinic acid branch↓, the KYNA branch↑	ACMSD↓	ACMSD inhibitors	Cisplatin	Katsyuba et al. (2018)
		KYNA↑	Exogenous supplementation with KYNA	I/R	Arora et al. (2014)
		KMO↓	KMO gene blockade	I/R	Zheng et al. (2019)
		NAD↑	PGC1α agonist	I/R	Tran et al. (2016)
	Arginine metabolism: arginase pathway↓	Arginase2↓	Arginase2 inhibitors	I/R	Hara et al. (2020)
	Arginine metabolism: nitric oxide synthase pathway↑	Arginase2	Exogenous administration of arginine	Sepsis	Tanuseputeroet al. (2020)
	Polyamine degradation↓	SAT↓, SMOX↓	Ablation of the SSAT or SMOX gene	Cisplatin, Sepsis	Zahedi et al. (2010); Zahedi et al. (2017)

FAO: CPT1A, Carnitine palmitoyltransferase 1 A; PGC1α, Peroxisome proliferator-activated receptor coactivator (PGC)-1 alpha; PPARγ, Peroxisome proliferator-activated receptor-gamma; PXR, pregnane X receptor; CYP450, Cytochrome P450; 20-HETE, 20-hydroxyeicosatetraenoic acid; PKM2, Pyruvate Kinase M2; SK-1, Sphingosine kinase 1; S1P, Sphingosine-1-phosphate; NAD, nicotinamide adenine dinucleotide; KYNA, kynurenine acid; KMO, Kynurenine 3-monooxygenase; SAT1/PAOX, Spermidine/spermine and by N1-acetylation and N1-acetylpolyamine oxidase; SMOX, spermine oxidase; ACMSD, aminocarboxymuconate semialdehyde decarboxylase; I/R:Ischemia/reperfusion. ↑, Up-regulation of the substance or metabolic pathway after the intervention; ↓, Down-regulation of the substance or metabolic pathway after the intervention.

renal TECs (Krupa et al., 2022). Furthermore, during AKI, upregulation of LPCAT3 leads to phospholipid peroxidation containing polyunsaturated fatty acids, which induces ferroptosis (Zhang et al., 2022). Kang et al. (2019) found that P53-mediated ferroptosis is associated with solute carrier family 7member 11 (SLC7A11) inhibition and upregulation of SAT1 and GLS2 in cancer cells. However, further research is needed to confirm if P53 can induce iron death in AKI renal TECs by regulating these substances.

4 Summary and perspectives

In summary, AKI leads to significant reprogramming of energy metabolism in renal TECs. This reprogramming involves not only the well-known down-regulation of FAO and up-regulation of glycolysis but also changes in the metabolism of cell membrane lipids, triglycerides, PPP, gluconeogenesis, and amino acids (Table 1; Figure 5). FAO plays a critical role in maintaining energy supply in PTECs, occurring not only in mitochondria but also in peroxisomes. Peroxisomes not only metabolize long-chain fatty acids into shorter chain products, but also serve as a sink for the ROS generated by mitochondria due to their abundant catalase and other ROS scavenging enzymes, protecting TECs from toxic accumulation of long-chain fatty acids. Up-regulating FAO in peroxisomes has been found to protect against AKI kidney injury. Cell membrane lipid metabolism also plays an important role in AKI. LPCAT can induce ferroptosis in renal TECs by regulating phospholipid metabolism. Additionally, the metabolism of AA derivative 20-HETE and sphingolipid-derived ceramides play a significant role in AKI. Furthermore, cholesterol and triglycerides accumulate in renal TECs during AKI, inducing autophagy. Nevertheless, the

abnormal accumulation of intracellular lipids hinders the autophagic clearance process. This, in turn, results in even more lipid buildup, further aggravating the impaired autophagic function. This establishes a detrimental cycle. During AKI, various changes occur in the glucose metabolism of renal TECs, including increased glycolysis, activated PPP, inhibited gluconeogenesis, and upregulated polyol metabolism. Inhibiting glycolysis and increasing PPP activity, as well as blocking the polyol pathway, may offer protective effects for the kidneys. Amino acid metabolism is also an important aspect of AKI metabolic reprogramming. Upregulated glutamine metabolism in AKI compensates for metabolic acidosis and supplements the TCA cycle. The tryptophan metabolism pathway in the kidneys mainly involves KYN, and inhibiting the PA branch of KYN metabolism while increasing the NAD branch and KYNA branch metabolism can alleviate AKI kidney injury. Moreover, the upregulation of arginase in renal TECs during AKI competes with nitric oxide synthase for the same substrate, arginine, leading to nitrosative stress and damaging cells. Branched-chain amino acid and polyamine metabolism are also closely related to AKI. These changes in energy metabolism pathways, metabolites, and key enzymes can further regulate autophagy, apoptosis, necroptosis, ferroptosis, and other pathways in renal TECs. Additionally, AKI triggers changes in nucleotide metabolism in renal TECs. Under ischemic and inflammatory conditions, ATP degrades into AMP to generate adenosine, which has been shown to have a protective effect on cells (Módis et al., 2009). Xanthine oxidoreductase (XOR) activity and purine degradation products were also found to be significantly elevated in AKI (Kosaki et al., 2022). Administering exogenous NAD and inhibiting poly ADP-ribosepolymerase (PARP) can restore renal tubular cell ATP, phosphocreatine (PCr), and NAD + levels, reducing renal TEC apoptosis (Liu et al., 2015). However, due to limited research, further experiments are needed to clarify the specific mechanisms.

Recent studies have shown that activating SIRT1 and AMPK/mToR through calorie and diet restriction enhances autophagy, counters the decrease of endothelial nitric oxide synthase (eNOS) and PGC-1α induced by I/R, and improves AKI (Lempiäinen et al., 2013; Robertson et al., 2015; Andrianova et al., 2021). Therefore, in the future, regulating the energy metabolism pathway, key enzyme activity, and metabolic product generation are potential strategies for regulating programmed cell death in renal TECs and improve AKI (Table 2). Dietary structure adjustments may also serve as supportive measures in the treatment of assist in the treatment of AKI.

Author contributions

LZ: Writing–original draft. YH: Investigation, Writing–review and editing. ST: Writing–review and editing. XH: Writing–review and editing. RL: Writing–review and editing. XZ: Writing–review and editing.

Funding

The author(s) declare financial support was received for the research, authorship, and/or publication of this article. This work was supported by grants from the National Natural Science Foundation of China (NSFC) (Grant Number 2F012021006), and Scientific Research Project Funded by International Students of Shanxi Province (2020-182).

Acknowledgments

The authors would like to thank all the reviewers who participated in the review and MJEditor (www.mjeditor.com) for its linguistic assistance during the preparation of this manuscript.

Conflict of interest

The authors declare that the research was conducted in the absence of any commercial or financial relationships that could be construed as a potential conflict of interest.

Publisher's note

References

Akhtar, S., Culver, S. A., and Siragy, H. M. (2021). Novel regulation of renal gluconeogenesis by Atp6ap2 in response to high fat diet via PGC1-α/AKT-1 pathway. *Sci. Rep.* 11, 11367. doi:10.1038/s41598-021-90952-7

Anderson, N. M., Hortelano, P., and Alleyne, G. A. (1982). Renal metabolism of glutamine in rats with acute renal failure. *Kidney Int.* 22, 640–642. doi:10.1038/ki.1982.223

Andres-Hernando, A., Li, N., Cicerchi, C., Inaba, S., Chen, W., Roncal-Jimenez, C., et al. (2017). Protective role of fructokinase blockade in the pathogenesis of acute kidney injury in mice. *Nat. Commun.* 8, 14181. doi:10.1038/ncomms14181

Andrianova, N. V., Buyan, M. I., Bolikhova, A. K., Zorov, D. B., and Plotnikov, E. Y. (2021). Dietary restriction for kidney protection: decline in nephroprotective mechanisms during aging. *Front. Physiol.* 12, 699490. doi:10.3389/fphys.2021.699490

Arora, S., Kaur, T., Kaur, A., and Singh, A. P. (2014). Glycine aggravates ischemia reperfusion-induced acute kidney injury through N-Methyl-D-Aspartate receptor activation in rats. *Mol. Cell Biochem.* 393, 123–131. doi:10.1007/s11010-014-2052-0

Bagnasco, S., Good, D., Balaban, R., and Burg, M. (1985). Lactate production in isolated segments of the rat nephron. *Am. J. Physiol.* 248, F522–F526. doi:10.1152/ajprenal.1985.248.4.F522

Bajwa, A., Rosin, D. L., Chroscicki, P., Lee, S., Dondeti, K., Ye, H., et al. (2015). Sphingosine 1-phosphate receptor-1 enhances mitochondrial function and reduces cisplatin-induced tubule injury. *J. Am. Soc. Nephrol.* 26, 908–925. doi:10.1681/ASN.2013121351

Becker, H. M., Mohebbi, N., Perna, A., Ganapathy, V., Capasso, G., and Wagner, C. A. (2010). Localization of members of MCT monocarboxylate transporter family Slc16 in the kidney and regulation during metabolic acidosis. *Am. J. Physiol. Ren. Physiol.* 299, F141–F154. doi:10.1152/ajprenal.00488.2009

Bellinghieri, G., Santoro, D., Mallamace, A., Di Giorgio, R. M., De Luca, G., and Savica, V. (2006). L-arginine: a new opportunity in the management of clinical derangements in dialysis patients. *J. Ren. Nutr.* 16, 245–247. doi:10.1053/j.jrn.2006.04.004

Bernard, K., Logsdon, N. J., Benavides, G. A., Sanders, Y., Zhang, J., Darley-Usmar, V. M., et al. (2018). Glutaminolysis is required for transforming growth factor-β1-induced myofibroblast differentiation and activation. *J. Biol. Chem.* 293, 1218–1228. doi:10.1074/jbc.RA117.000444

Bhargava, P., and Schnellmann, R. G. (2017). Mitochondrial energetics in the kidney. *Nat. Rev. Nephrol.* 13, 629–646. doi:10.1038/nrneph.2017.107

Burr, S. P., Costa, A. S., Grice, G. L., Timms, R. T., Lobb, I. T., Freisinger, P., et al. (2016). Mitochondrial protein lipoylation and the 2-oxoglutarate dehydrogenase complex controls HIF1α stability in aerobic conditions. *Cell Metab.* 24, 740–752. doi:10.1016/j.cmet.2016.09.015

Casero, R. A., and Pegg, A. E. (2009). Polyamine catabolism and disease. *Biochem. J.* 421, 323–338. doi:10.1042/BJ20090598

Chaudhary, K., Shinde, R., Liu, H., Gnana-Prakasam, J. P., Veeranan-Karmegam, R., Huang, L., et al. (2015). Amino acid metabolism inhibits antibody-driven kidney injury by inducing autophagy. *J. Immunol.* 194, 5713–5724. doi:10.4049/jimmunol.1500277

Chiba, T., Peasley, K. D., Cargill, K. R., Maringer, K. V., Bharathi, S. S., Mukherjee, E., et al. (2019). Sirtuin 5 regulates proximal tubule fatty acid oxidation to protect against AKI. *J. Am. Soc. Nephrol.* 30, 2384–2398. doi:10.1681/ASN.2019020163

Cienfuegos-Pecina, E., Ibarra-Rivera, T. R., Saucedo, A. L., Ramírez-Martínez, L. A., Esquivel-Figueroa, D., Domínguez-Vázquez, I., et al. (2020). Effect of sodium (S)-2-hydroxyglutarate in male, and succinic acid in female Wistar rats against renal ischemia-reperfusion injury, suggesting a role of the HIF-1 pathway. *PeerJ* 8, e9438. doi:10.7717/peerj.9438

Clark, A. S., and Mitch, W. E. (1983). Muscle protein turnover and glucose uptake in acutely uremic rats. Effects of insulin and the duration of renal insufficiency. *J. Clin. Invest.* 72, 836–845. doi:10.1172/JCI111054

Curthoys, N. P. (2001). Role of mitochondrial glutaminase in rat renal glutamine metabolism. *J. Nutr.* 131, 2491S–2495S; discussion 2496S-7S. doi:10.1093/jn/131.9.2491S

Dahdouh, F., Raane, M., Thévenod, F., and Lee, W. K. (2014). Nickel-induced cell death and survival pathways in cultured renal proximal tubule cells: roles of reactive oxygen species, ceramide and ABCB1. *Arch. Toxicol.* 88, 881–892. doi:10.1007/s00204-014-1194-x

Dany, M., and Ogretmen, B. (2015). Ceramide induced mitophagy and tumor suppression. *Biochim. Biophys. Acta* 1853, 2834–2845. doi:10.1016/j.bbamcr.2014.12.039

Decuypere, J. P., Ceulemans, L. J., Agostinis, P., Monbaliu, D., Naesens, M., Pirenne, J., et al. (2015). Autophagy and the kidney: implications for ischemia-reperfusion injury and therapy. *Am. J. Kidney Dis.* 66, 699–709. doi:10.1053/j.ajkd.2015.05.021

Dhillon, P., Park, J., Hurtado Del Pozo, C., Li, L., Doke, T., Huang, S., et al. (2021). The nuclear receptor ESRRA protects from kidney disease by coupling metabolism and differentiation. *Cell Metab.* 33, 379–394.e8. doi:10.1016/j.cmet.2020.11.011

Dupre, T. V., Doll, M. A., Shah, P. P., Sharp, C. N., Siow, D., Megyesi, J., et al. (2017). Inhibiting glucosylceramide synthase exacerbates cisplatin-induced acute kidney injury. *J. Lipid Res.* 58, 1439–1452. doi:10.1194/jlr.M076745

Eleftheriadis, T., Pissas, G., Golfinopoulos, S., Efthymiadi, M., Liakopoulos, V., and Stefanidis, I. (2022). Inhibition of malate dehydrogenase-2 protects renal tubular epithelial cells from anoxia-reoxygenation-induced death or senescence. *Biomolecules* 12, 1415. doi:10.3390/biom12101415

Eleftheriadis, T., Pissas, G., Sounidaki, M., Antoniadis, N., Antoniadi, G., Liakopoulos, V., et al. (2017). Preconditioning of primary human renal proximal tubular epithelial cells without tryptophan increases survival under hypoxia by inducing autophagy. *Int. Urol. Nephrol.* 49, 1297–1307. doi:10.1007/s11255-017-1596-9

Emma, F., Montini, G., Parikh, S. M., and Salviati, L. (2016). Mitochondrial dysfunction in inherited renal disease and acute kidney injury. *Nat. Rev. Nephrol.* 12, 267–280. doi:10.1038/nrneph.2015.214

Farmer, B. C., Kluemper, J., and Johnson, L. A. (2019). Apolipoprotein E4 alters astrocyte fatty acid metabolism and lipid droplet formation. *Cells* 8, 182. doi:10.3390/cells8020182

Fontecha-Barriuso, M., Lopez-Diaz, A. M., Guerrero-Mauvecin, J., Miguel, V., Ramos, A. M., Sanchez-Niño, M. D., et al. (2022). Tubular mitochondrial dysfunction, oxidative stress, and progression of chronic kidney disease. *Antioxidants (Basel).* 11, 1356. doi:10.3390/antiox11071356

Fontecha-Barriuso, M., Martin-Sanchez, D., Martinez-Moreno, J. M., Monsalve, M., Ramos, A. M., Sanchez-Niño, M. D., et al. (2020). The role of PGC-1α and mitochondrial biogenesis in kidney diseases. *Biomolecules* 10, 347. doi:10.3390/biom10020347

Fougeray, S., Mami, I., Bertho, G., Beaune, P., Thervet, E., and Pallet, N. (2012). Tryptophan depletion and the kinase GCN2 mediate IFN-γ-induced autophagy. *J. Immunol.* 189, 2954–2964. doi:10.4049/jimmunol.1201214

Garibotto, G., Sofia, A., Saffioti, S., Bonanni, A., Mannucci, I., and Verzola, D. (2010). Amino acid and protein metabolism in the human kidney and in patients with chronic kidney disease. *Clin. Nutr.* 29, 424–433. doi:10.1016/j.clnu.2010.02.005

Gatticchi, L., Bellezza, I., Del Sordo, R., Peirce, M. G., Sidoni, A., Roberti, R., et al. (2015). The Tm7sf2 gene deficiency protects mice against endotoxin-induced acute kidney injury. *PloS One* 10, e0141885. doi:10.1371/journal.pone.0141885

Gerich, J. E., Meyer, C., Woerle, H. J., and Stumvoll, M. (2001). Renal gluconeogenesis: its importance in human glucose homeostasis. *Diabetes Care* 24, 382–391. doi:10.2337/diacare.24.2.382

Gewin, L. S. (2021). Sugar or fat? Renal tubular metabolism reviewed in health and disease. *Nutrients* 13, 1580. doi:10.3390/nu13051580

Han, P., Qin, Z., Tang, J., Xu, Z., Li, R., Jiang, X., et al. (2017). RTA-408 protects kidney from ischemia-reperfusion injury in mice via activating Nrf2 and downstream GSH biosynthesis gene. *Oxid. Med. Cell Longev.* 2017, 7612182. doi:10.1155/2017/7612182

Hao, J., Wei, Q., Mei, S., Li, L., Su, Y., Mei, C., et al. (2017). Induction of microRNA-17-5p by p53 protects against renal ischemia-reperfusion injury by targeting death receptor 6. *Kidney Int.* 91, 106–118. doi:10.1016/j.kint.2016.07.017

Hara, M., Torisu, K., Tomita, K., Kawai, Y., Tsuruya, K., Nakano, T., et al. (2020). Arginase 2 is a mediator of ischemia-reperfusion injury in the kidney through regulation of nitrosative stress. *Kidney Int.* 98, 673–685. doi:10.1016/j.kint.2020.03.032

Hasegawa, K., Wakino, S., Yoshioka, K., Tatematsu, S., Hara, Y., Minakuchi, H., et al. (2010). Kidney-specific overexpression of Sirt1 protects against acute kidney injury by retaining peroxisome function. *J. Biol. Chem.* 285, 13045–13056. doi:10.1074/jbc.M109.067728

Hashimoto, T. (1996). Peroxisomal beta-oxidation: enzymology and molecular biology. *Ann. N. Y. Acad. Sci.* 804, 86–98. doi:10.1111/j.1749-6632.1996.tb18610.x

Hewitson, T. D., and Smith, E. R. (2021). A metabolic reprogramming of glycolysis and glutamine metabolism is a requisite for renal fibrogenesis-why and how? *Front. Physiol.* 12, 645857. doi:10.3389/fphys.2021.645857

Hoff, U., Lukitsch, I., Chaykovska, L., Ladwig, M., Arnold, C., Manthati, V. L., et al. (2011). Inhibition of 20-HETE synthesis and action protects the kidney from ischemia/reperfusion injury. *Kidney Int.* 79, 57–65. doi:10.1038/ki.2010.377

Houten, S. M., Violante, S., Ventura, F. V., and Wanders, R. J. (2016). The Biochemistry and physiology of mitochondrial fatty acid β-oxidation and its genetic disorders. *Annu. Rev. Physiol.* 78, 23–44. doi:10.1146/annurev-physiol-021115-105045

Hu, H., Zou, C., Xi, X., Shi, Z., Wang, G., and Huang, X. (2012). Protective effects of pioglitazone on renal ischemia-reperfusion injury in mice. *J. Surg. Res.* 178, 460–465. doi:10.1016/j.jss.2012.01.012

Idrovo, J. P., Yang, W. L., Nicastro, J., Coppa, G. F., and Wang, P. (2012). Stimulation of carnitine palmitoyltransferase 1 improves renal function and attenuates tissue damage after ischemia/reperfusion. *J. Surg. Res.* 177, 157–164. doi:10.1016/j.jss.2012.05.053

Jain, V., Raina, S., Gheware, A. P., Singh, R., Rehman, R., Negi, V., et al. (2018). Reduction in polyamine catabolism leads to spermine-mediated airway epithelial injury and induces asthma features. *Allergy* 73, 2033–2045. doi:10.1111/all.13472

Jiang, M., Wei, Q., Dong, G., Komatsu, M., Su, Y., and Dong, Z. (2012). Autophagy in proximal tubules protects against acute kidney injury. *Kidney Int.* 82, 1271–1283. doi:10.1038/ki.2012.261

Johnson, A. C., Stahl, A., and Zager, R. A. (2005). Triglyceride accumulation in injured renal tubular cells: alterations in both synthetic and catabolic pathways. *Kidney Int.* 67, 2196–2209. doi:10.1111/j.1523-1755.2005.00325.x

Johnson, R. J., Sanchez-Lozada, L. G., and Nakagawa, T. (2010). The effect of fructose on renal biology and disease. *J. Am. Soc. Nephrol.* 21, 2036–2039. doi:10.1681/ASN.2010050506

Jouret, F., Leenders, J., Poma, L., Defraigne, J. O., Krzesinski, J. M., and de Tullio, P. (2016). Nuclear magnetic resonance metabolomic profiling of mouse kidney, urine and serum following renal ischemia/reperfusion injury. *PloS One* 11, e0163021. doi:10.1371/journal.pone.0163021

Kang, R., Kroemer, G., and Tang, D. (2019). The tumor suppressor protein p53 and the ferroptosis network. *Free Radic. Biol. Med.* 133, 162–168. doi:10.1016/j.freeradbiomed.2018.05.074

Katsyuba, E., Mottis, A., Zietak, M., De Franco, F., van der Velpen, V., Gariani, K., et al. (2018). *De novo* NAD (+) synthesis enhances mitochondrial function and improves health. *Nature* 563, 354–359. doi:10.1038/s41586-018-0645-6

Kim, J., Devalaraja-Narashimha, K., and Padanilam, B. J. (2015). TIGAR regulates glycolysis in ischemic kidney proximal tubules. *Am. J. Physiol. Ren. Physiol.* 308, F298–F308. doi:10.1152/ajprenal.00459.2014

Kim, J., Kim, K. Y., Jang, H. S., Yoshida, T., Tsuchiya, K., Nitta, K., et al. (2009). Role of cytosolic NADP+-dependent isocitrate dehydrogenase in ischemia-reperfusion injury in mouse kidney. *Am. J. Physiol. Ren. Physiol.* 296, F622–F633. doi:10.1152/ajprenal.90566.2008

Klein, K. L., Wang, M. S., Torikai, S., Davidson, W. D., and Kurokawa, K. (1981). Substrate oxidation by isolated single nephron segments of the rat. *Kidney Int.* 20, 29–35. doi:10.1038/ki.1981.100

Kosaki, K., Kumamoto, S., Tokinoya, K., Yoshida, Y., Sugaya, T., Murase, T., et al. (2022). Xanthine oxidoreductase activity in marathon runners: potential implications

for marathon-induced acute kidney injury. *J. Appl. Physiol.* 133, 1–10. doi:10.1152/japplphysiol.00669.2021

Krupa, A., Krupa, M. M., and Pawlak, K. (2022). Indoleamine 2,3 dioxygenase 1-the potential link between the innate immunity and the ischemia-reperfusion-induced acute kidney injury? *Int. J. Mol. Sci.* 23, 6176. doi:10.3390/ijms23116176

Lan, R., Geng, H., Singha, P. K., Saikumar, P., Bottinger, E. P., Weinberg, J. M., et al. (2016). Mitochondrial pathology and glycolytic shift during proximal tubule atrophy after ischemic AKI. *J. Am. Soc. Nephrol.* 27, 3356–3367. doi:10.1681/ASN.2015020177

Lanaspa, M. A., Ishimoto, T., Cicerchi, C., Tamura, Y., Roncal-Jimenez, C. A., Chen, W., et al. (2014). Endogenous fructose production and fructokinase activation mediate renal injury in diabetic nephropathy. *J. Am. Soc. Nephrol.* 25, 2526–2538. doi:10.1681/ASN.2013080901

Laviad, E. L., Albee, L., Pankova-Kholmyansky, I., Epstein, S., Park, H., Merrill, A. H., Jr., et al. (2008). Characterization of ceramide synthase 2: tissue distribution, substrate specificity, and inhibition by sphingosine 1-phosphate. *J. Biol. Chem.* 283, 5677–5684. doi:10.1074/jbc.M707386200

Lee, K., Jang, H. R., Jeon, J., Yang, K. E., Lee, J. E., Kwon, G. Y., et al. (2022). Repair phase modeling of ischemic acute kidney injury: recovery vs. transition to chronic kidney disease. *Am. J. Transl. Res.* 14, 554–571.

Legouis, D., Faivre, A., Cippà, P. E., and de Seigneux, S. (2022). Renal gluconeogenesis: an underestimated role of the kidney in systemic glucose metabolism. *Nephrol. Dial. Transpl.* 37, 1417–1425. doi:10.1093/ndt/gfaa302

Legouis, D., Ricksten, S. E., Faivre, A., Verissimo, T., Gariani, K., Verney, C., et al. (2020). Altered proximal tubular cell glucose metabolism during acute kidney injury is associated with mortality. *Nat. Metab.* 2, 732–743. doi:10.1038/s42255-020-0238-1

Lempiäinen, J., Finckenberg, P., Mervaala, E. E., Sankari, S., Levijoki, J., and Mervaala, E. M. (2013). Caloric restriction ameliorates kidney ischaemia/reperfusion injury through PGC-1α-eNOS pathway and enhanced autophagy. *Acta Physiol. (Oxf).* 208, 410–421. doi:10.1111/apha.12120

Li, X., Zhao, X., Yao, Y., Guo, M., and Li, S. (2021). New insights into crosstalk between apoptosis and necroptosis co-induced by chlorothalonil and imidacloprid in *Ctenopharyngodon idellus* kidney cells. *Sci. Total Environ.* 780, 146591. doi:10.1016/j.scitotenv.2021.146591

Li, Y., Nourbakhsh, N., Pham, H., Tham, R., Zuckerman, J. E., and Singh, P. (2020). Evolution of altered tubular metabolism and mitochondrial function in sepsis-associated acute kidney injury. *Am. J. Physiol. Ren. Physiol.* 319, F229-F244–F244. doi:10.1152/ajprenal.00390.2019

Lin, Z., Liu, Z., Wang, X., Qiu, C., and Zheng, S. (2019). MiR-21-3p plays a crucial role in metabolism alteration of renal tubular epithelial cells during sepsis associated acute kidney injury via AKT/CDK2-FOXO1 pathway. *Biomed. Res. Int.* 2019, 2821731. doi:10.1155/2019/2821731

Liu, D., Shu, G., Jin, F., Qi, J., Xu, X., Du, Y., et al. (2020). ROS-responsive chitosan-SS31 prodrug for AKI therapy via rapid distribution in the kidney and long-term retention in the renal tubule. *Sci. Adv.* 6, eabb7422. doi:10.1126/sciadv.abb7422

Liu, S. B., Liu, J., Liu, D. W., Wang, X. T., and Yang, R. L. (2015). Inhibition of poly-(ADP-ribose) polymerase protects the kidney in a canine model of endotoxic shock. *Nephron* 130, 281–292. doi:10.1159/000435815

Liu, W., Gan, Y., Ding, Y., Zhang, L., Jiao, X., Liu, L., et al. (2022). Autophagy promotes GSDME-mediated pyroptosis via intrinsic and extrinsic apoptotic pathways in cobalt chloride-induced hypoxia reoxygenation-acute kidney injury. *Ecotoxicol. Environ. Saf.* 242, 113881. doi:10.1016/j.ecoenv.2022.113881

Lu, Y. A., Liao, C. T., Raybould, R., Talabani, B., Grigorieva, I., Szomolay, B., et al. (2021). Single-nucleus RNA sequencing identifies new classes of proximal tubular epithelial cells in kidney fibrosis. *J. Am. Soc. Nephrol.* 32, 2501–2516. doi:10.1681/ASN.2020081143

Luo, W., Hu, H., Chang, R., Zhong, J., Knabel, M., O'Meally, R., et al. (2011). Pyruvate kinase M2 is a PHD3-stimulated coactivator for hypoxia-inducible factor 1. *Cell* 145, 732–744. doi:10.1016/j.cell.2011.03.054

Lynch, M. R., Tran, M. T., Ralto, K. M., Zsengeller, Z. K., Raman, V., Bhasin, S. S., et al. (2019). TFEB-driven lysosomal biogenesis is pivotal for PGC1α-dependent renal stress resistance. *JCI Insight* 5, e126749. doi:10.1172/jci.insight.126749

Ma, H., Guo, X., Cui, S., Wu, Y., Zhang, Y., Shen, X., et al. (2022). Dephosphorylation of AMP-activated protein kinase exacerbates ischemia/reperfusion-induced acute kidney injury via mitochondrial dysfunction. *Kidney Int.* 101, 315–330. doi:10.1016/j.kint.2021.10.028

Maremonti, F., Meyer, C., and Linkermann, A. (2022). Mechanisms and models of kidney tubular necrosis and nephron loss. *J. Am. Soc. Nephrol.* 33, 472–486. doi:10.1681/ASN.2021101293

Melo, R. S., Visoná, I., Almeida, W. S., and Campos, A. H. (2010). Glucose-insulin infusion reduces kidney injury in an experimental model of ischemic nephropathy. *Am. J. Nephrol.* 32, 603–609. doi:10.1159/000319622

Módis, K., Gero, D., Nagy, N., Szoleczky, P., Tóth, Z. D., and Szabó, C. (2009). Cytoprotective effects of adenosine and inosine in an *in vitro* model of acute tubular necrosis. *Br. J. Pharmacol.* 158, 1565–1578. doi:10.1111/j.1476-5381.2009.00432.x

Morigi, M., Perico, L., Rota, C., Longaretti, L., Conti, S., Rottoli, D., et al. (2015). Sirtuin 3-dependent mitochondrial dynamic improvements protect against acute kidney injury. *J. Clin. Invest.* 125, 715–726. doi:10.1172/JCI77632

Nakamura, S., Shigeyama, S., Minami, S., Shima, T., Akayama, S., Matsuda, T., et al. (2020). LC3 lipidation is essential for TFEB activation during the lysosomal damage response to kidney injury. *Nat. Cell Biol.* 22, 1252–1263. doi:10.1038/s41556-020-00583-9

Nicholson, R. J., Holland, W. L., and Summers, S. A. (2022). Ceramides and acute kidney injury. *Semin. Nephrol.* 42, 151281. doi:10.1016/j.semnephrol.2022.10.007

Nilakantan, V., Maenpaa, C., Jia, G., Roman, R. J., and Park, F. (2008). 20-HETE-mediated cytotoxicity and apoptosis in ischemic kidney epithelial cells. *Am. J. Physiol. Ren. Physiol.* 294, F562–F570. doi:10.1152/ajprenal.00387.2007

Oates, J. R., McKell, M. C., Moreno-Fernandez, M. E., Damen, M., Deepe, G. S., Jr., Qualls, J. E., et al. (2019). Macrophage function in the pathogenesis of non-alcoholic fatty liver disease: the Mac Attack. *Front. Immunol.* 10, 2893. doi:10.3389/fimmu.2019.02893

O'Connor, P. M. (2006). Renal oxygen delivery: matching delivery to metabolic demand. *Clin. Exp. Pharmacol. Physiol.* 33, 961–967. doi:10.1111/j.1440-1681.2006.04475.x

Pagliarini, D. J., Calvo, S. E., Chang, B., Sheth, S. A., Vafai, S. B., Ong, S. E., et al. (2008). A mitochondrial protein compendium elucidates complex I disease biology. *Cell* 134, 112–123. doi:10.1016/j.cell.2008.06.016

Park, S. W., Kim, M., Kim, J. Y., Brown, K. M., Haase, V. H., D'Agati, V. D., et al. (2012). Proximal tubule sphingosine kinase-1 has a critical role in A1 adenosine receptor-mediated renal protection from ischemia. *Kidney Int.* 82, 878–891. doi:10.1038/ki.2012.224

Peeters, A., Shinde, A. B., Dirkx, R., Smet, J., De Bock, K., Espeel, M., et al. (2015). Mitochondria in peroxisome-deficient hepatocytes exhibit impaired respiration, depleted DNA, and PGC-1α independent proliferation. *Biochim. Biophys. Acta* 1853, 285–298. doi:10.1016/j.bbamcr.2014.11.017

Piret, S. E., Attallah, A. A., Gu, X., Guo, Y., Gujarati, N. A., Henein, J., et al. (2021a). Loss of proximal tubular transcription factor Krüppel-like factor 15 exacerbates kidney injury through loss of fatty acid oxidation. *Kidney Int.* 100, 1250–1267. doi:10.1016/j.kint.2021.08.031

Piret, S. E., Guo, Y., Attallah, A. A., Horne, S. J., Zollman, A., Owusu, D., et al. (2021b). Krüppel-like factor 6-mediated loss of BCAA catabolism contributes to kidney injury in mice and humans. *Proc. Natl. Acad. Sci. U. S. A.* 118, e2024414118. doi:10.1073/pnas.2024414118

Portilla, D., Li, S., Nagothu, K. K., Megyesi, J., Kaissling, B., Schnackenberg, L., et al. (2006). Metabolomic study of cisplatin-induced nephrotoxicity. *Kidney Int.* 69, 2194–2204. doi:10.1038/sj.ki.5000433

Quigley, R., Baum, M., Reddy, K. M., Griener, J. C., and Falck, J. R. (2000). Effects of 20-HETE and 19(S)-HETE on rabbit proximal straight tubule volume transport. *Am. J. Physiol. Ren. Physiol.* 278, F949–F953. doi:10.1152/ajprenal.2000.278.6.F949

Rardin, M. J., He, W., Nishida, Y., Newman, J. C., Carrico, C., Danielson, S. R., et al. (2013). SIRT5 regulates the mitochondrial lysine succinylome and metabolic networks. *Cell Metab.* 18, 920–933. doi:10.1016/j.cmet.2013.11.013

Regner, K. R., Zuk, A., Van Why, S. K., Shames, B. D., Ryan, R. P., Falck, J. R., et al. (2009). Protective effect of 20-HETE analogues in experimental renal ischemia reperfusion injury. *Kidney Int.* 75, 511–517. doi:10.1038/ki.2008.600

Reshef, N., Karn, A., Manns, D. C., Mansfield, A. K., Cadle-Davidson, L., Reisch, B., et al. (2022). Stable QTL for malate levels in ripe fruit and their transferability across Vitis species. *Hortic. Res.* 9, uhac009. doi:10.1093/hr/uhac009

Robertson, L. T., Treviño-Villarreal, J. H., Mejia, P., Grondin, Y., Harputlugil, E., Hine, C., et al. (2015). Protein and calorie restriction contribute additively to protection from renal ischemia reperfusion injury partly via leptin reduction in male mice. *J. Nutr.* 145, 1717–1727. doi:10.3945/jn.114.199380

Roman, R. J., Akbulut, T., Park, F., and Regner, K. R. (2011). 20-HETE in acute kidney injury. *Kidney Int.* 79, 10–13. doi:10.1038/ki.2010.396

Sauer, S. (2015). Ligands for the nuclear peroxisome proliferator-activated receptor gamma. *Trends Pharmacol. Sci.* 36, 688–704. doi:10.1016/j.tips.2015.06.010

Scantlebery, A. M., Tammaro, A., Mills, J. D., Rampanelli, E., Kors, L., Teske, G. J., et al. (2021). The dysregulation of metabolic pathways and induction of the pentose phosphate pathway in renal ischaemia-reperfusion injury. *J. Pathol.* 253, 404–414. doi:10.1002/path.5605

Schetz, M., Vanhorebeek, I., Wouters, P. J., Wilmer, A., and Van den Berghe, G. (2008). Tight blood glucose control is renoprotective in critically ill patients. *J. Am. Soc. Nephrol.* 19, 571–578. doi:10.1681/ASN.2006101091

Scholz, H., Boivin, F. J., Schmidt-Ott, K. M., Bachmann, S., Eckardt, K. U., Scholl, U. I., et al. (2021). Kidney physiology and susceptibility to acute kidney injury: implications for renoprotection. *Nat. Rev. Nephrol.* 17, 335–349. doi:10.1038/s41581-021-00394-7

Settembre, C., and Ballabio, A. (2014). Lysosome: regulator of lipid degradation pathways. *Trends Cell Biol.* 24, 743–750. doi:10.1016/j.tcb.2014.06.006

Settembre, C., De Cegli, R., Mansueto, G., Saha, P. K., Vetrini, F., Visvikis, O., et al. (2013). TFEB controls cellular lipid metabolism through a starvation-induced autoregulatory loop. *Nat. Cell Biol.* 15, 647–658. doi:10.1038/ncb2718

Sharma, V., and Patial, V. (2022). Peroxisome proliferator-activated receptor gamma and its natural agonists in the treatment of kidney diseases. *Front. Pharmacol.* 13, 991059. doi:10.3389/fphar.2022.991059

Simon, N., and Hertig, A. (2015). Alteration of fatty acid oxidation in tubular epithelial cells: from acute kidney injury to renal fibrogenesis. *Front. Med. (Lausanne)* 2, 52. doi:10.3389/fmed.2015.00052

Smith, J. A., Stallons, L. J., and Schnellmann, R. G. (2014). Renal cortical hexokinase and pentose phosphate pathway activation through the EGFR/Akt signaling pathway in endotoxin-induced acute kidney injury. *Am. J. Physiol. Ren. Physiol.* 307, F435–F444. doi:10.1152/ajprenal.00271.2014

Spurgeon, K. R., Donohoe, D. L., and Basile, D. P. (2005). Transforming growth factor-beta in acute renal failure: receptor expression, effects on proliferation, cellularity, and vascularization after recovery from injury. *Am. J. Physiol. Ren. Physiol.* 288, F568–F577. doi:10.1152/ajprenal.00330.2004

Standage, S. W., Xu, S., Brown, L., Ma, Q., Koterba, A., Lahni, P., et al. (2021). NMR-based serum and urine metabolomic profile reveals suppression of mitochondrial pathways in experimental sepsis-associated acute kidney injury. *Am. J. Physiol. Ren. Physiol.* 320, F984–F1000. doi:10.1152/ajprenal.00582.2020

Stegen, S., van Gastel, N., Eelen, G., Ghesquière, B., D'Anna, F., Thienpont, B., et al. (2016). HIF-1α promotes glutamine-mediated redox homeostasis and glycogen-dependent bioenergetics to support postimplantation bone cell survival. *Cell Metab.* 23, 265–279. doi:10.1016/j.cmet.2016.01.002

Stumvoll, M., Chintalapudi, U., Perriello, G., Welle, S., Gutierrez, O., and Gerich, J. (1995). Uptake and release of glucose by the human kidney. Postabsorptive rates and responses to epinephrine. *J. Clin. Invest.* 96, 2528–2533. doi:10.1172/JCI118314

Suryawan, A., Hawes, J. W., Harris, R. A., Shimomura, Y., Jenkins, A. E., and Hutson, S. M. (1998). A molecular model of human branched-chain amino acid metabolism. *Am. J. Clin. Nutr.* 68, 72–81. doi:10.1093/ajcn/68.1.72

Susztak, K., Ciccone, E., McCue, P., Sharma, K., and Böttinger, E. P. (2005). Multiple metabolic hits converge on CD36 as novel mediator of tubular epithelial apoptosis in diabetic nephropathy. *PloS Med.* 2, e45. doi:10.1371/journal.pmed.0020045

Szeto, H. H. (2017). Pharmacologic approaches to improve mitochondrial function in AKI and CKD. *J. Am. Soc. Nephrol.* 28, 2856–2865. doi:10.1681/ASN.2017030247

Tan, B., Chen, J., Qin, S., Liao, C., Zhang, Y., Wang, D., et al. (2021a). Tryptophan pathway-targeted metabolomics study on the mechanism and intervention of cisplatin-induced acute kidney injury in rats. *Chem. Res. Toxicol.* 34, 1759–1768. doi:10.1021/acs.chemrestox.1c00110

Tan, C., Gu, J., Li, T., Chen, H., Liu, K., Liu, M., et al. (2021b). Inhibition of aerobic glycolysis alleviates sepsis-induced acute kidney injury by promoting lactate/Sirtuin 3/AMPK-regulated autophagy. *Int. J. Mol. Med.* 47, 19. doi:10.3892/ijmm.2021.4852

Tanaka, Y., Kume, S., Araki, S., Isshiki, K., Chin-Kanasaki, M., Sakaguchi, M., et al. (2011). Fenofibrate, a PPARα agonist, has renoprotective effects in mice by enhancing renal lipolysis. *Kidney Int.* 79, 871–882. doi:10.1038/ki.2010.530

Tanuseputero, S. A., Lin, M. T., Yeh, S. L., and Yeh, C. L. (2020). Intravenous arginine administration downregulates NLRP3 inflammasome activity and attenuates acute kidney injury in mice with polymicrobial sepsis. *Mediat. Inflamm.* 2020, 3201635. doi:10.1155/2020/3201635

Tian, C., Liu, Y., Li, Z., Zhu, P., and Zhao, M. (2022). Mitochondria related cell death modalities and disease. *Front. Cell Dev. Biol.* 10, 832356. doi:10.3389/fcell.2022.832356

Tran, M. T., Zsengeller, Z. K., Berg, A. H., Khankin, E. V., Bhasin, M. K., Kim, W., et al. (2016). PGC1α drives NAD biosynthesis linking oxidative metabolism to renal protection. *Nature* 531, 528–532. doi:10.1038/nature17184

Trimble, M. E. (1982). Long chain fatty acid transport by the perfused rat kidney. *Ren. Physiol.* 5, 136–142. doi:10.1159/000172849

Uni, R., and Choi, M. E. (2022). Novel roles of necroptosis mediator receptor-interacting protein kinase 3 in kidney injury. *Nephron* 146, 259–263. doi:10.1159/000517732

Valdés, A., Lucio-Cazaña, F. J., Castro-Puyana, M., García-Pastor, C., Fiehn, O., and Marina, M. L. (2021). Comprehensive metabolomic study of the response of HK-2 cells to hyperglycemic hypoxic diabetic-like milieu. *Sci. Rep.* 11, 5058. doi:10.1038/s41598-021-84590-2

Van de Poll, M. C., Soeters, P. B., Deutz, N. E., Fearon, K. C., and Dejong, C. H. (2004). Renal metabolism of amino acids: its role in interorgan amino acid exchange. *Am. J. Clin. Nutr.* 79, 185–197. doi:10.1093/ajcn/79.2.185

Van Opdenbosch, N., and Lamkanfi, M. (2019). Caspases in cell death, inflammation, and disease. *Immunity* 50, 1352–1364. doi:10.1016/j.immuni.2019.05.020

Vasko, R. (2016). Peroxisomes and kidney injury. *Antioxid. Redox Signal* 25, 217–231. doi:10.1089/ars.2016.6666

Wang, T., Fu, X., Chen, Q., Patra, J. K., Wang, D., Wang, Z., et al. (2019). Arachidonic acid metabolism and kidney inflammation. *Int. J. Mol. Sci.* 20, 3683. doi:10.3390/ijms20153683

Wang, Z., Fu, Z., Wang, C., Xu, J., Ma, H., Jiang, M., et al. (2021). ZLN005 protects against ischemia-reperfusion-induced kidney injury by mitigating oxidative stress through the restoration of mitochondrial fatty acid oxidation. *Am. J. Transl. Res.* 13, 10014–10037.

Wee, H. N., Liu, J. J., Ching, J., Kovalik, J. P., and Lim, S. C. (2021). The kynurenine pathway in acute kidney injury and chronic kidney disease. *Am. J. Nephrol.* 52, 771–787. doi:10.1159/000519811

Wei, Q., Dong, G., Yang, T., Megyesi, J., Price, P. M., and Dong, Z. (2007). Activation and involvement of p53 in cisplatin-induced nephrotoxicity. *Am. J. Physiol. Ren. Physiol.* 293, F1282–F1291. doi:10.1152/ajprenal.00230.2007

Wood, P. L., Khan, M. A., Moskal, J. R., Todd, K. G., Tanay, V. A., and Baker, G. (2006). Aldehyde load in ischemia-reperfusion brain injury: neuroprotection by neutralization of reactive aldehydes with phenelzine. *Brain Res.* 1122, 184–190. doi:10.1016/j.brainres.2006.09.003

Wu, H. H., Hsiao, T. Y., Chien, C. T., and Lai, M. K. (2009). Ischemic conditioning by short periods of reperfusion attenuates renal ischemia/reperfusion induced apoptosis and autophagy in the rat. *J. Biomed. Sci.* 16, 19. doi:10.1186/1423-0127-16-19

Wu, J., Rong, S., Zhou, J., and Yuan, W. (2021). The role and mechanism of PKM2 in the development of LPS-induced acute kidney injury. *Histol. Histopathol.* 36, 845–852. doi:10.14670/HH-18-343

Xiong, W., Xiong, Z., Song, A., Lei, C., Ye, C., and Zhang, C. (2021). Relieving lipid accumulation through UCP1 suppresses the progression of acute kidney injury by promoting the AMPK/ULK1/autophagy pathway. *Theranostics* 11, 4637–4654. doi:10.7150/thno.56082

Xu, S., Jia, P., Fang, Y., Jin, J., Sun, Z., Zhou, W., et al. (2022). Nuclear farnesoid X receptor attenuates acute kidney injury through fatty acid oxidation. *Kidney Int.* 101, 987–1002. doi:10.1016/j.kint.2022.01.029

Yamamoto, T., Takabatake, Y., Takahashi, A., Kimura, T., Namba, T., Matsuda, J., et al. (2017). High-Fat diet-induced lysosomal dysfunction and impaired autophagic flux contribute to lipotoxicity in the kidney. *J. Am. Soc. Nephrol.* 28, 1534–1551. doi:10.1681/ASN.2016070731

Yamazaki, T., Wakabayashi, M., Ikeda, E., Tanaka, S., Sakamoto, T., Mitsumoto, A., et al. (2012). Induction of 1-acylglycerophosphocholine acyltransferase genes by fibrates in the liver of rats. *Biol. Pharm. Bull.* 35, 1509–1515. doi:10.1248/bpb.b12-00243

Yang, J., Zhou, R., and Ma, Z. (2019). Autophagy and energy metabolism. *Adv. Exp. Med. Biol.* 1206, 329–357. doi:10.1007/978-981-15-0602-4_16

Yang, X., de Caestecker, M., Otterbein, L. E., and Wang, B. (2006). Carbon monoxide: an emerging therapy for acute kidney injury. *Med. Res. Rev.* 40, 1147–1177. doi:10.1002/med.21650

Yu, X., Xu, M., Meng, X., Li, S., Liu, Q., Bai, M., et al. (2020). Nuclear receptor PXR targets AKR1B7 to protect mitochondrial metabolism and renal function in AKI. *Sci. Transl. Med.* 12, eaay7591. doi:10.1126/scitranslmed.aay7591

Yuan, F., Zhang, L., Cao, Y., Gao, W., Zhao, C., Fang, Y., et al. (2018). Spermidine/spermine N1-acetyltransferase-mediated polyamine catabolism regulates beige adipocyte biogenesis. *Metabolism* 85, 298–304. doi:10.1016/j.metabol.2018.04.007

Zager, R. A., Burkhart, K. M., Johnson, A. C., and Sacks, B. M. (1999). Increased proximal tubular cholesterol content: implications for cell injury and "acquired cytoresistance". *Kidney Int.* 56, 1788–1797. doi:10.1046/j.1523-1755.1999.00745.x

Zager, R. A., Johnson, A. C., and Becker, K. (2014). Renal cortical pyruvate depletion during AKI. *J. Am. Soc. Nephrol.* 25, 998–1012. doi:10.1681/ASN.2013070791

Zahedi, K., Barone, S., Destefano-Shields, C., Brooks, M., Murray-Stewart, T., Dunworth, M., et al. (2017). Activation of endoplasmic reticulum stress response by enhanced polyamine catabolism is important in the mediation of cisplatin-induced acute kidney injury. *PloS One* 12, e0184570. doi:10.1371/journal.pone.0184570

Zahedi, K., Barone, S., Kramer, D. L., Amlal, H., Alhonen, L., Jänne, J., et al. (2010). The role of spermidine/spermine N1-acetyltransferase in endotoxin-induced acute kidney injury. *Am. J. Physiol. Cell Physiol.* 299, C164–C174. doi:10.1152/ajpcell.00512.2009

Zahedi, K., Barone, S., and Soleimani, M. (2019). Polyamine catabolism in acute kidney injury. *Int. J. Mol. Sci.* 20, 4790. doi:10.3390/ijms20194790

Zhang, D., Xing, Y., Li, W., Yang, F., Lang, Y., Yang, J., et al. (2018). Renal tubules transcriptome reveals metabolic maladaption during the progression of ischemia-induced acute kidney injury. *Biochem. Biophys. Res. Commun.* 505, 432–438. doi:10.1016/j.bbrc.2018.08.111

Zhang, H., Wu, H., Qian, J., Sun, L., Sang, L., Wang, P., et al. (2022). The regulation of LPCAT3 by miR-124-3p.1 in acute kidney injury suppresses cell proliferation by

disrupting phospholipid metabolism. *Biochem. Biophys. Res. Commun.* 604, 37–42. doi:10.1016/j.bbrc.2022.03.009

Zhang, J. Y., Zhou, B., Sun, R. Y., Ai, Y. L., Cheng, K., Li, F. N., et al. (2021). The metabolite α-KG induces GSDMC-dependent pyroptosis through death receptor 6-activated caspase-8. *Cell Res.* 31, 980–997. doi:10.1038/s41422-021-00506-9

Zhang, P., Chen, J. Q., Huang, W. Q., Li, W., Huang, Y., Zhang, Z. J., et al. (2017). Renal medulla is more sensitive to cisplatin than cortex revealed by untargeted mass spectrometry-based metabolomics in rats. *Sci. Rep.* 7, 44804. doi:10.1038/srep44804

Zhao, X., Quan, J., Tan, Y., Liu, Y., Liao, C., Li, Z., et al. (2021). RIP3 mediates TCN-induced necroptosis through activating mitochondrial metabolism and ROS production in chemotherapy-resistant cancers. *Am. J. Cancer Res.* 11, 729–745.

Zheng, X., Zhang, A., Binnie, M., McGuire, K., Webster, S. P., Hughes, J., et al. (2019). Kynurenine 3-monooxygenase is a critical regulator of renal ischemia-reperfusion injury. *Exp. Mol. Med.* 51, 1–14. doi:10.1038/s12276-019-0210-x

Zhou, H. L., Zhang, R., Anand, P., Stomberski, C. T., Qian, Z., Hausladen, A., et al. (2019). Metabolic reprogramming by the S-nitroso-CoA reductase system protects against kidney injury. *Nature* 565, 96–100. doi:10.1038/s41586-018-0749-z

Glossary

AKI	Acute kidney injury; TECs, Tubular epithelial cells; PTECs, Proximal renal tubular epithelial cells
FAO	Fatty acid oxidation
PPP	Pentose phosphate pathway
IRI	Ischemia-reperfusion injury
ROS	Reactive oxygen species
FAs	Fatty acids
CPT	Carnitine palmitoyltransferase
Acyl-CoA	Acyl-Coenzyme A
TCA	Tricarboxylic acid
NADH	Nicotinamide adenine dinucleotide hydrogen
FADH	Flavin Adenine Dinucleotide hydrogen
Sirt	Sirtuin
PGC	Peroxisome proliferator-activated receptor coactivator
PGC1α	Peroxisome proliferator-activated receptor coactivator -1 alpha
PPAR	Peroxisome proliferator-activated receptor
CD36	Cluster of Differentiation 36
LPCAT	Lysophosphatidylcholine acyltransferase
20-HETE	20-hydroxyeicosatetraenoic acid
19-HETE	19-hydroxyeicosatetraenoic acid
I/R	Ischemia/reperfusion
FFAs	Free fatty acids
LPS	Lipopolysaccharide
LDH	Lactate dehydrogenase
HK	Hexokinase
PFK	Phosphofructokinase
PK	Pyruvate kinase
PDH	Pyruvate dehydrogenase
HIF-1α	Hypoxia-inducible factor-1α
PKM	Pyruvate kinase muscle isoform
NADPH	Nicotinamide adenine dinucleotide phosphate
GSH	Glutathione
G6PD	Glucose-6-phosphate dehydrogenase
αKG	α-ketoglutarate
NOS	Nitric oxide synthase
KYN	Kynurenine
NAD	Nicotinamide adenine dinucleotide
GLS	Glutaminase
KP	Kynurenine pathway
IDO	Indoleamine 2,3-dioxygenase
TDO	Tryptophan 2,3-dioxygenase
KYNA	Kynurenic acid
SAT1/ PAOX	Spermidine/spermine and by N1-acetylation and N1-acetylpolyamine oxidase

frontiers | Frontiers in Molecular Biosciences

TYPE Original Research
PUBLISHED 11 December 2023
DOI 10.3389/fmolb.2023.1214961

OPEN ACCESS

EDITED BY
Pablo Vicente Escriba,
University of the Balearic Islands, Spain

REVIEWED BY
Annayya R. Aroor,
University of Missouri, United States
John W. Steele,
Baylor College of Medicine, United States

*CORRESPONDENCE
Krzysztof Marycz,
krzysztof.marycz@upwr.edu.pl
Lynda Bourebaba,
lynda.bourebaba@upwr.edu.pl

RECEIVED 30 April 2023
ACCEPTED 14 November 2023
PUBLISHED 11 December 2023

CITATION
Bourebaba L, Kępska M, Qasem B, Zyzak M, Łyczko J, Klemens M, Mularczyk M and Marycz K (2023), Sex hormone-binding globulin improves lipid metabolism and reduces inflammation in subcutaneous adipose tissue of metabolic syndrome-affected horses. *Front. Mol. Biosci.* 10:1214961. doi: 10.3389/fmolb.2023.1214961

Sex hormone-binding globulin improves lipid metabolism and reduces inflammation in subcutaneous adipose tissue of metabolic syndrome-affected horses

Lynda Bourebaba[1]*, Martyna Kępska[1], Badr Qasem[1], Magdalena Zyzak[1], Jacek Łyczko[2], Marta Klemens[2], Malwina Mularczyk[1,3] and Krzysztof Marycz[1,3,4]*

[1]Department of Experimental Biology, Faculty of Biology and Animal Science, Wrocław University of Environmental and Life Sciences, Wrocław, Poland, [2]Department of Food Chemistry and Biocatalysis, Faculty of Biology and Animal Science, Wrocław University of Environmental and Life Sciences, Wrocław, Poland, [3]International Institute of Translational Medicine, Wisznia Mała, Poland, [4]Department of Surgical and Radiological Sciences, School of Veterinary Medicine, University of California, Davis, Davis, CA, United States

Equine metabolic syndrome (EMS) is a steadily growing endocrine disorder representing a real challenge in veterinary practice. As a multifactorial condition, EMS is characterized by three main metabolic abnormalities including insulin resistance, increased adiposity or obesity and hoof laminitis. Adipose tissue dysfunction is recognized as a core pathophysiological determinant of EMS, as it strongly participates to lipotoxicity and systemic metaflammation, both of which have been closely linked to the development of generalized insulin resistance. Besides, sex hormone binding globulin (SHBG) is an important sex steroids transporters that has been recently proposed as an important metabolic mediator. Therefore, the aim of this study was to verify whether SHBG treatment may ameliorate subcutaneous adipose tissue metabolic failure under EMS condition in terms of lipidome homeostasis, lipid metabolism programs, insulin signalling and local inflammation. Subcutaneous adipose tissue (SAT) biopsies were collected post-mortem from healthy (n = 3) and EMS (n = 3) slaughtered horses. SHBG protein has been applied to SAT samples from EMS horses for 24 h at a final concentration of 50 nM, while control groups (healthy and untreated EMS) were cultured in the presence of SHBG-vehicle only. Tissues from all groups were afterwards secured for downstream analysis of gene expression using RT-qPCR, protein levels by Western blot and ELISA assay and lipidomics through GC-MS technique. Obtained results showcased that SHBG intervention efficiently normalized the altered fatty acids (FAs) profiles by lowering the accumulation of saturated and trans FAs, as well as the pro-inflammatory arachidonic and linoleic acids. Moreover, SHBG showed promising value for the regulation of adipocyte lipolysis and engorgement by lowering the levels of perilipin-1. SHBG exerted moderated effect toward SCD1 and FASN enzymes expression, but increased the LPL abundance. Interestingly, SHBG exhibited a negative regulatory effect on pro-adipogenic stimulators and induced higher expression of KLF3, IRF3 and β-catenin, known as strong adipogenesis repressors. Finally, SHBG protein showed remarkable ability in restoring the

insulin signal transduction, IR/IRS/Pi3K/AKT phosphorylation events and GLUT4 transporter abundance, and further attenuate pro-inflammatory response by lowering IL-6 tissue levels and targeting the PDIA3/ERK axis. Overall, the obtained data clearly demonstrate the benefice of SHBG treatment in the regulation of adipose tissue metabolism in the course of EMS and provide new insights for the development of molecular therapies with potential translational application to human metabolic disorders.

KEYWORDS

EMS, SHBG, lipid metabolism, metaflammation, lipidome, insulin signaling

1 Introduction

Metabolic syndrome (MetS) or syndrome X is defined as a cluster of metabolic defects comprising insulin resistance, hypertension, dyslipidaemia, central obesity or regional adiposity. The pathogenesis of MetS englobes both genetic and environmental factors; however, lifestyle seems to be an equally important risk factor, especially when insulin resistance related to obesity and inflammation are considered (Rochlani et al., 2017). MetS is nowadays becoming a frequently diagnosed endocrine disorder not only in human beings but also among animals including horses. The pathogenesis of equine metabolic syndrome (EMS) reflects many similarities to MetS and therefore becomes a valuable large animal model for studying endocrine disorders. Indeed, EMS condition has been recognized as a similar endocrinopathy to human Metabolic Syndrome (MetS). Statements from the American College of Veterinary Internal Medicine (ACVIM) and the European College of Equine Internal Medicine (ECEIM) EMS consensus have highlighted the clinical, phenotypic, and molecular resemblances between EMS and the pathophysiology of human MetS. Shared mechanisms of these conditions involve irregular insulin regulation and resistance, abnormal fat distribution, and metaflammation, offering promising opportunities for utilizing EMS as a valuable experimental model in translational human medicine (Frank et al., 2010; Morgan et al., 2015; Durham et al., 2019; Ragno et al., 2019).

In both MetS and EMS central obesity or adiposity is regarded as a major determinant of the disease development and a serious factor promoting local and systemic inflammation that is often associated with cardiovascular diseases development or laminitis in horses. The latter is recognized among insulin resistance horses as the most debilitating, life-threatening disorder that is often diagnosed among obese horses (Ertelt et al., 2014). According to the Center of Disease Control and Prevention (CDC), obesity prevalence has increased by 35% in the last 15 years in the United States (Fahed et al., 2022). These alarming data are not alien to European countries where obesity is growing at a similar pace. Surprisingly, the same scenario has been observed among large animals; and obesity-related insulin resistance has been identified in more than 30% of horses in the territory of the United Kingdom. These data clearly show that obesity or adiposity is our century's devastating disorder that has a serious impact on health and in consequence, becomes a significant financial burden for many healthcare systems around the world (Rendle et al., 2018; Krzysztoszek et al., 2019).

Obesity is actually recognized as a worldwide epidemic and one of the most prevalent risk factors for insulin resistance, immune-mediated disorders, non-alcoholic fatty liver disease, cardiovascular affections (CVD), several types of cancer, and type 2 diabetes mellitus (T2D). As above mentioned, obesity is strongly associated with the development of many other disorders, and as a multifactorial chronic disease is recognized as a key player in the development of MetS or EMS (Pi-Sunyer, 2009). Adipose tissue is considered an is a metabolically dynamic endocrine organ that actively produces and secretes various humoral factors (adipokines), hormones, and cytokines that play a fundamental role in local and systemic insulin dysregulation, and insulin resistance development as well as inflammation. Adipose tissue insulin resistance is a key factor strongly impacting fat hypertrophy, which is believed to be closely associated to low-grade local and systemic inflammation (Zatterale et al., 2020). Impaired glucose uptake within adipocytes that is mediated by hampered glucose transporter 4 (GLUT-4) translocation, combined with the lower expression and phosphorylation of adipocytes' insulin receptor (IR) and its substrates (IRSs) have been found to play an important role in adipose tissue hyperinsulinemia and insulin resistance development in both human and horses (Reynolds et al., 2019; Ahmed et al., 2021). Metabolically impaired adipose tissue further displays altered lipid metabolism homeostasis, which subsequently aggravates the existing insulin resistance and metaflammation. Lipids play a pivotal role in the pathogenesis of insulin resistance and adipose tissue inflexibility. Once enlarged due to excess caloric intake, dysfunctional adipose tissue produces and releases toxic reactive lipids such as ceramides and diacyl-glycerides (DAG) that impede the insulin-mediated kinases phosphorylation and triggers various cellular stresses related to MAPK/NFκB pro-inflammatory pathway activation, excessive ROS generation, endoplasmic reticulum (ER) and mitochondrial disruption and cell apoptosis (Sears and Perry, 2015). Moreover, defects in lipolysis results in adipocytes engorgement, adipose tissue failure and excessive adipokines release, which promotes systemic insulin dysregulation (Guilherme et al., 2008). In EMS horses, adipocytes hypertrophy has been associated with increased expression of leptin and the inflammatory cytokines tumor necrosis factor (TNF)-α, IL1β and monocyte chemoattractant protein (MCP)-1 and typical fasting hyperinsulinemia, evoking the close relationship between flawed adipose tissue dynamics and insulin resistance progression (Reynolds et al., 2019).

Imbalanced saturated fatty acids levels deriving from cell surface-expressed lipases including the hormone-sensitive lipase

(HSL) depletion exerts direct stimulatory feedback to activate various pro-inflammatory cascades leading to adipose tissue infiltration by macrophages, higher expression of TNF-α, MCP-1, and IL-6. Although the exact molecular mechanisms underlying metaflammation unleashing are quite complex, a body of evidence indicate that FFAs such as palmitic acid initiate a TLR4-dependent gene expression program that facilitate the NF-κB/MAPK inflammatory cascade (Kawai et al., 2021). Elevated expression of TNF-α, MCP-1, or IL-6 has been further reported to significantly reduce the expression of GLUT4 and promote the compensatory hyperinsulinemia. Moreover, pro-inflammatory cytokines are critically involved in the induction of energy expenditure by binding to signaling receptors in adipose tissue and activating leptin expression. More specifically, it was found that TNF-α is involved in the regulation of leptin expression and activation in adipose tissue of MetS individuals, and thus promotes adipose tissue hypoxia that modulates adipose depots expansion (Caputo et al., 2017). Massive expansion and remodeling of adipose tissue significantly contributes to vascular dysfunction including arterial stiffening. Excessive deposition of AT around inner organs and at the periphery promotes the excessive infiltration of immune cells and secretion of various cytokines and vasoconstrictor mediators (Koenen et al., 2021). Oxidative stress and proinflammatory processes associated with secreted cytokines and adipokines englobing TNF-α, IL-6, angiotensinogen, aldosterone-stimulating factors, aldosterone, adiponectin, dipeptidylpeptidase 4 (DPP-4), leptin, resistin, and MCP-1 arousing from dysfunctional AT have been evidenced as key players participating in obesity-related vascular dysfunction (Fleenor et al., 2022). Moreover, suppressed insulin metabolic signaling in endothelial cells triggers reductions in nitric oxide (NO) production within the vasculature, which further initiates vascular stiffening (Aroor et al., 2018). Noteworthy, besides visceral and subcutaneous fat have been evoked as critical contributors of vascular stiffening in the course of obesity and metabolic disorders, perivascular fat tissue surrounding blood vessels, was similarly found to exert strong paracrine effects influencing the vasculature plasticity and remodling. Hence, hypertrophic perivascular adipocytes release a number of mediators such as IL-6, resistin and visfatin that enhance the deposition of collagen type 1, advanced glycation end products and calcium phosphate in the vascular wall (Para et al., 2021).

Recently, the correlation between serum sex hormone binding globulin (SHBG), inflammation, and insulin resistance has been demonstrated in obese and MetS human patients (Alinezhad and Jafari, 2019). It was found, that low serum SHBG correspond to increased body mass index (BMI), excessive liver fat, chronic obstructive pulmonary disease and diabetes incidence (Simó et al., 2015; Wang, 2021). SHBG is a 373-amino-acid glycoprotein produced in the liver and adipose tissue and excreted to the bloodstream where it binds sex steroids to regulate their bioavailability, and as reported recently, SHBG acts as an anti-inflammatory mediator suppressing inflammation and lipid accumulation in macrophages and adipocytes (Yamazaki et al., 2018). Albeit the exact mechanisms underlying SHBG interaction with cells and tissues in a context independent from sex hormones transport remains still under debate, latest research suggested the existence of an SHBG-specific membrane-bound megalin receptor (R_{SHBG}) which facilitates the endocytosis of SHBG. Interaction of SHBG with megalin has been proposed to activate a G-protein-coupled receptor second messenger system, which initiates the synthesis and release of cyclic adenosine monophosphate (cAMP) and subsequent activation of protein kinase A (Nakhla et al., 1999; Wallace et al., 2013). Interestingly, foregoing studies revealed that SHBG affinity to its receptor was highly decreased upon its fixation to sex steroids, and that the stronger the binding of a steroid to SHBG, the greater its capacity to hinder the interaction between SHBG and its receptor, suggesting the interplay of distinct signalling pathways mediating SHBG biological effects (Rosner et al., 2010). SHBG is thus gaining more attention as it might be a potential therapeutic factor in the treatment of obesity and associated inflammation and insulin resistance. Little is known regarding the eventual biological effects of SHBG in disease, however mounting evidence highlight the promising role of SHBG in reducing both oxidative and ER stress, which might be recognized as a primary mechanism involved in the modulation of adipose tissue insulin sensitivity (Kornicka-Garbowska et al., 2021). Although there is limited data documenting the direct effect of SHBG on adipose tissue and its molecular implications, recent investigation demonstrated that overexpression of SHBG in a model of SHBG-C57BL/ksJ-db/db mouse confers high protection against high fat diet-induced excessive weight gain while preventing metabolic profile deregulation by normalizing the glucose, insulin, leptin, resistin, adiponectin, cholesterol, FFA and TG plasma levels. Interestingly, the same study established a direct link between SHBG and adipose tissue turnover showing the ability of SHBG to activate lipolysis by promoting protein kinase A (PKA), extracellular signal-regulated kinase 1/2 (ERK-1/2), hormone-sensitive lipase (HSL) and perilipin (PLIN) expression and phosphorylation (Saez-Lopez et al., 2020). Noteworthy, our previously published findings illustrated similar effects of SHBG in HepG2 cells, where exposure of hepatocytes overloaded with palmitic acid to exogenous human SHBG resulted in a sharp decreased expression of FASN, ACLY, and peroxisome proliferator-activated receptor gamma (PPARγ), indicating the potential of SHBG to regulate liver metabolism by the inhibition of lipogenesis (Kornicka-Garbowska et al., 2021). Hence, it can be speculated that SHBG may exert favourable action on lipid metabolism in both liver and AT via similar mechanisms. Nevertheless, the exact molecular impact of SHBG on adipose tissue metabolism, inflammation and insulin resistance remains elusive, and more advanced investigations are needed to clarify the possible use of the glycoprotein as a therapeutic agent for metabolic disorders management.

For that purpose, this study aimed at investigating the impact of SHBG treatment on adipose tissue biopsies in terms of lipid metabolism and insulin sensitivity, and to further explore its role as a potential anti-inflammatory mediator in EMS condition. We have found that SHBG normalized the lipidome profile of EMS-derived adipose tissue, improved the insulin-kinases phosphorylation cascade and decreased the expression of IL-6 and MCP-1 mediated by the modulation of the PDIA3/ERK axis;

however, further clinical trials are necessary to confirm the applicability and effectiveness of SHBG in counteracting EMS pathological events.

2 Materials and methods

2.1 Tissue samples collection

Subcutaneous Adipose Tissue (SAT) biopsies were collected post-mortem from Polish cold-blooded healthy and EMS horses from a local slaughterhouse (Targowa, Rawicz, Poland). Animals that were euthanized for reasons unrelated to this study, were aged between 8 and 10 years, and qualified by experienced veterinarians on the basis of their clinical profiles and medical history following previously described procedure and established criterions that included body weight (BW), body condition score (BCS), cresty neck score (CNS) and fasting insulin levels (Henneke et al., 1983; Basinska et al., 2015; Marycz et al., 2016). The clinical assessment data of qualified healthy horses (n = 3) and EMS horses (n = 3) are summarized in Table 1.

2.2 Preparation of subcutaneous adipose tissue specimens

Freshly collected tissue fragments were transported in Dulbecco's Phosphate Buffered Saline (DPBS, Biowest) supplemented with 1% penicillin-streptomycin solution (PS, Biowest) to the cell culture facility. Within 2 h of collection, tissues were cut manually to smaller pieces (approximately 50 mg each) and washed twice in DPBS with 1% PS. The biopsies were transferred into 12-well plates containing a growth culture medium consisting of Dulbecco's Modified Eagle's Medium with 1,000 mg/L glucose, L-glutamine, and sodium bicarbonate (DMEM-LG, Biowest) supplemented with 0.2% bovine serum albumin (BSA, Sigma Aldrich) and 1% PS. In each well, six pieces of tissue (two from each horse) were cultured in 1.5 mL of growth medium under aseptic and standard conditions in a CO_2 incubator at 37°C. Specimens harvested from horses affected with EMS were split into control untreated group (Eq SAT_EMS) and experimental group treated with native sex hormone binding globulin (SHBG, Fitzgerald) at a concentration of 50 nM for 24 h (Eq SAT_EMS + SHBG), while SAT obtained from healthy horses were used as a normal control group (Eq SAT_HE). Then all tissue pieces from each group were pulled together, secured in appropriate reagents and subjected to further analysis as described below.

2.3 Gene expression analysis

Tissue fragments were lysed in 1 mL of Extrazol (Blirt). Total RNA was isolated from specimens according to the manufacturer's instructions using the chloroform/phenol method. To verify the quality and quantity of obtained RNA, absorbance at 260 and 280 nm were measured using an Epoch Take3 plate (BioTek). Any remaining DNA from the RNA samples was digested for 30 min at 37°C with DNase I RNase-free (ThermoFisher). DNA-free RNA was used for synthesizing complementary DNA (cDNA) using a PrimeScript RT Reagent Kit (Takara). Both digestion and reverse transcription were performed using a T100 Thermal Cycler (Bio-Rad). Obtained cDNA were used for pre-amplification of determined products using specific primers and annealing temperatures. The pre-amplification mixtures contained both forward and reverse primers at a concentration of 50 mM each (listed in Table 2), 6 ng of cDNA and reagent from SensiFAST SYBR and Fluorescein Kit (Bioline) at 50% of total volume. The pre-amplification based on polymerase chain reaction (PCR) consisted of: initial enzyme activation at 95°C for 2 min, followed by 18 cycles of denaturation at 95°C for 5 s, annealing for 3 min at a temperature dependent on the sequences of primers, and elongation at 72°C for 5 s. The obtained products were diluted in DEPC treated water in a 1:3 ratio and used for Quantitative Reverse-Transcription Polymerase Chain Reaction (RT-qPCR).

For each measurement, 2.5 µL of pre-amplified fragments of cDNA were mixed with forward and reverse primers at concentration of 500 nM each and SensiFAST SYBR and Fluorescein Kit at 50% of reaction total volume. qRT-PCR analysis was performed using a CFX Connect Real-Time PCR Detection System (Bio Rad) under the following thermal conditions: 95°C for 2 min, followed by 40 cycles of: 95°C for 15 s for denaturation, annealing in temperature gradient for 30 s, and extension at 72°C for 15 s with a single fluorescence measurement. The mRNA levels were normalized relative to GAPDH housekeeping gene and the relative gene expression was calculated using the $2^{-\Delta\Delta CT}$ algorithm.

TABLE 1 Healthy and EMS horses' qualification criteria.

Groups	Age	BW (kg)	BCS (1–9)	CNS (1–5)	Fasting insulin (mU/mL)	CGIT:GLU in 45 min (mg/dL)
Healthy Horses	8	569	6	1	8	74/n
	8	601	6	2	12	69/n
	10	542	7	2	10	73/n
Average ± SD	8.66 ± 1.15	570.66 ± 29.53	6.33 ± 0.57	1.66 ± 0.57	10 ± 2	72 ± 2.64
EMS Horses	9	710	8	3	83	144/p
	10	726	9	4	82	141/p
	10	760	9	5	89	137/p
Average ± SD	9.66 ± 0.57	732 ± 25.53	8.66 ± 0.57	4 ± 1	84.66 ± 3.78	140.5 ± 3.51

BW, body weight; BCS, body condition score; CNS, crest neck score; CGIT, combined glucose-insulin test; SD, standard deviation; GLU, glucose; p, positive test result; n, negative test result.

TABLE 2 Sequences of primers used in RT-qPCR.

Gene	Primers (5′→3′)		Length of amplicon	Accession no.
AKT1	**F**	AAGGAGATCATGCAGCACCG	**180**	XM_023628568.1
	R	CTCCATCGTGTCGTCTTGGT		
CEBPD	**F**	CTGTCTGCCGAGAACGAGAA	**186**	XM_023648662.1
	R	TCGGGTCTGAGGTATCGGTC		
COX4I1	**F**	GAATAGGGGCACGAACGAGT	**138**	XM_023637444.1
	R	GCCACCCACTCCTCTTCAAA		
COX7A1	**F**	GAAGAGGAGGACGCAGAATG	**289**	XM_014733609.2
	R	CTGTTTCAGGTCCTGTAGGC		
COX8A	**F**	TTCCCGACCTTGGGCTGTAG	**190**	XM_008541287.1
	R	GAGGTGAGCCCAATGGTGAC		
CTNNB	**F**	GAACCCAGCAGCAGTTTGTG	**219**	NM_001122762.1
	R	CAGCCTCTTTGTCCTGAGCA		
FASN	**F**	AAAGGAGGCTGCCCGAAAAA	**450**	XM_023651718.1
	R	CCACACGGAGTCTCGTTTCT		
GAPDH	**F**	GATGCCCCAATGTTTGTGA	**250**	NM_001163856.1
	R	AAGCAGGGATGATGTTCTGG		
GLUT4	**F**	TTTGTGGCATTCTTTGAGA	**65**	NM_001081866.2
	R	CTGAAGAGCTCAGCCACG		
IL6	**F**	CGTCACTCCAGTTGCCTTCT	**225**	NM_001082496.2
	R	GCCAGTACCTCCTTGCTGTT		
INSR	**F**	CCGTTTGAGTCTGAGGGGTC	**254**	XM_023644607.1
	R	ACCGTCACATTCCCGACATC		
IRF3	**F**	CCTATGCCCTCCACCTCTGA	**124**	XM_001504445.4
	R	GGTATCCCTTGCCATCCACG		
IRS1	**F**	GGTGCCCAAGGACAAGGAAGGA	**276**	XM_023650154.1
	R	GAGAGGGGGTGGCTGTTGGAAA		
IRS2	**F**	ATTCATGGTGGTCACGGGTC	**197**	XM_023621823.1
	R	CCCTGTGCGATGGTTTCTCT		
KLF7	**F**	TAAAGGCCCACCAGAGGACT	**253**	XM_003363309.4
	R	GTTTCCCTCAGACAACGGCT		
KLF15	**F**	CGGGTGTACCACATGCTGCCT	**248**	XM_023619835.1
	R	TTCACAGATGCCGGTGCCCTC		
KLF2	**F**	CACACCTGCAGCTACGC	**127**	XM_023625367.1
	R	CGAACTTCCAGCCGCAG		
KLF3	**F**	GGAAGAGACCGTTACCTGTGG	**280**	XM_023638230.1
	R	AGGTGGTCAGAGCGGGAAA		
KLF4	**F**	GCATGTGCCCCAAGATCAAG	**202**	XM_023629843.1
	R	GGATGACAGTCCCTGTTGCT		

(Continued on following page)

TABLE 2 (*Continued*) Sequences of primers used in RT-qPCR.

Gene	Primers (5′→3′)		Length of amplicon	Accession no.
KLF5	**F**	GAGAAACGGCGCATCCACT	**275**	XM_023621686.1
	R	GCTCAGTTCTGGTGCCTCTTC		
KLF9	**F**	TGTCTGCGAAGGGGAAACAC	**608**	XM_001916945.4
	R	GATCATGCTGGGGTGGAACT		
LPL	**F**	TCGCTCTGAGGACCCCTAAA	**297**	XM_005607650.3
	R	TGATAAACCGGGCCACATCC		
MCP1	**F**	ATTGGCCAAGGAGATCTGTG	**167**	NM_001081931.2
	R	ATATCAGGGGGCATTTAGGG		
PI3K	**F**	GACTTGCACTTGGGTGACATA	**152**	XM_023625590.1
	R	TAAGTTCCCGGAAAGTCCCC		
PLIN1	**F**	CAATGGCAGTGAACAAGGACCCG	**120**	XM_023650036.1
	R	TTTTCTGGAAGCACGCGCAGG		
PNPL2	**F**	CATGGAACATCTCGTTCGCC	**197**	XM_023654788.1
	R	CACCTCGATGATGTTGGCAC		
PPARA	**F**	GGCCTTCTAAACGTGGGACA	**135**	NM_001242553.1
	R	CCGGAGGTCTGCCATTTTCT		
PPARGC1A	**F**	TCTACCTAGGATGCATGG	**93**	XM_014738763.2
	R	GTGCAAGTAGAAACACTGC		
PPARGC1B	**F**	CAACTATCTTGCCGACACCC	**162**	XM_023617445.1
	R	ATGGGTTCAGTCTCGGGGTT		
PTGES2	**F**	GGCCAAGTACATGGGTGCAG	**334**	XM_023628980.1
	R	GCATCTTCCGTTGCCTCTCG		
SCD	**F**	ATGCTGATCCCCACAATGCC	**182**	XM_001500364.4
	R	GAAGCACAGCAACACGACAC		
SMAD2	**F**	AGGGTGGGGAGCAGAATACC	**89**	XM_023647764.1
	R	CCAACCACTGTAGGGGTCCA		
STAT5A	**F**	AGATGCTGGCCGAGGTCAAC	**212**	XM_023652507.1
	R	AGACTTGGCCTGCTGCTCAC		

AKT1, Protein kinase B; ***CEBPD***, CCAAT/enhancer-binding protein delta; ***COX4I1***, Cytochrome C Oxidase Subunit 4I1; ***COX7A1***, Cytochrome C Oxidase Subunit 7A1; ***COX8A***, Cytochrome C Oxidase Subunit 8A; ***CTNNB***, Catenin Beta; ***EBF1***, Early B cell factor-1; ***FASN***, Fatty Acid Synthase; ***GAPDH***, Glyceraldehyde-3-phosphate dehydrogenase protein; ***GLUT4***, Glucose transporter 4; ***GSK3B***, Glycogen Synthase Kinase 3beta; ***IL6***, Interleukin 6; ***INSR***, Insulin receptor; ***IRF3***, Interferon regulatory factor 3; ***IRS1***, Insulin receptor substrate 1; ***IRS2***, Insulin receptor substrate 1; ***KLF7***, Krueppel-like factor 7; ***KLF15***, Krueppel-like factor 15; ***KLF2***, Krueppel-like factor 2; ***KLF3***, Krueppel-like factor 3; ***KLF4***, Krueppel-like factor 4; ***KLF5***, Krueppel-like factor 5; ***KLF9***, Krueppel-like factor 9; ***LPL***, Lipoprotein lipase; ***MCP1***, Monocyte chemoattractant protein-1; ***PI3K***, Phosphatidylinositol 3-kinase; ***PLIN1***, Perilipin-1; ***PNPL2***, Patatin Like Phospholipase Domain Containing 2; ***PPARA***, Peroxisome proliferator activated receptor alpha; ***PPARGC1A***, Peroxisome proliferator-activated receptor gamma coactivator 1-alpha; ***PPARGC1B***, Peroxisome proliferator-activated receptor gamma coactivator 1-beta; ***PTGES2***, Prostaglandin E Synthase 2; ***SCD***, Stearoyl-CoA desaturase; ***SMAD1***, Mothers against decapentaplegic homolog 1; ***SMAD2***, Mothers against decapentaplegic homolog 2; ***SMAD5***, Mothers against decapentaplegic homolog 5; ***SMAD9***, Mothers against decapentaplegic homolog 9; ***STAT5A***, Signal Transducer And Activator Of Transcription 5A.

2.4 Protein isolation

Biopsies were collected following 24 h incubation in the presence or absence of SHBG protein, washed with ice-cold PBS and cut with scalpel on ice. Then each 100 mg of tissue was lysed in 500 µL of RIPA buffer containing 1% of protease and phosphatase inhibitor cocktail (Sigma Aldrich). The samples were blended with a mini handheld homogenizer and then incubated for 60 min on ice. Afterwards, the tissues were centrifuged at 12,000 × g, 4°C for 15 min. The upper layer containing fat was discarded and the supernatant was transferred with a syringe into a new tube. To remove excess fat from the sample, the procedure of centrifugation

TABLE 3 Antibodies used in Western blot analysis.

Protein	Manufacturer	Catalog number	Dilution
FASN	Affinity Biosciences	DF6106	1:500
Vinculin	Sigma Aldrich	V9264	1:8000
LPL	Affinity Biosciences	DF12534	1:500
SCD1	Affinity Biosciences	DF13253	1:500
ATGL	Aviva System Biology	OAEB02425	1:250
HSL	Affinity Biosciences	AF6403	1:500
PLIN1	Affinity Biosciences	DF7602	1:1000
p-PI3K	Biorbyt	orb544410	1:1000
p-AKT	Biorbyt	orb304681	1:1000
GLUT4	Abcam	ab33780	1:1000
p-IRS1	Invitrogen	PA1-1054	1:660
p-IRS2	Affinity Biosciences	AF8383	1:1000
SHBG	Biorbyt	orb11366	1:500
p-IR	Affinity Biosciences	AF3099	1:500
ERK1/2	Affinity Biosciences	AF1055	1:500
PDIA3	Aviva System Biology	ARP63565	1:250
Anti-mouse IgG, HRP conjugated	Jackson ImmunoResearch	115-035-146	1:8000
Anti-rabbit IgG, HRP conjugated	Sigma Aldrich	AP156P	1:2500
Anti-goat IgG, HRP conjugated	Jackson ImmunoResearch	805-035-180	1:8000

FASN, Fatty Acid Synthase; ***LPL***, Lipoprotein lipase; ***SCD1***, Stearoyl-CoA desaturase-1; ***ATGL***, Adipose triglyceride lipase; ***HSL***, Hormone-sensitive lipase; ***PLIN1***, Perilipin 1; ***p-PI3K***, Phosphorylated Phosphoinositide-3-kinase; ***p-AKT***, Phosphorylated Protein kinase B; ***GLUT4***, Glucose transporter 4; ***p-IRS1***, Phosphorylated Insulin receptor substrate 1; ***p-IRS2***, Phosphorylated Insulin receptor substrate 2; ***SHBG***, Sex hormone-binding globulin; ***p-IR***, Phosphorylated Insulin receptor; ***GSK3B***, Glycogen Synthase Kinase 3 Beta; ***ERK1/2***, extracellular signal-regulated protein kinase 1/2; ***PDIA3***, Protein disulfide isomerase associated 3; ***HRP***, Horseradish peroxidase.

was repeated two times more. Total content of protein was measured spectrophotometrically using the TaKaRa BCA Protein Assay Kit (Takara) and microplate spectrophotometer Epoch (BioTek).

2.5 Western blot analysis

The protein samples were mixed with 4× Laemmli Loading Buffer (Bio-Rad) and boiled for 5 min at 95°C. 10 µg of total protein from each specimen was separated by electrophoresis in sodium dodecyl sulphate-polyacrylamide gel at 110 V for 100 min using Mini-PROTEAN Tetra Vertical Electrophoresis Cell (Bio-Rad). Then, the proteins were transferred into previously activated with methanol PVDF membrane (Bio-Rad). The transfer was performed at 100 V for 60 min using the Mini Trans-Blot Cell (Bio-Rad). Afterwards, the membranes were blocked in 5% skimmed milk solution or 5% bovine serum albumin for 2 h at room temperature. After blocking, the membranes were washed once in Tris-buffered saline supplemented with 0.1% Tween-20 detergent (TBST) and then incubated overnight at 4°C with primary antibodies. Washing of membranes with TBST was performed five times for 5 min with TBST and then the membranes were incubated with the secondary antibodies for 2 h at room temperature. After incubation, the membranes were washed again five times for 5 min in TBST before adding the Clarity Western ECL Substrate (Bio-Rad) and visualization in ChemiDoc MP Imaging System (Bio-Rad). The relative adjusted density of protein bands was evaluated using the Image Lab Software (Bio-Rad). To determine the molecular weight of detected proteins, BLUeye Prestained Protein Ladder was used as a marker (Sigma Aldrich). Whole analysis of each protein (listed in Table 3) was performed in at least four repetitions.

2.6 Enzyme-linked immunosorbent assay

Concentrations of inflammatory factors (IL6, TNFA, PGE2, MCP1) in tissues were evaluated by enzyme linked immunosorbent assays (ELISA) in accordance with the manufacturers' instructions (IL6, TNFA and MCP1—BTLAB, PGE2—EIAab). For each assay, 7 µg of total protein solution were served per well as an antigen. Concentration of each marker was measured in four technical repetitions using microplate spectrophotometer Epoch (BioTek).

2.7 Lipidomics profiling

2.7.1 Extraction of FAs from subcutaneous adipose tissue specimens

The extraction of lipid metabolites was performed with Folsh method from 500 mg of SAT (Folch et al., 1957). Briefly, 2 mL of a chloroform: methanol (2:1) solution was added to each sample, and subjected to vigorous shaking for 2 h. Thereafter, the organic solvents were separated and the process was repeated. Then, the extraction solvent from particular samples were combined and evaporated with a rotary-vacuum evaporator. All samples were prepared in three repetitions.

2.7.2 Preparation of fatty acid methyl esters (FAMEs)

At the first step, 50 µg of C17:0 fatty acid (Sigma-Aldrich, Steinheim, Germany) was added as an internal standard (IS) to each sample. Then, the samples were hydrolyzed with 2 mL 0.5 M solution of potassium hydroxide (KOH) (POCH, Gliwice, Poland) in methanol (POCH, Gliwice, Poland) by boiling the flask content for 10 min under the reflux column. Then, after cooling, 1.5 mL of 14% (v/v) solution of boron trifluoride (BF3) in methanol (Sigma-Aldrich, Steinheim, Germany) was added and the esterification process was carried out for 10 min at 80°C under the reflux column. After cooling, 1 mL of saturated solution of sodium chloride (NaCl) (POCH, Gliwice, Poland) was added and the FAMEs were extracted with two portions, 1.5 mL each, of hexane (POCH, Gliwice, Poland). After the extraction, the hexane phases from particular samples were combined and dried above the anhydrous magnesium(II) sulphate(VI) ($MgSO_4$) (POCH, Gliwice, Poland). Thereafter, the samples were concentrated to approx. 200 µL with rotary-vacuum evaporator and transferred to chromatographical vials equipped with glass inserts.

2.7.3 Qualitative and quantitative analysis of the FAMEs profiles

For GC-MS analyses, a Shimadzu GCMS-QP2020 (Shimadzu, Kyoto, Japan) apparatus equipped with a ZB-FAME column (Phenomenex, Torrance, CA, United States) (60 m × 0.25 mm i. d. × 0.25 µm layer thickness) was used. 1 µL of each sample was injected at 80°C in split mode 2, and helium (1.8 mL·min^{-1}) was used as a carrier gaz. The GC thermal program was as follows: 80°C held for 2 min, then raised to 180°C at a rate of 3°C·min^{-1}, then to 240°C at a rate of 8°C·min^{-1} and held for 4 min. The MS operational conditions were as follows: interface temperature 240°C; ion source temperature 220°C; scanning mode 40–400 m/z.

The identification of FAMEs present in the samples was based on the reference analysis of Supelco 37 Component FAME Mix (Sigma-Aldrich, Steinheim, Germany). The quantification of the FAMes present in the samples was based on the amount of added IS.

2.8 Statistical analysis and bioinformatics

The data were presented as mean ± standard error of the mean (SEM). One-way analyses of variance (ANOVA) were conducted using GraphPad Prism 8 software (GraphPad Software, La Jolla, CA, United States) with a Tukey's correction. Differences with probability of $p < 0.05$ were indicated with an asterisk (*), those with $p < 0.001$ were marked with two asterisks (**), differences with $p < 0.001$ were represented with three asterisks (***), and differences with $p < 0.0001$ were showed with four asterisks (****).

Integrated peak areas are normalized by internal standard amount. The average and standard deviation for each individual molecular species is calculated. The data discrimination analysis using SIMCA-17 (Umetrics, Sweden) group-based models were constructed using 3D principal component analysis (PCA) and 2D partial least squares-discriminant analysis (PLS-DA) to identify differentially abundant fatty acids between groups. The loading plot of PCA was obtained to identify the lipids negative and positive association to the principal components (PCs). The most important fatty acids identified by PLS-DA model for control, EMS and SHBG-treated EMS groups were selected based on values of the variable importance in projection (VIP) plot score. Pathway enrichment and topology analysis was performed on the 13 assigned fatty acids. All matched pathways were plotted based on their *p*-value obtained from pathway enrichment analysis and pathway impact score. The significance of each pathway was indicated by a color gradient, with yellow representing higher *p*-values and red representing lower *p*-values. The pathway impact score was reflected in the size of the circle, with a larger circle indicating a higher impact score (Xia et al., 2015). Moreover, the pathways were also used to confirm their significance with p <0.05 and FDR≤0.05 by using the MetaboAnalyst software (http://www.metaboanalyst.ca/).

3 Results

3.1 SHBG normalizes the lipidome profile of EMS adipose tissue

We conducted GC-MS based lipidomics analysis on subcutaneous adipose tissue samples from a total of nine subjects, including control, EMS, and SHBG-treated EMS groups. A total of 25 fatty acids were successfully identified in the tissue samples (Figures 1, 2; Table 4).

To explore the changes in fatty acid composition, we generated 3D PCA and loading plots of the fatty acid dataset and built an OPLS-DA model to predict the total scores of the groups. The models were then validated and assessed using R^2X (cum), the predictive and orthogonal variation in X, R^2Y (cum), the total sum of variation in Y explained, and Q^2 (cum) the goodness of prediction, calculated by significant cross-validated predictive residuals (CV-ANOVA) *p*-values for the comparisons between the control, EMS, and SHBG groups (Table 4).

The results from SAT fatty acids profiling showed that 3D PCA model has a good separation between control, EMS and SHBG-treated EMS groups (Figure 3A). The PLS-DA model was rebuilt from variable importance in projection (VIP) score plot with VIP value above 1 and validated with statistical parameters [R^2X (cum), R^2Y (cum) and Q^2] by using just two PLS components and the cross-validated residuals (CV-ANOVA) of PLS-R model was significant (Figure 3B; Table 5). Moreover, the PCA-loading plot showed the fatty acids have negative contribution to PC1 including 8,11,14-eicosatrienoic acid, docosadienoate and

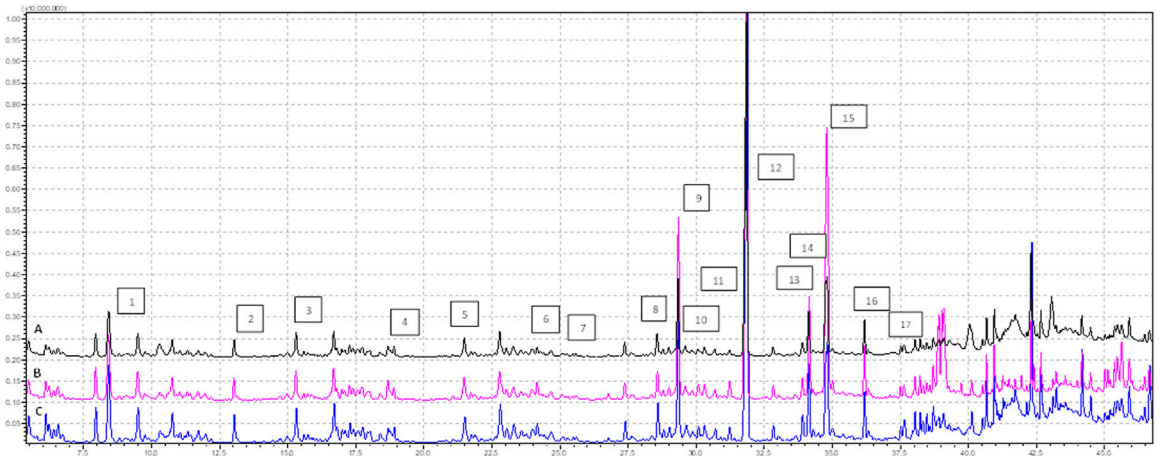

FIGURE 1
Profile of FAMEs identified in the tissues samples (analysis time 7.5 min—37.0 min), where **(A)** EMS tissue, **(B)** EMS + SHBG, **(C)** CRTL; 1—C8:0, 2—C10:0, 3—C11:0, 4—C12:0, 5—C13:0, 6—C14:0, 7—C14:1n5, 8—C15:1n5, 9—C16:0, 10—C16:1n7, 11—C17:0, 12—C17:1, 13—C18:0, 14—C18:1n9 (E), 15—C18:1n9 (Z), 16—C18:2n7, 17—C18:3n3.

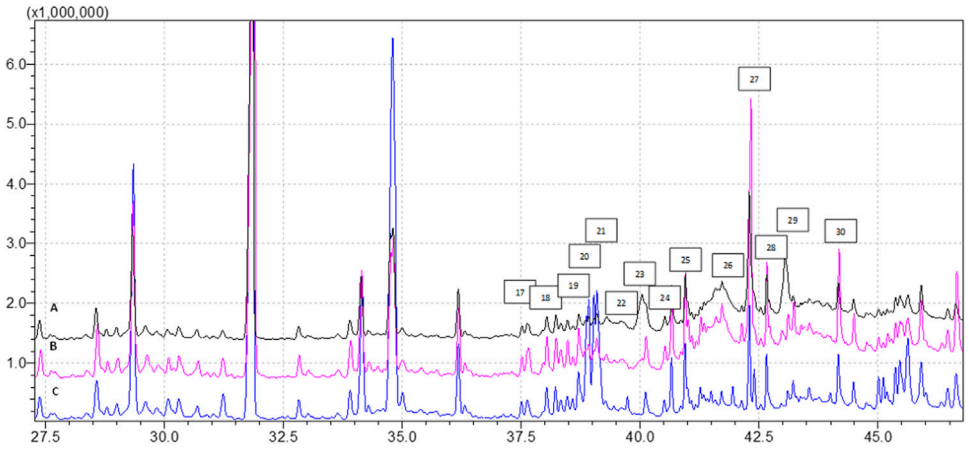

FIGURE 2
Profile of FAMEs identified in the tissues samples (analysis time 37.5 min—45.0 min), where **(A)** EMS tissue, **(B)** EMS + SHBG, **(C)** CRTL; 17—C18:3n3, 18—C20:0, 19—C20:1n9, 20—C20:2n6, 21—C21:0, 22—C20:3n6, 23—C20:4n6, 24—C22:0, 25—C20:5n3, 26—C22:2n6, 27—C24:0, 28—C25:1, 29—C24:1, 30—C22:6n3.

eicosadienoic acid. However, the remaining fatty acids have positive contribution to PC1 (Figure 3C). The 6 fatty acids with VIP (variable importance in projection) value above 1.00 were selected including 8,11,14-eicosatrienoic acid, linoelaidic acid, eicosenoic acid, alpha-Linolenic acid, palmitolinoleic acid and linoleic acid (Figure 3D).

We performed hierarchical clustering analysis using Euclidean distance and Ward D. linkage to identify any scattered samples. The resulting heatmap revealed distinct variations in the fatty acids among the control SAT, EMS SAT, and the SHBG-treated EMS SAT groups (Figure 4). The fatty acids were clearly grouped based on different percentages between groups. For example, 8,11,14-eicosatrienoic acid and linoelaidic acid were abundant in the control group but not in the EMS and EMS treated with SHBG groups. Conversely, Oleic acid, Linoleic acid, Heneicosanoic acid, Arachidonic acid, Tricosanoic acid, Tetracosanoic acid, Alpha-Linolenic acid, Eicosenoic acid, Caprylic acid, FAHFA (18:0/9-O-18:0) (9-hexadecanoyloxy-octadecanoic acid), Pentadecanoic acid, Methyl hexadecanoic acid, Undecylenic acid and Methyl dodecanoate were significantly more abundant in the EMS group but not in SHBG-treated EMS SAT.

The assigned fatty acids were tested by ANOVA, and showed different tendency between groups. For instance, ten fatty acids have downregulated by 55.5% from 18 significant fatty acids after SHBG treatment, with significant differences observed between the Eq SAT_EMS and Eq SAT_EMS + SHBG groups. These results suggest that the negative changes in the fatty acid profiles induced by EMS are reversible and can be effectively normalized by SHBG treatment such as undecylenic acid, methyl dodecanoate,

TABLE 4 Fatty acids composition of SAT-derived metabolites identified by GCMS- based lipidomics from control, EMS and EMS tissue with SHBG treatment samples.

Fatty acids (FAMEs)	Names	CTRL ($n = 3$) mean ± SD	EMS ($n = 3$) mean ± SD	SHBG ($n = 3$) mean ± SD	VIP value[a]
		[µg/500 mg tissue]			
Me20:3n3	8,11,14-Eicosatrienoic acid	0.0210 ± 0.000	0.0040 ± 0.0040	0.0060 ± 0.0010	**1.7530**
Me 18:2n6, Z,Z	Linoelaidic acid	1.7040 ± 0.1130	1.206 ± 0.0270	1.132 ± 0.2140	**1.6801**
Me20:1n9	Eicosenoic acid	0.0857 ± 0.0075	0.7493 ± 0.1595	0.2050 ± 0.0450	**1.2001**
Me 18:3n3	Alpha-Linolenic acid	0.4343 ± 0.0205	3.125 ± 0.6600	0.6997 ± 0.0675	**1.1327**
Me 16:1n7	Palmitolinoleic acid	0.4103 ± 0.0045	0.3990 ± 0.0440	0.2860 ± 0.0950	**1.1033**
Me 18:2n6, E,E	Linoleic acid	0.0030 ± 0.0030	0.0300 ± 0.0130	0.0037 ± 0.0035	**1.0128**
Me18:0	FAHFA(18:0/9-O-18:0)	8.128 ± 0.2935	10.27 ± 0.7750	4.759 ± 0.4335	0.9871
18:1n9,Z	Oleic acid	8.0280 ± 2.8080	31.56 ± 12.7800	6.245 ± 2.7290	0.9611
Me 14:0	Methyl tetradecanoate	1.6410 ± 0.272	1.787 ± 0.4075	1.030 ± 0.1215	0.9605
Me 11:0	Undecylenic acid	0.5803 ± 0.0385	1.855 ± 0.2410	0.2150 ± 0.0580	0.9342
Me 21:0	Heneicosanoic acid	0.1667 ± 0.0395	0.2093 ± 0.0405	0.0827 ± 0.0055	0.9316
Me 17:1, Z	(Z)-9-Heptadecenoic acid	0.0477 ± 0.0055	0.05367 ± 0.0295	0.0227 ± 0.0055	0.9262
Me 16:0	Methyl hexadecanoic acid	16.0900 ± 0.3765	24.94 ± 0.8955	10.35 ± 0.2405	0.9164
Me 15:0	Pentadecanoic acid	0.5597 ± 0.0165	0.7233 ± 0.0935	0.3937 ± 0.0275	0.9101
Me 12:0	Methyl dodecanoate	1.8430 ± 0.0585	3.892 ± 0.3670	0.7983 ± 0.2545	0.8962
Me 8:0	Caprylic acid	0.3220 ± 0.0720	0.4497 ± 0.03750	0.1743 ± 0.0465	0.8861
Me 10:0	Capric acid	0.4220 ± 0.0500	0.5453 ± 0.1245	0.2410 ± 0.0840	0.8645
Me 23:0	Tricosanoic acid	0.3037 ± 0.0685	0.4823 ± 0.0775	0.2250 ± 0.0580	0.8342
Me 18:1n9,E	Elaidic acid	0.0553 ± 0.0095	0.1460 ± 0.0830	0.0157 ± 0.0065	0.8179
Me 24:0	Tetracosanoic acid	1.7460 ± 0.4050	2.377 ± 0.3320	1.440 ± 0.4490	0.7945
Me 22:0	Behenic acid	1.9900 ± 0.4385	2.551 ± 0.6925	1.343 ± 0.4070	0.7684
Me 22:1n10	Erucic acid	0.8557 ± 0.0785	0.8787 ± 0.1375	0.7060 ± 0.2520	0.7582
Me 20:0	Arachidonic acid	1.2640 ± 0.3895	1.862 ± 0.4120	1.014 ± 0.1035	0.7481
Me 20:2n6	Eicosadienoic acid	0.8557 ± 0.0785	0.8787 ± 0.1375	0.7060 ± 0.2520	0.7228
Me 22:2n6	Docosadienoate (22:2n6)	0.0130 ± 0.0020	0.0103 ± 0.0105	0.0160 ± 0.0030	0.6862

[a]Variable importance in projection value from PLS-DA, model.
Me, Methyl esters; ***FAMEs***, Fatty acid methyl esters; The numerical symbol: total amount of (C)arbon atoms of the fatty acid, and the number of (D)ouble (unsaturated) bonds.

pentadecanoic acid, methyl hexadecanoic acid, FAHFA (18:0/9-O-18:0), oleic acid, linoleic acid, alpha-Linolenic acid, eicosenoic acid and tricosanoic acid (Figure 5).

Moreover, from ANOVA test we found six fatty acids have moderate differences between control and EMS groups including caprylic acid, capric acid, methyl tetradecanoate, elaidic acid, arachidonic acid and heneicosanoic acid. Additionally, only two fatty acids showed no significant differences between EMS and SHBG-treated groups such as linoelaidic acid and 8,11,14-eicosatrienoic acid (Figure 6).

We conducted pathway and enrichment analysis of the 25 identified fatty acids using Metaboanalyst 4.0, and the associated metabolic pathways are presented in Figure 7. We calculated the pathway impact value based on pathway topology analysis and identified potential target pathways. Alpha-Linolenic acid metabolism, Linoleic acid metabolism, biosynthesis of unsaturated fatty acids, and Arachidonic acid metabolism (Table 6; Figures 7A–F) were the primary fatty acid pathways affected by SHBG treatment.

3.2 SHBG modulates lipids metabolism-related mediators in EMS SAT

To investigate whether SHBG is involved in the regulation of lipid metabolism in equine SAT, the expression of mediators

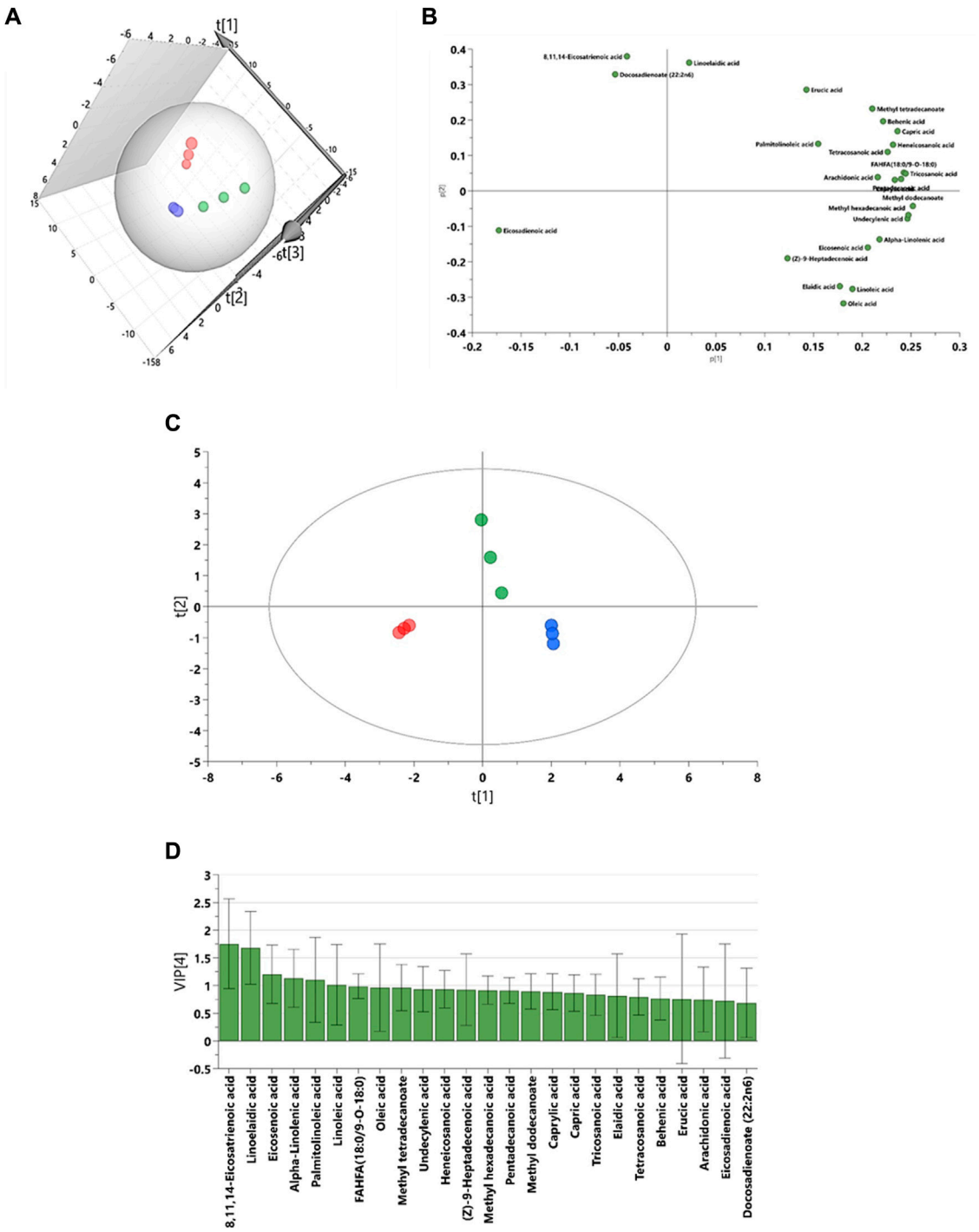

FIGURE 3
Graphical representation for lipidomic data driven models for subcutaneous adipose tissue. **(A)** The 3D principal component analysis (PCA) scores plot. **(B)** The partial least squares projections to latent structures discriminant analysis (PLS-DA). **(C)** The loadings plots for PCA model. **(D)** The variable importance in projection (VIP) score plot from PLS-DA model. Blue: control SAT (CTRL); Red: EMS SAT; Green: SHBG-treated EMS SAT.

involved in the regulation of this process was analyzed at the mRNA and protein level. The obtained data showed that the relative expression of LPL in EMS SAT was significantly downregulated compared to control tissue (Figure 8A; $p < 0.0001$), which has been subsequently upregulated following application of SHBG for 24 h (Figure 8A; $p < 0.01$). Relative expression of SCD in EMS SAT was drastically decreased when compared to the control tissue (Figure 8B; $p < 0.0001$) and remained unaffected after the SHBG treatment compared to the control ($p < 0.0001$) and EMS SAT (Figure 8B; $p < 0.001$). In contrast to these results, expression of PNPLA2 was significantly upregulated compared to the EMS group (Figure 8C; $p < 0.0001$), while exogenous SHBG treatment

TABLE 5 The multivariate analysis model summary of adipose tissue extract GCMS- based lipidomic in comparisons between control, EMS and SHBG treatment.

Group comparison	Model type	PC/LV	N =	R^2X (cum)	R^2Y (cum)	Q^2 (cum)	CV-ANOVA *p*-value
CTRL vs. EMS vs. EMS_SHBG	PCA-X	4	9	0.976	–	0.873	–
CTRL vs. EMS vs. EMS_SHBG	PLS-DA VIP>1	2	9	0.906	0.894	0.772	$\mathbf{1.24 \times 10^{-2}}$

PCA-X, Principal component analysis; ***PLS-DA***, Partial least squares-discriminant analysis; ***VIP***, Variable importance in projection; ***LV***, Latent variable; ***N***, Number of samples. ***$R^2X(cum)$/$R^2Y(cum)$***, Cumulative explained variation; ***$Q^2(cum)$***, Goodness of prediction; ***CV-ANOVA***, Cross-validated predictive residuals of a model.

drastically decrease its expression level when compared to control and EMS tissue (Figure 8C; $p < 0.0001$). Relative expression of PLIN1 was downregulated in SAT from EMS horses (Figure 8D; $p < 0.0001$) and similar tendency was observed after exposure to SHBG (Figure 8D). mRNA level of PPARA in EMS tissue was increased compared to control (Figure 8E; $p < 05$), and SHBG rescue enabled the restoration of normal PPARA expression levels (Figure 8E). Transcript level of FASN was significantly increased in SAT of EMS horses compared to the control healthy group (Figure 8F; $p < 0.0001$), and abrogated following SHBG treatment (Figure 8F; $p < 0.0001$). Basic regulators of lipids metabolism have been further analyzed at the protein level. EMS adipose tissue was characterized by comparable LPL protein level in regards to the control group (Figures 8G, N), however, the treatment of EMS tissue with exogenous SHBG resulted in a remarkable upregulation of the protein when we compared to the control tissue (Figure 8G). Similar to mRNA, PLIN1 protein level was upregulated in EMS group compared to the control (Figures 8H, N; $p < 0.01$). Exogenous

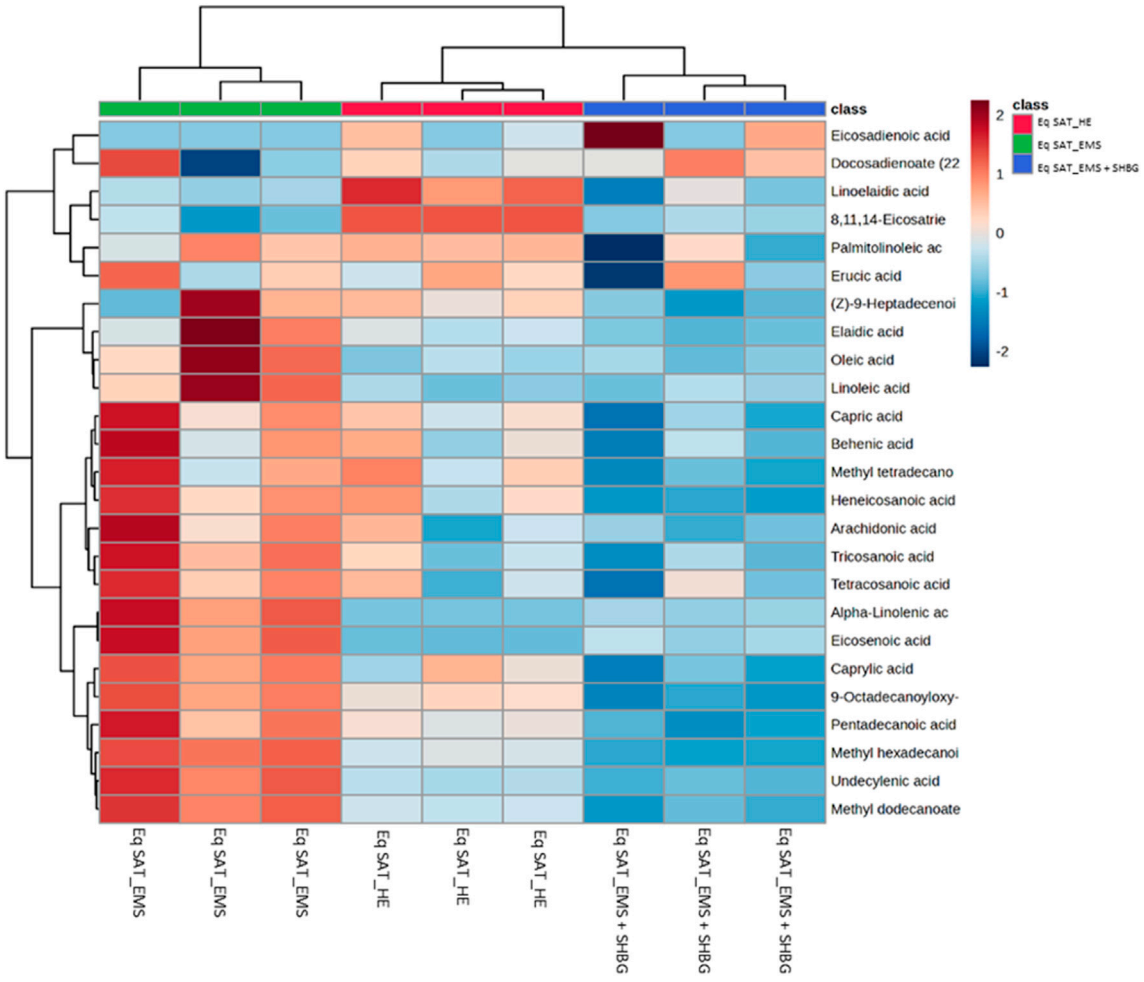

FIGURE 4
Hierarchical clustering heatmap analysis of fatty acids in equine subcutaneous adipose tissue. Each colored cell on the map corresponds to a concentration value. The top 25 features from the Eq SAT_HE, Eq SAT_EMS and Eq SAT_EMS + SHBG groups are presented and ranked by t-tests to retain the most contrasting patterns. Values are measured by Euclidean distance with a Ward clustering algorithm ($n = 3$ per group). *$p \leq 0.05$ for each comparison. Red color indicates high level, and blue color indicates low level.

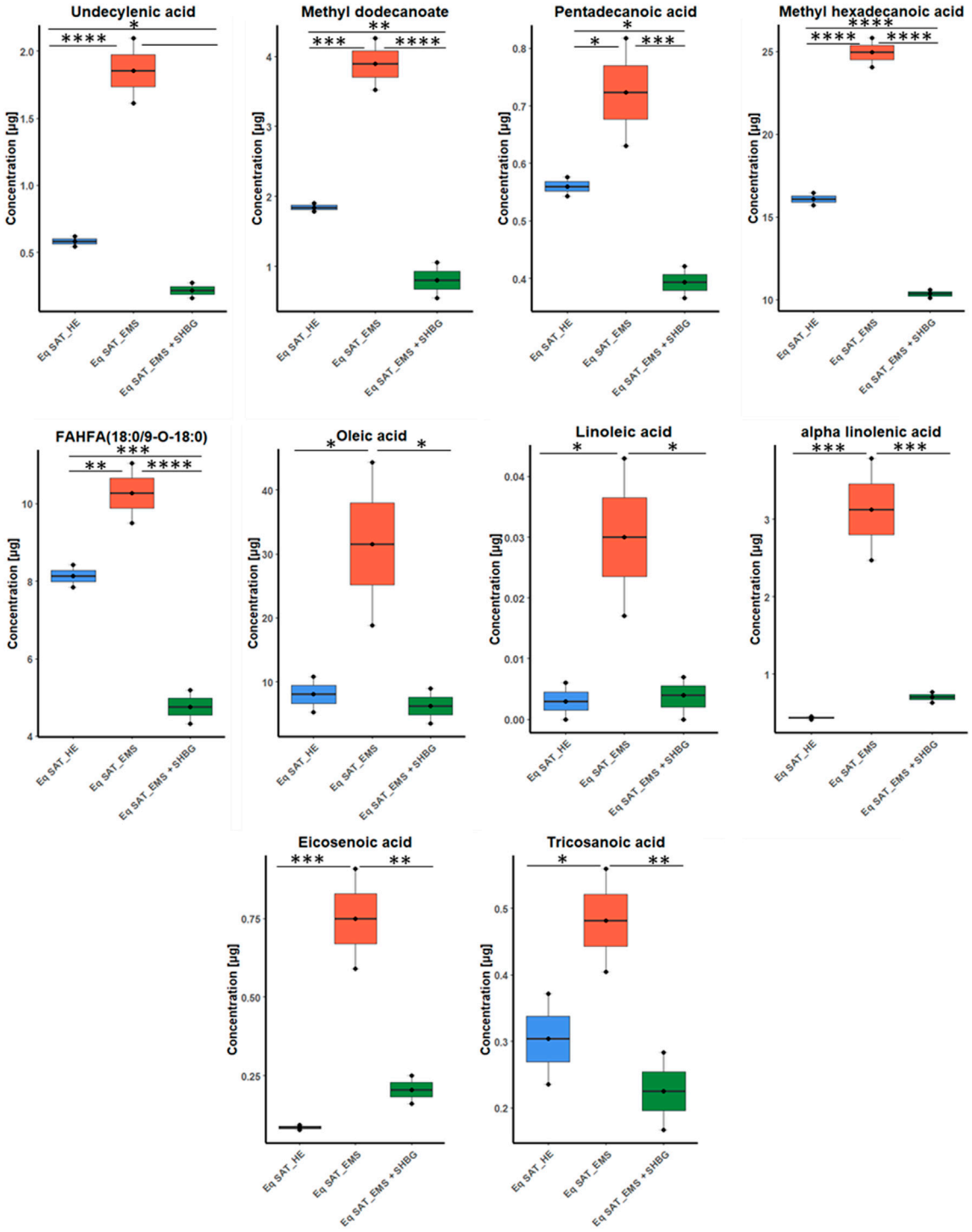

FIGURE 5
Boxplots for fatty acids sets showed efficacy of SHBG treatment, and after *p*-value adjustment. Whiskers—1.5 × interquartile range (IQR); bar—median; box—range between first quartile (Q1) and third quartile (Q3). Black points—data points. *Adjusted *p*-value <0.05.

SHBG treatment further decreased its expression to a level comparable to that of control tissue (Figure 8H; $p < 0.01$). In contrast to these results, FASN protein appeared markedly decreased in EMS SAT compared to control group (Figures 8H, N; $p < 0.0001$). Treatment of EMS SAT with exogenous SHBG induced slight augmentation of FASN protein level however of statistical insignificance compared to both control ($p < 0.01$) and EMS SAT ($p < 0.0001$). Significantly downregulated of SCD1 (Figures 8J, N; $p < 0.01$), ATGL (Figures 8K, L, N; $p < 0.01$ for 63 kDa subunit, $p < 0.001$ for 57 kDa subunit), and HSL

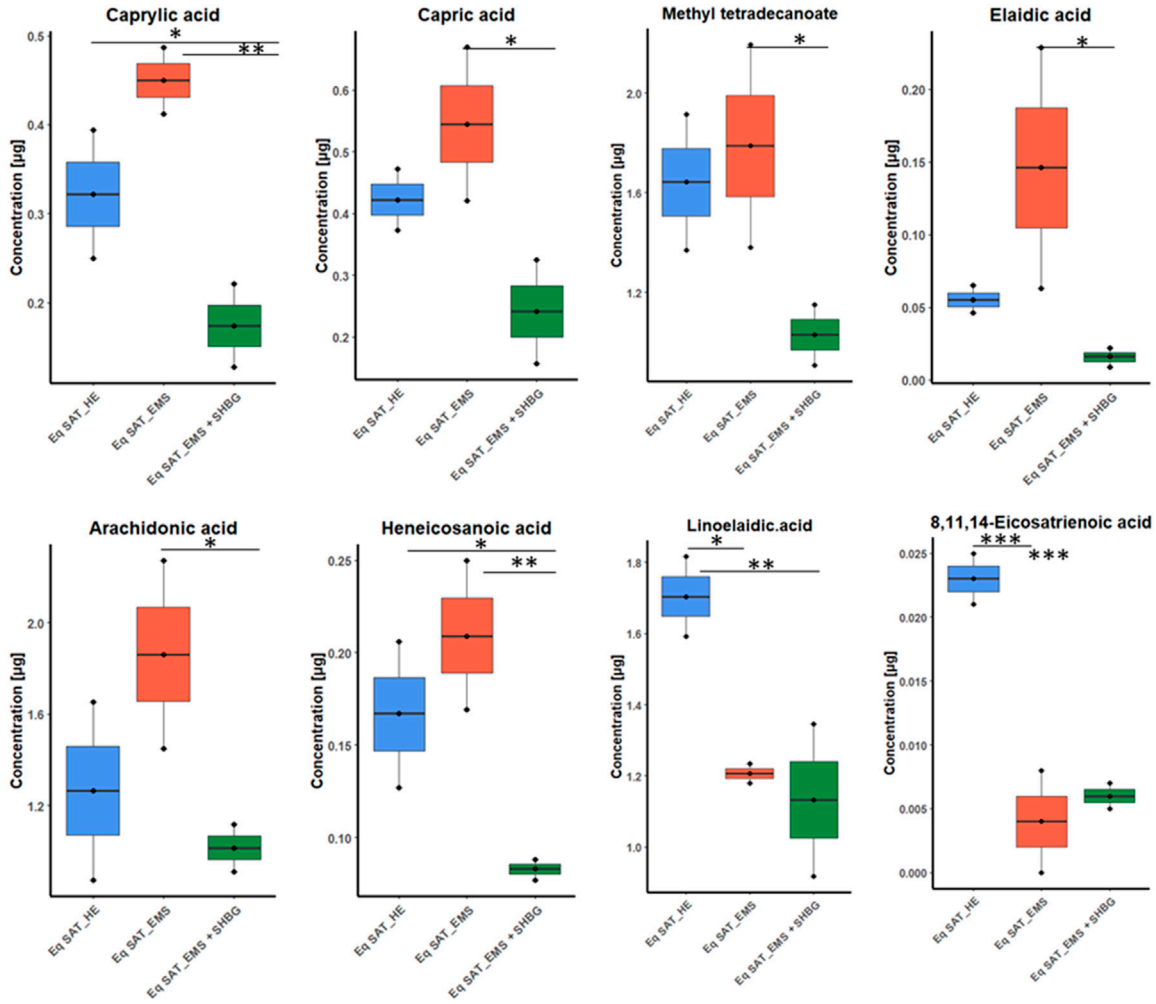

FIGURE 6
Boxplots for the ANOVA significant fatty acids showing different tendency between groups, and after *p*-value adjustment. Whiskers—1.5 × interquartile range (IQR); bar—median; box—range between first quartile (Q1) and third quartile (Q3). Black points—data points. *Adjusted *p*-value <0.05.

(Figures 8M, N; $p < 0.0001$) protein levels were also observed in EMS group in opposition to the control tissue. Moreover, application of exogenous SHBG induced a moderate elevation of SCD1 protein (Figure 8J), and the 57 kDa ATGL isoform (Figure 8L), while HSL level remained unchanged (Figure 8M).

3.3 SHBG promotes the expression of adipogenesis negative regulators in EMS SAT

To better investigate the relation between SHBG protein and adipose tissue turnover, an analysis of the expression of adipogenesis promotors (Figures 9A–J) and inhibitors (Figures 9H–K) was performed using RT-qPCR technique. At first, expression levels of kruppel-like factor family (KLF), promotors of adipogenesis were analyzed. The obtained results showed that KLF4 (Figure 9A) and KLF9 (Figure 9B) expression levels were significantly increased in EMS SAT compared to the control group ($p < 0.0001$). After treatment of the tissue with exogenous SHBG, the mRNA levels of these promoters were all downregulated. The level of KLF4 was emphatically reduced when compared to EMS SAT (Figure 9B; $p < 000.1$) and appeared at a similar level compared to control cells (Figure 9A). Similarly, treatment of EMS fat tissue with exogenous SHBG drastically reduced KLF9 levels relative to EMS group (Figure 9B; $p < 0.0001$), and compared to control (Figure 9B; $p < 0.0001$). However, no differences were observed in the KLF15 transcript level, both in EMS SAT and after treatment with exogenous SHBG compared to control group (Figure 9C). Obtained results additionally showed that in EMS SAT, the expression level of the pro-adipogenic CEBPD was drastically upregulated compared to control group (Figure 9D; $p < 0.0001$), which has been critically lowered upon SHBG treatment (Figure 9D; $p < 0.0001$). Similar levels were observed for STAT5A mRNA expression, that was found significantly activated in EMS-derived SAT compared to the control group (Figure 9F; $p < 0.0001$), and subsequently mitigated following SHBG application (Figure 9E; $p < 0.0001$).

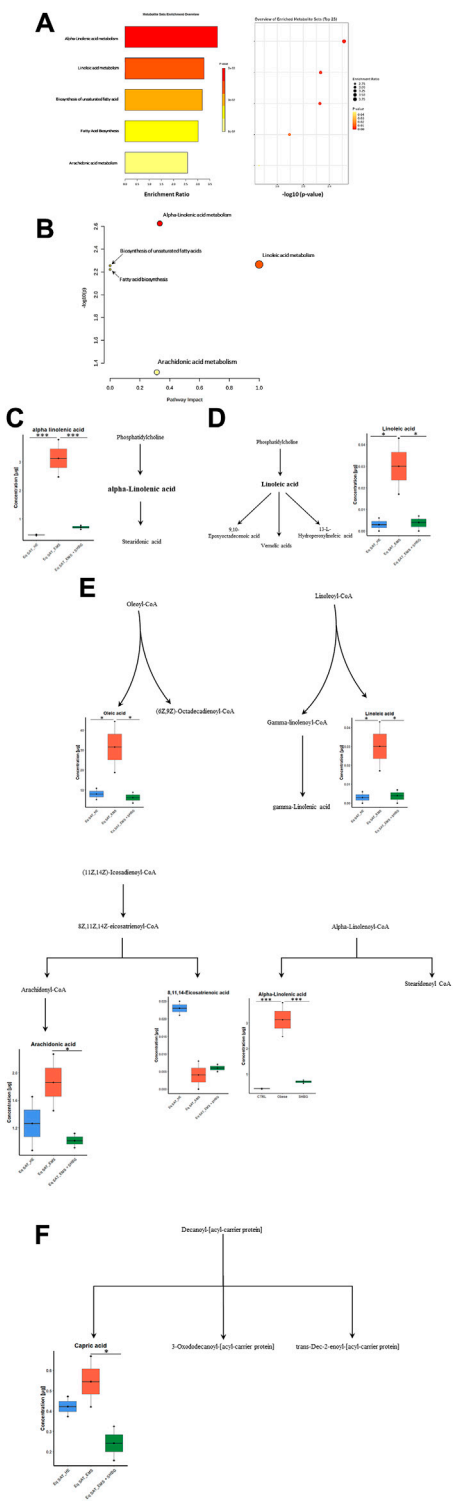

FIGURE 7
Graphical representations for GC-MS dataset driven models of adipose tissue lipidome. **(A)** Summary plot for Quantitative Enrichment Analysis (QEA). **(B)** Pathway enrichment and topology analysis was performed on the 13 identified metabolites. All matched pathways were plotted based on their *p*-value obtained from pathway enrichment analysis and pathway impact score. The significance of each pathway was indicated by a color gradient, with yellow representing higher *p*-values and red representing lower *p*-values. The pathway impact score was reflected in the size of the circle, with a larger circle indicating a higher impact score. **(C–F)** Altered fatty acids (*Continued*)

FIGURE 7 (Continued)
pathway to SHBG treatment with KEGG ID from the merged dataset KEGG and SMPDB reference pathways and interaction networks were generated in Metaboanalyst. **(C)** Alpha-Linolenic acid metabolism. **(D)** Linoleic acid metabolism. **(E)** Biosynthesis of unsaturated fatty acids. **(F)** Fatty acid biosynthesis. Bold text: detected fatty acids; control SAT (CTRL); Red: EMS SAT; Green: SHBG-treated EMS SAT.

Next, the expression patterns of factors negatively regulating adipogenesis were analyzed. The obtained data showed a critical loss in adipogenesis regulatory signals in EMS animals. The relative expression level of KLF2 and KLF7 was significantly downregulated in EMS tissue compared to control one (Figures 9F, J; $p < 0.0001$), and interestingly, further treatment of the tissues with SHBG reduced their expression when compared to EMS group (Figures 9F, J; $p < 0.0001$) and control group (Figures 9F, J; $p < 0.0001$). Next, the relative expression level of KLF3 was also found to be significantly downregulated in EMS SAT compared to control (Figure 9I; $p < 0.001$), however, subsequent treatment of EMS tissue with exogenous SHBG protein exerted a noticeable augmented expression of KLF3 by opposition to EMS group (Figure 9I; $p < 0.0001$) and was normalized to an equivalent level of that in control SAT (Figure 9I). In the case of the IRF3 inhibitor, mRNA level was similarly downregulated in EMS group when compared to the control tissues (Figure 9G; $p < 0.0001$). Exogenous SHBG application induced a visible increase in IRF3 level in relation to EMS SAT (Figure 9G; $p < 0.0001$), however it remained moderately lower than that observed in control SAT (Figure 9G; $p < 0.0001$). Analysis of CTNNB expression level showed no differences between control and EMS groups (Figure 9H). However, in EMS SAT treated with exogenous SHBG protein, a significant upregulation in the relative mRNA level of this gene was observed compared to both control (Figure 9H; $p < 0.0001$) and EMS tissues (Figure 9H; $p < 0.0001$).

3.4 SHBG enhances the expression of mitochondrial metabolism markers in SAT

To better investigate the relationship between SHBG protein and mitochondrial functions in the course of adipocytes metabolism, the main markers involved in the mitochondrial oxidative phosphorylation machinery have been analyzed at the mRNA level. The obtained results showed that the relative expression level of PPARGC1A remained unchanged in EMS tissue (Figure 10A), however, appeared elevated in SAT treated with exogenous SHBG, both relative to control (Figure 10A; $p < 0.0001$) and EMS fat (Figure 10A; $p < 0.0001$). On the other hand, EMS SAT had significantly downregulated PPARGC1B expression compared to the control group (Figure 2B; $p < 0.0001$). Next, the expression of mitochondrial cytochrome c oxidase (COX) family members was analyzed. The obtained results showed that the relative expression level of COX7A1 was significantly downregulated in EMS SAT (Figure 10C; $p < 0.0001$), and SHBG protein intervention drastically increased the mRNA level of this gene so that it was significantly higher compared to both control (Figure 10C; $p < 0.0001$) and EMS tissue (Figure 10C; $p < 0.0001$). A similar trend

TABLE 6 Summary of pathways analysis of fatty acids dataset.

Pathway name	Match status	*p*-Value	–log(p)	FDR	Impact
Alpha-Linolenic acid metabolism	1/13	0.002	2.626	0.008	0.333
Linoleic acid metabolism	1/5	0.005	2.266	0.008	1.000
Biosynthesis of unsaturated fatty acids	5/36	0.006	2.255	0.008	0.000
Fatty acid biosynthesis	2/47	0.006	2.221	0.008	0.000
Arachidonic acid metabolism	1/36	0.048	1.320	0.048	0.314

was observed for the COX4I1 expression level. While it appeared significantly downregulated in EMS fat (Figure 10D; $p < 0.0001$), exogenous SHBG application resulted in a substantial augmentation of its transcription rate compared to the control (Figure 10D; $p < 0.0001$) and EMS group (Figure 10D; $p < 0.0001$). A difference in expression levels between control cells and EMS SAT was not observed for COX8A expression (Figure 10E). However, treatment of EMS fat with exogenous SHBG reduced its mRNA levels relative to control (Figure 10E; $p < 0.0001$) and EMS tissue (Figure E10; $p < 0.0001$).

3.5 SHBG restores insulin signalling in EMS SAT

To thoroughly investigate the role of the SHBG protein in insulin signaling transduction, the gene expression and phosphorylation rates of the main factors involved in insulin cascade were investigated. EMS SAT displayed critical loss in expression efficiency of key insulin signaling mediators including PI3K (Figure 11A; $p < 0.0001$), AKT (Figure 11B; $p < 0.0001$) and IRS1/2 (Figures 11D, E; $p < 0.0001$). Nevertheless, expression levels of INSR and GLUT4 were found unaffected by the EMS condition (Figures 11C, F). Interestingly, SHBG intervention enabled to substantially enhance the transcription of PI3K, AKT, GLUT4 and IRS1/2 when compared to EMS untreated tissues as well as healthy controls.

To seek on the potential influence of SHBG on insulin-mediated phosphorylation cascades, Western blot analysis has been used for proteins profiling. Obtained data highlighted the profound defects in phosphorylation mechanisms underlying insulin signaling of EMS SAT. both phospho-Pi3K, -AKT and -IR levels were found slightly lowered under EMS condition when compared to control tissues (Figures 11G, H, M). Notably, EMS SAT also displayed a critical suppressed GLUT4 protein level (Figure 11I), evoking a reduced capacity for glucose uptake. Accordingly, treatment of EMS SAT with 50 nM SHBG exerted a potent insulin sensitizing effect by restoring proper phosphorylation levels of Pi3K, AKT, IR and IRS1/2 and by augmenting the expression level of GLUT4 protein in relation to EMS untreated group. Particularly, SHBG induced a stimulation of insulin-induced phosphorylation of its transducers at a higher level than the threshold observed for control tissue, suggesting its great potential as an insulin sensitizer agent.

Another interesting finding lies in the observed loss in endogenous SHBG protein in EMS SAT compared to healthy tissue (Figures 11L, P; $p < 0.01$), which confirms the critical importance of SHBG as a metabolic mediator.

3.5 SHBG mitigates inflammatory pathways by inhibiting the PDIA3/ERK axis

To investigate the effect of SHBG protein on inflammation in SAT, the levels of selected pro-inflammatory cytokines were evaluated at the tissue level using ELISA assays (Figures 12A–D). The obtained results showed that the concentration of IL-6 in EMS tissue was significantly higher compared to normal tissue (Figure 12A; $p < 0.001$), which has been substantially lowered following SHBG treatment application (Figure 12A; $p < 0.001$). Next, TNF-α has been evaluated at comparable levels in both control and EMS SAT (Figure 12B), and surprisingly, SHBG treatment further decreases TNF-α concentration in the EMS SAT compared to untreated EMS fat (Figure 12B; $p < 0.001$) and also control SAT (Figure 12B; $p < 0.001$). MCP-1 (Figure 12C) and PGE2 (Figure 12D) concentrations were found slightly increased in EMS SAT and lowered after SHBG intervention, however with statistical insignificance.

In order to further elucidate the possible molecular pathways, put in play of anti-inflammatory potential of SHBG, changes in PDIA3/ERK proteins have been tested. Western blots analysis showed that in EMS SAT, the level of ERK1 66 kDa protein was significantly increased when compared to control fat (Figures 12H, K; $p < 0.0001$), while in EMS tissue treated with exogenous SHBG resulted in a visible downregulated protein compared to untreated tissue (Figures 12H, K; $p < 0.001$), and reached comparable level to that of control SAT (Figures 12H, K). A similar tendency was noted for ERK2 46 kDa isoform, where EMS SAT exhibited higher ERK2 abundance compared to control (Figures 12I, K; $p < 0.01$), while exogenous SHBG protein addition triggered a sharp decrease in ERK2 amount with respect to EMS tissue (Figures 12I, K; $p < 0.001$) and was found furthermore normalized to control basal level (Figures 12I, K). Interestingly, an important augmented expression of PDIA3 protein was noted in EMS-derived adipose tissue by opposition to control group (Figures 12J, K; $p < 0.001$). Here also, SHBG intervention efficiently regulated and normalized the levels of PDIA3 protein in EMS SAT in connection to both EMS untreated group (Figure 12J; $p < 0.001$) and healthy fat tissue (Figures 12J, K), suggesting that SHBG might attenuate inflammatory responses via the inhibition of the PDIA3/ERK pathway.

4 Discussion

Adipose tissue is a fat storage and endocrine organ that plays a pivotal role in lipids and glucose homeostasis. The release of different adipokines including adiponectin, leptin, visfatin,

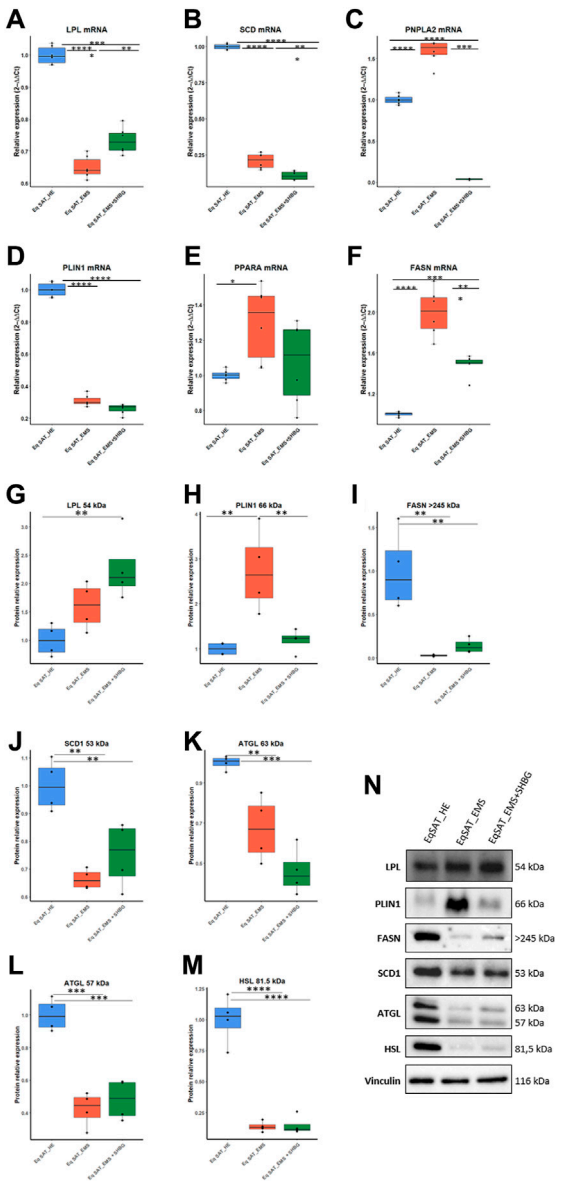

FIGURE 8
Influence of SHBG treatment of lipid metabolism related modulators interplay in SAT (A–N). The relative expression levels of LPL **(A)**, SCD **(B)**, PNPLA2 **(C)**, PLIN1 **(D)**, PPARA **(E)**, FASN **(F)** in SAT were analyzed by RT-PCR. Protein levels of LPL **(G)**, PLIN1 **(H)**, FASN **(I)**, SCD1 **(J)**, ATGL **(K, L)** and HSL **(M)** were analyzed by Western blot (**(N)**, representative membranes). Representative data are shown as mean ± SD. ** *p*-value <0.01, *** *p*-value<0.001 and **** *p*-value<0.0001.

resistin, tumor necrosis factor-α (TNF-α), and monocyte chemoattractant protein-1 (MCP-1) regulate and mediate the fate of both residing cells and non-adipogenic organs such as liver and pancreas (Jung and Choi, 2014). Many lines of evidence clearly indicated the implication of adipose tissue disease and malfunction in the development and progression of endocrine and inflammatory disorders including insulin resistance, making it an essential target for therapeutics. While EMS affected horses display profound altered adipose tissue metabolism and dysregulated lipids turnover, the loss in SHBG protein has been previously correlated with impaired insulin signalling and general metabolic disruption in the course of insulin resistance, systemic inflammation, obesity and metabolic syndrome (Reynolds et al., 2019; Bourebaba et al., 2022). Therefore, the impact of SHBG treatment on EMS subcutaneous adipose tissue (SAT) metabolic dynamics has been investigated. Obtained data demonstrated that *ex-vivo* SHBG application restores insulin sensitivity, regulates lipids metabolism programs and reduces inflammation in fat tissue biopsies derived from EMS affected horses.

The choice of SHBG as a therapeutic target was motivated by the existence of a certain number of reports having demonstrated a direct interrelation between the abnormal expansion and dysfunction of adipose tissue, whether visceral or subcutaneous, and the drop in SHBG levels. De Simone and others (De Simone et al., 2001), have thus found that massive visceral adipose tissue accumulation strongly associates with elevated circulating insulin levels and negatively correlates with serum SHBG level in obese adolescents. As well, Nielsen et al. (2007), demonstrated that excessive SAT was closely associated with declined SHBG levels in obese men patients. Likewise, Kim and collaborators (Kim et al., 2017), found that changes in both VAT and SAT were inversely related to changes in SHBG, and that reduction in both VAT and SAT results in higher levels of SHBG in both men and women with diabetes, suggesting SHBG as a valuable candidate for obesity-associates complications intervention.

Adipose tissue dysfunction is regarded as a major pathophysiologic component of metabolic syndrome. Besides releasing a large amount of reactive adipokines, malfunctioning adipose tissue strongly alters the lipid metabolism and turnover machinery. The untargeted lipidome analysis of EMS-derived adipose tissue evidenced a profound alteration in the lipidic profile with abnormal elevated levels of saturated (SFAs), polyunsaturated (PUFAs), trans and cis unsaturated fatty acids, as well as fatty acid hydroxy fatty acids (FAHFAs). Specifically, EMS SAT exhibited significant higher levels of palmitic, lauric, oleic, α-linoleic, elaidic, capric and caprylic acids. Excessive saturated and trans unsaturated fats intake has been previously evidenced as a major contributor of obesity and related diseases development (De Souza et al., 2015; Cena and Calder, 2020). The SFAs thus induce fundamental molecular changes that impair the metabolic capacity of cells. Weijers (2015), for example, reported that increased SFAs levels participates in insulin resistance and glucose intolerance onset as they induce an increase in membrane stiffness and a partial loss in glucose transporters (GLUTs) capacity. Moreover, SFAs such as palmitic acid (16:0) or lauric acid (12:0) can also elicit inflammatory responses by antagonizing the TLR4/NFκB/JNK/ERK axis, which subsequently alters the phosphorylation of the insulin receptor, leading to adipose tissue insulin resistance (Huang et al., 2012). In terms of the cis unsaturated oleic acid (18:1n9,Z), Malodobra-Mazur et al. (2019), showed in their research that oleic acid surplus induces excessive expression of leptin, lipids accumulation, adiponectin suppression and simultaneous insulin signalling and glucose utilization impairment in murine adipocytes; as far as Xie and co (Xie et al., 2006), who reported that high oleic acid levels trigger insulin resistance in adipocytes via the inhibition of Akt phosphorylation and Glut4 translocation. Adipose tissue malfunction and low-grade inflammation are associated to lipid metabolism disruption and increased circulating and ectopic PUFA

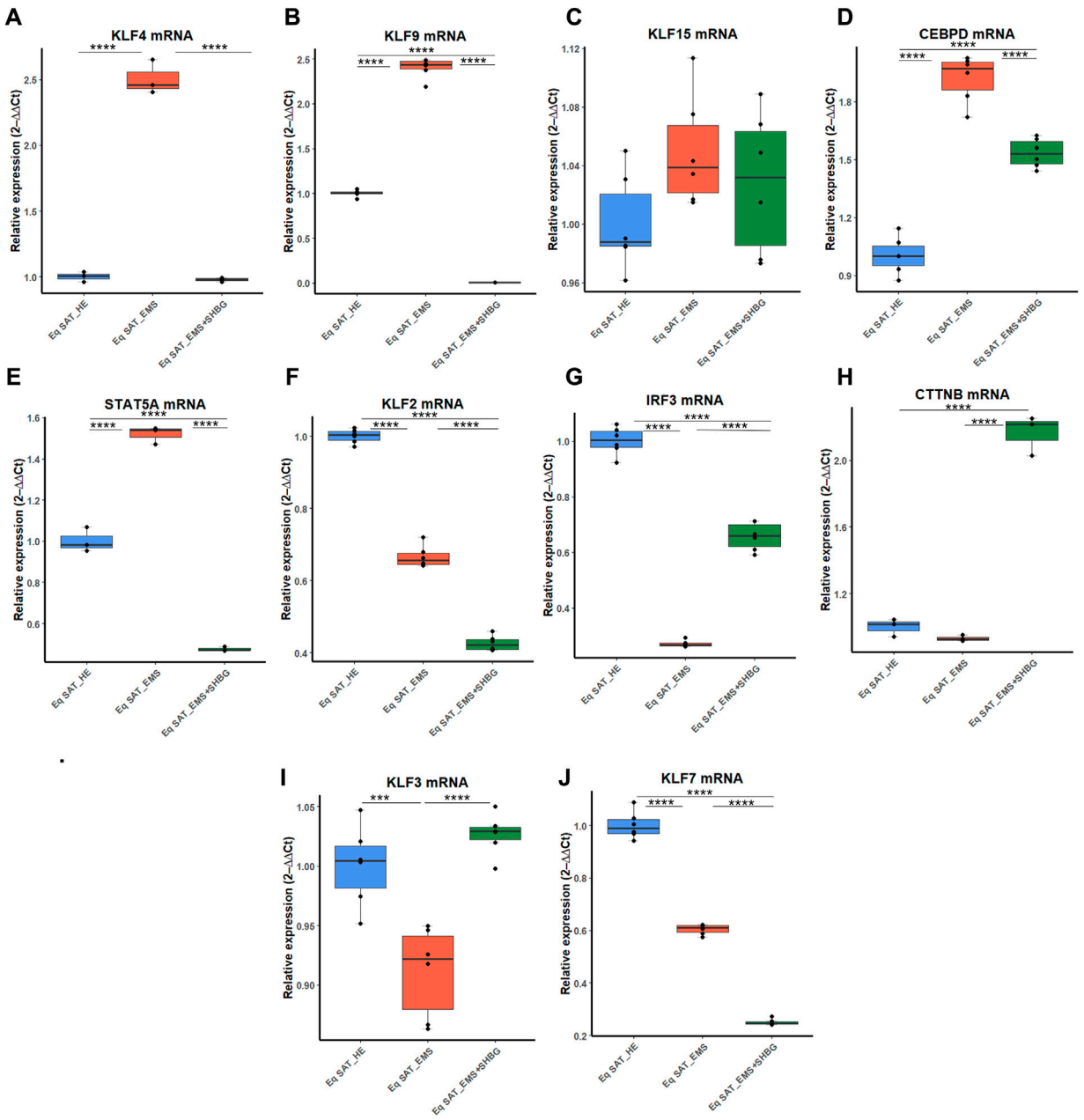

FIGURE 9
Representative graphs showing the relative expression levels of promotors (A–J) and inhibitors (K–P) of adipogenesis. The expression analysis of KLF4 **(A)**, KLF9 **(B)**, KLF15 **(C)**, CEBPD **(D)**, STAT5A **(E)**, KLF2 **(F)**, IRF3 **(G)**, CTNNB **(H)**, KLF3 **(I)**, KLF7 **(J)** was performed by RT-PCR tool. Representative data are shown as mean ± SD. *p-value < 0.05, ** p-value < 0.01, *** p-value < 0.001, ****p-value < 0.0001.

levels. A critical increase in delta-6 and -9 desaturases activities and reduction in delta-5 desaturase have been linked to reduced capacity to convert α-linoleic acid into EPA and DHA (ω-3 PUFA) pro-resolving mediators in overweight/obese subjects, suggesting a possible decreased rate of α-linoleic acid conversion to beneficial ω-3 PUFA in altered adipose tissue (Takic et al., 2022). In line with the observed lipids imbalance in EMS SAT, SHBG treatment showed remarkable ability to normalize the levels of the detected fatty acids by lowering the abundance of FAHFA, palmitic, lauric, oleic, elaidic, capric and caprylic acids. Modified SHBG levels has already been strongly associated with *de novo* lipogenesis alterations, increased pro-inflammatory dietary lipids intake and fatty acids subclasses imbalance (Wang et al., 2015; Simons et al., 2021; Liu et al., 2022). Accordingly, Bataille and others (Bataille et al., 2005), showcased SHBG as a central determinant in the regulation of lipids profile, in relation to is sex hormones bindings capacity and its significant association with insulin. Here, we showed for the first time the clear influence of SHBG on individual adipose tissue FFAs abundance under EMS condition, and bring the evidence for a possible regulatory effect of SHBG on lipid metabolism.

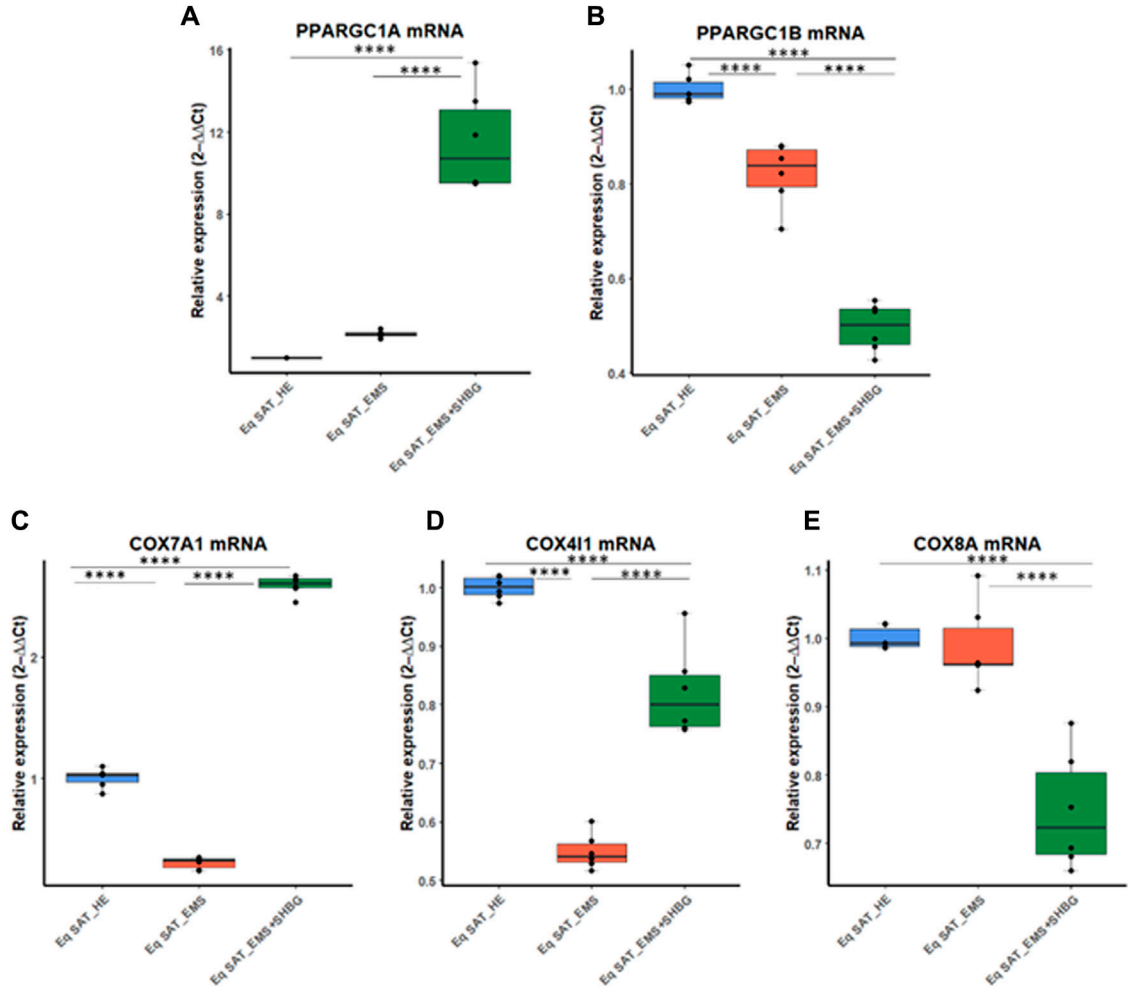

FIGURE 10
SHBG and mitochondrial metabolism markers interplay analysis. The relative expression levels of PPARGC1A **(A)**, PPARGC1B **(B)**, COX7A1 **(C)**, COX4I1 **(D)**, and COX8A **(E)** were analyzed by RT-PCR. Representative data are shown as mean ± SD. **** *p*-value < 0.0001.

To further illustrate the SHBG implication in adipose tissue lipid shift, the expression levels of key enzymes involved in lipolysis and lipogenesis has been investigated. EMS adipose tissue displayed significant dysregulated lipid metabolism master mediators with evidence of either transcriptional or posttranslational alterations. Indeed, a critical loss in lipoprotein lipase (LPL) and stearoyl CoA desaturase 1 (SCD1), has been observed at both mRNA and protein levels, while increased mRNA expression of fatty acid synthase (FASN), and adipose triglyceride lipase—ATGL (PNPLA2) were found to oppositely correspond to lower proteins levels. Conversely, the expression of perilipin-1 (PLN1) appeared upregulated at the protein level only. Previous investigations reported on the association of disrupted lipid metabolism and lipolysis mediators with metabolic disorders development. Lower FASN protein levels, a central lipogenesis enzyme that catalyses *de novo* saturated FA biosynthesis, has been associated with hyperglycaemia, insulin resistance and obesity (Mayas et al., 2010). Likewise, depleted expression of LPL, a rate-limiting enzyme regulating TG-FFAs absorption and storage has been observed in adipose tissue of obese, diabetic, atherosclerotic and dyslipidaemic patients (Kursawe et al., 2010; Serra et al., 2017). Interestingly, contradictory findings regarding SCD1 implication in metabolic syndrome development have demonstrated that while overactivation of SCD1 enzyme triggers insulin resistance and increased fat depots in rodents, SCD1 expression is inversely correlated with inflammation and insulin resistance in human patients (Peter et al., 2009; Gong et al., 2011), which strongly suggest that in horses, SCD1 loss is a hallmark of EMS and SAT metabolic instability. Moreover, elevated perilipin-1 (PLN1) protein abundance, a key lipolysis modulator has been found similarly to our observations in obese human subjects, which has been proposed as a compensatory mechanism limiting basal lipolysis (Kern et al., 2004). By contrast, triglyceride lipase (ATGL) deficiency has been reported to deteriorate the adipose tissue metabolic microenvironment, and consequently participate in obesity and hyperlipidaemia occurrence (Lai et al., 2022). Lipolysis plays a crucial role in maintaining lipid homeostasis and its alteration has been shown to trigger adipocyte hypertrophy and severe metabolic inflexibility (Li et al., 2022). Our obtained data evidenced the pro-lipolytic potential of SHBG by the selective perilipin 1 modulation. In white adipose tissue, perilipin

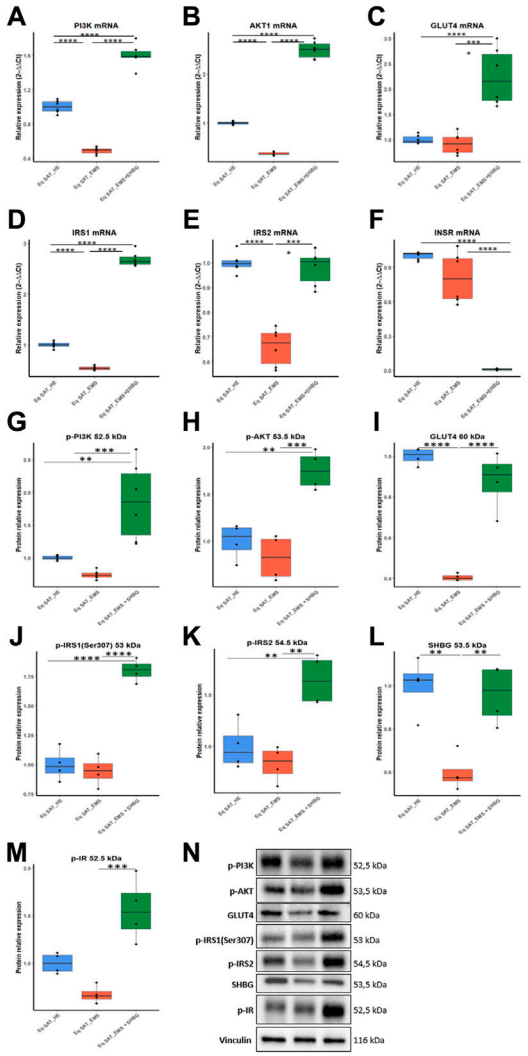

FIGURE 11
Involvement of SHBG in the insulin signaling pathway. Relative expression levels of PI3K **(A)**, AKT1 **(B)**, GLUT4 **(C)**, IRS1 **(D)**, IRS2 **(E)**, INSR **(F)** were analyzed by qRT-PCR. Protein levels of PI3K **(G)**, AKT **(H)**, GLUT4 **(I)**, IRS1 **(J)**, IRS2 **(K)**, SHBG **(L)**, IR **(M)** were analyzed by Western Blot. Representative immunoblots **(N)**. Representative data are shown as mean ± SD. ** p-value < 0.01, *** p-value < 0.001 and **** p-value < 0.0001.

1 restricts the access of cytosolic lipases to adipocytes lipid droplets to promote the storage of triacylglycerols (Sztalryd and Brasaemle, 2017). Treatment of EMS SAT with exogenous SHBG resulted in a substantial downregulation of perilipin 1 protein to a basal level. These observations are in contrast to a previous study showing that SHBG overexpression stimulates PLIN mRNA and protein expression in a model of human SHBG transgenic mice fed with HFD. However, the same study evidenced the ability of SHBG to activate lipolytic pathways and to prevent adipocytes hypertrophy by restoring HSL protein levels (Saez-Lopez et al., 2020). In the same vein, the response of human visceral adipocytes to SHBG treatment were in agreement with observed effects on mouse white adipose tissue, where a visible activation of HSL and ERK-1/2 phosphorylation have been observed, indicating that SHBG similarly promotes lipolysis in human mature visceral adipocytes (Saez-Lopez et al., 2020). These findings are in opposition to our obtained data demonstrating no significant regulatory effect of SHBG toward HSL and ATGL lipases expression. Such discrepancies maybe explained by the variation in the studied models and the already observed species differences of the regulatory mechanisms governing lipid turnover in rodents and horses (Breidenbach et al., 1998). Moreover, the absence of lipolysis stimuli in our *ex-vivo* model may explain the non-observable activation of lipases in EMS SAT, and obtained data could provide evidence of EMS-associated resistance to basal lipolysis mediated by increased expression of the gatekeeper perilipin which is reversed by SHBG treatment. In point of fact, PLIN1 deletion has been shown to minimize weight gain in HFD db/db mice and proposed as an obesity preventive mediator. Therewith, high expression of PLIN1 in fibroblasts resulted in a strong suppression of basal lipolytic rates (Tansey et al., 2004), suggesting its critical role in aberrant fats accumulation and storage, as well as the potential role of SHBG in limiting PLIN1 bioavailability in adipocytes. However, further investigation of stimulated lipolytic pathways is necessary to elucidate whether SHBG can promote the PLIN1 phosphorylation and HSL activation. Little is known regarding lipolytic pathways in equines, and to our best knowledge, this is the first study analysing the implication of SHBG in the modulation of lipid metabolism under EMS condition. Previous report showed that EMS adipose tissue is characterized by adipocytes hypertrophy and lipids engorgements, evoking defects in lipolysis as demonstrated in the present study (Reynolds et al., 2019). Other findings indicated on the loss in SHBG protein in the course of insulin resistance and metabolic syndrome (De Oya et al., 2009; Winters et al., 2014), which stays in line with the present investigation, where a marked SHBG protein downregulation has been observed in EMS SAT biopsies SHBG. Hence, the incubation of EMS SAT with SHBG protein induced a downregulation of the FASN gene expression and increased mRNA and protein levels of LPL. These results are in accordance with previous investigation demonstrating the suppressive effect of SHBG toward FASN transcript and the potential anti-lipogenic effect of SHBG which has been postulated to be at least partly related to its ability to increase intracellular cAMP (Yamazaki et al., 2018). However, it is not clear whether SHBG might exert its effects on a transcriptional level only rather than posttranslational, as no significant changes in FASN or SCD1 protein levels were observed in the present study.

While adipocyte hypertrophy has been clearly pointed as a pivotal contributor of obesity and metabolic syndrome associated adipose tissue dysfunction and systemic metabolic failure, hyperplasia derived from adipocytes precursors differentiation has been proposed as a potential anti-obesity protective mechanism, where increased number of adipocytes is believed to attenuate the lipids engorgement (Ghaben and Scherer, 2019). However, several lines of evidence also indicated that excessive adipogenesis may trigger immoderate fat accumulation and contribute to adipose tissue inflexibility (Jakab et al., 2021). In this investigation, EMS SAT displayed disrupted adipogenic regulatory network, where depleted expression of adipogenesis repressors has been observed in favour of pro-adipogenic

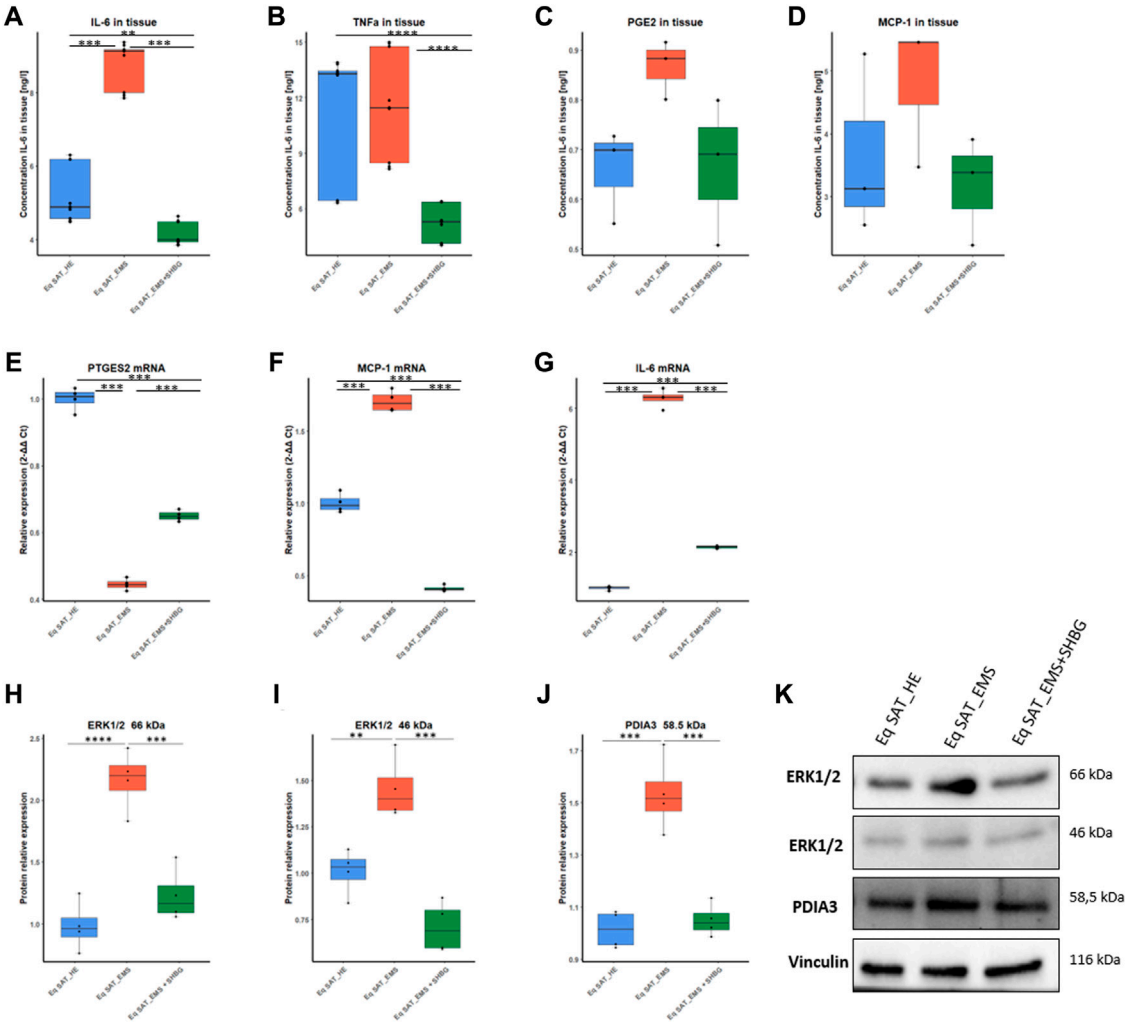

FIGURE 12
Involvement of SHBG in the inflammation pathway. Graphs showing the concentration of IL-6 **(A)**, TNF **(B)**, PGE2 **(C)**, and MCP-1 **(D)** in SAT analysed by ELISA tests. Relative expression levels of PTGES2 **(E)**, MCP-1 **(F)**, and IL-6 **(G)** were analysed by qRT-PCR. Protein levels of ERK1/2 **(H,I)** and PDIA3 **(J)** were analyzed by Western Blot. Representative blot membranes **(K)**. Representative data are shown as mean ± SD. ** p-value < 0.01, *** p-value < 0.001 and **** p-value < 0.0001.

initiators profusion. In the past few decades, several transcription factors have been identified as either stimulators or repressors for adipogenesis in white adipose tissue. Although C/EBP family members and peroxisome proliferator-activated receptor γ (PPARγ) are known as master adipogenesis mediators expressed at various differentiation stages, other important pathways are also involved in the initiation of adipogenic cascades. Among others, the Kruppel-like factors KLF4, -9, and -15 positively regulate the expression of pro-adipogenic genes including PPARγ and C/EBPα/β/δ (Ahmad et al., 2020). Likewise, the STAT5A protein has been implicated in the regulation of various cellular processes including adipogenic differentiation, by conveying the extracellular pro-adipogenic stimuli to the nucleus to initiate PPARγ transcription (Wakao et al., 2011). Conversely, other signaling molecules have been appointed as direct adipogenesis suppressors. KLF2, -3, -7 and -16, as well as β -catenin (CTNNB1) have thus been reported to specifically alter the expression of C/EBPα, PPARγ and sterol regulatory binding protein-1c (SREBP-1c) and inhibit the percussor cells commitment into mature adipogenic lineage (Pollak et al., 2018; Chen et al., 2020). Here we found that incubation of EMS SAT with exogenous SHBG promoted the expression of adipogenesis repressors, namely, KLF3, IRF3 and CTNNB1, while downregulating the regulators of PPARγ and C/EBPα that include KLF4, KLF9, STAT5A and CEBPD. These data suggest a potential antiadipogenic property of SHBG, which has been similarly reported by Yamazaki et al. (2018), in their study, where they showed that SHBG suppressed the expression of CEBPα, PPARγ, and SREBP1 as key transcription factors controlling adipogenesis in 3T3-L1 preadipocytes. In another study, lower SHBG levels have been strongly correlated with increased adipogenesis, however in liver tissue of patients with obesity and metabolic syndrome (Xing et al., 2022), providing a strong evidence for the potential regulatory effect of SHBG towards adipogenesis. To our best knowledge, this is the first study showing the influence of SHBG on the expression profile of pro- and anti-

adipogenic mediators in EMS white adipose tissue, and further investigations are needed to fully elucidate the exact molecular targets underlying the anti-adipogenic effects of SHBG.

Insulin signalling impairment as a core mechanism underlying EMS onset negatively impacts the lipid metabolism within adipocytes. A critical defect in post-insulin receptor' signalling events including tyrosine phosphorylation of IRS proteins and activation of Pi3K-Akt axis has been further reported in adipocytes derived from obese subjects (Czech et al., 2013). In this study, the disrupted lipid metabolism has been found accompanied with significant blunted insulin signalling in EMS SAT. Proteins profiling revealed a substantial decrease in both INSR, IRS1/2, Akt and Pi3K phosphorylation levels, indicating a strong insulin desensitization. Impaired lipolysis and resulting hypertrophy of adipocytes has been associated with systemic insulin resistance and elevated circulating insulin levels under metabolic syndrome condition (Arner et al., 2010). In subcutaneous adipose tissue, insulin is an important adipogenic hormone mediating the FFAs storage via triglycerides biosynthesis within the adipocytes (Gastaldelli et al., 2017). Thus, previous data demonstrated that IR and associated improper IRS/Pi3K/Akt transducers phosphorylation significantly hampers the activity of main lipogenic enzymes including LPL and FASN, and loss in insulin-mediated cascades trigger to profound defective triglyceride clearance and overall dysregulated fatty acids and triacylglycerol metabolism (Panarotto et al., 2002; Mayas et al., 2010; Wong and Sul, 2010). Interestingly, the observed ability of SHBG to regulate the levels of LPL and FASN has been with a visible amelioration of the IR, Pi3K, IRS1/2 and Akt phosphorylation status of EMS SAT. Furthermore, we found that application of SHBG to EMS SAT increased the protein level of Glut-4, suggesting a possible alleviation of insulin resistance and improvement of the glucose uptake capacity. Similarly to our observations, decreased SHBG mRNA and protein levels have been previously correlated to lower expression of insulin-associated effectors, namely, IRS-1, IRS-2, PI3Kp85α and GLUT-3 and GLUT-4, and has been further linked to the PI3K/AKT pathway-mediated systemic insulin resistance (Feng et al., 2018). Moreover, SHBG overexpression has been reported to enhance the Glut-1-mediated glucose uptake and utilization via cAMP/PKA/CREB1 pathways activation in a human model of insulin resistant placental trophoblasts (Chi et al., 2020). What is more, Robker and others (Robker et al., 2009), that obesity phenotype of granulosa and cumulus cells correlated with increased insulin levels and suppressed SHBG expression in combination to lower Glut-4 and IRS2 transcript abundance, evoking an IRS1/IRS2 axis deactivation and a resulting insulin resistance status. Remarkably, the same study evidenced an additional connection between depleted SHBG levels and loss in ChREBP and SREBP-1, two critical mediators involved in lipogenesis regulation and lipogenic enzymes modulation, substantiating the prospective ability of SHBG to enhance insulin and lipid homeostasis in EMS SAT.

Increased adiposity and hyperinsulinemia has been closely linked to low-grade systemic inflammation in the course of EMS, resulting from the excessive production and release of various adipokines including the proinflammatory cytokines IL-1, IL-6, and the tumor necrosis factor (TNF) α (Vick et al., 2007). Here we found that EMS SAT was characterized by significant increased levels of IL-6 and moderate elevated PGE2 and MCP-1. Additionally, lipidomic analysis showed a critical elevation in polyunsaturated fatty acids (PUFAs) notably arachidonic and linoleic acids as well as eicosanoids, all known as important inflammation contributors. Indeed, under metabolic syndrome and hyperglycaemic condition, linoleic acid has been proposed to influence inflammatory reactions upon its Lipoxygenases (LOX)-mediated oxidation to highly reactive derivatives, namely, hydroxyoctadecadienoic acids (HODEs), oxo-HODEs and epoxy-HODEs (Vangaveti et al., 2016). Linoleic acid is further engaged in arachidonic acid biosynthesis via its conversion to γ-linolenic acid by the Δ^6-desaturase (Norris and Carr, 2021). Under unfavourable conditions such as metabolic distress, arachidonic acid undergoes rapid conversion to endoperoxides that are used by cyclooxygenases to synthetise a pleiotropy of eicosanoids including prostaglandins, thromboxanes, leukotrienes, and lipoxins (Litwack, 2022). Arachidonic-derived eicosanoids have been reported as highly active pro-inflammatory mediators, and earlier investigations demonstrated that specific overactivation of cyclooxygenase 2 (COX2) triggers severe inflammatory response in the adipose tissue of obese subjects with high arachidonic acid levels. Likewise, upregulated COX2 has been correlated with an activation of the JNK/NFκB pathway leading to MCP-1 and IL-6 induction and immune cell infiltration into adipose tissue (Gartung et al., 2016). Hither, the *ex-vivo* treatment of EMS SAT with 50 nM SHBG exerted a potent anti-inflammatory effect as evidenced by the noticeable lowered levels of pro-inflammatory markers IL-6, TNF-α and MCP-1. The observed effect positively correlates with a number of reports that suggested the potential use of SHBG as an inflammation in the course of metabolic syndrome. Chronic inflammatory diseases such as polycystic ovary syndrome (PCOS), diabetes or obesity have been associated with low circulating SHBG levels in female patients (Ding et al., 2009). Withal, Yamazaki and collaborators (Yamazaki et al., 2018), in like manner found that SHBG efficiently abolished lipopolysaccharide- (LPS-) induced inflammatory response by suppressing the release of MCP-1, TNFα, and IL-6 cytokines in adipocytes and macrophages, along with phosphorylations of JNK and ERK. Interestingly, we also found that SHBG decreased the tissue levels of arachidonic and linoleic acids, which might have contributed to its observed anti-inflammatory effect, and further stands in line with the formerly underscored interrelation between high pro-inflammatory polyunsaturated fatty acids and low SHBG levels in adult human subjects (Liu et al., 2022).

Notably, our study evidenced the activation of both protein disulfide-isomerase A3 (PDI3A) stress and extracellular signal-regulated kinase 1/2 (ERK1/2) kinases in the SAT biopsies derived from EMS horses. Initially identified as a stress response molecule and a protein chaperone mediating the unfolded protein response (UPR), PDIA3 has been later showed to negatively impact various cellular processes in disease. Hence, accumulating evidence demonstrate that PDIA3 is promoting immune-activated hallmarks, and its depletion inhibits pro-inflammatory responses and oxidative damage (Wang et al., 2019). Besides, ERK1/2 plays an important role in determining cell survival or death, it has also been wildly described as an important regulator of pro-inflammatory gene expression including JNK/NF-κB signaling pathways, IL-1β, IL-6 and TNF-α cytokines (Li et al., 2016). Accordingly, SHBG treatment engendered a visible downregulation of both PDIA3 and ERK1/2 in the EMS SAT, which might represent a possible molecular mechanism underlying the anti-inflammatory activity of SHBG. In point of fact, SHBG has been thus far described as a direct inhibitor of ERK pathway markers activation (Wang et al., 2020). Moreover, previous data emphasized the

stimulatory effect of PDIA3 toward ERK1/2 activation, as PDIA3 silencing results in a critical ERK depletion (Ye et al., 2018). Taken together, these findings infer that SHBG may exert its biological functions by regulating the ERK pathway components through PDIA3 modulation.

5 Conclusion

Equine metabolic syndrome strongly impairs the endocrine properties of subcutaneous adipose tissue by altering lipid metabolism homeostasis and promoting low-grade inflammation, which collectively trigger insulin resistance in relation to depleted SHBG levels. In this investigation, we evidenced the great potential of SHBG treatment in restoring proper SAT physiology by enhancing the expression of lipogenic enzymes and regulating the overall lipid profile. Moreover, SHBG application exerted a strong insulin sensitizing effect and showed remarkable anti-inflammatory potential through the modulation of the pro-inflammatory cytokines IL-6, TNF-α and MCP-1 and the reduction of arachidonic and linoleic acids levels. Interestingly, we demonstrated for the first time that SHBG may target the PDIA3/ERK axis to attenuate the exaggerated inflammatory responses and aberrant lipid metabolism inflexibility. This research therefore contributes to understanding the possible intercorrelation between SHBG protein and equine metabolic syndrome, and provides new molecular insight into the mechanism by which SHBG exerts its metabolic regulatory action.

Data availability statement

The original contributions presented in the study are included in the article/supplementary material, further inquiries can be directed to the corresponding author.

Ethics statement

Ethical approval was not required for the study involving animals in accordance with the local legislation and institutional requirements because Tissue samples were obtained from a local slaughterhouse post-mortem and did not require any approval. No living animals were used in this study, and horses from which tissues were collected were slaughtered for reasons unrelated to the study before the tissue collection.

Author contributions

LB participated in experiment conceptualization, data curation, formal analysis, investigation, methodology, software, supervision, validation, writing–original draft, writing–review and editing. MK participated in investigation, data curation and writing–original draft. BQ participated in lipidomics analysis, formal analysis, bioinformatics, software, writing–original draft. MZ participated in formal analysis, writing–original draft. JL participated in lipidomics analysis, methodology, formal analysis, software. MK participated in lipidomics analysis. MM participated in obtaining materials and resources. KM participated in experiment conceptualization, supervision, funding acquisition, methodology, formal analysis, project administration, resources, validation, writing–original draft. All authors contributed to the article and approved the submitted version.

Funding

The work was financed by the National Science Centre in Poland over the course of the realization of the project: “Exploring the role and therapeutic potential of sex hormone binding globulin (SHBG) in the course of insulin resistance, inflammation, lipotoxicity in adipose stem progenitor cells and adipocytes in equine metabolic syndrome (EMS) mares” (No 2019/35/B/NZ7/03651). The APC was co-financed by Wrocław University of Environmental and Life Sciences.

Conflict of interest

The authors declare that the research was conducted in the absence of any commercial or financial relationships that could be construed as a potential conflict of interest.

Publisher’s note

References

Ahmad, B., Serpell, C. J., Fong, I. L., and Wong, E. H. (2020). Molecular mechanisms of adipogenesis: the anti-adipogenic role of AMP-activated protein kinase. *Front. Mol. Biosci.* 7, 76. doi:10.3389/fmolb.2020.00076

Ahmed, B., Sultana, R., and Greene, M. W. (2021). Adipose tissue and insulin resistance in obese. *Biomed. Pharmacother.* 137, 111315. doi:10.1016/j.biopha.2021.111315

Alinezhad, A., and Jafari, F. (2019). The relationship between components of metabolic syndrome and plasma level of sex hormone-binding globulin. *Eur. J. Transl. Myology* 29 (2), 8196. doi:10.4081/ejtm.2019.8196

Arner, E., Westermark, P. O., Spalding, K. L., Britton, T., Rydén, M., Frisén, J., et al. (2010). Adipocyte turnover: relevance to human adipose tissue morphology. *Diabetes* 59 (1), 105–109. doi:10.2337/db09-0942

Aroor, A. R., Jia, G., and Sowers, J. R. (2018). Cellular mechanisms underlying obesity-induced arterial stiffness. *Am. J. Physiology-Regulatory, Integr. Comp. Physiology* 314 (3), R387–R398. doi:10.1152/ajpregu.00235.2016

Basinska, K., Marycz, K., Śmieszek, A., and Nicpoń, J. (2015). The production and distribution of IL-6 and TNF-α in subcutaneous adipose tissue and their correlation with serum concentrations in Welsh ponies with equine metabolic syndrome. *J. Veterinary Sci.* 16 (1), 113–120. doi:10.4142/jvs.2015.16.1.113

Bataille, V., Perret, B., Evans, A., Amouyel, P., Arveiler, D., Ducimetière, P., et al. (2005). Sex hormone-binding globulin is a major determinant of the lipid profile: the PRIME study. *Atherosclerosis* 179 (2), 369–373. doi:10.1016/j.atherosclerosis.2004.10.029

Bourebaba, N., Ngo, T., Śmieszek, A., Bourebaba, L., and Marycz, K. (2022). Sex hormone binding globulin as a potential drug candidate for liver-related metabolic disorders treatment. *Biomed. Pharmacother.* 153, 113261. doi:10.1016/j.biopha.2022.113261

Breidenbach, A., Fuhrmann, H., Busche, R., and Sallmann, H.-P. (1998). Studies on equine lipid metabolism. 1. A fluorometric method for the measurement of lipolytic activity in isolated adipocytes of rats and horses. *J. Veterinary Med. Ser. A* 45 (1–10), 635–643. doi:10.1111/j.1439-0442.1998.tb00868.x

Caputo, T., Gilardi, F., and Desvergne, B. (2017). From chronic overnutrition to metaflammation and insulin resistance: adipose tissue and liver contributions. *FEBS Lett.* 591 (19), 3061–3088. doi:10.1002/1873-3468.12742

Cena, H., and Calder, P. C. (2020). Defining a healthy diet: evidence for the role of contemporary dietary patterns in health and disease. *Nutrients* 12 (2), 334. doi:10.3390/nu12020334

Chen, M., Lu, P., Ma, Q., Cao, Y., Chen, N., Li, W., et al. (2020). *CTNNB1/β -catenin* dysfunction contributes to adiposity by regulating the cross-talk of mature adipocytes and preadipocytes. *Sci. Adv.* 6 (2), eaax9605. doi:10.1126/sciadv.aax9605

Chi, X., Feng, C., Wang, X., and Jin, Z. (2020). Sex hormone-binding globulin regulates glucose metabolism in human placental trophoblasts via cAMP/PKA/CREB1. *J. Obstetrics Gynaecol. Res.* 46 (11), 2340–2346. doi:10.1111/jog.14429

Czech, M. P., Tencerova, M., Pedersen, D. J., and Aouadi, M. (2013). Insulin signalling mechanisms for triacylglycerol storage. *Diabetologia* 56 (5), 949–964. doi:10.1007/s00125-013-2869-1

De Oya, I., Schoppen, S., Lasunción, M. A., Lopez-Simon, L., Riestra, P., De Oya, M., et al. (2009). Sex hormone-binding globulin levels and metabolic syndrome and its features in adolescents. *Pediatr. Diabetes* 11 (3), 188–194. doi:10.1111/j.1399-5448.2009.00559.x

De Simone, M., Verrotti, A., Iughetti, L., Palumbo, M., Farello, G., Di Cesare, E., et al. (2001). Increased visceral adipose tissue is associated with increased circulating insulin and decreased sex hormone binding globulin levels in massively obese adolescent girls. *J. Endocrinol. Investigation* 24 (6), 438–444. doi:10.1007/BF03351044

De Souza, R. J., Mente, A., Maroleanu, A., Cozma, A. I., Ha, V., Kishibe, T., et al. (2015). Intake of saturated and trans unsaturated fatty acids and risk of all cause mortality, cardiovascular disease, and type 2 diabetes: systematic review and meta-analysis of observational studies. *BMJ* 351, h3978. doi:10.1136/bmj.h3978

Ding, E. L., Song, Y., Manson, J. E., Hunter, D. J., Lee, C. C., Rifai, N., et al. (2009). Sex hormone–binding globulin and risk of type 2 diabetes in women and men. *N. Engl. J. Med.* 361 (12), 1152–1163. doi:10.1056/NEJMoa0804381

Durham, A. E., Frank, N., McGowan, C. M., Menzies-Gow, N. J., Roelfsema, E., Vervuert, I., et al. (2019). ECEIM consensus statement on equine metabolic syndrome. *J. Veterinary Intern. Med.* 33 (2), 335–349. doi:10.1111/jvim.15423

Ertelt, A., Barton, A.-K., Schmitz, R. R., and Gehlen, H. (2014). Metabolic syndrome: is equine disease comparable to what we know in humans? *Endocr. Connect.* 3 (3), R81–R93. doi:10.1530/EC-14-0038

Fahed, G., Aoun, L., Bou Zerdan, M., Allam, S., Bou Zerdan, M., Bouferraa, Y., et al. (2022). Metabolic syndrome: updates on pathophysiology and management in 2021. *Int. J. Mol. Sci.* 23 (2), 786. doi:10.3390/ijms23020786

Feng, C., Jin, Z., Chi, X., Zhang, B., Wang, X., Sun, L., et al. (2018). SHBG expression is correlated with PI3K/AKT pathway activity in a cellular model of human insulin resistance. *Gynecol. Endocrinol.* 34 (7), 567–573. doi:10.1080/09513590.2017.1411474

Fleenor, B. S., Carlini, N. A., Ouyang, A., and Harber, M. P. (2022). Perivascular adipose tissue-mediated arterial stiffening in aging and disease: an emerging translational therapeutic target? *Pharmacol. Res.* 178, 106150. doi:10.1016/j.phrs.2022.106150

Folch, J., Lees, M., and Sloane Stanley, G. H. (1957). A simple method for the isolation and purification of total lipides from animal tissues. *J. Biol. Chem.* 226 (1), 497–509. doi:10.1016/s0021-9258(18)64849-5

Frank, N., Geor, R. J., Bailey, S. R., Durham, A. E., Johnson, P. J., and American College of Veterinary Internal Medicine (2010). Equine metabolic syndrome: equine metabolic syndrome. *J. Veterinary Intern. Med.* 24 (3), 467–475. doi:10.1111/j.1939-1676.2010.0503.x

Gartung, A., Zhao, J., Chen, S., Mottillo, E., VanHecke, G. C., Ahn, Y.-H., et al. (2016). Characterization of eicosanoids produced by adipocyte lipolysis: implication of cyclooxygenase-2 in adipose inflammation. *J. Biol. Chem.* 291 (31), 16001–16010. doi:10.1074/jbc.M116.725937

Gastaldelli, A., Gaggini, M., and DeFronzo, R. A. (2017). Role of adipose tissue insulin resistance in the natural history of type 2 diabetes: results from the san antonio metabolism study. *Diabetes* 66 (4), 815–822. doi:10.2337/db16-1167

Ghaben, A. L., and Scherer, P. E. (2019). Adipogenesis and metabolic health. *Nat. Rev. Mol. Cell Biol.* 20 (4), 242–258. doi:10.1038/s41580-018-0093-z

Gong, J., Campos, H., McGarvey, S., Wu, Z., Goldberg, R., and Baylin, A. (2011). Genetic variation in stearoyl-CoA desaturase 1 is associated with metabolic syndrome prevalence in Costa Rican adults. *J. Nutr.* 141 (12), 2211–2218. doi:10.3945/jn.111.143503

Guilherme, A., Virbasius, J. V., Puri, V., and Czech, M. P. (2008). Adipocyte dysfunctions linking obesity to insulin resistance and type 2 diabetes. *Nat. Rev. Mol. Cell Biol.* 9 (5), 367–377. doi:10.1038/nrm2391

Henneke, D. R., Potter, G. D., Kreider, J. L., and Yeates, B. F. (1983). Relationship between condition score, physical measurements and body fat percentage in mares. *Equine Veterinary J.* 15 (4), 371–372. doi:10.1111/j.2042-3306.1983.tb01826.x

Huang, S., Rutkowsky, J. M., Snodgrass, R. G., Ono-Moore, K. D., Schneider, D. A., Newman, J. W., et al. (2012). Saturated fatty acids activate TLR-mediated proinflammatory signaling pathways. *J. Lipid Res.* 53 (9), 2002–2013. doi:10.1194/jlr.D029546

Jakab, J., Miškić, B., Mikšić, Š., Juranić, B., Ćosić, V., Schwarz, D., et al. (2021). Adipogenesis as a potential anti-obesity target: a review of pharmacological treatment and natural products. *Diabetes, Metabolic Syndrome Obes. Targets Ther.* 14, 67–83. doi:10.2147/DMSO.S281186

Jung, U., and Choi, M.-S. (2014). Obesity and its metabolic complications: the role of adipokines and the relationship between obesity, inflammation, insulin resistance, dyslipidemia and nonalcoholic fatty liver disease. *Int. J. Mol. Sci.* 15 (4), 6184–6223. doi:10.3390/ijms15046184

Kawai, T., Autieri, M. V., and Scalia, R. (2021). Adipose tissue inflammation and metabolic dysfunction in obesity. *Am. J. Physiology-Cell Physiology* 320 (3), C375–C391. doi:10.1152/ajpcell.00379.2020

Kern, P. A., Di Gregorio, G., Lu, T., Rassouli, N., and Ranganathan, G. (2004). Perilipin expression in human adipose tissue is elevated with obesity. *J. Clin. Endocrinol. Metabolism* 89 (3), 1352–1358. doi:10.1210/jc.2003-031388

Kim, C., Dabelea, D., Kalyani, R. R., Christophi, C. A., Bray, G. A., Pi-Sunyer, X., et al. (2017). Changes in visceral adiposity, subcutaneous adiposity, and sex hormones in the diabetes prevention program. *J. Clin. Endocrinol. Metabolism* 102 (9), 3381–3389. doi:10.1210/jc.2017-00967

Koenen, M., Hill, M. A., Cohen, P., and Sowers, J. R. (2021). Obesity, adipose tissue and vascular dysfunction. *Circulation Res.* 128 (7), 951–968. doi:10.1161/CIRCRESAHA.121.318093

Kornicka-Garbowska, K., Bourebaba, L., Röcken, M., and Marycz, K. (2021). Sex hormone binding globulin (SHBG) mitigates ER stress in hepatocytes *in vitro* and *ex vivo*. *Cells* 10 (4), 755. doi:10.3390/cells10040755

Krzysztoszek, J., Laudańska-Krzemińska, I., and Bronikowski, M. (2019). Assessment of epidemiological obesity among adults in EU countries. *Ann. Agric. Environ. Med.* 26 (2), 341–349. doi:10.26444/aaem/97226

Kursawe, R., Eszlinger, M., Narayan, D., Liu, T., Bazuine, M., Cali, A. M. G., et al. (2010). Cellularity and adipogenic profile of the abdominal subcutaneous adipose tissue from obese adolescents: association with insulin resistance and hepatic steatosis. *Diabetes* 59 (9), 2288–2296. doi:10.2337/db10-0113

Lai, H.-H., Yeh, K.-Y., Hsu, H.-M., and Her, G. M. (2022). Deficiency of adipose triglyceride lipase induces metabolic syndrome and cardiomyopathy in zebrafish. *Int. J. Mol. Sci.* 24 (1), 117. doi:10.3390/ijms24010117

Li, N., Liu, B.-W., Ren, W.-Z., Liu, J.-X., Li, S.-N., Fu, S.-P., et al. (2016). GLP-2 attenuates LPS-induced inflammation in BV-2 cells by inhibiting ERK1/2, JNK1/2 and NF-κB signaling pathways. *Int. J. Mol. Sci.* 17 (2), 190. doi:10.3390/ijms17020190

Li, Y., Li, Z., Ngandiri, D. A., Llerins Perez, M., Wolf, A., and Wang, Y. (2022). The molecular brakes of adipose tissue lipolysis. *Front. Physiology* 13, 826314. doi:10.3389/fphys.2022.826314

Litwack, G. (2022). "Eicosanoids," in *Hormones* (Netherlands: Elsevier), 195–212. doi:10.1016/B978-0-323-90262-5.00005-6

Liu, N., Feng, Y., Luo, X., Ma, X., and Ma, F. (2022). Association between dietary inflammatory index and sex hormone binding globulin and sex hormone in U.S. Adult females. *Front. Public Health* 10, 802945. doi:10.3389/fpubh.2022.802945

Malodobra-Mazur, M., Cierzniak, A., and Dobosz, T. (2019). Oleic acid influences the adipogenesis of 3T3-L1 cells via DNA Methylation and may predispose to obesity and obesity-related disorders. *Lipids Health Dis.* 18 (1), 230. doi:10.1186/s12944-019-1173-6

Marycz, K., Kornicka, K., Basinska, K., and Czyrek, A. (2016). Equine metabolic syndrome affects viability, senescence, and stress factors of equine adipose-derived mesenchymal stromal stem cells: new insight into EqASCs isolated from EMS horses in the context of their aging. *Oxidative Med. Cell. Longev.* 2016, 4710326–4710417. doi:10.1155/2016/4710326

Mayas, M. D., Ortega, F. J., Macías-González, M., Bernal, R., Gómez-Huelgas, R., Fernández-Real, J. M., et al. (2010). Inverse relation between FASN expression in human adipose tissue and the insulin resistance level. *Nutr. Metabolism* 7 (1), 3. doi:10.1186/1743-7075-7-3

Morgan, R., Keen, J., and McGowan, C. (2015). Equine metabolic syndrome. *Veterinary Rec.* 177 (7), 173–179. doi:10.1136/vr.103226

Nakhla, A. M., Leonard, J., Hryb, D. J., and Rosner, W. (1999). Sex hormone-binding globulin receptor signal transduction proceeds via a G protein. *Steroids* 64 (3), 213–216. doi:10.1016/S0039-128X(98)00084-1

Nielsen, T. L., Hagen, C., Wraae, K., Brixen, K., Petersen, P. H., Haug, E., et al. (2007). Visceral and subcutaneous adipose tissue assessed by magnetic resonance imaging in relation to circulating androgens, sex hormone-binding globulin, and luteinizing hormone in young men. *J. Clin. Endocrinol. Metabolism* 92 (7), 2696–2705. doi:10.1210/jc.2006-1847

Norris, D. O., and Carr, J. A. (2021). "Synthesis, metabolism, and actions of bioregulators," in *Vertebrate endocrinology* (Netherlands: Elsevier), 43–90. doi:10.1016/B978-0-12-820093-3.00003-4

Panarotto, D., Rémillard, P., Bouffard, L., and Maheux, P. (2002). Insulin resistance affects the regulation of lipoprotein lipase in the postprandial period and in an adipose tissue-specific manner: insulin resistance and postprandial lipoprotein lipase. *Eur. J. Clin. Investigation* 32 (2), 84–92. doi:10.1046/j.1365-2362.2002.00945.x

Para, I., Albu, A., and Porojan, M. D. (2021). Adipokines and arterial stiffness in obesity. *Medicina* 57 (7), 653. doi:10.3390/medicina57070653

Peter, A., Weigert, C., Staiger, H., Machicao, F., Schick, F., Machann, J., et al. (2009). Individual stearoyl-CoA desaturase 1 expression modulates endoplasmic reticulum stress and inflammation in human myotubes and is associated with skeletal muscle lipid storage and insulin sensitivity *in vivo*. *Diabetes* 58 (8), 1757–1765. doi:10.2337/db09-0188

Pi-Sunyer, X. (2009). The medical risks of obesity. *Postgrad. Med.* 121 (6), 21–33. doi:10.3810/pgm.2009.11.2074

Pollak, N. M., Hoffman, M., Goldberg, I. J., and Drosatos, K. (2018). Krüppel-like factors: crippling and un-crippling metabolic pathways. *JACC Basic Transl. Sci.* 3 (1), 132–156. doi:10.1016/j.jacbts.2017.09.001

Ragno, V. M., Zello, G. A., Klein, C. D., and Montgomery, J. B. (2019). From table to stable: a comparative review of selected aspects of human and equine metabolic syndrome. *J. Equine Veterinary Sci.* 79, 131–138. doi:10.1016/j.jevs.2019.06.003

Rendle, D., McGregor Argo, C., Bowen, M., Carslake, H., German, A., Harris, P., et al. (2018). Equine obesity: current perspectives. *UK-Vet Equine* 2 (5), 1–19. doi:10.12968/ukve.2018.2.S2.3

Reynolds, A., Keen, J. A., Fordham, T., and Morgan, R. A. (2019). Adipose tissue dysfunction in obese horses with equine metabolic syndrome. *Equine Veterinary J.* 51 (6), 760–766. doi:10.1111/evj.13097

Robker, R. L., Akison, L. K., Bennett, B. D., Thrupp, P. N., Chura, L. R., Russell, D. L., et al. (2009). Obese women exhibit differences in ovarian metabolites, hormones, and gene expression compared with moderate-weight women. *J. Clin. Endocrinol. Metabolism* 94 (5), 1533–1540. doi:10.1210/jc.2008-2648

Rochlani, Y., Pothineni, N. V., Kovelamudi, S., and Mehta, J. L. (2017). Metabolic syndrome: pathophysiology, management, and modulation by natural compounds. *Ther. Adv. Cardiovasc. Dis.* 11 (8), 215–225. doi:10.1177/1753944717711379

Rosner, W., Hryb, D. J., Kahn, S. M., Nakhla, A. M., and Romas, N. A. (2010). Interactions of sex hormone-binding globulin with target cells. *Mol. Cell. Endocrinol.* 316 (1), 79–85. doi:10.1016/j.mce.2009.08.009

Saez-Lopez, C., Villena, J. A., Simó, R., and Selva, D. M. (2020). Sex hormone-binding globulin overexpression protects against high-fat diet-induced obesity in transgenic male mice. *J. Nutr. Biochem.* 85, 108480. doi:10.1016/j.jnutbio.2020.108480

Sears, B., and Perry, M. (2015). The role of fatty acids in insulin resistance. *Lipids Health Dis.* 14 (1), 121. doi:10.1186/s12944-015-0123-1

Serra, M. C., Ryan, A. S., and Goldberg, A. P. (2017). Reduced LPL and subcutaneous lipid storage capacity are associated with metabolic syndrome in postmenopausal women with obesity. *Obes. Sci. Pract.* 3 (1), 106–114. doi:10.1002/osp4.86

Simó, R., Sáez-López, C., Barbosa-Desongles, A., Hernández, C., and Selva, D. M. (2015). Novel insights in SHBG regulation and clinical implications. *Trends Endocrinol. Metabolism* 26 (7), 376–383. doi:10.1016/j.tem.2015.05.001

Simons, P. I. H. G., Valkenburg, O., Telgenkamp, I., Van Der Waaij, K. M., De Groot, D. M., Veeraiah, P., et al. (2021). Relationship between *de novo* lipogenesis and serum sex hormone binding globulin in humans. *Clin. Endocrinol.* 95 (1), 101–106. doi:10.1111/cen.14459

Sztalryd, C., and Brasaemle, D. L. (2017). The perilipin family of lipid droplet proteins: gatekeepers of intracellular lipolysis. *Biochimica Biophysica Acta (BBA) - Mol. Cell Biol. Lipids* 1862 (10), 1221–1232. doi:10.1016/j.bbalip.2017.07.009

Takic, M., Pokimica, B., Petrovic-Oggiano, G., and Popovic, T. (2022). Effects of dietary α-linolenic acid treatment and the efficiency of its conversion to eicosapentaenoic and docosahexaenoic acids in obesity and related diseases. *Molecules* 27 (14), 4471. doi:10.3390/molecules27144471

Tansey, J., Sztalryd, C., Hlavin, E., Kimmel, A., and Londos, C. (2004). The central role of perilipin A in lipid metabolism and adipocyte lipolysis. *IUBMB Life (International Union Biochem. Mol. Biol. Life)* 56 (7), 379–385. doi:10.1080/15216540400009968

Vangaveti, V. N., Jansen, H., Kennedy, R. L., and Malabu, U. H. (2016). Hydroxyoctadecadienoic acids: oxidised derivatives of linoleic acid and their role in inflammation associated with metabolic syndrome and cancer. *Eur. J. Pharmacol.* 785, 70–76. doi:10.1016/j.ejphar.2015.03.096

Vick, M. M., Adams, A. A., Murphy, B. A., Sessions, D. R., Horohov, D. W., Cook, R. F., et al. (2007). Relationships among inflammatory cytokines, obesity, and insulin sensitivity in the horse. *J. Animal Sci.* 85 (5), 1144–1155. doi:10.2527/jas.2006-673

Wakao, H., Wakao, R., Oda, A., and Fujita, H. (2011). Constitutively active Stat5A and Stat5B promote adipogenesis. *Environ. Health Prev. Med.* 16 (4), 247–252. doi:10.1007/s12199-010-0193-7

Wallace, I. R., McKinley, M. C., Bell, P. M., and Hunter, S. J. (2013). Sex hormone binding globulin and insulin resistance. *Clin. Endocrinol.* 78 (3), 321–329. doi:10.1111/cen.12086

Wang, Q., Kangas, A. J., Soininen, P., Tiainen, M., Tynkkynen, T., Puukka, K., et al. (2015). Sex hormone-binding globulin associations with circulating lipids and metabolites and the risk for type 2 diabetes: observational and causal effect estimates. *Int. J. Epidemiol.* 44 (2), 623–637. doi:10.1093/ije/dyv093

Wang, W.-T., Sun, L., and Sun, C.-H. (2019). PDIA3-regulted inflammation and oxidative stress contribute to the traumatic brain injury (TBI) in mice. *Biochem. Biophysical Res. Commun.* 518 (4), 657–663. doi:10.1016/j.bbrc.2019.08.100

Wang, X., Chi, X., Feng, C., Zhang, X., and Jin, Z. (2020). Sex hormone-binding globulin regulates the activity of the ERK pathway in the placentas of patients with gestational diabetes mellitus. *Biochem. Biophysical Res. Commun.* 532 (4), 613–619. doi:10.1016/j.bbrc.2020.08.100

Wang, Y. (2021). Definition, prevalence, and risk factors of low sex hormone-binding globulin in US adults. *J. Clin. Endocrinol. Metabolism* 106 (10), e3946–e3956. doi:10.1210/clinem/dgab416

Weijers, R. N. M. (2015). Membrane flexibility, free fatty acids, and the onset of vascular and neurological lesions in type 2 diabetes. *J. Diabetes and Metabolic Disord.* 15 (1), 13. doi:10.1186/s40200-016-0235-9

Winters, S. J., Gogineni, J., Karegar, M., Scoggins, C., Wunderlich, C. A., Baumgartner, R., et al. (2014). Sex hormone-binding globulin gene expression and insulin resistance. *J. Clin. Endocrinol. Metabolism* 99 (12), E2780–E2788. doi:10.1210/jc.2014-2640

Wong, R. H., and Sul, H. S. (2010). Insulin signaling in fatty acid and fat synthesis: a transcriptional perspective. *Curr. Opin. Pharmacol.* 10 (6), 684–691. doi:10.1016/j.coph.2010.08.004

Xia, J., Sinelnikov, I. V., Han, B., and Wishart, D. S. (2015). MetaboAnalyst 3.0—making metabolomics more meaningful. *Nucleic Acids Res.* 43 (1), W251–W257. doi:10.1093/nar/gkv380

Xie, W., Hamilton, J. A., Kirkland, J. L., Corkey, B. E., and Guo, W. (2006). Oleate-induced formation of fat cells with impaired insulin sensitivity. *Lipids* 41 (3), 267–271. doi:10.1007/s11745-006-5096-4

Xing, C., Zhang, J., Zhao, H., and He, B. (2022). Effect of sex hormone-binding globulin on polycystic ovary syndrome: mechanisms, manifestations, genetics, and treatment. *Int. J. Women's Health* 14, 91–105. doi:10.2147/IJWH.S344542

Yamazaki, H., Kushiyama, A., Sakoda, H., Fujishiro, M., Yamamotoya, T., Nakatsu, Y., et al. (2018). Protective effect of sex hormone-binding globulin against metabolic syndrome: *in vitro* evidence showing anti-inflammatory and lipolytic effects on adipocytes and macrophages. *Mediat. Inflamm.* 2018, 3062319–3062412. doi:10.1155/2018/3062319

Ye, Q., Fu, P., Dou, J., and Wang, N. (2018). Downregulation of PDIA3 inhibits proliferation and invasion of human acute myeloid leukemia cells. *OncoTargets Ther.* 11, 2925–2935. doi:10.2147/OTT.S162407

Zatterale, F., Longo, M., Naderi, J., Raciti, G. A., Desiderio, A., Miele, C., et al. (2020). Chronic adipose tissue inflammation linking obesity to insulin resistance and type 2 diabetes. *Front. Physiology* 10, 1607. doi:10.3389/fphys.2019.01607

frontiers | Frontiers in Molecular Biosciences

TYPE Original Research
PUBLISHED 11 January 2024
DOI 10.3389/fmolb.2023.1250423

OPEN ACCESS

EDITED BY
Or Kakhlon,
Hadassah Medical Center, Israel

REVIEWED BY
Monserrat Olea-Flores,
University of Massachusetts Medical School, United States
Michael Rehman,
Yale University, United States
Marianna Caterino,
University of Naples Federico II, Italy

*CORRESPONDENCE
Peter Hoffmann,
Peter.Hoffmann@unisa.edu.au
Sarawut Jitrapakdee,
sarawut.jit@mahidol.ac.th

RECEIVED 30 June 2023
ACCEPTED 27 December 2023
PUBLISHED 11 January 2024

CITATION
Sukjoi W, Young C, Acland M, Siritutsoontorn S, Roytrakul S, Klingler-Hoffmann M, Hoffmann P and Jitrapakdee S (2024), Proteomic analysis of holocarboxylase synthetase deficient-MDA-MB-231 breast cancer cells revealed the biochemical changes associated with cell death, impaired growth signaling, and metabolism.
Front. Mol. Biosci. 10:1250423.
doi: 10.3389/fmolb.2023.1250423

Proteomic analysis of holocarboxylase synthetase deficient-MDA-MB-231 breast cancer cells revealed the biochemical changes associated with cell death, impaired growth signaling, and metabolism

Witchuda Sukjoi[1], Clifford Young[2], Mitchell Acland[3], Siraprapa Siritutsoontorn[1], Sittiruk Roytrakul[4], Manuela Klingler-Hoffmann[2], Peter Hoffmann[2]* and Sarawut Jitrapakdee[1]*

[1]Department of Biochemistry, Faculty of Science, Mahidol University, Bangkok, Thailand, [2]Clinical and Health Sciences, University of South Australia, Adelaide, SA, Australia, [3]Adelaide Proteomics Centre, School of Biological Sciences, The University of Adelaide, Adelaide, SA, Australia, [4]Functional Proteomics Technology Laboratory, National Center for Genetic Engineering and Biotechnology, National Science and Technology Agency, Pathumthani, Thailand

We have previously shown that the holocarboxylase synthetase (HLCS) is overexpressed in breast cancer tissue of patients, and silencing of its expression in triple-negative cancer cell line inhibits growth and migration. Here we investigated the global biochemical changes associated with HLCS knockdown in MDA-MB-231 cells to discern the pathways that involve HLCS. Proteomic analysis of two independent HLCS knockdown cell lines identified 347 differentially expressed proteins (DEPs) whose expression change > 2-fold ($p < 0.05$) relative to the control cell line. GO enrichment analysis showed that these DEPs were mainly associated with the cellular process such as cellular metabolic process, cellular response to stimulus, and cellular component organization or biogenesis, metabolic process, biological regulation, response to stimuli, localization, and signaling. Among the 347 identified DEPs, 64 proteins were commonly found in both HLCS knockdown clones, confirming their authenticity. Validation of some of these DEPs by Western blot analysis showed that plasminogen activator inhibitor type 2 (SerpinB2) and interstitial collagenase (MMP1) were approximately 90% decreased in HLCS knockdown cells, consistent with a 50%–60% decrease in invasion ability of knockdown cells. Notably, argininosuccinate synthase 1 (ASS1), one of the enzymes in the urea cycle, showed approximately a 10-fold increase in the knockdown cells, suggesting the crucial role of HLCS in supporting the urea cycle in the triple-

negative cancer cell line. Collectively, our proteomic data provide biochemical insights into how suppression of HLCS expression perturbs global changes in cellular processes and metabolic pathways, impairing cell growth and invasion.

KEYWORDS

holocarboxylase synthetase, biotin carboxylases, breast cancer, proteomics, metabolism, breast cancer

Introduction

Cancer cells exhibit several profound changes in cellular and biochemical pathways that enable them to grow and invade other tissues or organs (Hanahan, 2022). Metabolic reprogramming constitutes one of the cancer hallmarks and has received much attention in recent years. Metabolic reprogramming is defined as the specific adjustment of metabolic pathways which supports biomass synthesis and bioenergetic requirements during oncogenic transformation. These changes include increased aerobic glycolysis (Warburg effect), pentose phosphate pathway activity, glutaminolysis, and *de novo* synthesis of lipids, nucleotides, and amino acids (Pavlova and Thompson, 2016; Vander Heiden and DeBerardinis, 2017), all of which are regulated by p53, c-Myc, and HIF-1α (Dang et al., 2008; DeBerardinis and Chandel, 2016). Therefore, inhibiting these metabolic pathways by small molecules or enzyme inhibitors hold promise for novel anti-cancer drugs (Vander Heiden, 2011; Stine et al., 2022).

The biotin-dependent carboxylases (BDCs), including acetyl-CoA carboxylase 1 and 2 (ACC1 and ACC2), methylcrotonyl-CoA carboxylase (MCC), propionyl-CoA carboxylase (PCC), and pyruvate carboxylase (PC) play pivotal roles in various intermediary metabolism including lipogenesis, gluconeogenesis, odd-chain fatty acid catabolism, and branched-chain amino acid catabolism (Tong, 2017). All BDCs have been reported to be overexpressed in several types of human cancer (Milgraum et al., 1997; Phannasil et al., 2015; Sellers et al., 2015; Svensson et al., 2016; Liu et al., 2019; Ngamkham et al., 2020; Du et al., 2021; Gondas et al., 2022); only the pro-oncogenic roles of ACC1 and PC have been studied extensively. Pharmacological inhibition or genetic ablation of these enzymes attenuates cancer growth, invasion and metastasis (Phannasil et al., 2015; Sellers et al., 2015; Davidson et al., 2016; Svensson et al., 2016; Shinde et al., 2018; Stoiber et al., 2018). Although attenuating the activity or expression of BDC is ideal for inhibiting the growth of cancers, inhibiting the BDC regulator may be more effective. The holocarboxylase synthetase (HLCS) regulates BDC activity through the covalent attachment of a biotin moiety to the specific lysine residue at the C-terminus of the biotin carboxyl carrier domain, in a process known as biotinylation (Leon-Del-Rio et al., 2017; Sternicki et al., 2017). Inhibition of biotinylation abrogates the carboxylase activity, thus lowering all BDC activities simultaneously. We have previously shown that HLCS is upregulated in breast cancer tissues, and its expression is correlated with lymph node invasion and poor prognosis (Sukjoi et al., 2020). Elevated expression of HLCS in breast cancer tissues is believed to support biotin carboxylase activities required for oncogenic growth and metastasis (Sukjoi et al., 2020). Pharmacological inhibition of biotin incorporation into biotin carboxylases can inhibit HLCS activity, thus providing an alternative means to block cancer growth (Yoon et al., 2021; Siritutsoontorn et al., 2022). We have recently shown that suppressing HLCS expression in both low and highly-invasive breast cancer cell lines, MCF-7 and MDA-MB-231, respectively, inhibits their growth and migration, accompanied by cell cycle arrest, indicating the pro-oncogenic role of HLCS (Siritutsoontorn et al., 2022). Although the growth defect observed in both MCF-7 and MDA-MB-231 cells primarily results from the lowered carboxylase activities, it is unclear how the impaired carboxylase activities globally perturb biological pathways in breast cancer cells. Here we performed a proteomic analysis of HLCS knockdown MDA-MB-231 cells and demonstrated that suppression of HLCS expression perturbs various biological processes associated with cell survival and affects several key metabolic enzymes.

Materials and Methods

Holocarboxylase synthetase knockdown cells and maintenance

The two previously described HLCS knockdown MDA-MB-231 cell lines, KD 868 and KD 1950, and scrambled control cell lines were used in this study (Siritutsoontorn et al., 2022). They were cultured in Minimal Essential Medium (MEM) supplemented with 10% (v/v) fetal bovine serum (FBS) and 1% (v/v) penicillin/streptomycin. Cells were cultured at 37°C with 5% CO_2 and routinely sub-cultured every 3 days.

Clonogenic assay

Five hundred cells of HLCS knockdown and scrambled control cell lines were seeded into a 100-mm culture dish containing MEM supplemented with 10% (v/v) fetal bovine serum and maintained at 37°C with 5% CO_2. Following 10 days, the culture media were removed, and the colonies were washed with phosphate buffer saline (PBS). Cells were fixed with 100% (v/v) methanol for 20 min at room temperature and gently washed with water. The colonies were stained with 0.5% (w/v) crystal violet in 25% (v/v) methanol for 45 min at room temperature in the dark, rinsed with water, air-dried overnight, and counted.

Invasion assay

Approximately 1×10^6 cells/mL were suspended in MEM media supplemented with 0.1% (v/v) BSA and incubated with 1 μg/mL of

fluorogenic calcein-AM (Invitrogen) for 30 min at room temperature in the dark. Cells were then centrifuged at 1,500 rpm for 5 min, washed three times with MEM supplemented with 0.1% (v/v) BSA, and resuspended at the density of 8×10^5 cells/mL with MEM containing 0.1% (v/v) BSA. Afterwards, 4×10^4 cells were suspended in 49 mL of MEM before placing onto the filter (12-µm pore size) of 96-well ChemoTx® chemotaxis system (Neuro Probe), which was pre-coated with Geltrex (Life Technologies). Cells were allowed to migrate from the filter to the bottom compartment containing 29 µL of MEM supplemented with 10% (v/v) FBS at 37°C for 6 h. The non-migrated cells on the top of the filter were gently removed with a paper towel before the fluorescence intensity generated from the calcein-labeled cells in the bottom compartment was measured with excitation and emission wavelength at 485 and 520 nm, respectively, in a Triad series multimode detector (Dynex Technologies).

SDS-PAGE and Western blot analysis

Whole-cell lysates of HLCS knockdown and scramble MDA-MB-231 cells were extracted in 100 µL of 1x radioimmunoprecipitation assay (RIPA) buffer containing 50 mM Tris-HCl pH 7.4, 1% (v/v) NP-40, 0.25% (w/v) sodium deoxycholate, 150 mM NaCl, 1 mM EDTA, and 1x protease inhibitor cocktail (Roche) on ice for 30 min before centrifugation at 12,000 × g for 15 min at 4°C. Protein concentrations were determined using Bradford regent (Bio-Rad). Protein (30 µg) was separated on a 7.5% discontinuous SDS-PAGE mini gel using 1x glycine buffer (25 mM Tris-HCl pH 8.3, 193 mM glycine, 0.1% (w/v) SDS) under reducing conditions. The protein was transferred from polyacrylamide gel to polyvinylidene difluoride membranes by Trans-Blot®Turbo™ Transfer system (Bio-Rad) with 1x transfer buffer (25 mM Tris-HCL pH 8.3, 192 mM glycine, 0.1% (w/v) SDS and 20% (v/v) methanol) at constant 25 V for 20 min. Then, the membranes were blocked in a blocking buffer containing 5% (w/v) skim milk and 1% (v/v) Tween 20 in 1x PBS pH 7.4 at 4°C overnight. The blots were then incubated with appropriate primary antibodies: 5 µg of rabbit anti-HLCS antibody (Bailey et al., 2010), 1:1,000 dilution of rabbit anti-MMP1 polyclonal antibody (E9S9N) (Cell Signaling Technologies), or 1: 5,000 dilution of rabbit anti-SerpinB2 polyclonal antibody (ab47742, Abcam) at room temperature for 2 h. Excess antibodies were washed four times with 1x PBS buffer containing 1% Tween 20 before incubating with 1: 20,000 dilution of mouse anti-rabbit IgG conjugated with horseradish peroxidase (Dako) at room temperature for 1 h. The immunoreactive bands representing each protein were detected using a chemiluminescence substrate (Merck, Millipore). Following MMP1 detection, the blot was incubated with stripping buffer (20 mM glycine, 0.1% SDS and 1% Tween 20, pH 2.2) and blocked in a blocking buffer at room temperature for 1 h. The membrane was incubated with 1:1,000 dilution of rabbit anti-ASS1 polyclonal antibody (D4O4B) (Cell Signaling Technologies) at room temperature for 2 h. Then, the membrane was incubated with a secondary antibody and developed as above.

Proteomic analysis

Sample preparation

The proteomics analysis was performed with three sample groups, including scrambled control and two HLCS knockdown cell lines: KD 868 and KD 1950. Each sample group was performed in three biological replicates, each with two technical replicates. HLCS knockdown cell lines were grown to 90% confluence in MEM supplemented with 10% (v/v) FBS and 1% (v/v) penicillin/streptomycin. Cells were trypsinized and harvested by centrifugation at 1,500 × g for 5 min. The supernatant was discarded, and the cell pellet was washed three times with PBS. The cell pellet was snap-frozen at −80°C and suspended in 200 µL of RIPA buffer supplemented with 1x protease inhibitor cocktail (Sigma-Aldrich). Cells were disrupted by passing cell suspension through a 26.5-gauge needle 5 times. The lysates were centrifuged at 20,000 × g for 30 min at 4°C, and the supernatant was collected. Four volumes of cold acetone (Chem-Supply) were added to the supernatant before storing at −20°C overnight. The proteins were precipitated by centrifugation at 20,000× g for 20 min at −9°C. The pellet was washed with 200 µL of cold acetone and dried on ice for 30 min before resuspending in 40 µL of 8 M urea (Merck) in 50 mM ammonium bicarbonate (Fluka Analytical). Protein concentration was determined by tryptophan fluorescence.

Trypsin digestion

Protein samples (100 µg) were subjected to disulfide bond reduction with 10 mM dithiothreitol (Sigma-Aldrich) and incubated at room temperature for 1 h. The samples were then alkylated with 15 mM 2-chloroacetamide (Sigma-Aldrich) at room temperature for 30 min in the dark before 10-fold diluted with 50 mM ammonium bicarbonate. Trypsin (Mass spectrometry grade, Promega) was added to the protein at a ratio of 1:50, and the digestion was performed at 37°C in a ThermoMixer (Eppendorf) with 500 rpm agitation for 18 h. Approximately 10 µL of formic acid (LC-MS grade, Merck) was added to each sample before centrifugation at 20,000 × g for 10 min. The supernatant was transferred to a new tube, and the peptides quantitated by tryptophan fluorescence. The resulting samples were desalted using a 1 cc Sep-Pak C18 cartridge (Waters). The stationary phase was flushed with 1 mL of methanol, 3 mL of 80% (v/v) acetonitrile in 0.1% (v/v) formic acid, and then 4 mL of 0.1% (v/v) formic acid to equilibrate the columns before the samples were loaded. The samples were washed with 3 mL of 0.1% (v/v) formic acid, eluted with 1 mL of 50% (v/v) acetonitrile in 0.1% (v/v) formic acid, and dried under vacuum centrifugation (Christ AVC 2–25 CD plus) at 50°C.

Liquid chromatography-mass spectrometry

LC-MS analysis was performed on an Ultimate 3000 RSLC-nano system connected to an Orbitrap Exploris 480 mass spectrometer (Thermo Scientific, Bremen, Germany). Approximately 1 µg of each peptide sample was resuspended in 0.1% (v/v) formic acid and loaded onto a 25 cm fused silica column heated to 50°C. The internal diameter (75 µm) of the column was packed with 1.9 µm C18 particles. Peptides were separated over 70 min with a linear gradient of 3%–20% acetonitrile in 0.1% formic acid at a flow rate of 300 nL/min. Compensation voltages (−50 and −70 V) were applied from a FAIMS Pro interface (Thermo Scientific) to regulate the entry of ionized peptides into the mass spectrometer. MS scans (m/z 300–1500) were acquired at resolution 60,000 (m/z 200) in positive ion mode, with MS/MS scans of fragment ions measured at

15,000 resolution after applying 27.5% higher-energy collision dissociation. A dynamic exclusion period of 40 s was specified.

Data processing and bioinformatic analysis

Raw data was processed with Proteome Discoverer v2.4 (Thermo Scientific). Searches were performed against the human FASTA database using the SEQUEST HT search engine, with the precursor and fragment mass tolerances set to 10 ppm and 0.02 Da, respectively. Two missed cleavage sites were allowed, with the minimum peptide length specified at 6 amino acids. Oxidation (+15.995), deamidation (+0.984), N-terminal acetylation (+42.011), N-terminal methionine loss (−131.040) and N-terminal methionine loss and acetylation (−89.030) were included as variable modifications, and cysteine carbamidomethylation was included as a fixed modification. To understand the differentially expressed proteins (DEPs) involvement in various biological processes, molecular functions, and cellular components, a list of all DEPs was subjected to gene annotation analysis using PANTHER database analysis tool version 16.0 (http://www.pantherdb.org/) (Thomas et al., 2003).

Statistical analysis

All experiment results are expressed as means ± S.D. The statistical analysis was performed using GraphPad Prism software (version 8.4.0; GraphPad Software, Inc., La Jolla, CA). Significant differences between the sample groups were calculated by one-way factorial analysis of variance (ANOVA), followed by Dunnett's test. A p-value of <0.05 indicated statistically significant.

Results

Quantitative analysis of the proteome of holocarboxylase synthetase knockdown MDA-MB-231 cells

Two previously generated independent HLCS knockdown MDA-MB-231 cell lines (KD 868 and KD 1950) were used for proteomic analysis. These two HLCS knockdown cell lines possessed approximately 70%–80% reduction of HLCS protein corresponding to 86, 82, and 72 kDa isoforms (Bailey et al., 2010) (Figure 1A) compared to the scrambled control cell line. The decreased HLCS expression in these two knockdown clones was accompanied by 40%–60% reduction of clonogenic growth (Figure 1B). To gain further insight into how suppression of HLCS expression impacted global cellular changes, proteomic analysis was performed on the knockdown cells using LC-MS. The proteomic study was performed on these two HLCS knockdown cell lines to eliminate the clonal bias compared to the scrambled control cell line. All LC-MS data were obtained from three biological replicates, each with two technical replicates. According to the 1% false discovery rate (FDR) criteria with at least one unique peptide (Zhang et al., 2018; Yang et al., 2019), 5,306 proteins were identified across samples. Figure 2A shows the heat map of expression profiles and hierarchical clustering analysis of 5,306 proteins identified in all samples. Principle component analysis of all samples revealed a distinct cluster of scrambled control and HLCS knockdown clones KD 868 and KD 1950, respectively. The greatest component of variation of the data (PC1, 22.4%) showed a clear separation between the scrambled control and the knockdown groups, whereas the distinct cluster-based PC2 (16.4%) separation indicated a variable biological response between HLCS knockdown clones, KD 868 and KD 1950 (Figure 2B). Figure 2C shows the volcano plots of differentially expressed proteins identified between control and each HLCS knockdown cell lines [control vs. KD 868 (left panel) and control vs. KD 1950 (right panel)], separately. With the cut-off threshold of minimal 2-fold change with p-value <0.05, 196 proteins were considered differentially expressed. Of this number, 95 proteins were downregulated (spots in green box), while 101 proteins were upregulated (spots in red box). For the KD 1950 cell line, 151 proteins were differentially expressed, with 59 proteins being downregulated (spots in green box) and 92 proteins being upregulated (spots in red box).

Functional annotation of biological pathways associated with DEPs

To gain further insights into the biological response in HLCS knockdown, the functional annotation of the DEPs in each HLCS knockdown cell line was performed using the GO annotation tool. Based on the biological processes classification, the top three biological response changes associated with the downregulation of DEPs in the KD 868 clone were cellular process (GO:0009987, 30%), metabolic process (GO:0008125, 24%), and biological regulation (GO:00650007, 15%), with the other individual processes accounting for less than 10% (Figure 3A, left panel). Likewise, most changes associated with the downregulation of DEPs in the KD 1950 clone were cellular process (32%), metabolic process (24%), and biological regulation (16%), with the other processes listed similar to those of the KD 868 clone (Figure 3A, right panel). Regarding the upregulated proteins, the three most biological changes associated with the KD 868 clone were cellular process (GO: 0009987, 29%), metabolic process (GO: 0008152, 20%), and biological regulation (GO: 0065007, 16%). For the KD 1950 clone, the upregulated proteins were associated with cellular process (27%), metabolic process (18%), and biological regulation (16%).

According to the molecular function classification, the downregulated proteins in both HLCS knockdown clones were mostly involved in catalytic activity (GO:0003824; 65% in KD 868 (Figure 3B, left panel), and 42% in KD 1950 (Figure 3B, right panel), followed by binding activity (GO:0005488, 22% in KD 868, and 36% in KD 1950), and molecular function regulator (GO: 0098772, 9% in KD 868, and 19% in KD 1950). However, the molecule transducer activity and structural molecule activity were molecular functions that exclusively related to the downregulated proteins in KD 868 and KD 1950, respectively. In contrast, the upregulated proteins in both knockdown clones were predominantly related to the binding activity (GO:0005488; 41% in KD 868, and 36% in KD 1950), followed by catalytic activity (GO:0003824; 33% in KD 868, and 28% in KD 1950), and molecular function regulator (GO:0098772; 15% in KD 868, and 23% in KD 1950).

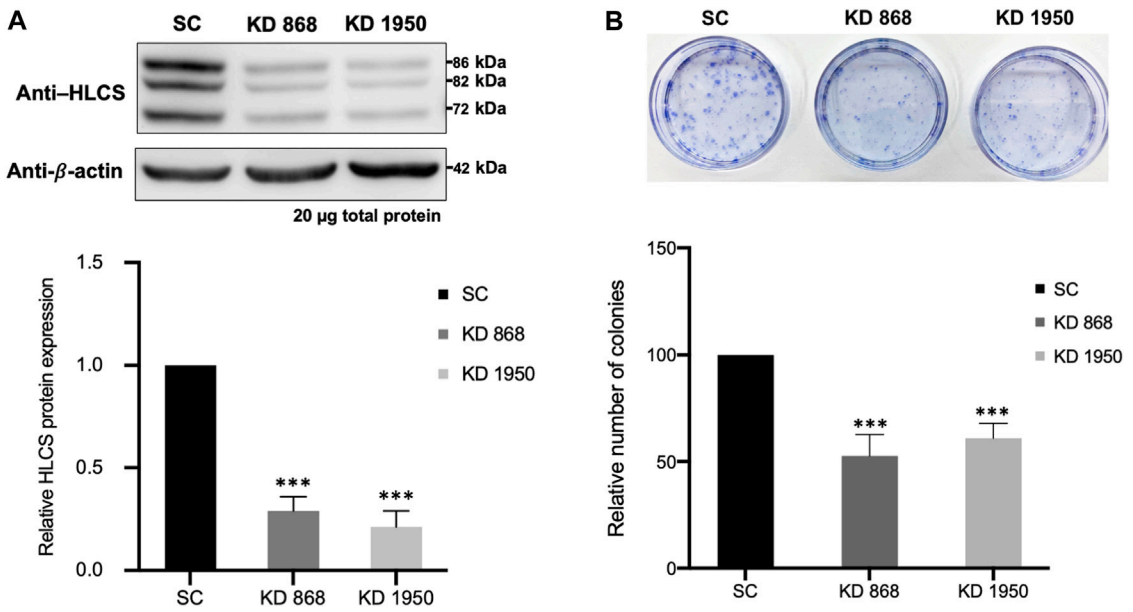

FIGURE 1
HLCS knockdown MDA-MB-231 cell lines show impaired clonogenic growth **(A)** Western blot analysis of HLCS protein in two HLCS knockdown clones, KD 868 and KD 1950 (top panel), and their expression level relative to that of the scrambled control cell line (SC) which was arbitrarily set to 1 (bottom panel). **(B)** Crystal violet staining of HLCS knockdown colonies following 10 days of clonogenic growth (top panel) and the relative number of clones (bottom panel). ***$p < 0.001$.

Common DEPs: MMP1, SerpinB2, and ASS1

To see whether the affected pathway changes in both HLCS knockdown cell lines were mediated through common proteins, the Venn diagram of DEPs of both knockdown clones was generated (Figure 3C). Both HLCS knockdown clones shared 64 common DEPs, with 23 being downregulated and 41 being upregulated. The list of these upregulated and downregulated and common proteins and their associated biological processes are shown in Table 1 and Table 2, respectively. According to the candidate proteins shown in Table 1, suppression of HLCS expression appears to be associated with increased programmed cell death, as shown by the increased expression of proteins involved in apoptosis [Apoptotic protease-activating factor 1 (APAF1)], immunogenic cell death [caspase-1 (CASP1)], autophagy [stimulator of interferon genes protein, (STING1)] and increased expression of proteins that possess tumor suppressor function such as tetraspanin-6 (TSPAN6), mitogen-activated protein kinase 6 (MAPK6), protein sprouty homolog 2 (SPRY2), HAUS augmin-like complex subunit 4 (HAUS4). The other common DEPs include those involved in metabolic processes, transcriptional regulation, cellular transport. Regarding the downregulated DEPs (Table 2), these proteins were associated with cell motility, such as myosin ID (MYO1D), leupaxin (LPXN), Interleukin-1β (IL-1β), plastin-2 (LCP1), transglutaminase 2 (TGM2), metallothionein 1X (MT1X), small p97/VCP-interacting protein (SVIP), and peroxiredoxin-like 2A (PRXL2A). The other affected biological processes include metabolic processes, cellular organization and biogenesis, and DNA-binding proteins.

To validate some of the candidate proteins shown in both Tables 1, 2, some candidates from both upregulated proteins and downregulated which showed the most significant fold changes, including argininosuccinate synthase 1 (ASS1) ($\log_2$ + 3.3 and + 2.8-fold in KD 868 and KD 1950 cells, respectively), plasminogen activator inhibitor 2 (SerpinB2) (−3.0 and −2.2-fold), interstitial collagenase/matrix metalloproteinase-1 (MMP1) (−2.2 and −1.5-fold) were validated by Western blot analysis. ASS1, one of the urea cycle enzymes, catalyzes the condensation of citrulline and L-aspartate to form argininosuccinate, and this enzyme is downregulated in many types of cancer (Hajaj et al., 2021). SerpinB2 has been shown to regulate stroma remodeling and metastasis (Harris et al., 2017), and MMP1 is one of the metalloproteases involved in cell invasion (Liu et al., 2012). As shown in Figure 4A, ASS1 expression level was extremely low in the scrambled control cell line, while it was markedly increased in both KD 868 and KD 1950 cell lines ($p = 0.005$ and $p = 0.004$, respectively). SerpinB2 expression was reduced by 95% in the KD 868 and was reduced by 75% in KD 1950 ($p < 0.001$) (Figure 4B). Similar to SerpinB2, MMP1 expression level was barely detectable in KD 868 and decreased by approximately 94% ($p = 0.00001$) in KD 1950 (Figure 4C). The marked reduction of MMP1 was accompanied by 40% decrease of invasion in both HLCS knockdown clones (Figure 4D).

Discussion

We have previously shown that suppression of HLCS expression lowers biotinylation of carboxylases accompanied by impaired growth, migration and invasion, and cell cycle arrest in both luminal subtype (MCF-7) and triple-negative subtype (MDA-MB-231) breast cancer cell lines (Siritutsoontorn et al., 2022). Although these phenotypic defects were solely attributed to the lowered carboxylase activities, how reduced carboxylase activities perturb the biological and metabolic processes is largely unknown, leading to growth retardation.

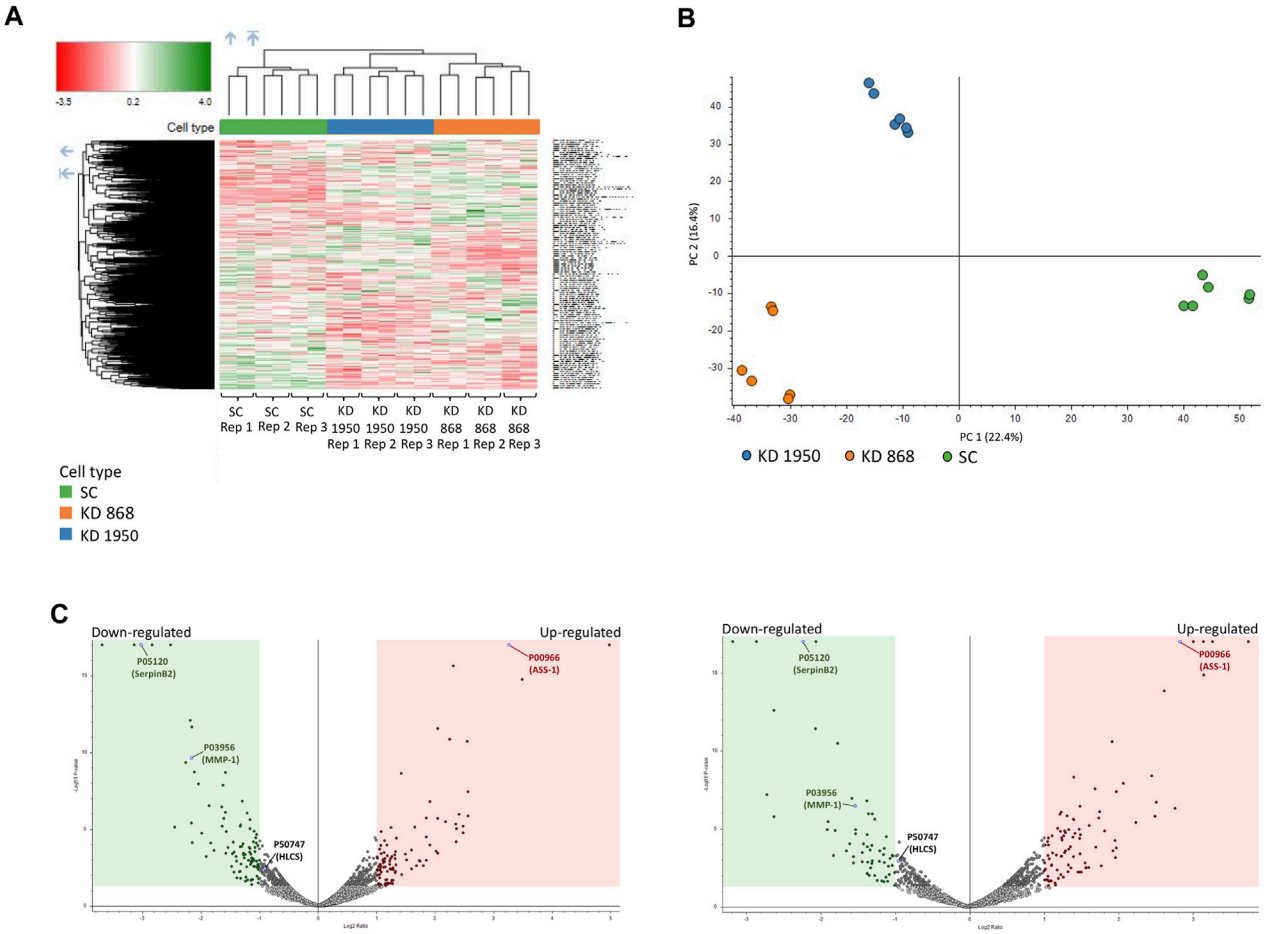

FIGURE 2
Proteomic analysis of HLCS knockdown MDA-MB-231 cells. Three biological replicates (REP1, REP2, REP3) of scrambled (SC) and two HLCS knockdown cell lines (KD 868 and KD 1950), each with two technical replicates, were performed. **(A)** Heat map and hierarchical clustering of 5,306 proteins identified in all samples. Color intensity indicates protein expression level. Green and red is upregulation and downregulation, respectively. **(B)** PCA analysis of proteomics data set. PC scores are based on individual proteomic data between scrambled control and KD 868 and KD 1950 clones. **(C)** Volcano plot of protein expression in HLCS knockdown KD 868 (left panel) and KD 1950 (right panel). Each colored dot represents a protein that displays a large magnitude of fold change relative to the scrambled control cell line (*X*-axis) and statistical significance (*Y*-axis). Green dots represent downregulated proteins, red dots represent upregulated proteins, and grey dots represent the unchanged proteins relative to those of the scrambled control cell line. Green and red squares indicate significant protein abundance differences ($p < 0.05$) less than $\log_2$FC = −1 or greater than $\log_2$FC = 1, respectively. ASS1, HLCS, SerpinB2, and MMP1 are shown in blue dots.

Holocarboxylase synthetase knockdown promotes program cell death and tumor suppressor proteins

GO analysis indicates that HLCS knockdown mainly affects cell death and other biological processes associated with cell motility and metabolic pathways. Regarding cell death, several proteins implicated in cell death pathways were increased—for example, the APAF1, CASP1, and STING1 (Table 1). APAF1 is a core component of the apoptosome, essential for caspase-9 activation (Pop et al., 2006). Increased APAF1 expression is well-described in many types of cancer exposed to chemotherapeutic drugs (Yuan et al., 2019; Xiang et al., 2020; Bakhshoudeh et al., 2021). CASP1 is a pro-inflammatory cytokine that cleaves pro-IL-1β, and pro-IL-18 to their active forms. This activity is essential for pyroptosis, a cell death process triggered by inflammation. A recent study shows that the chemotherapeutic drug, cisplatin, induces CASP1-mediated pyroptosis in MDA-MB-231 cells (Yan et al., 2021). CASP1-deficient mice showed enhanced colon epithelial and tumor proliferation, indicating its role as a tumor-suppressor protein (Hu et al., 2010). STING1, an ER-bound protein, is crucial for autophagy and programmed cell death (Zhang et al., 2021a). A recent study shows that Eribulin, an anti-cancer drug used to treat breast cancer and liposarcoma, triggers cancer cell death via the STING1-dependent signaling axis (Fermaintt et al., 2021; Takahashi-Ruiz et al., 2022), indicating its role as a cell-death-promoting factor. Upregulation of these pro-apoptotic proteins may be induced in response to HLCS suppression.

The reduced clonogenic growth of MDA-MB-231 herein may be attributed to the upregulation of some tumor suppressor proteins such as TSPAN6, MAPK6, SPRY2, HAUS4, stomatin (STOM) and

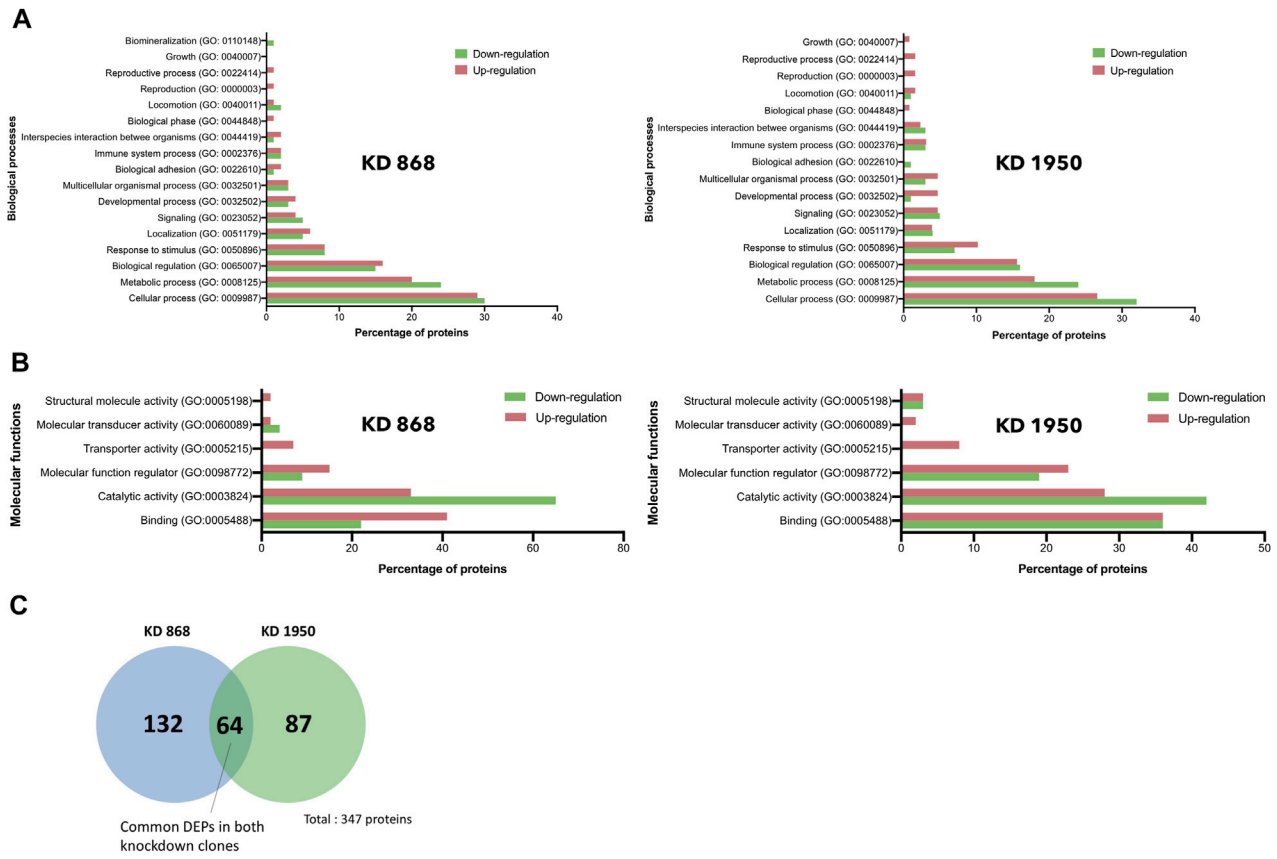

FIGURE 3
Gene ontology and pathway analysis of DEPs in HLCS knockdown MDA-MB-231 cells. Histograms depicting the percentage of pathway changes associated with HLCS knockdown in **(A)** Biological processes and **(B)** Molecular functions in KD 868 (left panel) and KD 1950 (right panel) clones. Green boxes indicate downregulated proteins, and red boxes indicate upregulated proteins. **(C)** Venn diagram showing distinct and common DEPs in both HLCS KD clones 868 and 1950.

conserved oligomeric golgi complex subunit 8 (COG8) (Table 1). TSPAN6, a tetraspanin family member, is a tumor suppressor protein that interferes with TGF-α signaling in colorectal cancer (Andrijes et al., 2021). Similarly, MAPK6 or ERK3, an atypical MAPK member, controls cell growth (Chen et al., 2000). A recent study shows that MAPK6/ERK3 exerts its tumor suppressor function by inhibiting cell cycle progression (Julien et al., 2003) and proliferation and invasion of melanoma (Chen et al., 2019a). SPRY2, a receptor tyrosine kinase inhibitor, has been shown to interfere with oncogenic signaling by antagonizing the ERK signaling pathway (Fong et al., 2006). Overexpression of SPRY2 in several types of cancer inhibits their growth and progression (Kawazoe and Taniguchi, 2019). HAUS4 is part of the HAUS augmin-like complex, which contributes to mitotic spindle assembly, maintenance of chromosome integrity, and completion of cytokinesis. Avelar et al., 2020 showed that elevated HAUS4 expression is associated with senescence and a tumor-suppressor gene. Stomatin, an integral membrane, regulates ion channels and transporter (Rahman et al., 2021). A recent study showed that stomatin suppresses proliferation and induces apoptosis by inhibiting Akt signaling in prostate cancer (Rahman et al., 2021; Sato et al., 2021). The decreased stomatin expression was associated with poor prognosis of prostate, breast, and non-small cell lung cancer patients, indicating its role as a tumor suppressor protein (Chen et al., 2016; An et al., 2019; Rahman et al., 2021). COG8 is the structural component of golgi-apparatus that functions in intracellular transport and glycosylation. COG8 level is negatively correlated with the survival of renal clear carcinoma patients (Zhang et al., 2021b).

Holocarboxylase synthetase knockdown perturbs cellular function by down-regulating MMP1 and other cytoskeletal proteins

Extracellular matrix detachment is a fundamental process for cancer cell migration. This process involves metalloproteinase secretion and other proteases such as urokinase plasminogen activator. MMP1 is a member of matrix metalloproteinases, which degrades extracellular matrix during an invasion, while SerpinB2 regulates stromal remodeling, local invasion and metastasis (Valiente et al., 2014; Harris et al., 2017). Overexpression of MMP1 is associated with tumor invasion and metastasis (Chambers and Matrisian, 1997) and is highly expressed

TABLE 1 Abundance ratios (Log2) of upregulated proteins that are common in both knockdown clones relative to scrambled control cells.

Accession	Protein abbreviation	Protein name	KD 868		KD 1950	
			Fold change (Log2)	*p*-value (-Log10)	Fold change (Log2)	*p*-value (-Log10)
		Regulation of biological process				
C9JLV4	APAF1	Apoptotic protease-activating factor 1	2.0	3.6	1.6	2.5
D3DSM0	ITGB2	Integrin beta	1.3	1.7	2.0	3.8
H7C224	IRAK1	Interleukin-1 receptor-associated kinase 1	2.4	4.2	1.8	2.6
O43597	SPRY2	Protein sprouty homolog 2	1.2	1.7	1.8	4.9
O43657	TSPAN6	Tetraspanin-6	2.4	5.3	1.9	3.6
P29466	CASP1	Caspase-1	1.1	3.0	1.1	3.5
Q10589	BST2	Bone marrow stromal antigen 2	2.3	15.7	1.9	10.6
Q16659	MAPK6	Mitogen-activated protein kinase 6	1.3	2.7	1.2	3.3
Q86WV6	STING1	Stimulator of interferon genes protein	2.4	6.0	1.5	2.2
Q9H6D7	HAUS4	HAUS augmin-like complex subunit 4	2.2	10.9	1.4	4.5
Q9H9A7	RMI1	RecQ-mediated genome instability protein 1	1.2	1.1	1.5	1.5
Q9NQ25	SLAMF7	SLAM family member 7	2.0	3.4	2.5	5.8
		Metabolic process				
P00966	ASS1	Argininosuccinate synthase 1	3.3	17.0	2.8	17.0
P04114	APOB	Apolipoprotein B-100	1.0	1.5	1.3	2.7
P14618-2	PKM1	Isoform M1 of Pyruvate kinase PKM	1.1	2.7	1.7	7.6
P17900	GM2A	Ganglioside GM2 activator	1.9	5.7	2.1	7.9
Q8WV93	AFG1L	AFG1-like ATPase	1.3	2.2	1.0	1.7
Q9NXS2	QPCTL	Glutaminyl-peptide cyclotransferase-like protein	2.5	4.8	2.0	3.2
U3KPX1	ACYP2	Acylphosphatase	1.2	2.5	2.6	13.8
		Transcriptional regulation				
A0A0U1RRL5	ELF1	ETS-related transcription factor Elf-1	1.8	3.0	2.5	6.7
M0R3F3	MED29	Mediator of RNA polymerase II transcription subunit 29	1.7	3.0	1.1	1.6

(Continued on following page)

10.3389/fmolb.2023.1250423

TABLE 1 (*Continued*) Abundance ratios (Log2) of upregulated proteins that are common in both knockdown clones relative to scrambled control cells.

Accession	Protein abbreviation	Protein name	KD 868		KD 1950	
			Fold change (Log2)	*p*-value (-Log10)	Fold change (Log2)	*p*-value (-Log10)
O60907	TBL1X	F-box-like/WD repeat-containing protein	2.6	7.4	1.2	1.8
O95365	ZBTB7A	Zinc finger and BTB domain-containing protein 7A	1.2	1.5	1.6	2.5
Q16594	TAF9	Transcription initiation factor TFIID subunit 9	1.7	2.6	3.1	14.9
Q5JXX2	MORF4L2	Mortality factor 4-like protein 2	1.9	6.8	1.1	2.7
Q8IWI9	MGA	MAX gene-associated protein	1.8	2.6	2.8	6.3
Q969E4	TCEAL3	Transcription elongation factor A protein-like 3	1.1	4.3	1.1	4.5
		Protein involved in transport				
H3BQV3	COG8	Conserved oligomeric Golgi complex subunit 8	1.3	1.5	1.1	1.7
K7EPV6	SLC44A2	Choline transporter-like protein 2	2.5	10.7	1.7	6.1
P27105	STOM	Stomatin	1.0	2.6	1.3	4.9
Q13303	KCNAB2	Voltage-gated potassium channel subunit beta-2	1.7	5.1	1.2	3.3
Q9BZI7	UPF3B	Regulator of nonsense transcripts 3B	2.2	5.5	1.7	3.8
Q9Y6M7-7	SLC4A7	Isoform 7 of Sodium bicarbonate cotransporter 3	1.2	1.7	1.2	3.2
Q9Y6M9	NDUFB9	NADH:ubiquinone oxidoreductase subunit B9	1.1	3.0	1.3	4.8
		Metal-ion binding				
E7EV05	ZFAND2B	AN1-type zinc finger protein 2B	1.9	4.0	3.1	17.0
F8WCD0	RNF149	E3 ubiquitin-protein ligase RNF149	1.6	2.4	1.5	2.2
P33764	S100A3	Protein S100-A3	1.8	4.5	3.0	17.0
		Transmembrane protein				
A0A075B6H3	TMCO4	Transmembrane and coiled-coil domain-containing protein 4	1.2	1.5	1.5	2.8
		Receptor				
A0A1B0GVW0	ATP6AP2	Renin receptor	1.2	2.7	1.3	3.5
		Unknown function				
O60732	MAGEC1	Melanoma-associated antigen C1	1.3	3.2	1.3	5.0
U3KQP1	-	Uncharacterized protein	1.6	3.6	1.6	5.2

10.3389/fmolb.2023.1250423

10.3389/fmolb.2023.1250423

TABLE 2 Abundance ratio (Log2) of downregulated proteins that are common in both knockdown clones relative to scrambled control cells.

Accession	Protein abbreviation	Protein name	KD 868		KD 1950	
			Fold change (Log2)	*p*-value (-Log10)	Fold change (Log2)	*p*-value (-Log10)
		Biological process				
J3QRN6	MYO1D	Myosin ID	−1.5	2.6	−1.6	3.2
O60711	LPXN	Leupaxin	−2.8	17.0	−1.3	6.0
P01584	IL1B	Interleukin-1 beta	−1.1	1.7	−1.6	2.8
P03956	MMP1	Interstitial collagenase	−2.2	9.6	−1.5	6.5
P05120	SERPINB2	Plasminogen activator inhibitor 2	−3.0	17.0	−2.2	17.0
P13796	LCP1	Plastin-2	−2.5	17.0	−2.9	17.0
P21980	TGM2	Transglutaminase 2	−1.3	6.8	−1.8	10.5
P80297	MT1X	Metallothionein 1X	−1.3	3.4	−2.6	12.6
Q8N668	COMMD1	Copper metabolism domain containing 1	−1.6	3.4	−1.2	2.9
Q8NHG7	SVIP	Small VCP/p97-interacting protein	−1.6	4.9	−1.4	3.9
Q9BRX8	PRXL2A	Peroxiredoxin-like 2A	−1.3	4.0	−1.6	7.0
		Metabolic process				
A0A087WYS9	SURF1	SURF1-like protein	−1.1	3.1	−1.1	3.1
M0QXB5	ETHE1	Persulfide dioxygenase ETHE1, mitochondrial	−1.6	6.1	−1.4	6.8
P36269	GGT5	Glutathione hydrolase 5 proenzyme	−1.2	2.7	−1.5	4.7
Q16719	KYNU	Kynureninase	−3.1	17.0	−2.1	11.4
Q96AD5	ATGL	Adipocyte triglyceride lipase	−1.6	5.2	−1.4	4.6
Q96GK7	FAHD2A	Fumarylacetoacetate hydrolase domain-containing protein 2A	−2.2	12.1	−2.1	17.0
		Cell organization and biogenesis				
P0CG12	CHTF8	Decreased expression in renal and prostate cancer protein	−1.3	3.1	−1.0	2.2
Q96AY3	FKBP10	Peptidyl-prolyl cis-trans isomerase FKBP10	−2.0	7.9	−1.3	3.6
		DNA-binding protein				
Q96KM6	ZNF512B	Zinc finger protein 512B	−1.9	3.2	−1.3	2.0
Q9BQ70	TCF25	Transcription factor 25	−2.2	5.4	−1.9	5.5
		Unknown function				
P43363	MAGEA10	Melanoma-associated antigen 10	−3.7	17	−3.2	17.0
Q9NS25	SPANXB1	Sperm protein associated with the nucleus on the X chromosome B1	−2.1	8.7	−1.5	5.0

in triple-negative breast cancer (Wang et al., 2019). The decreased abundances of MMP1 and SerpinB2 in HLCS knockdown cells are consistent with impaired cell invasion and migration (Siritutsoontorn et al., 2022). The reduced cell invasion of HLCS deficient cells may also be associated with the decreased expression of cytoskeletal proteins, including SerpinB2, LPXN, MYO1D, LCP1, or their regulators, such as IL1B and TGM2 (Table 2). LPXN, a focal adhesion adaptor protein, is essential for cell adhesion and migration (Alpha et al., 2020). Recent studies show that LPXN is overexpressed in many cancers (Kaulfuss et al., 2008; Kaulfuss et al., 2015; Hou et al., 2018). Depletion of LPXN expression reduces prostate cell migration and invasion, while its overexpression promotes prostate cancer progression (Kaulfuss et al., 2009). MYO1D, a member of the myosin motor protein, controls cell movement (Diaz-Valencia et al., 2022) and promotes the growth and invasion of cancer cells (Amcheslavsky et al., 2018). MYO1D

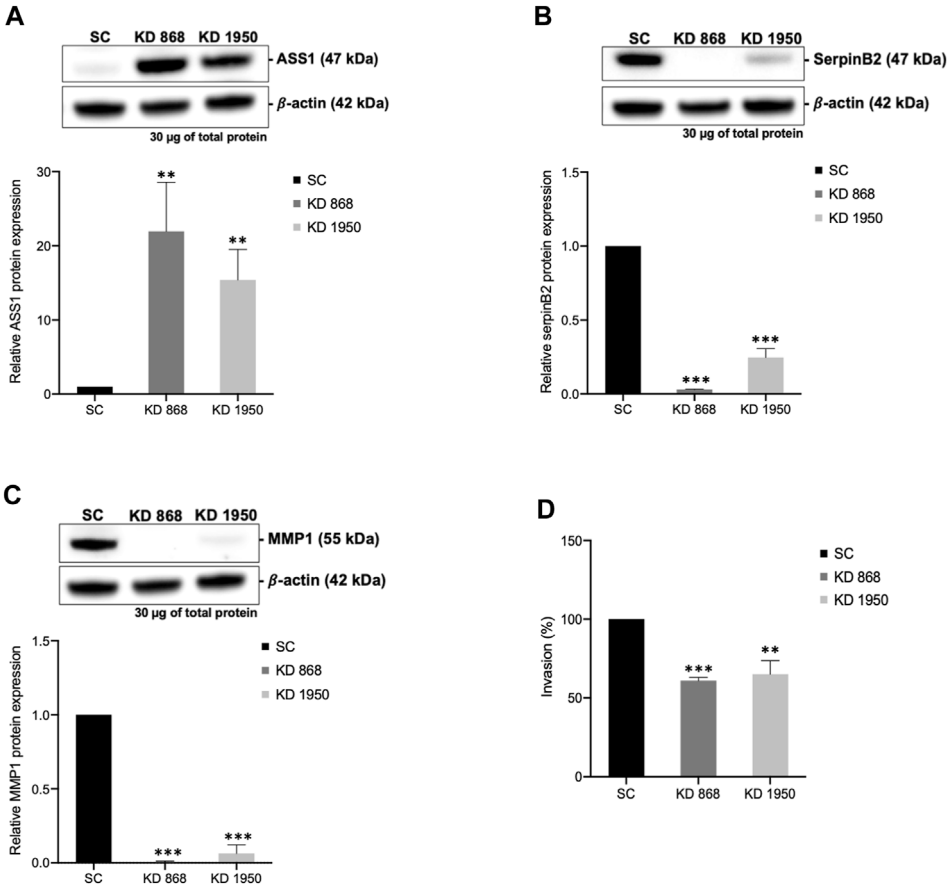

FIGURE 4
The marked induction of ASS1 and reduction of SerpinB2 and MMP1 expression in HLCS knockdown cells. Western blot analysis of ASS1 **(A)**, SerpinB2 **(B)**, and MMP1 **(C)**, and their expression levels relative to those of scrambled control cell line (bottom panel). **(D)** *In vitro* invasion assay of HLCS knockdown clones KD 868 and KD 1950. The number of invaded cells was relative to that of the scrambled control cell line, which was arbitrarily set as 100. $^{**}p < 0.01$, $^{***}p < 0.001$.

interacts with EGFR and contributes to oncogenesis (Ko et al., 2019; Mu et al., 2022). IL-1B plays various roles in physiological processes, including inflammation, cell adhesion, migration, and angiogenesis (Rebe and Ghiringhelli, 2020). Although IL-1B is primarily produced from immune cells, it can be synthesized and secreted from several types of solid tumors (Jin et al., 1997; Wu et al., 2016), where it stimulates the expression of IL-6 and COX-2, which are promoting factor for breast cancer aggressiveness (Reed et al., 2009; Oh et al., 2016). Plastin-2 (LCP1), an actin-binding protein, regulates cytoskeleton movement. Plastin-2 is overexpressed in most types of cancer (Park et al., 1994; Tiedemann et al., 2019), supporting invasion and metastasis (Foran et al., 2006). TGM2 catalyzes the posttranslational modification of glutamine residue-bound proteins. TGM2 also plays a non-enzymatic function by interacting with fibronectin and integrin to stabilize ECM structure (Condello et al., 2022). TGM2 is overexpressed in many types of cancer (Agnihotri and Mehta, 2017), promoting proliferation, migration, and invasion (Wang et al., 2016).

In addition, HLCS suppression also downregulates some proteins involved in intracellular transport and stress response, i.e., copper metabolism domain containing 1 (COMMD1), SVIP, and PRXL2A. COMMD1 is a copper-binding protein with additional non-copper-related function (Weiskirchen and Penning, 2021). COMMD1 was elevated in lymphoma, and its level was correlated with poor prognosis (Taskinen et al., 2014). SVIP involves the ER-associated protein degradation of misfolded proteins. In cancer cells, SVIP was overexpressed in prostate cancer tissue, while its inhibition reduces migration and malignant transformation (Erzurumlu and Ballar, 2017). PRXL2A is a member of the peroxiredoxin antioxidant protein and functions in removing reactive oxygen species. PRXL2A is an essential protein in cancer stem cells that modulates redox status and maintains stemness properties. PRXL2A was overexpressed in oral squamous cell carcinoma and renal clear cell carcinoma, where high PRXL2A was associated with poor prognosis (Chen et al., 2019b; Ren et al., 2021). MT1X, a member of the metallothionein family, functions as a copper/zinc binding protein to maintain metal homeostasis and control oxidative stress and DNA damage (Krizkova et al., 2018). MT1X supports proliferation while inhibiting apoptosis and p53 expression in several types of cancer (Liu et al., 2018).

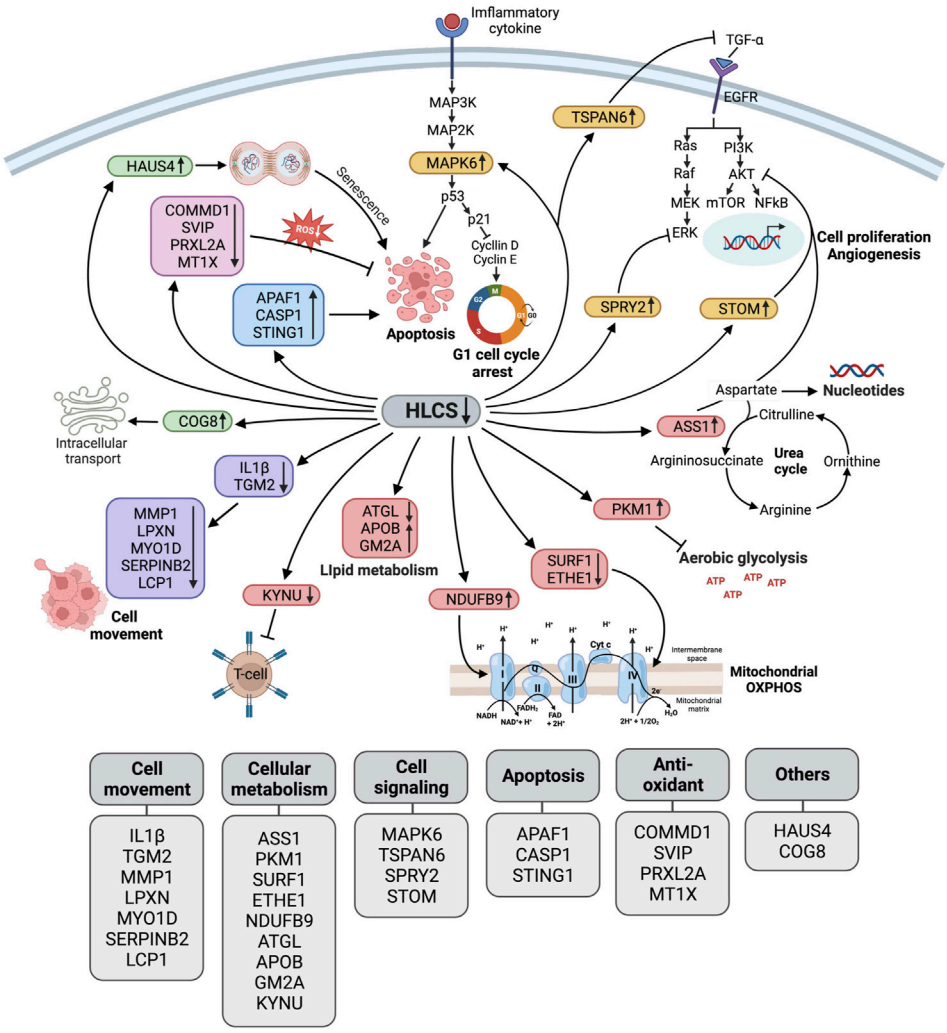

FIGURE 5
Schematic diagram illustrating the biological pathway changes in response to HLCS knockdown. Based on proteomic data, HLCS suppression promotes proteins involved in cell death (APAF1, CASP1, STING1 as shown in the blue box) and senescence (HAUS4 and COG8 as shown in the green box) while decreasing expression of antioxidant proteins (COMMD1, SVIP, PRXL2A, and MT1X as shown in the pink box), oncogenic signaling (MAPK6, TSPAN6, SPRY2, and STOM as shown in the yellow box).These changes probably contribute to growth restriction, oxidative stress, and cell death. Downregulation of the cytoskeleton and its regulatory proteins (IL1B, TGM2, MMP1, LPXN, MYO1D, SerpinB2, and LCP1, as shown in purple) likely result in impaired migration and invasion. Depletion of HLCS perturbs metabolic pathways (shown in red box) via increased expression of ASS1, which regulates the aspartate pool available for nucleotide synthesis, and PKM1, which antagonizes aerobic glycolysis. Other metabolic disruptions include the downregulation of proteins that support respiratory chain activities (SURF1, ETHE1, and NDUFB9), lipid metabolism (ATGL, APOB, and GM2A), and attenuating kynurenine metabolism (KYNU).

MT1X was overexpressed in many cancers, including breast cancer (Si and Lang, 2018), and was a prognostic marker for invasive ductal carcinoma (Zhang et al., 2000) and renal carcinoma (Ding et al., 2022).

As HLCS knockdown cells showed marked reduction of invasion accompanied by reduced MMP1 expression, we checked whether these defective phenotypes were attributed to impaired epithelial-mesenchymal transition program and stemness of cancer cells. Western blot analysis of vimentin and Oct4 showed that the levels of these two proteins were unchanged, suggesting the impaired clonogenic growth and invasion were not due to the loss of EMT and stemness (Supplementary Figure S1).

Holocarboxylase synthetase suppression perturbs the expression of metabolic enzymes

In addition to the changes in cellular processes, HLCS knockdown also affects metabolic pathways related to both glycolysis and mitochondrial metabolism. One of the most apparent changes is the increased expression of ASS1, suggesting that the urea cycle may be compromised in response to HLCS knockdown. The urea cycle is not only a cycle that disposes ammonium from amino acid catabolism, but it is also linked to the TCA cycle through aspartate. Transamination of oxaloacetate produces L-aspartate, which enters the urea cycle, where it condenses with L-citrulline to form argininosuccinate mediated by

ASS1. Because L-aspartate is an essential nitrogen donor for purine biosynthesis, modulation of ASS1 expression would determine the cellular aspartate pool, which supports nucleotide synthesis during proliferation. ASS1 also plays a non-metabolic role by suppressing Akt signaling and attenuating cancer growth (Miyamoto et al., 2017). Growing evidence indicates that many cancers inactivate urea cycle enzymes, including ASS1 (Rabinovich et al., 2015; Lee et al., 2018b), so the L-aspartate is available for nucleotide synthesis. Ectopic expression of the ASS1 gene in cancer cells inhibits their growth, indicating its role as a tumor suppressor enzyme (Khare et al., 2021; Kim et al., 2021). The marked increase of ASS1 expression in HLCS knockdown cells suggests that urea cycle activity may be increased as previously reported in hepatocytes of liver-specific PC knockout mice (Cappel et al., 2019). The increased ASS1 expression can also affect immediate downstream reactions in the urea cycle, i.e., the conversion of argininosuccinate to arginine catalyzed by arginosuccinate lyase. Because arginine is a precursor of nitric oxide, a chief mediator of inflammatory cytotoxicity, elevated arginine levels due to increased ASS1 would enhance NO production (Kim et al., 2021). Interestingly, PC KO pancreatic cells showed elevated urea cycle activity accompanied by increased arginine and NO production (Fu et al., 2020). The increased NO, in turn, promotes oxidative stress in PC KO pancreatic beta cells, contributing to cell death (Fu et al., 2020). Because HLCS regulates PC activity through biotinylation, it is not unexpected to see a similar perturbation of urea cycle activity in both HLCS and PC-deficient cells. However, it is still unclear how suppression of HLCS expression induces ASS1 expression. Although the expression of ASS1 was markedly increased in MDA-MB-231 cells, we did not see the same response in HLCS knockdown MCF-7 cells (Supplementary Figure S2). However, this outcome was anticipated as the basal level of ASS1 expression in MCF-7 cell line was already high. The lack of ASS1 change in HLCS knockdown MCF-7 cells may recapitulate the early stage of cancer, where ASS1 may not be essential during early stage of tumor progression. This is consistent with previous studies demonstrating that not all breast cancer subtypes inactivate ASS1 expression to enhance their oncogenic property (Qiu et al., 2014; Zou et al., 2021). Qiu et al. (2014) showed that highly invasive MDA-MB-231 cells regulate their oncogenic property by down-regulating ASS1 expression, but this is not the case for low invasive cell lines, i.e., MCF-7 and T47D, which possess much higher levels of endogenous ASS1. This indicates that the low and high invasive breast cancer cell lines regulate their oncogenic potentials via ASS1 differently (Qui et al., 2014). Qui et al. also showed that breast cancer patients with stage 0-I possess higher ASS1 expression, while those with advanced stage (III and IV) possess considerably lower ASS1 levels, suggesting the inactivation of ASS1 expression may occur during the transition from low to advanced stages of breast cancer.

In addition to the urea cycle, HLCS knockdown cells showed increased pyruvate kinase M1 (PKM1) isoform expression. While PKM1 is a highly active isoform, most cancers expressed PKM2 rather than PKM1 to promote Warburg's effect. The increased PKM1 level in HLCS knockdown could attenuate cancer growth, as reported in prostate adenocarcinoma, where inhibiting receptor tyrosine kinase signaling induces the expression of PKM1 and attenuates the growth of glioblastoma (Yang et al., 2022). The tumor suppressor role of PKM1 was also reported in breast cancer (Choksi et al., 2021) and prostate adenocarcinoma (Davidson et al., 2022).

HLCS knockdown also negatively affects lipid metabolism by altering expression of adipocyte triglyceride lipase (ATGL) (Table 2) and apolipoprotein B-100 (APOB) (Table 1). ATGL catalyzes the hydrolysis of triglycerides to free fatty acid and diacylglycerol. ATGL was overexpressed in several types of cancer, suggesting that fatty acid catabolism is essential to support the growth of tumors (Iftikhar et al., 2021; Yin et al., 2021; Zhang et al., 2022). APOB, a component of low-density lipoprotein, functions in triglyceride transport. APOB has recently been reported to play a role as tumor suppressor protein. The loss of APOB expression in several types of cancers is also associated with the upregulation of oncogenes and poor prognosis (Lee et al., 2018a; He et al., 2022). Mechanistically, overexpression of APOB in MDA-MB-231 cells inhibits their growth and invasion by depleting the lipid supply to the breast cancer cells (Ben Hassen et al., 2020).

The reduced growth of HLCS knockdown cells may result from the perturbation of mitochondrial oxidative phosphorylation, causing mitochondrial stress and apoptosis via downregulation of SURF1-like protein (SURF1), persulfide dioxygenase (ETHE1), and NADH: ubiquinone oxidoreductase subunit B9 (NDUFB9) (Tables 1, 2). SURF1 encodes an assembly factor of cytochrome oxidase of respiratory complex IV. The reduced expression of SURF1 can potentially impair cytochrome C oxidase activity, accelerating mitochondrial apoptosis in response to oxidative stress (Pequignot et al., 2001; Schull et al., 2015). ETHE1, a mitochondrial enzyme, detoxifies hydrogen persulfide, a harmful agent for cytochrome C oxidase. A recent study showed that ETHE1 is overexpressed in colorectal cancer, promoting aerobic glycolysis and mitochondria biogenesis (Witherspoon et al., 2019). Depleting ETHE1 expression induces oxidative stress, which aligns with the increased apoptosis of HLCS knockdown cells. NDUFB9 is a component of NADH dehydrogenase in the respiratory chain complex I. NDUFB9 was downregulated in highly metastatic breast cancer and silencing its expression in MDA-MB-231 cells promotes proliferation, migration, and invasion (Li et al., 2015). This inhibitory effect of NDUFB9 on tumor growth may be attributed to enhanced aerobic glycolysis in cancer cells (Li et al., 2015). The upregulation of NDUFB9 expression may be partly responsible for restricting MDA-MB-231 cell growth in response to HLCS suppression. The ganglioside GM2 activator (GM2A) activator protein is a specific glycolipid transport that binds to ganglioside GM2 and facilitates degradation. GM2A is associated with a programmed-cell death via interaction with tumor-necrosis receptor 1 receptor (Mahata et al., 2015). The increased abundance of GM2 activator may be attributed to the increased apoptosis in HLCS knockdown cells.

Kynureninase (KYNU) is an enzyme that catalyzes the reversible conversion of kynurenine to anthranilate and L-alanine. Kynurenine serves as the immunomodulant that protects cells against strong immune reactions. A recent study indicates that tumor cells hijack the kynurenine pathway to promote their growth and protect them from immune surveillance (Venkateswaran and Conacci-Sorrell, 2020). Kynurenine supports tumor growth by acting as the ligand for the aryl hydrocarbon receptor-transcription factor that activates oncogenic growth. Regarding immunomodulation, kynurenine suppresses T-lymphocyte proliferation by modulating their metabolism (Siska et al., 2021). Kynurenin was overexpressed in ductal and renal carcinoma, which confers ferroptosis-cell death (Liu et al., 2023).

Figure 5 summarizes the biological changes in response to HLCS knockdown. As previously reported, these combined effects likely

contribute to growth retardation, migration, invasion, cell cycle arrest, and apoptotic induction.

Data availability statement

The datasets presented in this study can be found in online repositories. The names of the repository/repositories and accession number(s) can be found in the article/Supplementary Material.

Ethics statement

Ethical approval was not required for the studies on humans in accordance with the local legislation and institutional requirements because only commercially available established cell lines were used.

Author contributions

WS designed and performed experiments, analyzed data, and wrote the original version of the manuscript. CY performed the LC-MS analyses and edited the manuscript. MA and SR provided useful suggestions and edited the manuscript. SS performed one experiment and generated an illustration. MK-H and PH designed experiments, provided supervision and resources. SJ contributed to project administration, designed experiments, provided supervision, edited the manuscript, and acquired financial support. All authors contributed to the article and approved the submitted version.

Funding

This work was supported by the International Research Network grant (IRN59W0003) from the Thailand Science Research and Innovation (TSRI) to SJ, and WS was supported by the Ph.D. scholarship from IRN59W0003 grant.

Conflict of interest

The authors declare that the research was conducted in the absence of any commercial or financial relationships that could be construed as a potential conflict of interest.

Publisher's note

All claims expressed in this article are solely those of the authors and do not necessarily represent those of their affiliated organizations, or those of the publisher, the editors and the reviewers. Any product that may be evaluated in this article, or claim that may be made by its manufacturer, is not guaranteed or endorsed by the publisher.

Supplementary material

The Supplementary Material for this article can be found online at: https://www.frontiersin.org/articles/10.3389/fmolb.2023.1250423/full#supplementary-material

References

Agnihotri, N., and Mehta, K. (2017). Transglutaminase-2: evolution from pedestrian protein to a promising therapeutic target. *Amino Acids* 49 (3), 425–439. doi:10.1007/s00726-016-2320-2

Alpha, K. M., Xu, W., and Turner, C. E. (2020). Paxillin family of focal adhesion adaptor proteins and regulation of cancer cell invasion. *Int. Rev. Cell Mol. Biol.* 355, 1–52. doi:10.1016/bs.ircmb.2020.05.003

Amcheslavsky, A., Wang, S., Fogarty, C. E., Lindblad, J. L., Fan, Y., and Bergmann, A. (2018). Plasma membrane localization of apoptotic caspases for non-apoptotic functions. *Dev. Cell* 45 (4), 450–464. doi:10.1016/j.devcel.2018.04.020

An, H., Ma, X., Liu, M., Wang, X., Wei, X., Yuan, W., et al. (2019). Stomatin plays a suppressor role in non-small cell lung cancer metastasis. *Chin. J. Cancer Res.* 31 (6), 930–944. doi:10.21147/j.issn.1000-9604.2019.06.09

Andrijes, R., Hejmadi, R. K., Pugh, M., Rajesh, S., Novitskaya, V., Ibrahim, M., et al. (2021). Tetraspanin 6 is a regulator of carcinogenesis in colorectal cancer. *Proc. Natl. Acad. Sci. U. S. A.* 118 (39), e2011411118. doi:10.1073/pnas.2011411118

Avelar, R. A., Ortega, J. G., Tacutu, R., Tyler, E. J., Bennett, D., Binetti, P., et al. (2020). A multidimensional systems biology analysis of cellular senescence in aging and disease. *Genome Biol.* 21 (1), 91. doi:10.1186/s13059-020-01990-9

Bailey, L. M., Wallace, J. C., and Polyak, S. W. (2010). Holocarboxylase synthetase: correlation of protein localisation with biological function. *Arch. Biochem. Biophys.* 496 (1), 45–52. doi:10.1016/j.abb.2010.01.015

Bakhshoudeh, M., Mehdizadeh, K., Hosseinkhani, S., and Ataei, F. (2021). Upregulation of apoptotic protease activating factor-1 expression correlates with anti-tumor effect of taxane drug. *Med. Oncol.* 38 (8), 88. doi:10.1007/s12032-021-01532-8

Ben Hassen, C., Gutierrez-Pajares, J. L., Guimaraes, C., Guibon, R., Pinault, M., Fromont, G., et al. (2020). Apolipoprotein-mediated regulation of lipid metabolism induces distinctive effects in different types of breast cancer cells. *Breast Cancer Res.* 22 (1), 38. doi:10.1186/s13058-020-01276-9

Cappel, D. A., Deja, S., Duarte, J. A. G., Kucejova, B., Inigo, M., Fletcher, J. A., et al. (2019). Pyruvate-carboxylase-mediated anaplerosis promotes antioxidant capacity by sustaining TCA cycle and redox metabolism in liver. *Cell Metab.* 29 (6), 1291–1305. doi:10.1016/j.cmet.2019.03.014

Chambers, A. F., and Matrisian, L. M. (1997). Changing views of the role of matrix metalloproteinases in metastasis. *J. Natl. Cancer Inst.* 89 (17), 1260–1270. doi:10.1093/jnci/89.17.1260

Chen, C. Y., Yang, C. Y., Chen, Y. C., Shih, C. W., Lo, S. S., and Lin, C. H. (2016). Decreased expression of stomatin predicts poor prognosis in HER2-positive breast cancer. *BMC Cancer* 16 (1), 697. doi:10.1186/s12885-016-2681-7

Chen, G., Hitomi, M., Han, J., and Stacey, D. W. (2000). The p38 pathway provides negative feedback for Ras proliferative signaling. *J. Biol. Chem.* 275 (50), 38973–38980. doi:10.1074/jbc.M002856200

Chen, M., Myers, A. K., Markey, M. P., and Long, W. (2019a). The atypical MAPK ERK3 potently suppresses melanoma cell growth and invasiveness. *J. Cell Physiol.* 234 (8), 13220–13232. doi:10.1002/jcp.27994

Chen, Y. F., Wei, Y. Y., Yang, C. C., Liu, C. J., Yeh, L. Y., Chou, C. H., et al. (2019b). miR-125b suppresses oral oncogenicity by targeting the anti-oxidative gene PRXL2A. *Redox Biol.* 22, 101140. doi:10.1016/j.redox.2019.101140

Choksi, A., Parulekar, A., Pant, R., Shah, V. K., Nimma, R., Firmal, P., et al. (2021). Tumor suppressor SMAR1 regulates PKM alternative splicing by HDAC6-mediated deacetylation of PTBP1. *Cancer Metab.* 9 (1), 16. doi:10.1186/s40170-021-00252-x

Condello, S., Prasad, M., Atwani, R., and Matei, D. (2022). Tissue transglutaminase activates integrin-linked kinase and β-catenin in ovarian cancer. *J. Biol. Chem.* 298 (8), 102242. doi:10.1016/j.jbc.2022.102242

Dang, C. V., Kim, J. W., Gao, P., and Yustein, J. (2008). The interplay between MYC and HIF in cancer. *Nat. Rev. Cancer* 8 (1), 51–56. doi:10.1038/nrc2274

Davidson, S. M., Papagiannakopoulos, T., Olenchock, B. A., Heyman, J. E., Keibler, M. A., Luengo, A., et al. (2016). Environment impacts the metabolic dependencies of ras-driven non-small cell lung cancer. *Cell Metab.* 23 (3), 517–528. doi:10.1016/j.cmet.2016.01.007

Davidson, S. M., Schmidt, D. R., Heyman, J. E., O'Brien, J. P., Liu, A. C., Israelsen, W. J., et al. (2022). Pyruvate kinase M1 suppresses development and progression of prostate adenocarcinoma. *Cancer Res.* 82 (13), 2403–2416. doi:10.1158/0008-5472.CAN-21-2352

DeBerardinis, R. J., and Chandel, N. S. (2016). Fundamentals of cancer metabolism. *Sci. Adv.* 2 (5), e1600200. doi:10.1126/sciadv.1600200

Diaz-Valencia, J. D., Estrada-Abreo, L. A., Rodriguez-Cruz, L., Salgado-Aguayo, A. R., and Patino-Lopez, G. (2022). Class I Myosins, molecular motors involved in cell migration and cancer. *Cell Adh Migr.* 16 (1), 1–12. doi:10.1080/19336918.2021.2020705

Ding, Y., Fang, J., Chen, M., Xu, Y., Liu, N., Fang, S., et al. (2022). MT1X is an oncogene and indicates prognosis in ccRCC. *Biosci. Rep.* 42 (10). doi:10.1042/BSR20221128

Du, Z., Zhang, X., Gao, W., and Yang, J. (2021). Differentially expressed genes PCCA, ECHS1, and HADH are potential prognostic biomarkers for gastric cancer. *Sci. Prog.* 104 (2), 368504211011344. doi:10.1177/00368504211011344

Erzurumlu, Y., and Ballar, P. (2017). Androgen mediated regulation of endoplasmic reticulum-associated degradation and its effects on prostate cancer. *Sci. Rep.* 7, 40719. doi:10.1038/srep40719

Fermaintt, C. S., Takahashi-Ruiz, L., Liang, H., Mooberry, S. L., and Risinger, A. L. (2021). Eribulin activates the cGAS-STING pathway via the cytoplasmic accumulation of mitochondrial DNA. *Mol. Pharmacol.* 100 (4), 309–318. doi:10.1124/molpharm.121.000297

Fong, C. W., Chua, M. S., McKie, A. B., Ling, S. H., Mason, V., Li, R., et al. (2006). Sprouty 2, an inhibitor of mitogen-activated protein kinase signaling, is down-regulated in hepatocellular carcinoma. *Cancer Res.* 66 (4), 2048–2058. doi:10.1158/0008-5472.CAN-05-1072

Foran, E., McWilliam, P., Kelleher, D., Croke, D. T., and Long, A. (2006). The leukocyte protein L-plastin induces proliferation, invasion and loss of E-cadherin expression in colon cancer cells. *Int. J. Cancer* 118 (8), 2098–2104. doi:10.1002/ijc.21593

Fu, A., Alvarez-Perez, J. C., Avizonis, D., Kin, T., Ficarro, S. B., Choi, D. W., et al. (2020). Glucose-dependent partitioning of arginine to the urea cycle protects β-cells from inflammation. *Nat. Metab.* 2 (5), 432–446. doi:10.1038/s42255-020-0199-4

Gondas, E., Kralova Trancikova, A., Baranovicova, E., Sofranko, J., Hatok, J., Kowtharapu, B. S., et al. (2022). Expression of 3-methylcrotonyl-CoA carboxylase in brain tumors and capability to catabolize leucine by human neural cancer cells. *Cancers (Basel)* 14 (3), 585. doi:10.3390/cancers14030585

Hajaj, E., Sciacovelli, M., Frezza, C., and Erez, A. (2021). The context-specific roles of urea cycle enzymes in tumorigenesis. *Mol. Cell* 81 (18), 3749–3759. doi:10.1016/j.molcel.2021.08.005

Hanahan, D. (2022). Hallmarks of cancer: new dimensions. *Cancer Discov.* 12 (1), 31–46. doi:10.1158/2159-8290.CD-21-1059

Harris, N. L. E., Vennin, C., Conway, J. R. W., Vine, K. L., Pinese, M., Cowley, M. J., et al. (2017). SerpinB2 regulates stromal remodelling and local invasion in pancreatic cancer. *Oncogene* 36 (30), 4288–4298. doi:10.1038/onc.2017.63

He, Y., Chen, J., Ma, Y., and Chen, H. (2022). Apolipoproteins: new players in cancers. *Front. Pharmacol.* 13, 1051280. doi:10.3389/fphar.2022.1051280

Hou, T., Zhou, L., Wang, L., Kazobinka, G., Chen, Y., Zhang, X., et al. (2018). Leupaxin promotes bladder cancer proliferation, metastasis, and angiogenesis through the PI3K/AKT pathway. *Cell Physiol. Biochem.* 47 (6), 2250–2260. doi:10.1159/000491536

Hu, B., Elinav, E., Huber, S., Booth, C. J., Strowig, T., Jin, C., et al. (2010). Inflammation-induced tumorigenesis in the colon is regulated by caspase-1 and NLRC4. *Proc. Natl. Acad. Sci. U. S. A.* 107 (50), 21635–21640. doi:10.1073/pnas.1016814108

Iftikhar, R., Penrose, H. M., King, A. N., Samudre, J. S., Collins, M. E., Hartono, A. B., et al. (2021). Elevated ATGL in colon cancer cells and cancer stem cells promotes metabolic and tumorigenic reprogramming reinforced by obesity. *Oncogenesis* 10 (11), 82. doi:10.1038/s41389-021-00373-4

Jin, L., Yuan, R. Q., Fuchs, A., Yao, Y., Joseph, A., Schwall, R., et al. (1997). Expression of interleukin-1beta in human breast carcinoma. *Cancer* 80 (3), 421–434. doi:10.1002/(sici)1097-0142(19970801)80:3<421::aid-cncr10>3.0.co;2-z

Julien, C., Coulombe, P., and Meloche, S. (2003). Nuclear export of ERK3 by a CRM1-dependent mechanism regulates its inhibitory action on cell cycle progression. *J. Biol. Chem.* 278 (43), 42615–42624. doi:10.1074/jbc.M302724200

Kaulfuss, S., Grzmil, M., Hemmerlein, B., Thelen, P., Schweyer, S., Neesen, J., et al. (2008). Leupaxin, a novel coactivator of the androgen receptor, is expressed in prostate cancer and plays a role in adhesion and invasion of prostate carcinoma cells. *Mol. Endocrinol.* 22 (7), 1606–1621. doi:10.1210/me.2006-0546

Kaulfuss, S., Herr, A. M., Buchner, A., Hemmerlein, B., Gunthert, A. R., and Burfeind, P. (2015). Leupaxin is expressed in mammary carcinoma and acts as a transcriptional activator of the estrogen receptor α. *Int. J. Oncol.* 47 (1), 106–114. doi:10.3892/ijo.2015.2988

Kaulfuss, S., von Hardenberg, S., Schweyer, S., Herr, A. M., Laccone, F., Wolf, S., et al. (2009). Leupaxin acts as a mediator in prostate carcinoma progression through deregulation of p120catenin expression. *Oncogene* 28 (45), 3971–3982. doi:10.1038/onc.2009.254

Kawazoe, T., and Taniguchi, K. (2019). The Sprouty/Spred family as tumor suppressors: coming of age. *Cancer Sci.* 110 (5), 1525–1535. doi:10.1111/cas.13999

Khare, S., Kim, L. C., Lobel, G., Doulias, P. T., Ischiropoulos, H., Nissim, I., et al. (2021). ASS1 and ASL suppress growth in clear cell renal cell carcinoma via altered nitrogen metabolism. *Cancer Metab.* 9 (1), 40. doi:10.1186/s40170-021-00271-8

Kim, S., Lee, M., Song, Y., Lee, S. Y., Choi, I., Park, I. S., et al. (2021). Argininosuccinate synthase 1 suppresses tumor progression through activation of PERK/eIF2α/ATF4/CHOP axis in hepatocellular carcinoma. *J. Exp. Clin. Cancer Res.* 40 (1), 127. doi:10.1186/s13046-021-01912-y

Ko, Y. S., Bae, J. A., Kim, K. Y., Kim, S. J., Sun, E. G., Lee, K. H., et al. (2019). MYO1D binds with kinase domain of the EGFR family to anchor them to plasma membrane before their activation and contributes carcinogenesis. *Oncogene* 38 (49), 7416–7432. doi:10.1038/s41388-019-0954-8

Krizkova, S., Kepinska, M., Emri, G., Eckschlager, T., Stiborova, M., Pokorna, P., et al. (2018). An insight into the complex roles of metallothioneins in malignant diseases with emphasis on (sub)isoforms/isoforms and epigenetics phenomena. *Pharmacol. Ther.* 183, 90–117. doi:10.1016/j.pharmthera.2017.10.004

Lee, G., Jeong, Y. S., Kim, D. W., Kwak, M. J., Koh, J., Joo, E. W., et al. (2018a). Clinical significance of APOB inactivation in hepatocellular carcinoma. *Exp. Mol. Med.* 50 (11), 1–12. doi:10.1038/s12276-018-0174-2

Lee, J. S., Adler, L., Karathia, H., Carmel, N., Rabinovich, S., Auslander, N., et al. (2018b). Urea cycle dysregulation generates clinically relevant genomic and biochemical signatures. *Cell* 174 (6), 1559–1570. doi:10.1016/j.cell.2018.07.019

Leon-Del-Rio, A., Valadez-Graham, V., and Gravel, R. A. (2017). Holocarboxylase synthetase: a moonlighting transcriptional coregulator of gene expression and a cytosolic regulator of biotin utilization. *Annu. Rev. Nutr.* 37, 207–223. doi:10.1146/annurev-nutr-042617-104653

Li, L. D., Sun, H. F., Liu, X. X., Gao, S. P., Jiang, H. L., Hu, X., et al. (2015). Down-regulation of NDUFB9 promotes breast cancer cell proliferation, metastasis by mediating mitochondrial metabolism. *PLoS One* 10 (12), e0144441. doi:10.1371/journal.pone.0144441

Liu, D., Liang, C. H., Huang, B., Zhuang, X., Cui, W., Yang, L., et al. (2023). Tryptophan metabolism acts as a new anti-ferroptotic pathway to mediate tumor growth. *Adv. Sci. (Weinh)* 10 (6), e2204006. doi:10.1002/advs.202204006

Liu, H., Kato, Y., Erzinger, S. A., Kiriakova, G. M., Qian, Y., Palmieri, D., et al. (2012). The role of MMP-1 in breast cancer growth and metastasis to the brain in a xenograft model. *BMC Cancer* 12, 583. doi:10.1186/1471-2407-12-583

Liu, Y., Yuan, Z., and Song, C. (2019). Methylcrotonoyl-CoA carboxylase 2 overexpression predicts an unfavorable prognosis and promotes cell proliferation in breast cancer. *Biomark. Med.* 13 (6), 427–436. doi:10.2217/bmm-2018-0475

Liu, Z., Ye, Q., Wu, L., Gao, F., Xie, H., Zhou, L., et al. (2018). Metallothionein 1 family profiling identifies MT1X as a tumor suppressor involved in the progression and metastastatic capacity of hepatocellular carcinoma. *Mol. Carcinog.* 57 (11), 1435–1444. doi:10.1002/mc.22846

Mahata, B., Biswas, S., Rayman, P., Chahlavi, A., Ko, J., Bhattacharjee, A., et al. (2015). GBM derived gangliosides induce T cell apoptosis through activation of the caspase cascade involving both the extrinsic and the intrinsic pathway. *PLoS One* 10 (7), e0134425. doi:10.1371/journal.pone.0134425

Milgraum, L. Z., Witters, L. A., Pasternack, G. R., and Kuhajda, F. P. (1997). Enzymes of the fatty acid synthesis pathway are highly expressed in *in situ* breast carcinoma. *Clin. Cancer Res.* 3 (11), 2115–2120.

Miyamoto, T., Lo, P. H. Y., Saichi, N., Ueda, K., Hirata, M., Tanikawa, C., et al. (2017). Argininosuccinate synthase 1 is an intrinsic Akt repressor transactivated by p53. *Sci. Adv.* 3 (5), e1603204. doi:10.1126/sciadv.1603204

Mu, J., Yuan, P., Luo, J., Chen, Y., Tian, Y., Ding, L., et al. (2022). Upregulated SPAG6 promotes acute myeloid leukemia progression through MYO1D that regulates the EGFR family expression. *Blood Adv.* 6 (18), 5379–5394. doi:10.1182/bloodadvances.2021006920

Ngamkham, J., Thuwajit, C., Thuwajit, P., Khamwachirapithak, P., Lertsuwan, K., Charoensawan, V., et al. (2020). Overexpression of pyruvate carboxylase is correlated with colorectal cancer progression and supports growth of invasive colon cancer HT-29 cell line. *Anticancer Res.* 40 (11), 6285–6293. doi:10.21873/anticanres.14649

Oh, K., Lee, O. Y., Park, Y., Seo, M. W., and Lee, D. S. (2016). IL-1β induces IL-6 production and increases invasiveness and estrogen-independent growth in a TG2-dependent manner in human breast cancer cells. *BMC Cancer* 16 (1), 724. doi:10.1186/s12885-016-2746-7

Park, T., Chen, Z. P., and Leavitt, J. (1994). Activation of the leukocyte plastin gene occurs in most human cancer cells. *Cancer Res.* 54 (7), 1775–1781.

Pavlova, N. N., and Thompson, C. B. (2016). The emerging hallmarks of cancer metabolism. *Cell Metab.* 23 (1), 27–47. doi:10.1016/j.cmet.2015.12.006

Pequignot, M. O., Dey, R., Zeviani, M., Tiranti, V., Godinot, C., Poyau, A., et al. (2001). Mutations in the SURF1 gene associated with Leigh syndrome and cytochrome C oxidase deficiency. *Hum. Mutat.* 17 (5), 374–381. doi:10.1002/humu.1112

Phannasil, P., Thuwajit, C., Warnnissorn, M., Wallace, J. C., MacDonald, M. J., and Jitrapakdee, S. (2015). Pyruvate carboxylase is up-regulated in breast cancer and essential to support growth and invasion of MDA-MB-231 cells. *PLoS One* 10 (6), e0129848. doi:10.1371/journal.pone.0129848

Pop, C., Timmer, J., Sperandio, S., and Salvesen, G. S. (2006). The apoptosome activates caspase-9 by dimerization. *Mol. Cell* 22 (2), 269–275. doi:10.1016/j.molcel.2006.03.009

Qiu, F., Chen, Y. R., Liu, X., Chu, C. Y., Shen, L. J., Xu, J., et al. (2014). Arginine starvation impairs mitochondrial respiratory function in ASS1-deficient breast cancer cells. *Sci. Signal* 7 (319), ra31. doi:10.1126/scisignal.2004761

Rabinovich, S., Adler, L., Yizhak, K., Sarver, A., Silberman, A., Agron, S., et al. (2015). Diversion of aspartate in ASS1-deficient tumours fosters *de novo* pyrimidine synthesis. *Nature* 527 (7578), 379–383. doi:10.1038/nature15529

Rahman, N. I. A., Sato, A., Tsevelnorov, K., Shimizu, A., Komeno, M., Ahmat Amin, M. K. B., et al. (2021). Stomatin-mediated inhibition of the Akt signaling Axis suppresses tumor growth. *Cancer Res.* 81 (9), 2318–2331. doi:10.1158/0008-5472.CAN-20-2331

Rebe, C., and Ghiringhelli, F. (2020). Interleukin-1β and cancer. *Cancers (Basel)* 12 (7), 1791. doi:10.3390/cancers12071791

Reed, J. R., Leon, R. P., Hall, M. K., and Schwertfeger, K. L. (2009). Interleukin-1beta and fibroblast growth factor receptor 1 cooperate to induce cyclooxygenase-2 during early mammary tumourigenesis. *Breast Cancer Res.* 11 (2), R21. doi:10.1186/bcr2246

Ren, X., Ma, L., Wang, N., Zhou, R., Wu, J., Xie, X., et al. (2021). Antioxidant gene signature impacts the immune infiltration and predicts the prognosis of kidney renal clear cell carcinoma. *Front. Genet.* 12, 721252. doi:10.3389/fgene.2021.721252

Sato, A., Rahman, N. I. A., Shimizu, A., and Ogita, H. (2021). Cell-to-cell contact-mediated regulation of tumor behavior in the tumor microenvironment. *Cancer Sci.* 112 (10), 4005–4012. doi:10.1111/cas.15114

Schull, S., Gunther, S. D., Brodesser, S., Seeger, J. M., Tosetti, B., Wiegmann, K., et al. (2015). Cytochrome c oxidase deficiency accelerates mitochondrial apoptosis by activating ceramide synthase 6. *Cell Death Dis.* 6 (3), e1691. doi:10.1038/cddis.2015.62

Sellers, K., Fox, M. P., Bousamra, M., 2nd, Slone, S. P., Higashi, R. M., Miller, D. M., et al. (2015). Pyruvate carboxylase is critical for non-small-cell lung cancer proliferation. *J. Clin. Invest* 125 (2), 687–698. doi:10.1172/JCI72873

Shinde, A., Wilmanski, T., Chen, H., Teegarden, D., and Wendt, M. K. (2018). Pyruvate carboxylase supports the pulmonary tropism of metastatic breast cancer. *Breast Cancer Res.* 20 (1), 76. doi:10.1186/s13058-018-1008-9

Si, M., and Lang, J. (2018). The roles of metallothioneins in carcinogenesis. *J. Hematol. Oncol.* 11 (1), 107. doi:10.1186/s13045-018-0645-x

Siritutsoontorn, S., Sukjoi, W., Polyak, S. W., Akekawatchai, C., and Jitrapakdee, S. (2022). Differential growth inhibition, cell cycle arrest and apoptosis of MCF-7 and MDA-MB-231 cells to holocarboxylase synthetase suppression. *Biochem. Biophys. Res. Commun.* 593, 108–115. doi:10.1016/j.bbrc.2022.01.049

Siska, P. J., Jiao, J., Matos, C., Singer, K., Berger, R. S., Dettmer, K., et al. (2021). Kynurenine induces T cell fat catabolism and has limited suppressive effects *in vivo*. *EBioMedicine* 74, 103734. doi:10.1016/j.ebiom.2021.103734

Sternicki, L. M., Wegener, K. L., Bruning, J. B., Booker, G. W., and Polyak, S. W. (2017). Mechanisms governing precise protein biotinylation. *Trends Biochem. Sci.* 42 (5), 383–394. doi:10.1016/j.tibs.2017.02.001

Stine, Z. E., Schug, Z. T., Salvino, J. M., and Dang, C. V. (2022). Targeting cancer metabolism in the era of precision oncology. *Nat. Rev. Drug Discov.* 21 (2), 141–162. doi:10.1038/s41573-021-00339-6

Stoiber, K., Naglo, O., Pernpeintner, C., Zhang, S., Koeberle, A., Ulrich, M., et al. (2018). Targeting *de novo* lipogenesis as a novel approach in anti-cancer therapy. *Br. J. Cancer* 118 (1), 43–51. doi:10.1038/bjc.2017.374

Sukjoi, W., Siritutsoontorn, S., Chansongkrow, P., Waiwitlikhit, S., Polyak, S. W., Warnnissorn, M., et al. (2020). Overexpression of holocarboxylase synthetase predicts lymph node metastasis and unfavorable prognosis in breast cancer. *Anticancer Res.* 40 (8), 4557–4565. doi:10.21873/anticanres.14461

Svensson, R. U., Parker, S. J., Eichner, L. J., Kolar, M. J., Wallace, M., Brun, S. N., et al. (2016). Inhibition of acetyl-CoA carboxylase suppresses fatty acid synthesis and tumor growth of non-small-cell lung cancer in preclinical models. *Nat. Med.* 22 (10), 1108–1119. doi:10.1038/nm.4181

Takahashi-Ruiz, L., Fermaintt, C. S., Wilkinson, N. J., Chan, P. Y. W., Mooberry, S. L., and Risinger, A. L. (2022). The microtubule destabilizer Eribulin synergizes with STING agonists to promote antitumor efficacy in triple-negative breast cancer models. *Cancers (Basel)* 14 (23), 5962. doi:10.3390/cancers14235962

Taskinen, M., Louhimo, R., Koivula, S., Chen, P., Rantanen, V., Holte, H., et al. (2014). Deregulation of COMMD1 is associated with poor prognosis in diffuse large B-cell lymphoma. *PLoS One* 9 (3), e91031. doi:10.1371/journal.pone.0091031

Thomas, P. D., Campbell, M. J., Kejariwal, A., Mi, H., Karlak, B., Daverman, R., et al. (2003). PANTHER: a library of protein families and subfamilies indexed by function. *Genome Res.* 13 (9), 2129–2141. doi:10.1101/gr.772403

Tiedemann, K., Sadvakassova, G., Mikolajewicz, N., Juhas, M., Sabirova, Z., Tabaries, S., et al. (2019). Exosomal release of L-plastin by breast cancer cells facilitates metastatic bone osteolysis. *Transl. Oncol.* 12 (3), 462–474. doi:10.1016/j.tranon.2018.11.014

Tong, L. (2017). Striking diversity in holoenzyme architecture and extensive conformational variability in biotin-dependent carboxylases. *Adv. Protein Chem. Struct. Biol.* 109, 161–194. doi:10.1016/bs.apcsb.2017.04.006

Valiente, M., Obenauf, A. C., Jin, X., Chen, Q., Zhang, X. H., Lee, D. J., et al. (2014). Serpins promote cancer cell survival and vascular co-option in brain metastasis. *Cell* 156 (5), 1002–1016. doi:10.1016/j.cell.2014.01.040

Vander Heiden, M. G. (2011). Targeting cancer metabolism: a therapeutic window opens. *Nat. Rev. Drug Discov.* 10 (9), 671–684. doi:10.1038/nrd3504

Vander Heiden, M. G., and DeBerardinis, R. J. (2017). Understanding the intersections between metabolism and cancer biology. *Cell* 168 (4), 657–669. doi:10.1016/j.cell.2016.12.039

Venkateswaran, N., and Conacci-Sorrell, M. (2020). Kynurenine: an oncometabolite in colon cancer. *Cell Stress* 4 (1), 24–26. doi:10.15698/cst2020.01.210

Wang, Q. M., Lv, L., Tang, Y., Zhang, L., and Wang, L. F. (2019). MMP-1 is overexpressed in triple-negative breast cancer tissues and the knockdown of MMP-1 expression inhibits tumor cell malignant behaviors *in vitro*. *Oncol. Lett.* 17 (2), 1732–1740. doi:10.3892/ol.2018.9779

Wang, X., Yu, Z., Zhou, Q., Wu, X., Chen, X., Li, J., et al. (2016). Tissue transglutaminase-2 promotes gastric cancer progression via the ERK1/2 pathway. *Oncotarget* 7 (6), 7066–7079. doi:10.18632/oncotarget.6883

Weiskirchen, R., and Penning, L. C. (2021). COMMD1, a multi-potent intracellular protein involved in copper homeostasis, protein trafficking, inflammation, and cancer. *J. Trace Elem. Med. Biol.* 65, 126712. doi:10.1016/j.jtemb.2021.126712

Witherspoon, M., Sandu, D., Lu, C., Wang, K., Edwards, R., Yeung, A., et al. (2019). ETHE1 overexpression promotes SIRT1 and PGC1α mediated aerobic glycolysis, oxidative phosphorylation, mitochondrial biogenesis and colorectal cancer. *Oncotarget* 10 (40), 4004–4017. doi:10.18632/oncotarget.26958

Wu, T., Hong, Y., Jia, L., Wu, J., Xia, J., Wang, J., et al. (2016). Modulation of IL-1β reprogrammes the tumor microenvironment to interrupt oral carcinogenesis. *Sci. Rep.* 6, 20208. doi:10.1038/srep20208

Xiang, Y., Chen, Y. J., Yan, Y. B., Liu, Y., Qiu, J., Tan, R. Q., et al. (2020). MiR-186 bidirectionally regulates cisplatin sensitivity of ovarian cancer cells via suppressing targets PIK3R3 and PTEN and upregulating APAF1 expression. *J. Cancer* 11 (12), 3446–3453. doi:10.7150/jca.41135

Yan, H., Luo, B., Wu, X., Guan, F., Yu, X., Zhao, L., et al. (2021). Cisplatin induces pyroptosis via activation of MEG3/NLRP3/caspase-1/GSDMD pathway in triple-negative breast cancer. *Int. J. Biol. Sci.* 17 (10), 2606–2621. doi:10.7150/ijbs.60292

Yang, L. N., Pu, J. C., Liu, L. X., Wang, G. W., Zhou, X. Y., Zhang, Y. Q., et al. (2019). Integrated metabolomics and proteomics analysis revealed second messenger system disturbance in Hippocampus of chronic social defeat stress rat. *Front. Neurosci.* 13, 247. doi:10.3389/fnins.2019.00247

Yang, Y., Tu, Y., Lu, J., Chen, Q., Zhu, Z., Peng, W., et al. (2022). PT109, a novel multi-kinase inhibitor suppresses glioblastoma multiforme through cell reprogramming: involvement of PTBP1/PKM1/2 pathway. *Eur. J. Pharmacol.* 920, 174837. doi:10.1016/j.ejphar.2022.174837

Yin, H., Li, W., Mo, L., Deng, S., Lin, W., Ma, C., et al. (2021). Adipose triglyceride lipase promotes the proliferation of colorectal cancer cells via enhancing the lipolytic pathway. *J. Cell Mol. Med.* 25 (8), 3963–3975. doi:10.1111/jcmm.16349

Yoon, J., Grinchuk, O. V., Kannan, S., Ang, M. J. Y., Li, Z., Tay, E. X. Y., et al. (2021). A chemical biology approach reveals a dependency of glioblastoma on biotin distribution. *Sci. Adv.* 7 (36), eabf6033. doi:10.1126/sciadv.abf6033

Yuan, W., Zhou, R., Wang, J., Han, J., Yang, X., Yu, H., et al. (2019). Circular RNA Cdr1as sensitizes bladder cancer to cisplatin by upregulating APAF1 expression through miR-1270 inhibition. *Mol. Oncol.* 13 (7), 1559–1576. doi:10.1002/1878-0261.12523

Zhang, R., Kang, R., and Tang, D. (2021a). The STING1 network regulates autophagy and cell death. *Signal Transduct. Target Ther.* 6 (1), 208. doi:10.1038/s41392-021-00613-4

Zhang, R., Meng, J., Yang, S., Liu, W., Shi, L., Zeng, J., et al. (2022). Recent advances on the role of ATGL in cancer. *Front. Oncol.* 12, 944025. doi:10.3389/fonc.2022.944025

Zhang, R., Zhang, H., Wei, H., and Luo, X. (2000). Expression of metallothionein in invasive ductal breast cancer in relation to prognosis. *J. Environ. Pathol. Toxicol. Oncol.* 19 (1-2), 95–97.

Zhang, Y., Lai, H., and Tang, B. (2021b). Abnormal expression and prognosis value of COG complex members in kidney renal clear cell carcinoma (KIRC). *Dis. Markers* 2021, 4570235. doi:10.1155/2021/4570235

Zhang, Y., Yuan, S., Pu, J., Yang, L., Zhou, X., Liu, L., et al. (2018). Integrated metabolomics and proteomics analysis of Hippocampus in a rat model of depression. *Neuroscience* 371, 207–220. doi:10.1016/j.neuroscience.2017.12.001

Zou, Z., Hu, X., Luo, T., Ming, Z., Chen, X., Xia, L., et al. (2021). Naturally-occurring spinosyn A and its derivatives function as argininosuccinate synthase activator and tumor inhibitor. *Nat. Commun.* 12 (1), 2263. doi:10.1038/s41467-021-22235-8

Frontiers in
Cell and Developmental Biology

Explores the fundamental biological processes of life, covering intracellular and extracellular dynamics.

The world's most cited developmental biology journal, advancing our understanding of the fundamental processes of life. It explores a wide spectrum of cell and developmental biology, covering intracellular and extracellular dynamics.

Discover the latest Research Topics

See more →

Frontiers

Avenue du Tribunal-Fédéral 34
1005 Lausanne, Switzerland
frontiersin.org

Contact us

+41 (0)21 510 17 00
frontiersin.org/about/contact